



2023-1

Tagungsbericht

DGMK/ÖGEW-Frühjahrstagung

Exploring the subsurface potential - make the energy
transition happen



DGMK und Autor(en) haben alle Sorgfalt walten lassen, um vollständige und akkurate Informationen in diesem Buch zu publizieren. Der Verlag übernimmt weder Garantie noch die juristische Verantwortung oder irgendeine Haftung für die Nutzung dieser Informationen, für deren Wirtschaftlichkeit oder fehlerfreie Funktion für einen bestimmten Zweck. Die DGMK übernimmt keine Gewähr dafür, dass die beschriebenen Verfahren, Programme usw. frei von Schutzrechten Dritter sind.

Alle Rechte vorbehalten

© DGMK e.V., Hamburg, 2023

Für Copyright in Bezug auf das verwendete Bildmaterial siehe Quellenangaben in den Abbildungsunterschriften.

Abbildungen ohne Quellenangabe sind von den Autoren.

Das Werk einschließlich aller seiner Teile ist urheberrechtlich geschützt. Jede Verwertung außerhalb der engen Grenzen des Urheberrechtsgesetzes ist ohne Zustimmung der DGMK unzulässig und strafbar. Das gilt insbesondere für Vervielfältigungen, Übersetzungen, Mikroverfilmungen und die Einspeicherung und Verarbeitung in elektronischen Systemen.

The work including all its parts is protected by copyright. Any use outside the narrow limits of the German Copyright Law without the consent of the DGMK is prohibited and punishable by law. This applies in particular to reproduction, translation, microfilming and storage and processing in electronic systems.

Umschlaggestaltung: DIE NEUDENKER®, Darmstadt | DGMK e.V., Hamburg

Titelfotografie: LiteHeavy/Shutterstock

ISSN 1433-9013

ISBN 978-3-947716-52-4

<https://www.dgmk.de>

| | | |
|---------------------------|--|--------------|
| Inhaltsverzeichnis | | Seite |
|---------------------------|--|--------------|

H2 Storage

| | |
|---|---|
| Über die Ermittlung der Anwendbarkeit von Stählen für Wasserstofftransport und -speicherung <i>G. Mori, B. Loder, C. Fournier, A. Reveillere, A.</i> | 1 |
| HySTORAGE: Preliminary investigations of possible hydrogen losses with focus on a planned hydrogen storage field test in Bierwang <i>Strobel, G., Kosack, C., Bombach, P., Fischer, A., Hagemann, B., Hogeweg, S.</i> | 2 |
| Netzbrücken - Dual-Direktionale Kavernen als verbindendes Element zwischen Strom- und Gasnetzen <i>Fischer, K., Wischert, J., Lüdtke, C., Lindemann, P., Feller, O.</i> | 3 |
| Characterization of OCTG material for the application in underground hydrogen storage caverns <i>Klarner, J., Schnideritsch, H., Friess, B., Kepplinger, J., Horvath, B., Haydl, R.</i> | 5 |

Digitale Transformation

| | |
|---|----|
| Vision4SRP: Digital monitoring system for sucker-rod pumps – an example for collaborative project development through co-creation <i>Fischer, D., Buchebner, M., Allmaras, M.</i> | 22 |
| Datenmanagement im Rahmen des Energie Management Systems der EMPG <i>Bauschulte, S.</i> | 28 |
| Möglichkeiten der Optimierung von Bohrplanungsprozessen durch Nutzung von Machine Learning <i>Ulumaskan, I.</i> | 31 |
| AI Use Cases for Asset Failure Prediction <i>Kisslinger, F., Hildinger, M., Möller, J.</i> | 32 |

Drilling Technology

| | |
|---|----|
| A discussion on the state of drillstring vibrations control: Industry vs Research <i>Sharma, A., Abid, K., Teodoriu, C.</i> | 39 |
| 100% Core Recovery in Potassium Salt Layers – Our Experience with MgCl₂-Mud-Systems <i>Schimmrigk, L.</i> | 49 |

| | |
|--|-----------|
| A new well shape with direct application to geothermal drilling in order to reduce costs and improve lifetime of the well | 50 |
| <i>Teodoriu, C.</i> | |

| | |
|--|-----------|
| Experimental Analysis of Cyclic Loading Effect on Seal Integrity of Cement Sheath | 55 |
| <i>Wu, X., Hou, Z., Li, Z., Xie, Y., Liu, J., Song, W., Li, J., Sun, W.</i> | |

HSE

| | |
|--|-----------|
| Life Saving Rules and Actions (LSRA) bei EMPG | 63 |
| <i>Hahn, C.</i> | |

| | |
|--|-----------|
| Geosteering Mittelplate (NW Deutschland) – Besondere Herausforderung während der Corona-Einschränkungen | 64 |
| <i>Bolten, H., Dellepiane, S., Schwarz, D., Berger, P.</i> | |

| | |
|----------------------------------|-----------|
| Process Safety Competency | 65 |
| <i>Schmid, S.</i> | |

| | |
|---|-----------|
| Human Performance Konzept bei EMPG | 66 |
| <i>Beyer, J. L.</i> | |

Energy Storage

| | |
|---|-----------|
| Gas Mixing Behavior and Flow Processes in Porous Media During the Conversion of Natural Gas Storage Facilities to Hydrogen Storage | 67 |
| <i>Toufighi, S. R., Moeininia, N., Bültemeier, H.</i> | |

| | |
|---|-----------|
| Compressed Air Energy Storage (CAES) Solutions | 89 |
| <i>Scheller, T.</i> | |

| | |
|--|-----------|
| Speicherung mechanischer Energie über künstliche Risse in gering durchlässigen Gesteinsformationen des tiefen Untergrunds | 91 |
| <i>Tischner, T., Krug, S., Jung, R.</i> | |

Geoscience

| | |
|--|-----------|
| Aspekte einer auf bohrlochgeophysikalischen Daten basierten Endlagersuche | 99 |
| <i>Strobel, J., Schöner, N., Zühlke, R.</i> | |

| | |
|---|------------|
| Systematische Integration von Bohrungsdaten zum Zweck der Identifizierung und Charakterisierung von geeigneten geologischen Barriere-Formationen | 102 |
| <i>Alles, S.</i> | |

| | |
|---|------------|
| Verbreitung von Sandsteinen der Unterkreide in Niedersachsen – neue Karten und Daten für die Geothermie | 103 |
| <i>Pierau, R., Schöner, R.</i> | |
| Speicherung von Kohlendioxid unter der Nordsee | 104 |
| <i>Wallmann, K.</i> | |
| CCS-Monitoring mit Gravimetrie – eine Sensitivitätsstudie | 105 |
| <i>Grobys, N., Roth, T., Petersen, S., Krieger, M.</i> | |
| Ein neues generalisiertes geologisches 3D-Modell für Niedersachsen (TUNB3D-NI) | 110 |
| <i>Helms, M., Sattler, S., Wangenheim, C., Ziesch, J., Schöner, R.</i> | |
| Das Geologiedatengesetz (GeolDG) - Zusammenspiel zwischen E&P-Industrie und den Staatlichen Geologischen Diensten am Beispiel des LBEG | 112 |
| <i>Brauner, H.-J.</i> | |

Production Engineering

| | |
|---|------------|
| Surfactant-based Diverting Agent for Acidizing: Lab Evaluation and Treatment of an Injector Well in a German Oil Field | 113 |
| <i>Lummer, N.</i> | |
| Entwicklung und Erprobung eines Tools zur Scaleentfernung in Rohren mittels Elektro-Impuls-Verfahren | 117 |
| <i>Anders, E., Klein, S.</i> | |
| Use of hydrogen as a fuel towards the decarbonization of gas turbines | 118 |
| <i>Zindel, E.</i> | |

Monitoring

| | |
|---|------------|
| Health, Safety and Environment – Positive impact on HSE using drones | 119 |
| <i>Wirth, S., Dinu, I.</i> | |
| Öffentliche Beteiligung im Geomonitoring – Der Erfolg am Untergrundgasspeicher Epe | 129 |
| <i>Rudolph, T., Goerke-Mallet, P., Müterthies, A., Teuwsen, S., Tomlik, C., Yang, C.-H.</i> | |
| Monitoring induzierter Seismizität in Niedersachsen aus operativer Sicht | 135 |
| <i>Bartels, T.</i> | |

Underground Storage Technology

| | |
|---|------------|
| Rekomplettierung von Ölkavernen zur Schaffung eines Überwachungsfähigen Ringraums am Kavernenspeicher Etzel <i>Patzer, S., Reekers, C.</i> | 137 |
| Planung und Durchführung einer Kavernenflutung unter Berücksichtigung der geologischen Rahmenbedingungen und nachgeschalteter Gaskonditionierung <i>Geisweller, M., Buzogany, R., Donadei, S., Gaßner, A.</i> | 138 |
| Aktuelle Forschungsaktivitäten zu gebirgsmechanischen Aspekten in Verbindung mit der Wasserstoffspeicherung in Salzkavernen <i>Lux, K.-H., Pan, T., Sun-Kurczinski, J., Zhao, J.</i> | 139 |
| Dry Recompletion of two gas storage cavern wells in UK <i>Lennox, A., Sloan, A., McMichael, C.</i> | 140 |

Petroleum Engineering

| | |
|--|------------|
| Exploring for unlocked subsurface potential by integration of historic and modern data: The case of a forgotten Flysch reservoir within the Vienna Basin (Austria) discovered almost a century ago <i>Moebius, R., Gauer, A. L., Tosoratti, F.</i> | 157 |
| Geological realization screening using Python script for reservoir simulation: First results of application on Mittelplate simulation model <i>Lin, L.</i> | 161 |
| EOR Barenburg: Pilot-Verlauf & -Ergebnisse <i>Kalunka, J.</i> | 163 |
| CO2-EOR in stark zerklüfteten Karbonatlagerstätten – Eine Fallstudie <i>Amro, M., Reichmann, S., Freese, C., Alkan, H.</i> | 164 |

Geothermal Energy

| | |
|---|------------|
| Stimulation der Geothermiebohrung Geretsried – Operativer Ablauf und Herausforderungen beim Technologietransfer aus der KW-Industrie <i>Tegeler, R., Backers, T.</i> | 169 |
| Geothermische Nachnutzung von Kohlenwasserstoffbohrungen durch tiefe Erdwärmesonden <i>Koltzer, N., Sporleder, M., Schoenherr, J., Steininger, S., Wellmann, F., Bracke, R., Kukla, P. A.</i> | 170 |

| | |
|--|------------|
| Large scale heat pumps and geothermal energy – an ideal couple for a greener heating scenario | 171 |
| <i>Schäfer, J., Wenn, N., Hüttl, C.</i> | |

| | |
|---|------------|
| Lessons learned from a geothermal well test with associated sour gas in the Vienna Basin | 172 |
| <i>Maierhofer, M., Romich, N., Hollmann, T.</i> | |

CC(U)S

| | |
|--|------------|
| Influence of Capillarity on Salt Precipitation during Primary CO₂-Brine Displacement | 177 |
|--|------------|

Jammernegg, B., Schollenberger, T., Hommel, J., Flemisch, B., Ott, H.

| | |
|--|------------|
| Development of a Well Delivery Process for CO₂ Injection Wells | 178 |
|--|------------|

Krueckert, K.

| | |
|--|------------|
| Importance of Proper Curing and Aging of Cements in Laboratory Testing for CCS Applications | 179 |
|--|------------|

Mandt, T., Czuprat, O., Fogden, A.

| | |
|---|------------|
| Comprehensive guidelines on the suitability criteria of cementitious materials for carbon capture and storage (CCS) in oil wells | 189 |
|---|------------|

Congiu, E., Mandt, T., Dideriksen, K., Canonico, F., Plack, H., Boccaleri, E., Cassino, C., Paul, G.

Performing while Transforming

| | |
|---|------------|
| Decentralised energy supply with fuel cells and green hydrogen | 196 |
|---|------------|

Lehmann, F., Michael, M., Beyer, U., Scheffler, S.

| | |
|--|------------|
| Reaktivierung Transition im Nachbergbau: Wie gelingt ein erfolgreicher Umschwung von traditioneller Ressourcennutzung zu erneuerbaren Energien? | 205 |
|--|------------|

Tiganj, J.

| | |
|---|------------|
| Digitale Transformation – Wie neue Technologie die Mitarbeiter inspirierte, den Betrieb eines mehr als 80 Jahre alten Öl Gasfeld zu modernisieren! | 206 |
|---|------------|

Bernold, M.

Postersession

| | |
|---|------------|
| Flood-induced seismicity in the Ruhr area – a geomechanics perspective | 207 |
| <i>Niederhuber, T., Müller, B., Röckel, T., Rische, M., Schilling, F.</i> | |
| The importance of studies on the mitigation of environmental impacts in the Santos Basin Region: Focus on pre-salt oil and gas activities. | 208 |
| <i>Oliveira, F., Oliveira, M., Nascimento, A.</i> | |
| Celsius Energy: An industrial, digital native geoenergy solution to accelerate the deployment of low-carbon heating and cooling | 219 |
| <i>Sosio, G., Merino, C.</i> | |
| Numerical Simulation of Bio-Geo-Reactive Transport during UHS - A Modelling Approach | 221 |
| <i>Hogeweg, S., Hagemann, B., Ganzer, L.</i> | |
| Experimental investigations and development of a correlation to characterize the diffusion process of hydrogen and methane during UHS | 231 |
| <i>Michelsen, J., Hogeweg, S., Hagemann, B., Langanke, N., Ganzer, L.</i> | |
| Biostratigraphic evaluation of data from the Mittelplate oilfield (NW Germany) | 246 |
| <i>Holstein, B., Schneider, C. A., Bolten, H.</i> | |
| Anforderungen und Realisierung eines Monitoringsystem zur Überwachung der Axiallastsituation in Bohrungs- Komplettierungen. Beschreibung der zum Einsatz kommenden Systeme | 254 |
| <i>Pfeifer, K., Hansen-Stichel, A., Maut, D.</i> | |
| Aktueller Forschungsstand zur thermischen Wasserstoffgewinnung aus ausgefördernten Erdöllagerstätten | 265 |
| <i>Bauer, J. F., Amro, M. M.</i> | |
| Verfolgung der Flüchtigen 200° Isotherm in Norddeutschland | 280 |
| <i>Heins, W. A., Masterton, S. M.</i> | |
| Diagenetic controls and reservoir quality of tight limestones from the Upper Cretaceous | 281 |
| <i>Ölmez, J. A., Busch, B., Hilgers, C.</i> | |
| Visualisation of microbial activities in reservoirs during UHS based on real-rock micromodels | 282 |
| <i>Cheng, C., Busch, B., von Dollen, M., Oelmez, J. A., Hilgers, C.</i> | |
| Comparative Analysis of Well Drilling Techniques for Natural Resources Access and Energy Recovery | 283 |
| <i>Maluf, T., Nascimento, N., Nascimento, A.</i> | |
| Drilling Geothermal wells, challenges, and solutions. | 284 |
| <i>Zapata Bermudez, F., Zajaczkowski, J.</i> | |

| | |
|--|------------|
| Optimize and de-risking the execution of Geothermal wells through real-time drilling interpretation | 293 |
| <i>Ferrando, P., Abolins, N.</i> | |
| Experimental determination of the capillary pressure to assess hydrogen integrity in completion systems | 304 |
| <i>Perozo, N., Jaeger, P.</i> | |
| Einsatz der FMEA-Methode zur Bewertung der Integrität untertägiger Kavernenspeicher | 305 |
| <i>Bachmann, N., Boernecke, D.</i> | |
| Experimental simulation of bit-rock interaction to study and analyze the effect of stick-slip vibrations on a drillstring | 307 |
| <i>Sharma, A., Teodoriu, C.</i> | |
| Large-scale underground energy storage: A key technology for carbon neutrality in China and Germany | 310 |
| <i>Xie, Y., Wu, X., Hou, M., Li, Z., Luo, J., Lüddeke, C., Huang, L., Sun, W.</i> | |
| Fluvio-deltaic facies interpretation using 3D-seismic attributes analysis and unsupervised machine-learning algorithm: Strategy to reduce geothermal exploration risk in the North German Basin | 322 |
| <i>Bello, L., von Hartmann, H., Franz, M., Moeck, I.</i> | |
| Hydrothermal und petrothermal: “TRENDS” – und ein Rückblick | 323 |
| <i>Behrens, H., Ghergut, J., Sauter, M., Haas, C., Winter, T., Zosseder, K.</i> | |
| Lithiumgewinnung im Thermalwasserkreislauf – wie es mitunter zu Fehlprognosen kommt | 332 |
| <i>Ghergut, J., Wiegand, B., Behrens, H., Sauter, M.</i> | |
| CompReact: Compositional Simulation of Reactive Transport in CO₂ Storage | 336 |
| <i>M. Wirth, W. Yan</i> | |

Keynote:

Über die Ermittlung der Anwendbarkeit von Stählen für Wasserstofftransport und -speicherung

G. Mori¹, B. Loder¹, C. Fournier², A. Reveillere²

¹Montanuniversität Leoben, Leoben, Österreich, ²Geostock SAS, Rueil-Malmaison Cedex Frankreich

Im Rahmen des Horizon2020-Projekts HyStorIES (Hydrogen Storage in European Subsurface) wurde ein umfangreiches experimentelles Versuchsprogramm zur Ermittlung der Anwendbarkeit von Stählen unter Hochdruckwasserstoff für die Gasspeicherung durchgeführt.

In praxisnahen Versuchen unter konstanter Last wurden gegenüber der Praxis deutlich aggressivere Bedingungen gewählt, so dass Aussagen über die Anwendbarkeit in Wasserstoffatmosphären erfolgen können. Es wurden die gängigen Stähle J55, K55, beide auch im geschweißten Zustand, L80 und höher feste Qualitäten untersucht.

Zusätzlich existiert eine Reihe von anderen Prüfmethoden (Langsamzugversuche, zyklische Versuche sowie bruchmechanische Tests). Alle haben ihre Berechtigung, keine dieser Prüfmethoden weist ausschließlich Vorteile auf. Die Prüfmethoden und Ergebnisse ausgewählter anderer Forschungsgruppen werden vorgestellt und kritisch miteinander verglichen.

HySTORAGE: Preliminary investigations of possible hydrogen losses with focus on a planned hydrogen storage field test in Bierwang

G. Strobel¹, C. Kosack¹, P. Bombach², A. Fischer², B. Hagemann³, S. Hogeweg³

¹Uniper Energy Storage GmbH, Düsseldorf, Germany, ²Isodetect GmbH, Leipzig, Germany, ³TU Clausthal, Institute of Subsurface Energy Systems, Clausthal-Zellerfeld, Germany

As part of the commitment archiving net zero by 2030, the interest in storing hydrogen in the subsurface has risen strongly. In order to conclude the technical feasibility of storing hydrogen in porous storage, a field trial is planned, where different hydrogen concentrations are mixed into a natural gas stream and stored in a porous formation. The three different concentrations (5%, 10%, 25% H₂) lead to three different sub-tests, each containing an injection, storage, and withdrawal phase and each sub-test with a total duration of ca. four months. Consequently, the field test is scheduled for at least 12 months. In detail, 150,000 m³ of natural-gas hydrogen mixture is injected, and withdrawn via the same well per one sub-test. In order to conclude the hydrogen recovery during the withdrawal phase and the overall operation of hydrogen storage, the existing operational monitoring is complemented by online gas composition measurement. During the preparation and execution of the field test, safe operation is ensured through implemented technical and organizational measures.

Besides the primary field test, accompanying and partly preliminary studies are performed to investigate and predict hydrogen losses, focusing on hydro-dynamical and microbiological effects. The complete research consists of experimental investigations before and during the field test, tracer tests, and reservoir simulations, including microbial conversion and mixing behavior.

Based on the literature, potential microbial metabolisms leading to a conversion of hydrogen are sulfate-reduction, methanation, and acetogenesis. To study the reactions, microbial growth experiments are performed before and during the field test. The pre-experiments with the formation water and the hydrogen-natural gas mixture show a significant hydrogen reduction in the reactors. Further, additional experiments are conducted with deuterium as a tracer to test its feasibility for a growth indicator in the reservoir.

As the first growth tests indicate a possible conversion of hydrogen, a change of hydrogen concentration during the field test can not be directly linked to the mixing of injected and the initial gas because microbial and mixing effects could overlap. Therefore it is planned to add a defined amount of helium to the injected gas mixture. As helium acts as an inert tracer, its concentration changes can be used to study the mixing behavior in the reservoir.

Based on the growth experiments and changes in gas composition, reservoir simulations are performed, which coupled the microbial activity with diffusion and dispersion effects. In the first step, a dynamic model is implemented to predict those effects and the performance of the field test.

Netzbrücken - Dual-Direktionale Kavernen als verbindendes Element zwischen Strom- und Gasnetzen

K. Fischer, J. Wischert, C. Lüdtke, P. Lindemann, O. Feller
Stablegrid Group, Schlagsdorf, Germany

Abstract

Durch den wachsenden Anteil erneuerbarer Energiequellen wie Onshore- und Offshore-Windenergie unterliegt das deutsche Stromnetz einer stark volatilen Leistungsbereitstellung. Aufgrund von Netzengpässen müssen regelmäßig maßgebliche Mengen elektrischer Leistung aus erneuerbaren Energien vom Netz genommen werden. Die Stablegrid Group und ihre Projektpartner planen, an ausgewählten Standorten in Niedersachsen und Mecklenburg-Vorpommern Elektrolyseanlagen zur stromerzeugungsoptimierten Wasserstoffproduktion mit angeschlossener untertägiger Speichereinheit zu errichten. Ziel ist es, einen Beitrag zur Netzstabilisierung zu leisten, indem bisher abgeregelte elektrische Energie bei Bedarf aus dem Netz entnommen und in Form von Wasserstoff in Salzkavernen eingespeichert wird. Der eingespeicherte Wasserstoff soll anschließend bedarfsgesteuert dem bestehenden Erdgasnetz beigemischt oder dem zukünftigen Wasserstoffnetz zugeführt werden. Als „Netzbrücke“ zwischen Strom- und Gasnetz versteht sich das Konzept als Instrument der unabhängigen Sektorenkopplung.

Für den Netzanschluss wird eine Stromleitung von einem geeigneten Anschlusspunkt zum Standort des Elektrolyseurs verlegt und die entnommene elektrische „Überschussenergie“ für die Produktion von Wasserstoff eingesetzt.

Aktuelle Herausforderungen

Nach dem Netzentwicklungsplan 2023 (NEP 2023) der Übertragungsnetzbetreiber, steigt der Bruttostromverbrauch bis 2045 um den Faktor zwei. Demnach muss die Erzeugung analog steigen und hierbei soll der Großteil vom Ausbau der Solar- und Windenergieanlagen bereits 2037 abgeschlossen sein. Eine erhöhte Erzeugung durch Erneuerbare Energien bewirkt gleichzeitig eine erhöhte Beanspruchung des Stromnetzes im Sinne der Volatilität.

Infolgedessen sollten weitere netzstabilisierende Maßnahmen getroffen werden. Denn schon jetzt zeigt sich, dass nördliche und östliche Bundesländer vergleichsweise deutliche Erzeugungsüberschüsse aufweisen. Aktuell ist deswegen ein verstärkter Netzausbau, vor allem in Norddeutschland vorgesehen. Darüber hinaus sind Speichertechnologien mit über 100 GW zur Unterstützung der Integration erneuerbarer Energien vorgesehen.

Besonders dem Wasserstoff wird eine wichtige Rolle zugesprochen. Die Verwendung des aus der Elektrolyse hergestellten Wasserstoffs als sekundären Energieträger ermöglicht eine zeitliche und örtliche Verschiebung der energetischen Nutzung.

Der Abruf der Anlagen erfolgt durch den Übertragungsnetzbetreiber im ausschließlichen Sinne der Netzdienlichkeit des Stromnetzes. Die neusten Regularien der EU erlauben in diesem Zusammenhang die Produktion von grünem Wasserstoff aus gelbem Überschussstrom [Delegated Act of 10.02.23; C(2023) 1087 final].

Gemäß NEP 2023 entfällt auf Schleswig-Holstein, Niedersachsen und Mecklenburg-Vorpommern über die Hälfte der deutschen Wasserstoffproduktion. Die hohe Wasserstoffproduktion kann den Erzeugungsüberschuss ausgleichen.

In den Szenarien des NEP 2023 wird davon ausgegangen, dass bis 2037 eine umfassende Wasserstoffinfrastruktur besteht. Bis spätestens 2045 soll Erdgas als Brennstoff für

Gaskraftwerke vollständig durch Wasserstoff ersetzt werden. Um dies zu erreichen, soll die installierte Leistung der Elektrolyseure zwischen 2037 und 2045 verdoppelt werden.

Die bislang angenommenen Standorte ergeben sich aus einer reinen Betrachtung im Sinne des Stromnetzes. Im weiteren Verfahren sollten die Standorte auch unter Einbeziehung der Anforderung des Gasnetzes und der Speicherung überprüft werden.

Konzept

Die Netzbrücke hat das grundsätzliche Ziel die Energie des überschüssigen Stroms in Wasserstoff umzuwandeln und in Salzkavernen einzuspeisen. Hierbei wird sowohl die großvolumige saisonale als auch die kurzzeitige Speicherung im Sinne der Netzglättung berücksichtigt.

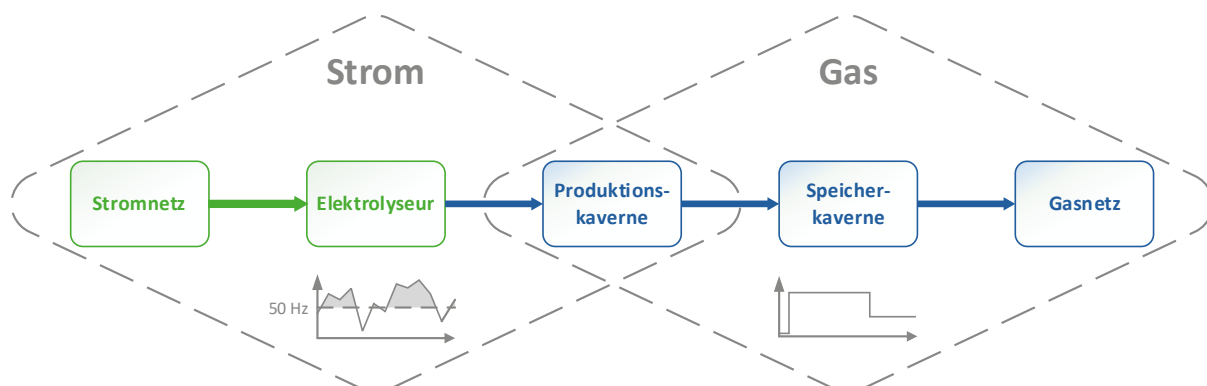


Abbildung 1: Schematische Darstellung der Netzbrücke.

Aus dem Elektrolyseur gelangt der produzierte Wasserstoff über einen Vorverdichter zunächst in eine „Produktionskaverne“. Diese ist dual-direktonal ausgelegt, das heißt sie besitzt zwei georedundante Leitungen zum Ein- und Ausspeichern, was eine vollständige Entkopplung dieser Vorgänge ermöglicht. Dadurch kann eine permanente und kurzfristige Einspeicherung jederzeit und unabhängig vom Ausspeichervorgang erfolgen. Dies berücksichtigt insbesondere die unterschiedlichen Ansprüche der beiden gekoppelten Energienetze Strom und Gas. Zur weiteren Verwendung gelangt der Wasserstoff aus der Produktionskaverne über eine zentrale Verteileinheit in die Speicherkavernen. Dieser modulare Aufbau ermöglicht zudem die Einbindung von zusätzlichen externen Wasserstoffimporten in das Gesamtkonzept.

Bei großen Elektrolyseleistungen spielt die Bereitstellung des benötigten Prozesswassers eine maßgebliche Rolle. Aus umwelttechnischen Gründen wird auf eine Verwendung des Grundwassers verzichtet und eine Seewasseraufbereitung unter Nutzung von Prozessabwärme konzeptioniert.

Fazit

Das vorgestellte Konzept stellt in unserer Wahrnehmung eine geeignete Maßnahme dar, um den im NEP 2023 beschriebenen Rahmenbedingungen nachzukommen. Der durch die Elektrolyseure hergestellte Wasserstoff kann saisonal gespeichert und wieder verstromt werden.

Darüber hinaus bietet eine Netzbrücke die Möglichkeit zur kurzzeitigen Glättung von Leistungsspitzen, wenn ein Erzeugungsüberschuss besteht, der durch das Netz temporär nicht aufgenommen werden kann.

Die Vermeidung von Redispatch Maßnahmen soll nach dem Delegated Act als Indikator zur sinnvollen Sektorenkopplungen gewertet werden. Netzbrücken können in diesem Sinne in letzter Konsequenz Möglichkeiten zur sinnvollen gemeinschaftlichen Netzgestaltung des Strom- und Gasnetzes zur Verfügung stellen.

Characterization of OCTG material for the application in underground hydrogen storage caverns

Klarner, J.¹; Schnideritsch, H.¹; Friess, B.¹; Kepplinger, J.²; Horvath, B.²; Haydl, R.²

¹voestalpine Tubulars GmbH & Co KG, Kindberg-Aumuehl, Austria

²DEEP.KBB GmbH, Hannover, Germany

Abstract

One key factor for decarbonization strategies of the industry is the use of hydrogen as renewable energy source. Due to the discontinuous availability of renewable primary energy for hydrogen production and energy demand, the underground storage of hydrogen plays an essential role in future. There are many activities worldwide to develop new or re-utilize existing salt caverns or porous media reservoirs for the application as an underground hydrogen storage under high gas pressure conditions. The filling and storage operation of these gas storages is done by applying typically subsurface completion equipment including low alloyed OCTG pipes.

In a first application in a Dutch pilot project regarding the storage of hydrogen in a salt cavern well a 4 ½" L80-1 VAhyper pipe string with approximately 1500 m total length was used for debrining as well for filling of the well with hydrogen. Moreover, through this first of its kind application and setup, the hydrogen gas-tightness and hence integrity of the string and the used premium connections was successfully demonstrated at pressures of up to 220 bar of 100 % pure gaseous hydrogen. Furthermore, within the project also the first snubbing operation under pressurized pure hydrogen retrieving the 4 ½" L80-1 VAhyper pipe string was accomplished successfully and in a save manner.

This paper briefly describes the performed field application and related overall setup of the applied technology and well installations. Majorly the paper covers the discussion of the comprehensive material characterization of the utilized steel pipes. The pipe material was thoroughly tested after manufacturing before installation, after the first mechanical integrity test of the salt cavern well with 20 days of hydrogen exposure and after the second field application (32 days) with pure 100 % hydrogen. The material characterization at each stage was performed according to a defined extensive material test program consisting of standard material testing methods as well as sour service and specific hydrogen testing methods. Amongst them constant load tests up to 140 bar hydrogen, including determination of the hydrogen content in the steel after the test and hydrogen permeation measurements have been conducted. Overall, next to the successful field application the material also showed a very good resistance against hydrogen during all stages of this field in the consecutive feasibility study including the aforementioned enhanced testing sequence. These first results are very promising for the use of threaded steel pipes for such hydrogen applications in future. Finally, further steps and possibilities for material tests under high pressure hydrogen loading of steel pipe materials will be described.

Introduction

In consideration of the European climate protection targets and the associated decarbonization of energy sources, an expansion of renewable energies in Europe is deemed indispensable. However, fluctuations in renewable electricity generation currently remain one of the major obstacles for the transition to an energy system with a high share of renewable energy. Due to the discontinuous availability of renewable primary energy, large-scale energy storage plays an essential role in future. Therefore, also hydrogen from renewable energy sources is going to play an important role as energy carrier in making the industry more sustainable.

As one of the first movers of this energy transition N.V. Nederlandse Gasunie (Gasunie) works on the implementation of the first large-scale project for underground hydrogen storage in salt caverns in the Netherlands. As part of the Dutch hydrogen backbone, the HyStock project was established in Zuidwending to demonstrate the technical aspects and a safe hydrogen storage operation.

The existing cavern field Zuidwending near Veendam in the north of the Netherlands is located in an enormous underground salt dome. Various salt caverns have been leached for brine production, and additionally, five caverns have already been created and utilized for the purpose of natural gas storage. Therefore, within the HyStock project a hydrogen storage pilot project was carried out at the cavern well A8A.

The general concept for the implementation of this pilot project was developed by Gasunie together with DEEP.KBB GmbH (DEEP.KBB). Overall, the pilot project consists of two stages: Firstly, in conducting a mechanical integrity test (MIT) to check the tightness of the well related to hydrogen exposure. Secondly, to execute a systematic hydrogen storage test run over a certain period of time to check the “H₂-readiness” of the relevant subsurface equipment, involved services and the related operational setup.

The filling and storage operation of salt caverns is typically done by applying subsurface completion equipment including low alloyed OCTG pipes. At the well Zuidwending A8A, a 4 ½" L80-1 pipe with VAhyper premium gas tight threads has been used during MIT and for the initial gas filling / debrining process of the pilot project. In this context also a set of different material tests has been performed on the applied OCTG product. These started already with taking of reference samples during pipe manufacturing. The related test results have been compared with those samples taken from the pipe material after the MIT execution and in a separate step also after the snubbing out operation of the debrining string. Within all test phases 100% hydrogen was applied at high gas pressures.

The initial material selection for the low alloyed high strength steel OCTG pipes within this project was based on the experience and knowledge of voestalpine Tubulars (VAT). This was combined with the requirements defined by DEEP.KBB with regard to the field application within the pilot project. Furthermore, the aforementioned investigation program for the tested material samples has been jointly agreed and developed.

There have been many studies and investigations in corrosion science dedicated to the influence of hydrogen (atomistic and molecular) on steels. In the oil & gas industry primarily Q&T (quenched & tempered) steel grades are used when the combination between high strength and corrosion resistance is needed. These grades are based on the API and NACE standards, where the last ones are mainly focusing on sour service (H₂S) and CO₂ resistance. The base for the corrosive attack of these media is that hydrogen is always dissolved as H⁺ in aqueous solutions with different concentrations depending on various parameters like e.g., the pH value or partial pressure of gas components. Therefore, the intention of this paper is to extend the knowledge about the behavior of molecular gaseous hydrogen in low alloyed martensitic steel grades and the effect on the material performance.

Field application and well installation

The cavern well A8A was drilled in the year 2010 and equipped with a 13 3/8"/13 5/8"-LCC. Subsequently, the borehole remained filled with brine and was pressure monitored. Since no further cavern development and intervention took place, the cavern well A8A offered favorable conditions for the demonstration project of hydrogen storage. As result of the long service life, the well cavern particularly offers practical and stable conditions in relation to the temperature behavior. A more detailed discussion of the setting of the project and the initial findings of the pilot project can be found in [1].

Project Stage 1

In stage 1, a MIT was performed at the maximum allowable pressure at LCCS before switching to the storage operations and was considered to be an essential part of the demonstration project. The following pressures were applied during the two-stage MIT at the wellhead:

- Maximum wellhead pressure (nitrogen): 194 bars (2,814 psi),
- Maximum wellhead pressure (hydrogen): 218 bars (3,162 psi).

Because of the well conditions with limited geometric volume (compared to a fully developed cavern), the brine was displaced during the test gas injection. This was done firstly to adjust the test gas-brine interface below the last cemented casing shoe but mainly to avoid causing damage to the salt formation through any overpressure scenario.

Therefore, a 4 1/2"- test string was installed with gas tight VAhyper connections for the brine discharge as part of the MIT sequence execution. To apply an adequate MIT test method and thus benefit from the advantages of a continuous interface measurement, the test gas (first stage nitrogen and second stage hydrogen) was further injected in the annulus between the test string and the last cemented casing. Within this sequence, an equivalent amount of brine was discharged through the 4 1/2" pipe. Next, a bypass at the wellhead was used to create a short circuit between the annulus filled with test gas and the brine filled test string. By this, the fluid interface level in the annulus and the test string was adjusted at a same depth by pressure equalization. In Figure 1 the applied general test setup is graphically shown.

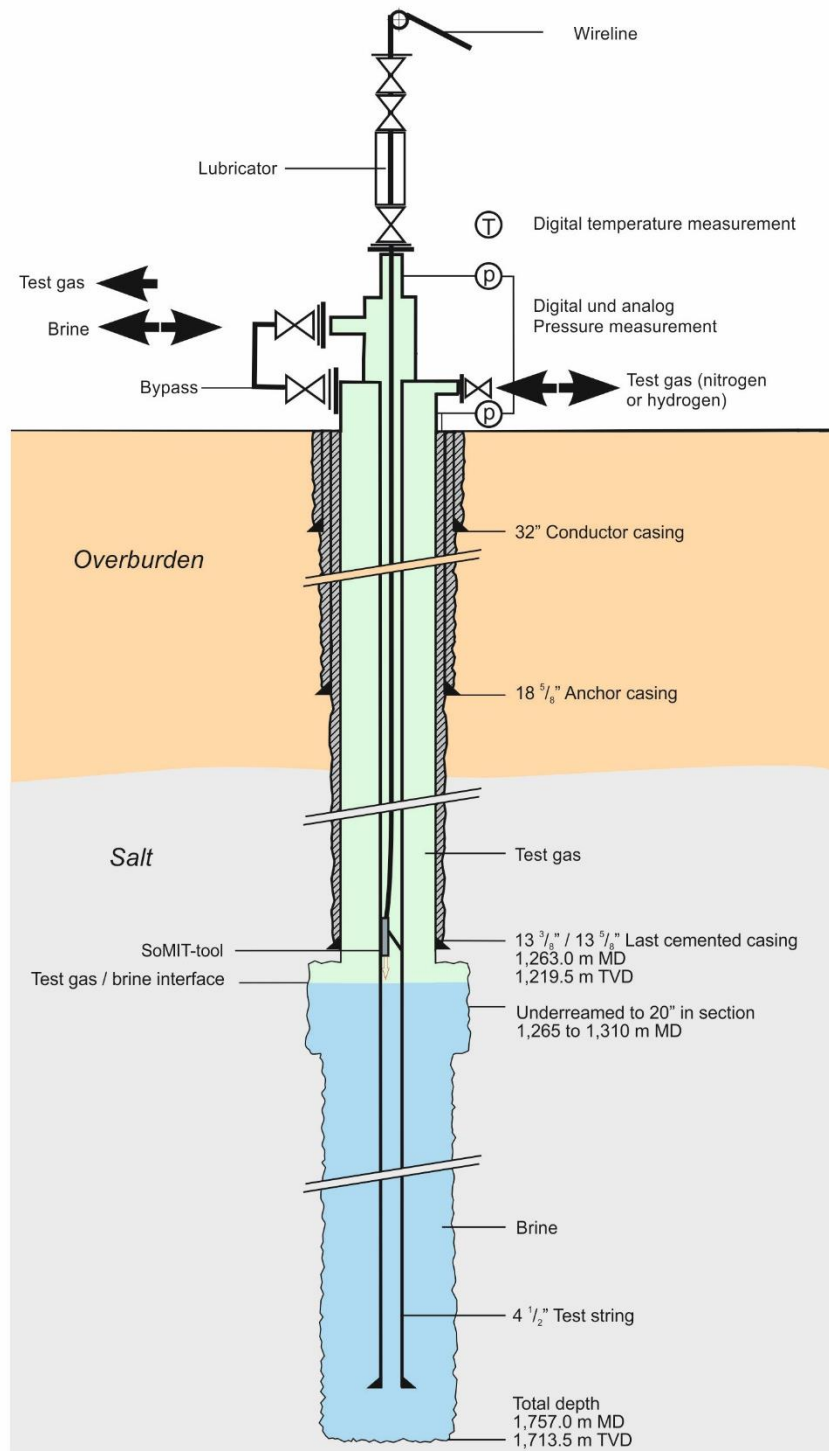


Figure 1: Well sketch including the general test setup

During this stage of the pilot project the 4 1/2" pipe was exposed to 100 % hydrogen within the salt cavern well environment at about 220 bars over a period of 21 days. Within this step, the pipe was mainly exposed to hydrogen at in-situ conditions from inside and outside.

Project Stage 2

After verifying the general integrity of the well, major aim of the hydrogen storage demonstration project at well A8A was to show the “H₂-readiness” of the setup and the involved subsurface installations for a salt cavern storage with focus on a large-scale and hence realistic approach.

The overall sequence of the execution and related interventions of the demonstration project has been drafted as a concept and further addressed in a detailed engineering phase beforehand (see [1]). The following main operational phases have been engineered and executed during the course of the project:

1. Installation of subsurface completion items
2. Hydrogen filling and brine withdrawal operation
3. Snubbing out of debrining string
4. Main pilot storage phase: hydrogen cycle operation and shut-in period
5. Hydrogen withdrawal and brine filling operation
6. Retrieval of subsurface completion items

In the first phase of the pilot project the subsurface completion of the well has been installed within the existing last cemented casing to ensure a safe gas operation during the pilot hydrogen storage phase. This included the installation of the following equipment which is also depicted in Figure 2 below:

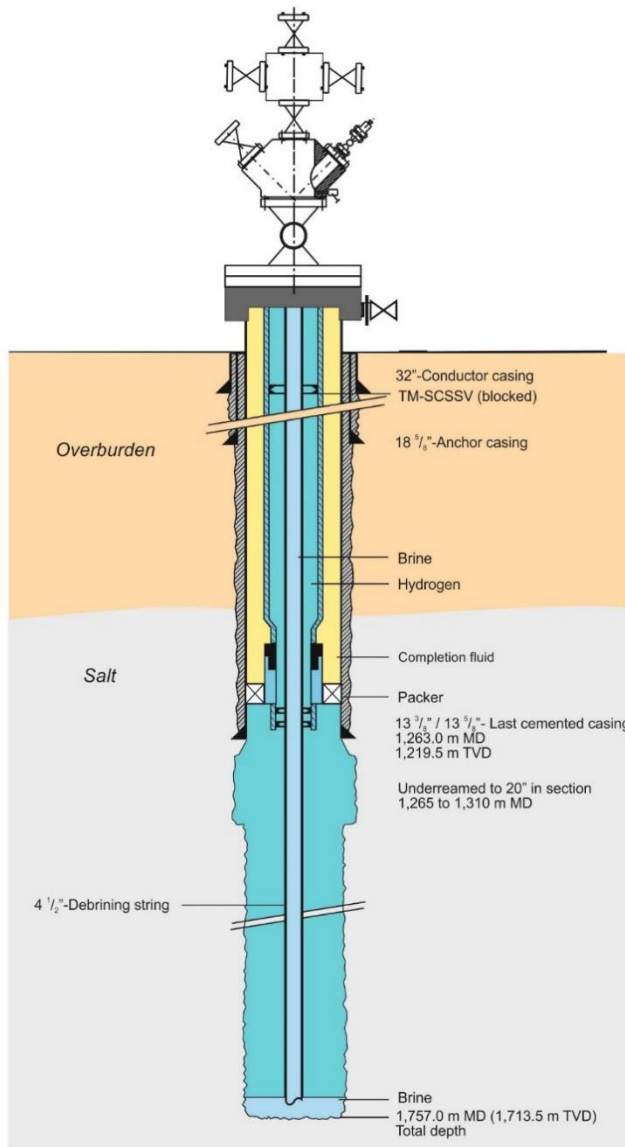


Figure 2: Schematic illustration of the completion of the pilot project ZW A8A

During this phase of the pilot project, the 4 1/2" debrining string was applied for the process to fill the cavern well initially with hydrogen. In a subsequent step the pipe was snubbed out from the hydrogen filled well. Hence, this covered steps 1-3 of the aforementioned sequence. In this second stage of the project, the 4 1/2" pipe was exposed to 100 % hydrogen within the salt cavern well environment at about 200 bars over a period of 32 days. The inner part of the 4 1/2" debrining string remained brine filled, and the hydrogen was situated at the outside of the pipe. As an initial result (observed from constant pressure monitoring), no leakage through the pipe and the introduced VAhyper premium threads has been observed during this time.

Test methods for hydrogen resistance of OCTG steel grades

In underground storage applications hydrogen can be involved in two ways in the corrosion processes of steel pipes. One is dissolved as hydrogen ion H⁺ in aqueous solutions and the other form is as molecule H₂ in gaseous mixtures. Many investigations and scientific studies focus on the dissolved hydrogen and are the basis for the developments of test methods in NACE standards like NACE TM0177 (Method A and Method D) for stress corrosion cracking or NACE TM0284 for hydrogen induced cracking. When gaseous H₂ is involved in the process,

especially with high strength steels, the effect of hydrogen embrittlement must be considered [2]. This phenomenon has been intensively studied over the last decades. By the contact of gaseous H₂ with steel surfaces there are two principles paths of getting hydrogen into the steel matrix. Zafraa et al. [3] describe these two paths for reproducing such conditions in laboratory tests by:

1. In-situ testing in high pressure gas or testing with external hydrogen
2. Testing in air after pre-charging the specimens in a gaseous hydrogen medium or testing with internal hydrogen

As the first method replicates the real field conditions very closely, there is also the disadvantage of using high pressurized hydrogen gas with the enormous safety requirements at the test lab linked with high testing costs. Compared to this the second test method is quite simple in implementation and running of tests. The results of the comparison from both test methods show a much better and realistic fatigue crack growth rate at the in-situ testing by having a constant high pressure of the hydrogen test media at process zone during the whole test [2]. The fracture initiated by hydrogen under certain conditions leads to the degradation of the material. There are many widely accepted mechanisms describing the crack growth inside the material like e.g., hydrogen enhanced local plasticity model (HELP) or hydrogen enhanced decohesion mechanism (HEDE). Most of the time the crack propagation is a combination of mechanisms. In general, the material susceptibility, the stress level, and the environment are the main factors being responsible for hydrogen embrittlement in materials [4]. In metallic materials the microstructure, grain boundaries, grain size, dislocations and precipitation are influencing the resistance of the material against hydrogen embrittlement.

For the material testing under hydrogen environment, beside the stress corrosion test methods from NACE standards the intention in this project was to get the test environment as close to the real field conditions as possible. The focus was on the following two methods:

- Hydrogen permeation test method for the determination of the diffusion coefficient inside the material and
- Constant load test for the evaluation of the hydrogen uptake and the material degradation under hydrogen environment

NACE TM0177 – Method A and D

Method A, which is part of NACE TM0177 standard, provides information on the resistance of materials to sulfide stress cracking (SSC) when subjected to tensile stress for a specified test time or, conversely, determines the critical stress value at which SSC occurs. If the specimen passes the test for 720 hours without fracture, the material or specimen is considered resistant to SSC. Instead to Method A, which delivers only an “yes or no” result to SSC resistant, Method D allows a quantitative characterization and comparison of the materials behavior regarding SSC. For this purpose, a double-cantilever-beam-sample with a fine-milled Chevron-notch or an electro-discharge-machined notch is used. After crack initiating and wedging the entire sample is immersed into the test fluid for 14 days. At the end of the test period the specimen will be cracked, the total crack length evaluated, and the appropriated K_{ISSC} value calculated. For details (specimen geometry, testing rig and procedure, etc.) of both methods, refer to the appropriate chapters of NACE TM0177 standard. [5], [6]

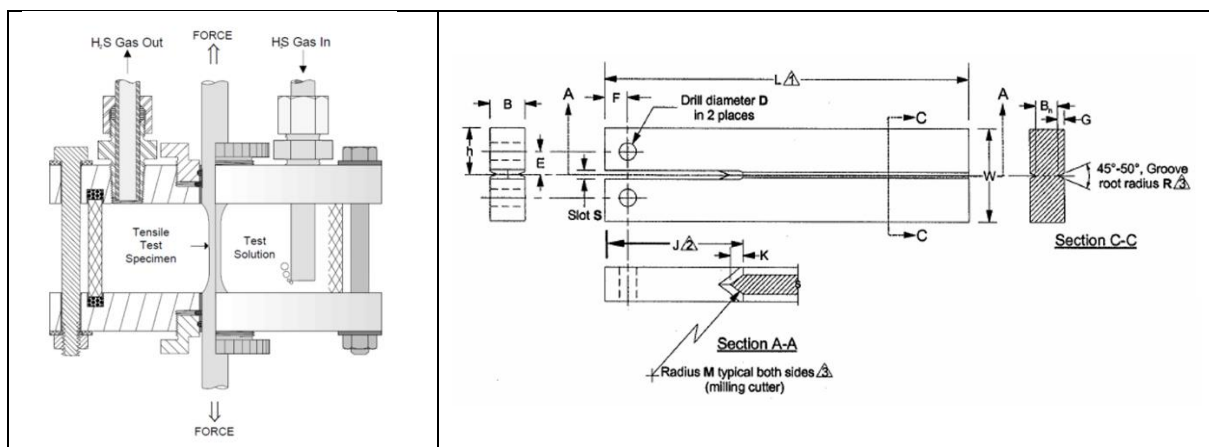


Figure 3: Test arrangement of Method A (left) and sample geometry of Method D (right) according to NACE TM0177 [5]

Hydrogen permeation test method (PT)

The hydrogen permeation test method according to ASTM G148-1997 or EN ISO 17081, developed in the early 1960s by Devanathan and Stachurski [7], is the most popular used electrochemical method to evaluate the hydrogen diffusion behavior in materials like aluminum, nickel, steel, and iron. By means of an electrochemical double cell, consisting of a charging and oxidation cell as well as the appropriate electrode systems (see Figure 4) allows to determine the hydrogen diffusivity, amount, and type of traps as well as the specific activation energy in the material.

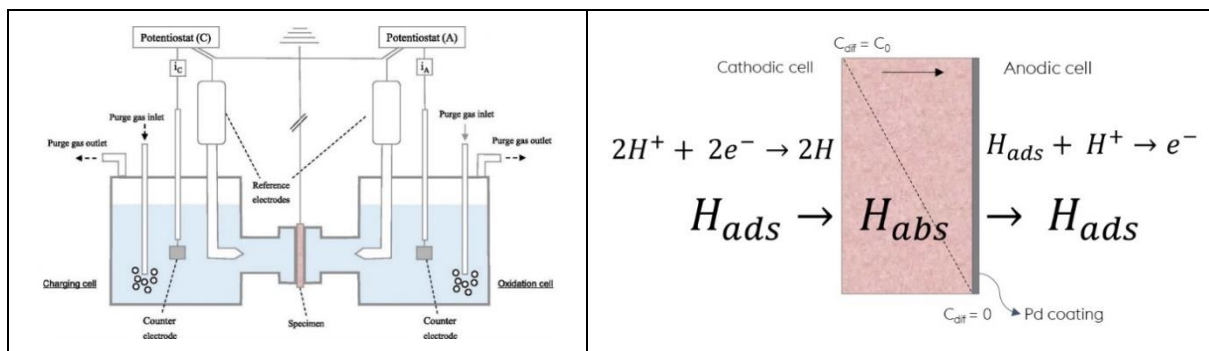


Figure 4: Schematic of a hydrogen permeation test unit (left) and charging reactions at the specimen surface (right)

The specimen itself (in the presented studies in the dimension of 40 x 40 x 1 mm) is one sided coated with Pd and is fixed between both cells. For charging a 3.5 % NaCl solution with 1 g/l thiourea at room temperature was used.

Constant load test (CLT)

The aim of constant load test is to verify the hydrogen uptake as well as the hydrogen embrittlement resistance of different materials under high pressure conditions in combination with an aqueous and/or gaseous media. The CLT is part of a combined testing sequence consisting of three small specimens: (1) the CLT specimen itself, (2) an immersion sample to determine the hydrogen uptake and (3) a coupon for investigation of corrosion phenomenon to the material. The CLT is based on a 3 mm diameter tensile specimen, which is mechanically preloaded by a special mount up to 90 % to the specific yield strength (SMYS). The mount for the test consists of a high alloyed spring, ceramic nuts, and PTFE-inserts to prevent electrochemical effects between the parts. Trautmann et al. [8] describe the hydrogen uptake and hydrogen embrittlement in different low alloyed steel grades based on this test method.

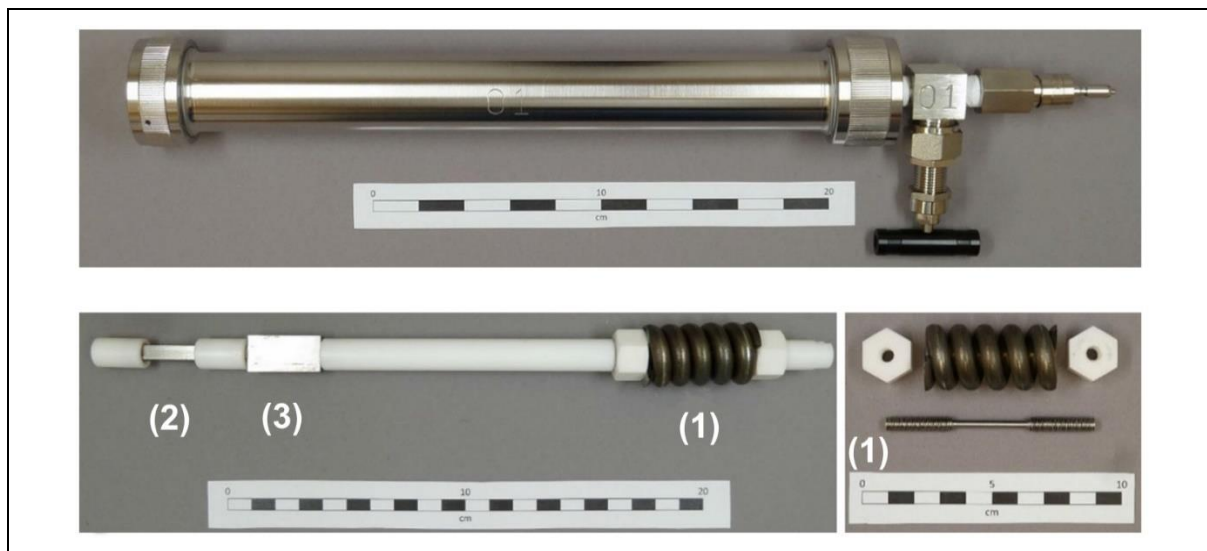


Figure 5: Autoclave for combined high-pressure testing (1) CLT specimen (2) immersion sample, (3) test coupon for corrosion effect analysis [8]

Testing procedure and material characterization

As described in the previous chapter the basic plan was to retrieve pipes for material characterization after each stage of the test program. Based on this primarily objective and the requirements from the field application a comprehensive test procedure was developed to investigate the material performance and under relevant loads. Table 1 summarizes the executed enhanced test procedure with all applied test methods and reference to the test standards. Additional to standard testing, as required according to the quality assurance procedures for these products, further testing with supplementary test methods have been defined before the pipes have been produced and installed. The supplementary tests can be divided into extended testing to get a statistical basis of relevant material properties and additional testing with application-oriented test methods.

There are pipes with three different conditions through the whole test period:

- Pipes in delivery condition (after manufacturing)
- Pipes after project stage 1 (after MIT)
- Pipes after project stage 2 (after gas fill and snubbing)

Figure 6 gives an impression from the condition of the retrieved pipes after project stage 2.



Figure 6: Retrieved pipes for investigation after project stage 2

Table 1: Test procedure for comprehensive material characterization

| Field of knowledge | Standard testing | Extended testing | Additional testing |
|--|--|--|--|
| Mechanical properties | Tensile testing acc. ASTM A370 | Tensile testing acc. ASTM A370 | |
| | Charpy test acc. ASTM E23 (at +20°C and -20°C) | Charpy test acc. ASTM E23 (at +20°C and -20°C) | |
| | Hardness test acc. ASTM E18 (4 quadrants) | Hardness test acc. ASTM E18 (4 quadrants) | |
| Chemical analysis | Chemical analysis acc. ASTM A415 | | Chemical analysis acc. ASTM A415 |
| Structural analysis | | | Metallographically investigation at imagination of 100x, 200x and 500x |
| Structural analysis | | | Metallographically investigation at imagination of 100x, 200x and 500x |
| Corrosion resistance (Sour Service) | | SSC test acc. NACE TM0177: Method A | SSC test acc. NACE TM0177: Method D |
| | | | HIC test acc. NACE TM0284 |
| Corrosion resistance (Hydrogen resistance) | | | Constant Load Tests (CLT) (in aqueous NaCl solution, 15000 mg/L Chloride and hydrogen at 90% SMYS) |
| | | | H ₂ permeation tests |

Table 2 summarizes the overview of the complete pipe string in numbers of tested pipes and

specimens. Where each tensile, hardness and NACE test specimens consists of one specimen, a Charpy-V test set consists of three specimens. Additional for the structural analysis also three specimens across one pipe have been taken.

Table 2: Overview on tested pipes and specimen

| Condition | Total number of pipes | Number of additional tested pipes | Number of test specimens |
|--------------------|-----------------------|-----------------------------------|--|
| Delivery condition | 196 pipes | 6 pipes | 18 tensile tests 12 Charpy-V sets 6 hardness tests 9 NACE TM0177:A 6 NACE TM0177:D 6 NACE TM0284:HIC 18 metallography 5 CLT 4 PT |
| Project stage 1 | 150 pipes | 4 pipes 4 couplings | 8 tensile tests 16 Charpy-V sets 8 hardness tests 9 NACE TM0177:A 6 NACE TM0177:D 6 NACE TM0284:HIC 16 metallography 4 CLT |
| Project stage 2 | 186 pipes | 3 pipes 3 couplings | 6 tensile tests 12 Charpy-V sets 6 hardness tests 9 NACE TM0177:A 6 NACE TM0177:D 3 NACE TM0284:HIC 12 metallography 4 CLT |

Test results and summary

The test results for material characterization are based on the methodology described in the previous chapter. The following figures (Figure 7 to Figure 11) summarize the main results from the material characterization according to the relevant test standards.

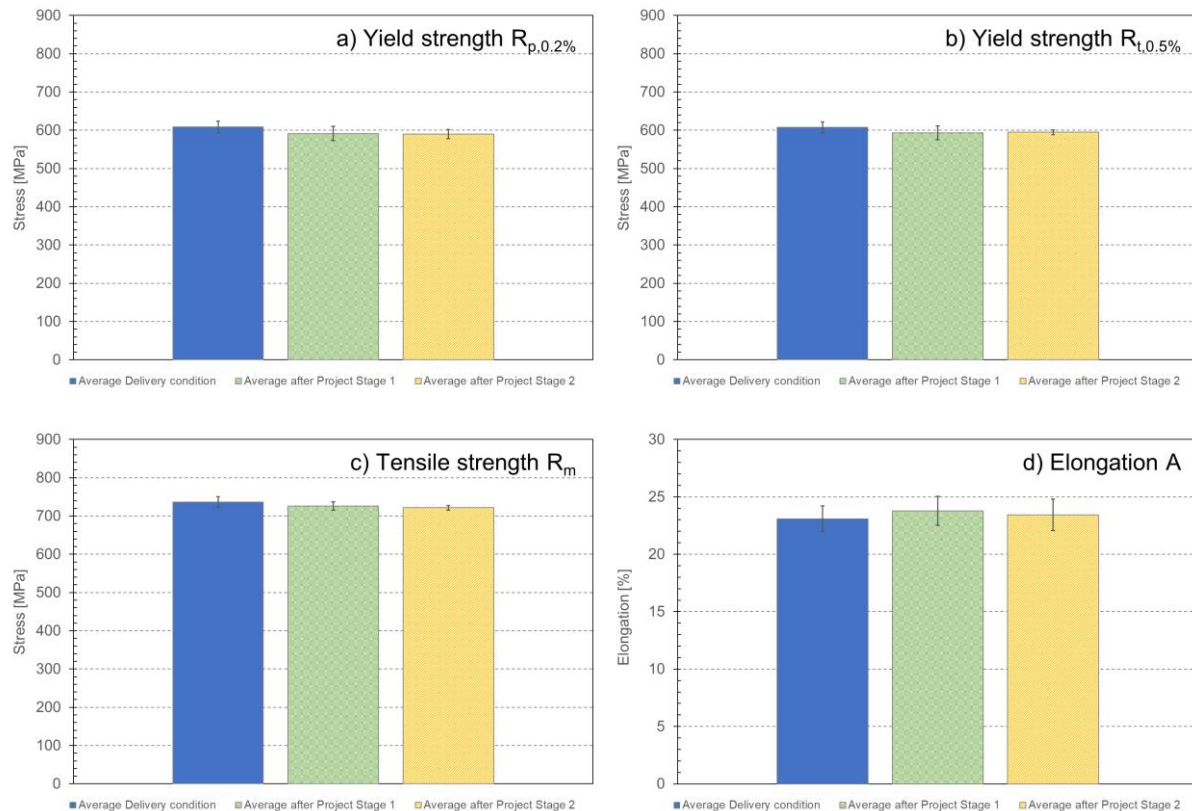


Figure 7: Overview of mechanical test results (yield strength, tensile strength, and elongation) from pipes in delivered condition, after Project Stage 1 and Project Stage 2

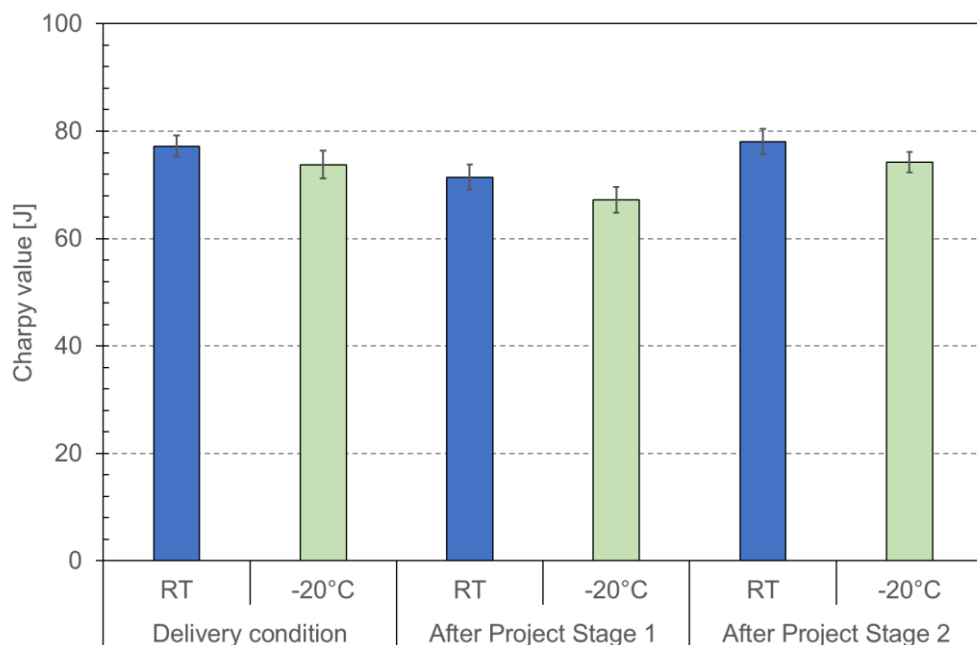


Figure 8: Overview of Charpy test results from pipes in delivered condition, after Project Stage 1 and Project Stage 2

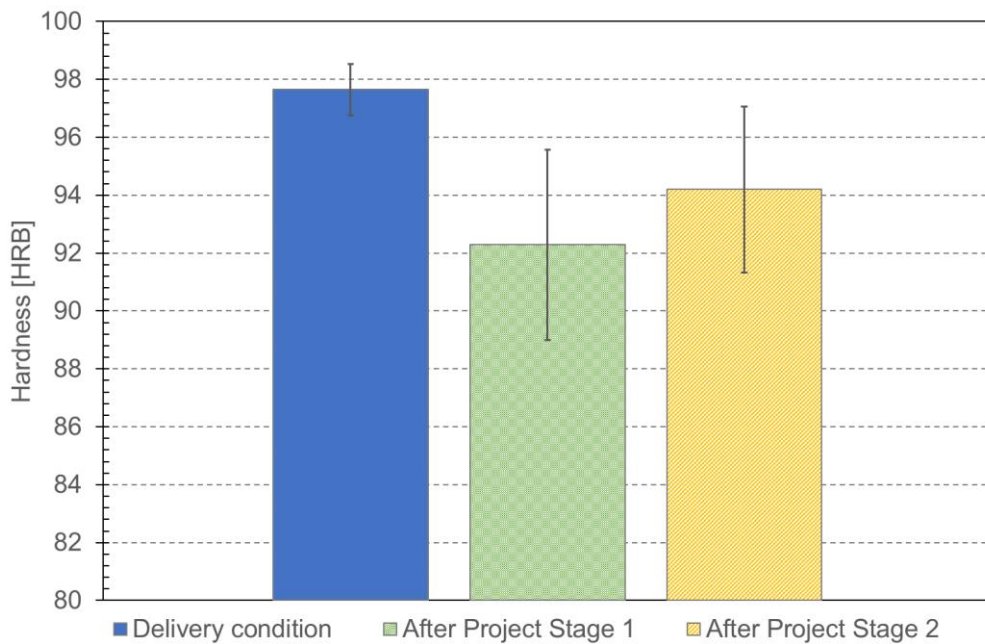


Figure 9: Overview of hardness test results from pipes in delivered condition, after Project Stage 1 and Project Stage 2

The comparison of the mechanical properties yield strength, tensile strength and elongation shows very consistent properties at all investigated conditions. The average strength values have a maximum scatter of 20 MPa, so no effect of any degradation of the material is evident. With a standard deviation of maximum 2.54 J the Charpy values are also very consistent throughout all evaluated conditions. The hardness variation in Figure 9 seems to be a little bit too high; but considering the measuring inaccuracy and the standard deviation at each condition all measured values are within the normal scatter of production lots.

The metallographic analysis was done on several samples machined from pipes number 1, 80 and 38 longitudinally as well as transversely at different magnifications (shown in Figure 10). All samples from delivery condition, after project stage 1 and stage 2 show an annealed martensite structure without any minor changes due to the testing conditions.

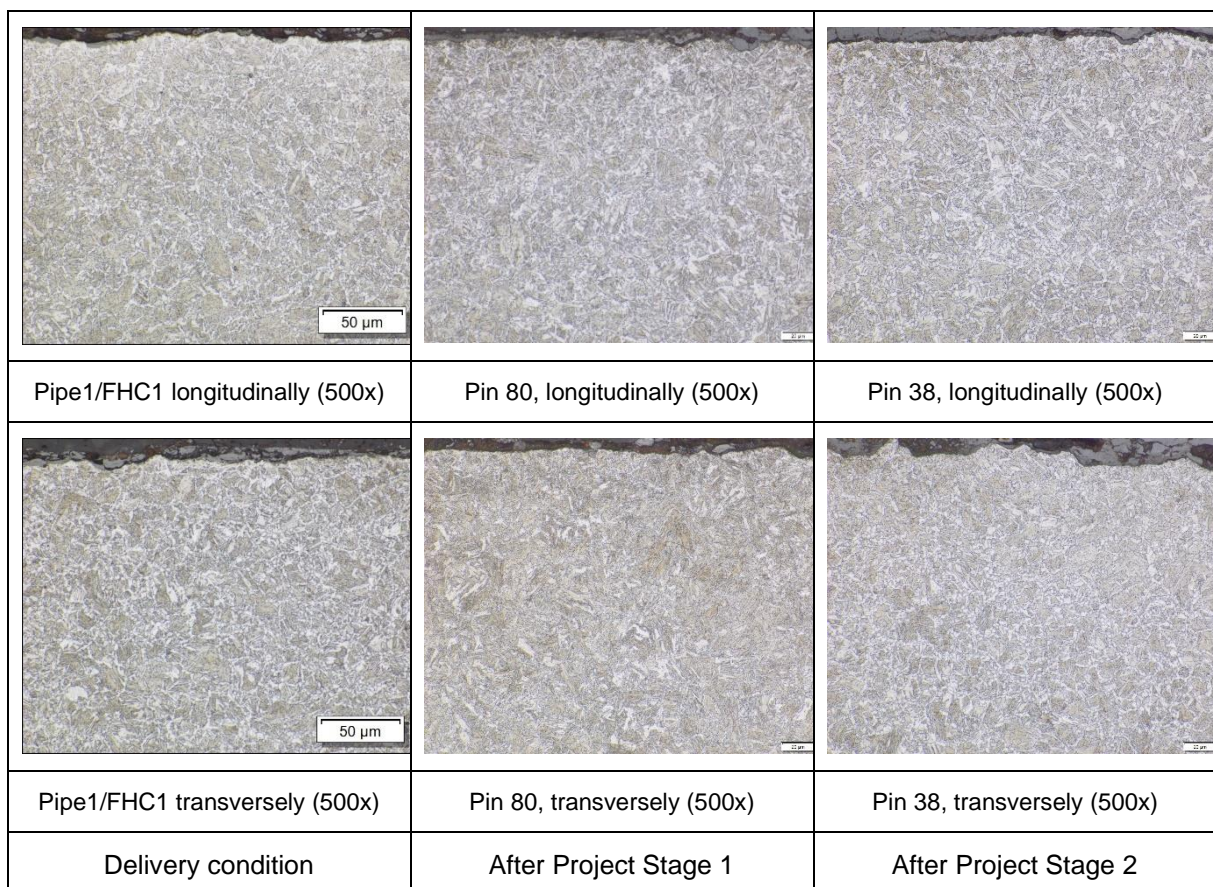


Figure 10: Metallographic characterization of a reference specimen, longitudinally/transversely (500x), at delivery condition and after project stage 1 and project stage 2

For the evaluation of the corrosion resistance of the materials it must be distinguished between sour gas (H_2S) resistance and resistance against hydrogen embrittlement (H_2). The sour gas resistance tests according to NACE TM0284 showed no hydrogen-induced cracks (0 % crack rate) in all tested specimen.

For stress corrosion cracking all specimens from all three conditions tested according to NACE TM0177: Method A passed the whole test time of 720 days at 72 % SMYS (specified minimum yield strength) stress level in test solution A (100 % H_2S). No difference between the material in delivery condition and after each project stage was evident.

Further fracture mechanical testing of the material according to NACE TM0177: Method D has been performed. The measured stress intensity factor K_{ISSC} in NACE test solution A with 100 % H_2S was between 31 to 34 $MPa \cdot \sqrt{m}$ over all three conditions. The diagram in Figure 11 shows the stress intensity factor referenced to the measured hardness of each specimen. The regression line with reduced K_{ISSC} by increasing hardness shows the standard behavior of steel grades at this stress level.

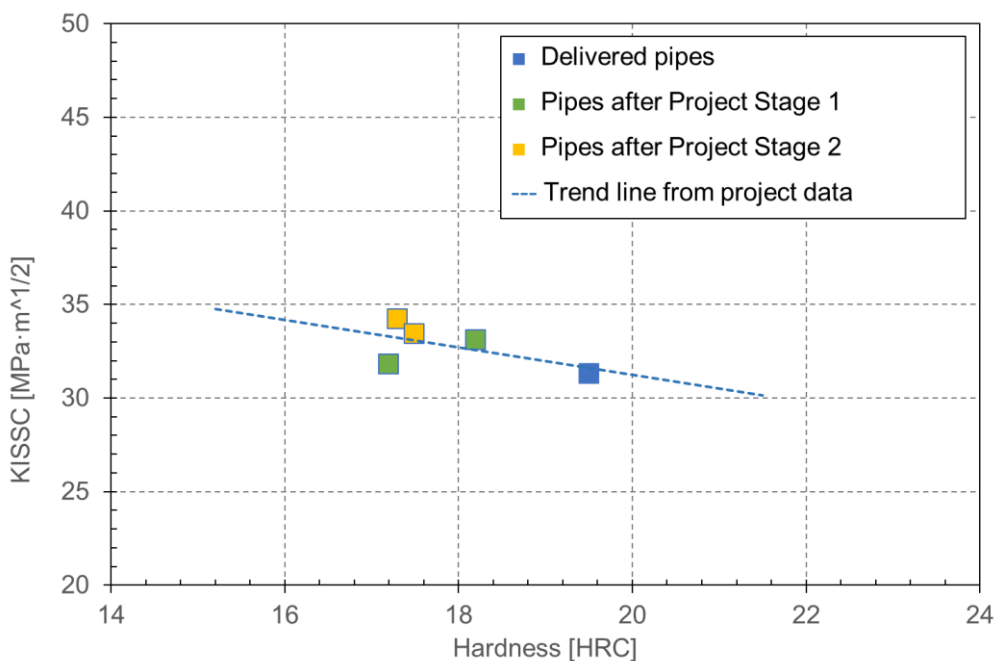


Figure 11: Comparison of Kissc results acc. NACE TM0177: Method D testing from pipes in delivered condition, after Project Stage 1 and Project Stage 2

For the evaluation of the corrosion resistance of the material under high-pressurized hydrogen environment permeation tests, as described in previous chapter, were performed with the result of an average diffusion coefficient of $1.5 \times 10^{-6} \text{ cm}^2/\text{s}$ for the material as delivered. Further with the material from all three conditions constant load tests under aqueous conditions with 15 g/l NaCl and hydrogen gas at 100 and 140 bar have been performed. No fracture of any specimen during the test time of 720 hours occurred. Figure 12 shows the measured hydrogen content in the specimens after these tests. In total the measured hydrogen content was between 0.2 and 0.6 ppm and all single values show a normal scatter of the hydrogen content, as the measuring error of this method is about +/- 0.2 ppm.

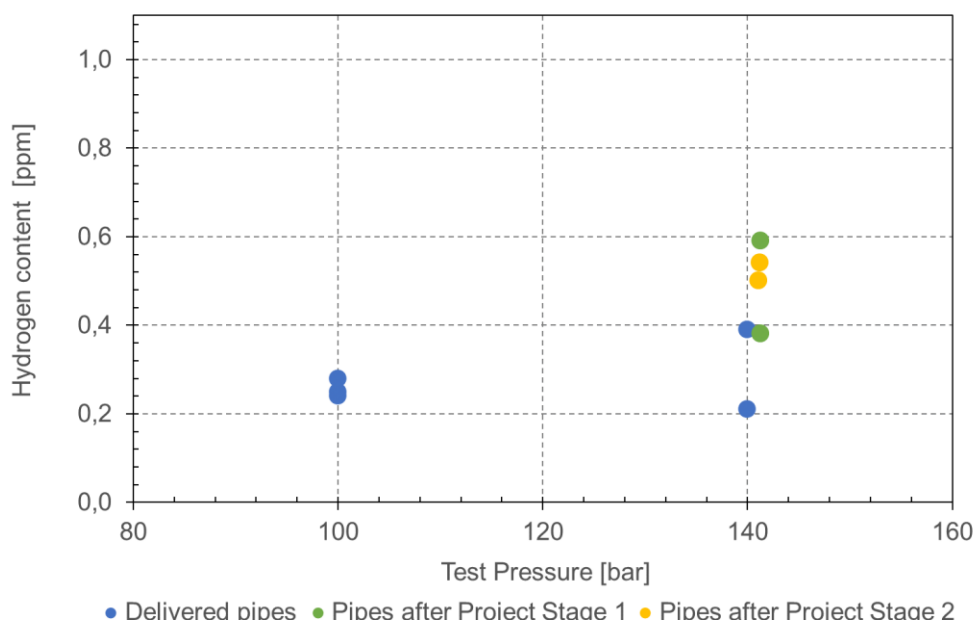


Figure 12: Comparison of hydrogen content after constant load tests from pipes in delivered condition, after Project Stage 1 and Project Stage 2

Conclusion

The 4 ½" VAhyper premium OCTG pipes introduced as test and debrining string has been successfully applied within one of the first pilot projects in Europe with aim to demonstrate the "H₂-readiness" of salt caverns in the context of large-scale hydrogen storage. During the application of the 4 ½" pipe within the hydrogen storage phase of the pilot project and the exposure of 100 % hydrogen at in-situ conditions (up to approx. 200 bar) over a period of 21 days (MIT phase) / 32 days (initial filling phase and snubbing) no leakage through the VAhyper premium threaded connections has been observed.

Furthermore, a range of different material tests and subsequent analysis have been conducted during the course of this pilot project. The holistic approach of the test sequence of the applied OCTG pipes started with the manufacturing process and covered also essential phases of the field application within the demonstration project dealing with the hydrogen filled salt cavern well Zuidwending A8A.

The comprehensive material characterization of specimens through the whole duration of the project did not indicate any degradation of the material exposed to hydrogen and any other media during the whole process. The characterization covered next to standard testing methods for general quality assurance aspects also application-oriented testing like stress corrosion testing under H₂S environment and constant load testing for resistance against hydrogen embrittlement and high hydrogen pressure. During the evaluation period the constant load testing equipment was only able for test pressures up to 150 bar. Meanwhile the equipment was extended and can test up to 1000 bar high-pressurized hydrogen. The same material grade L80-1, but not based on samples from this project, was also tested under these high pressures without any fracture of the specimens.

Based on all achieved results of this comprehensive testing project on pipe applied in a real field application for hydrogen storage in salt caverns it can be summarized that due to the absence of any negative results according to the material performance under high-pressurized hydrogen loading and for the hydrogen tightness of the pipe connection the results are very promising for the future safe application of such underground hydrogen storage operations supporting the decarbonization strategies of the industry.

Literature/References

- [1] Roordink, P., Horváth, B., Kepplinger, J., Haydl, R.: Hydrogen Storage in the Netherlands – Latest findings from demonstration project HyStock for underground storage of hydrogen in salt caverns; SMRI Fall 2022 Technical Conference, 26-27 September 2022, Chester, United Kingdom.
- [2] Trautmann, A., Mori, G., Oberndorfer, M., Bauer, S.: Susceptibility of Selected Steel Grades to Hydrogen Embrittlement – Simulating Field Conditions by Performing Laboratory Wheel Tests with Autoclaves, NACE Corrosion Conference & Expo 2022, NACE paper no. 13402 (2019)
- [3] Zafraa, A., Álvarez, G., Benoitb, G., Hénaffb, G., Rodríguezc, C., Belzuncea, J.: Influence of hydrogen on the fatigue crack growth rate of 42CrMo4 steel welds: a comparison between pre-charge and in-situ testing, Procedia Structural Integrity 39, pp. 128–138 (2022)
- [4] Dwivedi, S.K., Vishwakarma, M.: Hydrogen embrittlement in different materials: A review, International Journal of Hydrogen Energy, 43, pp. 21603-21616 (2018)
- [5] Moderer, L.: Sauergasbeständigkeit neuer hochfester Stähle für die Erdöl- und Erdgasindustrie, Dissertation, Montanuniversität Leoben, Leoben (2012)
- [6] NACE International: Laboratory Testing of Metals for Resistance to Sulfide Stress Cracking and Stress Corrosion Cracking in H₂S Environments, ANSI/NACE TM0177-2016, ISBN 1-57590-036-X, Houston (2016)
- [7] Devanathan, M.A.V, Stachurski, Z.: The adsorption and diffusion of electrolytic hydrogen in palladium, Proceedings Royal Society (London), Volume 270, Issue 1340 (1962)
- [8] Trautmann, A., Mori, G., Loder, B.: Hydrogen Embrittlement of Steels in High Pressure H₂ Gas and Acidified H₂S-saturated Aqueous Brine Solution, BHM - Berg- und Hüttenmännische Monatshefte, Vol. 166 (9), pp. 450-457 (2021)

Vision4SRP: Digital monitoring system for sucker-rod pumps – an example for collaborative project development through co-creation

D. Fischer¹, M. Buchebner², M. Allmaras³

¹ExxonMobil Production Deutschland GmbH

²Wintershall Dea Deutschland GmbH

³Siemens Energy Global GmbH & Co. KG

Abstract

Monitoring of remote well sites is a critical task for operators of sucker-rod pumps (SRPs) that is often carried out manually through recurring site visits for ensuring correct operation of pumps. The Vision4SRP system was born from the idea to improve the monitoring of well sites by combining video surveillance technology with advanced computer vision algorithms to determine arising issues automatically on-site. This reduces the time for detection of potential issues, optimise the site visits and helps to prevent costly downtime.

The Vision4SRP system has been developed in a joined effort of ExxonMobil, Wintershall Dea and Siemens Energy. While ExxonMobil came up with the original idea, the software and algorithms have been developed by Siemens Energy, and the system was piloted and refined at Wintershall DEA's Emlichheim oil field and ExxonMobil's Röhlermoor site.

Introduction

Sucker-rod pumps are complex systems combining mechanical, electrical, automation and communication components that are required to operate continuously in remote locations and under adverse environmental conditions. Monitoring of pump operation hence is a critical task to avoid downtime and costly repairs. In addition, equipment defects may lead to oil spillages that pose serious health and environmental hazards.

Traditionally, pump operation has been monitored through regular site visits by responsible lease pumper. Even though basic telemetry has subsequently been introduced at many well-sites, there remain many conditions that cannot be readily measured by sensors, such as slowly seeping leakages through the well-head stuffing box.

Solution concept

The desire to monitor pump operation more efficiently has led to the idea of a vision-based surveillance system that not only records video streams from pump sites, but also processes the video locally on-site in order to derive some higher-level indicators for operational health. By using advanced computer vision algorithms, metrics such as readings of pressure gauges and detection of oil stains on the polished rod can be derived that could otherwise not easily be obtained. The system should operate independently from the pump control and automation system, such that it could be easily retrofitted to existing pumps regardless of the specific local setup. This was the starting point for developing the Vision4SRP (*Vision for Sucker Rod Pump*) system.

System Architecture

The video stream recorded by the camera is processed by advanced computer vision algorithms to read gauge values and quantify amount of visible oil on the pump rod. These metrics together with an annotated image from the camera are sent via wireless broadband connection to a central cloud application. In each customer's private area of the cloud

application, a web dashboard is hosted that can be customized by each pumper to show the indicator relevant for him. Thresholds can be defined on gauge readings and the amount of oil stains, and when thresholds are exceeded, pumpers will receive notifications via SMS that they should check the pump's condition.

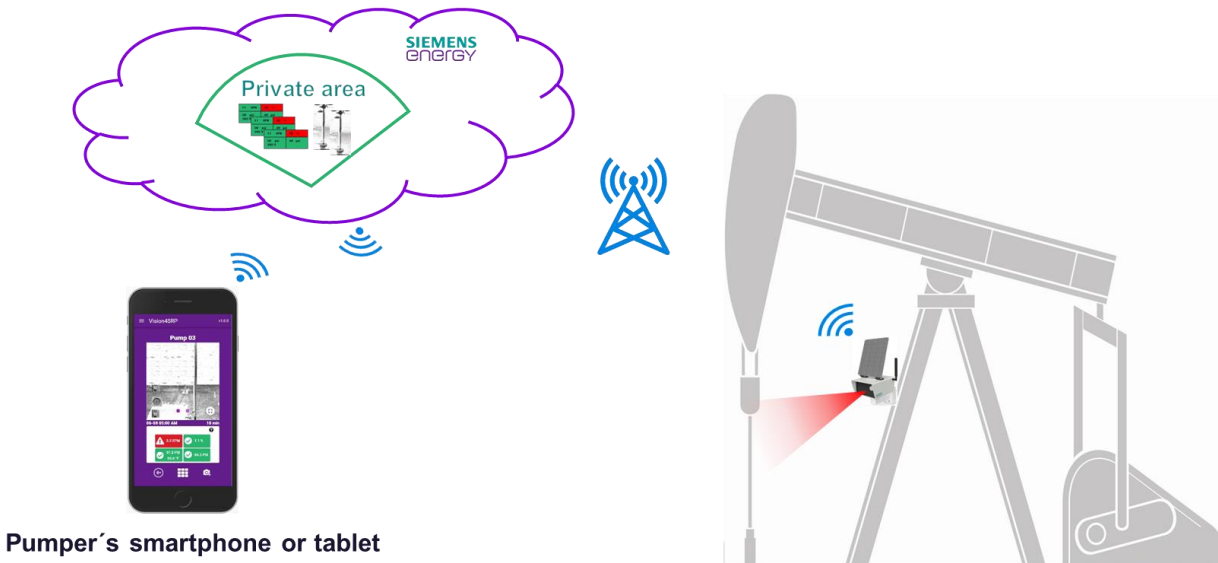


Figure 1 – General system structure

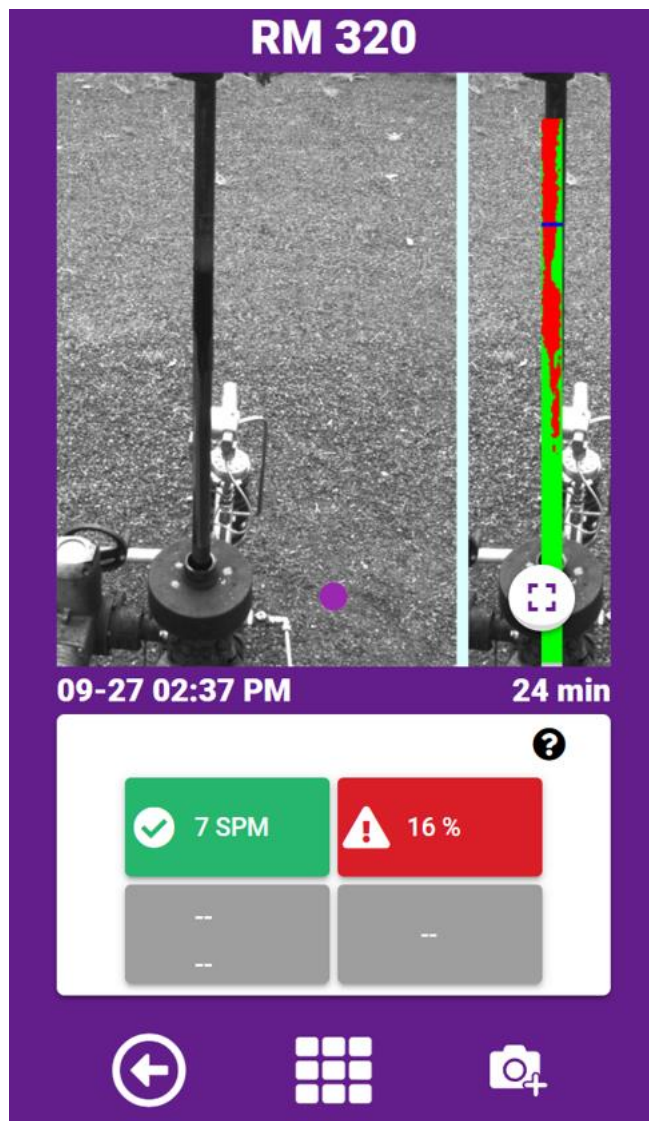


Figure 2 – Detailed view of leakage indicators in the pumper's dashboard

Prototypes and Pilots

Development of the initial prototype started in 2018 and consisted of a dedicated cubicle containing camera, processing board, communication, and IO-hardware, see Figure 1. The algorithmic development initially focused on the automatic reading of gage values. The prototype was installed and tested at Röhlermoor field. With initial results being promising, it was time to make the hardware setup more compact and extend the capability of the algorithms.



Figure 3 – Initial prototype at Röhlermoor field, 2019

For the next version of the system, a custom case was designed for mounting directly on the pump post. The compact case integrated camera, edge compute device and modem with an external cellular antenna. On the software side, a computer vision algorithm was implemented for detecting and quantifying visible oil stains on the pump rod. Development of this version finished in 2021 and was piloted for 10 pumps at Röhlermoor site. A solar version with additional solar panel and integrated battery was developed for use in off-grid scenarios.



Figure 4 – Second version with custom case; solar powered variant (middle), placement of components inside the case (right)

In order to allow the system to operate at night and in low-level scenarios, various ways of illuminating gauges and pump rods at night were tested, out of which IR illumination was found to be the most reliable. Also, having all electronic mounted on the pump post meant it was subject to changing environmental conditions, which made the durable design of the case complicated and limited the choice of components.

For the next version developed in 2022, a COTS outdoor surveillance camera was mounted on the pump post and connected via ethernet to the compute device, modem and IO-modules which were placed in control racks located close to the pumps. Figure 3 shows this version of the system with the camera mounted on a pump post, and the electronic devices mounted on a base plate in the control cabinets. The system is equipped with IR illuminators for night vision and the algorithm has been extended to cope with the specifics of IR-illuminated video footage.

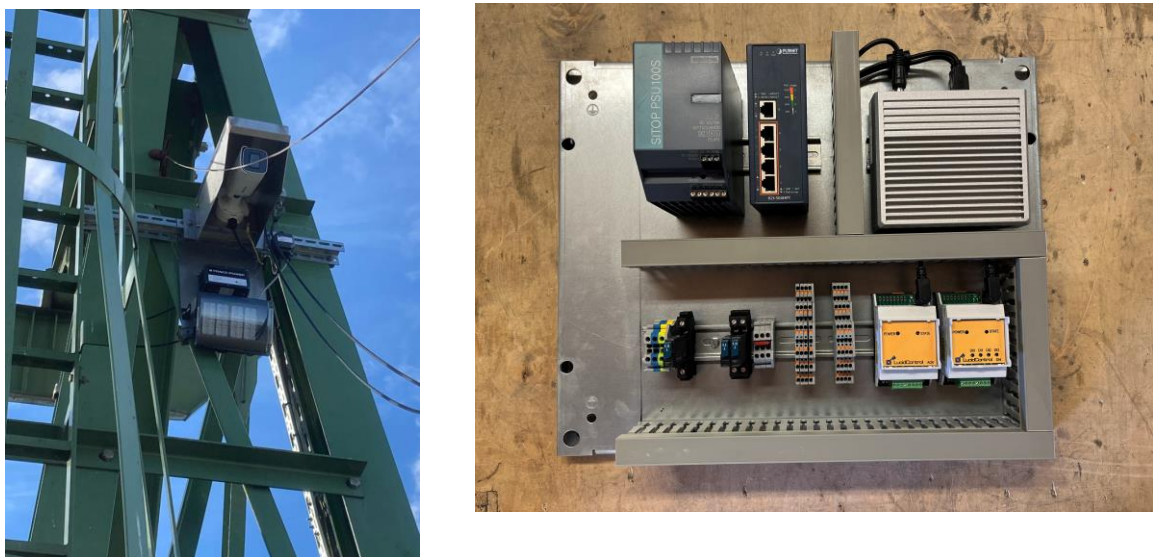


Figure 5 – Third version installed at Emlichheim field, 2022. Separate camera with weather-proof case (left), baseplate with compute device, switch, and IO-modules for placement inside the control rack (right)

This generation of the Vision4SRP system was commissioned and piloted for 12 SRPs at Emlichheim oil field, where it is since monitoring pump operation 24/7 around the clock.

Testing and validation

Throughout the pilot phases, a large number of experiments were carried out to investigate impact of the following factors on the detection accuracy:

- weather and environmental conditions,
- position and orientation of the camera,
- frame rate and camera settings,
- different position, orientation and lenses for the IR illuminator at night.

Multiple leakage experiments were conducted in which oil was externally applied to the stuffing box and results of the leak detection algorithm were analysed. In some experiments, stuffing boxes were loosened in order to simulate slowly developing leaks.

Results were recorded and discussed among the partners, and incremental changes to the setup were implemented in order to improve prediction accuracy. It was found that under most conditions, visibility was good enough to allow the system to accurately determine the amount of oil visible on the pump rod. Under a few weather- and lighting-induced conditions, a reliable detection of oil spills on the road turned out to be not feasible, and in these cases, care was taken in order to minimize the number of reported false positives.

The system is currently planned to be rolled out to a larger number of pump sites, and provisions are in progress to make this roll-out as efficient as possible.

Datenmanagement im Rahmen des Energie Management Systems der EMPG

S. Bauschulte

ExxonMobil Production Deutschland GmbH, Großkenneten

Abstract

Die Revision der DIN ISO EN 50001:2018 führte bei der EMPG zu einer Neustrukturierung des Energie Management Systems (EnMS). Wo bisher einfache Verhältniszahlen auf Basis von monatlichen Werten für die Beschreibung des Energiebedarfs und die Ermittlung der Energieeffizienz ausreichend waren, wurden diese von Bereichen mit wesentlichen Energieeinsatz (SEU's) und deren Energieleistungskennzahlen (EnPI's) abgelöst, welche auf statistischen oder ingenieurwissenschaftlichen Modellen basieren. Diese Modelle berücksichtigen relevante Einflussgrößen auf den Energieverbrauch und erlauben damit eine bessere Bewertung der Energieeffizienz.

Diese Anforderungen führten zu einer signifikanten Zunahme an benötigten Messgrößen, zeitlicher Auflösung, Berechnungen und somit zu einem geänderten Datenmanagement im Energie Management System.

Introduction

Die digitale Transformation des Datenmanagement lässt sich auf fünf wesentliche Schritte eingrenzen:

1. Bestandsaufnahme und Analyse
2. Entwicklung einer Strategie
3. Vorbereitung und Information
4. Umsetzung der Strategie
5. Kontinuierliche Verbesserung

Ausgangslage und Umsetzung

Die Standorte und Lagerstätten der Erdgas und Erdöl Förderung der EMPG sind breitflächig über Norddeutschland verteilt.

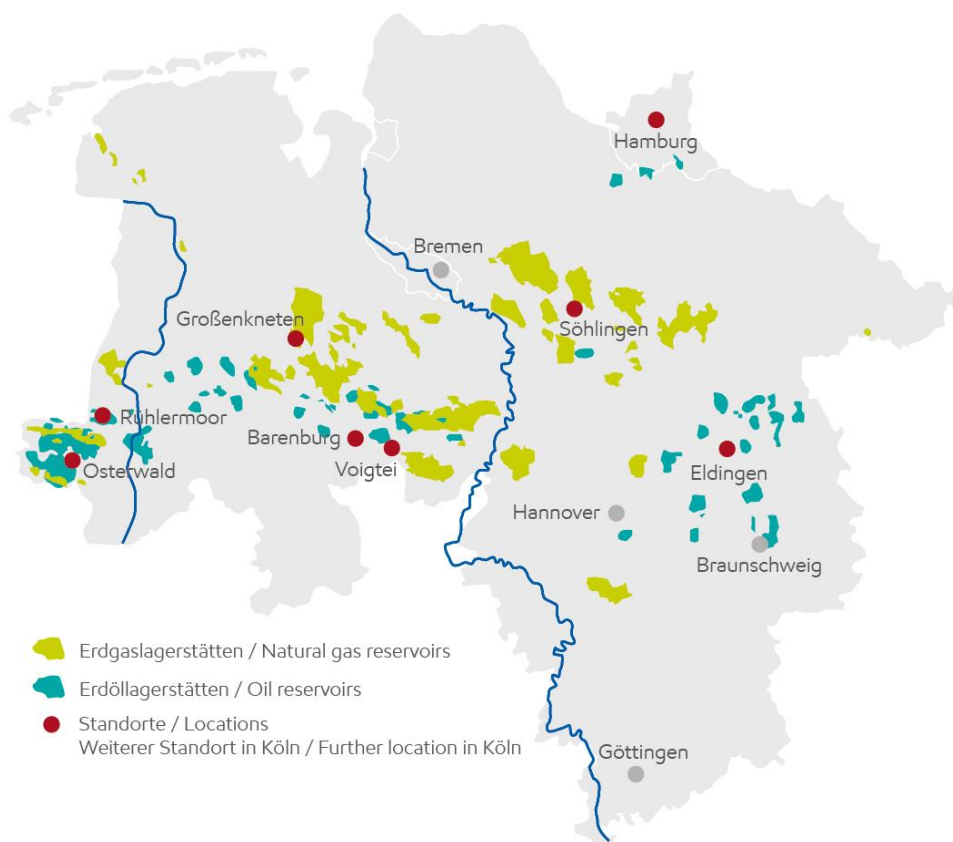


Bild Quelle : EMPG

Als erster Schritt wurde eine Bestandsaufnahme und Analyse in einem Top-Down Ansatz nach Energiebedarf der Standorte durchgeführt

- Identifikation der Energiebedarfs SEU's, EnPI's, Lage und Größe
- Analyse der Infrastruktur (IT Office Bereich, IT Prozesstechnik)
- Bestimmung der notwendigen Messgrößen und Modelle für das EnMS
- Stärken, Schwächen des Standortes und welche Herausforderungen bei der Umsetzung zu erwarten sind.

Der zweite Schritt war Entwicklung einer Strategie auf der Grundlage der Ergebnisse der Bestandsaufnahme

- Analyse der bislang genutzten Energiemanagement-Software auf Verwendbarkeit
- Abbildung der Standorte, SEU's und EnPI's über Dashboards, Berichte
- Anforderungen an IT-Infrastruktur, Datenmengen, Zykluszeiten
- Entwicklung eines Zeitplans zur Umsetzung an den Standorten
- Identifizierung der notwendigen Ressourcen und Budgetplanung zur Umsetzung

Kommunikation und Zusammenarbeit waren als dritter Schritt ein wesentlicher Schlüssel, um die Umsetzung der Strategie vorzubereiten.

- Die Mitarbeiter an den Standorten müssen in Bezug auf die Technologien und Prozesse geschult und informiert werden
- Führungspositionen müssen zeigen, dass Sie aktiv an der Umsetzung beteiligt sind und Mitarbeiter ermutigen, neue Ideen und Technologien einzubringen

Im vierten Schritt erfolgte dann die Umsetzung unter Berücksichtigung der in Schritt 1 und 2 gefunden Stärken und Schwächen innerhalb des identifizierten Budgets und entsprechender Ressourcen

- Überwachung und Bewertung des Fortschritts am einzelnen Standort.
- Identifizierung von Abweichungen/Herausforderungen, die eine Anpassung entweder für den Standort oder andere Standorte bedingen.

Der fünfte und letzte Schritt ist die Identifizierung von Abweichungen/Herausforderungen und führt zu einer Feedback-Schleife, um kontinuierliche Verbesserungen vorzunehmen und sicherzustellen.

Die digitale Transformation des Datenmanagements ermöglicht seither eine kontinuierliche Berechnung und Bewertung der wesentlichen Energieleistungskennzahlen bei EMPG. Dazu werden komplexe statistische Regressionen genutzt die im Tool Energie Manager Pro implementiert sind. Die Darstellung findet mittels Dashboards im Intranet der EMPG statt und ermöglicht den betrieblichen Energiemanagement-Beauftragten, die Einhaltung von Grenzen zu überwachen sowie im Fall von auftretenden Abweichungen entsprechende Gegenmaßnahmen einzuleiten und letztlich den Energiebedarf der EMPG zu optimieren.

Möglichkeiten der Optimierung von Bohrplanungsprozessen durch Nutzung von Machine Learning

I. Ulumaskan

Wintershall Dea Deutschland GmbH, Business & Information Management Ressort - Data & Information Management Department, Hamburg, Germany

Das Ziel der vorliegenden Arbeit ist es, zu untersuchen, ob Machine Learning zur Optimierung von Bohrplanungsprozessen genutzt werden kann.

Um diese Frage zu beantworten, werden Daten aus 47 Bohrungen eines bestehenden Erdölfeldes als Grundlage für eine explorative Datenanalyse und zum Trainieren und Evaluieren von Machine Learning Modellen genutzt, mit dem Ziel die Bohrgeschwindigkeit; englisch rate of penetration (ROP) vorauszusagen. Verschiedene Machine Learning (ML)-Techniken werden vorgestellt und ihre Auswirkungen auf die Performance der Modelle in Experimenten untersucht.

Die Ergebnisse der Experimente zeigten, dass eine explorative Datenanalyse wichtige Hinweise zur Gestaltung der Vorverarbeitung von Daten gibt. Die Qualität und Quantität der zum Trainieren von Modellen zugrundeliegenden Daten ist entscheidend für die Modellperformance. Außerdem wurde gezeigt, dass eine fehlerhafte Methodik bei der Umsetzung von Regressionsprojekten zu unrealistischen Ergebnissen führen kann. Auf Grundlage der bisher bei Bohrungen traditionell gesammelten Daten ist eine präzise Modellierung von ROP zur Optimierung von Bohr-, geschweige denn Bohrplanungsprozessen nicht möglich. Für die Anwendung von ML zur Optimierung des Bohrprozesses ist es notwendig, eine umfangreiche Datenbank anzulegen und zu pflegen, die jede Information enthält, die über historische Bohrungen vorliegen und für den Bohrprozess relevant sein können.

Für die Zukunft ist es notwendig, zu definieren, welche ergänzenden Daten für eine erfolgreichere Anwendung von ML notwendig sind, das Sammeln dieser Daten sicherzustellen und sie in einem integrativen Datensystem mit den historischen Daten zu verknüpfen.

AI Use Cases for Asset Failure Prediction

F. Kisslinger, M. Hildinger, J. Möller
Siemens AG, Karlsruhe

Abstract

Using predictive and proactive maintenance methods for critical equipment and processes in industry can help reduce unplanned downtimes and improve process availability and stability. Artificial intelligence (AI) methods for process data analysis can provide plant operators with much-needed insights for decision support and predictive plant maintenance strategies. In this article, we provide a guideline for implementing AI methods in the process industry using the AI-based application Siemens Predictive Analytics (SiePA) and present the results of a SiePA application in a petrochemical plant.

1 Introduction

The development of artificial intelligence (AI) for process monitoring has been ongoing since the mid-1980s [1, 2], but AI has not been widely adopted until very recently. With the rapid evolution of computational capacity, AI has reached a considerable level of maturity and is increasingly applied in many areas of process analysis and optimization as well as asset management [3–5]. However, until recently, the application of AI-based methods was largely limited to the awareness level of the Gartner AI Maturity Model [6]; 75% of the companies included in a 2018 Gartner survey were at Level 1: Awareness – being interested in AI but applying it only to select use cases or pioneering AI techniques. A similar situation is seen in Russia [7], where surveys show that only one company in three has chosen and implemented a digital transformation strategy.

One factor contributing to AI hesitancy in industry is the need to upload process and plant data to a cloud for the purpose of training the AI, which raises security and safety concerns among many users. On a more technical level, the application of AI-based data analysis methods to process data is often impeded by a lack of connection between AI-based process analysis systems and the systems at the process level (e.g., maintenance/engineering systems), as well as a lack of data contextualization (e.g., a lack of connection between metadata about the process from SAP and process data). However, these challenges are counterbalanced by the need to reduce operational costs by improving process and equipment performance, for which AI techniques can be used. As a result, companies in the process industry could benefit greatly from a proven, secure, and easy-to-implement approach for introducing AI-based data analyses to their processes. In this paper, we describe the approach of consulting the customer and co-creating a solution based on the Siemens Predictive Analytics (SiePA) application.

2 Tools and methods

The aim of the project was to develop an AI-based solution for predictive maintenance of a rock grinding mill using SiePA, an application for equipment predictive analytics developed by Siemens AG [8]. SiePA is a software application for model training based on the integration of machine learning with domain expertise. It can be used to support for pre-alerting/predicting critical equipment conditions and identifying issues based on natural language processing. SiePA also provides an integrated dashboard to support user interaction and data visualization, enabling users to monitor the equipment sensors grouped by subsystem.

2.1 Defining anomalies for the purpose of process optimization

Using SiePA, the project aimed to enable the plant operator to anticipate failures at several points in the process based on correlations among sensors. Many failures of process-critical equipment are preceded by anomalies in the process data, and SiePA is designed to identify such anomalies. This identification is enabled by deriving predictive models from historical data through advanced machine learning algorithms.

Various methods of detecting outliers in data sets have long been used to identify errors, system faults, and fraud [9]. Gaussian mixture models (GMMs) can be used to find clusters of process states in a data set that share common characteristics, and these models have been applied to signal evaluation in the process industry for many years. However, their application has been limited to specific tasks, because (a) anomaly detection itself is not a well-defined problem, as the question “What is an anomaly?” has no general answer; (b) data must be labeled and contextualized, often (semi-)manually; and (c) the interpretation of the results is difficult.

The assessment of the potentially large number of anomalies based on many variables in a common process requires the involvement of domain experts, so we have complemented the SiePA data analysis tool with domain expertise and consulting services to facilitate the definition of anomalies in a given process. Moreover, focusing anomaly detection on those process variables that are especially relevant to equipment or the process performance reduces the complexity and increases the usability in many applications. This can be further supported by a semantic grouping of anomaly detection models into so-called modules.

2.2 Calculating correlations and creating models

Based on historical data, the SiePA system automatically calculates how sensors correlate with each other in order to define a starting point for the modeling procedure. The correlation analysis considers time-independent and time-shifted dependencies between sensors. Moreover, the analysis uses different kinds of correlation coefficients (Pearson, Spearman, Kendall, etc.) to consider different types of dependencies. After the correlations have been established, the results are evaluated and enriched with the support from a domain expert to integrate domain knowledge into the modeling procedure and create high-quality models that will be able to detect potential risks better than just relying on the correlations.

Whenever a model is being built, as the first step, the user should choose the most important sensor or the indicating sensor (key performance indicator) that they usually monitor to determine the equipment status. This sensor is called the target sensor. This could be either a data-driven choice based on correlations or a choice based on experience and domain knowledge.

For each chosen target sensor, a model must be built by learning the normal behavior of the sensor from historical data. These models are based on extended GMMs, as described in Sect. 2.1. The GMM fits a sum of weighted multivariate Gaussian distributions to the historical sensor values with normal behavior. Afterward, the models evaluate the real-time

sensor values for each time point to decide whether the sensor is still in normal operation. Therefore, our algorithm uses Bayesian inference.

If these estimated values are near to the measured sensor values, the equipment is still in normal condition. However, if the difference between these values is large, the equipment's behavior is considered abnormal. To define a tolerance for the expected values, the system calculates a confidence band. As long as the measured values are within the confidence band, the equipment is still in normal condition. As soon as the measured values exceed the limits of the confidence band, the system issues an alert, which informs the operator about the equipment's condition. The user can adjust the tolerated range by configuring the width of the confidence band and, therefore, the sensitivity of the model, by an intuitive scaling factor.

2.3 Training models

Since SiePA's purpose is to inform the user whenever a target sensor is behaving abnormally, we must know what the sensor's normal behavior is. Therefore, the system needs to be trained with historical operational data from the "healthy" periods of equipment operation to learn what normal behavior looks like. These data must be provided by the equipment operator. Using this technique also avoids the challenges of enumerating complicated rules, especially considering all the relevant factors that may affect the result. As the problem is usually multivariate, the potential number of possibilities scales with the power of the number of variables. As opposed to that, the complexity of the problem can be reduced when different variables are correlated. SiePA enables the use of several training periods to ensure that the system achieves the highest level of accuracy.

2.4 Configuring the algorithms

New models can be created, and existing models can be adjusted by changing the number of correlated sensors within a model or adding training periods to a model. The accuracy of the models is influenced by the combination of sensors, the number of defined training periods, and the configuration of the confidence band. As part of the modeling processes, the constellation of the variables is changed and the impact on the models is assessed to ensure the best results for the application. This functionality is provided by Siemens as a service and is not part of the application itself.

2.5 Creating modules

To enable the visualization of results in a dashboard, multiple target sensors are grouped into modules. These modules can be used to represent a subsystem and help the operators organize their target sensors in semantic groups. In the event of an alert, this grouping supports a faster assessment and root cause analysis of the underlying deviation.

2.6 Dashboard and alerts

When the system is set up, operators can monitor their subsystems on the dashboard. If an anomaly is detected, the system issues an alert. The alerts are categorized as low- or high-risk alerts.

In general, the system provides an overview of all monitored equipment along with a modern dashboard showing detailed status information.

The overview (Fig. 1) shows statistics relating to overall asset health status. In particular, as described in Sect. 2.5, modules can represent subsystems or assets. The health index is calculated for each module.

The index itself is described as a percentage value, whereby the percentage is the share of the last 24 hours when no alerts were active. So, 100% represent a fully functional module (subsystem or asset), and 75% means that there were 6 hours of active alerts.



Figure 1 SiePA dashboard with target sensors grouped into modules (sunburst charts), a timeline with the status, and bar charts (as DNA charts) for target sensor deviation.

3 Data requirements

As a tool to support advanced data analysis for predictive maintenance, SiePA requires sufficient data from and about the asset or process equipment for analysis.

Historical data

To train the models, SiePA requires a historical data set in which normal operation modes are labeled. The amount of data required depends on the type of process as well as the frequency of anomalies, the number of failures, and whether the model needs to account for long-term effects on data (e.g., seasonal variations in process conditions). This data set must include both historical sensor data and distributed control system (DCS) alarm data, and it must also include all operation modes that should be treated as normal behavior of the equipment, as only those operation modes that are included in the historical data set can be reasonably monitored with the app. An example of different operation modes would be the distinction between plant operation during winter and summer due to the different ambient air temperatures.

Failure modes

To test different types of equipment failure, examples labeled with dates and background information should be provided. The provided qualified examples of failures should cover the relevant failure cases and the variation of data within one type of failure.

Training periods

SiePA uses supervised machine learning and therefore needs to have specific periods identified for training the models. Training periods for each piece of equipment must be provided or defined during co-creation of the solution.

Charts and data overviews

For a better understanding of the process in question, an overview of the instrumentation of all sensor tags related to the equipment to be monitored should be provided. This overview can be provided as a diagram, sketches, etc. Also, a mapping table, such as a piping and instrumentation diagram, for the sensors included in the overview is required.

Data format

A predefined format is used for the historical data with a time resolution down to 30 seconds, including information about the time zone of the plant.

Data preprocessing and model selection

The data provided are checked for quality and compatibility. This step is required because both the amount of available data and the number of sensors must be adequate for the specific application. As mentioned above, many companies still have not reached data and AI maturity [6], so data quality can be a challenge, especially in brownfield plants. This review includes checking the data for gaps, inconsistencies, and conflicts. Following the data preprocessing, we then select the suitable models for each process or equipment issue to be analyzed.

4 Implementation

The methods and tools described in Sect. 2 were applied to a compressor. Figure 2 presents an overview of the process as provided by the DCS. Data scientists and in-house domain experts performed the analysis of the process and assets in plant.

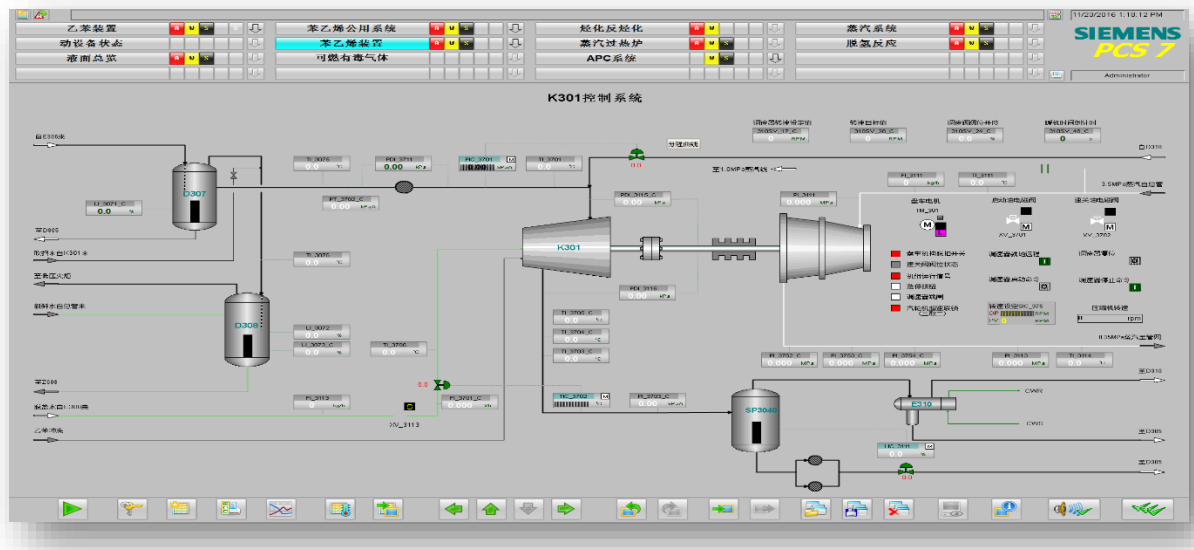


Figure 2. DCS Screen of the styrene unit, where the compressor was monitored.

The four goals of the equipment data analysis were as follows:

1. To identify correlations between the sensors using correlation coefficients based on historical data and domain know-how and provide the results as a scatter plot with correlation coefficients

2. To identify normal plant behavior based on alarms, domain know-how, and data analysis
3. To train the model based on normal behavior data
4. To monitor the target sensors and trigger an alert when abnormal behavior is detected, with the alert displayed on a dashboard using radar and DNA charts

Using eight months of data provided for the compressor, data scientists and in-house domain experts analyzed the operation with SiePA. Because the plant is a typical brownfield installation, this analysis also required matching tags to the positions of the probes in the process as well as identifying missing data and ensuring consistency in data naming and values.

5 Summary and future work

Following the training on the process data, the SiePA solution can generate early warnings of sensor failures or equipment deterioration and detect slow changes to the process in a system of multiple correlated sensors. These early warnings and the ability of the app to connect with different maintenance, repair, and overhaul (MRO) systems can be used as a trigger for specific preventive maintenance workflows.

The presented approach resolves the problem of lack of data contextualization and questions like “What is an anomaly?” in a certain process context by involving domain experts and data scientists. Furthermore, the application supports future changes in the process by means of interactive data labeling and retraining procedures during operations. The next step will be to refine these tools and methods to extend the AI capabilities beyond anomaly detection and to streamline the data analysis process. For example, classification of failures based on historical failures will be implemented to improve the ability to identify the root cause of a failure with less domain expertise. Another area of research is refining the models so that they can be used to recommend adjustments to optimize process parameters to return the process back to normal behavior.

Abbreviations

| | |
|-------|------------------------------|
| AI | artificial intelligence |
| DCS | distributed control system |
| GMM | Gaussian mixture model |
| SiePA | Siemens Predictive Analytics |

References

- [1] G. Stephanopoulos, *Chem. Eng. Prog.* **1987**, 83 (9), 44–51.
- [2] S. Rich, V. Venkatasubramanian, *Comput. Chem. Eng.* **1987**, 11 (2), 111–122. DOI: 10.1016/0098-1354(87)80012-1
- [3] V. Venkatasubramanian, C. Zhao, G. Joglekar, A. Jain, L. Hailemariam, P. Sureshbabu, P. Akkisetty, K. Morris, G. Reklaitis, *Comput. Chem. Eng.* **2006**, 30 (10–12), 1482–1496.
- [4] <https://www.ge.com/news/reports/deep-machine-learning-ge-and-bp-will-connect-2> (Accessed on May 06, 2021)
- [5] J. Mattioli, P. Perico, P. Robic, in *2020 IEEE 15th Int. Conf. of System of Systems Engineering (SoSE)*, Budapest, Hungary, **2020**, 151–156. DOI: 10.1109/SoSE50414.2020.9130505
- [6] S. Sicular, B. Elliot, W. Andrews, P. den Hamer, *Artificial Intelligence Maturity Model*, Gartner, Stamford, CT **2020**.
- [7] T. Lezina, O. Stoianova, V. Ivanova, L. Gadasina, in *Digital Economy: Emerging Technologies and Business Innovation* (Eds: R. Jallouli, M. A. Bach Tobji, D. Bélisle, S. Mellouli, A. Farid, I. H. Osman), Springer Nature Switzerland AG, Cham, Switzerland **2019**. DOI: 10.1007/978-3-030-30874-2_1
- [8] <https://industry-suites.siemens.com/all/operation-suites/ensure-asset-uptime/drives-turbines/predictive-analytics-for-process-industries> (Accessed on April 16, 2021)
- [9] V. Hodge, J. Austin, *Artif. Intell. Rev.* **2004**, 22, 85–126.

A discussion on the state of drillstring vibrations control: Industry vs Research

A. Sharma, K. Abid, C. Teodoriu
The University of Oklahoma

Abstract

The process of drilling for hydrocarbon extraction and geothermal applications involves creating a borehole in the earth by crushing through the rock formations to access the energy source. Vibrations and shocks are drilling dynamic phenomenon that are unavoidable and are detrimental to the equipment and pose a threat to rig safety. Understanding the drillstring vibration is the essential first step to control/mitigate the harmful vibrations and for this reason different modeling techniques have been used to model the drillstring vibrations. Lumped parameter models, distributed parameter models, neutral-type time delay models and coupled PDE-ODE models are some of the modeling methods used to model the drillstring dynamics. These models once derived are further used to design control algorithms to help cure drillstring vibrations. Although in literature several drillstring models have been formulated and a number of controllers have been designed, they have not been standardized and applied to the field. The industry to this date mostly uses a stiff PI controller or a SoftTorque system to control vibration, both of which are over two decade old techniques. This paper discusses the state of drillstring vibration control, controllers that have been proposed in the recent years and why they still haven't made it to the field. A hybrid approach involving the integration of system modeling, experimental investigation and machine learning has been proposed to aid in design of robust and practical controller.

Introduction

Drilling is a destructive process. It involves crushing the rock formation to create a borehole, which acts as a conduit to access the subsurface hydrocarbon and geothermal resources. To achieve this, rotational mechanical energy from an electric motor is transmitted through the drillstring to a drill bit which chips/crushes the rock formation and creates a borehole. The drillstring, which is composed of a series of slender tubes called drillpipes and the bottom hole assembly, can be thousands of feet in length, thus making it elastic. Non-linear friction is experienced throughout the length of the drillstring and at the interface between the drill bit and the rock formation. The elastic nature of the drillstring and the disturbance introduced in the system, due to the friction, leads to vibrations. Other factors like bent drill pipes and misaligned drillstring can induce or increase the severity of the vibration ([Sotomayor et al. 1997](#)). Vibrations experienced during drilling result in substantial loss of drilling energy and are a major concern as they have the tendency to damage drilling tools and equipment ([Abbassian and Dunayevsky 1998](#)) ([Reckmann, et al. 2010](#)), severely impacts the well bore integrity ([Macpherson et al. 1993](#)), increase Non-Productive Time (NPT), and lower the rate of penetration. It is reported that about 25% of the NPT is caused by the vibrations and shocks every year which reduces the overall drilling efficiency ([Dong and Chen 2016](#)) and increases the drilling cost by 10% ([Jardine et al. 1994](#)).

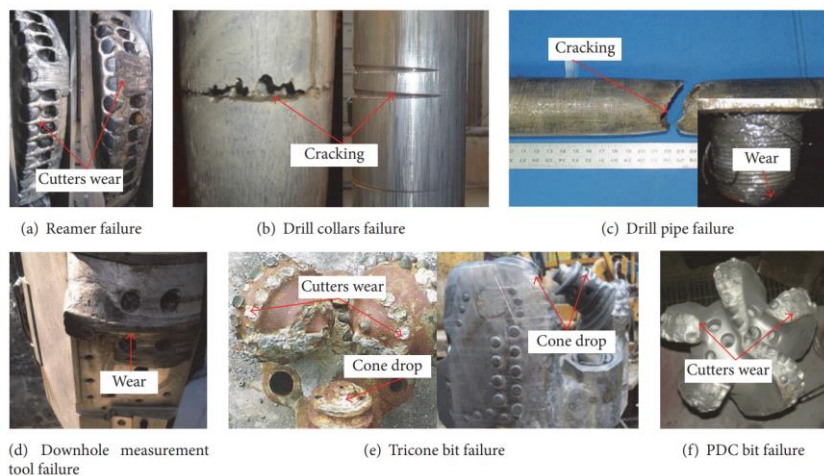


Figure 1. Drilling tool damage due to drillstring vibrations (Dong and Chen 2016)

Drilling vibrations can be classified into three modes: axial, lateral and torsional. Axial vibration causes irregular motion of the drillstring in the longitudinal/rotational axis leading to a phenomenon known as bit bounce. Lateral vibrations are a result of off-centered rotation of the drillstring, i.e. when the center of rotation of the drillstring does not coincide with the center of the well. This is commonly known as whirl. Torsional vibrations are characterized by fluctuation of the rotational speed of the BHA and the bit because of the oscillation that occurs due to low torsional stiffness of the drilling pipes. Stick-slip is a type of self-excited torsional vibration in which even though the surface RPM is constant, the bit periodically stops to rotate followed by a sudden spike in the bottom hole RPM which can be 10 to 15 times the surface RPM ([Dufeyte and Henneuse 1991](#)) ([Sharma et al. 2020](#)). Stick slip is a commonly occurring drilling dysfunction and it was reported by Dufeyte and Henneuse ([Dufeyte and Henneuse 1991](#)) that stick-slip occurred almost 50% of the drilling time during 3,500 hours of drilling in four different fields.

Control/mitigation of drilling vibrations is essential for increasing the overall efficiency of the drilling process. Analysis and control of drilling dynamics is an active area of research and over the years a number of numerical and experimental studies have been carried out to respect to this. This paper provides an overview of the analysis and control of drilling vibrations and discusses the state of vibration control in the industry focused towards stick-slip vibrations.

Modeling Drillstring Vibrational Dynamics

When modeling a physical system two approaches are commonly followed: (i) numerical modeling and, (ii) experimental modeling. Numerical modeling involves the use of mathematical equations to represent the system behavior. A numerical model is not unique to a given system, i.e., a system can be represented in numerous ways and may have a number of mathematical models. On the other hand, physical modeling involves building a physical model of the system. A combination of sensors, actuators and controllers is put together and up-scaling or down-scaling is performed if needed, to form a physical system that behaves in a way similar to the real system. Both these approaches have been applied by various researchers to study the behavior of a drillstring.

Numerical Modeling

Two popular numerical modeling techniques used to model the drillstring are lumped parameter modeling and distributed parameter modeling.

In lumped parameter modeling technique the drillstring is represented as a mass-spring-damper system. The dependent variables of interest are a function of time only. This makes it possible to describe the system mathematically using ordinary differential equations and making the analysis simpler. Lumped parameter models of the drillstring with one or multiple degrees-of-freedom (DOF) have been developed ([Brett 1992](#)) ([Lin and Wang 1991](#)) ([Jansen and van den Steen 1995](#)) ([Abdulgail and Siguerdidjane 2005](#)) ([Navarro-López and Cortés 2007](#)). Models with higher DOF have higher accuracy. The lumped parameter models of the drillstring are comparatively simpler but they ignore the distributed nature of the drilling system. The drillstring can be modeled more accurately with a distributed parameter modeling approach especially when an oscillatory system behavior is involved ([Aarrestad et al. 1986](#)) ([Tucker and Wang 1999](#)) ([Challamel 2000](#)) ([Sagert, et al. 2013](#)) ([Bresch-Pietri and Krstic 2014](#)). Here the dependent variables of interest are a function of time and one or more spatial variables. A beam subjected to axial and/or torsional forces represents the drillstring and partial differential equations are used to describe the system. This modeling approach is more accurate but has a higher level of complexity.

During drilling friction forces act on the drillstring. The drillstring experiences contact friction with the borehole, viscous friction due to drilling fluids and bit-rock interaction forces. Friction models like the Coulomb friction, Stribeck friction and Karnoop's model are used to model friction encountered by the drillstring. A comprehensive review of mechanical friction models can be found in ([Armstrong-Hélouvy et al. 1994](#)).

Experimental Modeling

Over the years, mathematical models of the drillstring have evolved from basic models to sophisticated models. Although extensive research has been done to understand the drilling dynamics mathematical, the models still have shortcomings and are often based on assumptions and simplification. Many non-linearities involved in the drilling process are ignored to help ease the computational expense ([Ghasemloonia et al. 2015](#)).

An alternate approach to study drillstring dynamics is the physical modeling approach in which experimental laboratory scaled rigs are developed to simulate the process of drilling. A detailed review of the experimental rigs can be found in ([Patil and Teodoriu 2013](#)) ([Srivastava and Teodoriu 2019](#)).

When designing an experimental setup of the drilling rig the choice of an appropriate downscaling factor is essential. With appropriate downscaling of the geometric, kinematic and dynamic properties, the behavior of the setup can be close to real scale drilling rig behavior. Although downscaling might seem straightforward, there are some constraints that must be considered. For example, downscaling the length of the drillpipe might see straightforward at first but when the diameter of the drillpipe has to be downscaled with the same factor it becomes impractical after a certain point. This is because of the slenderness of the drillstring. However downscaled experiments are providing valuable data for model validation and verification.

Drilling Vibrations Control

Drilling vibration control techniques are classified into two categories: passive and active. Passive control techniques deal with the physical manipulation of downhole tools. On the other hand, active control involves making decisions/changing drilling parameters (RPM, WOB etc.) in real-time. This section consists of a brief overview of passive and active control techniques presented by various researchers.

Active Control

Monitoring and control of the dynamic drilling parameters is essential in preventing drilling dysfunctions thus increasing the efficiency. Changing drilling parameters actively have been shown to help in suppression of drillstring vibrations (Sananikone et al. 1992) (Pavone and Desplans 1994) (Efteland, et al. 2015) (Vogel and Creegan 2016). Rate of penetration (ROP) can be maximized by controlling parameters like the WOB and RPM can keep the drilling process in an optimal zone as shown in figure 2 (Wu, et al. 2010).

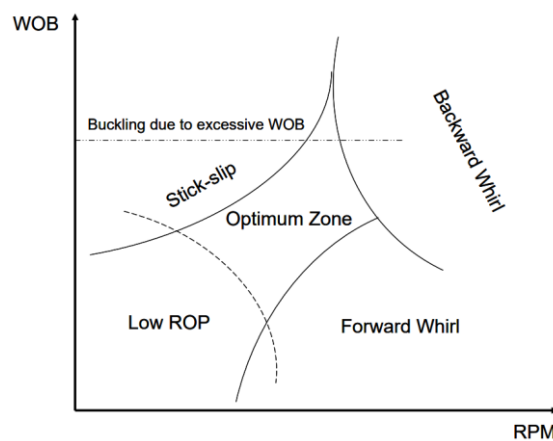


Figure 2. Optimal drilling zone (Wu, et al. 2010)

The first implementation of active control system for drilling vibrations can be traced back to (Halsey, Kyllingstad and Kylling 1988). They proposed an active control approach to control the surface torque and rotary speed to perform smooth drilling and cure stick-slip. Testing was carried out on a full scale drilling rig to demonstrate the performance of the technique. (Shuttleworth, et al. 1998), demonstrated the use of a MWD tool for downhole vibration detection to abate the destructive effects of downhole vibrations. (Serrarens, et al. 1998) used the H_∞ control technique to design a controller to suppress stick-slip. The controller was shown to tackle stick-slip on a scaled experimental rig and with simulations. Yigit and Christoforou proposed models that account for fully coupled torsional, axial, and lateral drillstring vibrations and designed a linear quadratic regulator (LQR) controller (Christoforou and Yigit 2001) based on these models to control stick-slip vibrations. Their simulation results also showed that axial vibrations reduce stick-slip severity and have a positive effect in suppressing stick-slip. (Al-Hiddabi, Samanta and Seibi 2003) highlighted the non-linear nature of the drilling system and proposed a controller design based on a coupled non-linear model and a dynamic inversion approach to mitigate stick-slip. (Abdulgalil and Siguerridjane 2005) also applied non-linear control approach to design a backstepping control. The control approach showed a quick response time of less than three seconds, and robustness to uncertainties of drillstring length and damping when tested using simulations. Sliding mode control, which is a popular non-linear control technique, was first applied to drilling vibration control by (Navarro-López and Cortés 2007). The controller was effective during simulation testing in the presence of dry friction and weight-on-bit variations under stick-slip conditions. Active control of weight-on-bit to counter stick-slip was proposed (Canudas-de-Wit et al. 2008). They named this mechanism

D-OSKIL (drilling oscillation killer). (Karkoub, et al. 2010) demonstrated the use μ -synthesis control design technique to tackle the drillstring stick-slip control problem. (Vromen, et al. 2014) used the finite element method (FEM) with eighteen elements to modelled a jack-up drilling rig. They employed an observer-based controller design strategy for Lur'e-type systems with discontinuities for mitigating stick-slip. Simulations showed the design to be effective, whereas an existing industrial PI controller was unsuccessful in mitigating stick-slip under same conditions. (Hong et al. 2016) put forward a control system design consisting of a Kalman estimator to estimate downhole states, and a linear quadratic regulator to control the vibrations. To validate the controller numerical simulations were performed and the results demonstrated the control scheme to be capable of controlling stick-slip. (Fu, et al. 2019) proposed an observer and reference governor-based control design. The observer estimates the downhole drilling parameters and the non-linear friction torque based on the reference governor changes the reference inputs to a PI controller. A super-twisting sliding mode controller was employed by (Krama, et al. 2021) to cure stick-slip. The performance of this controller was compared to a sliding mode controller using numerical simulations and hardware-in-loop testing. It was concluded that the former had better tracking, improved robustness, chatter-free implementation and faster convergence. (Laib, et al. 2022) proposed a hybrid fuzzy PID control scheme in which an interval type-2 fuzzy logic controller (IT2FC) was combined with a conventional PID controller. Particle swarm optimization (PSO) algorithm was utilized to set the optimal parameters for the controller. Simulations, and experimental testing with a hardware in loop (HIL) system were performed to validate the scheme and comparisons were made to the sliding mode controller and the PID controller. The proposed control scheme had a comparatively faster response time but had small overshoots.

Discussions

Drilling vibrations still continues to be a challenge for the drilling industry. Many different active control techniques have been proposed in literature but hardly any make it to the field application. The reasons behind this are discussed here.

One of the main drawbacks of using numerical models for studying complex systems like drillstring dynamics is that the modeling involves many assumptions and simplifications. With changing drilling conditions and geology for a localized application, the assumption can be violated resulting in inaccurate system representation by the model being used. Some assumptions like absence of contact friction between the drillstring and the wellbore, laminar flow of the drilling fluid etc. are made. On top of this many system dynamics are neglected. For example, the dynamics of the motor used to provide rotational energy to the drillstring, and the time delays in the system are ignored in most system models. Lumped parameter models with four or lesser degrees of freedom are the most popular when modeling drillstring dynamics and it is a well-known fact that lesser the degrees of freedom lesser is the model accuracy. Furthermore, the lumped parameter models may be acceptable when modeling a vertical well but their efficacy has not yet been proven when considering directional wells (Tang, et al. 2020). In an experimental study (Sharma et al. 2021) it was shown that the performance of a PID based RPM controller changes with a change in well configuration. Therefore, considering the well geometry is essential in system modeling and controller design. There are many non-linearities in a drilling system which are very difficult to model one of them being the friction experienced by the drillstring. The drillstring experiences contact friction throughout the wellbore (which as mentioned before is mostly neglected in the models) and bit-rock interaction forces. These forces are normally represented by the Coulomb friction, Stribeck friction and Karoop's models which are much simplified when compared to the actual friction forces on the drillstring and the bit.

To test the performance of the controllers computer simulations are employed. Only a handful of studies (Serrarens, et al. 1998) ([Krama, et al. 2021](#)) ([Laib, et al. 2022](#)) reported testing on experimental setups and even lesser on actual full scale drilling rigs ([Jansen and van den Steen 1995](#)). As a result, these controllers can only perform well in restricted conditions and have a limited band of operation. Absence of real-time downhole data is another limitation. Even if downhole data is available using MWD tools the data sampling rate is 1Hz or less which is low for vibration detection in real-time. ([Srivastava et al. 2023](#)) highlighted the need of surface and downhole data sampled at higher sampling frequencies and suggested a sampling frequency of at least 10Hz for stick-slip vibration detection.

The industry is still dominated by a stiff PI controller or the Shell SoftTorque ([Jansen and van den Steen 1995](#)). These vibration control systems have been around since the 1980s and 1990s. NOV SoftSpeed ([Kyllingstad and Nessjøen 2009](#)) and Z-Torque (Dwars 2015) are the other two active control strategies that have made it to the field. Although these industrial controllers have been shown to control stick-slip, they still have limitations. The stiff PI controller manages to reduce the magnitude of the oscillations but cannot always mitigate stick-slip. SoftTorque has a narrow band of operation and is vulnerable to frequency mistuning. SoftSpeed is sensitive to time delays in the feedback loops. Z-Torque, which is also developed by Shell, performs better than the original SoftTorque system and has a wider band of operation, but is still sensitive to time delays. Kyllingstad ([Kyllingstad, 2017](#)) and Aarsnes et.al. ([Aarsnes et al. 2018](#)) presented comparative studies on the industrial stick-slip controllers.

In the last two decades, numerous studies have been conducted that have used data driven approaches and machine learning for drilling applications ([Zhong et al. 2022](#)). With advances in sensor and data acquisition technology new tools have been designed which enable high frequency drilling data acquisition, thus catering to the use of data driven approaches for drilling applications. Machine learning techniques have been applied to tackle drilling vibrations and have been proven successful in categorizing and classifying vibrations and their severity ([Zha and Pham 2018](#)) ([Hegde et al. 2019](#)) ([Millan, et al. 2019](#)) ([Alsaihati and Alotaibi 2022](#)).

Moving forward, a hybrid approach involving numerical modeling, data driven approaches and experimental analysis is suggested. Numerical approaches and mathematical modeling of the system can be used to design controllers but models that better represent the dynamics of directional wells have to be developed. Machine learning techniques can be used to predict the severity of drilling vibrations and based on it the controller gains and/or set points can be changed. Finally, experimental testing of the controllers on physical setups can also help in simulating drilling dynamics that might be difficult to simulate numerically.

Conclusions

Currently the stick slip control is caught in complex dilemma: the limited number of parameters being used versus the limited amount of data being sampled.

Our paper have shown that new active controller will require high sampling rate as well as integration of multiparameter controllers.

Hybrid approaches may be the next step for future drilling vibration controls.

References

- Arrestad, Thor Viggo , Harald Tonnesen, and Age Kyllingstad. 1986. "Drillstring Vibrations: Comparison Between Theory and Experiments on a Full-Scale Research Drilling Rig." *IADC/SPE Drilling Conference*. Dallas, Texas.
- Aarsnes, U. J. F. , F. di Meglio, and R. J. Shor. 2018. "Benchmarking of Industrial Stick-Slip Mitigation Controllers." *IFAC-PapersOnLine* 51 (8): 233-238.
- Abbassian, Fereidoun, and V. A. Dunayevsky. 1998. "Application of Stability Approach to Torsional and Lateral Bit Dynamics." *SPE Drilling & Completion* 13 (2): 99-107.
- Abdulgalil, Farag, and Houria Siguerdidjane. 2005. "Backstepping design for controlling rotary drilling system." *Proceedings of 2005 IEEE Conference on Control Applications*. IEEE. 120-124.
- Al-Hiddabi, S.A., B. Samanta, and A. Seibi. 2003. "Non-linear control of torsional and bending vibrations of oilwell drillstrings." *Journal of Sound and Vibration* 401-415.
- Alsaihati, Ahmed, and Bader Alotaibi. 2022. "Determining Severity of Lateral and Torsional Downhole Vibrations While Drilling Surface Holes Using Three Machine Learning Techniques." *SPE Journal* 27 (3): 1493–1503.
- Armstrong-Hélouvy, Brian, Pierre Dupont, and Carlos Canudas De Wit. 1994. "A survey of models, analysis tools and compensation methods for the control of machines with friction." *Automatica* 30 (7): 1083-1138.
- Bailey, J.R.. R. , and S.M.. M. Rempert. 2010. "Managing Drilling Vibrations Through BHA Design Optimization." *SPE Drill & Compl* 25 (04): 458-471.
- Bresch-Pietri, Delphine, and Miroslav Krstic. 2014. "Adaptive output feedback for oil drilling stick-slip instability modeled by wave PDE with anti-damped dynamic boundary." *2014 American Control Conference*. Portland, OR: IEEE. 386-391.
- Brett, J. F. . 1992. "The Genesis of Torsional Drillstring Vibrations." *SPE Drill Eng* 7 168–174.
- Canudas-de-Wit, Carlos , Francisco R. Rubio, and Miguel Angel Corchero. 2008. "D-OSKIL: A New Mechanism for Controlling Stick-Slip Oscillations in Oil Well Drillstrings." *IEEE Transactions on Control Systems Technology* 16 (6): 1177-1191.
- Challamel, Noël. 2000. "Rock destruction effect on the stability of a drilling structure." *Journal of sound and vibration* 233 (2): 235-254.
- Christoforou, Andreas P. , and Ahmet S. Yigit. 2001. "Active control of stick-slip vibrations: The role of fully coupled dynamics." *SPE Middle East Oil Show*. Manama, Bahrain: SPE .
- Dong, Guangjian, and Ping Chen. 2016. "A Review of the Evaluation, Control, and Application Technologies for Drill String Vibrations and Shocks in Oil and Gas Well." *Shock and Vibration* 2016 .
- Dufeyte, M-P. , and H. Henneuse. 1991. "Detection and Monitoring of the Slip-Stick Motion: Field Experiments." *SPE/IADC Drilling Conference*. Amsterdam, Netherlands.
- Dwars, Sicco. 2015. "Recent Advances in Soft Torque Rotary Systems." *SPE/IADC Drilling Conference and Exhibition*. London, England, UK: SPE.

- Efteland, F., A. Creegan, L. Jordan, and C. Caraway. 2015. "The Significance of Pro-active Online Monitoring with Stick-slip Mitigation." *bu Dhabi International Petroleum Exhibition and Conference*. Abu Dhabi, UAE: SPE.
- Fear, M. J., F. Abbassian, S. H. L. Parfitt, and A. McClean. 1997. "The Destruction of PDC Bits by Severe Slip-Stick Vibration." *SPE/IADC drilling conference*. Amsterdam, Netherlands: SPE/IADC.
- Fu, Meng, Ping Zhang, Jianghong Li, and Yafeng Wu. 2019. "Observer and reference governor based control strategy to suppress stick-slip vibrations in oil well drill-string." *Journal of Sound and Vibration* 37-50.
- Ghasemloonia, Ahmad, D. Geoff Rideout, and Stephen D. Butt. 2015. "A review of drillstring vibration modeling and suppression methods." *Journal of Petroleum Science and Engineering* 131: 150-164.
- Halsey, G.W. , A. Kyllingstad, and A. Kylling. 1988. "Torque Feedback Used to Cure Slip-Stick Motion." *SPE Annual Technical Conference and Exhibition*. Houston, Texas: SPE .
- Hegde, Chiranth, Harry Millwater, and Ken Gray. 2019. "Classification of drilling stick slip severity using machine learning." *Journal of Petroleum Science and Engineering* 179 : 1023-1036.
- Hong, Liu, Irving P. Girsang, and Jaspreet S. Dhupia. 2016. "Identification and control of stick-slip vibrations using Kalman estimator in oil-well drill strings." *Journal of Petroleum Science and Engineering* 119-127.
- Huang, Zhiqiang , Dou Xie, Bing Xie, Wenlin Zhang, Fuxiao Zhang, and Lei He. 2018. "Investigation of PDC bit failure base on stick-slip vibration analysis of drilling string system plus drill bit." *Journal of Sound and Vibration* 417 (1): 97-109.
- Jansen, J.D. 1991. "Non-linear rotor dynamics as applied to oilwell drillstring vibrations." *Journal of Sound and Vibration* 115-135.
- Jansen, J.D., and L. van den Steen. 1995. "Active damping of self-excited torsional vibrations in oil well drillstrings." *Journal of Sound and Vibration* 179 (4): 647-668.
- Janwadkar, S. S. , D. G. Fortenberry, G. K. Roberts, M. Kramer, D. K. Trichel, T. Rogers, S. A. Privott, B. Welch, and M. R. Isbell. 2006. "BHA and Drillstring Modeling Maximizes Drilling Performance In Lateral Wells of Barnett Shale Gas Field of N. Texas." *SPE Gas Technology Symposium*. Calgary, Alberta, Canada.
- Karkoub, M., M. Zribi, L. Elchaar , and L. Lamont. 2010. "Robust μ -synthesis controllers for suppressing stick-slip induced vibrations in oil well drill strings." *Multibody System Dynamics* 23 (2): 191–207.
- Krama, Abdelbasset, Mohamed Gharib, Shady S. Refaat, and Alan Palazzolo. 2021. "Design and Hardware in-the-Loop Validation of an Effective Super-Twisting Controller for Stick-Slip Suppression in Drill-String Systems." *Journal of Dynamic Systems, Measurement, and Control* 143 (11): 111008 (12 pages).
- Kyllingstad, , A. 2017. "A Comparison of Stick-Slip Mitigation Tools." *SPE/IADC Drilling Conference and Exhibition*. The Hague, The Netherlands.

- Kyllingstad, Åge , and Pål Jacob Nessjøen. 2009. "A New Stick-Slip Prevention System." *SPE/IADC Drilling Conference and Exhibition*. Amsterdam, The Netherlands: SPE.
- Laib, Abdelbaset, Billel Talbi, Abdelbasset Krama, and Mohamed Gharib. 2022. "Hybrid Interval Type-2 Fuzzy PID+I Controller for a Multi-DOF Oilwell Drill-String System." *IEEE Access* 10: 67262-67275.
- Lin, Yao-Qun , and Yu-Hwa Wang. 1991. "Stick-Slip Vibration of Drill Strings." *Journal of Engineering for Industry* 113 (1): 38-43.
- Mahyari, M F , M Behzad, and G R Rashed. 2010. "Drill string instability reduction by optimum positioning of stabilizers." *Journal of Mechanical Engineering Science* 224 (3): 647-653.
- Millan, Ekaterina , Maurice Ringer , Riadh Boualleg, and Denis Li. 2019. "Real-Time Drillstring Vibration Characterization Using Machine Learnin." *SPE/IADC International Drilling Conference and Exhibition*. The Hague, The Netherlands.
- Navarro-López, Eva M., and Domingo Cortés. 2007. "Sliding-mode control of a multi-DOF oilwell drillstring with stick-slip oscillations." *American control conference*. New York, NY, USA: IEEE.
- Ortiz, Blas , Cesar Casallas, and Hector Parra. 1996. "Improved Bit Stability Reduces Downhole Harmonics (Vibrations) ." *SPE/IADC Asia Pacific Drilling Technology*. Kuala Lumpur, Malaysia.
- Patil, Parimal Arjun , and Catalin Teodoriu. 2013. "A comparative review of modelling and controlling torsional vibrations and experimentation using laboratory setups." *Journal of Petroleum Science and Engineering* 112: 227-238.
- Pavone, D.R., and J.P. Desplans. 1994. "Application of High Sampling Rate Downhole Measurements for Analysis and Cure of Stick-Slip in Drilling." *SPE Annual Technical Conference and Exhibition*. New Orleans, Louisiana: SPE.
- Reckmann, Hanno, Pushkar Jogi, Franck Kpetehoto, Sridharan Chandrasekaran, and John Macpherson. 2010. "MWD failure rates due to drilling dynamics." *IADC/SPE Drilling Conference and Exhibition*. New Orleans, Louisiana, USA.
- Sagert, C., F. Di Meglio, M. Krstic, and P. Rouchon. 2013. "Backstepping and flatness approaches for stabilization of the stick-slip phenomenon for drilling." *IFAC Proceedings Volumes* 46 (2): 779-784.
- Sananikone, Prasert , Osamu Kamoshima, and D.B. White. 1992. "A Field Method for Controlling Drillstring Torsional Vibrations." *IADC/SPE Drilling Conference*. New Orleans, Louisiana: SPE.
- Serrarens, A. F. A., M. J. G. van de Molengraft, J. J. Kok , and L. van den Steen. 1998. " H^∞ control for suppressing stick-slip in oil well drillstrings." *IEEE Control Systems Magazine* 19-30.
- Sharma, Aditya , Saket Srivastava, and Catalin Teodoriu. 2020. "Experimental Design, Instrumentation, and Testing of a Laboratory-Scale Test Rig for Torsional Vibrations—The Next Generation." *Energies* 13 (18): 4750.

- Sharma, Aditya, Saket Srivastava, Catalin Teodoriu , and Marius Stan. 2021. "Experimental Comparison of PID Based RPM Control for Long Horizontal vs. Vertical Drillstring." *Preprints* .
- Shuttleworth, N.E. , E.J. van Kerkoerle, D.R. Folmer, and N. Foekema. 1998. "Revised Drilling Practices, VSS-MWD Tool Successfully Addresses Catastrophic Bit/Drillstring Vibrations." *IADC/SPE Drilling Conference*. Dallas, Texas: IADC/SPE.
- Srivastava, Saket , Aditya Sharma, and Catalin Teodoriu. 2023. "Optimizing Sampling Frequency of Surface and Downhole Measurements for Efficient Stick-Slip Vibration Detection." *Petroleum*.
- Srivastava, Saket , and Catalin Teodoriu. 2019. "An extensive review of laboratory scaled experimental setups for studying drill string vibrations and the way forward." *Journal of petroleum Science and Engineering* 182: 106272.
- Tang, L. , B. Guo, X. Zhu, C. Shi , and Y. Zhou. 2020. "Stick–slip vibrations in oil well drillstring: A review." *Journal of Low Frequency Noise, Vibration and Active Control* 39 (4): 885-907.
- Tian, Jialin , Yi Zhou, Lin Yang, and Shuhui Hu. 2020. "Analysis of stick-slip reduction." *Journal of Multi-Body Dynamics* 1 (234): 82-94.
- Tucker, Robin W., and Charles Wang. 1999. "On the effective control of torsional vibrations in drilling systems." *Journal of Sound and Vibration* 224 (1): 101-122.
- Vogel, Stephen K., and Andrew P. Creegan. 2016. "Case Study for Real Time Stick/Slip Mitigation to Improve Drilling Performance." *SPE/IADC Middle East Drilling Technology Conference and Exhibition*. Abu Dhabi, UAE: OnePetro.
- Vromen, T. G. M., N. van de Wouw, A. Doris, P. Astrid, and H. Nijmeijer. 2014. "Observer-based output-feedback control to eliminate torsional drill-string vibrations." *53rd IEEE Conference on Decision and Control*. Los Angeles, CA, USA: IEEE. 872-877.
- Wu, Sean Xianping, Luis Paez, Uyen Partin, and Mukul Agnihotri. 2010. "Decoupling Stick-Slip and Whirl to Achieve Breakthrough in Drilling Performance." *IADC/SPE Drilling Conference and Exhibition*. New Orleans, Louisiana, USA.
- Zha, Yang, and Son Pham. 2018. "Monitoring downhole drilling vibrations using surface data through deep learning." *SEG International Exposition and Annual Meeting*. Anaheim, California, USA.
- Zhong , Ruizhi , Cyrus Salehi , and Ray Johnson Jr. 2022. "Machine learning for drilling applications: A review." *Journal of Natural Gas Science and Engineering* 108: 104807.

100% Core Recovery in Potassium Salt Layers – Our Experience with MgCl₂-Mud-Systems

L. Schimmrigk

UGS GmbH, Engineering, Drilling / P&A, Mittenwalde, Germany

A common fluid design in solution mining for drilling through salt formations is a fully NaCl saturated mud system. When facing complex salt structures consisting of alternating layers of Halite and Potassium, uncontrolled leaching of potassium layers will happen due to solubility equilibriums of the present cations. This can lead to wellbore stability issues as well as to potential drilling problems and poor recovery rates when acquiring cores from those formations/layers.

Utilizing a fully saturated mixed-salt mud system (NaCl, KCl) with an accurate equilibrium and to maintain it during operation is often impracticable. Furthermore it excludes the feasibility of performing a Spectral-Gamma-Ray-Logging-Run in the desired section, which can be crucial in complex salt structures for placing the future cavern and for determining the optimal production casing depth. The alternative of using an oil-based mud system may involve a huge environmental impact and can lead to high costs.

In a proactive effort to prevent the aforementioned issues and to ensure an optimal cavern placement UGS-GmbH cooperated with a client in terms of using a Magnesium chloride (MgCl₂) saturated, water-based mud for drilling through potassium salt rich formations, particularly when these alternating layers are to be expected. Utilizing this MgCl₂-mud system data- and core-acquisition has demonstrated a remarkable improvement in the rate of success when encountering complex soil formations. This method has been used successfully in numerous cavern wells throughout Germany.

The implementation of the fully saturated MgCl₂ Mud System, however, has posed some additional challenges. Due to an increased potential for corrosion, as well as a high level of reactivity between the mud and cement, several adaptions of the overall working program and handling of the equipment and materials had to be implemented.

This presentation will give a critical overview of the outcomes, challenges, and lessons learned with the aim of offering a general understanding of utilizing MgCl₂ saturated water-based mud when drilling through complex potassium salt formations.

A new well shape with direct application to geothermal drilling in order to reduce costs and improve lifetime of the well

C. Teodoriu

The University of Oklahoma

Introduction

Geothermal wells are currently drilled using the long-established drilling and well construction technology that has been borrowed from oil and gas wells. The geothermal well construction is thus based on the telescopic design in which a larger diameter hole is drilled, followed by a casing run and cementing. The process is continued by adding smaller and smaller sizes until the final depth is achieved. This technology uses the rotary drilling process: the bit is rotated while pushed against the rock and a drilling fluid is circulated in order to transport to the surface the cuttings generated during the rock breaking process. The result of this procedure is usually a round hole with some minor imperfections. Because geothermal wells need high temperature, depth is critical and thus, the deeper the well the higher the temperature. If the temperature is low, the production flow rate must be increased and this process requires larger hole and casing diameters (Fichter et al., 2010). However, using current geothermal drilling methods and well construction, the deeper the well is the smaller the final casing (production) will become. As a result, it is impossible to meet geothermal requirements without high drilling costs which are not favorable to geothermal development.

Project *gebo* demonstrated that monobore well construction is possible if new technologies are adapted to meet geothermal needs. Some of these technologies are folded and expanded tubulars, large diameter coiled tubing drilling applications, welding as replacement to threaded connections and automation. Originally, the project was focused on creating a circular wellbore shape as in oil and gas circular shape. However, the main outcome of *gebo* was that the use of novel technologies makes possible a monobore well construction.

In this paper, the monobore well construction is a well in which the ID of the casing string is the same size from top to bottom. This was described by Teodoriu (2013) and Varahram (2011), see figure 1.

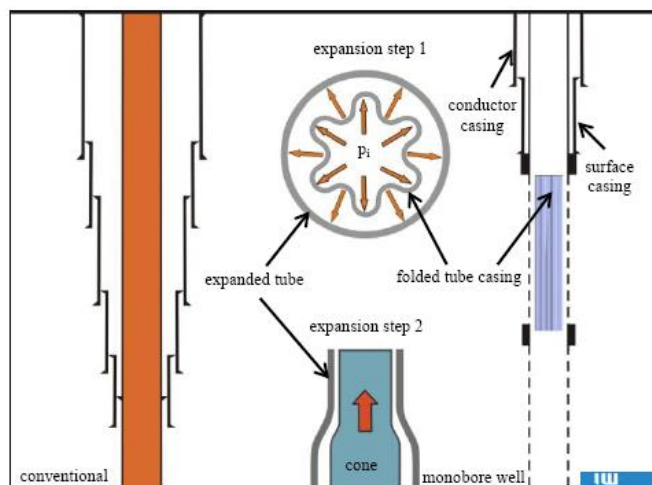


Figure 1. Conventional and *gebo* monobore well design, after Varahram et al. (2011)

Lavrov et al. (2014) discussed the stability of non-circular boreholes in highly inclined wells and showed that a non-circular well shape can be beneficial for the improvement of the drilling process and long-term wellbore stability. Figure 2 shows the well shape proposed by Lavrov et al. (2014). Oyedokun and Schubert (2022) have also studied the stability of non-circular wellbore by using an elliptical shape. They demonstrated that circular and near-circular wellbores are more stable than elliptical shaped borehole in both shear and tension.

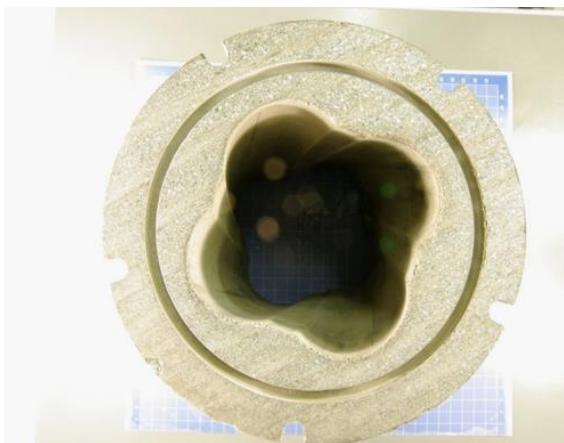


Figure 2. Non-circular well shape as proposed by Lavrov et al. (2014)

The new approach

In this paper, we investigate the possibility of using a different well shape instead of the classical circular shape as drilled today. The main reason for this approach lies in the fact that circular well shapes are always prone to deformations. Thus, the real well shape is far from the perfect theoretical well shape, especially for tubulars that need to withstand high external pressure loads. Furthermore, since geothermal production wells require a high flow area, we propose a combination of possible technical and operational solutions that one day could revolutionize the geothermal well construction.

Our non-circular wellbore as proposed in this paper has an eight shape or infinity shape, as shown in figure 3. Such a well can be drilled with two drill bits in parallel.

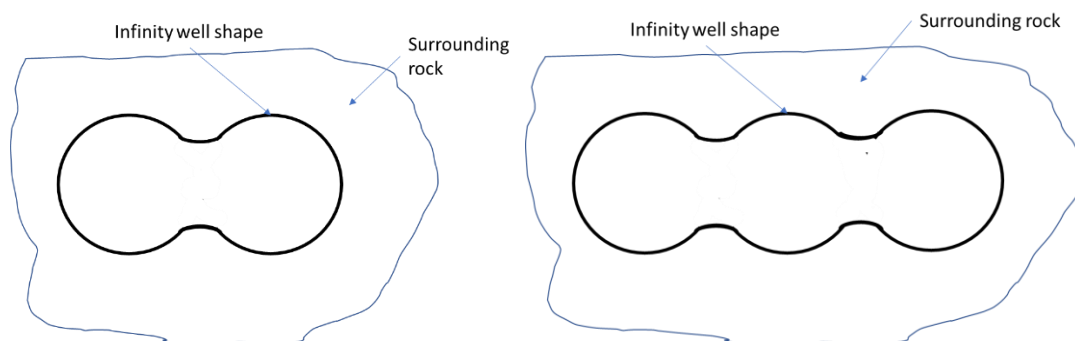


Figure 3. A possible shape for non-circular well construction

A new bottom hole assembly is required to drill such a non-circular well shape. Since gebo demonstrated that large OD coiled tubing rigs can be used for drilling deep geothermal wellbores, figure 4 shows a possible use of two coiled tubing units in tandem. A smart way to build such a concept will also allow replacing the bits individually, for example by using a retrievable bit assembly.

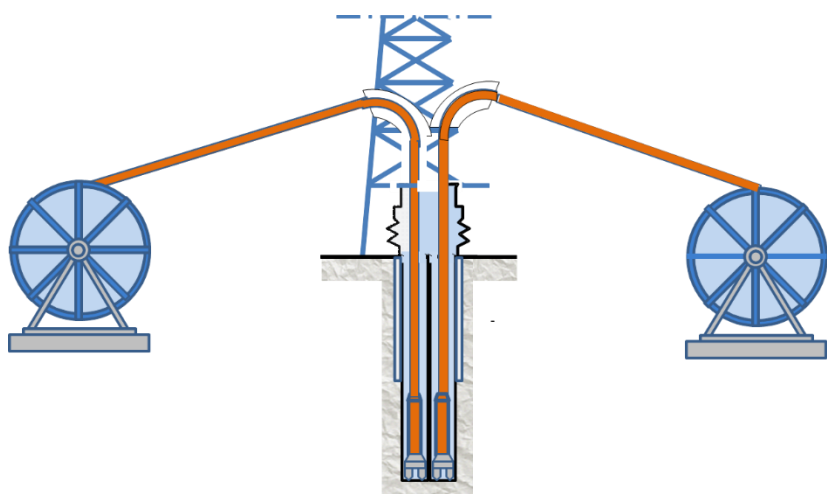


Figure 4. Dual coiled tubing rig to drill a non-circular well construction

Discussions

Drilling large wellbores to compensate for the geothermal need of high flow rates (100 l/s) is cost intensive and increases exponentially with depth. The new concept will allow the use of the fastest bit sizes on the market while creating an area which is double the size. Several studies have pointed out that a sweet spot exists for drill bit sizes between 8 and 10 $\frac{3}{4}$ ". Thus, the new proposed non-circular shape could lead to a higher rate of penetration hence reducing drilling costs. Subproject W6 of the *gebo* project investigated various foldable pipe solutions, including one that could fit the new well shape as presented in this paper, see Figure 5. The ability to manufacture foldable pipes with multilobes actually opens the way to complex non-circular wellbore geometries. However, for the purpose of this paper the double lobe foldable pipe geometry is considered.

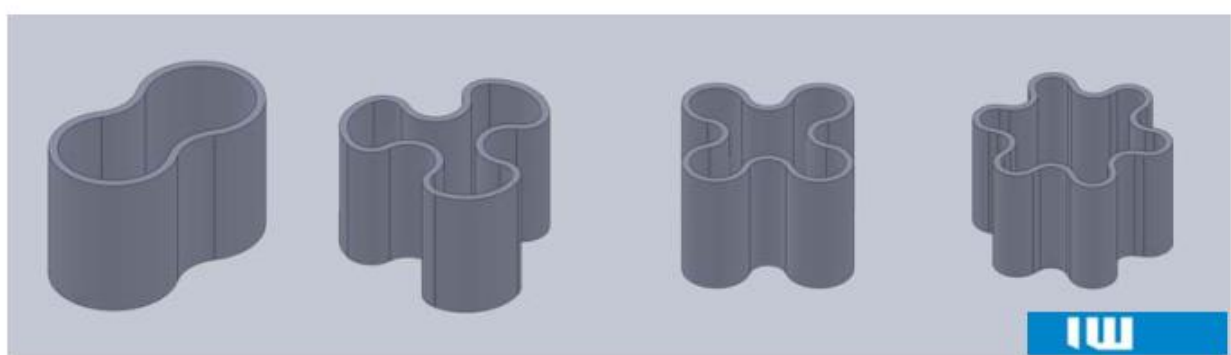


Figure 5. Foldable pipe geometry with application to monobore well construction, after Varahram et al. (2011)

Conclusions

The ability of future geothermal applications to replace base load electricity demand requires revisiting geothermal well construction.

This paper discusses the option to drill large cross-sectional wellbore areas using existing conventional drill bits that are smaller in diameter.

Using the *gebo* outcome, the construction of a non-circular deep monobore well for geothermal applications is one step nearer, but still requires intensive research and technology development.

Increasing the wellbore cross sectional area will enable higher flow rates in geothermal wellbore and thus increase the energy output per well.

References

Fichter, C., Reinicke, K.M., Teodoriu, C., Wang, Y., Lotz, U. 2009. Influences and limiting parameters of casing design on the success of hydrogeothermal projects - a new approach for the design of geothermal wells, Geothermal Congress - "Der Geothermiekongress 2009", Bochum, Germany, November 17-19.

A. Lavrov, A. Taghipour, J.D. Ytrehus, J. Mårdalen, H. Lund, T. Vrålstad, B. Lund, I.M. Carlsen, A. Saasen, S. Wold, J. Abdollahi, A. Torsvoll, A. Reyes, J.R. Næumann, J.C. Melchiorse, P. Skalle, Numerical and experimental study of the stability of non-circular boreholes in high-permeability formations, International Journal of Rock Mechanics and Mining Sciences, Volume 68, 2014, Pages 128-135, ISSN 1365-1609

Oluwafemi Oyedokun, Jerome Schubert. Stability of highly inclined non-circular wellbores in isotropic formations, 10 May 2022, PREPRINT (Version 1) available at Research Square [<https://doi.org/10.21203/rs.3.rs-1639301/v1>]

Teodoriu, C., 2013, Monobore Well Drilling: Definition, Advantages and Future Deep Drilling Concepts, 9. International Geothermal Conference Freiburg, May 16th, 2013

Varahram, A., Bach, W., Hassel, T., 2011 *gebo* intermediate report

Experimental Analysis of Cyclic Loading Effect on Seal Integrity of Cement Sheath

Xuning Wu^{1,2}, Zhengmeng Hou¹, Zaoyuan Li², Yachen Xie¹, Jian Liu², Weitao Song², Jin Li², Wei Sun^{3,4}

¹ Research Centre of Energy Storage Technologies, Clausthal University of Technology, Goslar, Germany

² National Key Laboratory of Oil and Gas Reservoir Geology and Exploitation, Southwest Petroleum University, Chengdu, China

³ Faculty of Land and Resources Engineering, Kunming University of Science and Technology, Kunming, China

⁴ Yunnan Key Laboratory of Sino-German Blue Mining and Utilization of Special Underground Space, Kunming, China

Abstract

The cement sheath is the first barrier of well integrity, and plays a critical role in maintaining the zonal isolation and ensuring the safety of oil and gas wells. Once the cement sheath seal fails, it will lead to issues such as fluid leakage and sustained casing pressure. Cyclic loading will cause cumulative plastic strain and strength degradation of cement stone, which is a relatively dangerous working condition for the downhole cement sheath. In this research, the laboratory experiment method was used to carry out the uniaxial and triaxial compressive strength tests of cement systems with conventional density (1.9 g/cm^3). Seal integrity tests under cyclic loading were then carried out on the mold-cured cement sheath. X-ray CT scanning was performed on the cement sheath sample after the cyclic loading test to observe the form of sealing failure. The research shows that the failure modes of the cement sheath under cyclic loading are mainly interface debonding and tensile cracks. After the internal pressure of the casing was loaded to the upper limit for the first time, the gas channelling flow was monitored, indicating that the cement sheath had lost its sealing performance. After that, the gas flow rate gradually increased with each additional cycle. Under multiple cycles, the cement sheath is compacted and its deformation capacity is weakened. Due to the accumulated plastic deformation, micro-annulus is generated at the casing-cement sheath interface. The cyclic loading also caused multiple cracks in the cement sheath sample, including penetrating cracks from the bulk to the interface. The research results are beneficial to understand the influence of cyclic loading on cement sheath and guide the design of cement sheath system.

1 Introduction

The utilization of underground resources and space through drilling methods has become increasingly diversified, encompassing activities such as the extraction of oil and gas, hydrates, and geothermal energy, as well as carbon dioxide sequestration and underground energy storage. In order to maintain the long-term safe and sustainable production of wells, ensuring the integrity of the wells is of paramount importance [1, 2]. After completing a stage of drilling and casing installation, cement slurry is injected into the annulus apace between the casing and wellbore from the bottom of a casing string to the surface. Then, the cement slurry solidifies in the wellbore, a continuous and robust cement sheath is formed. As a major element of well integrity, the cement sheath plays an important role in providing mechanical and hydraulic isolation between the wellbore and surrounding rock formations, and preventing the migration of fluids or gases from one zone to another.

However, the complex downhole conditions impose varying loads on the cement sheath, which increases the risk of its failure. One significant issue is the cyclic loading caused by multistage hydraulic fracturing. The failure of cement sheaths due to changes in temperature and pressure of the wellbore or formation is very common. The most apparent problem is the sustained casing pressure (SCP), manifested as a pressure in well annulus that is

measurable at the wellhead and rebuilds when bled down. To address SCP issues, measures such as well shut-in and wellbore remediation are required, and in severe cases, well abandonment may be necessary, which poses a serious threat to the safe and sustainable production of wells.

N. K. Combs [3] The study selected a representative shale area in the United States, collected and analyzed historical data on cementing, completion, and production operations that caused SCP in the shale area. As shown in Figure 1 (a), The analysis indicated that 86.5% of wells drilled manifested SCP of some magnitude. 36.7% of study wells with no SCP exhibited signs of SCP occurrence after fracturing operations. 49.8% of study wells exhibited SCP prior to fracturing; and all of those wells were affected by stimulation operations. Another study [4] pointed out that the proportion of annular pressure-bearing wells in the Fuling shale gas field in China reached 79.52%. Before and after multi-stage fracturing, the proportion of annular pressure-bearing wells at the first casing head (between production casing and technical casing) increased from 14.85% to 50.05%, while the proportion of annular pressure-bearing wells at the second casing head (between technical casing and surface casing) increased from 15.84% to 53.01% (Figure 1 (b)). It is indisputable that the cyclic loading (temperature and stress cycling) caused by multi-stage fracturing has a significant impact on the integrity of the cement sheath.

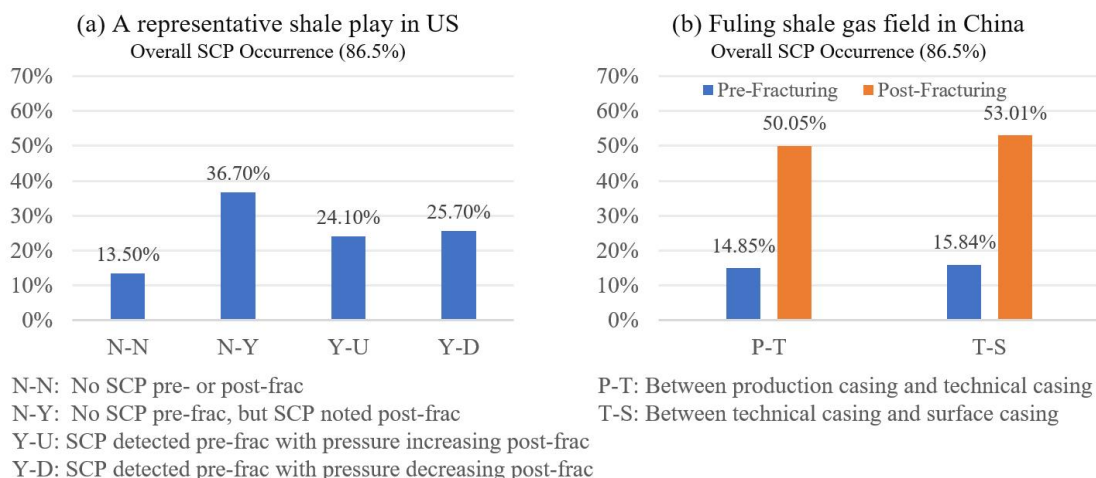


Figure 1. Overall occurrence of SCP in different regions.

The barrier of a wellbore is mainly composed of casing and cement sheath. Casing is made of metallic material and has good elastic deformation ability, which is not easily damaged under cyclic loads. However, cement sheath is a brittle material, and although the confining pressure underground can enhance its elastic-plastic deformation ability [5], it is still the most vulnerable part of the wellbore barrier under cyclic loads. Some research has been conducted on the influence of cyclic loads on the cement sheath integrity. Jackson and Murphey [6] (1993) used an experimental apparatus close to full size to study the effect of cyclic pressure inside the casing on the sealing ability of cement sheath. The tests showed increased gas flow through the annulus after cyclic application and bleed off of casing differential pressure greater than 5000 psi. Arash and Jerome [7] (2014) cured cement samples in a newly developed high-temperature and high-pressure rheometer and then conducted cyclic loading tests under HPHT conditions. The experiment found that Cement sheath made of H-class cement plus 35% silica developed failures such as radial cracking, debonding and disking occurred due to cyclical loadings. Geng Yanan [8] (2020) used a cement sheath integrity evaluation device to conduct tests on the sealing integrity of cement sheath under different casing internal pressure cyclic loads of 5~40MPa. The test found that the cement sheath was prone to seal failure during unloading, and the number of cycles required for seal failure decreased with the increase of casing internal pressure cyclic loads. Li Jun [9] (2020) used a new full-size physical simulation experimental facility to simulate the hydraulic fracturing construction process, applied 70MPa internal pressure inside the casing, and then unloaded it to 0 cyclically. The experimental results demonstrated that micro-

annulus emerged in the casing-cement sheath interface and became the pathway for gas migration.

Although some experimental phenomena can be obtained from the above experimental apparatuses, there are still some limitations. Some cannot apply confining pressure or temperature, which cannot meet the requirements of complex testing conditions. Some are full-size devices, and the testing cost is too high, which is not conducive to batch testing. Therefore, this paper adopts a non-full-size high-temperature and high-pressure cement sheath integrity evaluation device to conduct tests on the sealing integrity of cement sheath under cyclic loads. The X-ray CT scanning method is used to visualize the failure forms of cement sheath integrity and analyze the failure mechanism. This will help to design new cement systems and improve the continuous production capacity of oil and gas wells.

2 Materials and Methods

2.1 Raw materials

The cement slurry system used in this study is conventional density (1.9 g/cm^3), and the detailed formula is as follows: Grade G cement + dispersant + stabilizer + fluid loss agent + defoamer (W/S is 0.38). The curing mold of the cement sheath and the cement sheath sample after curing are shown in the figure 2. Put the entire mold into a high-temperature and high-pressure curing kettle, and cure it for 72 hours under the condition of $60^\circ\text{C} \times 20.07 \text{ MPa}$. The cement sheath sample shown in Figure 2 (c) was obtained, and its physical parameters are shown in Table 1.

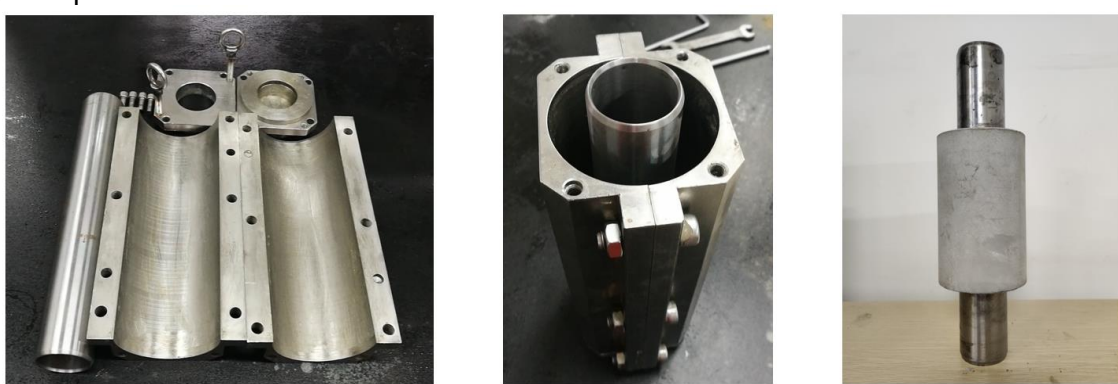


Figure 3. Curing mold and cement sheath samples

Table 1 Physical parameters of cement sheath samples

| Table 11 Physical parameters of cement sheath samples | | | |
|---|-------|------------------------|--------|
| Parameter | Value | Parameter | Value |
| Casing inner diameter | 44mm | Casing Young's modulus | 210GPa |
| Casing outer diameter | 50mm | Casing length | 300mm |
| Cement sheath outer diameter | 92mm | Cement sheath length | 150mm |

2.2 Cement sheath integrity evaluation device and method

The equipment used in this study is a high-temperature and high-pressure cement sheath integrity evaluation device designed by the Cementing Research Office of Southwest Petroleum University in China. As shown in Figure 3, the evaluation device is mainly composed of four parts: pressure control system, data monitor and display system, well integrity test system and N₂ cylinder. The experimental device could control the working temperature between 0-200 °C and the working pressure between 0-100 MPa. The pressure control system could provide pressure cycling in the casing and gas pressure (0.5-1 MPa N₂) in the inlet of the annulus space between the casing and formation. The data monitor and display system recorded the temperature, internal pressure, confining pressure, inlet and outlet pressure, flow rate, and cycle times. The sealing integrity of the cement sheath could be evaluated using the monitoring pressure and flow rate at the outlet of the annulus space.

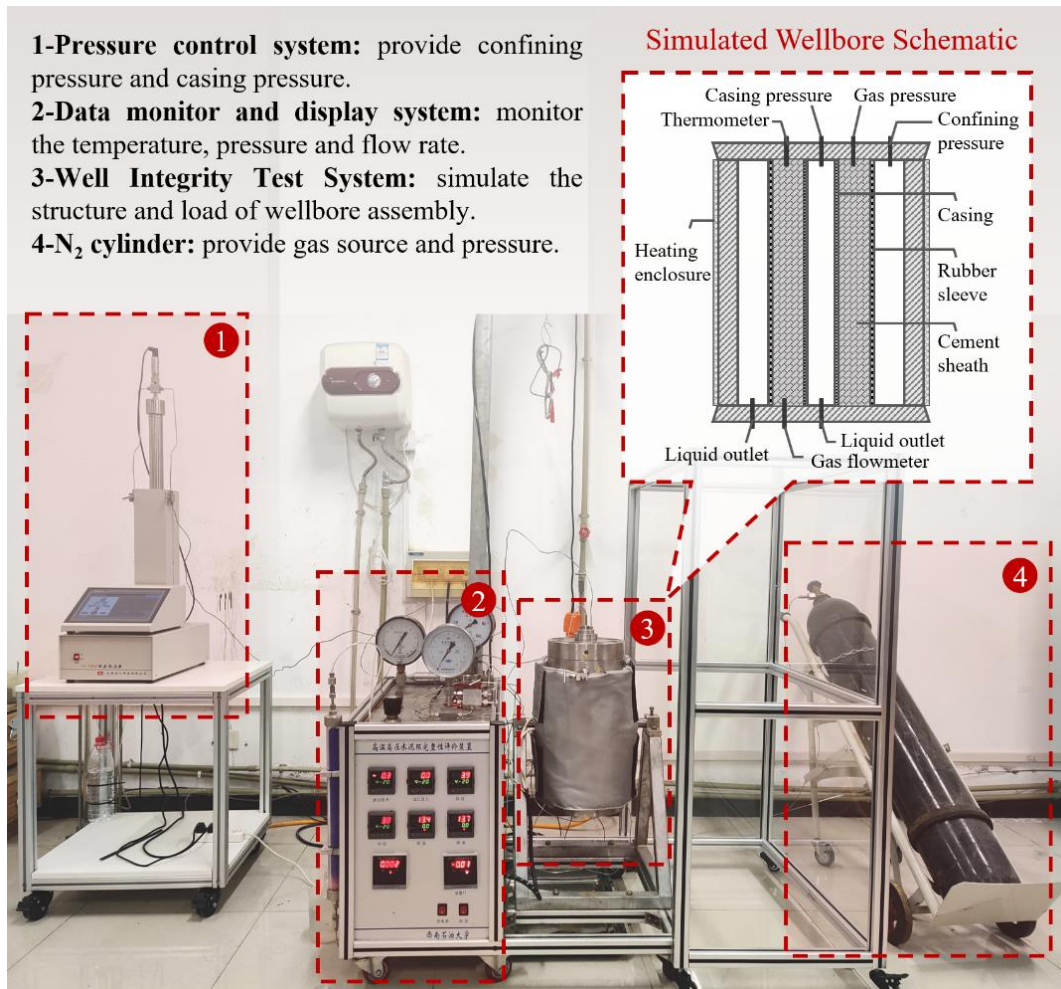


Figure 3. High temperature and high pressure cement sheath integrity evaluation device. The main purpose of the experiment was to test the seal integrity of the cement sheath samples under cyclic loading conditions. The specific experimental method is as follows:

Step 1: A rubber sleeve is wrapped around the outer circumference of the cement sheath sample to form a combination of casing-cement sheath-rubber sleeve. When the confining pressure is applied to the rubber sleeve, the sealing of the outer periphery of the cement sheath can be maintained and downhole stresses can be simulated.

Step 2: Apply a certain amount of confining pressure (3 MPa) and internal pressure (0.5 MPa) to the "casing-cement sheath-rubber sleeve" assembly, and inject nitrogen gas pressure (0.5 MPa) into the annular space on top of the cement sheath to verify the initial sealing performance of the assembly.

Step 3: Use a heating enclosure to raise the temperature of the vessel to 60°C, increase the external pressure to 10 MPa, and adjust the nitrogen gas pressure to 1 MPa.

Step 4: Apply 20 cycles of loading and unloading to the assembly according to the process shown in Figure 4. The internal pressure loading and unloading rate is 10 MPa/min. After each loading or unloading, maintain the pressure for 3 minutes to reach a steady state.

Step 5: During the cyclic loading process, monitor the generation and fluctuation of nitrogen gas in the bottom annulus using a gas flow meter. If gas flow is detected, it indicates that the sealing integrity of the casing-cement sheath-rubber sleeve assembly has failed.

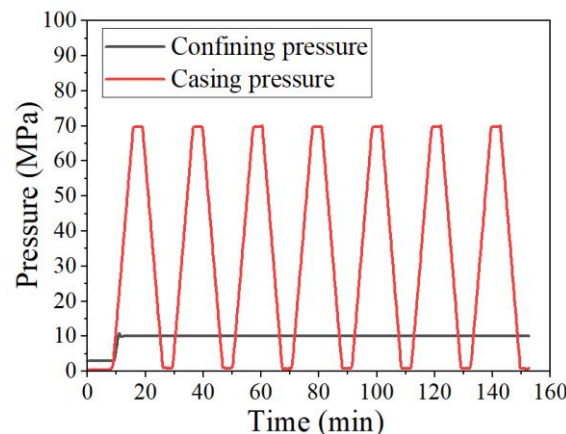


Figure 4. Pressure control process of cyclic loading and unloading.

3 Results and Discussion

3.1 Uniaxial and Triaxial Compressive Strength Tests of Cement Stone

The stress and strain measurement of cement stone was conducted using the GCTS RTR-1000 rapid rock triaxial testing system, a servo-controlled system for rock mechanics. The local linear variable differential transformer (LVDT) was used as the strain measurement sensor, which has an accuracy of 0.25%. The loading rate was 0.25 ± 0.05 MPa/s, and test data were automatically collected by a monitoring system, starting after the base had contact stress.

For consistent observations, cylindrical specimens with a height-to-diameter ratio between 1.8 and 2.2 were used for uniaxial and triaxial tests, in accordance with ASTM C39/C39M-01 [10]. As depicted in Figure 5, the specimens had a height and diameter of 50 ± 1 mm and 25 mm, respectively. The specimen's end surface was polished using a stone grinding machine, and the dimensions were measured using a Vernier caliper. The end surface was ground until the height values measured along the 0° and 90° directions had an error of less than 0.05 mm.



Figure 5. Rapid rock triaxial testing system and cement stone specimen.

The uniaxial and triaxial compressive strength test results of cement stone are shown in Figure 6. The mechanical properties of cement stone were significantly affected by confining pressure, which increased its strength and extended the nonlinear deformation stage, leading to a significant increase in strain. Unlike the brittleness observed under uniaxial conditions, confining pressure induced cement stone to exhibit the ductile characteristics of ductile materials. Many scholars have reported on this observation [11-13].

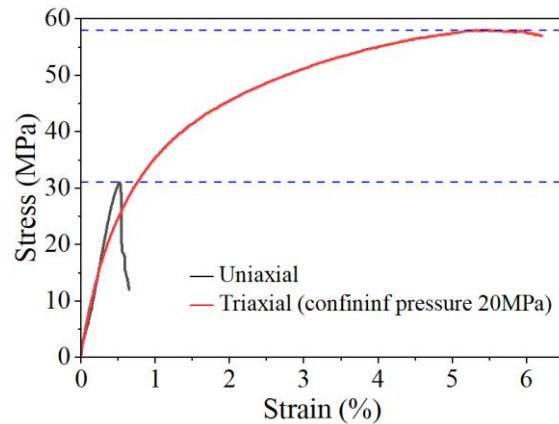


Figure 6. Uniaxial and triaxial compressive strength test results of cement stone.

3.2 Effect of Cyclic Loading on Sealing Integrity of Cement Sheath

The cement sheath is subjected to stress not only from the increase in internal pressure of the casing but also from the influence of rock formation stress. During the process of increasing internal pressure of the casing, the cement sheath is squeezed and may undergo plastic deformation or tensile failure. The results of the high temperature and high pressure integrity evaluation experiment of the cement sheath are shown in Figure 7.

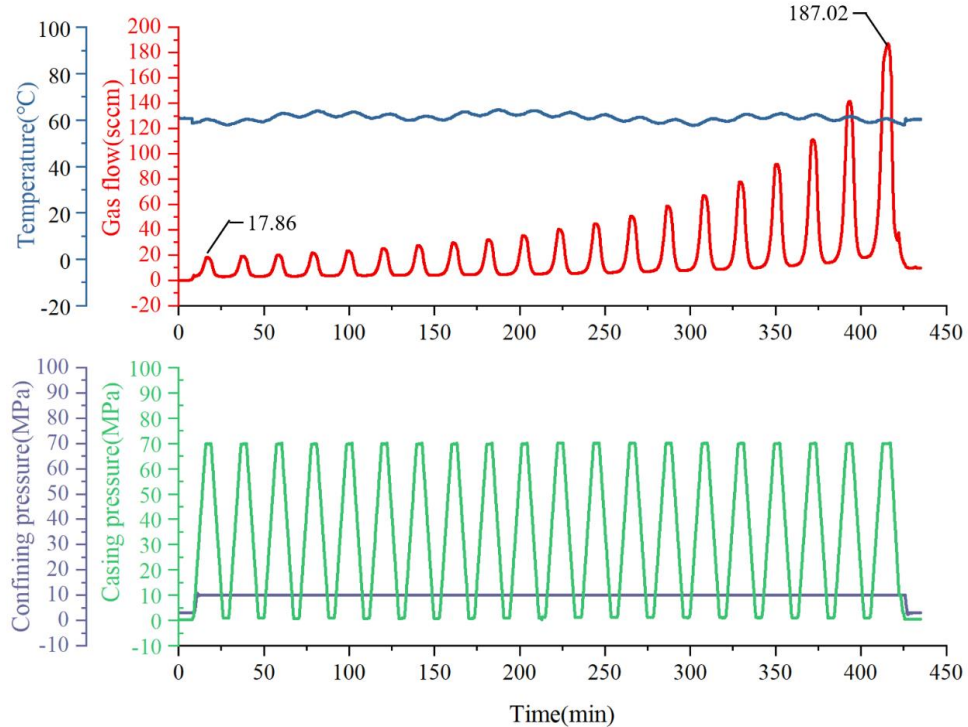


Figure 7 HTHP integrity evaluation test results of cement sheath.

Under low confining pressure (3 MPa) and low internal pressure (0.5 MPa) conditions, no gas seepage was detected, indicating good initial sealing performance of the cement sheath sample. As the internal pressure of the casing increased, gas seepage was detected and increased with the number of cycles, indicating that the cement sheath lost its sealing performance under cyclic loading. After CT scanning the tested samples with a resolution of 61.83 μm , the scan results of the sliced cement sheath internal seepage channel area are shown in Figure 8.

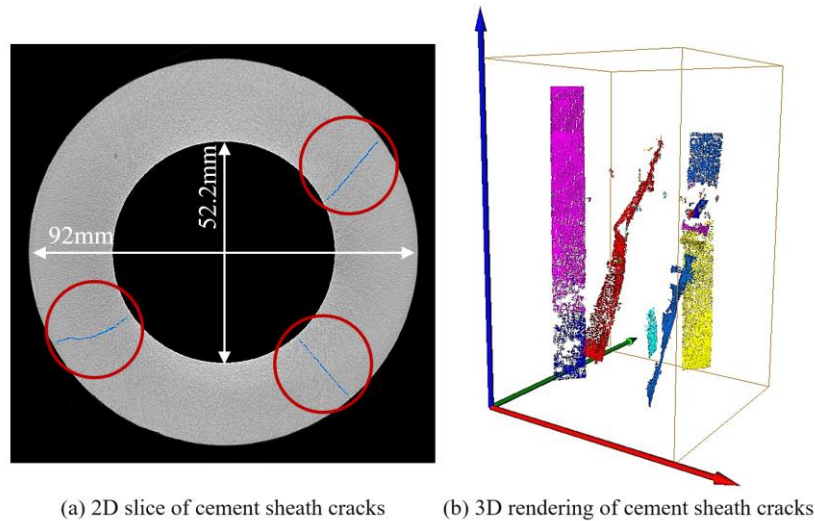


Figure 8. CT scan results of cement sheath after integrity evaluation test.

The following findings can be drawn from Figures 7 and 8:

1. After the internal pressure of the casing was loaded to the upper limit for the first time, gas channeling flow was monitored ($17.86 \text{ cm}^3/\text{min}$), indicating that the cement sheath had lost its sealing performance. With each additional cycle, the gas flow rate gradually increased, reaching a maximum of $187.02 \text{ cm}^3/\text{min}$ after 20 cyclic loads. This shows that the cyclic loads have gradually damaged the integrity of the cement sheath.
2. Under multiple cycles, the cement sheath becomes compacted and its deformation capacity is weakened. The cement sheath body suffered from tensile failure after repeated loading, resulting in multiple cracks, including penetrating cracks from the bulk to the interface, as shown in the red circle in Figure 8 (a).
3. Under the effect of cyclic load, the casing and the cement sheath expand and deform when the internal pressure of the casing increases. During the pressure unload process, the expansion deformation of the casing can be fully restored, but the cement sheath has entered a state of plastic deformation and cannot fully return to its original state after pressure unload. The uncoordinated deformation of the casing and cement sheath leads to micro-annulus at the casing-cement sheath interface. As shown in Figure 8 (b), the inner diameter of the cement sheath is increased by 2.2 mm due to accumulated plastic deformation, resulting in micro-annulus formation at the casing-cement sheath interface.
4. The micro-annulus at the interface of the cement sheath and the micro-cracks in the body together constitute the channel for gas channeling, which can cause harmful gas leakage or annular pressure phenomenon, affecting environmental safety and engineering benefits.

In summary, the failure modes of the cement sheath under cyclic loading are mainly interface debonding and tensile cracking, corresponding to the deformability and strength of the cement sheath, respectively. A cement sheath with higher deformability can better recover from deformation during cyclic loading, while a cement sheath with higher strength can withstand higher casing pressure. Therefore, to improve the sealing ability of the cement sheath under cyclic loading, its strength should be increased and its elastic modulus should be decreased.

5. Conclusion

uniaxial and triaxial compressive strength tests, as well as integrity evaluation tests under cyclic loading, were carried out on conventional density cement slurry systems. CT scans of the sample after the high-temperature and high-pressure seal integrity test visualized the seal failure mode of the cement sheath. The main conclusions obtained are as follows:

- (1) Under the effect of confining pressure, the strength of the cement stone increases significantly, and the nonlinear deformation stage of cement stone is obviously extended, with greatly increased strain.
- (2) The failure modes of the cement sheath under cyclic loading are mainly interface

debonding and tensile cracking, with interfacial debonding mainly caused by uncoordinated deformation of the casing and cement sheath. The cement sheath in a plastically deformed state cannot completely return to its original state after pressure relief. However, the strength of the cement sheath is not enough to withstand the upper limit of the internal pressure of the casing, and tensile failure will occur, resulting in cracks in the cement sheath body. The micro-annulus at the interface of the cement sheath and the micro-cracks in the body together constitute the channel for gas channelling.

(3) The initial sealing performance of the experimental device is satisfactory, which indicates that the design of the device is appropriate. However, the generated gas flow rate gradually increases with an increase in the cycle period, indicating that the integrity of the cement sheath is progressively damaged by cyclic loading.

Acknowledgment

This work is funded by Henan Institute for Chinese Development Strategy of Engineering & Technology (No. 2022HENZDA02), the Science & Technology Department of Sichuan Province (No. 2021YFH0010), High-End Foreign Experts Program of the Yunnan Revitalization Talents Support Plan of Yunnan Province, and the China Scholarships Council (No. 202008080235).

References:

- [1] Wu X., Liu J., Li Z., Song W., Liu Y., Shi Q., Chen R.: Failure Analysis of Cement Sheath Mechanical Integrity Based on the Statistical Damage Variable. *ACS Omega*. 8. 2128 [2023].
- [2] Su D., Wu X., Li Z., Huang S., Li J., Sun J., Zheng G.: Theoretical Analysis of the Micro Annulus of an Oil-Well Cement Sheath Formed via Cooling under Acid-Fracturing Conditions. *Processes*. 10. 966 [2022].
- [3] Combs N.K., Sabins F., Watters J., Watters. L.T. Preventing Sustained Casing Pressure in Shale Wells. *AADE National Technical Conference and Exhibition*. Houston, Texas: [2017].
- [4] Xi Y., Li J., Tao Q., Guo B., Liu G.: Experimental and numerical investigations of accumulated plastic deformation in cement sheath during multistage fracturing in shale gas wells. *Journal of Petroleum Science and Engineering*. 187. 106790 [2020].
- [5] Liu J., Wu X., Li Z., Song W., Liu Y., Shi Q., Chen R.: Mechanical properties and nonlinear deformation description model of cement stone. *Geoenergy Science and Engineering*. 223. 211578 [2023].
- [6] Jackson P.B., Murphrey. C.E. Effect of Casing Pressure on Gas Flow Through a Sheath of Set Cement. *SPE/IADC drilling conference*. Amsterdam: [1993].
- [7] Arash S., Schubert J., Amani M., Teodoriu C. HPHT Cement Sheath Integrity Evaluation Method for Unconventional Wells. *SPE International Conference on Health, Safety, and Environment*. California, USA: [2014].
- [8] Yanan G., Lulu Q., Jiaping Y., Zhiqiang H., Zhiqiang W., Shuangjin Z.: Experimental study on the influence of cyclic load on the sealing integrity of cement sheath under complex temperature and pressure conditions (In Chinese). *MINERAL EXPLORATION*. 11. 1066 [2020].
- [9] Li J., Xi Y., Tao Q., Li Y., Qu G.: Experimental investigation and numerical simulation of the emergence and development of micro-annulus in shale gas wells subjected to multistage fracturing. *Journal of Natural Gas Science and Engineering*. 78. 103314 [2020].
- [10] ASTM. Standard Test Method for Compressive Strength of Cylindrical Concrete Specimens. C 39/C 39M–01. West Conshohocken, PA, USA.
- [11] Zhou S., Liu R., Zeng H., Zeng Y., Zhang L., Zhang J., Li X.: Mechanical characteristics of well cement under cyclic loading and its influence on the integrity of shale gas wellbores. *Fuel*. 250. 132 [2019].
- [12] Lima V.N., Silva F.D.A., Skadsem H.J., Beltrán-Jiménez K., Sunde J.K.: Effects of confinement pressure on the mechanical behavior of an oil well cement paste. *Journal of Petroleum Science and Engineering*. 208. 109769 [2022].
- [13] Yang H., Bu Y., Guo S., Liu H., Du J., Cao X.: Effects of in-situ stress and elastic parameters of cement sheath in salt rock formation of underground gas storage on seal integrity of cement sheath. *Engineering Failure Analysis*. 123. 105258 [2021].

Life Saving Rules and Actions (LSRA) bei EMPG

C. Hahn

ExxonMobil, SHE, Hannover, Germany

Der positive Trend der Sicherheitsleistung konnte bei EMPG über die letzten Jahre fortgesetzt werden. Einen wesentlichen Punkt zur Vermeidung von Unfällen stellt dabei die sehr gute Vorbereitung und Durchführung der Arbeiten dar, was erst durch ein strukturiertes Workmanagementsystem (WMS) ermöglicht wird. Die Steuerung der Prozesse und eindeutige Beschreibung der einzelnen Arbeitsschritte sowie die Beschreibung und Prüfung der Sicherheitsmaßnahmen bilden resistente Barrieren, um Unfälle zu verhindern.

Allerdings zeigt sich im weltweiten Bereich, dass die Anzahl der schweren Verletzungen mit Ausfallzeiten oder Todesfolge weitestgehend konstant bleibt. Aus diesem Grund wurden bereits vor Jahren bei EMPG die „Maßnahmen, die Ihr Leben schützen“ (international: Life Saving Actions – LSA) eingeführt. Diese LSA fokussierten auf die Schwerpunkte des Workmanagementsystems und berücksichtigen risikoreichere Tätigkeiten wie zum Beispiel „Energiesperrung“, „Öffnen von Systemen“, „Heißarbeiten“, „Höhenarbeiten“ oder „Heben von Lasten“. Themengerichtete Checklisten, die die Arbeitsgenehmigung ergänzen, ermöglichen den Arbeitsteams, die Sicherheitsmaßnahmen vor Beginn der Arbeiten zu überprüfen und sicherzustellen.

In der Industrie sind diese „Lebensretter“ oder goldenen Regeln weit verbreitet und helfen insgesamt dabei, dass Unfallgeschehen positiv zu beeinflussen. Dabei variieren die Themenbereiche, die Anzahl der Module und natürlich die Anwendung bzw. der Umgang mit den Regeln. Eine Vereinheitlichung der LSRA durch IOGP würde insbesondere für Auftragnehmer, die bei unterschiedlichen Öl- und Gasunternehmen tätig sind, zu Vereinfachungen in der Anwendung führen.

Aus diesem Grund hat ExxonMobil sich dazu entschlossen, als neue Basis die neun „Life Saving Rules“ der IOGP* zu wählen und diese um die Regeln „Line of Fire“, „Driving“ und „Working around mobile Equipment“ zu ergänzen. Außerdem wurden ergänzende Aktionen formuliert, die als Hilfestellung in den Tool Box Meetings besprochen und -wenn anwendbar- als Barriere vor Ort angewandt und überprüft werden.

Der Schwerpunkt bei den LSRA liegt in der Kommunikation und Diskussion innerhalb des Arbeitsteams vor Ort. Jeder im Team muss über die Gefährdungen und die entsprechenden Minderungsmaßnahmen informiert sein. Die erfolgreiche Umsetzung der Minderungsmaßnahmen muss vor Arbeitsbeginn vom Arbeitsteam bestätigt werden, erst danach erfolgt der sichere Start. Zur Anwendung der LSRA gehört ebenfalls das Anhalten von Arbeiten, wenn sich Randbedingungen ändern oder Minderungsmaßnahmen nicht mehr volumnäßig wirksam sind. Dabei sind alle gleichberechtigt. Denn nur im Team können wir Fehler, die zu schweren Unfällen führen könnten, verhindern.

Die Einführung und der Umgang der **LSRA** wird im Beitrag vorgestellt.

Geosteering Mittelplate (NW Deutschland) – Besondere Herausforderung während der Corona-Einschränkungen

H. Bolten, S. Dellepiane, D. Schwarz, P. Berger

Wintershall Dea Deutschland GmbH, Hamburg, Germany

Mittelplate ist Deutschlands größtes und produktivstes Ölfeld. Es liegt 100 Kilometer nordwestlich von Hamburg in der Elbmündung und befindet sich damit im Nationalpark und UNESCO-Weltnaturerbe Wattenmeer. Das Feld ging 1987 in Produktion und fördert aus vier Lagerstätten – den Dogger Beta-, Gamma-, Delta- und Epsilon-Sandsteinen – insgesamt wurden bis heute mehr als 70 Bohrungen (inklusive Ablenkungen) abgeteuft. Zur weiteren Erschließung des Feldes wurde und wird Geosteering eingesetzt, um während der aktiven Bohrphase den Bohrpfad anzupassen. Damit ist es möglich, auch in einem maturen Feld neue Bohrungen optimal zu platzieren.

Die eigentlichen Herausforderungen und Aufgaben des Geosteerings liegen in der Navigation zu den gewünschten Reservoirsanden und dem Aufschluss dieser gemäß der Entwicklungsstrategie des Feldes. Bei der Komplexität der Struktur und den geringmächtigen Reservoirsanden werden für diese Aufgaben HighTech-Tools genutzt, welche durchgehend Live-Daten liefern.

Zur normalen Arbeitsweise gehört ein Geosteering-Raum, der während der Geosteering-Phase 24/7 mit zwei Personen in drei Schichten besetzt ist. Diese nutzen die eingehenden Live-Daten, um den Bohrpfad entsprechend der angetroffenen Geologie anzupassen.

Corona und die damit einhergegangenen Kontaktbeschränkungen haben eine neue Herausforderung hinzugefügt. In den Jahren 2021/ 2022 musste auf die Nutzung des Geosteering-Raums verzichtet werden. Via Microsoft Teams wurden unterschiedliche virtuelle Räume eingerichtet, in denen zu dieser Zeit die Diskussionen stattgefunden haben. Ebenso mussten alle anderen für die Operations nötigen Anwendungen nun im Homeoffice funktionieren, um das Team in die Lage zu versetzen, die nötigen Entscheidungen zu treffen. Diese virtuelle Art der Zusammenarbeit bietet auch in Zukunft viele Möglichkeiten der Anwendung, jedoch ist der Nutzen eines Geosteering-Raumes nicht zu unterschätzen.

Process Safety Competency

S. Schmid

ExxonMobil Production Deutschland GmbH, Hannover, Germany

A key component of managing higher consequence process safety risk is the application of Scenario Management. At ExxonMobil Corporation this includes the identification and proactive management of major hazards, the associated scenarios that might lead to an event, and the safeguards that prevent or mitigate the consequence of this event. Equally vital to managing process safety is competency, both for team members and supervisors.

To ensure full understanding of the relevant Scenario Management aspects, ExxonMobil Corporation is now making competency demonstration a requirement for operations supervisors. Leaders need to demonstrate process safety competency for their role at the beginning of their assignments. These demonstrations will focus on ten key areas. For each of those focus areas, essential process safety competency expectations have been defined and include items such as:

- Understanding the process and the hazards associated with deviating from an operating procedure
- Knowing the appropriate considerations when approving Management of Change

Team members in key Operations and Maintenance positions are required to continually demonstrate their knowledge of process safety hazards, scenarios and safeguards, and their role in preventing and mitigating process safety events. Verification of this knowledge is periodically reinforced through training, drills, interviews, and demonstrations. This approach is referred to as "Process Safety Knowledge Verification" (PSKV) and includes several components. Utilizing PSKV ensures team members understand high consequence process safety scenarios for their specific areas of responsibilities and how their specific actions act as a safeguard to prevent or mitigate the process safety scenario.

Human Performance Konzept bei EMPG

J. L. Beyer

ExxonMobil Production Deutschland GmbH, SSHE, Hannover, Germany

ExxonMobil's Ziel ist eine stetige Verbesserung der Arbeitssicherheit. Während in der Vergangenheit die sichere Gestaltung von Anlagen und die Einführung eines Sicherheitsmanagementsystems einen guten Fortschritt in der Verringerung von Arbeitsunfällen bewirkt haben, stand in den letzten Jahren insbesondere der verhaltensbasierte Ansatz im Mittelpunkt.

Ein konsequenter Schritt der weiteren Entwicklung stellt das Human Performance (HP) Konzept dar.

Bei Human Performance geht es darum zu verstehen, wie Menschen mit Anlagen, Prozessen und untereinander interagieren – als Teil eines Systems – um Risiken zu identifizieren, zu minimieren und so sicher zu arbeiten.

HP ist eine risikobasierte Betrachtungsweise, die berücksichtigt, dass Fehler Teil des menschlichen Verhaltens sind und dass Organisations-, Aufgaben- und individuelle Faktoren die Handlungen eines Individuums oder einer Gruppe stark beeinflussen.

Oder kurz gesagt – „Menschen machen Fehler“ und dies muss im Arbeitsumfeld berücksichtigt werden. Selbstredend, aber doch ein Paradigmenwechsel in unserem Denken, wenn von dem Standpunkt „Menschen sind das Problem“ zu dem Punkt „Menschen sind die Lösung“ übergegangen wird.

Menschliche Fehler werden bei HP daher als Symptome oder Auslöser gesehen, die tiefer in einem System liegen. HP ist das Ergebnis unseres Verständnisses menschlicher Fähigkeiten und auch deren Grenzen. Es ist die Berücksichtigung dieses Verständnisses auf die Interaktionen zwischen Menschen, Geräten und Prozessen und führt zum Aufbau fehlertoleranter Systeme, die die Abhängigkeit von Menschen als „letztem Sicherheitsfilter“ verringern und die HP Prinzipien nutzen, um die Wahrscheinlichkeit und die Auswirkungen von Fehlern dort zu reduzieren, wo es am wichtigsten ist.

Dabei keine neuen Werkzeuge zu erfinden, sondern die vorhandenen Sicherheitssysteme zu nutzen und diese an der richtigen Stelle in den Arbeitablauf zu integrieren, ist eine Aufgabe für das gesamte Team. Vom Leadership zu den einzelnen Teams, von der Projektplanung, von Aufsichtspersonen zu den Fachkräften vor Ort, vom Safety Team.

Der Vortrag erläutert die HP Prinzipien, die Integration des Konzepts sowie die Herausforderungen auf dem weiteren Weg zu „Nobody Gets Hurt“.

Gas mixing behavior and flow processes in porous media during the conversion of natural gas storage facilities to hydrogen storage

R. Toufighi, N. Moeininia, H. Bültemeier

DBI-Gruppe, Gas Production / Gas Storage Department

Abstract

Hydrogen, as a promising alternative to fossil fuels, requires new research in various aspects of the gas infrastructure. Long-term storage in underground gas storage (UGS) facilities has significantly attracted research interest, as this is considered a major asset to system stability and security of supply. For porous UGS facilities, the complexity of the gas mixing, flow processes, and the interactions between hydrogen, cushion gas, and reservoir water are currently insufficiently known and must be explicitly investigated. The present work intends to provide a preliminary sensitivity analysis and detailed assessment of involved mechanisms by reservoir simulation. The developed insights can serve as a basis for future research on the topic and operation planning.

Two generic reservoir models (2D and 3D homogenous) are generated according to the average reservoir properties of German UGS facilities. By employing compositional numerical simulation (CMG-GEM), the main mechanisms including physical dispersion, solubility, and hysteresis in underground hydrogen storage (UHS) are successfully modeled. Additionally, a comprehensive sensitivity analysis is conducted aiming to elaborate on the parameters influencing the gas mixing process.

The hydrogen-cushion gas mixing zone and hydrogen production efficiency are monitored in the defined experiments. In general, strong gravity segregation results from the high-density contrast between the hydrogen and the cushion gas. The gas mixing zone extent and gravity overriding are varied in the carried-out sensitivity analysis due to their dependency on porosity, permeability, and slope of structure. Lower porosity and permeability experiments in combination with the physical dispersion effect can elevate hydrogen recovery efficiency and gas mixing compared to high porosity and permeability experiment (3D conceptual models). Furthermore, mechanical dispersion plays a substantial role in gas mixing behavior at high flow rates. The share of molecular diffusion in overall hydrodynamic dispersion and gas mixing increases considerably at low flow rates or shut-in periods. In the deeper reservoir with solubility effect, the variation of physical properties and solubility can lead to higher gas mixing while slightly changing hydrogen recovery efficiency. The factor of injection rate in the 3D experiment with a single well, which located in the crest of the reservoir, contributes insignificantly to the mixing behavior.

Numerical dispersion is a truncation error contributing vastly to simulating miscible displacement. Two methods are investigated to minimize this calculation error by discretizing grid cells and time-step size and also implementing the second-order upstream weighting scheme calculation method. The second method can efficiently minimize numerical dispersion to an acceptable level. Moreover, the great importance of using this method is time and cost-effective simulation runs in field-scale models. Including the TVD flux limiter can enable more realistic concentration calculation at cell borders. Accordingly, it can prevent the overestimation of mechanical dispersion.

Introduction

Hydrogen is a key contributor to energy transition and net-zero emissions by 2050. The number of innovative hydrogen technologies has recently increased to facilitate and support the energy transition. Hydrogen can potentially lead the smooth energy transition to clean, affordable, and secure energy in the future. Due to the seasonal fluctuation of renewable energy, there is a necessity to store hydrogen to fill seasonal gaps between hydrogen production and demand. The subsurface porous medium could be a storage option for a large amount of energy over long storage cycles. Thus, it can substantially mitigate shortages in energy supply. The vast existing reservoir volumes as suitable candidates in Germany could be utilized for storing green hydrogen. Depleted gas reservoirs and natural gas storages are advantageous due to the availability of remaining gas in the reservoirs which is considered cushion gas. Cushion gas can play an important role in preserving reservoir pressure and preventing further hydrogen trapping. Nonetheless, serious challenges can be encountered when converting underground natural gas storage to hydrogen storage. The mixing between hydrogen and cushion gas is inevitable during the injection of hydrogen and displacement processes, and this miscible displacement leads to less hydrogen purity in production streams which requires subsequent adjustment in gas treatment. Flow process and front breakthrough can be also challenging to determine an appropriate operation schedule.

The integration of UHS with UGS facilities appears to be conceptually feasible (Tarkowski 2019). Compared to natural gas or methane, different hydrogen properties such as density, viscosity, and reactivity can cause unanticipated behavior (Feldmann et al. 2016). By injecting hydrogen as working gas into the porous medium, the interactions between cushion gas, hydrogen, and formation water are inevitable. Thus, this conversion necessitates extensive research to fill knowledge gaps. This work aims to provide a preliminary insight and technical outlook into simulation challenges and required precautions for UGS conversion. The mineralogical-chemical reactions are excluded from this study.

Hydrogen properties in the context of underground storage

Hydrogen properties change in various states depending on pressure and temperature (Tarkowski 2019). The knowledge of the physicochemical properties of hydrogen can help in achieving a successful storage operation and further adaptation at storage sites if required (Table 1).

Table 1: Comparison of physicochemical properties of hydrogen and methane (Tarkowski 2019)

| Properties | Hydrogen | Methane |
|--|-----------|---------|
| Molecular mass (g/mol) | 2.016 | 16.043 |
| Density at NTP (kg/m³) | 0.08375 | 0.6682 |
| Dynamic viscosity at 20 °C (Pa·s) | 0.88 | 1.1 |
| Gas constant (J/kg K) | 4142.2 | 518.28 |
| Specific gravity (air = 1) (-) | 0.07 | 0.55 |
| Critical temperature (°C) | -239.96 | -82.59 |
| Critical pressure (bar) | 13.13 | 45.99 |
| Critical density (kg/m³) | 31.43 | 162.7 |
| Solubility in water (g/100g) | 0.00016 | 0.0023 |
| Net heating value (MJ/kg) | 120-141.7 | 50-55.5 |

Simulation Approach

The used compositional reservoir simulator, CMG-GEM, couples the advection-dispersion transport equation and physical dispersion into reservoir simulation models. Compositional models associated with the Equation of State (EOS) are used for predicting reservoir performance. PVT model describes the fluid phase behavior by handling fluids with different compositions in reservoir simulation, which is implemented in the Winprop module of CMG. Further tuning phase behavior model must be carried out based on real measurements which are lacking in this work.

Simultaneously, GEM allows the monitoring of macro-scale mixing phenomena. The efficient displacement can be potentially complicated by viscous fingering and gravitational segregation due to large density and viscosity differences in the multi-phase flow system. CMG-GEM is useful to numerically simulate the front displacement of hydrogen-cushion gas and assist to understand better the impact of various factors on the front stability.

In this assessment, two established conceptual models are initially filled with trapped natural gas or methane and connate water in rock pores. Therefore, the development of a miscible gas zone is foreseeable in a single gas-gas phase flow system. Differences in physical properties over displacement can make a gas-gas interface balance out over time. Advective-dispersive processes are determined as the main contributors to the rate of growing mixing zone and extent of front propagation as described in the following equation:

$$\emptyset \frac{\partial C}{\partial t} + \nabla C \cdot u - \nabla (D_h \nabla C) \emptyset = 0$$

where,

\emptyset = Porosity

$\nabla C \cdot u$ = Description of the advective process

$\nabla (D_h \nabla C) \emptyset$ = Description of the dispersive-diffuse process

D_h = Physical dispersion or hydrodynamic dispersion

– Hydrodynamic Dispersion

The substantial role of hydrodynamic dispersion as a scale-dependent process is prominent in the mixing process. Two key parameters that characterize fluid and solute transport in porous media are flow velocities and hydrodynamic dispersion coefficients. The velocity variation is caused by three factors: microscopic heterogeneity, variation in pore sizes, and variation in path length. The hydrodynamic dispersion (Physical dispersion) equation is defined by the sum of mechanical dispersion (D_m) and effective molecular diffusion (D_e) as follows:

$$D_h = D_m + D_e = \alpha * u + D_0 \emptyset^m$$

The dispersivity (α) in porous media is described as a function of heterogeneity and tortuosity (m). u term implies the velocity of the fluid (m/s). Effective molecular diffusion contains diffusion coefficient (D_0) (m^2/s), porosity (\emptyset), and cement factor (exponent m in (\emptyset^m)).

Mechanical dispersion in porous media refers to flow velocity and dispersivity as below equation (Scheidegger 1957):

$$\tilde{D}_{disp,L} = a_L * \|v\| \quad \& \quad \tilde{D}_{disp,T} = a_T * \|v\|$$

where,

| | |
|------------------------|---|
| $a_L =$ | Longitudinal dispersivity, local variation of velocity in a porous medium (m) |
| $a_T =$ | Transverse dispersivity, local variation of velocity in a porous medium (m) |
| $\ \nu\ =$ | Fluid velocity (m/s) |
| $\tilde{D}_{disp,L} =$ | Longitudinal mechanical dispersion (m^2/s) |
| $\tilde{D}_{disp,T} =$ | Transverse mechanical dispersion (m^2/s) |

The dispersion coefficient in the longitudinal direction (1 to 100 m) is superior to the dispersion coefficient in the transverse direction (one or two orders of magnitude less) (Tek 1989). Transverse dispersion is not accounted for further investigation.

Molecular diffusion described by Fick's first law is driven by concentration gradient. Diffusion in a porous medium differs from aqueous solution and occurs through tortuous and irregularly shaped pores. In this work, Fuller's method is used to calculate the diffusion coefficient between hydrogen gas and methane gas (Poling et al. 2001) as described below:

$$D_{AB} = \frac{0.00143 T^{1.75}}{PM_{AB}^{(1/2)} \left[(\sum v)_A^{1/3} + (\sum v)_B^{1/3} \right]^2} \quad \& \quad M_{AB} = 2 \left[\left(\frac{1}{M_A} \right) + \left(\frac{1}{M_B} \right) \right]^{-1}$$

where,

| | |
|--------------|---|
| $D_{AB} =$ | Diffusion coefficient between gas A and B (cm^2/s) |
| $T =$ | Temperature ($^{\circ}K$) |
| $P =$ | Pressure (bar) |
| $M_A, M_B =$ | Molecular weights of A and B (g/mol) |
| $\sum v =$ | Sum of the atomic diffusion volumes of the individual molecules |

The presented approach is advantageous to predict binary gas phase diffusivities and has relative reliability compared to other correlations. However, the presence of the solid media (grains) is neglected in this method. The diffusion coefficient and effective diffusion coefficient are interrelated with the term ϕ^m according to the hydrodynamic dispersion equation. The dimensionless factor m is caused by the pore networks in the combination of various lithologies. This factor is varied between 1.3 and 5 (Dr. Li Li 2020). Thus, the coupling of the diffusion coefficient between gases with porosity and cement factor can prevent the overestimation of effective molecular diffusion. (Hagemann 2017) reported the molecular diffusion coefficient of hydrogen gas in the order of $10E-06 m^2/s$. At static conditions or very low injection rates, the magnitude of dispersion can vary due to the solute dependence of diffusion. In contrast, the contribution of mechanical dispersion is significant due to its velocity dependency. Thus, the growth rate of the mixing zone and front propagation is dependent on advective and diffusive forces during operation cycles (Terstappen 2021).

GEM can solve also the following material balance equation for component i and phase m (Shiralkar and Stephenson 1991):

$$\frac{\partial}{\partial t} (\varphi \sum_{m=1}^{n_p} \rho_m S_m C_{im}) = \sum_{m=1}^{n_p} \nabla \cdot k \rho_m \lambda_m C_{im} (\nabla p_m - \rho_m g \nabla d) + \sum_{m=1}^{n_p} \nabla \cdot \alpha_m |\vec{v}_m| \rho_m \nabla C_{im}$$

– Numerical Dispersion

Modeling coupled processes of multiphase fluid flow and tracer transport in realistic large-scale reservoir models remains a mathematical challenge. One of the main concerns in solving advection-dispersion governing equations for handling tracer transport is numerical dispersion when dealing with irregular or multidimensional coarse grids. Thus, another dominant factor influencing the development of the mixing front is numerical dispersion which demands further analysis. Generally, the simulator solves the advection-dispersion equation and assigns the concentration of each fluid to the center of the grid blocks. Indeed, numerical dispersion as truncation error occurs during concentration calculation by using various weighting schemes and assigning concentration at the cell borders conforming with grid block centers. The importance of discretization is to minimize this calculation error to an acceptable level. Therefore, the size of grid blocks and time steps are primarily reduced to monitor the gas mixing behavior in this work.

The second method of reducing the effects of numerical dispersion is to use upstream higher-order weighting schemes for numerical dispersion control (Shrivastava et al. 2005). In the upstream weighting scheme, extra grid points of neighboring cells are incorporated into the calculation that enables more reliable concentration estimation at the cell boundary with a less smearing front (Terstappen 2021).

GEM simulator allows controlling numerical simulation by employing a total variation diminishing (TVD) flux limiter scheme. The TVD flow restrictor prevents the generation of excessive oscillations. This methodology is subsequently compared with spatial and temporal discretization to ensure the accuracy of simulation results and a proxy to the physical dispersion.

– Solubility

Hydrogen solubility is recognized as one source of hydrogen loss during UHS and is generally a slower process compared to hysteresis in the reservoir. At the gas-water interface, a certain amount of gas can dissolve in the aqueous phase until the system reaches equilibrium. In GEM, the solubility model is based on the equality of the two phases' fugacities at equilibrium using Henry's law:

$$f = x * H$$

According to Henry's law, the concentration of gas in the aqueous phase is proportional to its partial pressure in the gas phase above the liquid at a constant temperature. In this work, the (Li and Nghiem 1986) method is used to model the solubility of hydrogen in the aqueous phase. This method assumes a small temperature gradient within the reservoir (aquifer) and also a small temperature difference between injected H_2 and the reservoir fluid. Henry's constant is calculated as a function of pressure by the following equation:

$$\ln H_i = \ln H_i^* + \frac{\bar{v}_i}{RT} (p - p^*)$$

where,

- | | |
|---------------|---|
| $H_i =$ | Henry's constant at varied p and T |
| $H_i^* =$ | Henry's constant at reference p^* and T |
| $\bar{v}_i =$ | Partial molar volume of i in brine |

Solubility is mainly defined as a function of pressure, temperature, and salinity of water formation. Higher temperatures and salinity can reduce gas solubility in the aqueous phase while increasing pressure can boost adversely gas solubility. The effect of salinity on hydrogen solubility in GEM is calculated by (Cramer 1982):

$$\log_{10} \left(\frac{H_{salt,i}}{H_i} \right) = k_{salt,i} m_{salt}$$

where:

| | |
|----------------|--|
| $H_{salt,i}$ = | Henry's constant of component i in brine |
| H_i = | Henry's constant of component i in freshwater |
| $k_{salt,i}$ = | Salting-out coefficient for component i |
| m_{salt} = | Molality of dissolved salt (mol/kg H ₂ O) |

– Fluid density

The density of hydrogen increases significantly with pressure and relatively with temperature. In contrast to methane density, hydrogen density is less responsive to temperature and pressure impacts (Figure 1). This density difference can lead to the gravity segregation effect during UHS operation, resulting in gravity override or hydrogen upward movement to the upper reservoir layer or beneath the caprock. The following plots show the isothermal density behavior of methane and hydrogen calculated based on Peng-Robinson EOS. The large density ratio between two gases at higher pressure can accommodate a larger potential for gravitational segregation.

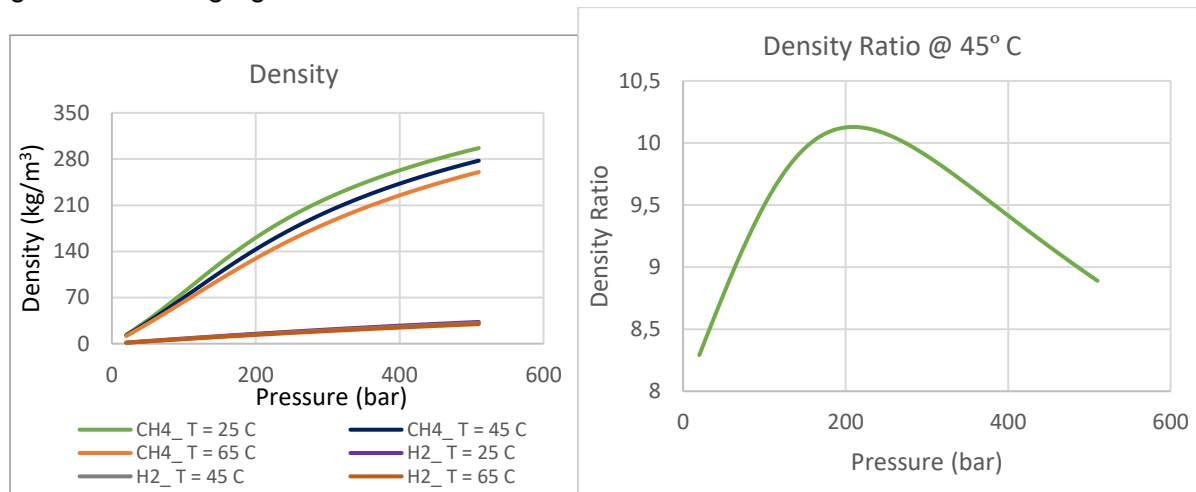


Figure 1: H₂ and CH₄ isothermal densities (left) and CH₄/H₂ density ratio at 45°C (right)

– Fluid Viscosity

Fluid viscosity is defined as one of the main criteria in the concept of displacement efficiency substantially affecting the mobility ratio. The mobility ratio is an indicator of flow stability in a displacement process that is highly dependent on the effective phase permeability and phase viscosity. In practical terms, a high mobility ratio (higher than one) potentially leads to viscous fingering recognized as an unstable front. Thus, an unfavorable mobility ratio can adversely affect the areal sweep efficiency and create conformance problems. Hydrogen viscosity is affected by temperature and pressure. However, viscosity change is not significant compared to CH₄ as shown in Figure 2. The viscosity model calculation is carried out according to Jossi-Stiel-Thodos Correlation. In this equation, the term $\mu_{low,i}$ is computed from the (Yoonm and Thodos 1970) correlation.

$$\mu (mix) = \frac{\sum_{i=1}^{nc} \mu (low, i) x(i) \sqrt{M(i)}}{\sum_{i=1}^{nc} (i) \sqrt{M(i)}}$$

where:

$\mu (mix)$ = Viscosity for hydrocarbon mixture (applicable for low pressures)

$\mu (low, i)$ = Viscosity for component i (applicable for low pressures)

$M(i)$ = Molar mass of component i

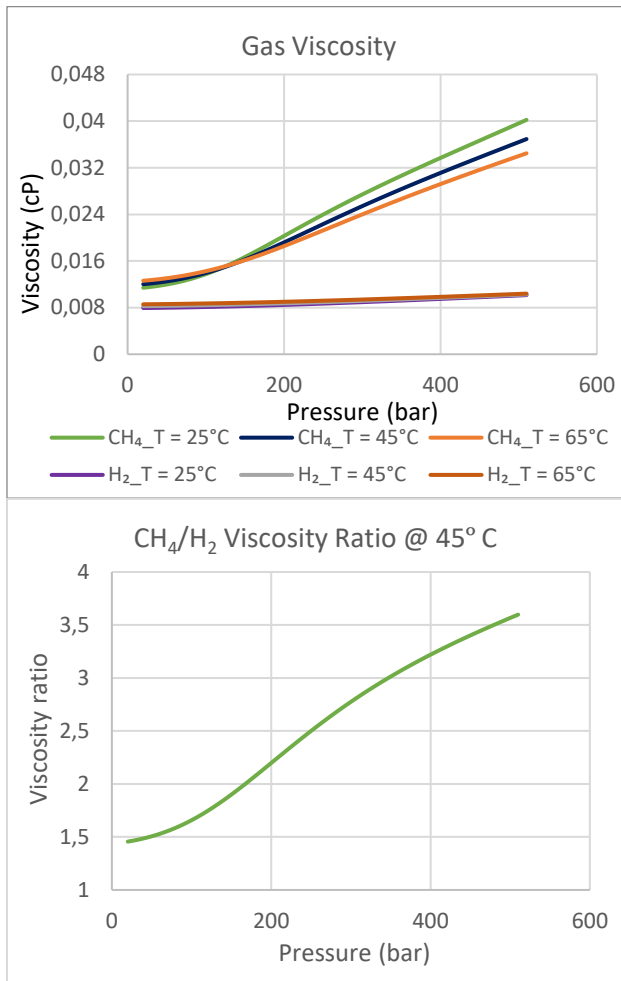


Figure 2: H₂ and CH₄ isothermal viscosities (left) and CH₄/H₂ viscosity ratio at 45°C (right)

– Hysteresis

In addition to the physical dispersion process, it is essential to incorporate hysteresis on the non-wetting phase behavior into reservoir simulation to obtain accurate reservoir performance predictions. Hysteresis phenomenon influences the ultimate fluid distribution and production performance during multi-cycle of gas injection-withdrawal. Hysteresis refers to the dependence of relative permeability and capillary pressure on saturation path and history (Spiteri and Juanes 2005). In the pore-scale process, two sources are key to hysteresis: contact angle and trapping of the nonwetting phase (gas). The majority of relative permeability models are generally based on the trapping model proposed by Land (1968). In this empirical trapping model, the trapped non-wetting phase saturation is formulated as below:

$$S_{grh} = \frac{S_{gh} - S_{gcrit}}{1 + C (S_{gh} - S_{gcrit})}$$

where,

- S_{gcrit} = Critical gas saturation
- S_{gh} = Gas saturation at the flow reversal
- C = Land coefficient

The Land trapping parameter (Figure 3) depending on the type of rock and fluid is computed from the bounding drainage and imbibition curves as follows:

$$C = \frac{1}{S_{gt,max} - S_{gc}} - \frac{1}{S_{g,max} - S_{gc}}$$

where $S_{g,max}$ refers to the maximum gas saturation and $S_{gt,max}$ refers to the maximum trapped gas saturation associated with the imbibition curve or bounding water-flood curve (Spiteri and Juanes 2005).

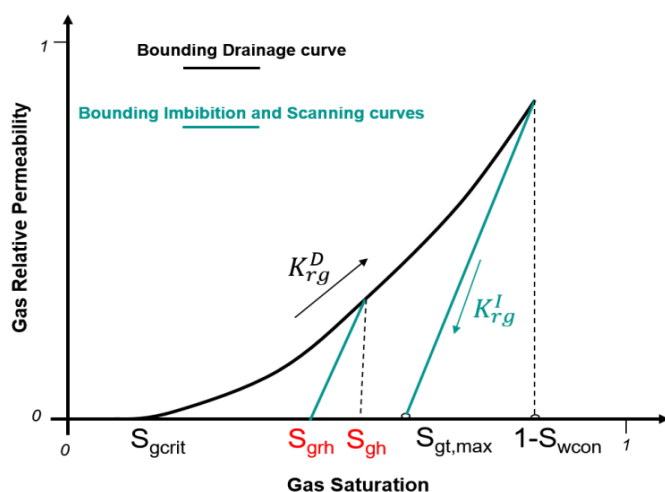


Figure 3: Gas relative permeability hysteresis effect based on Land's trapping model

GEM can consider the hysteresis effect by including the maximum trapped gas saturation and accordingly, calculating the trapped gas saturation by using Land's Model.

Simulation of a 2D homogeneous conceptual model

When injecting hydrogen into a reservoir formation filled with natural gas, the smearing out of the miscible front could be foreseeable due to diffusive or dispersive flow. Additionally, the heterogeneity of the reservoir, mobility ratio, and density differences could play roles in the overall process (Hagemann 2017). Thus, the goal of this study is to evaluate the impact of influencing parameters in gas mixing behavior and flow process. To quantify the extent of the mixing zone, the below description is applied:

$$\text{Mixing Degree} = \frac{\text{Number of Grid cells of Mixing Area between 10--90 percent}}{\text{Number of Grid cells in entire Reservoir}}$$

The 2D base case is established with homogeneous distributions of reservoir properties taken from existing UGS and gas reservoirs in Germany. A couple of potential influencing criteria are considered for this investigation. The operating scenario is set up for two years of hydrogen injection with an injection rate of 500 (m^3/day), followed by two more years of shut-in period (one cycle). This reservoir model is initialized by methane with a weak aquifer. The reservoir temperature is 45 °C. A more detailed setup of experiments is provided in Table 2:

Table 2: Experiment definition in the 2D conceptual model

| Characteristics | Base | 2D.1 | 2D.2 | 2D.3: | 2D.4 | 2D.5 | 2D.6 |
|---|---------------------------------|---|---------------------------|------------------------------|----------------------------------|--|------|
| Thickness (m) | 40 | 40 | 40 | 40 | 20, 40, 100, 200, 450 | 40 | 40 |
| Initial reservoir pressure (bar) | 131 | 131 | 131 | 50, 131, 200, 318 | 131 | 131 | 131 |
| Porosity (-) | 0.2 | 0.2 | 0.05, 0.2, 0.3 | 0.2 | 0.2 | 0.2 | 0.2 |
| Permeability K_h (md) | 740 | 37, 74, 370, 740, 1480, 3000 | 740 | 740 | 740 | 740 | 740 |
| K _v /K _h | 0.1 | 0.1 | 0.1 | 0.1 | 0.1 | 0.1 | 0.1 |
| Inclination (°) | 0 | 0 | 0 | 0 | 0 | -20, -10, -5, 0, +5, +10, +20 | 0 |
| Density Model | Peng Robinson EOS Model | | | | SRK | | |
| Viscosity Model | Jossi-Stiel- Thodos Correlation | | | | Peder- son | | |

To evaluate the gas mixture compositions over the withdrawal period, 2 years monitoring period is substituted by 2 years of production with a constant rate of 500 (m³/day). The preliminary presented results describe the mixing degree quantification with several parameter variations (Figure 4). Hydrogen saturation maps and production plots are presented for a couple of sensitivity sets. The recovered volume fraction is not violated by the production and pressure rate constraints. The spatial hydrogen distribution and mixing region extent are visualized after one and two years of hydrogen injection and at the end of production (Figure 5).

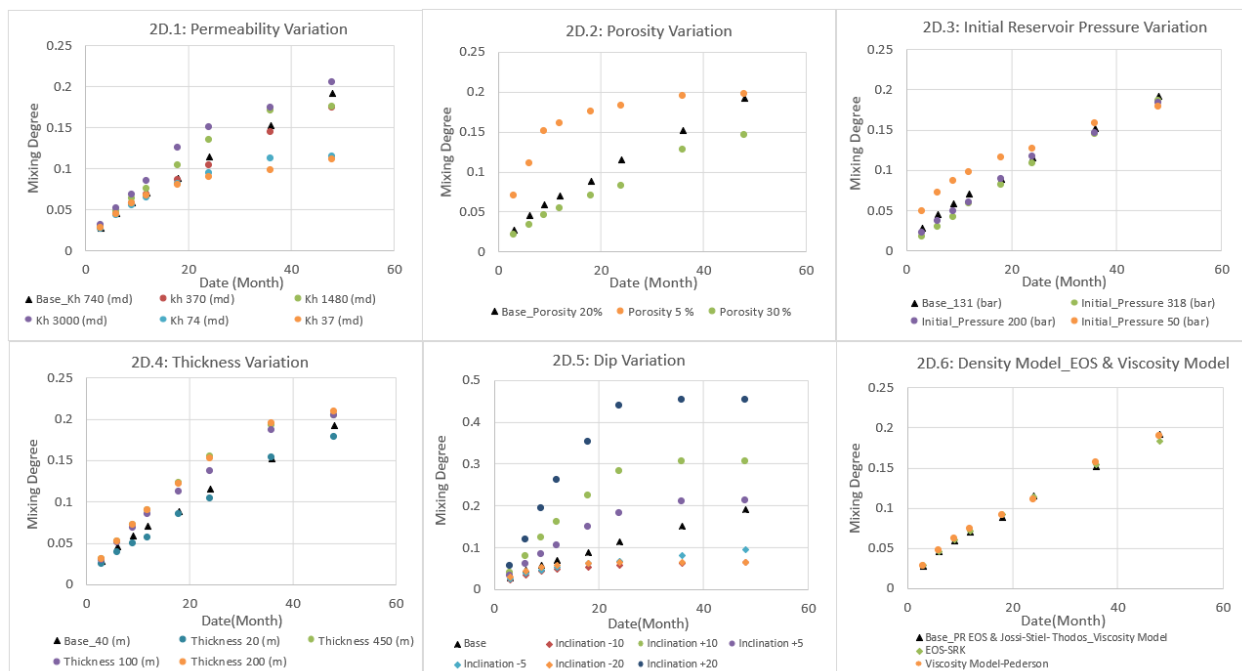


Figure 4: Influence of various geological and dynamic factors on gas mixing degree

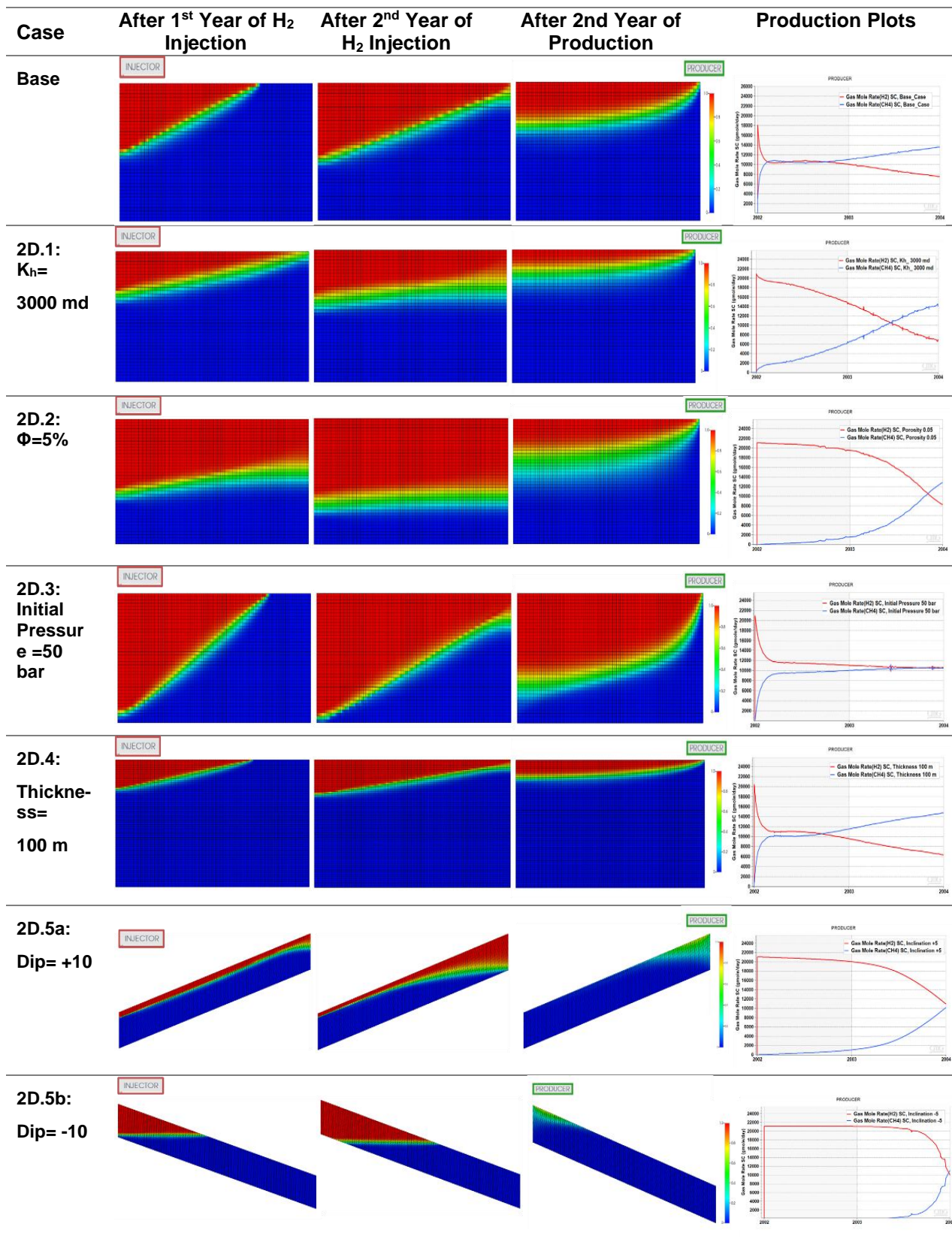


Figure 5: Cross-sectional view of hydrogen saturation in the sensitivity analysis of the 2D conceptual model

Higher horizontal permeability can lead to faster gas movement laterally (Figure 5) and higher gas mixing degrees (Figure 4). Porosity reduction can increase pore pressure and subsequently, faster front flow during the injection process leading to higher gas mixing. Hydrogen purity in both sets is significantly enhanced compared to the base case. As a result, the impact of the heterogeneity factor is significant when mixing hydrogen with methane. In both cases, strong gravity segregation is detectable.

By decreasing depth and pressure, the hydrogen front moves faster and is also distributed widely compared to the base case (Figure 5). A higher mixing extent is observed while minor changes in hydrogen purity can be distinguished from the production plot. The reservoir thickness may vary from a few to hundreds of meters. From the presented figures, it is evident that the distribution of gas can be affected by thickness change. Gravitational segregation occurs to a larger extent in higher thicknesses. Gas compositions in production streams are slightly changed.

Dip angle as another structural geological feature is investigated in this work by varying from negative to positive slope, which represents syncline and anticline, respectively. In the positive dip, the injector is located at the deepest depth of the structure (down-dip injection) and hydrogen moves rapidly from the upper layer to reach the crest. A high tendency of mixing can be observed at the top of the reservoir in experiment 2D.5a (Figure 4). In contrast, less mixing between the gases and strong gravity segregation can be distinguished in the negative slope with up-dip injection (when injecting gas at the crest of a reservoir, up-dip injection is analog to negative slope). In the experiment setup 2D.5b, no further change is observed by negatively increasing the dip angle. In this experiment, it is assumed to shift the producer to the injector location. High hydrogen recovery is predicted over the production phase in both experimental setups (Figure 5). Therefore, the dip of the structure is considered to be a critical factor in terms of the gravity segregation effect, hydrogen front flow, and gas mixing behavior in the reservoir.

Two other experiments referring to viscosity, and density models present relatively negligible impacts on the mixing degree and hydrogen recovery efficiency (Figure 4).

Moreover, gas overriding is demonstrated vividly through all experimental approaches except the high dip injection setup. Accordingly, the override of injected hydrogen can induce severe gravity segregation in the reservoir formation, thereby substantially limiting the application of pure hydrogen. The gravitational segregation effect can be intensified by heterogeneity change. It is visible that the hydrogen distribution and front flow affect dramatically in hydrogen recovery in all experimental setups (Figure 5).

Another main goal is to gain better insight into the effect of physical and numerical dispersive processes on the gas mixing zone (Table 3). The additional experiments are conducted on the base case setup. The investigation of numerical dispersion is primarily carried out by discretizing grid cells and timestep sizes, further followed by employing the high-order upstream weighting method.

Table 3: Experiment definition for evaluating numerical and dispersion in the 2D conceptual model

| Parameters | Base | New Base | 2D.7a | 2D.7b | 2D.7c | 2D.8a | 2D.8b | 2D.9 | 2D.10 |
|--------------------------------------|------|----------|--------------|--------|---------------|-------|-------|------|-------|
| Time step size (days) (DTMAX) | 30 | 30 | 1, 0.1, 0.01 | - | - | 30 | 30 | 30 | 30 |
| Grid size in l (m) | 5 | 5 | - | 2.5, 1 | - | 5 | 5 | 5 | 5 |
| Grid size in k (m) | 1 | 1 | - | - | 0.5, 0.2, 0.1 | 0.2 | 1 | 1 | 1 |

| Parameters | Base | New Base | 2D.7a | 2D.7b | 2D.7c | 2D.8a | 2D.8b | 2D.9 | 2D.10 |
|--|------|----------|-------|-------|-------|-------|-------|----------------|------------------------------------|
| TVD flux limiter | - | On | - | - | - | Off | On | On | On |
| Fully implicit method | - | On | - | - | - | - | - | On | On |
| Mechanical dispersion (m) | - | - | - | - | - | - | - | 1, 2, 5, 10 | - |
| Molecular diffusion (cm ² /s) | - | - | - | - | - | - | - | - | 2.34E-06, 5.86E-05, 2.93E-4, |

The results of all experiments conducted on physical and numerical dispersion are shown Figure 6.

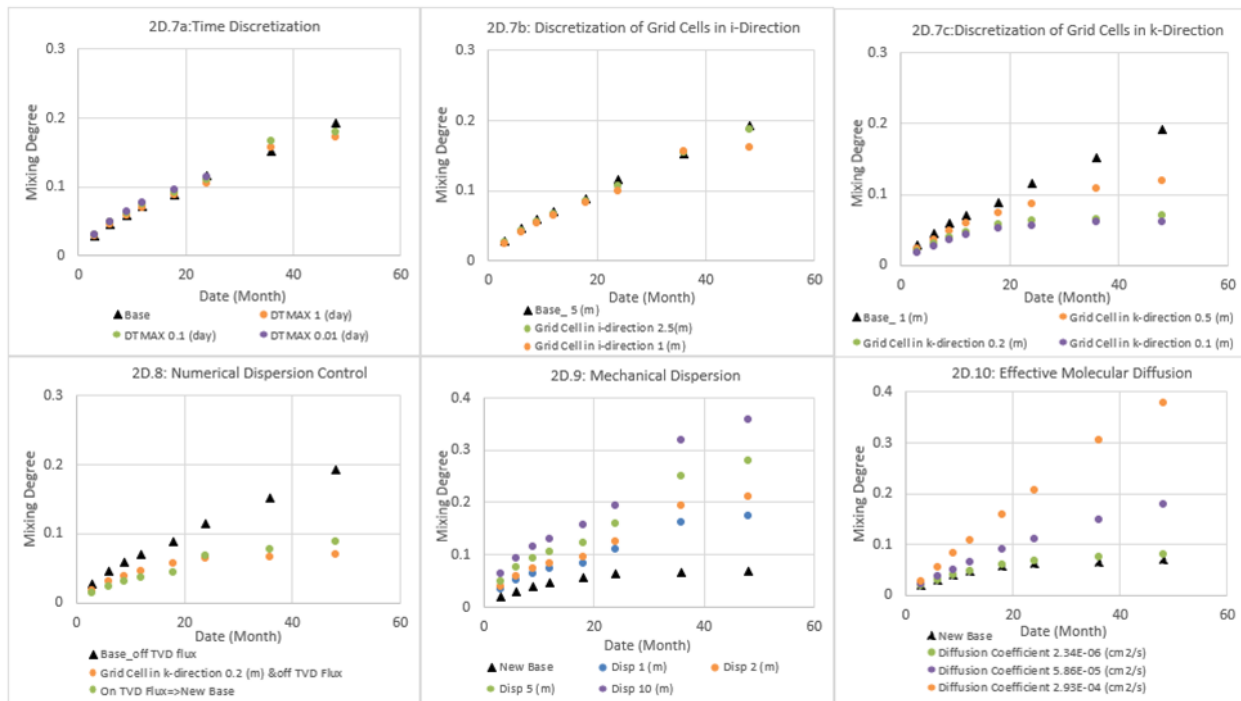


Figure 6: Effect of numerical and physical dispersion on the mixing degree in the 2D conceptual model

All presented plots in 2D.7 experiments indicate the inevitable involvement of numerical dispersion with simulation runs caused by grid cell and timestep size (Figure 6). This calculation error can influence at various extent on the mixing zone. In the first experiment 2D.7a, time-step discretization imposes long computation times with slightly insignificant changes in the degree of mixing. In the experiment, 2D.7b, grid block size reduction to 1 meter in the i-direction can boost running time while having a relatively minor impact on the mixing degree compared to the grid size reduction in the k-direction. In the 2D.7c experiment, the consequential impact on the mixing degree cannot be overlooked when decreasing cell height from 1 to 0.2 m. However, the effect of numerical dispersion on gas mixing degree is negligible by further discretization of grid cell size to 0.1 m.

In experiment 2D.8a, grid size refinement in the k-direction to 0.2 m is used for further comparison (Figure 6). On the one hand, this refining in the k-direction represents minimum numerical dispersion. On the other hand, it can increase unfavorably running time. The 2D.8b experiment setup is to activate the numerical dispersion control keyword regardless of discretizing either timestep or grid block size. Accordingly, a TVD flux limiter can eliminate the numerical dispersion and capture the trend of result in discretizing of k-direction (2D.8a) to an

acceptable level. The use of the second-order scheme calculation method is practically preferable since this activation can have great importance on time and cost-effective simulation runs in field-scale models. Consequently, the setup model with a TVD flux limiter is used for minimizing numerical dispersion when assessing physical dispersion (Figure 6).

A step-by-step approach is followed by evaluating all potential influential criteria in the gas mixing process. The next experiment runs are aligned with the incorporation of physical dispersion including mechanical dispersion and molecular diffusion (Figure 6). Numerical inconsistency is recognized as a major concern of mechanical dispersion inclusion occurring mainly in the vicinity of the injector due to the flow velocity dependency of mechanical dispersion. To mitigate material balance errors and run simulation models smoothly, a fully implicit calculation method is integrated into further simulation models.

In experiment 2D.9, no effective molecular diffusion is set in the simulation model and the impact of various dispersivity values is only examined (Figure 6). The simulated results show purely the effect of mechanical dispersion while the numerical dispersion and material balance error are eliminated. Accordingly, simulation models can capture more realistically the gas mixing and flow process. The varied parameter in experiment 2D.10 is the molecular diffusion coefficient. This coefficient is estimated based on 20 % porosity with various cementation factors referring to clean sandstone to compacted sandstone and limestone.

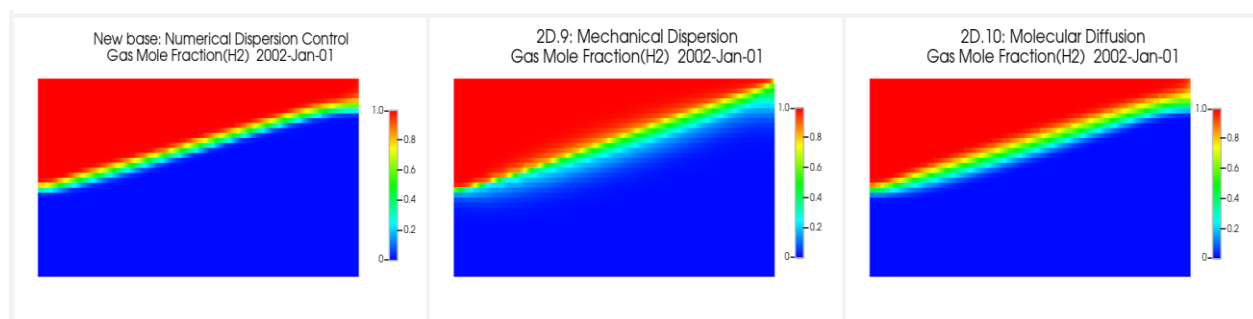


Figure 7: Cross-sectional view of hydrogen saturation in experiments 2D.8, 2D.9 and 2D.10

The width growth of the mixing zone depends dramatically on mechanical dispersion and molecular diffusion. By injecting hydrogen, the flow velocity dependency of mechanical dispersion dominantly controls the proportion of hydrogen spreading and mixing zone (Figure 7). In the assumed setup, due to the extremely low hydrogen injection rate, even coupling of molecular diffusion can affect mixing behavior.

Over the monitoring phase, hydrogen distribution and mixing zone are changed in the porous medium until reaching pressure equilibrium in the reservoir model and accordingly, molecular diffusion driven by concentration gradients is identified as the most dominant mechanism in the mixing process.

Simulation of a 3D homogeneous conceptual model

The second step is to conceptually study the functioning of the mixing process and the involved limitations related to capturing realistically gas mixing behavior in the 3D field-scale conceptual simulation model. The experiment setups are introduced with their accompanying reservoir parameters and settings in Table 4. In a 3D homogeneous conceptual model, one anticline with the average reservoir properties of the Detfurth reservoir formation is initialized with typical Russian natural gas composition. One single well located at the crest of the structure is used for consequent injection and withdrawal (Huff and Puff technique).

Table 4: Experiment definition in the 3D conceptual model

| Characteristics | Base | 3D.0 | 3D.1 | 3D.2 | 3D.3 | 3D.4 |
|---|---------------------|---------------------|---------------------|---------------------------|-----------------------|---------------------|
| Grid size (m*m*m) | 50*50*2 | 50*50*2 | 50*50*2 | 50*50*2 | 50*50*2 | 50*50*2 |
| Thickness (m) | 30 | 30 | 30 | 30 | 30 | 30 |
| Top of Reservoir (m) | 920 | 920 | 920 | 920 | 920 | 1420 |
| Porosity | 0.15 | 0.15 | 0.1, 0.25 | 0.15 | 0.15 | 0.15 |
| K_h (md) | 425 | 425 | 150, 800 | 425 | 425 | 425 |
| K_v (md) | K _h *0.1 | K _h *0.1 | K _h *0.1 | K _h *0.1 | K _h *0.1 | K _h *0.1 |
| Inclination (°) | 8 | 8 | 8 | 8 | 8 | 8 |
| GWC (m) | 1040 | 1040 | 1040 | 1040 | 1040 | 1540 |
| Temperature (°C) | 45 | 45 | 45 | 45 | 45 | 70 |
| Initial Pressure (bar) | 98 | 98 | 98 | 98 | 98 | 148 |
| Number of cycles | 5 | 5 | 5 | 5 | 1 | 1 |
| Max. BHP (bar) | 110 | 110 | 110 | 110 | 110 | 160 |
| Max. injection rate (m³/day) | 110,000 | 110,000 | 110,000 | 110,000 | 55,000-165,000 | 110,000 |
| Injection Duration (days) | 160 | 160 | 160 | 160 | 320- 106 | 160 |
| Production Duration (days) | 160 | 160 | 160 | 160 | 160 | 160 |
| Shut-in Time (days) | 45 | 45 | 45 | 45 | 45 | 45 |
| Min. BHP (bar) | 92 | 92 | 92 | 92 | 92 | 148 |
| Max. production rate (m³/day) | 110,000 | 110,000 | 110,000 | 110,000 | 110,000 | 110,000 |
| Dispersivity (m) | 1 | 1 | 5, 10 | 5, 10 | 1 | 1 |
| Molecular Diffusion (cm²/s) | 2.47E-05 | 2.47E-05 | 2.47E-05 | 2.47E-05, 1.68E-04 | 2.47E-05 | 2.47E-05 |
| Solubility | On/off | On | On | On | On | On/off |
| TVD Flux Limiter | On | On/off | On | On | On | On |

Solubility (calculation is based on Henry's law) and hysteresis effect (Land's Model) are incorporated into the simulation model to consider also potential trapping mechanisms in the base model. In addition, the second-order upstream weighting scheme is used to diminish the effect of numerical truncation errors. Besides that, the fully implicit method in GEM as a compositional simulation is activated to avoid convergence errors relating to dispersivity when simulating high gas injection rates and miscible flow processes. In this section, the results are shown in the most informative way for further comparison. The presented bar charts are indicative of mole fractions from pure hydrogen to the mixture (filtered between 0.01 to 0.99).

The prominent development of gas mixing is visible in subsequent injections (Figure 8). As a mixing between hydrogen and natural gas is inevitable, the sweeping strategy can potentially lead to various gas compositions and hydrogen purity in the production stream. Gas injection-

production plot indicates that hydrogen purity can be extensively improved over multi-cycle despite vast gas mixing over time. The unrecovered hydrogen in each cycle can prompt higher hydrogen recovery in all subsequent cycles.

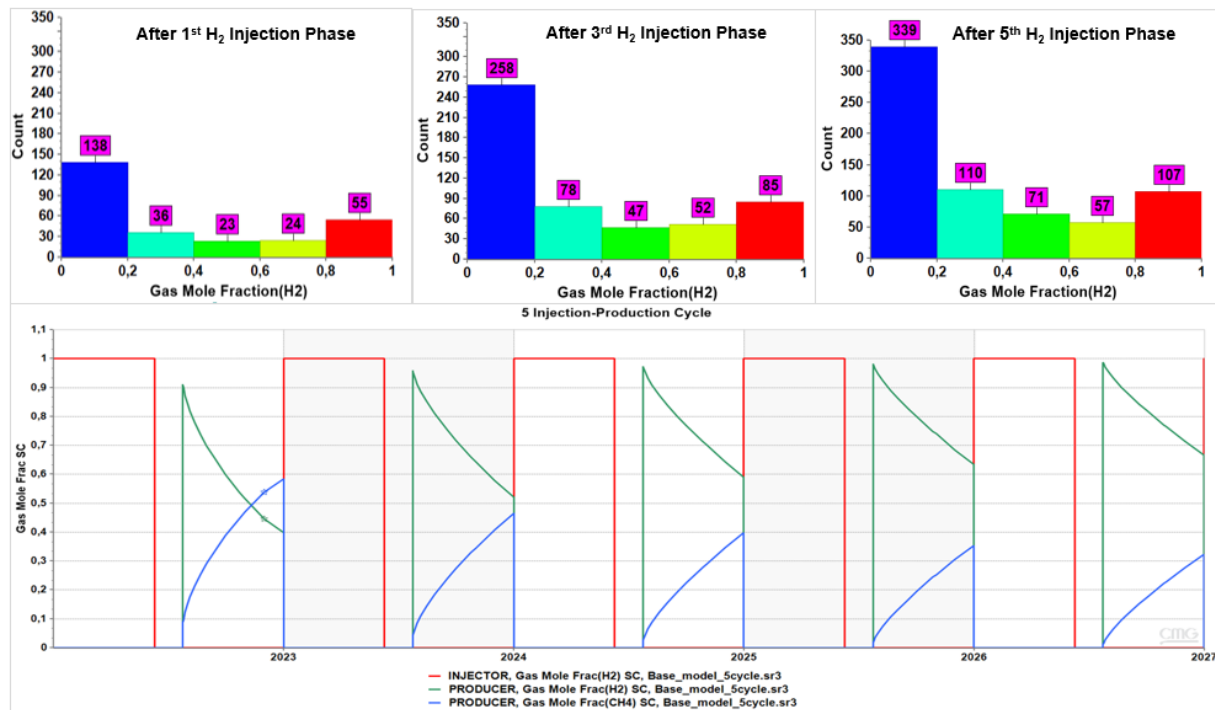


Figure 8: Hydrogen mixing bar chart at subsequent hydrogen injection cycles and injection-production cycle of the base case model with solubility in the 3D conceptual model

As we discussed earlier, the TVD Flux limiter is used for minimizing calculation errors. Since the accuracy of concentration calculation has great importance to mixing zone extent, the first attempt is to visualize the difference of base model including/excluding the TVD Flux limiter in this 3D conceptual model. Thus, the base simulation model with physical dispersion runs fully implicitly regardless of minimizing numerical dispersion. The large density differences between natural gas and hydrogen can accommodate strong gravitational segregation (Figure 9). Moreover, a large discrepancy can be observed in the mixing zone extent at the end of 1st injection phase by excluding the TVD Flux limiter. The front smear out further in the base model with numerical dispersion due to less accurate concentration calculations at the cell borders.

Hydrogen saturation is variably distributed at the end of 1st production phase (Figure 9), subsequently, the produced gas components are predicted more realistically showing higher recovery efficiency of hydrogen (Figure 10). Therefore, the involvement of numerical dispersion can overestimate mechanical dispersion leading to less accurate mixing extent and produced gas compositions.

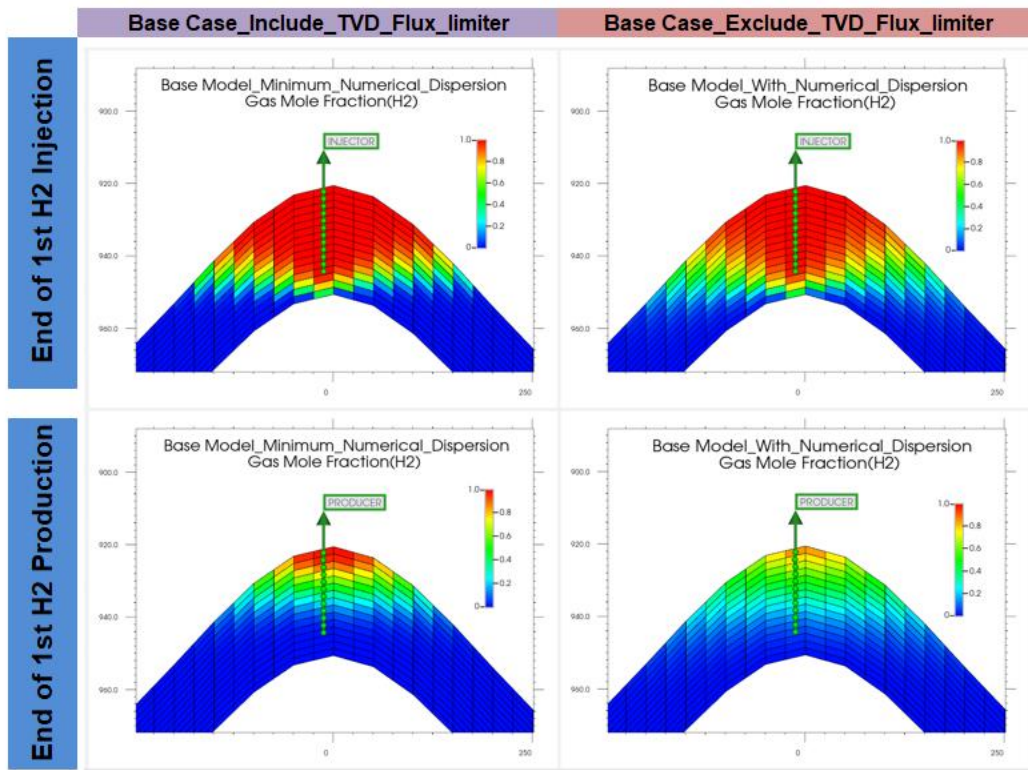


Figure 9: Cross-sectional view of hydrogen saturation after the end of injection and production in experiment 3D.0, comparing the base case model with/without TVD flux limiter

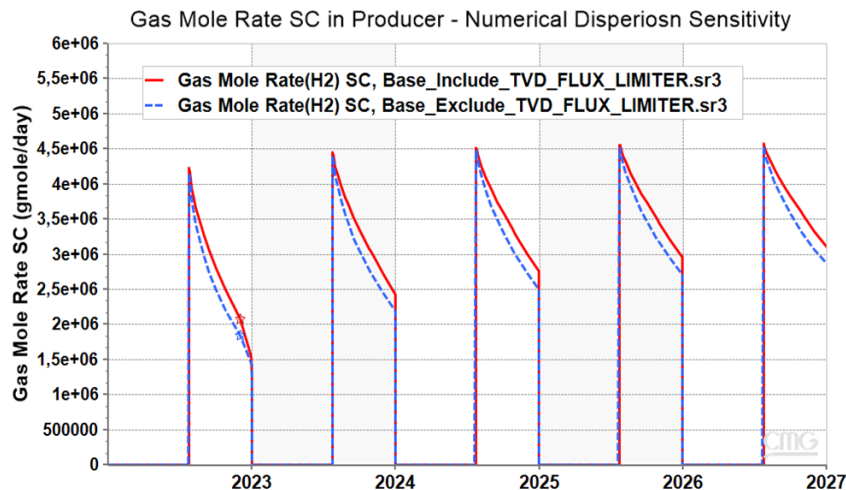
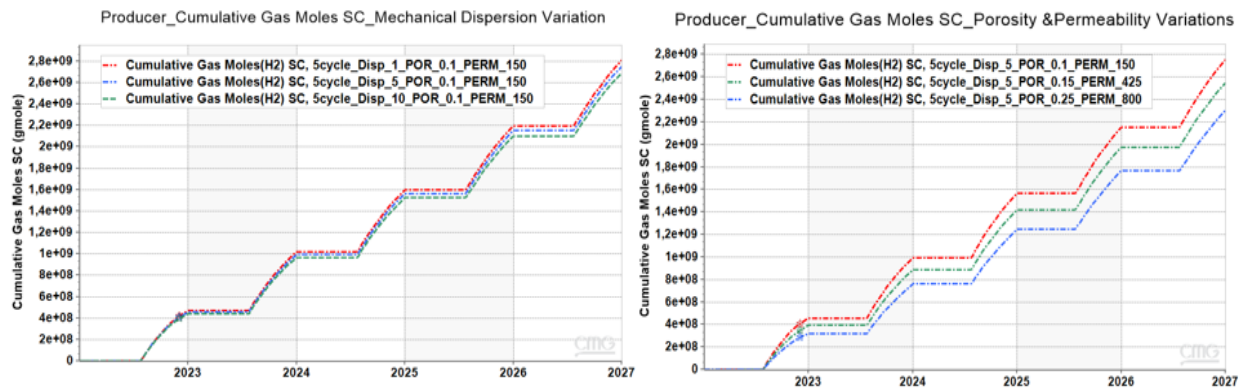


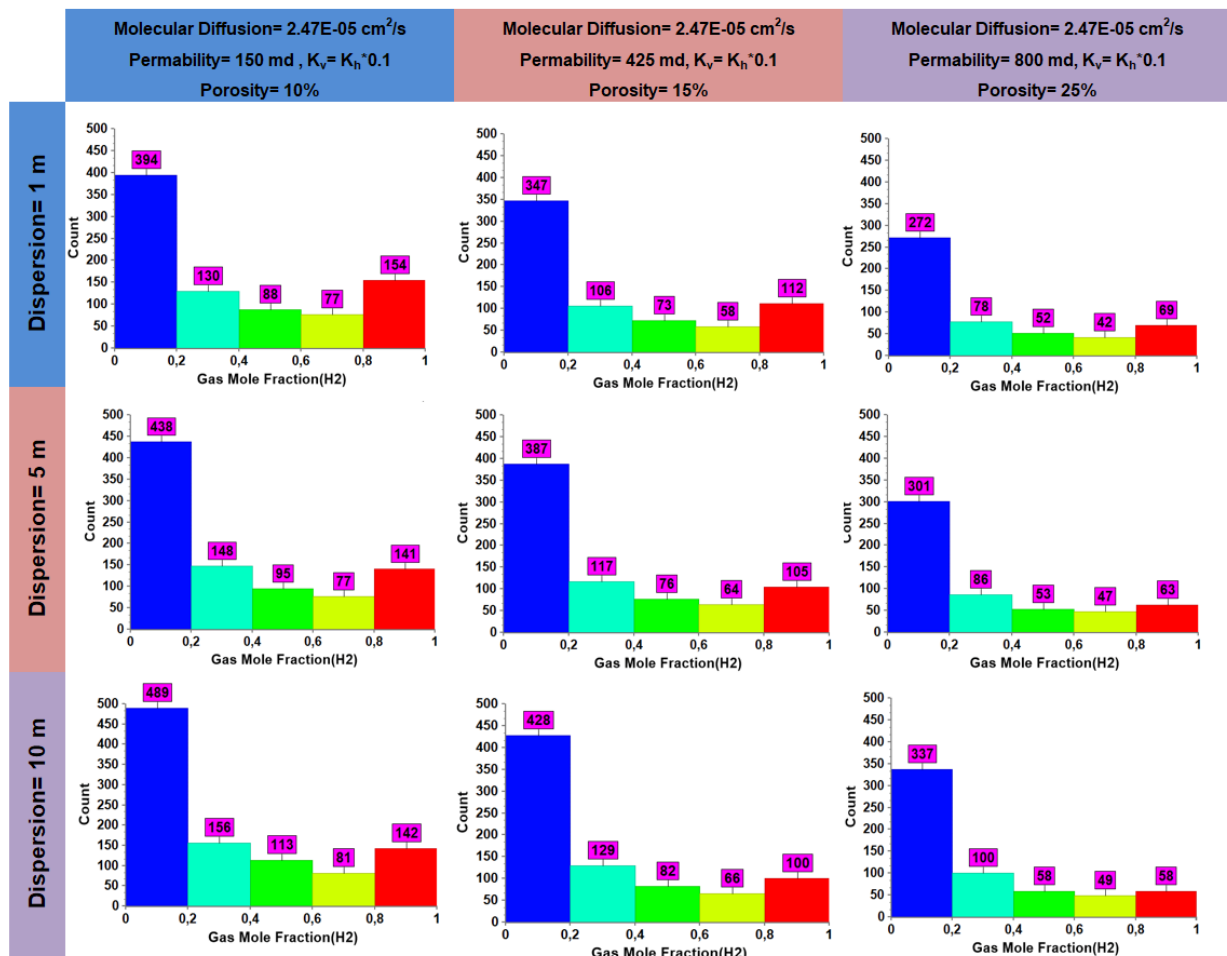
Figure 10: Hydrogen production plot in experiment 3D.0, comparing the base case model with/without TVD flux limiter

In other experiment setups, the TVD flux limiter is involved with reservoir simulation models so that the minimization of numerical dispersion can prevent the overestimation of mechanical dispersion (Figure 9).

Further research approaches are focused on combining different influencing factors that clearly manifest distinct trends in mixing behavior and hydrogen recovery.

Figure 11: Cumulative H₂ moles in producer over 5 cycles of injection-withdrawal in experiment 3D.1

In experiment 3D.1, the first observed trend in the right plot of Figure 11 shows the adverse relationship between porosity-permeability change and hydrogen volume recovery. The recovered mole fraction of hydrogen is mainly affected by heterogeneity. Opposed to heterogeneity, mechanical dispersion variation can slightly contribute to hydrogen recovery efficiency. Thus, less physical dispersion causing less mixing can desirably promote the recovered hydrogen volume in the successive injection-production cycles.

Figure 12: Hydrogen mixing bar chart at the end of the 5th hydrogen injection cycle in experiment 3D.1

The bar graphs corresponding to experiment set 3D.1 are presented at the last hydrogen injection phase (5th cycle) by varying mechanical dispersion, porosity, and permeability with constant molecular diffusion (Figure 12). Two noticeable trends can be observed. Lower porosity and permeability can elevate the mixing between hydrogen and natural gas. In addition, higher dispersivity is another substantial trigger to accelerate gas mixing.

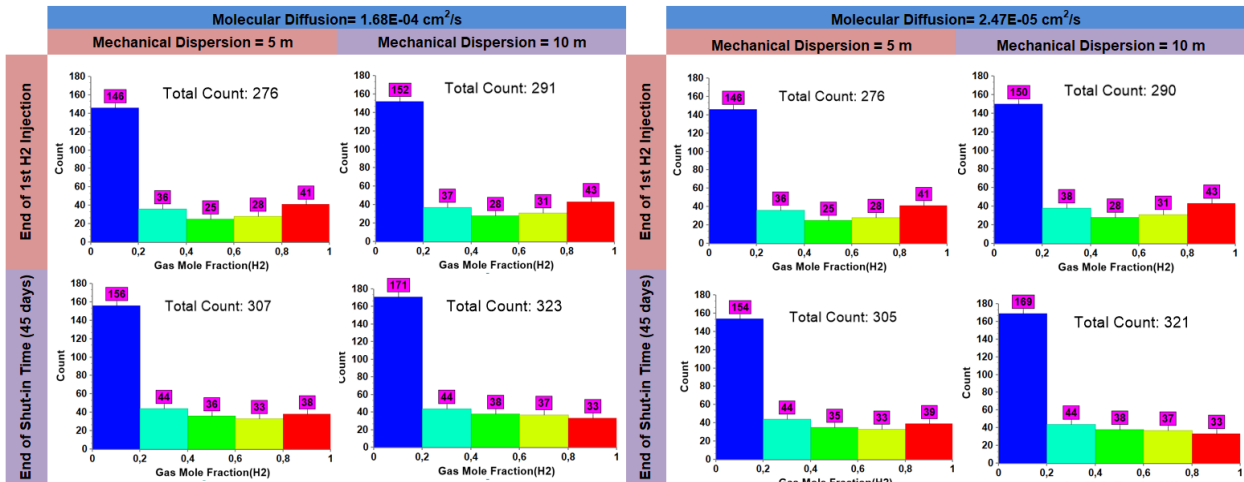


Figure 13: Hydrogen mixing bar chart at the beginning and end of the shut-in period in the 1st cycle in experiment 3D.2

During the injection phase, the mechanical dispersion phenomenon is the dominant process. Therefore, the impact of molecular diffusion on the mixing process, which is at least two orders of magnitude less than mechanical dispersion, can be mainly monitored during the shut-in time when the flow velocity is absent. The presented bar graphs illustrate an increasing number of grid blocks containing the gas mixture during the shut-in period (Figure 13). Thus, the mixing zone can be potentially enlarged during shut-in periods. Higher molecular diffusion in this experiment leads to a slight change in gas mixing.

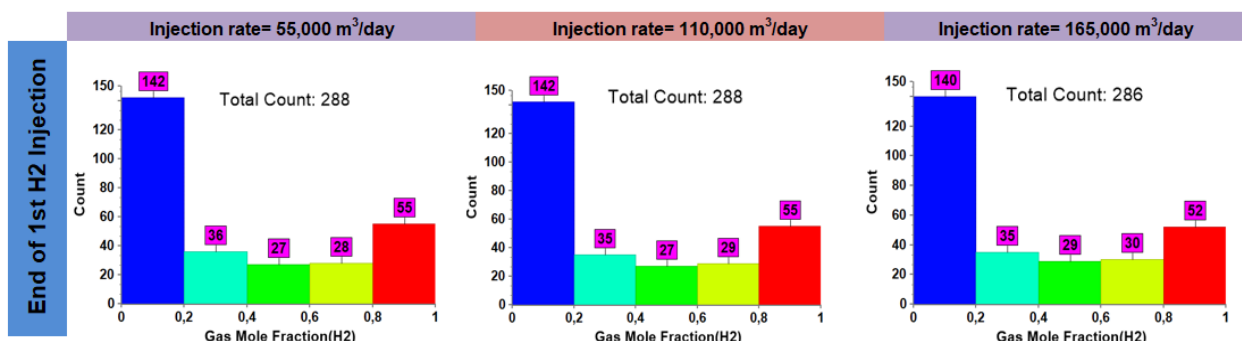
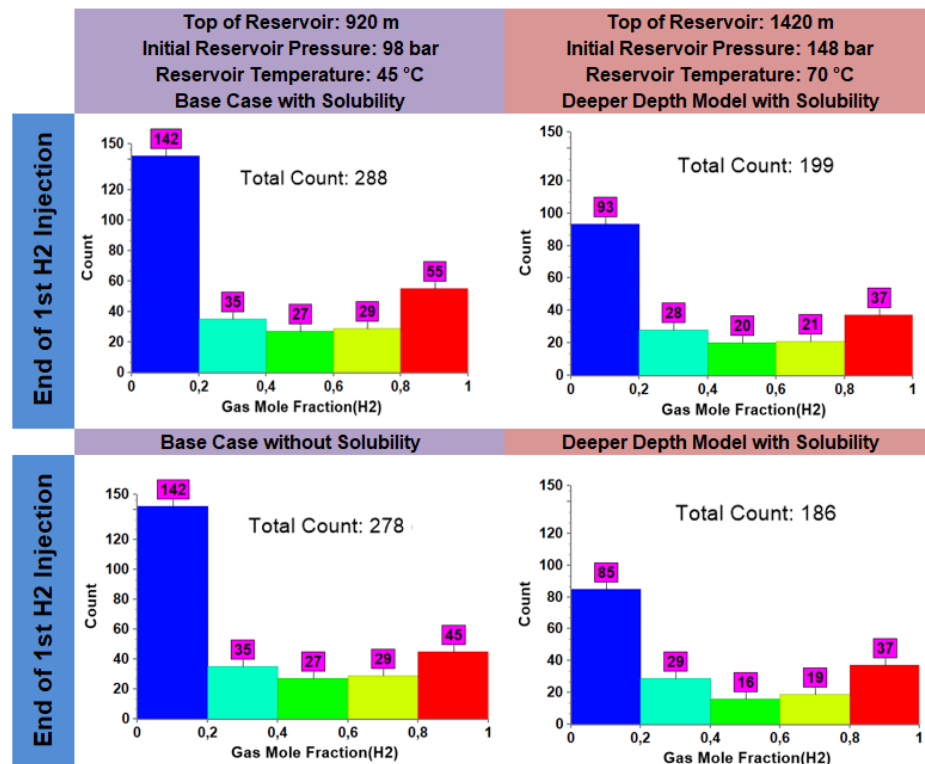


Figure 14: Hydrogen mixing bar chart at the end of 1st injection cycle in experiment 3D.3

Experiment 3D.3 investigates the extent of the impact of injection rate on gas mixing behavior. The negligible frequency of different hydrogen mole fractions is recognizable by comparing all injection scenarios that imply an insignificant change in the gas mixing zone (Figure 14).

Figure 15: Hydrogen mixing bar chart at the end of 1st injection cycle in experiment 3D.4

Experiment 3D.4 examines the initial pressure-temperature change affecting directly the density, viscosity, and solubility in the deeper depth. To compare gas mixing, the results of the higher pressure-temperature reservoir to the base case experiment with/without solubility are presented (Figure 15). In the base model with /without solubility, hydrogen recovery has relatively negligible variation despite the observed increase in gas mixing. Higher reservoir pressure with/ without solubility can reduce gas mixing while producing a higher amount of hydrogen at the later subsequent cycles (Figure 16).

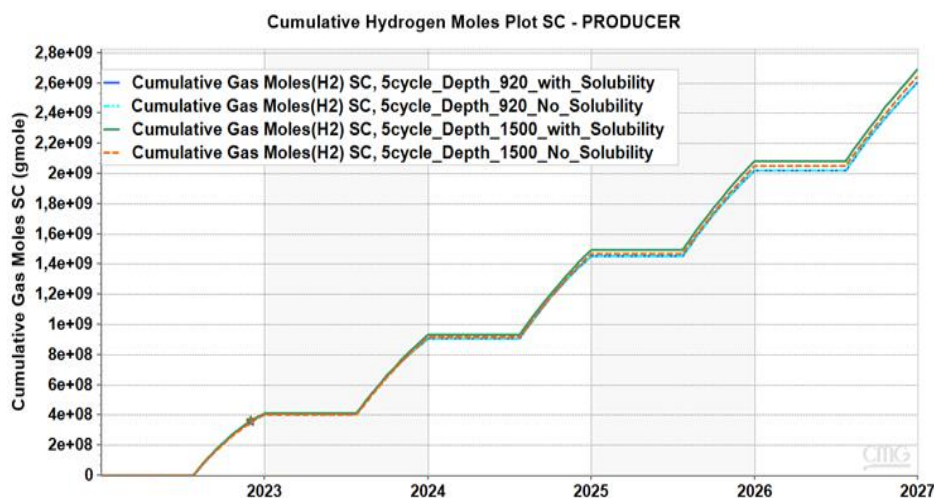


Figure 16: Hydrogen production plot over 5 cycles of injection-withdrawal in experiment 3D.4

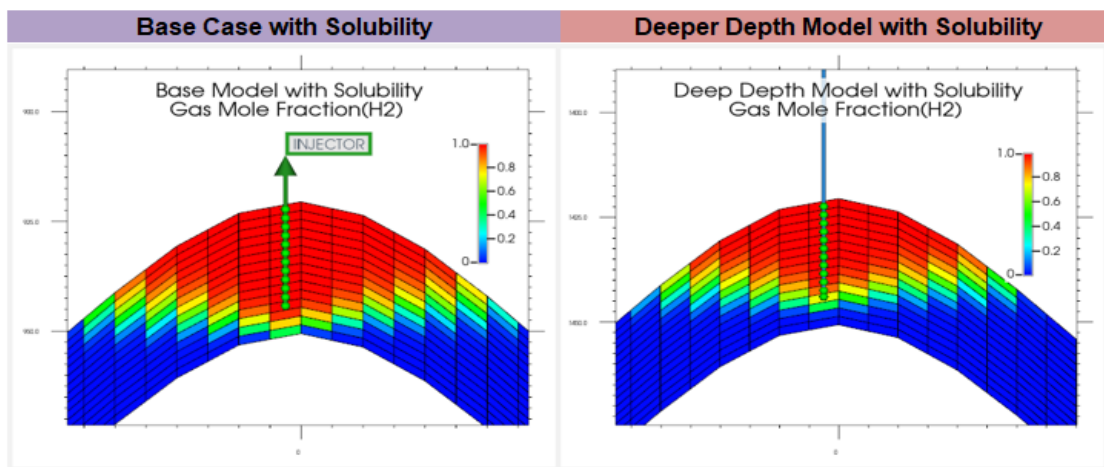


Figure 17: Cross-sectional view of hydrogen saturation after the end of injection in experiment 3D.4, comparing the base model and deeper depth model with solubility

Due to the change in physical properties of gas components in deeper depth, the gas mixing zone is influenced significantly (Figure 17). Strong gravitational segregation is observed in this sensitivity while hydrogen saturation is distributed differently.

Conclusion and Recommendation

In the 2D conceptual homogeneous model, the main controlling parameters involved in gas mixing extent as geological features include permeability, porosity, and structural dip. Further analysis indicates that after hydrogen injection, the system is prone to gravity segregation in all conducted experiments due to the large density contrast between CH_4 and H_2 . This effect can be intensified by increasing permeability. At very low injection rates in this sensitivity analysis, gravity override takes place as a function of density difference, especially occurring in down-dip injection when hydrogen can move rapidly upward and an early working gas breakthrough to the producer can be predicted. In up-dip injection, the width of the mixing zone remains relatively constant, and no further variation can be detected over the operation schedule (the upper part of the zone is only perforated). Despite a high mobility ratio between $\text{H}_2\text{-CH}_4$, the mixing front displacement is stabilized due to gas miscibility. Subsequently, the viscous fingering effect can be observed in none of the experiment results due to the possible low injection rate.

Apart from reservoir properties, physical dispersion is of great significance in the mixing process. One of the main simulation challenges that arise is numerical dispersion caused by temporal and spatial discretization. The numerical dispersion can overestimate dispersivity models and must be eliminated. Numerical dispersion, which is controlled by a second-order upstream weighting scheme, is significantly cost- and time effective compared to discretizing grid cells and timestep sizes. By minimizing numerical dispersion, the simulation model can realistically capture physical dispersion at an acceptable level.

Hydrodynamic dispersion consists of effective molecular diffusion and mechanical dispersion. Moreover, effective molecular diffusion is incorporated into 2D simulation runs and calculated based on cementation factor, porosity, and diffusion between H_2 and CH_4 to represent precise values of molecular diffusion in porous media. Due to the low injection rate, the contribution of this mechanism becomes significant during the injection phase as well as the shut-in phase. The effect of molecular diffusion is prominent in mixing behavior during the shut-in time. Nonetheless, this effect cannot be overlooked during very low injection rates. Thus, the front

stability and distribution may depend on molecular diffusion at a low injection rate and shut-in time. Mechanical dispersion is flow velocity and scale-dependent in porous media, leading to non-uniform velocity distribution, which is linked to tortuosity and anisotropy in the reservoir. As a result, this dispersive flux is also regarded as the substantial mechanism that can amplify the mixing between H₂ and CH₄.

In this work, the effect of discretization in the 3D conceptual model is omitted to evaluate numerical dispersion prior to adding physical dispersion. Subsequently, the achieved result of mitigating numerical dispersion from 2D conceptual models, which rely on using the TVD flux limiter, is applied to the sensitivity analysis in 3D cases. Nonetheless, the numerical dispersion effect on the mixing zone is assessed in combination with and without the TVD flux limiter when employing the base case model associated with physical dispersion. When numerical dispersion is involved with the simulation run, the simulated effect of mechanical dispersion is overshadowed. Moreover, the gas compositions in production streams are changed. Thus, minimizing the numerical dispersion effect can avoid further overestimating mechanical dispersion. Furthermore, the large density contrast between natural gas and hydrogen can accommodate strong gravitational segregation.

In the 3D conceptual homogeneous model, the effect of numerical dispersion and numerical error at a high injection rate near to injector is already mitigated. A combination of influencing factors is considered for further evaluation. The achieved result can enrich the understanding of various phenomena and involved mechanisms or even concerns in simulating field-scale reservoir models. In the carried-out experiment with lower reservoir properties (porosity and permeability) and physical dispersion effect, the result shows elevating dramatically hydrogen recovery efficiency and gas mixing compared to the experiment with higher permeability and porosity. Mechanical dispersion stimulates more mixing at the high flow injection rate while contributing slightly to produced gas components over successive injection-withdrawal cycles. Less mixing due to lower mechanical dispersion accompanied by constant reservoir properties can relatively amplify hydrogen volume in the production stream. Over shut-in time, molecular diffusion is more visible due to the absence of flow velocity. Thus, prolongation of the shut-in period can potentially enlarge the mixing zone with specific molecular diffusions in the carried-out experiments. Accordingly, mechanical dispersion has a key role in the mixing process at high injection rates. On the contrary, molecular diffusion behaves dominantly in static conditions. The factor of injection rate in this evaluation has an insignificant impact on the mixing zone due to the well location and using a single well. The solubility involvement in the deeper reservoir compared to the base model indicate a large discrepancy in hydrogen saturation at the end of the first injection caused by density, viscosity, and solubility variations. Solubility plays a role in mixing behavior in experiments with and without solubility. In the deeper reservoir, gas mixing is dramatically decreased due to varying physical properties and solubility while it has a minor impact on hydrogen recovery efficiency.

All achieved results from this work cannot be simply generalized to other reservoir cases. Since all reservoir models are homogeneously established with case-specific parameters in this research approach, which cannot be fully representative of real reservoirs with high heterogeneity, the results can be potentially varied.

The effect of discretization is not assessed in this 3D conceptual model to realize to what extent this coarse grid can capture accurately the flow front profile and mixing process. Hence, it is recommended to carry out one sensitivity analysis for providing a solid foundation in the field of UHS simulations. Furthermore, the microbial activity effect is neglected in this study and can be incorporated into further research approaches in UHS simulations. In this study, the

research focus is only the use of one well situated at the crest of the reservoir in the 3D conceptual model. Further study can also aim for the use of two different wells (injector and producer) and evaluate well patterns and well optimization.

Publication bibliography

- Cramer, S. D., The solubility of methane, carbon dioxide, and oxygen in brines from 0 deg to 300 deg c. Report of investigations. Bureau of Mines, Avondale, MD (USA). (1982)
- Dr. Li Li, Reactive Transport In The Subsurface. pennsilvania college of earth and mineral sciences. (2020)
- Feldmann, F.; Hagemann, B.; Ganzer, L.; Panfilov, M., Numerical simulation of hydrodynamic and gas mixing processes in underground hydrogen storages. In Environmental Earth Sciences 75 (16), p. 1165. (2016)
- Hagemann, Birger, Numerical and Analytical Modeling of Gas Mixing and Bio-Reactive Transport during Underground Hydrogen Storage. (2017)
- Li, Yau-Kun; Nghiem, Long X., Phase equilibria of oil, gas and water/brine mixtures from a cubic equation of state and henry's law. In Can. J. Chem. Eng. 64 (3), pp. 486–496. (1986)
- Poling, B. E.; Prausnitz, J. M.; O'Connell, J. P. , The Properties of Gases and Liquids: McGraw-Hill (Chemical engineering). (2001)
- Shiralkar, Gautam S.; Stephenson, Robert E., A General Formulation for Simulating Physical Dispersion and a New Nine-Point Scheme. In SPE Res Eng 6 (01), pp. 115–120. (1991)
- Shrivastava, Vijay; Nghiem, L. X.; Moore, R. G.; Okazawa, T., Modelling Physical Dispersion in Miscible Displacement-Part 1: Theory and the Proposed Numerical Scheme. In Journal of Canadian Petroleum Technology - 44. (2005)
- Sinan, Z.; Junchang, S.; Guoqi, W.; Dewen, ZH., Jieming, W., Numerical simulation-based correction of relative permeability hysteresis in water-invaded underground gas storage during multi-cycle injection and production 48 (1), pp. 190–200. (2021)
- Spiteri, E. J.; Juanes, R., Impact of relative permeability hysteresis on the numerical simulation of WAG injection 50, pp. 115–139. (2005)
- Tarkowski, Radoslaw, Underground hydrogen storage: Characteristics and prospects. In Renewable and Sustainable Energy Reviews 105, pp. 86–94. (2019)
- Tek, M. R., Underground Storage of Natural Gas: Theory and Practice. With assistance of North Atlantic Treaty Organization. Scientific Affairs Division: Springer Netherlands (E): [Nato ASI series]. (1989)
- Terstappen, R. J., Analysis of mixing during hydrogen store in gas reservoirs. Delft University of Technology. (2021)
- Yoonm, Poong; Thodos, George, Viscosity of nonpolar gaseous mixtures at normal pressures. In *Aiche Journal* 16, pp. 300–304. (1970)

Compressed Air Energy Storage (CAES) Solutions

T. Scheller

Siemens Energy, Business Owner CAES, Nürnberg, Germany

Subsurface storage of media like natural gas in caverns is widely used today. Many caverns are available in the area of the North Sea including its neighboring countries. In light of the political pledge to even stronger increase the addition of new renewable energy like wind power and photovoltaic from most recent level, the need for appropriate long duration energy storage (LEDS) is becoming more and more important.

Compressed Air Energy Storage solution can easily be deployed building on existing subsurface storages or even repurposing existing gas pipelines as storages. With mature and proven components this represents a low risk, high impact, readily available solution. So honestly, we have to talk about Compressed Air Energy Storage!



Compressed Air Energy Storage is already known since the 1970ies when the first plant has been built in Huntorf / Germany. A second plant has been built in the early 1990ies in McIntosh / Alabama, USA. Only most recently a new build plant has been commissioned in China. In the Western hemisphere we recognize a strong and increasing interest in this solution, with the first projects to potentially enter operation as early as 2026/27.

There are two different variants of Compressed Air Energy Storage solutions. The first is the already known (diabatic) version as it can be seen in Huntorf or McIntosh. Air from environment is compressed by means of several compressors and stored in an underground salt cavern. When favorable, the air is released thru an expander consisting of a HP Air Expander and a modified LP Gas Turbine Expander. The LP Gas Turbine Expander is required to heat up the air before expansion to avoid damages to the expander train.

As the above version, due to its nature using natural gas, is subject to emissions like CO₂ and NO_x, a second (adiabatic) version is readily developed: the heat that is produced during

compression will be stored in a separate heat storage. While expanding the stored heat will be used to reheat the air. Subsequently this will constitute a 100% emission free solution.

Siemens Energy is in a unique position to offer both of the aforementioned variants of Compressed Air Energy Storage solutions comprising proprietary equipment. For the diabatic version we are on track of soon using 100% H₂. In addition, we are looking into different type of storages for the adiabatic version, e.g. pipeline storage as well as hybrid models combining adiabatic and diabatic expansion.

Speicherung mechanischer Energie über künstliche Risse in gering durchlässigen Gesteinsformationen des tiefen Untergrunds

T. Tischner¹, S. Krug¹, R. Jung²

¹ Bundesanstalt für Geowissenschaften und Rohstoffe (BGR), Hannover

² Jung-Geotherm, Isernhagen

Zusammenfassung

Angeregt durch aktuelle Entwicklungen in den USA wird in diesem Beitrag die Speicherung von mechanischer Energie über künstliche Risse im tiefen Untergrund diskutiert.

Es werden hydraulische Untersuchungen an der BGR-Forschungsbohrung Horstberg neu bewertet. Die dort durchgeführten Injektions- und Fördertests zeigen, dass ein erheblicher Teil der für die Injektion von Wasser aufgewandten hydraulischen Pumpenergie bei einer Rückförderung wieder nutzbar ist. Entscheidend für die Energiespeicherung ist hier ein großflächiger künstlicher Riss im geringpermeablen Buntsandstein, der gleichzeitig dem effizienten Transport in das umliegende Gestein als auch der Speicherung von Wasser dient. Bei der Rückförderung fließt das Wasser vollständig und unter hohem Druck wieder zurück, so dass über eine Turbine und Generator eine Stromerzeugung möglich wäre. Für die Injektion des Wassers wurden bis zu 200 MWh an mechanischer Energie aufgewandt. Der Energieaufwand liegt damit in der gleichen Größenordnung wie die Speicherkapazität großer Batteriespeicher. Etwa die Hälfte der in den hydraulischen Tests aufgewandten Strommenge wäre rückgewinnbar gewesen.

Neben der Schaffung von hochpermeablen künstlichen Rissflächen sind für die Speicherung von mechanischer Energie überhydrostatische Druckbedingungen und gering durchlässige Gesteine vorteilhaft bzw. erforderlich. Im tiefen Untergrund von Sedimentbecken, wie dem Norddeutschen Becken, liegen diese Bedingungen vielfach vor.

Durch die Erzeugung mehrerer paralleler Risse aus einer Horizontalbohrung heraus können die Kapazität und die Effizienz der Speicherung erheblich gesteigert werden.

Für die Umsetzung dieses Speicherkonzepts sind die Untersuchung und Klärung erschließungstechnischer sowie verfahrenstechnischer Fragestellungen erforderlich. Insbesondere für die Nachnutzung von ehemaligen Gasbohrungen in Norddeutschland kann die Speicherung mechanischer Energie eine sinnvolle Alternative darstellen. Die Existenz von Altbohrungen, der Windenergieausbau verbunden mit temporären Stromüberschüssen sowie die geologischen Verhältnisse im Untergrund bieten in Norddeutschland gute Rahmenbedingungen für die Umsetzung dieses Speicherkonzepts.

Einleitung

Aufgrund der wetterabhängig fluktuierenden Stromverfügbarkeit steigt die Bedeutung der Energiespeicherung. Zur Speicherung elektrischer Energie über kurze Zeiträume, bis zu einigen Tagen, werden gewöhnlich Batteriespeicher als wichtigste Option angesehen. Bis 2030 wird in Deutschland eine Steigerung der Speicherkapazität stationärer Batterien auf 100 GWh_{el}¹ und damit auf etwa das Zwanzigfache der derzeitigen Kapazität erwartet (Wille-

¹ Die Indizes el, me, th werden als Abkürzung für elektrische, mechanische, thermische Energie verwendet.

Haussmann et al. 2022). Für die Speicherung größerer Energiemengen wird vermutlich die stoffliche Speicherung in Form von Wasserstoff oder Methan eine entscheidende Rolle spielen. Daneben können aber auch andere Optionen zur Energiespeicherung im Untergrund, wie die Druckluftspeicherung, an Bedeutung gewinnen. So verfolgt z.B. die Fa. Hydrostar ein neuartiges Konzept zur Druckluftspeicherung unter zusätzlicher Nutzung der entstehenden Abwärme bei der Kompression (Hydrostor 2022). Auf die Energiespeicherung in künstlichen Rissen zielt das Verfahren der Fa. Quidnet (Quidnet 2022). Es wird Wasser in einen Riss injiziert, das Fluid im Riss sowie im umgebenden Gestein werden elastisch komprimiert und bei Rückförderung wieder dekomprimiert.

Basierend auf den Experimenten an der Bohrung Horstberg wird in diesem Beitrag ein ähnliches Konzept wie das der Fa. Quidnet präsentiert und diskutiert. Die Untersuchungen an der Bohrung Horstberg zielten primär auf die Wärmegewinnung aus gering permeablen Sedimentgesteinen. Als Nebeneffekt lieferten diese wichtige Einblicke in die Option der mechanischen Energiespeicherung über künstliche Risse im Sedimentgestein. In diesem Beitrag werden die Untersuchungen an der Bohrung Horstberg im Hinblick auf die Speicherung mechanischer Energie dargestellt sowie Chancen und Herausforderungen dieser Form der Energiespeicherung diskutiert. Die Abbildung 1 illustriert das grundsätzliche Verfahren.

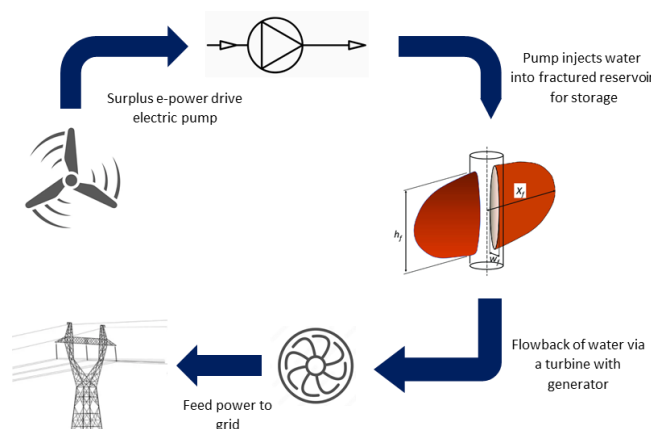


Abbildung 1: Schematische Darstellung der Speicherung von Überschussstrom als mechanische Energie über einen künstlichen Riss im Untergrund sowie die Rücktransformation zu Strom.

Bohrung Horstberg

Die Forschungsbohrung Horstberg Z1 liegt ca. 80 km nordöstlich von Hannover (Abb. 2) und erschloss ursprünglich gasführende Sandsteine des Rotliegenden. Nach Teilverfüllung der Gaserkundungsbohrung wurde der Mittlere Buntsandstein als potentielle Zielformation für geothermische Untersuchungen ausgewählt (Abb. 3). Mehr Informationen zur Bohrung und zu den hier durchgeföhrten geothermischen Untersuchungen sind z.B. in Jung et al. (2005) und Tischner et al. (2020) zu finden.

Der Mittlere Buntsandstein erstreckt sich zwischen 3636 und 3926 m Tiefe und erreicht eine Temperatur von ca. 145°C. Der Zugang zu einzelnen Abschnitten dieser Formation wurde durch Perforation erzielt. Für die nachfolgend dargestellten Untersuchungen sind nur die Perforation und der hydraulische Zugang zum Detfurth-Sandstein relevant. Dieser wurde bei 3787-3791 m perforiert, ist ca. 6 m mächtig und weist eine geringe Permeabilität von 2-3 mD bei ca. 8% Porosität auf.

Der Mittlere Buntsandstein steht an der Bohrung Horstberg unter einem überhydrostatischen Porenwasserdruck. Im hydraulischen Gleichgewicht und mit Formationswasser in der Bohrung (Dichte: 1,25 kg/l) beträgt der statische Bohrlochkopfdruck etwa 140 bar. Die Produktion von Formationswasser, wenn auch mit geringen Raten, ist damit einfach durch Öffnen der Bohrung möglich.

Produziertes Wasser aus dem Buntsandstein wurde in den hier diskutierten hydraulischen Tests in eine Kalkarenitschicht (Arenitfazies des Maastrichtium; Oberkreide) in ca. 1100 m Tiefe injiziert. Die Injektion erfolgte über den Ringraum derselben Bohrung (siehe Abb. 3).

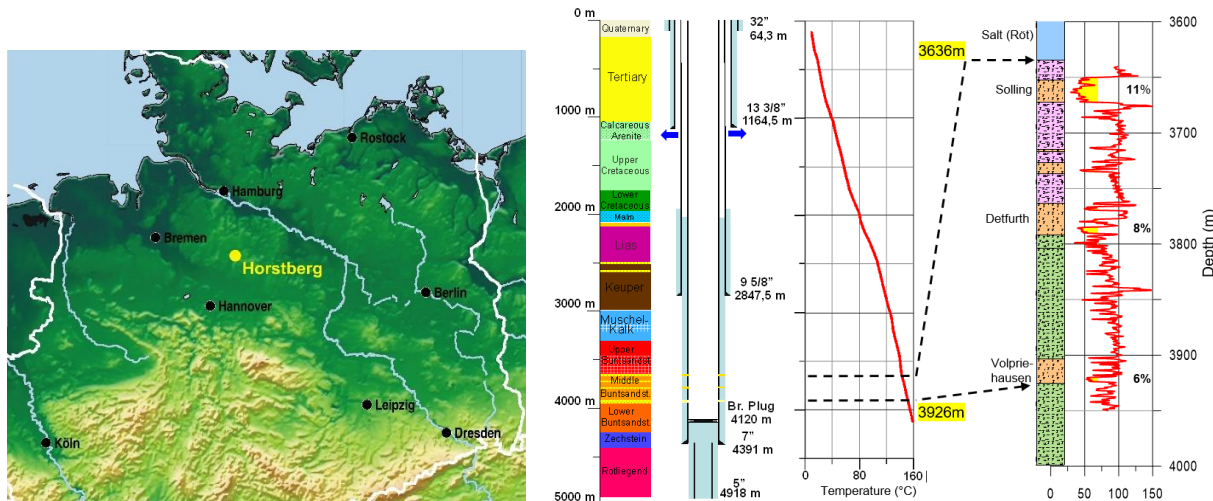


Abbildung 2: Lage der Bohrung Horstberg Z1 in Norddeutschland.

Abbildung 3: Lage, Stratigrafie, Bohrlochausbau und Temperaturprofil sowie Lithologie und Gamma-Log im Mittleren Buntsandstein. Im Gamma-Log sind Sandsteine gelb markiert (cut-off: 70 API) mit zugehörigen Porositätsangaben. Die blauen Pfeile kennzeichnen den Reinjektionshorizont über den Ringraum.

Hydraulische Tests im Detfurth-Sandstein

Nach der Ermittlung hydraulischer Parameter des Detfurth-Sandsteins in einem initialen Fördertest wurde eine Fracoperation durchgeführt. Etwa 20.000 m³ Frischwasser ohne Additive wurden in drei Stufen injiziert (Abb. 4).

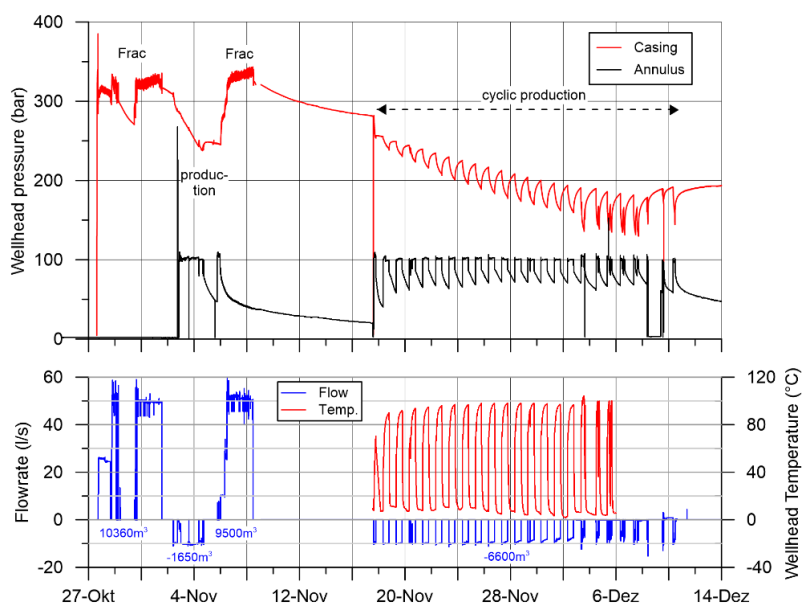


Abbildung 4: Druckverlauf während der Stimulation im Detfurth-Sandstein und bei nachfolgenden zyklischen Fördertests im Jahr 2003. Der Bohrlochkopfdruck im Casing (Detfurth) und im Ringraum (Annulus: Reinjektion) sind dargestellt. Negative (positive) Raten bedeuten Injektion (Produktion).

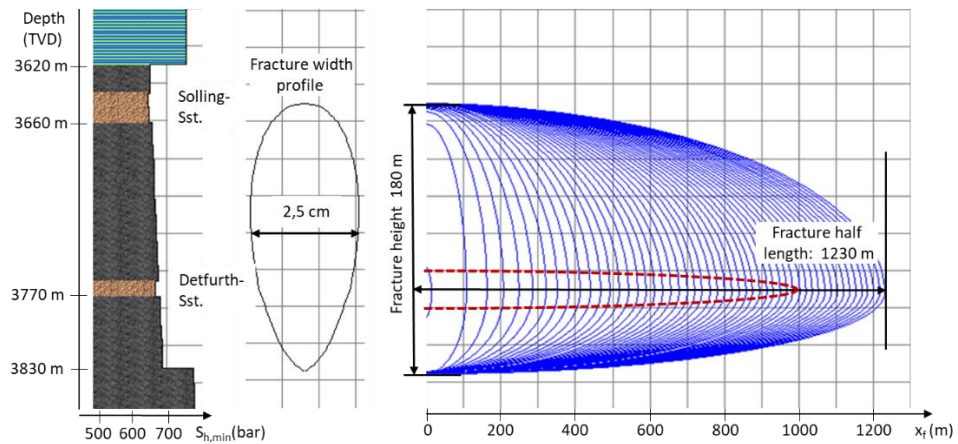


Abbildung 5: Berechnete Rissausbreitung für die Stimulation im Detfurth-Sandstein mit der Software FIELDPRO™ (Fa. RESnet). Die blauen Linien zeigen die Rissausbreitung in zweistündigen Intervallen. Die Berechnung wurde für ein Volumen von 20.000 m³ bei einer Rate von 50 l/s sowie dem links dargestellten Spannungsprofil durchgeführt. Die Rissweite in der Mitte wird für das Ende der Injektion gezeigt. Die rote Ellipse symbolisiert den Bereich des verbleibenden hochpermeablen Risses. x_f : fracture half length.

Die mechanische Pumpenergie für diese Fracoperation betrug ca. 180 MWh_{me}. Verschiedene Abschätzungen führen zu einer geschaffenen Rissfläche zwischen 200.000 und 500.000 m² (Abb. 5), wobei ein erheblicher Teil dieser Rissfläche auch bei Druckabsenkung unter den statischen Reservoirdruck hydraulisch hochleitfähig bleibt. Eine sehr gute hydraulische Anbindung des Risses an die Bohrung wurde nachgewiesen (Tischner et al. 2020).

Nach der Fracoperation und einer neuntägigen Einschlusssphase startete ein zyklischer Fördertest. Während dieses Tests wurden etwa 6.600 m³ Wasser unter hohem Druck zurückgefördert. Die Fließrate wurde hierbei auf ca. 10 l/s eingestellt. Aufgrund von technischen Problemen musste dieser Test jedoch nach 15 Zyklen beendet werden. Der Bohrlochkopf von ca. 190 bar am Ende der letzten Einschlusssphase hätte aber die Rückförderung von deutlich mehr Wasser bei erhöhtem Druck erlaubt. Demnach wäre es möglich gewesen, einen signifikanten Anteil der eingesetzten hydraulischen Pumpenergie von 180 MWh_{me} wieder zurück zu gewinnen, sofern eine Turbine mit Generator installiert gewesen wäre.

Ein weiterer wichtiger Test wurde 2004 durchgeführt (Abb. 6). Hierbei wurden ca. 2.600 m³ Frischwasser injiziert und innerhalb von fünf Tagen bei erhöhtem Druck wieder rückgefördert. Es wurden dieselbetriebene Pumpen eingesetzt. Um die Option zur Energiespeicherung quantitativ zu untersuchen, wird für diesen Test angenommen, dass die Pumpen elektrisch betrieben wurden. Ebenso wird für die Rückförderung angenommen, dass eine Turbine mit Generator die Stromrückgewinnung gewährleistet hätte. Eine Umwandlungseffizienz von 90 % wird für die Umwandlung von Strom zu mechanischer (hydraulischer) Energie in hocheffizienten Pumpen unterstellt. Für die Rückwandlung von mechanischer Energie über eine Turbine und Generator werden 80 % Effizienz angenommen. Dies bedeutet, dass das Maximum der Speichereffizienz ca. 70 % beträgt, allein bedingt durch die notwendige zweifache Energiekonversion.

In der Injektionsphase erreichte der Kopfdruck ca. 320 bar und damit etwa das gleiche Niveau wie bei der Fracoperation zuvor. Dies bedeutet, dass während der Injektion eine Wiederöffnung des zuvor geschaffenen Risses erfolgte. In den nachfolgenden Förderperioden fiel der Druck von ca. 290 bar bis auf ca. 140 bar am Ende der letzten Periode (Abb. 6). Nimmt man jeweils den mittleren Druck und die mittlere Fließrate in jeder Förderperiode, so wären ca. 11 MWh_{el} wieder rückgewinnbar gewesen (Tab. 1). Dies

bedeutet eine beachtliche Rückgewinnungsrate von ca. 45 %, obwohl die Testdurchführung nicht auf die Speicherung von Energie ausgelegt war. Betrachtet man nur die mechanischen Prozesse im Untergrund, so betrug dessen Effizienz etwa 60 % (Zeile 2 und 3 in Tab. 1). Das heißt, 60 % der eingesetzten mechanischen Pumpenergie wurden elastisch im Gestein/Riss gespeichert und wären rückgewinnbar gewesen.

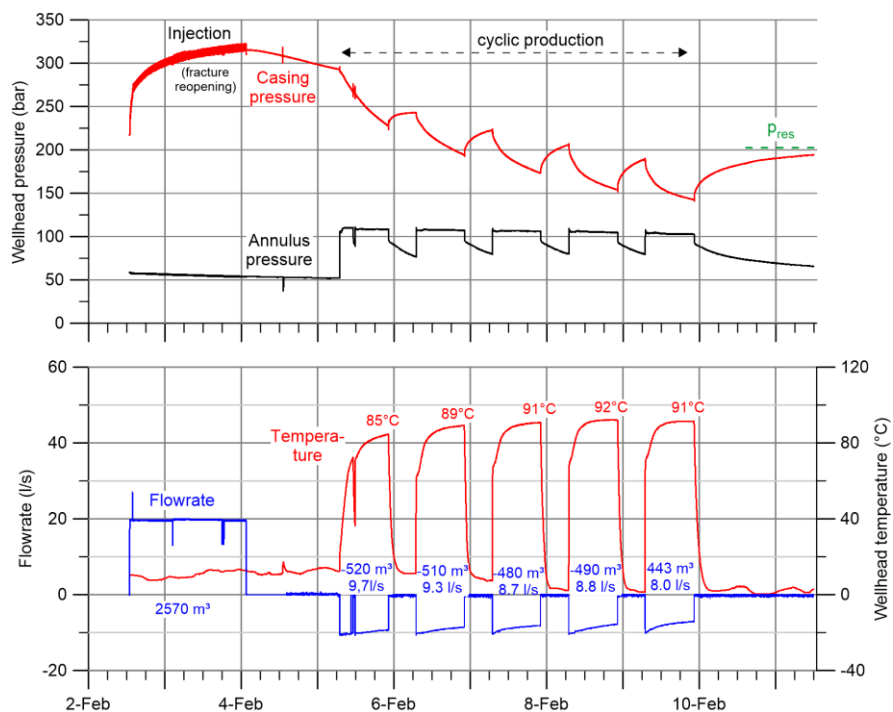


Abbildung 6: Druck, Fließrate und Temperatur bei einem Injektionstest in den Detfurth-Sandstein im Jahr 2004, gefolgt von der zyklischen Rückförderung. Das rückgeforderte Wasser wurde aus der Bohrung (Casing) direkt in den Ringraum der Bohrung (Annulus) reinjiziert. Im unteren Diagramm sind das Wasservolumen, die mittlere Fließrate und die maximale Temperatur für jede Fließperiode angegeben. Negative (positive) Rate bedeutet Injektion (Produktion). Der statische Bohrlochkopfdruck bei der mittleren Dichte der Fluidsäule von 1,1 kg/l ist dargestellt (grün gestrichelte Linie, oben)

Tabelle 1: Energiebilanz für den Test in Abbildung 6. Die Angaben zur elektrischen Energie wurden aus dem mechanischen Energieaufwand abgeleitet, da real Dieselpumpen eingesetzt wurden und kein Strom erzeugt wurde.

| Nr. | Prozess | Energie (MWh) | Erläuterung |
|-----|------------------------|---------------|---|
| 1 | Injektion, elektrisch | -24,1 | Erforderliche elektrische Pumpenergie zur Injektion – siehe Zeile 2 - bei Annahme einer Umwandlungseffizienz von 90 % (elektrisch zu mechanisch) |
| 2 | Injektion, mechanisch | -21,7 | Mechanische Pumpenergie für die Injektion mit 19,8 l/s über 36 h bei einem mittleren Kopfdruck von 305 bar; mechanische Leistung: 604 kW _{me} |
| 3 | Produktion, mechanisch | 13,4 | Verfügbare mechanische Energie bei der Rückförderung (5 Phasen à 15 h), basierend auf den mittleren Werten für Rate und Druck in jeder Phase |
| 4 | Produktion, elektrisch | 10,7 | Möglicher Rückgewinn an elektrischer Energie bei einer Umwandlungseffizienz von 80 % (mechanisch zu elektrisch) |
| 5 | Thermische Energie | 82,7 | Möglicher thermischer Energiegewinn bei der Rückförderung, kalkuliert für die mittlere Fließrate von 9 l/s, einer Fördertemperatur von 90°C und einer angenommenen Abkühlung auf 60°C. Mittlere thermische Leistung: 1,1 MW _{th} |

Während jeder Förderperiode stieg die Fluidtemperatur am Bohrlochkopf bis auf etwa 90°C an, obwohl gerade einige Tage zuvor 2600 m³ Wasser mit einer Temperatur von ca. 5°C injiziert worden waren (ungestörte Reservoirtemperatur: 145°C). Die entnommene thermische Energiemenge betrug 83 MWh_{th} bezogen auf eine Referenztemperatur von 60°C (siehe Tab. 1). Aus ökonomischer und ökologischer Sicht ist daher die Nutzung der thermischen Energie in Kombination mit dem Speicherkonzept geboten.

Diskussion

Die Experimente am Standort Horstberg zeigen, dass über künstliche Risse in geringpermeablem Gestein erhebliche Mengen an mechanischer Energie gespeichert werden können. Die Speichereffizienz hängt wesentlich von einem großen und hydraulisch gut leitfähigem Riss ab. Dieser dient als Fließweg für das Wasser vom Bohrloch zur Formation und gleichzeitig als Fluidspeicher. Der Riss öffnet und weitet sich während der Injektion und entspannt sich entsprechend bei Rückförderung. Insbesondere wenn bei Rückförderung das Druckniveau nicht wesentlich unter den Fracdruck sinkt, wird der Riss auch bei Rückförderung eine sehr hohe hydraulische Leitfähigkeit beibehalten. In Horstberg wurde sogar bis unterhalb des natürlichen Porenwasserdruks ein hochleitfähiger ("infinite conductive") Riss nachgewiesen.

Überhydrostatische Druckbedingungen sind vorteilhaft oder sogar notwendig für dieses Speicherkonzept. Je höher der statische Porenwasserdruk im Reservoir ist, desto mehr Energie kann bei gleicher Wassermenge gespeichert werden. Darüber hinaus ermöglicht ein hoher statischer Überdruck die vollständige Rückgewinnung des eingepressten Wassers unter hohem Druck. Formationen mit statischem Porenwasserüberdruck sind in tiefen Sedimentbecken weit verbreitet (Lindberg et al., 1980; Zhao et al., 2018). Am Versuchsstandort Horstberg im Norddeutschen Becken beträgt der statische Überdruck am Bohrlochkopf 140 bar (230 bar), wenn sich natürliches Formationswasser (Süßwasser) im Bohrloch befindet.

Durch die Erzeugung mehrerer paralleler Risse aus einer Horizontalbohrung heraus können die Kapazität und die Effizienz der Speicherung erheblich gesteigert werden. Ein System mit multiplen Rissen verhält sich ähnlich wie ein geschlossenes Reservoir. Während der Injektion wird die Flüssigkeitsbewegung zwischen den Rissen eingeschränkt, und die Energie wird überwiegend als elastische Energie im Gestein und im Wasser zwischen den Rissen gespeichert. Exemplarische Berechnungen auf Basis der petrophysikalischen Parameter im Buntsandstein der Bohrung Horstberg zeigen, dass hierdurch die Effizienz der mechanischen Energiespeicherung im Untergrund von den beobachteten 60 % mit einem Einzelriss bis auf ca. 90 % bei 10 parallelen Rissen gesteigert werden kann. Die Gesamteffizienz wird dann überwiegend von der Umwandlung von elektrischer Energie in mechanische und zurück limitiert.

In Sedimentbecken mit geringer tektonischer Aktivität ist die Wahrscheinlichkeit für das Auftreten spürbarer seismischer Ereignisse sehr gering. So ist nicht bekannt, dass im Norddeutschen Becken im Zusammenhang mit Fracoperationen oder Flüssigkeitsinjektionen jemals spürbare seismische Ereignisse getriggert wurden. Zur Überwachung der Rissöffnung bzw. Rissausbreitung ist aber auch in solchen Regionen ein seismisches Monitorig geboten. Hiermit kann in den Injektionsphasen nachgewiesen werden, dass sich der Riss nur innerhalb der gewünschten Schichten ausbreitet und vorgegebene Limits der Rissausbreitung nicht überschritten werden.

Wasser, das aus dem tiefen Untergrund gefördert wird, enthält Salze, gelöste Feststoffe und Gase. In Horstberg wurde bereits kurz nach der Frischwasserinjektion in dem dargestellten zyklischen Test Wasser mit einem Salzgehalt von über 50 g/l gefördert. Wenn salzhaltiges Wasser an der Oberfläche mit der Atmosphäre in Kontakt kommt, können sich Ablagerungen aus Eisenoxiden und anderen Mineralien bilden. Die Reinkjection von partikelbeladenem Wasser kann zu hydraulischen Limitierungen am Risseinlass oder im Reservoir führen. Daher erfordert die Zwischenlagerung des produzierten Salzwassers in Kontakt mit der Atmosphäre zusätzliche Mittel zum Filtern und Behandeln vor der Reinkjection. Eine Option

zur Vermeidung von Scaling-Problemen ist die Lagerung in geschlossenen Tanks an der Oberfläche unter einer Schutzgasatmosphäre (Stickstoff). Eine andere Option ist die Speicherung des geförderten Wassers in einem "flachen" Aquifer. Diese Aquifer muss deutlich tiefer liegen als Grundwasserleiter, die für die Trinkwassernutzung verwendet werden. Am Versuchsstandort Horstberg treten solche Aquifere in Tiefen von ca. 400 m (Neuengammer Sand) und 600 m (Brüsseler Sand) auf. Für weite Bereiche des Norddeutschen Beckens sind Aquifere bekannt, die potentiell zur Speicherung des produzierten Salzwassers genutzt werden können. Die Speicherung des rückgeförderten Wassers im Untergrund führt zu zusätzlichen Druck- und Energieverlusten. Die Entscheidung über die am besten geeignete Methode zur Zwischenspeicherung des produzierten Wassers sollte standortspezifisch unter Abwägung der relevanten geochemischen, technischen und finanziellen Aspekte getroffen werden.

Die Temperatur des produzierten Wassers in den zyklischen Tests von Horstberg erreichte mehr als 90°C, obwohl kurz zuvor Frischwasser mit einer Temperatur von etwa 5°C injiziert wurde. Diese Ergebnisse und durchgeführte numerische Simulationen zeigen, dass das thermische Energiepotential höher sein kann als das mechanische Speicherpotential. Die thermische Nutzung des geförderten Wassers ist daher wichtig, führt aber zu einer Einschränkung potenzieller Projektstandorte, da die Wärmeerzeugung in räumlicher Nähe zu einem Wärmenetz erfolgen muss. Eine weitere Einschränkung ergibt sich aus den unterschiedlichen Anforderungen an die zeitliche Verfügbarkeit von Strom und Wärme. Um beide Anwendungen zeitlich zu entkoppeln, kann die Speicherung des rückgeförderten Wassers in einem Aquifer (siehe oben) bei gleichzeitiger Nutzung als Aquiferwärmespeicher sein. Durch ein oder mehrere Bohrungen in den erwärmten Bereich des Aquifers kann dann Wärme entnommen werden, wenn Wärme benötigt wird, unabhängig von der Stromerzeugung bzw. Energiespeicherung.

Die vorgeschlagene Umwandlung elektrischer Energie und deren Speicherung als mechanische Energie im Untergrund muss mit anderen Speichermöglichkeiten konkurrieren, vor allem mit Batteriespeichern, die derzeit im Fokus der Energieversorger stehen.

Der Systemwirkungsgrad moderner Batteriespeicher kann über 90 % betragen (Zablocki, 2019). Im Vergleich dazu ist der maximale Wirkungsgrad des Rissspeichers geringer, kann aber etwa 60 % erreichen, was wiederum deutlich höher ist als die etwa 30 % eines Power-to-Power-Zyklus mit Wasserstoff oder Methan als chemischem Speichermedium (Ausfelder et al., 2015). Die Kapazität großer Batteriespeicher liegt im Bereich von einigen 100 MWh_{el} (VDI, 2021) und damit in der Größenordnung potenzieller Risspeicher.

Wesentliche Vorteile der Risspeicherung können die Kosten und die Unabhängigkeit von wertvollen Rohstoffen sein. Die Investitionskosten für Batterien liegen im Bereich von 200 USD/kWh_{el} (George 2020). Dementsprechend benötigt ein Batteriespeicher mit einer Leistung von 100 MWh_{el} etwa 20 Mio. USD der Investition. Wenn andererseits eine aufgegebene tiefe Gasbohrung rekomplettiert und für die Speicherung "gefract" wird, sollten etwa 5-10 Mio. USD Investition hierfür ausreichend sein, einschließlich Oberflächenausrüstung und einer weiteren "flachen" Bohrung zur Wasserspeicherung. Zudem stützt sich die Energiespeicherung über künstliche Risse auf lokale Ressourcen und ist nahezu unabhängig vom Import wertvoller oder kritischer Rohstoffe (Li, Co, Ni, ...), ein großer Vorteil, der aber kaum quantifizierbar ist.

Der Norden Deutschlands ist eine Schwerpunktregion für den Ausbau der Windenergie. Hier sind viele neue Windparks im Bau oder in der Planungsphase. Neue Stromübertragungsleitungen werden gebaut, um den Strom in den Süden zu transportieren, und der Bedarf an Stromspeichern in der Nähe seiner Erzeugung steigt. In Norddeutschland gibt es zudem viele Altbohrungen aus der Kohlenwasserstoffförderung. Diese Bohrungen könnten nachgenutzt und zu moderaten Kosten für die Risspeicherung verwendet werden. Schließlich sind im tiefen Untergrund des Norddeutschen Beckens Formationen bekannt, die einen erhöhten Porenwasserdruck aufweisen. Diese vier Punkte: Ausbau der Windenergie, steigender Bedarf an Stromspeichern, vorhandene Altbohrungen und überhydrostatischer Porendruck sind gute Argumente für die Entwicklung dieses Speicherkonzepts im Norden Deutschlands.

Literaturverzeichnis

- Ausfelder, F., Beilmann, C., Bertau, M., Bräuninger, S., Heinzel, A., Hoer, R., Koch, W., Mahlendorf, F., Metzelthin, A., Peuckert, M., Plass, L., Räuchle, K., Reuter, M., Schaub, G., Schiebahn, S., Schwab, E., Schüth, F., Stolten, D., Teßmer, G., Wagemann, K. and Ziegahn, K.-F. (2015): Energiespeicherung als Element einer sicheren Energieversorgung. *Chemie Ingenieur Technik*, 87, 1-2: 17-89. <https://doi.org/10.1002/cite.201400183>
- George, J.F. (2020): Kostenentwicklungsprognose stationärer Batteriespeichertypen. Strommarkttreffen Stationäre Stromspeicher, 21.02.2020, Berlin. https://www.strommarkttreffen.org/2020-02-21_George_Kostenentwicklungsprognose_stationaerer_Batteriespeichertypen.pdf
- Hydrostor (2022): Advanced Compressed Air Energy Storage. <https://www.hydrostor.ca/technology/> Company Hydrostor, Toronto, Canada, accessed on December 20th, 2022.
- Jung, R., Orzol, J., Tischner, T., Jatho, R. and Kehrer, P. (2005): The geothermal project GeneSys – Results of massive waterfrac-tests in the Bunter sandstone formation in the Northern German Basin. *Proceedings*, 30th Workshop on Geothermal Reservoir Engineering, 31.01.-2.02.2005, Stanford University, CA. <https://pangea.stanford.edu/ERE/pdf/IGAstandard/SGW/2005/jung.pdf>
- Lindberg, P., Riise, R. and Fertl, W.H. (1980): Occurrence And Distribution Of Overpressures In The Northern North Sea Area. *SPE Annual Technical Conference and Exhibition*. SPE-9339-MS. <https://doi.org/10.2118/9339-MS>
- Quidnet (2022): Modular Pumped Storage, Enabling the Zero-Carbon Grid. <https://www.quidnetenergy.com/> Company Quidnet Energy Houston, US, accessed on December, 20th, 2022.
- Tischner, T., Hassanzadegan, A., Krug, S., Stechern, A., Tzoufka, K. and Jung, R. (2020): Productivity enhancement by hydraulic fracturing and circulation of thermal water at the test site Horstberg in the North German Basin. *Proceedings*, World Geothermal Congress 2020+1, April-October 2021, Reykjavík, Iceland. <http://www.geothermal-energy.org/pdf/IGAstandard/WGC/2020/31109.pdf>
- VDI (2021): Batterie: Die größten Energiespeicher der Welt. VDI Verlag GmbH; Düsseldorf. Accessed on December, 22th, 2022. <https://www.ingenieur.de/technik/fachbereiche/energie/batterie-die-groessten-energiespeicher-der-welt>
- Wille-Haussmann, B., Biener, W., Brandes, J., Jülich, V. and Wittwer, C. (2022): Batteriespeicher an ehemaligen Kraftwerksstandorten. Fraunhofer-Institut für Solare Energiesysteme, ISE, Freiburg, Position paper, BAT4CPP: 20; <https://www.ise.fraunhofer.de/content/dam/ise/de/documents/publications/studies/Fraunhofer-ISE-Batteriespeicher-an-ehemaligen-Kraftwerkstandorten.pdf>
- Zhao, J., Li, J. and Xu, Z. (2018): Advances in the origin of overpressures in sedimentary basins. *Petroleum Research*, 3, 1: 1-24. DOI: <https://doi.org/10.1016/j.ptlrs.2018.03.007>
- Zablocki, A. (2019): Energy storage. White Papers - Fact Sheets and Issue Briefs, Environmental and Energy Study Institute; Washington, US. 10.01.2023. <https://www.eesi.org/papers/view/energy-storage-2019>

Aspekte einer auf bohrlochgeophysikalischen Daten basierten Endlagersuche

J. Strobel, N. Schöner, R. Zühlke

Bundesgesellschaft für Endlagerung mbH (BGE), Peine

Zusammenfassung

Die Grundlage für die aktuelle Suche nach dem bestmöglichen Endlagerstandort für hochradioaktive Abfälle ist das im Jahr 2017 novellierte Standortauswahlgesetz (StandAG). Der BGE obliegt es als Vorhabenträgerin im Standortauswahlverfahren nach den gesetzlich festgelegten Kriterien geeignete Standorte zu ermitteln und vorzuschlagen. Zum derzeitigen Stand des Standortauswahlverfahrens wird eine Bewertung der Teilgebiete im Rahmen der repräsentativen vorläufigen Sicherheitsuntersuchungen durchgeführt, um Standortregionen für die übertägige Erkundung zu ermitteln.

Tongestein ist neben Steinsalz und kristallinem Wirtsgestein eines der möglichen Wirtsgesteine für die Endlagerung hochradioaktiver Abfälle in Deutschland. Ein wichtiges Kriterium für die Bewertung des Wirtsgesteinsbereiches mit Barrierefunktion stellt die Homogenität der sedimentologischen Abfolge dar. Bohrlochgeophysikalische Logs zeichnen diese in vertikaler Richtung auf. Für die Berechnung der Diffusionslänge für Radionuklide ist die effektive, den Ionen zugängliche, Porosität, wie sie auch aus Logs errechnet werden kann, ein wichtiger Eingangsparameter.

Bohrlochdaten spielen daher im Standortauswahlverfahren eine wichtige Rolle zur Umsetzung einer evidenzbasierten Bewertung von Kriterien, die am Ende zu einer Eignungsaussage von Gebieten führen.

Einführung

Die Basis für die aktuelle Suche nach dem bestmöglichen Endlagerstandort für hochradioaktive Abfälle ist das im Jahr 2017 novellierte Standortauswahlgesetz (StandAG). Gemäß § 1 StandAG ist der Standort mit der bestmöglichen Sicherheit derjenige Standort, der im Zuge eines vergleichenden Verfahrens, ausgehend von einer weißen Deutschlandkarte bestimmt wird und der einen dauerhaften Schutz von Mensch und Umwelt vor ionisierender Strahlung und sonstigen schädlichen Wirkungen für einen Zeitraum von einer Million Jahren gewährleistet.

Der BGE obliegt es als Vorhabenträgerin im Standortauswahlverfahren nach den gesetzlich festgelegten Kriterien geeignete Standorte zu ermitteln und vorzuschlagen. Das Verfahren verläuft dabei in drei Phasen, in denen der Standort mit der bestmöglichen Sicherheit in mehreren Eingrenzungsschritten identifiziert werden. Am Ende jeder Phase werden die Ergebnisse und Vorschläge der BGE durch das Bundesamt für die Sicherheit der nuklearen

Entsorgung geprüft. Zum derzeitigen Stand des Standortauswahlverfahrens wird eine Bewertung der Teilgebiete im Rahmen der repräsentativen vorläufigen Sicherheitsuntersuchungen durchgeführt.

Unterteilung in Teilgebiete

Die bisher ausgewiesenen Teilgebiete umfassen alle potenziellen Wirtsgesteine: Tongestein, kristallines Wirtsgestein und Steinsalz, sowohl in steiler als auch in stratiformer Lagerung. Die weitere geowissenschaftliche Bearbeitung erfordert die Sichtung und Bewertung der verfügbaren Geodaten, dazu gehören auch insbesondere bohrlochgeophysikalische Daten.

Die Wirtsgesteine Steinsalz in stratiformer Lagerung oder Tongestein können eine horizontale Kontinuität der Eigenschaften zeigen. Diese wird auf Basis von Schichtenverzeichnissen und maßgeblich von geophysikalischen Logs bewertet. Darüber hinaus ermöglicht eine Interpretation geophysikalischer Daten die quantitative Beschreibung von einschlussrelevanten Eigenschaften dieser Gesteine.

Anwendung der Bohrlochgeophysik

Ein wichtiges Kriterium für die Bewertung des Wirtsgesteinsbereiches mit Barrierefunktion stellt die Homogenität der sedimentologischen Abfolge dar. Logs zeichnen diese in vertikaler Richtung auf. Obwohl eine visuelle Einstufung der Variation der Eigenschaften durch z. B. eine GammaRay Kurve einfach erscheint, ist jedoch die Quantifizierung einer Varianz im statistischen Sinne eine Herausforderung. Klassische „Cut-off“ Methoden könnten eingesetzt werden, verlangen aber nach objektiven Kriterien. Als vorteilhaft hat sich die Betrachtung einer residualen Variation die sich nach Subtraktion einer niederfrequenten Grundkomponente oder eines Trends ergibt, erwiesen. Basierend auf den Ablagerungszyklen differiert die praktische Anwendung zwischen Evaporiten und klastischen Sedimenten, aber das Anwendungsprinzip ist identisch. Auch vertikale Variogramme sind prinzipiell geeignet, Heterogenität zu charakterisieren. Diese Methode zeigt im Ergebnis jedoch eher größere Zyklen mit Spannen oberhalb von fünf Metern.

In Gebieten mit hoher Datendichte können Zusammenhänge zwischen der Mächtigkeit einer Schicht und seiner Homogenität beobachtet werden, die eine flächenhafte Abschätzung der Wirtsgesteinsgüte erlauben.

Eine im Rahmen der repräsentativen vorläufigen Sicherheitsuntersuchungen zu berechnende Kenngröße stellt die Diffusionslänge radioaktiver Ionen im Betrachtungszeitraum von einer Millionen Jahre dar. Für die Berechnung der Diffusionslänge für Radionuklide ist die effektive, den Ionen zugängliche, Porosität ein wichtiger Eingangsparameter. Diese kann aus der Ton-Porosität heraus abgeleitet werden wie sie an einer bei 105 C getrockneten Probe gemessen wird (Boisson, 2005).

Nur die wenigsten geophysikalischen Logs messen den Wasseranteil eines Gesteines direkt. Dazu gehören die (epithermische) Neutronenporosität und die Abklingzeit der magnetischen Resonanz. Die Bestimmung der Mineralogie durch Neutronenaktivierung kann über den Anteil

der Tonminerale einen Beitrag zur Bestimmung einer Tonporosität leisten (Strobel 1998). Die klassischen Log-Messungen wie GammaRay, Dichte und Laufzeit erlauben keine direkte Quantifizierung. Zwar gibt es für die Interpretation von Widerstandsmessungen sogenannte „Shaly-Sand“ Gleichungen – diese gelten aber, wie der Name sagt, nur für Sandsteine mit einem mittleren Tonanteil.

Innerhalb der zu betrachtenden Gebiete gibt es Bohrungen, die eine Vielzahl der genannten Messungen enthalten. Aus diesen Daten wird ein Multi-Mineral Model zusammengestellt, welches das Log-Antwortverhalten mit den Kernanalysen verknüpft. Dieses Model wird durch Reduzierung der Eingangsdaten schrittweise modifiziert, um auch an Bohrungen mit geringer Datenmenge Ergebnisse zu erzielen um die Anzahl der nutzbaren Bohrungen zu erhöhen. Die Zusammenschau der so ermittelten Tonporositäten erlaubt eine grobe Regression über die Teufe innerhalb der Grenzen eines einheitlichen Ablagerungsraums. Durch diese Vorgehensweise können genetisch zusammenhängende Gebiete mit unterschiedlicher Datenlage hinsichtlich der Variationsbreite der Gesteinsabfolge bewertet werden.

Verfügbarkeit bohrlochgeophysikalische Daten

Die Anwendung der genannten Methoden setzt einen effizienten Zugang zu Bohrungsdaten voraus. Da bohrlochgeophysikalische Daten in sehr unterschiedlichen Formaten (von analog bis digital) vorliegen, ist die Datenaufbereitung in vielen Gebieten sehr zeitintensiv.

Eine gute Ausgangssituation bezüglich digital vorhandener bohrlochgeophysikalischer Daten liegt im Bereich der Teilgebiete zur Unteren Meeresmolasse vor. Über Profillinien und Log basierten Analysen kann die Eignung dieses Gebiets auf Basis der vorhandenen Daten bewertet werden.

Bohrlochdaten spielen im Standortauswahlverfahren eine wichtige Rolle zur Umsetzung einer evidenzbasierten Bewertung von Kriterien, die am Ende zu einer Eignungsaussage von Gebieten führen. Die Verfügbarkeit von Bohrlochdaten stellt ein hohes gesellschaftliches Gut dar.

Literatur

Boisson JY (2005): Clay Club Catalogue of Characteristics of Argillaceous Rocks. NEA No.4436, ISBN 92-64-01067-X.

StandAG: Standortauswahlgesetz vom 5. Mai 2017 (BGBI. I S. 1074), das zuletzt durch Artikel 1 des Gesetzes vom 7. Dezember 2020 (BGBI. I S. 2760) geändert worden ist

Strobel J, Win P, Wouters L, Hagood M (1998): Groundwater Permeability Correlations in the Boom Clay using Wireline Logs. Paper presented at the International High-Level Nuclear Waste Conference, Las Vegas 1998.

Geschäftszeichen: SG01201/26-1/9-2022#13 – Objekt-ID: 9025963 – Stand: 08.12.2022
www.bge.de

Systematische Integration von Bohrungsdaten zum Zweck der Identifizierung und Charakterisierung von geeigneten geologischen Barriere-Formationen

S. Alles

ExxonMobil Production Deutschland GmbH, Hannover, Germany

Im Verlauf der erdgeschichtlichen Entwicklung konnten sich auch im NW-deutschen Raum zahlreiche potenzielle geologische Barriere-Formationen ausbilden. Die Eigenschaften dieser -im Wesentlichen aus Ton-, Schiefer- und Evaporitgesteinen bestehenden Formationen- sind sehr variabel, so dass die Integration der zur Verfügung stehenden Bohrungsdaten geboten ist. Dies umfasst ausdrücklich nicht nur quantitative Daten und/oder direkte petrophysikalische Bohrlochmessungen, sondern auch verschiedenste qualitative Informationen und Beobachtungen, die -gerade in älteren Bohrungen- häufig einen stark subjektiven Charakter haben.

Per Definition besteht die Kernaufgabe einer wirksamen geologischen Barriere darin, den Umstieg und Transport/Migration von Fluiden in andere Formationen oder bis an die Erdoberfläche wirksam zu verhindern. Bei EMPG untersuchte Kriterien für die Eignung einer geologischen Barriere sind:

Geringe Durchlässigkeit bzw. Permeabilität gegenüber anstehenden Formationsfluiden
Geomechanische Eignung bzw. Gesteinsfestigkeit gegenüber einem sich möglicherweise über geologische Zeiträume wiedereinstellenden initialen Lagerstättendruck
Kumulative Mächtigkeit der identifizierten Formationen

Die Ergebnisse der geologischen Barriere-Bewertung sind ein wichtiges Element u.a für das Erstellen von „Rock-to-Rock“ Verfüllungskonzepten und stellen ein wichtiges Kriterium in der Bewertung möglicher Umstiegs- und Migrationsszenarien dar. Darüber hinaus werden geeignete geologische Barrieren z.B. im Zusammenhang mit der Untertagespeicherung von CO₂ zunehmend an Bedeutung gewinnen.

Es wird ein Workflow vorgestellt, an dessen Ende eine systematische und möglichst reproduzierbare Charakterisierung der o.g. Barriere-Eigenschaften sowie eine standardisierte Darstellung aller relevanten Bohrlochdaten steht.

Verbreitung von Sandsteinen der Unterkreide in Niedersachsen – neue Karten und Daten für die Geothermie

R. Pierau, R. Schöner

Landesamt für Bergbau, Energie und Geologie, Hannover, Germany

Im Niedersächsischen Becken sind Sandsteine der Unterkreide aus Aufschlüssen im Leinebergland und aus den vielen Bohrungen der Kohlenwasserstoff-Industrie bekannt. Karten zu den Sandstein-Einheiten der Bückeberg-Gruppe (Ober-Berriasium) und des Valanginium im Niedersächsischen Becken wurden vom Landesamt für Bergbau, Energie und Geologie erstellt und sind im NIBIS-Kartenserver online abrufbar. Die Karten enthalten eine Darstellung der Verbreitung und der hydraulischen Eigenschaften dieser Sandsteine als mögliche Zielhorizonte für eine geothermische Nutzung.

Für die Entwicklung der Karten wurden Schichtenverzeichnisse, Bohrkernproben, biostratigraphische Daten und Bohrlochmessungen verwendet. Aus den Schichtenverzeichnissen und vorhandenen Bohrkernen wurden Angaben zur Lithologie, Korngröße und zu Sedimentstrukturen entnommen. Die Ergebnisse der Kernuntersuchungen wurden zur Auswertung der zugehörigen Bohrlochmessungen (entweder Eigenpotential oder Gamma-Ray-Logs) herangezogen. So konnten mittels eines charakteristischen „Referenzmusters“ der Bohrlochmessungen kartierbare Einheiten identifiziert und deren Verbreitung durch vernetzte Profilschnitte ermittelt werden.

Insgesamt können fünf relevante, regional verbreitete Sandsteineinheiten kartiert werden. Die Sandsteine der Barsinghausen-Subformation aus dem mittleren Teil der Bückeberg-Gruppe sind in den Höhenzügen des Leineberglandes (z.B. „Obernkirchener Sandstein“) aufgeschlossen und finden ihre Fortsetzung im tiefen Untergrund in der Schaumburger- und Deister-Mulde sowie in einem lokal begrenzten Nordost-Südwest ausgerichteten Gebiet zwischen Celle und Hannover. Die Sandsteine können als Küstenablagerungen im Übergangsbereich zwischen Festland und einem sehr flachen Binnenmeer gedeutet werden. Der Kopf-Sandstein der Fuhse-Formation stellt die jüngste Sandstein-Einheit im oberen Teil der Bückeberg-Gruppe dar. Die Ablagerung des Kopf-Sandstein erfolgte im küstennahen Bereich eines Binnenmeeres. Im Valanginium können drei zeitlich und räumlich getrennte Sandstein-Einheiten kartiert werden. Der Bentheim Sandstein im westlichen Teil des Beckens sowie der Hauptsandstein als sein zeitlichen Äquivalent im Ostteil des Beckens wurden während des Untervalanginium abgelagert. Während des Obervalanginium wurde im zentralen Becken als jüngste Sandstein-Einheit der Dichotomiten-Sandstein abgelagert. Für alle Sandsteine des Valanginium wird eine Ablagerung in einem flachen Meeresbereich nahe der Küste angenommen.

Auf regionalem Maßstab erfüllen die Sandsteine der Bückeberg-Gruppe aufgrund der häufig moderaten hydraulischen Eigenschaften nur mit Einschränkungen die Voraussetzungen für eine geothermische Nutzung. Geeignete Nutzungsbedingungen könnten jedoch lokal vorhanden sein. Die Sandsteine des Valanginium erfüllen weitgehend die Mindestanforderungen an einen geothermisch nutzbaren Aquifer und könnten ein Ziel für die weitere geothermische Exploration in Niedersachsen darstellen.

Speicherung von Kohlendioxid unter der Nordsee

K. Wallmann

GEOMAR Helmholtz-Zentrum für Ozeanforschung Kiel

Die Abscheidung von Kohlendioxid (CO_2) mit anschließender Speicherung im geologischen Untergrund kann einen Beitrag zur Reduktion von CO_2 -Emissionen leisten. In Europa, wird diese Technologien bisher nur in Norwegen in industriellem Maßstab angewendet. Das CO_2 wird dabei unter dem Meeresboden verpresst. Viele europäische Firmen erschließen zurzeit weitere CO_2 -Speicher unter der Nordsee, um dort CO_2 aus industriellen Quellen zu entsorgen. In einer Reihe von europäischen Forschungsprojekten konnte gezeigt werden, dass bei der geologischen CO_2 -Speicherung unter dem Meeresboden nur geringe Risiken bestehen, die durch eine geeignete Regulierung weiter minimiert werden können. Die Speicherkapazität unter der Nordsee ist ausreichend groß, um CO_2 , das in Zukunft in Europa abgeschieden werden muss, sicher zu entsorgen. Die Gesetzgebung in Deutschland soll im Jahr 2024 aktualisiert werden, um auch hier die CO_2 -Speicherung zumindest für bestimmte Anwendungen zu ermöglichen. Im BMBF-geförderten GEOSTOR-Projekt werden zurzeit die Chancen und Risiken der CO_2 -Speicherung in der deutschen Nordsee untersucht. Die laufenden GEOSTOR-Arbeiten zeigen, dass in der deutschen Ausschließlichen Wirtschaftszone erhebliche Speicherkapazitäten und potentiell geeignete Standorte vorhanden sind. Zudem untersucht GEOSTOR offene Fragen zu den Umweltrisiken, dem rechtlichen Rahmen, der Meeresraumplanung, der Speicherüberwachung sowie den Kosten für den CO_2 -Transport und die Speicherung, um den Weg für zukünftige industrielle CO_2 -Speicherprojekte in der deutschen Nordsee zu ebnen.

CCS-Monitoring mit Gravimetrie – eine Sensitivitätsstudie

N. Grobys¹, T. Roth¹, S. Petersen², M. Krieger²

¹ Wintershall Dea AG, ²TERRASYS Geophysics

Abstract

Carbon Capture and Storage (CCS) ist eine zunehmend wichtige Technologie zur Verringerung einer der Hauptursachen des Klimawandels – dem Eintrag von Kohlendioxid in die Atmosphäre. Bei der Planung von CCS-Projekten ist die Gewährleistung der sicheren CO₂-Speicherung von zentraler Bedeutung. Eine effektive und kostengünstige Überwachungsmethode der Verteilung des Kohlendioxids im Untergrund spielt hierbei eine entscheidende Rolle. Geophysikalische Methoden, insbesondere 4D-Seismik, sind gut zur Überwachung des Kohlendioxids im Speichergestein geeignet. Ein Monitoring der Sättigungsänderungen stellt dabei jedoch eine Herausforderung dar, für die sich 4D-Gravimetrie als vielversprechende und kostengünstigere Lösung anbietet. In der Studie wurden Berechnungen mit vereinfachten Modellen durchgeführt, um den Einfluss verschiedener Parameter (wie zum Beispiel Tiefe) auf gravimetrische Änderungen durch die Erhöhung der CO₂-Sättigung zu untersuchen. Es wurde auch geprüft, welche prinzipiell in Frage kommenden Messverfahren eine dafür geeignete Auflösung bieten. Die Ergebnisse zeigen, dass stationäre gravimetrische Messungen notwendig sind, um die Veränderungen im Reservoir zuverlässig zu erfassen. Um entscheiden zu können, in welchen Fällen 4D-Gravimetrie als vergleichsweise kosteneffektive und umweltfreundliche Methode für CCS-Projekte infrage kommt, ist im Vorwege immer eine detailliertere Modellierung des Speichers notwendig.

Einführung

Die Kohlendioxidspeicherung in geologischen Formationen wird zunehmend wichtiger, um die Ursachen des Klimawandels zu verringern. Ein wesentlicher Aspekt bei der Planung von CCS-Projekten ist es, eine sichere CO₂-Speicherung gewährleisten zu können.

Eine frühzeitige Evaluierung geeigneter Überwachungsmethoden, die auf die spezifischen Oberflächen- und Untergrundbedingungen des Speichers zugeschnitten sind, ist hierbei entscheidend. Methoden zum Monitoring der CO₂-Ausbreitung spielen dabei eine wesentliche Rolle. 4D-Seismik ist ein wichtiges und häufig verwendetes Werkzeug, das wegen des starken Geschwindigkeitskontrastes zwischen dem mit Sole und dem mit überkritischem CO₂ gefüllten Porenraum Hinweise zur Ausbreitung des Kohlendioxids liefern kann. Die Überwachung von Sättigungsänderungen ist mit dieser Methode schwieriger, weil die Geschwindigkeitsänderung mit zunehmender Sättigung weniger ausgeprägt ist. Durch den linearen Zusammenhang zwischen Sättigung und Dichte eignet sich die 4D-Gravimetrie, um die Informationslücke zu schließen.

4D-Gravimetrie ist bisher keine Standarduntersuchungsmethode für CO₂-Monitoring, wurde aber schon erfolgreich im Sleipner-Feld eingesetzt (Furre et al., 2016). Es ist zu erwarten, dass diese Methode nicht für alle CCS-Projekte zielführend ist, jedoch einen Mehrwert generieren kann, wenn das Reservoir über eine geeignete Kombination verschiedener Parameter verfügt. Als Entscheidungsgrundlage, ob es lohnenswert ist, 4D-Gravimetrie als Komponente eines CCS-Monitoring-Plans detaillierter zu evaluieren, wurde eine systematische Sensitivitätsstudie mit vereinfachten Modellen durchgeführt.

Überblick über das Auflösungsvermögen unterschiedlicher gravimetrischer Messmethoden

Für die Erfassung von gravimetrischen Daten stehen unterschiedliche Messverfahren zur Verfügung, die in statische und dynamische Systeme unterteilt werden (Tabelle 1).

Im Allgemeinen bewegen sich die Auflösungswerte von dynamischen Messsystemen in der Luft im Bereich von etwa 150 µGal, die je nach äußeren Einflüssen innerhalb eines Spektrums von 100 bis 300 µGal variieren können. Vergleichbare Auflösungen von 120 µGal (im Bereich von 100-250 µGal) lassen sich mit marinen Systemen erreichen. Dabei ist zu beachten, dass diese Angaben stets gemeinsam mit der Wellenlänge der aufzulösenden Anomalie betrachtet werden müssen, die wiederum von der Geschwindigkeit der Messplattform, der Messfrequenz und den angewandten Filtern abhängt; ferner wurden optimale und identische Bedingungen für die Wiederholungsmessungen angenommen. Diese vereinfachte Betrachtung ist für die hier relevante Fragestellung allerdings ausreichend.

Im Vergleich dazu können mit statischen Messsystemen deutlich bessere Auflösungen erreicht werden: 5-20 µGal für Land/Boden-Gravimeter und 3-10 µGal für Messungen am Meeresboden.

| Gravity survey type | Typical resolution | Resolution range |
|---------------------|--------------------|------------------|
| Airborne | 150 µGal | 100-300 µGal |
| Marine | 120 µGal | 100-250 µGal |
| Ground | 10 µGal | 5-20 µGal |
| Seafloor | 5 µGal | 3-10 µGal |
| Borehole | 3 µGal | a few µGal |

Tabelle 1: Übersicht über die Auflösung der Schweremessungen nach Beobachtungssystem, basierend auf Herstellerangaben. Unterteilung in dynamische (hellblau) und statische (grün) Messsysteme.

Methodik

Anhand von Beispielszenarien wurde der Einfluss von Tiefe und Größe des CO₂-Speichers auf die Messbarkeit von Schwereänderungen aufgrund von CO₂ Einspeicherung untersucht. Um verschiedene Szenarien leicht vergleichbar zu machen, wurden stark vereinfachte Dichtemodelle mit einer Größe von 107.000 m x 107.000 m x 3.500 m erstellt. Das Speichergestein wurde dabei als ein quaderförmiger Körper angenommen. Diese dreidimensionalen Modelle sind in Prismen unterteilt, deren Gravitationseffekte für jeden Beobachtungspunkt numerisch berücksichtigt werden. Im Ergebnisgebiet (54.800 m x 54.800 m) wurden im Abstand von 200 m Schwerewerte berechnet. Es wurden folgende Annahmen getroffen:

- Die Dichte des Hintergrundmodells bleibt zeitlich unverändert.
- Durch die kontinuierliche Injektion von überkritischem CO₂ ändert sich die Dichte der Porenraumfüllung.
- Die Porositätsverteilung innerhalb der Lagerstätte wird als konstant angenommen.
- Das injizierte CO₂ ist ideal homogen verteilt.

Damit wurde der gravimetrische Effekt der relativen Dichtevariation berechnet, die durch unterschiedliche CO₂-Sättigungsgrade entsteht.

Ergebnisse

Die Studie untersuchte gravimetrische Änderungen durch CO₂-Sequestrierung für

beispielhafte Untergrundspeicher mit Hilfe von vereinfachten geologischen Modellen. Für die Berechnungen wurden verschiedene Kombinationen von Tiefe, Mächtigkeit, Ausdehnung und Porosität verwendet. Wir zeigen hier exemplarisch drei Szenarien, die die Einflüsse verschiedener Parameter verdeutlichen:

| | Depth | Extension | Thickness | Porosity |
|-------------------|----------|-----------------|-----------|----------|
| Scenario A | < 2 km | 0,5 km x 2,5 km | 12 m | 35% |
| Scenario B | > 2,5 km | 3 km x 15 km | 140 m | 20% |
| Scenario C | < 2 km | 10 km x 20 km | 60 m | 14% |

Tabelle 2: Zusammenfassung der Beispilszenarien

Für alle Beispiele wurde die CO₂-Sättigung variiert und daraufhin die Schwereänderung (Abbildung 1-3) berechnet und deren Amplitude mit dem Auflösungsvermögen verschiedener gravimetrischer Beobachtungsmethoden und Messhöhen verglichen. Da Sole durch leichteres überkritisches CO₂ ersetzt wird, ergibt sich eine negative Dichteänderung, deren Gravitationswirkung ebenfalls negativ ist. Zur besseren Darstellbarkeit wird hier deren Absolutwert (positiv) illustriert. Sowohl dynamische Messungen an Bord von Schiffen, Hubschraubern oder Flugzeugen als auch stationäre an Land und am Meeresboden wurden betrachtet. Es zeigte sich deutlich, dass nur mit stationären Messungen aussagekräftige Informationen für die Szenarien B und C zu erwarten sind (vgl. Tabelle 1). Für Szenario A ergeben sich keine messbaren Schwereänderungen, was ein gravimetrisches Monitoring für einen vergleichbaren CO₂-Speicher ausschließen würde.

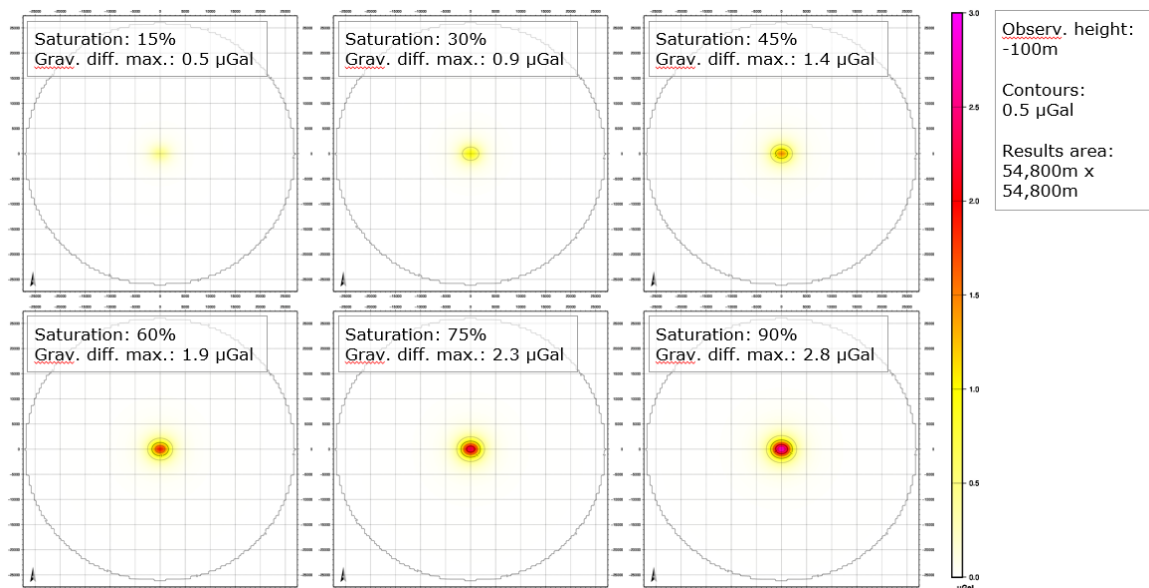


Abbildung 1: Gravimetrische Differenz mit steigender Sättigung für Szenario A.

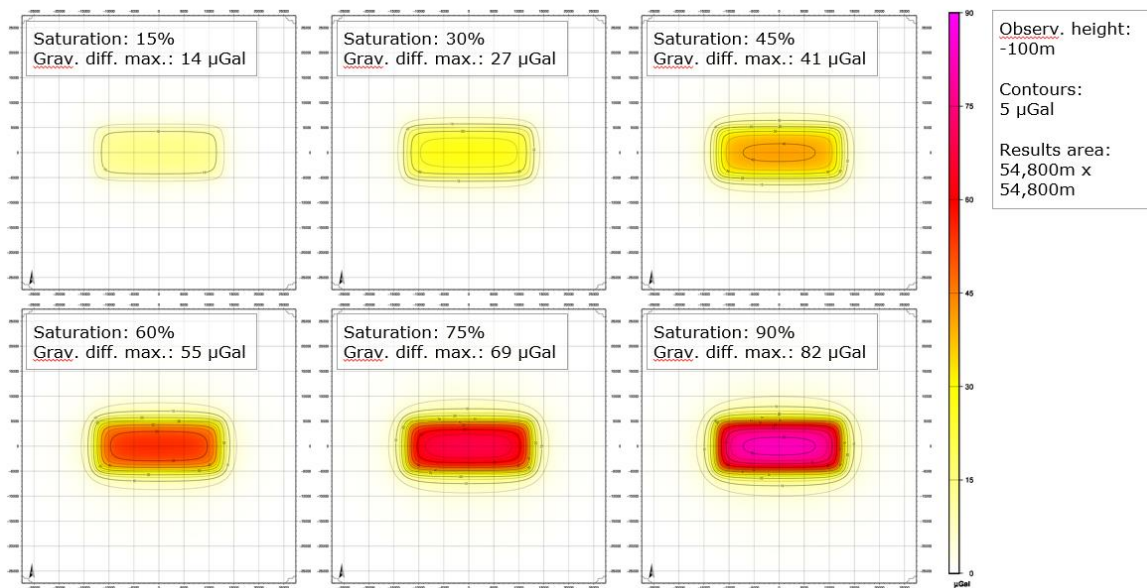


Abbildung 2: Gravimetrische Differenz mit steigender Sättigung für Szenario B.

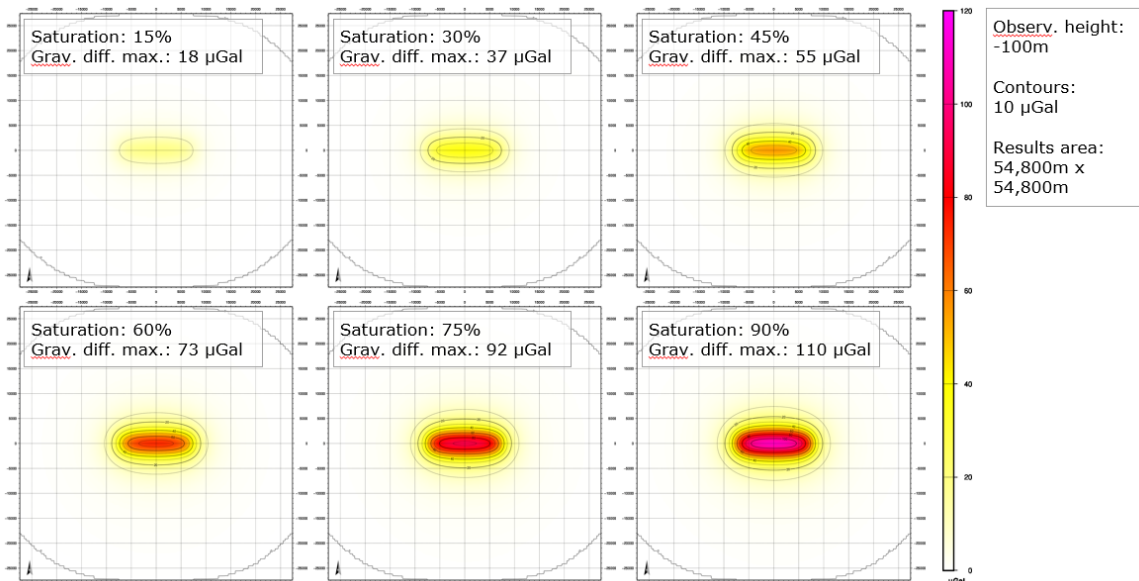


Abbildung 3: Gravimetrische Differenz mit steigender Sättigung für Szenario C.

Durch eine vereinfachte Geometrie und die Annahme einer homogenen, aber veränderlichen Sättigung ist es möglich, den Einfluss der einzelnen Speicher-Parameter systematisch zu untersuchen. Die hier angeführten Beispiele zeigen, dass besonders Mächtigkeit und die Größe des Speichergesteins einen Einfluss darauf haben, ob eine gravimetrisch messbare Wirkung entsteht. Auch in größerer Tiefe kann bei einem mächtigen Speichergestein eine auflösbare Differenzschwelle erreicht werden, die Konturen des Modellkörpers (hier ein Quader) sind jedoch durch die große Distanz zum Messniveau nicht mehr deutlich erkennbar (Abbildung 3).

Zusammenfassung

Die Sensitivitätsstudie zeigt, dass die gravimetrische Wirkung von Dichteänderungen durch die CO₂-Speicherung unter bestimmten Voraussetzungen mit statischen Messverfahren

detektierbar ist. Dabei haben besonders die Mächtigkeit und die Größe des Speichers einen Einfluss, ob ein messbarer Effekt bei Wiederholungsmessungen über einen längeren Zeitraum zu erwarten ist. Diese Studie hat stark vereinfachte Modelle verwendet, um eine Vergleichbarkeit zu erreichen und eine schnelle Übertragbarkeit auf andere potentielle CO₂-Speicher zu gewährleisten. Wenn 4-D Gravimetrie als Teil des Überwachungskonzepts für einen Speicher identifiziert wurde, sind detaillierte Modellierungen empfohlen, um eine genauere Ausgestaltung der Messungen planen zu können.

Literaturverzeichnis

Furre et al., 20 years of monitoring CO₂-injection at Sleipner, 13th International Conference on Greenhouse Gas Control Technologies, November 2016, Lausanne, Switzerland

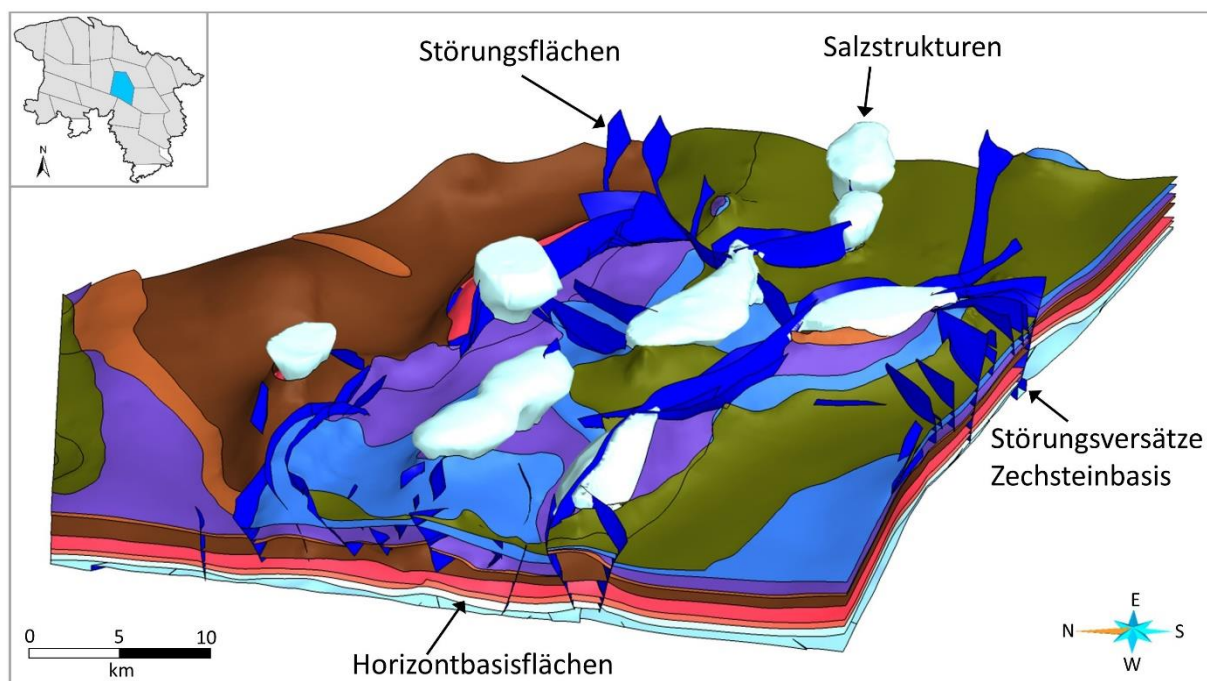
Ein neues generalisiertes geologisches 3D-Modell für Niedersachsen (TUNB3D-NI)

M. Helms, S. Sattler, C. Wangenheim, J. Ziesch, R. Schöner
Landesamt für Bergbau, Energie und Geologie, Hannover, Germany

Im Verbundprojekt TUNB (Tieferer Untergrund Norddeutsches Becken) haben die staatlichen geologischen Dienste Norddeutschlands gemeinsam mit der Bundesanstalt für Geowissenschaften und Rohstoffe (BGR) ein abgestimmtes und weitgehend grenzüberschreitend harmonisiertes geologisches 3D-Modell für ihre jeweiligen Landesgebiete erstellt.

Ziel dieses Vortrages ist es, die Vorgehensweise bei der Entwicklung des generalisierten geologischen 3D-Modells „Tieferer Untergrund Norddeutsches Beckens“ für Niedersachsen und Bremen (TUNB3D-NI) zu beschreiben [LIT01]. Eine der Herausforderungen war dabei der Umgang mit heterogenen und inkonsistenten Daten. Die Datengrundlage bildeten das Vorgängermodell „Geotektonischer Atlas von Niedersachsen und dem deutschen Nordseesektor als geologisches 3D-Modell“ (GTA3D) [LIT02], digital verfügbare Bohrlochdaten, tiefenmigrierte 2D- und 3D-seismische Daten aus der privatwirtschaftlichen Erkundung auf Kohlenwasserstoffe und Erdwärme und ergänzende Daten wie Mächtigkeits- und Strukturkarten lithostratigraphischer Einheiten.

Die geologische 3D-Modellierung wurde mit SKUA-GOCAD™ (AspenTech) unter Berücksichtigung der projektbezogenen Generalisierungsvorgaben und der geologischen Plausibilität durchgeführt. Das Modellergebiet wurde aufgrund seiner Größe in 20 Kacheln aufgeteilt; die Kachelgrenzen orientieren sich dabei am Strukturbau Niedersachsens. Es wurden Horizontbasisflächen, Salzstrukturen, horizontübergreifende Störungsflächen und senkrechte Störungsversätze an der Basis Zechstein als Modellbestandteile erstellt.



TUNB3D-NI, Modellkachel VER (Verden), Basishorizonte von Zechstein bis Jura, Salzstrukturen (hellblau) und Störungen (dunkelblau) (Darstellung 1,5-fach überhöht).

Automatisierte Verfahren waren nicht geeignet, um angemessen mit den Inkonsistenzen in den Eingangsdaten umzugehen, die aufgrund unterschiedlicher Quellen, Quantität und Qualität auftreten. Vielmehr erforderte dies die geologische Expertise des Modellierenden, der unter Berücksichtigung der regionalen geologischen Gegebenheiten die Daten gewichtete und ein plausibles, möglichst widerspruchsfreies Modell erstellte. Dabei wurden die geologisch unplausiblen Horizontüberschneidungen des GTA3D korrigiert. Aus senkrechten Störungsversatzflächen des GTA3D wurden mit Ausnahme der Basis Zechstein horizontübergreifende generalisierte Störungsflächen erstellt. Die Genauigkeit des Modells in Bezug auf die Bohrdaten konnte, im Vergleich zum Vorgängermodell, wesentlich bis um den Faktor 10 verbessert werden.

References:

- [LIT01] Bombien, H., Hoffers, B., Breuckmann, S., Helms, M., Lademann, M., Lange, M., Oelrich, A., Reimann, R., Rienäcker, J., Schmidt, C., Slaby, M. & Ziesch, J. , (2012), Der Geotektonische Atlas von Niedersachsen und dem deutschen Nordseesektor als geologisches 3D-Modell, ARGE GMIT, Geowissenschaftliche Mitteilungen, Bonn, 6-13, 48, <https://doi.org/10.23689/fidgeo-3901>
- [LIT02] Sattler, S., Helms, M. & Wangenheim, C. , (2022), Geologisches 3D-Modell Tieferer Untergrund Norddeutsches Becken für Niedersachsen und Bremen (TUNB3D-NI) – Abschlussbericht und Dokumentationen zu den Modellkacheln. Mit Beiträgen von Rienäcker-Burschil, J., Stehle, M., Wolf, M., Bombien, H. & Ziesch, Landesamt für Bergbau, Energie und Geologie (LBEG), Hannover, 230, <https://doi.org/10.48476/tunb3d-ni>

Das Geologiedatengesetz (GeolDG) - Zusammenspiel zwischen E&P-Industrie und den Staatlichen Geologischen Diensten am Beispiel des LBEG

H.-J. Brauner

LBEG, Hannover, Germany

Das im Juni 2020 in Kraft getretene Geologiedatengesetz (GeolDG) löst das Lagerstättengesetz von 1934 ab. Das Gesetz regelt die staatliche geologische Landesaufnahme, die Übermittlung, die dauerhafte Sicherung und die öffentliche Bereitstellung geologischer Daten sowie die Zurverfügungstellung geologischer Daten zur Erfüllung öffentlicher Aufgaben, um den nachhaltigen Umgang mit dem geologischen Untergrund gewährleisten und Geogefahren erkennen und bewerten zu können (§1, 1. Satz GeolDG). Das GeolDG regelt somit den Umgang mit „Geologischen Untersuchungen“ und beschreibt die Pflichten der Auftraggeber bzw. Ausführenden solcher Untersuchungen sowie der zuständigen Behörden. Dies sind i.d.R. die Staatlichen Geologischen Dienste (SGD) der Bundesländer.

So müssen z.B. die Geologischen Untersuchungen im Vorfeld bei dem zuständigen SGD angezeigt und im Nachgang die Daten und Ergebnisse umfänglich abgeliefert werden. Die SGD archivieren die Daten und stellen sie je nach Datenkategorie nach definierten Fristen der Öffentlichkeit bereit. Digitale Systeme zur Anzeige von Geologischen Untersuchungen sowie entsprechende Workflows zur Behandlung der abgelieferten Daten werden in den SGD aktuell erstellt. Richtlinien für die Kategorisierung von Nachweis-, Fach- und Bewertungsdaten (§3 GeolDG) wurden in den SGD erarbeitet und die praktische Umsetzung mit Hilfe von entsprechenden Bescheiden umgesetzt. Bezuglich des Umfangs und digitaler Formate von Daten und Ergebnissen Geologischer Untersuchungen wurden Merkblätter überarbeitet und mit der Erdöl-Erdgas-Industrie diskutiert, so dass ein pragmatisches, gesetzkonformes Vorgehen etabliert werden kann. Durch das GeolDG werden auch Daten früherer Geologischer Untersuchungen für die Öffentlichkeit über Kartenserver, Downloads oder spezifischen Anfragen bei den zuständigen SGD verfügbar und können in eigene Arbeiten einbezogen werden, über die wiederum berichtet werden muss.

In der Präsentation werden die Grundlagen des GeolDG, Aktivitäten der SGD, Pflichten der Industrie sowie Möglichkeiten zur Nutzung von Daten und Ergebnissen von Geologischen Untersuchungen vorgestellt.

Surfactant-based Diverting Agent for Acidizing: Lab Evaluation and Treatment of an Injector Well in a German Oil Field

N. Lummer

Fangmann Energy Services GmbH & Co. KG

Introduction

Employing diverting agents to prevent acids from leaking into the most permeable sub-layer of the target zone is common practice. These additives function by creating a temporary blocking effect which causes fluid diversion facilitating homogeneous and successful acidizing.

This paper focuses on a surfactant-based product with a tendency of forming rodlike micelles in acidic solutions. Here, a chaotic worm-like arrangement of dissolved molecules leads to a viscosity increase (see *Figure 1*). The use of a special breaker system effectively reduces said diverter viscosity and helps preventing formation damage.

After contact with acid systems, this surfactant-based diverting agent generates high viscous fluids

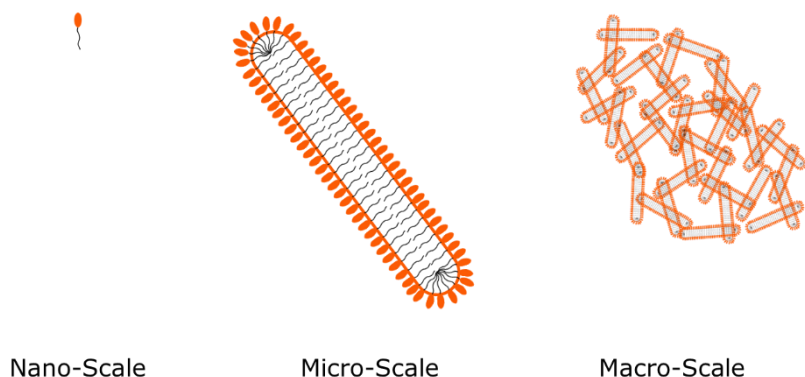


Figure 1: Working mechanism of surfactant-based diverting agent in acidic solutions.

Lab Testing

Lab experiments conducted prior to the field application included rheology measurements at bottomhole temperature (for test parameters, see *Figure 2*), corrosion testing with representative steel coupons, core flooding with sandstone samples, and breaker fluid optimization.

Rheology



Test parameters

- Test temperature: 60°C
- Differential pressure: 400 psi
- Rotational speed: 300 rpm
- R1 / B5 combination
- 1:1 Mixture of
 - 15% HCl + 5 L/m³ SCI-123
 - 100 L/m³ Diverting Agent SSD-550

Figure 2: Test parameters for rheology measurements at bottomhole temperature.

As shown in *Figure 3*, the viscosity of the acidic diverting agent system declines with time.

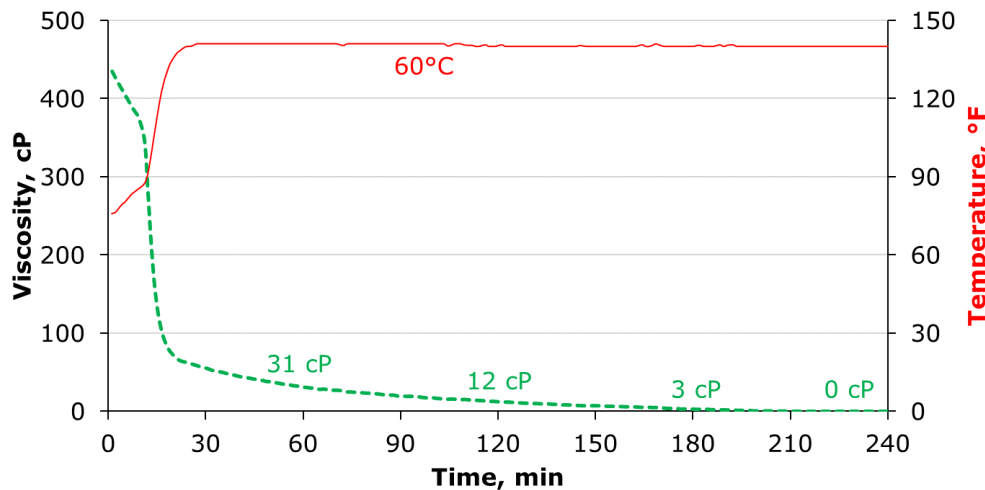


Figure 3: Viscosity of 7.5% HCl + 2.5 L/m³ SCI-123 + 50 L/m³ SSD-550, as measured at 60°C and 400 psi.

Core Flooding

As expected, pumping the viscous diverting agent system through the core resulted into a continuous increase in differential pressure. For test parameters, please consult *Figure 4*.

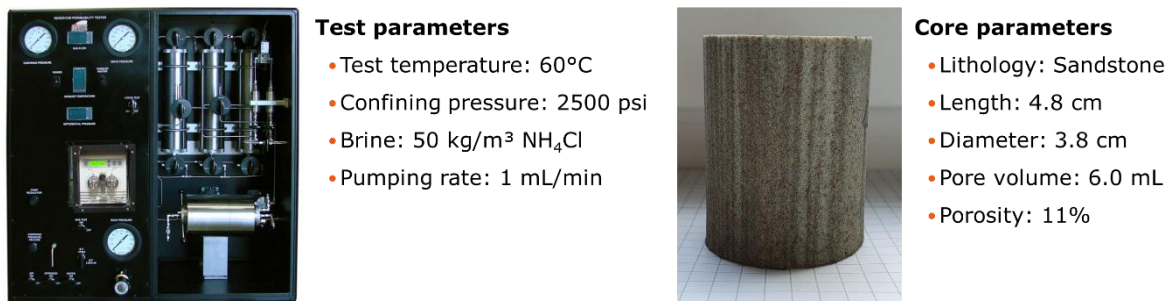


Figure 4: Test parameters for core flooding and characteristics of core specimen.

As visualized by *Figure 5*, the use of an optimized breaker system results into 95% regained permeability.

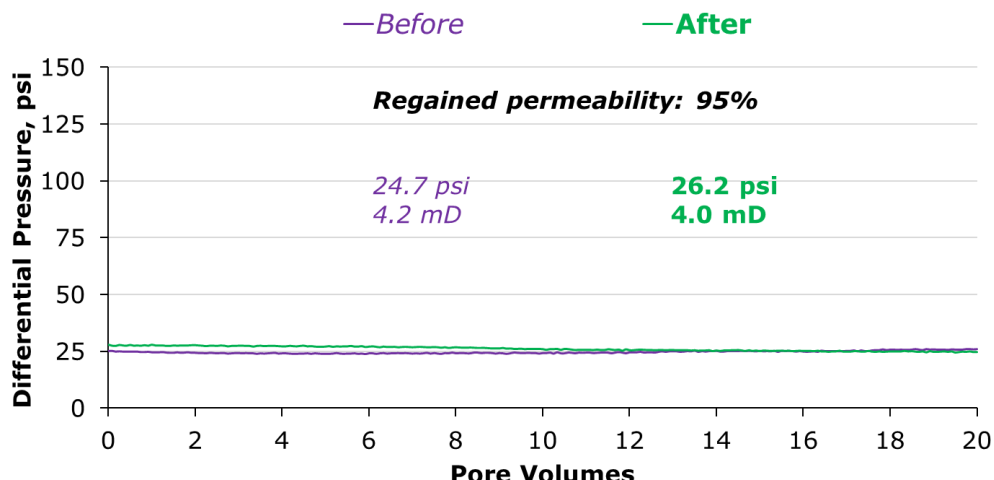


Figure 5: Results of core flooding tests before and after pumping an optimized breaker system.

Field Trial

For the actual treatment of the injector well in a Dogger formation, we alternated between acid and diverter steps in a volume-wise increasing approach. In total, 12 m³ of 15% HCl containing an adequate corrosion inhibitor dosage were pumped through tubing to a measured depth of approx. 1,400 m. Descaling of the two perforation zones with a length of 14 and 8 meters, respectively, was the goal of this application. 1 m³ / 2 m³ of the surfactant-based system followed each acid step for effective fluid diversion. Finally, 5 m³ of a special breaker concluded the acidizing job reducing diverter viscosity and hence counteracting formation damage.

Pumping Schedule and Fluid Composition

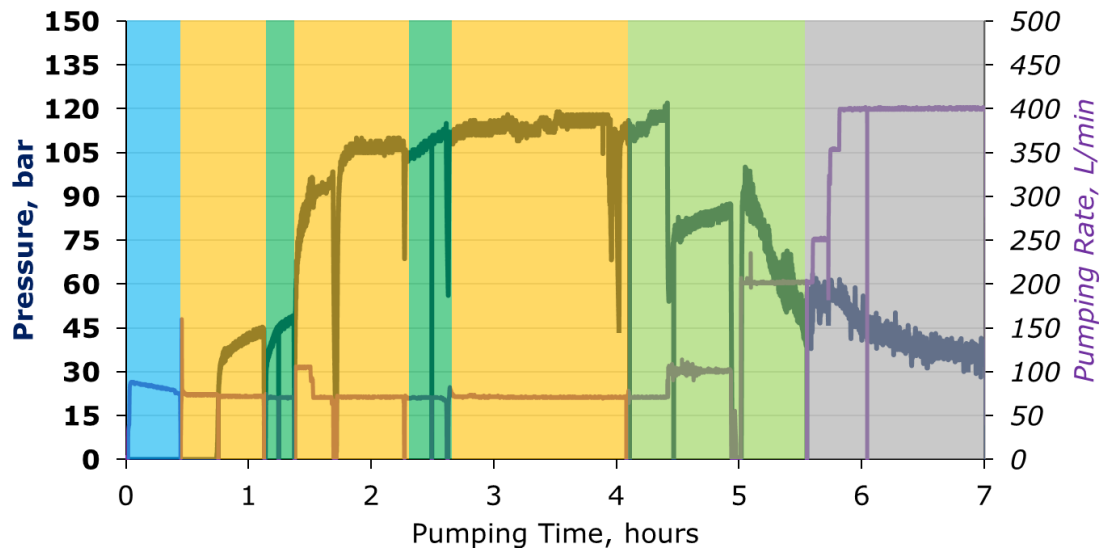
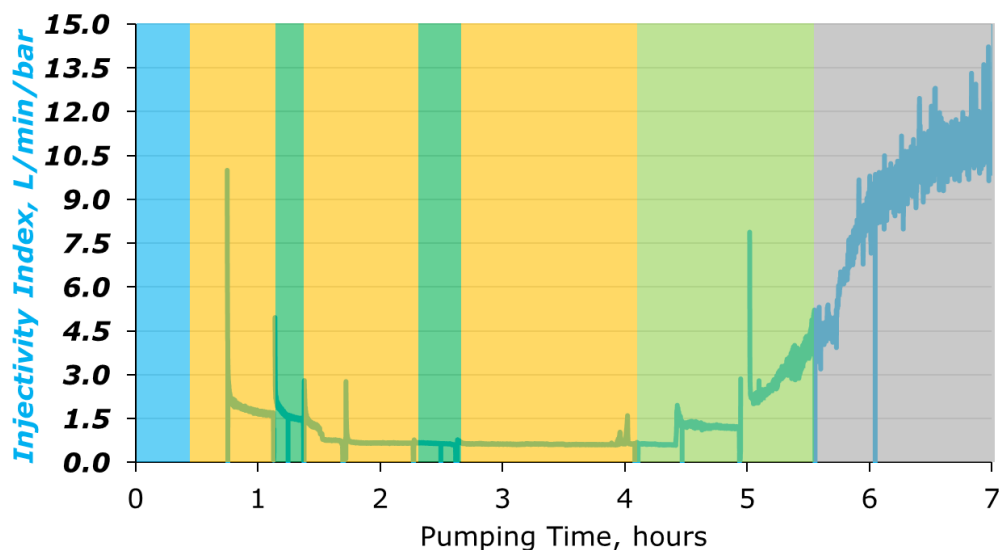
| Step | Fluid | Function | Volume | Composition | | |
|------|-------|------------|-------------------|-----------------|--------------------------------|--------------------------------|
| 1 | 1 | Pre-Flush | 2 m ³ | Water | + 100 L/m ³ SMS-300 | + 30 kg/m ³ SCC-220 |
| 2 | 2 | Acid | 3 m ³ | 15.0% HCl | + 5.0 L/m ³ SIC-123 | |
| 3 | 3 | Diverter | 1 m ³ | 7.5% HCl | + 2.5 L/m ³ SIC-123 | + 50 L/m ³ SDA-550 |
| 4 | 2 | Acid | 4 m ³ | 15.0% HCl | + 5.0 L/m ³ SIC-123 | |
| 5 | 3 | Diverter | 2 m ³ | 7.5% HCl | + 2.5 L/m ³ SIC-123 | + 50 L/m ³ SDA-550 |
| 6 | 2 | Acid | 5 m ³ | 15.0% HCl | + 5.0 L/m ³ SIC-123 | |
| 7 | 4 | Breaker | 5 m ³ | Water | + 500 L/m ³ SBR-300 | |
| 8 | 5 | Over-Flush | 40 m ³ | Formation water | | |

Equipment on Site



*Figure 6: FES-Equipment on site.***Short-term Results**

For evaluating treatment efficiency, we injected 40 m³ of formation water at ever increasing pumping rates and recorded the resulting pressure. Based upon these values, we determined a significant improvement of injectivity index directly after the job (see *Figure 7* and *Figure 8*).

*Figure 7: Recorded pressure and pumping rates during the application. Here, fluids are colour-coded as shown in the pumping schedule.**Figure 8: Calculated injectivity index. Here, fluids are colour-coded as shown in the pumping schedule.***Conclusion**

Long-term surveillance of well performance confirmed a two-fold increase in injection rate at constant pressure. Thus, lab and field results impressively proved the premium effectiveness of this surfactant-based diverting agent for acidizing. In close cooperation with our clients, we are currently planning additional applications in Germany.

Entwicklung und Erprobung eines Tools zur Scaleentfernung in Rohren mittels Elektro-Impuls-Verfahren

E. Anders¹, S. Klein²

¹TU Dresden, Professur für Baumaschinen, Dresden, Germany, ²TU Bergakademie Freiberg, Institut für Bohrtechnik und Fluidbergbau, Freiberg, Germany

Bei der Förderung von Thermalwässern, Trinkwasser sowie Erdöl und Erdgas aus Tiefbohrungen werden neben den gewünschten Rohstoffen meist auch Begleitstoffe in gelöster oder fester Form zutage gefördert. Durch die erhebliche Senkung von Druck und Temperatur im Förderstrang kommt es zu Ausfällungen und Ablagerungen dieser Stoffe in den Rohren. Es bilden sich sogenannte Scales. Diese können aus mehreren Schichten und Komponenten bestehen. Die Förderung kann durch das Scale-Wachstum innerhalb kurzer Zeit erheblich beeinträchtigt und die Wirtschaftlichkeit der Anlage entsprechend gefährdet werden. Außerdem kann es zu einer wesentlichen Erhöhung des Rohreigengewichts kommen.

Bis heute sind die Möglichkeiten zur Beseitigung von Scales auf chemische und mechanische Verfahren begrenzt und teilweise sehr ineffektiv. Beide Verfahren haben in Abhängigkeit vom Ort des Auftretens der Scales und deren physikochemischen Eigenschaften eigene spezifische Einsatzgebiete. Besonders schwer sind z. B. Baryt (BaSO_4) oder Galenit (PbS) Ablagerungen zu entfernen. Sie sind sowohl gegenüber chemischen als auch mechanischen Verfahren sehr widerstandsfähig. Deshalb ist eine Weiterentwicklung der vorhandenen Methoden bzw. die Entwicklung neuer Methoden zur schnelleren und effektiveren Entfernung von Ablagerungen erforderlich. Ein gänzlich neuer Ansatz zum Entfernen mineralischer Scales stellt dabei das Elektro-Impuls-Verfahren (EIV) dar.

Beim EIV werden Hochspannungsentladungen genutzt, um die Scales zu lösen. Es handelt sich hierbei um eine Weiterentwicklung eines Verfahrens aus der Tiefbohrtechnik, mit dem Hartgestein effektiver als bisher erbohrt werden kann. In dem vom BMWi geförderten Projekt „Entwicklung und in-situ Erprobung eines EIV-Bohrsystems (ISEB)“ wurde eine entsprechende Prototyp-Bohrgarnitur entwickelt. Diese Technologie kann, bei entsprechender Anpassung, grundsätzlich auch für Aufwältigungsarbeiten eingesetzt werden.

Die Stromversorgung ist bei dem neuen System gegenüber dem bereits entwickelten Bohrsystem sogar deutlich einfacher realisierbar. Da bei Work-Over-Arbeiten ein Stromversorgungskabel mitgeführt und die Ladespannung oberägig zur Verfügung gestellt werden kann, ist keine unterägige Stromerzeugung erforderlich, sondern lediglich ein Impulsspannungsgenerator zur Erzeugung der Hochspannungsimpulse.

Die konstruktive Herausforderung des zu entwickelnden Prototyps besteht darin, alle EIV-Komponenten von einem 12 1/4“ Rohrdurchmesser auf 4 1/2“ Rohrdurchmesser herunter zu skalieren. Nach erfolgter Konstruktion, Entwicklung und Durchführung von Funktionstests einzelner Komponenten, wurde das Prototyp-System gefertigt und in ersten Tests in Rohrsegmenten mit Scales auf einer institutseigenen Bohranlage bzw. Versuchsstand erprobt. Der Beitrag behandelt die Entwicklung und experimentelle Erprobung des Prototyps, sowie einen Ausblick auf die Fortführung des Projektes.

Use of hydrogen as a fuel towards the decarbonization of gas turbines

E. Zindel

Siemens Energy, Erlangen, Germany

Hydrogen combustion in gas turbines and combined cycle power plants is emerging as the preferred technology to cover the residual load during longer periods of "dark doldrums" (unavailability of both wind and solar energy) in a fully decarbonized power system. This applies as well for gas turbines used for mechanical drive (like in pipelines), where -in addition to a trend towards electrification of compression stations- we will continue to see the use of turbo compressor sets, which will need to be decarbonized in the next 10-20 years.

However, it needs to be noted that there are some locations in the world where it must be assumed that a connection to a hydrogen backbone network will not be possible or the required amounts of carbon-neutral hydrogen molecules at an acceptable price for re-electrification will not be made possible at the power plant fence.

As a consequence, and in addition to hydrogen, other fully or partially carbon-neutral fuels are also moving into the focus of gas turbine designers: Apart from various fuels of biogenic origin, hydrogen derivatives such as e-ammonia and e-methanol should also be mentioned here.

The presentation will show the current development situation of hydrogen combustion in gas turbines at Siemens Energy and will also present the first operating experiences from pilot plants. In addition, an outlook on other greenhouse gas-neutral fuels will be given. Finally, an update on reference plants and the latest status on "H2 readiness" (preparation for subsequent conversion to hydrogen) will be shown.

Health, Safety and Environment – Positive impact on HSE using drones

Stefan Wirth¹, Iulian Dinu²

¹Christof Industries Global GmbH, Graz, Austria; ²J Christof Industries E&P Services SRL, Bucharest, Romania

Abstract

For several years now, Christof Industries Romania, a subsidiary of Christof Industries Global, engaged in the inspection of pipelines for the timely detection of leaks. Due to the terrain (off road, hilly, forests) such inspections were carried out until recently almost exclusively by foot. These activities, repeatedly, resulted in incidents - Tick and dog bites to name a few. Additionally, the environment is a challenge when it comes to the rescue and transport of injured persons.

Due to this, since commencement of this type of activity, there was a drive to improve the way the task is performed, leading to a safer work environment for the employees but at the same time making the leak detection more reliable while staying within the budget limitations imposed by the existing contract with the client.

The rapid developments in the field of UAVs (Unmanned Aerial Vehicle), commonly referred to as Drones, very quickly showed off to be the ideal solution. Christof Industries Romania invested in this technology and developed the necessary inhouse competences. Since about a year, a big portion of pipeline inspection are now carried out by drones, with a significant positive impact on our HSE KPIs.

This paper is describing the used UAVs and the associated camera and sensor technology. The advantages and limitations of this technology will be discussed and the impact on HSE explained. Also, an outlook will be given on potential applications in the future. Finally, a look will be taken on the financial side to demonstrate that once again investment in safety also leads to cost reduction.

Introduction

Romania is a country of tremendous natural beauty with a wide spread of encountered landscapes. It is home to the largest natural forest still to exist in Europe, its south is dominated by the flat lands of Valahia with its huge crop fields, to the east it is bordered by the Black Sea, while its central parts are dominated by the mountains that form the eastern Carpathians. What might not be so commonly known is that Romania also represents the cradle of the Oil and Gas Industry, with the world's first refinery established in 1858 in Ploesti, north of Bucharest, making Bucharest the first capital city where oil lamps were illuminating the streets at night. Due to this long history in O&G, the country, that is 2/3 the size of Germany, has a wide-spread infrastructure that allows for the production, transport and refinement of oil and gas.

On the O&G transport side, large portions of the country are covered by a net of pipelines, connecting wells to gathering stations, tank farms to refineries, etc. While there is a constant effort by operators to maintain and replace old pipelines the average age of this infrastructure is on the high-end side. This, together with good operating practices, require for a constant verification of pipeline integrity via a variety of methods. One – until recently – irreplaceable

method is the inspection of the pipeline by individual inspectors (called Liniori) that walk along the pipeline. Their task is to look for any indications that the pipeline would suffer from a leak. As these pipelines are more often than not running through natural environments, these inspections can become quite difficult, and the evolved personnel are exposed to a variety of risks.



Figure 1: Actual Pipeline-Route in a forest in west Romania

Christof Industries Romania (CIR), who is performing such inspection services for a leading Romanian operator in the O&G sector, has therefore encountered multiple incidents in the past, including several Loss Time Incidents (LTI).

The major reason for incidents comes from the wildlife. Stray dogs are still a common sight in parts of Romania, and they can exhibit a rather violent behaviour, especially if paired with rabies. Occasionally wild dogs are “trained” by locals to scare away or even attack strangers. This resulted in several LTIs related to dog bites. Much smaller but not less dangerous can be the exposure to certain insects, bees, ticks, and there like, but also snakes are a common sight. CIR reacted to this by different means, from behavioural training of the Liniori, over adaption of the Personal Protective Equipment (PPE) to vaccinations and emergency communication means.

With all these measures in place a certain risk remains, and CIR was committed to reduce this risk even further. It quickly became clear that only the removal of the human component in this type of activity would allow for a further risk reduction and the technological advances from the recent years allowed for a few options. Finally, we settled for the UAVs as they seemed to offer the most flexibility for the task.

The UAVs used in CIR

The project consists in full-service and take over responsibility of every stage along the inspection cycle through our 360° approach.

UAV used: DJI Matrice 300 RTK with 4 sets of battery available

Inspection modules used:

- DJI H20T main camera
- Sniffer 4D V2 gas sensor
- Flir VUE TZ20-R thermal camera
- DJI Matrice Wingsland Z15 LED Spotlight
- DJI U10 laser methane detector

1. The DJI Matrice 300 RTK is a professional-grade, industrial drone, designed for commercial and industrial applications. It features a maximum flight time of up to 55 minutes, and a payload capacity of up to 2.7kg. It can fly in harsh weather conditions with its IP45 rating (Protected from low pressure water jets from any direction). The drone has advanced safety features, such as obstacle avoidance sensors and an ADS-B receiver for detecting nearby aircraft. It is also equipped with DJI's RTK technology for centimeter-level accuracy in mapping and surveying applications. The Matrice 300 RTK is widely used for industrial inspections, search and rescue operations, and agriculture applications.
2. The DJI H20T is a high-end, multi-sensor camera system designed for commercial drones. It features a 20 MP zoom camera with a 6.83-119.94 mm (equivalent: 31.7-556.2 mm) lens, a 12 MP wide-angle camera, a radiometric thermal camera with a 640x512 resolution, and a laser rangefinder with a range of up to 1200m. The H20T also has a 1/1.7-inch CMOS sensor, 3-axis gimbal stabilization, and can capture 1920x1080 video at 30fps. The H20T is primarily used for aerial inspections, search and rescue operations, and surveying applications.
3. The Sniffer 4D V2 gas sensor is a highly sensitive and accurate device (0,01 PPM sensitivity) used for detecting and measuring the concentration of various gases in the air. It uses a proprietary sensor technology that allows for real-time, simultaneous detection of up to four different gases, such as carbon monoxide, methane, hydrogen sulfide, and H2S and more. The Sniffer 4D V2 has a compact and rugged design,

making it suitable for use in harsh industrial environments. It also has wireless connectivity, enabling remote monitoring and data logging. The gas sensor is commonly used in applications such as environmental monitoring, industrial safety, and leak detection.



Figure 2: UAV Matrice 300 RTK with controls, cameras and sensors

4. The Flir VUE TZ20-R is a high-resolution thermal imaging camera designed for use in industrial and commercial applications. It features a 640x512 resolution thermal sensor, which can detect temperature differences as small as 0.03°C, and a 20x zoom lens, allowing for precise and detailed imaging from a distance. The camera has a built-in radiometric system that allows for accurate temperature measurement and analysis. The Flir VUE TZ20-R is also equipped with a digital video output for real-time streaming and recording of thermal footage. The camera is commonly used in applications such as building inspections, search and rescue operations, and industrial monitoring.
5. Wingsland Z15 is an advanced LED spotlight designed for use with DJI Matrice series drones. It features a powerful 3-axis gimbal system that can rotate up to 360 degrees. The spotlight has a maximum output of 48,000 lumens. It is controlled through the drone's remote controller, and can be adjusted for brightness, color temperature, and light projection angle. The Wingsland Z15 LED spotlight is commonly used for nighttime inspections, search and rescue operations, and cinematography.
6. The DJI U10 methane sensor is a high-precision methane detection device designed for use in industrial and environmental applications. It uses a non-dispersive infrared

(NDIR) sensor to detect methane gas with a concentration range of 0-5% volume. The sensor is integrated with DJI's Matrice series drones, allowing for remote detection and mapping of methane emissions from a safe distance. The U10 methane sensor is lightweight and easy to operate and has a maximum detection range of up to 100m. The sensor is commonly used in applications such as oil and gas pipeline inspections, landfill monitoring, and environmental research.

Operational Benefits and Limitations

Benefits

Besides the HSE benefits, that are discussed in the following section, the use of the UAVs has demonstrated several benefits.

Inspections are carried out significantly faster. While a Liniori manages in average five to six kilometers of pipeline per 8h shift, the common inspection length for one drone is 120km at the same time. It must be mentioned that this is only achieved if no leak indication is found. If the operator would see leak indications, the drone is used at much lower speed and altitude in order to verify the leak and its exact position.

As the drone is airborne it can naturally inspect objects (e.g. inside of facilities) that are hard or impossible to reach on foot. Accurate positioning via GPS ensures that the drone can hover at very exact location and revisit them with minimal deviation. Points can be set up in a flight program, allowing for a fully automated inspection flight. Similarly, the leaks can be measured in location very accurately, both in 2D and in 3D.

Of practical importance is the significantly faster flow of information. As the drone is constantly connected to the mobile operator station the reaction time between leak detection and information to the pipeline operator is substantially reduced and practically almost instant. Due to this constant communication and the multiple sensors / cameras, a wealth of data is available and enables in detail analysis and comprehensive documentation.

Operating the UAVs for over a year now, the ongoing operations have demonstrated that high quality results are obtained regardless of the light situation or the season. It is however necessary to utilize the sensors and cameras accordingly and to look for partly different leak indications.

Limitations

Besides these obvious benefits there are some limitations to keep in mind. From legal side, drone operations are not possible over or adjacent to flight control zones that can often be encountered at airports, military installations, or critical infrastructure. Besides that, it is not permitted to fly over inhabited areas without a specific flight authorization. Throughout the European Union it is in general required to constantly maintain visual sight of the drone, compromising a full autonomous flight. There is in general the possibility to seek for a permit to fly drones out of sight, but this is depending on the country a lengthy process and not always successful.

On the technical side a limiting factor is the battery lifetime. Standard operations allow for approximately 45 minutes of airtime, due to safety considerations batteries are however never used to below 30% charge, hence the practical airtime is about 30 minutes.

An important role also plays the encountered wind speed and as per the manufacturers instructions no flights are performed at wind speeds above 50km/h. Practically this has led to one non-operational days in the last 7 months out of about 140 operational days.

The vast amount of data collected is streamed live over GSM to the mobile operator station.

In locations where no or only very weak GSM signal is available, the drone stores all data on an internal storage card that can in such cases be collected during the change of the batteries. This however means that data is available only with a delay and might lead to additional time delays if leak indications are found within the offline data and the drone needs to return to this location for more detailed inspection.

Finally, it is to be mentioned, that servicing of the drones with the manufacturer / retailer currently takes quite long.

Impact on HSE Performance

As already mentioned, the impact on HSE was the major driver for CIR to establish its drone team and operations. At this point we like to take a closer look on what this means.

Health

Many companies in Romania, including CIR, are suffering from the fact that many young Romanians decide to seek for a career abroad. Especially the O&G sector is looking at a work force of a very high average age. This of course comes with natural challenges when talking about the health of the work force. Every worker that is not used for inspecting the pipelines will experience a positive health impact due to elimination of the risk for:

- Heat stroke / heat exhaustion
- Dehydration
- Frostbite
- Allergic reactions (Insects, pollen, contact to plants)
- Diseases transmitted by animals and insects (e.g. rabies, tick born encephalitis)
- Exhaustion

Safety

The pipeline inspections are most of the time carried out by one person. Due to the remoteness and partial roughness of the terrain, a variety of safety risks exist for this task:

- Slips trips and falls on the uneven terrain
- Fall from height
- Cuts and bruises
- Animal attacks (dogs, wolfs, bears, etc.)
- Exposure to pipeline medium

These risks are paired with the issue of alerting emergency services and the possibilities to quickly reach an injured person in a remote location.

Fortunately, CIR never had any fatalities in these services, however, as indicated before, we had several LTIs and multiple Medical Treatment and First Aid incidents.

Environment

The task of inspecting the pipelines serves an important environmental purpose, the timely and accurate detection of leaks that would lead to an environmental pollution. As the drones are much faster in their work, this enables to increase inspection frequencies. Additionally, the bird eye view gives a different possibility for easy detection of plant life anomalies that could be an indication for a leak. The well-trained drone data interpreters are able to use the vast amount of data generated by the drone's cameras and sensors, paired with the in house developed software for data screening and interpretation to find leaks that ground bound inspectors do not. This has already been demonstrated in our operation's multiple times. As already mentioned, there are limitations and therefore specific applications where a Liniori is

still needed, but for the vast majority of cases the drone detection is superior.

As a side note, a drone does not disturb the natural wildlife when flying in 50m altitude above ground and naturally also does not damage plant life like a human inspector, even when being careful, would do.

Risks

To conclude on the HSE aspects one shall not forget that there are of course some new risks introduced by using the drones. There is a small possibility that a fault in the drone or a misjudgment of the drone operator could lead to an uncontrolled crash. With the weight of the drone of max 9 kg, considering a normal working altitude of 50m, such a crash would most definitely lead to a fatality in case a human would get hit directly. Rules set up by the European Union are however in place to minimize such risk and we are not only strictly obeying to them but are performing our own risk assessments for all the routes we service.

Another risk comes from bird strike, that may or may not lead to a drone crash and would likely lead to a severe if not fatal injury of the bird. While the drones are equipped with an automatic anti-collision system, a bird strike from the side cannot be completely ruled out.

A final work on the risk of explosion, which is always a relevant risk to look at in the O&G industry. The drone by itself is not EX-proof, however the camera and sensor systems allow for a distance to the inspection object of up to 100m. Given the maximum wind speed of 50km/h at which a drone operation is possible and a maximum working altitude of 50m, there does not exist the physical possibility that a falling drone would crash into the test object. Nevertheless, especially for more complex facilities it is imperative to carefully select flight routes to ensure that even in a crash land scenario no hazardous areas are compromised. Also keep in mind that for a crash landing an ATEX proof drone would not help as the impact may lead to sparks and faulty batteries to sparks or excess heat and even flames.

Financial Considerations

While the drone and its attached cameras/sensors come with a significant investment need, the savings obtained for the application of inspecting pipelines that shall be discussed here, quickly bring in these investments.

As indicated above, one Liniori manages in average to inspect 6km of pipeline per 8h shift. For the drone we assume 90km per 8h, as it will not always operate at the maximum speed. This means, the drone achieves the workload of 15 Liniori.

For each Liniori the following monthly costs accumulate:

| | |
|---|-----------|
| Salary, including all taxes and contributions and allowances: | 1400 Euro |
| Transport, PPE, communication, tools and sensors: | 100 Euro |
| Total: | 1500 Euro |

Therefore, the traditional approach creates costs of 22500 Euro per month for 15 Liniori.

Looking at the costs for one drone per month we can consider:

| | |
|---|-----------|
| Insurance: | 200 Euro |
| Transport and follow vehicle, including leading, fuel, maintenance: | 1100 Euro |
| Software license: | 200 Euro |
| Average drone maintenance: | 475 Euro |

| | |
|-------------------------------------|-----------|
| Personnel (1 Operator, one Driver): | 4700 Euro |
| Total: | 6675 Euro |

This demonstrates that running costs are only 1/3rd when comparing drones with Liniori. To put it differently, one drone for this application saves approximately 15800 Euro per month.

Considering the upfront investments:

| | |
|--|----------|
| Drone: | 50k Euro |
| DJI H20T main camera: | included |
| Sniffer 4D V2 gas sensor: | included |
| Flir VUE TZ20-R thermal camera: | included |
| DJI Matrice Wingsland Z15 LED Spotlight: | included |
| DJI U10 laser methane detector: | 45k Euro |
| Total: | 95k Euro |

With this we are looking at a repay time of about 6 month or in half of a year! This does not take in account other effects like depreciation.

Note: the above shows numbers based on Romanian salary levels, naturally the results will vary in different countries depending on them.

Note: Christof Industries does not lay off personnel due to technological advances. The employees are used for more sophisticated tasks instead and are also given the opportunity for developing their skills.

Outlook on future fields of application

As already indicated, there are multiple fields of application and CIR has only started on its journey to explore potentials for its customers. Besides application in Oil & Gas like

- Leak detection on pipelines
- Power line inspection
- Facility inspection
- Metal detection
- Firefighting assist
- OGMP 2.0

There also exists applications in other industries and for society:

- Renewable energy (solar and wind farms)
- Agriculture
- Infrastructure inspection
- Search & Rescue
- Cinematography & Photography
- Industrial real estate
- Forestry
- Telecommunication and power lines
- Traffic control

While there is still much to explore, at this point two potential future activities that CIR is looking into shall be briefly described:

Solar and Wind Parks

The DJI Matrice 300 RTK can be used in inspections for both solar farms and wind farms to collect aerial data and conduct visual inspections of critical components. For solar farms, the Matrice 300 RTK can capture high-resolution images and videos of solar panels, cables, and support structures, allowing inspectors to identify potential issues such as damage, defects, or anomalies. The drone's RTK technology enables it to capture accurate data for 3D mapping and modeling of the solar farm, including terrain mapping and topographical analysis. Additionally, the Matrice 300 RTK can be equipped with thermal imaging cameras or other sensors to detect hotspots, electrical faults, or other anomalies that may not be visible to the naked eye.

For wind farms, the Matrice 300 RTK can be used to inspect wind turbines and their components, including blades, towers, and nacelles. The drone can capture high-resolution images and videos of these components from a safe distance, allowing inspectors to identify potential issues such as cracks, corrosion, or damage. Additionally, the Matrice 300 RTK can be equipped with thermal imaging cameras or other sensors to detect hotspots or other anomalies that may indicate problems with the turbines. Using the Matrice 300 RTK for inspections in both solar farms and wind farms can increase the efficiency and accuracy of maintenance and repair efforts, leading to cost savings and improved performance of the renewable energy assets.

Agriculture

The DJI Matrice 300 RTK can be used in agriculture to collect aerial data and perform various tasks that can improve crop yields and efficiency. Here are some examples of how the Matrice 300 RTK can be used in agriculture:

- **Mapping and Surveying:** The Matrice 300 RTK can be used to create high-resolution maps of farms and fields, which can help farmers to identify problem areas, track crop growth, and plan their operations more effectively.
- **Crop Health Monitoring:** The drone can be equipped with multispectral or thermal imaging cameras to monitor crop health and detect issues such as pests, diseases, or irrigation problems.
- **Precision Agriculture:** The Matrice 300 RTK can be used for precision agriculture tasks such as crop spraying, seeding, or fertilization.
- By using drones to perform these tasks, farmers can reduce the use of chemicals and water, save time and money, and improve crop yields.
- **Livestock Management:** The drone can be used to monitor and track livestock, including counting animals, detecting health issues, and identifying escapees.
- **Infrastructure Inspections:** The Matrice 300 RTK can be used to inspect agricultural infrastructure such as buildings, fences, and water systems, allowing farmers to identify and address issues more quickly.

Overall, the DJI Matrice 300 RTK can provide farmers with valuable insights and data to help them make more informed decisions and improve their operations.

Conclusion

With over one year of practical experience in the industrial application, Christof Industries can confirm that the use of drones in the Oil & Gas industry is beneficial for efficiency and flexibility, but foremost for safety reasons. This is coupled with financial savings. For us a clear win-win situation. There are of course significant investments necessary, these however quickly pay off. What this initiative also demonstrates is the necessary transition away from labor that requires for less competence but a high amount of work force toward

labor that comes with very high competency requirements but only for a few employees.

The applications for this technology are many and we are certain that innovative thinking will lead to even more in the near future.

Öffentliche Beteiligung im Geomonitoring – Der Erfolg am Untergrundgasspeicher Epe

T. Rudolph¹, P. Goerke-Mallet¹, A. Müterthies², S. Teuwsen², C. Tomlik¹, C.-H. Yang

¹Forschungszentrum Nachbergbau (FZN) der Technischen Hochschule Georg Agricola (THGA), Bochum,

²EFTAS Fernerkundung Technologietransfer GmbH MünsterInstitutions

Abstract

Integrated geo- and environmental monitoring in the provision of geo-resources represents a high-dimensional challenge (location, altitude/depth, time, sensors). This process is already challenging for experts, but poses major problems for a multitude of stakeholders and affected parties to build up a complete understanding of the process here. The research cooperation Epe has the goal to make the ground movement at the cavern storage Epe explainable with a public participation process and to build transparency in the influencing factors of the ground movements. For this purpose, the research cooperation was founded by the City of Gronau, the citizens' initiative Kavernenfeld Epe e.V., the company EFTAS GmbH, Münster and the Research Center of Post-Mining of the Technische Hochschule Georg Agricola, Bochum. In addition, this project is supported by the operators in the cavern field. In the research cooperation, the mine survey maps will be merged with the results of the areal radar interferometry (SBAS method) and with the public geodata available on site in order to obtain an extended overall picture. At the same time, this technical work is accompanied by a public participation process. The results show that, in addition to mining-induced ground motion, other processes influence the movement of the day surface, especially at the edge of the mining impact area. The scientific-neutral research cooperation thus represents a direct bringing together of the most diverse participants in a mining-related project. With the applied tools, the mine surveying-technical monitoring develops towards an integrated geo- and environmental monitoring with the development of an extended, transparent process understanding.

Introduction

The provision of georesources represents an intervention in nature and the environment, in which the intervention and the consequences become visible on the surface. But, in the case of underground gas storage, the provision only partially visible. Mine surveying, geo- and environmental monitoring serve to technically monitor and to build up an understanding of the process, thus supporting public participation. This public participation process goes beyond simple communication ("communication of results") and represents a multilateral participation of the different stakeholders.

The cavern field Epe – Public perception

The rural and former bog area of the Epe cavern field is located in the north-west of North Rhine-Westphalia in the German-Dutch border area of Gronau (D) and Enschede (NL). On 24 July 1964, the Epe-1 well was drilled and the Zechstein salt discovered (Figure 1). The salt layer was then developed and is now used for underground brine extraction and product storage (Natural gas, Helium, Hydrogen) in more than 114 caverns. The mining-induced ground movements in the cavern field proceed very slowly and evenly, with a seasonal overprint recognisable (withdrawal, injection, weather).

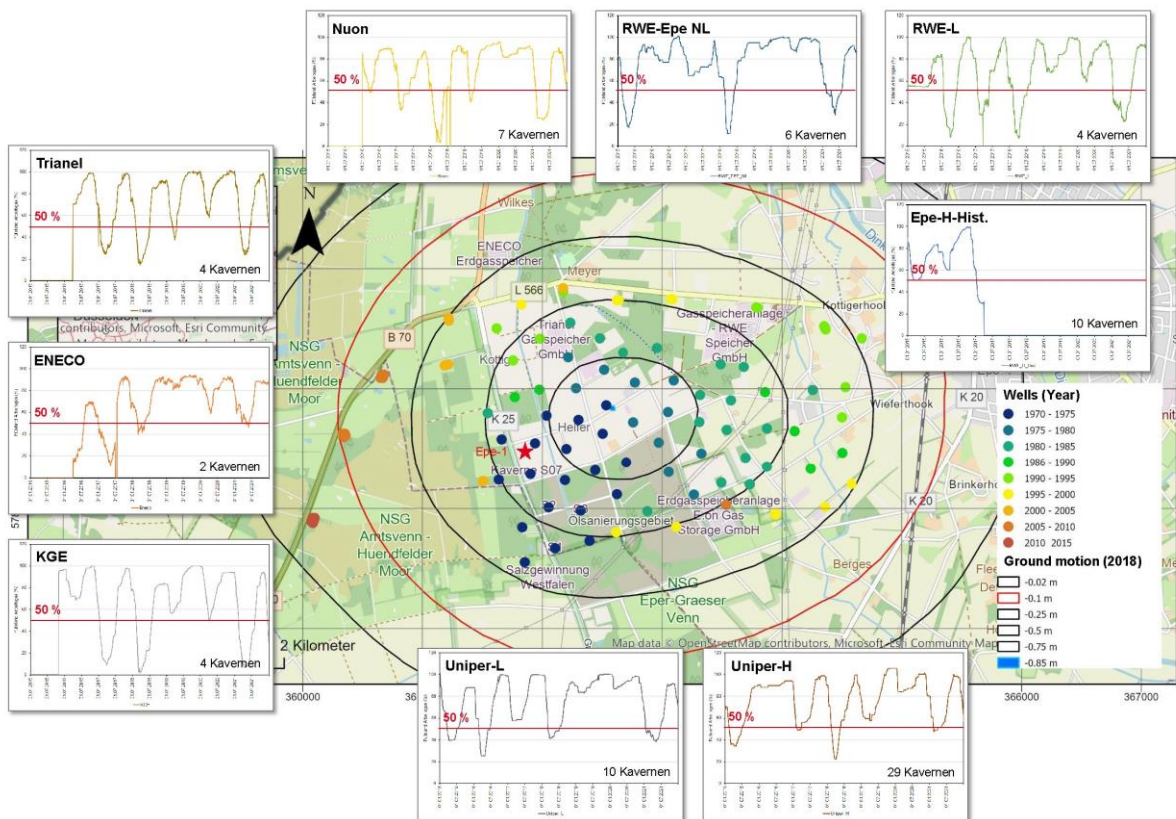


Figure 1: Location of the cavern field and its subsidence bowl and operational data (rough location) (AGSI+ 2022, SGW 2018).

On 12 April 2014, a serious operational accident occurred in the operation of the cavern field, which caused damage to nature and the environment (BezReg 2014). This accident triggered a broad public discussion on the monitoring of cavern storage facilities and the ground movement. The entire process is closely watched by the local citizens' initiative "BI-Kavernenfeld Epe e.V."

This public discussion gave rise to the "Epe Research Cooperation" with the cooperation partners City of Gronau, BI-Kavernenfeld e.V., EFTAS GmbH, Münster and the Research Center of Post-Mining Technische Hochschule Georg Agricola, Bochum. A resolution was passed by the Committee for Mobility, Environment and Climate Protection (A-MUK), which was unanimously accepted by the representatives and has the objectives:

1. Deepening a technical understanding of borehole mining and underground storage in the context of ground motion and determining the area of impact.
2. Use of methods of radar-satellite remote sensing (EU-Copernicus programme) to increase the areal monitoring frequency as well as the retrospective time series analysis using the documentation of the mine surveyor, GNSS measurements of Geobasis NRW, open geodata (e.g. Geobasis NRW, Geoportal NRW) as well as on-site analyses
3. Integrated understanding of ground movements at the edge of the subsidence bowl
4. Development of an understanding of the hydrological and hydrogeological development of the cavern field, especially from the point of view of flood protection with in the subsidence bowl
5. Bringing together competences, stakeholders and citizens for on-site analysis and science transfer
6. Scientific-technical and independent processing of the questions

Public participation

Social trust - especially in science - is a valuable asset that should be built up and continuously maintained. This is especially true in projects of the mining life cycle with an influence of the nature and the environment plus at the same time a change in social perception as well as the rapid availability of information (via the internet, social media). This made it necessary to actively build up transfer measures to generate understanding for the scientific working methods and the results obtained, and to maintain the social and subjective trust of the citizens. The challenges lay primarily in communicating scientific and technical content to the target group of citizens with their different requirements and experiences and also established opinion. The secondary goal was to stimulate an understanding that would enable a fact-based assessment of the past, present and future developments of the cavern use.

As an essential link, a website (www.monitoring-epc.de) was set up to communicate openly the content, the dates and the results of the research cooperation. Also very active press relations were developed (Figure 2). In this way, transparency is achieved for the (sub-)surface work and trust is built up. As an important tool for participation, the website included a WebGIS with publicly available and official geodata and a public poll to submit questions and remarks.

Success story geomonitoring

The integrated workflow, taken from post-mining projects, with the evaluation of the mine surveys, the available, public geodata plus an extensive internet and literature research showed an overlapping of different effects that can trigger ground movement in the area of the cavern field Epe (Figure 2).

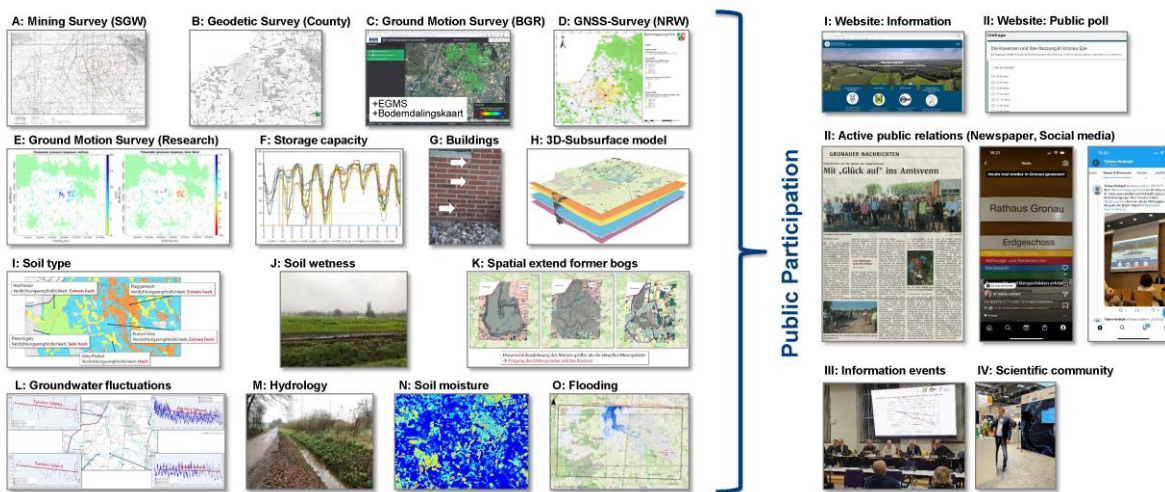


Figure 2: Presentation of the results of the geodata fusion (AGSI+ 2022, Biologische Station Zwillbrock 2010, BBD 2023, ELWAS 2022, EO-Browser 2022, GeoBasisNRW 2022, GeoPortal 2022, SGW 2018, SUBI 2022, Theis 2020).

The consequences of climate change also play an important role here. The reasons of the ground movement which could lead to possible damage to buildings are:

1. Underground cavern operations (mining induced)
2. The residual bogs of the Amtsvenn-and Hündtfelder-Moor with the partly peat cut and agriculturally used areas
3. Strong fluctuations of the groundwater level
4. Decomposition of biomass through air supply to the soil
5. Former floodplain areas along the receiving waters with water level fluctuations

6. Locally very differently developed, settlement-sensitive soils with a strong tendency to form waterlogging
7. Old scattered settlements, some of which are >60 years old, with modern upgrading of building envelopes and extensions.

Conclusions

The production of brine and the underground storage of chemical products represents an intervention in nature and the environment and thus has a direct impact on the surface and on the public. In this respect, borehole mining is a special case, as the processes take place underground and is therefore not visible. Only the surface effects, such as ground movements, represent a visible effect that can trigger immediate changes to buildings and infrastructure or even to water bodies.

The changes in the nature of public perception, climate change, but also the changed need to ensure security of supply for Germany, make extended geo- and environmental monitoring and intensive participation formats necessary in addition to the classic, mine surveying. This public participation makes it possible to bring transparency into these complex geoscientific-technical processes in order to make the underground use of space more resilient.

The evaluation of the available geodata for the Epe cavern field shows that the geoscientific-technical situation here is complex. Part of the cavern field is covered with a bog area and soils with a high organic content. The soils are very sensitive to subsidence. At the same time, the groundwater level is very low and the strong groundwater level fluctuations lead to buoyancy loss and decomposition in the soil, which again triggers ground movements.

The spatial radar interferometry (SBAS) is an important addition to the ground movement in the mine survey. The application of this method provided spatially and temporally highly resolved ground movements and made it possible to clearly separate the influencing variables of ground movement for the Epe cavern field (Figure 3). Thus, the results of the time series analysis show the direct influence of the changed precipitation and soil types.

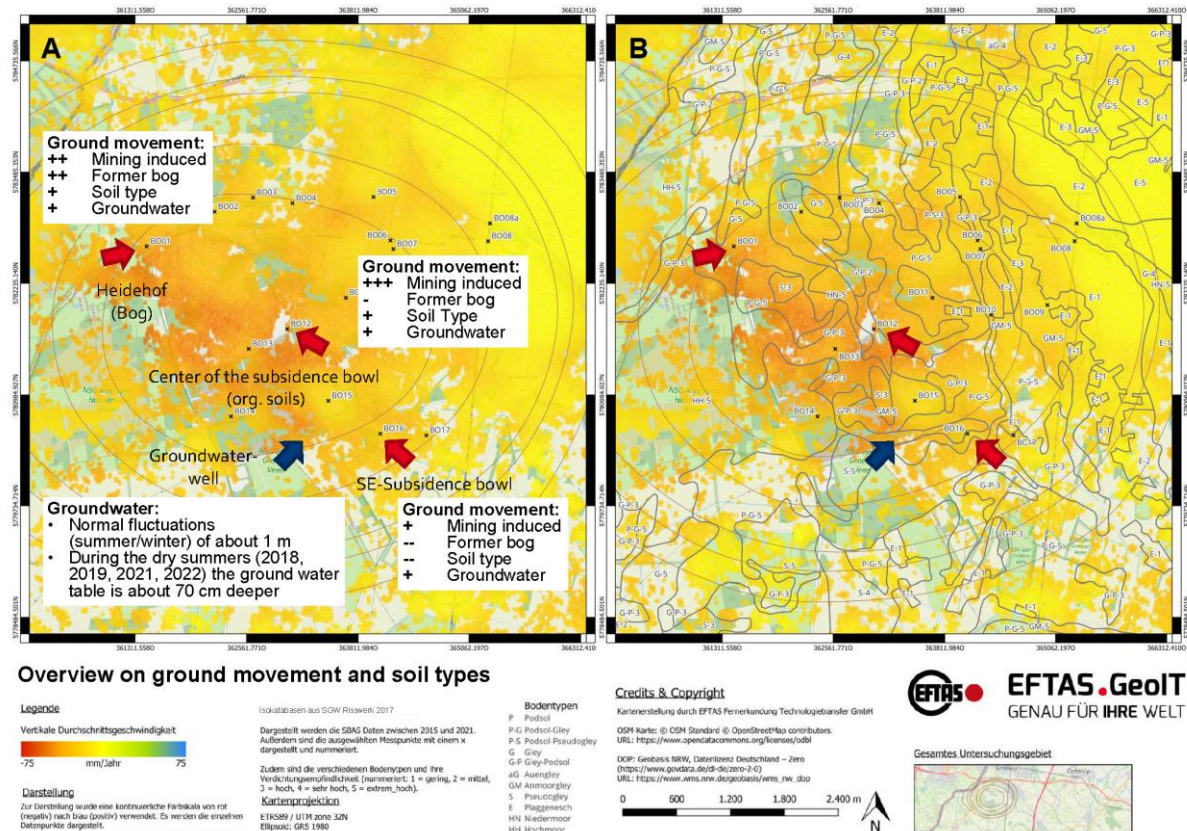


Figure 3: The results of the cumulative ground movement (2015-2021) (A) in comparison with the map of local soil types (B).

The visits over the course of the year of the research cooperation have shown the seasonal changes and also the interaction with the influence of climate change (reduced precipitation) and the prevailing hydro-(geo-)logical conditions. These fundamental findings are important in order to evaluate the results from radar satellite remote sensing in the future and to expand the mine survey with this.

For the first time in German mining, the Epe research cooperation with its partners represents a modern and innovative format for confidence building. Only through direct and open as well as scientifically neutral cooperation could a deeper understanding be achieved here among all those involved in borehole mining at the cavern field Epe. This integrated workflow, taken from post-mining projects, with the fusion of the mine survey, the use of radar interferometry, geodata and experience towards an integrated geo- and environmental monitoring could make the process of ground movement at the Epe cavern site explainable. The complexity and the approach to the processing show that a future continuation of the questions also at other sites where geo-resources are provided is necessary for the development of social operator responsibility.

Acknowledgements

The authors would like to thank the city of Gronau, in particular the mayor Mr. Rainer Doetkotte, the city planning officer Mr. Ralf Groß-Holtick and the other colleagues in the administration and the council for their support and professional exchange (contract 23.7.2021). The District Government of Arnsberg, Department 6, Mining and Energy in NRW, the District Government of Cologne, GeoBasis NRW and the District of Borken - FB62 Geoinformation and Real Estate are thanked for their support during the process. The members of the citizens' initiative Kavernenfeld Epe e.V., especially the chairman Mr. Holger Perrevort, are thanked for the good and intensive cooperation. Thanks are due to the

Chairman of the Committee for Mobility, Environment and Climate Protection in the City Council of Gronau, Mr. Josef Krefter, and the Deputy Chairman, Mr. Wolfgang Rövekamp, for their cooperation in the steering committee. Special thanks are due to Mr. Markscheider Stefan Meyer of the Salzgewinnungsgesellschaft Westfalen mbH for the technical exchange, the provision of data sets and the inspection of the site. We would also like to thank the various operators of gas storage facilities in the cavern field and their members in the operators' group for the diverse discussions. Special thanks go to Mr. Jost Müller and his colleagues from Uniper Energy Storage GmbH for the opportunity to visit the cavern facility. Please insert the text of your manuscript and figures here.

References

- AGSI+ (2022): Aggregated Gas Storage Inventory – Remit Storage Data; <https://agsi.gie.eu/#/>; 17. April 2023
- BezReg (2015): Jahresbericht 2014 der Bergbehörden des Landes Nordrhein-Westfalen. – 140 S.; https://www.bra.nrw.de/system/files/media/document/file/jahresbericht_2014_berg.pdf; 17. April 2023
- Biologische Station Zwillbrock (2010): Schutz für Moor und Heide – Die Naturschutzgebiete Amtsvenn und Hündfelder Moor. 2. S., <https://www.bszzwillbrock.de/fileadmin/dateiverzeichnis/wir/publikationen/amtsvennflyer.pdf>, 17. March 2010
- BBD (2023): BodenBewegungsdienst Deutschland.; <https://bodenbewegungsdienst.bqr.de/>; 17. April 2023
- ELWAS (2022): Fachinformationssystem ELWAS für die Wasserwirtschaftsverwaltung in NRW; <https://www.elwasweb.nrw.de/elwas-web/index.xhtml>; 17. April 2023
- EO Browser (2022): Sentinel Hub; <https://apps.sentinel-hub.com/eo-browser/>; 17. April 2023
- GeoBasis NRW (2022): Produkte und Dienstleistungen; https://www.bezreg-koeln.nrw.de/brk_internet/geobasis/wir-ueber-uns/index.html; 17. April 2023
- Geoportal NRW (2022): Webservice Geodaten NRW; <https://www.geoportal.nrw/>; 17. April 2023
- SGW (2018): Salzbergwerk Epe / Untergrundspeicher – Bodenbewegungsriß Gesamtsenkung 1972 – 2018. Karte im Maßstab 1:10.000
- SUBI (2022): SUBI - Safety of Underground Gas Storage Sites - Sicherheit von Untertagespeichern bei zyklischer Belastung: Funktionalität, Integrität und Überwachung von Speichern und Bohrungen; <https://www.subi-ugs.de/index.php>, 17. April 2023
- Theis, K.-P. (2020): Bodenbewegung im Bereich der SGW in Gronau Epe - 17.08.2020 Ausschuss für Verkehr, Energie und Tierschutz der Stadt Gronau, https://gronau.ratsinfomanagement.net/tops/?_U=UGhVM0hp2NXNFDcExjZX-c0a0xSEAOmcl7Mb_AOQg, 17. April 2023

Monitoring induzierter Seismizität in Niedersachsen aus operativer Sicht

T. Bartels

Wintershall Dea Deutschland GmbH

Abstract

Bei einem durch die Gasförderung induziertem Ereignis in Niedersachsen, ist es möglich, dass es zu Erschütterungen kommt, die zu leichten Gebäude Schäden wie z.B. Putzrissen führt. Zur Beweissicherung solcher Schäden werden im Raum Völkersen die Erschütterungen mit Hilfe eines Monitoring Netzes aufgezeichnet und ausgewertet. Diese Datengrundlage wird genutzt, die Schäden schnell und unbürokratisch zu regulieren.

Der Vortrag beschreibt das Vorgehen der Wintershall Dea aus operativer Sicht.

Introduction

Seit Beginn der Förderung 1992 wurden im Bereich des Gasfeldes Völkersen mehr als 20 seismische Ereignisse registriert. Etwa weniger als die Hälfte dieser Ereignisse waren an der Oberfläche spürbar, d.h. mit einer Schwinggeschwindigkeit $> 0.3 \text{ mm/s}$, die anderen Ereignisse wurden nur mittels installierter Sensoren aufgezeichnet.

Die fünf stärksten Ereignisse aus den Jahren 2008, 2012, 2016, 2019 und 2021 erreichten Magnituden zwischen 2,8 und 3,1. Die maximal gemessene Schwinggeschwindigkeit im Bereich des Feldes Völkersen betrug 5,25 mm/s.

Eine solche Schwinggeschwindigkeit kann zu leichten Schäden an Gebäuden führen (feine Risse im Putz, Bodenfliesen und Fugen). Wintershall Dea hat Verantwortung übernommen und Schäden innerhalb des vom LBEG festgelegten Einwirkungsbereiches unbürokratisch und zeitnah reguliert.

Das Monitoring Netzwerk

Zur Dokumentation und zur Beweissicherung werden die norddeutschen Gasfelder mit Hilfe des Bergschadenkundlichen Beweis Sicherungssystem (BBS System) des BVEG überwacht. Das Messsystem umfasst ein Netzwerk aus Seismometern sowie zusätzlich an der Oberfläche in Gebäuden installierten Schwingungsmessgeräten.

Die Seismometer dienen der Ortung der seismischen Ereignisse. Vor dem Hintergrund einer entsprechenden behördlichen Auflage ermöglicht die Auflösung des Systems die Ortung aller

seismischen Ereignisse mit Magnituden ≥ 2 mit einer Genauigkeit von ± 500 m horizontal und ± 1000 m vertikal.

Die Schwingungsmessgeräte an der Oberfläche erfassen die Bodenschwinggeschwindigkeiten oberhalb der Gasfelder. Sie dienen der Beweissicherung im Falle eines Ereignisses. Ihre Daten können gemäß DIN 4150 ausgewertet werden.

Das Messnetz ist in der Lage seismische Ereignisse automatisch zu detektieren. Es kann dabei zwischen Oberflächenerschütterungen durch Tätigkeiten an der Oberfläche, wie z.B. Baustellen und seismischen Wellen aus der Tiefe zu unterscheiden. Die aufgezeichneten Daten werden der Öffentlichkeit in Echtzeit auf einer Website (www.seis-info.de) zur Verfügung gestellt, auf Nachfrage wird der komplette Datensatz in digitaler Form Behörden und Forschungsinstituten bereitgestellt um Detailauswertungen zu ermöglichen.

Isoseistenkarten

Im Bereich Völkersen wurde das seismische Messnetz von Wintershall Dea sukzessive ausgebaut. Diese verbesserte Datenbasis ermöglicht eine genaue Bestimmung der Schwinggeschwindigkeiten an der Oberfläche. Durch die erhöhte Anzahl von Messgeräten und der damit verbesserten Datendichte ist es möglich, eine genaue Berechnung von Isoseisten durchzuführen. Isoseisten sind Linien gleicher Schwinggeschwindigkeiten. Diese dienen als Datenbasis für die Aufsichtsbehörde für die Bestimmung eines Einwirkungsbereichs (EWB). Innerhalb des EWB gilt eine Beweislastumkehr, der Bereich wird für den Regulierungsprozess bei möglichen Schäden genutzt. Aufgrund unterschiedlicher Herdpositionen der Ereignisse muss die Berechnung des EWBs für jedes stärkere seismische Ereignis erneut durchgeführt werden, da sich die Bereiche erhöhter Erschütterungen mit jedem Ereignis verschieben.

Rekomplettierung von Ölkavernen zur Schaffung eines Überwachungsfähigen Ringraums am Kavernenspeicher Etzel

S. Patzer¹, C. Reekers²

¹ESK GmbH, Freiberg, Germany, ²STORAG ETZEL GmbH, Friedeburg, Germany

Die Storag Etzel baut, betreibt und vermietet am Standort Etzel seit 1971 Kavernen. Zurzeit sind 51 Gasspeicher- und 24 Ölspeicherkavernen mit einem Speichervolumen von 4,3 Mrd. m³ Gas bzw. 10 Mio. m³ Rohöl in Betrieb.

Im Rahmen von turnusmäßigen Workover-Arbeiten an Kavernenbohrungen sollte zusätzlich ein überwachungsfähiger Ringraum nachgerüstet werden. Die zusätzliche Barriere verhindert einen direkten Kontakt des Speichermediums Rohöl mit der letzten zementierten Rohrtour und erhöht damit die Betriebssicherheit der Kaverne zusätzlich.

Eine wesentliche Zielstellung bei der Planung der neuen Komplettierung war die hydraulische Optimierung des Gesamtsystems, um Einbußen der Leistungsfähigkeit (Ein- und Auslagerungsraten) zu minimieren. Für die zu installierende Rohrtour waren darüber hinaus die auftretenden Beanspruchungen des Speicherbetriebs zu analysieren und die Auslegung der Rohre dementsprechend vorzunehmen.

Die am Standort Etzel vorhandenen Kavernen wurden zunächst in Typkavernen unterteilt (Teufenlage, Bohrpfad, Dimension IzRT), um mögliche Dimensionen der Schutzrohrtour zielgerichtet und effizient zu ermitteln. Im Anschluss an die Dimensionierung des Rohrmaterials folgten Detailbetrachtungen aus denen geeignete Verbinder abgeleitet wurden und die Bewertung der gesamten Komplettierung hinsichtlich Erfüllung der hydraulischen und mechanischen Anforderungen. Zusätzlich war in diesem Prozess auch das Packersystem auszuwählen und die hieraus resultierenden Anforderungen an die Gesamtkomplettierung ebenfalls zu berücksichtigen. Zur Auswahl der Vorzugsvariante(n) der gesamten Komplettierung wurden auch die erforderlichen Abläufe der Installation analysiert, gegenübergestellt und detailliert bewertet.

Der Vortrag gibt einen Einblick in die Entwicklung des Rekomplettierungskonzeptes. Weiterhin wird über die Realisierung der Maßnahme berichtet und Optimierungsmaßnahmen einzelner Arbeitsschritte, nach mittlerweile 14 rekomplettierten Bohrungen, vorgestellt.

Planung und Durchführung einer Kavernenflutung unter Berücksichtigung der geologischen Rahmenbedingungen und nachgeschalteter Gaskonditionierung

M. Geisweller¹, R. Buzogany², S. Donadei², A. Gaßner³

¹wesernetz Bremen GmbH, Bremen, Germany, ²DEEP.KBB GmbH, Hannover, Germany, ³Nord-West Kavernengesellschaft mbH, Wilhelmshaven, Germany

Am Standort Bremen-Lesum hat die wesernetz Bremen GmbH (wesernetz) über Jahrzehnte eine Speicheranlage mit zwei Gasspeicherkavernen betrieben. Im Zuge der Übergabe der Kavernen an den Erdölbevorratungsverband (EBV) wurden die Kavernen geflutet, um das in den Kavernen befindliche L-Gas aus den Kavernen zu entnehmen und eine Zustandsprüfung der Verrohrung im Bohrloch durchzuführen. Beide Flutungsmaßnahmen der wesernetz wurden von der DEEP.KBB GmbH (DEEP.KBB) ingenieurtechnisch geplant und begleitet.

Die Flutung der Kaverne L203 weist im Vergleich zu Flutungen anderer Kavernen Besonderheiten auf, da sie zeitlich nach der Umstellung des Gasnetzes in Bremen von L-Gas auf H-Gas durchgeführt wurde. Da L-Gas einen geringeren Brennwert aufweist und somit nicht mehr den Anforderungen an die Gasqualität entsprach, konnte das ausgelagerte L-Gas aus der Kaverne nicht ohne Weiteres in das Gasnetz eingespeist werden. Um das L-Gas entsprechend der Netzanforderung energetisch aufzuwerten, wurde nachgeschaltet über eine Konditionierungsanlage LPG (Propan/Butan) beigemengt. Die Gasauslagerung aus der Kaverne war folglich mit den betrieblichen Möglichkeiten der Konditionierungsanlage sowie mit der Verfügbarkeit von LPG abzustimmen.

Im unteren Kavernenbereich entstand während des Solprozesses eine unruhige Kavernenkontur. Um einen weiteren unregelmäßigen Solprozess in diesem Bereich zu vermeiden, wurde der untere Kavernenbereich mit gesättigter Sole geflutet, während der obere Kavernenbereich mit Wasser aus der benachbarten Lesum geflutet wurde.

Die Flutung der Kaverne L203 wurde nach einem Zeitraum von ca. einem Jahr im Mai 2022 erfolgreich abgeschlossen. Insgesamt wurden ca. 192.000 m³ Sole und 105.000 m³ Lesumwasser in die Kaverne verpumpt und ca. 30 Millionen Nm³ L-Gas aus der Kaverne produziert und energetisch aufgewertet.

Der Beitrag gibt einen Überblick über die Planung und Umsetzung des Flutungsprozesses. Dabei wird insbesondere auf die operativen Besonderheiten im Hinblick auf die energetische Aufwertung des L-Gases zu H-Gas und die speziellen geologischen Gegebenheiten eingegangen.

Aktuelle Forschungsaktivitäten zu gebirgsmechanischen Aspekten in Verbindung mit der Wasserstoffspeicherung in Salzkavernen

K.-H. Lux, T. Pan, J. Sun-Kurczinski, J. Zhao

TU Clausthal, Lehrstuhl für Geomechanik und multiphysikalische Systeme, Clausthal-Zellerfeld, Germany

Im Rahmen der Energiewende kann die Wasserstoffspeicherung in Salzkavernen aufgrund der großen Speicherkapazität, der hohen Förderleistung, des geringen Landschaftsverbrauchs und der relativ niedrigen Investitionskosten dieser untertägigen Anlagen einen wesentlichen Beitrag zur auch zukünftigen Versorgungssicherheit leisten. Bei der Umstellung von der Speicherung von fossilen Energieträgern zur Speicherung von grünem Wasserstoff sind auch gebirgsmechanische Aspekte zu betrachten – aufgrund der komplexen Prozesse in Kavernen und umgebendem Salinargebirge sowohl aus thermodynamischer wie auch thermohydromechanischer Sicht. In diesem Artikel werden in einer ersten Forschungsaktivität die potentielle Kapazität und Leistungsfähigkeit der Wasserstoffspeicherung in bestehenden Salzkavernen in Niedersachsen vorgestellt. Im Rahmen dieses Forschungsprojektes werden u.a. Grundlagen aus gebirgsmechanischer Sicht zum Potential der Wasserstoffspeicherung in niedersächsischen Salzkavernen erarbeitet, die dann in einem größeren Rahmen für energiepolitische Planungen und Entscheidungen herangezogen werden können.

Unabhängig von einem Neubau oder einer Umrüstung von Kavernen wird die technische Sicherheit der Gesamtanlage Salzkaverne und Zugangsbohrung vorausgesetzt. Die Zustandsanalyse des Bohrungsausbaus der Zugangsbohrung, insbesondere einer schon bestehenden Bohrung im Fall einer bereits langjährig betriebenen und für Wasserstoff umzurüstenden Kaverne, ist daher für das weitere Integritätsmanagement von zentraler Bedeutung. In einem zweiten Forschungsprojekt wird daher die Bohrungsintegrität aus gebirgsmechanischer Sicht unter besonderer Berücksichtigung von Überzugswirkungen aus der Kaverne analysiert. Im Beitrag werden zentrale Aspekte betrachtet, die bei der mechanischen Analyse und Bewertung der Bohrungsintegrität von Bedeutung sind.

Bei der Ermittlung derartiger Überzugswirkungen auf den Bohrungsausbau sind zwei Situationen zu betrachten: die Konvergenzbedingten Einwirkungen aus der eigenen Kaverne und die Einwirkungen aus Nachbarkavernen im Rahmen großräumiger Gebirgsbewegungen. Damit geht es dann in einem dritten Forschungsprojekt u.a. auch um die Validierung von Simulationsmodellen, um die Kavernenkonvergenz möglichst realitätsnah zu erfassen.

Ein vierter Forschungsprojekt schließlich betrifft den Dichtheitstest (MIT). Mit dem Dichtheitstest muss zukünftig nunmehr auch für Wasserstoff belegt werden, dass zu Beginn des Speicherbetriebes die Bohrungsintegrität gegeben ist. Vor diesem Hintergrund wird versucht, die während des Dichtheitstests ablaufenden hydromechanischen Prozesse zu identifizieren und rechnerisch nachzuvollziehen, um auf diese Weise ein verbessertes Verständnis für die auf Prozess- und Systemebene während des Testes ablaufenden Phänomene zu erarbeiten, vielleicht auch später die Auswertungsgrundlagen zu erweitern.

Dry Recompletion of two gas storage cavern wells in UK

A. Lennox, A. Sloan, C. McMichael
Atkins Ltd

Abstract

Client: Confidential

A client had removed two gas storage caverns from service due to integrity issues with the original completions. The client requested that Atkins develop plans for the recompletion of the wells to return the caverns to service. During concept development Atkins proposed recompleting the wells utilising the “dry” recompletion method by isolating the well from the cavern with plugs to remove the need to rewater the cavern to “wet” recomplete as has historically been conducted. This concept was approved by the client and after detailed design and procurement of equipment and services, the Atkins project team managed and supervised operations on site for the duration of the project. The project was complex and took place while the gas plant remained operational throughout the project. Both wells returned to gas storage service, ahead of schedule and on budget with no HSE incident during the workovers at the Tier 1 COMAH site.

In 2022 Atkins provided a multi-disciplinary team of engineers and project support staff to deliver the project to ensure the caverns were available for use during the peak winter months.

It is intended to present the technical aspects related to the “dry” recompletion and the process that Atkins undertook to plan and enact these.

Key words: Gas Storage Caverns, United Kingdom, Dry, Wet, Recompletion, Completion Design, Workover.

Introduction

A gas storage operator in the UK requested that Atkins review remediation options for two of their natural gas storage cavern wells that had sustained annulus pressure (SAP) within the A-annulus. Leak detection logs were run which confirmed that the leak was through the production packer on both wells. On discussion with the client, it was agreed that both wells required recompletion due to a failure of the well's primary barrier envelope.

The client requested that Atkins develop plans to recomplete the wells, to return the caverns to service. Atkins reviewed the “Wet” and “Dry” recompletion concepts (Lennox et al, 2020) and proposed that the “dry” recompletion method would be the optimal solution for the client to return both natural gas storage caverns to service.

The “dry” recompletion workover involved isolating the natural gas within the cavern from the well with mechanical plugs. This permitted the recovery of the existing completion with a hydraulic workover (HWO) unit and removal of the existing tubing spool and the installation of a new tubing spool, completion and tree valves.

The project was successfully completed in 2022 with the recovery of the mechanical plugs and final commissioning / gas testing of the control panel and plant control systems.

This paper discusses the key design choices made in the planning for the “dry” recompletion and reviews the outcomes of these choices during the “dry” recompletion operation. The following key aspects are reviewed:

- The recompletion concept, “wet” vs “dry”
- The selection and testing of the Mechanical Plugs.
- The selection and testing of the HWO unit blow out preventer (BOP)
- The “dry” recompletion operation (plug installation, recompletion, plug recovery and operational performance and conclusions).

Recompletion Concept

In general, there are two options available for the recompletion of a gas storage cavern completion:

1. “wet” recompletion - The removal of the cavern gas inventory by rewatering, prior to recompletion as presented by (Bernhardt, 2014).
2. “dry” recompletion - Isolating the stored gas in the cavern with mechanical barriers, prior to recompletion as discussed by (Engmann, 2018).

The fundamental difference between “dry” and “wet” recompletion operations is the need to remove gas from the cavern prior to the recompletion and then the refilling of the cavern with gas after the recompletion. The effect of this can be seen when comparing the high-level operational steps of the “wet” vs the “dry” recompletion concepts, as presented in Table 1,

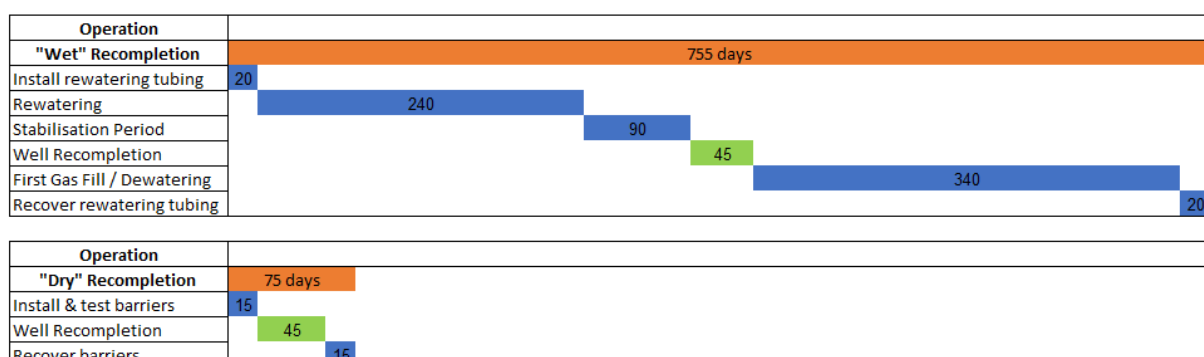
Table 2 and Figure 1 below:

Table 1 - “Wet” recompletion high-level operational steps

| # | Operational Steps | Estimated Days |
|----|--|----------------|
| 1 | Installation of the rewatering wellhead | 20 |
| 2 | Snubbing the rewatering tubing into the cavern, using a snubbing unit. | |
| 3 | Rewatering by pumping water into the cavern and export of natural gas via the gas plant. | 240 |
| 4 | Cavern monitoring / nitrogen purging to ensure that as much as possible of the gas has been removed from the cavern. This ensures that as far as reasonably practicable, gas has been purged from the cavern and that it is in a stable condition for recompletion operations. | 90 |
| 5 | Removal of the rewatering tubing with a workover unit. | |
| 6 | Removal of the rewatering wellhead | |
| 7 | Recompletion operations (recovery of the existing completion, logging of the existing production casing, the installation and testing of the new completion and tree) with a workover unit. | |
| 8 | Installation of the dewatering wellhead | 340 |
| 9 | Installation of the dewatering tubing with a workover unit | |
| 10 | Gas First Fill/Dewatering of the cavern by injecting natural gas via the gas plant | |
| 11 | Snubbing out the rewatering tubing from the well, using a snubbing unit. | 20 |
| 12 | Removal of the dewatering wellhead | |

Table 2 - “Dry” recompletion high-level operational steps

| # | Operational Steps | Estimated Days |
|---|---|----------------|
| 1 | Installation & testing of the mechanical barriers using wireline intervention tools. | 15 |
| 2 | Recompletion operations (recovery of the existing completion, logging of the existing production casing, the installation and testing of the new completion and tree) with a workover unit. | 45 |
| 3 | Recovery of the mechanical barriers using wireline intervention tools. | 15 |

**Figure 1 - Time Schedule Comparison "Wet" vs "Dry" Recompletion**

In addition to the requirement to perform the extra operations listed for the “wet” recompletion, the flooding of the cavern with water (or brackish water) would result in additional leaching of the cavern. This leaching would result in an increase in free volume, which would bring an increase in storage volume and potential revenues but brings additional risks due to the geometrical changes. This additional leaching can result in:

- Reduced pillar distance between adjacent caverns
- New geometry affecting the geomechanical stability of a cavern.
- Non-halite formations impacting cavern stability and geometrical development.
- Damage to the last cemented casing shoe (LCCS).

Since the “wet” recompletion method will result in geometrical changes to the cavern, there is a requirement to assess the expected new cavern shape and the geomechanical stability of this anticipated geometry. It is noted that during any rewatering operation the actual shape of the cavern will be periodically measured with sonar logging tools and the actual geometrical shape of the cavern assessed and modelled for geomechanical stability.

The “dry” recompletion concept was determined to be the optimal solution for the site due to:

- Removal of the risk of non-halite salts altering the caverns shape during a “wet” recompletion operations,
- Reduced Health & Safety impact as there is a significant reduction in scope when using the “dry” recompletion method.
- Reduction in the project unknowns as there is a need for a cavern stabilisation period prior to recovery of the completion, during the “wet” recompletion method. Due to the

complexities of thermal expansion of the cavern fluid and cavern convergence, this period could not be refined accurately.

- Reduced the duration of the recompletion operations as the cavern would not require rewatering and dewatering post recompletion.
- Reduced costs due to the reduced scope of the “dry” recompletion method.

“Dry” Recompletion Barriers

Through the design and risk assessment process it was identified that the cavern would have to be isolated from the well with two barriers and would also require a shearable barrier suitable for cutting and sealing the production tubing.

Mechanical Barriers

A review of the planned plug differential pressure requirements, well geometry and the supply chain for expandible and inflatable plugs, determined that the only suitable retrievable plug for the tubular configuration, was a high expansion type bridge plug. The bridge plug OEM confirmed that their high expansion bridge plug had previously been successfully deployed within similar tubulars on a European gas storage sites and had been used extensively in the oil & gas sector, providing confidence in the selection of this system for the “dry” recompletion barriers. The selected plug had to have the ability to be run through the original completion shown in Figure 2 and recovered through the new completion, the restrictions for each stage are detailed in Table 3 below.

Table 3 - Completion Restrictions

| Completion Stage | Minimum Restriction | Setting Diameter |
|---------------------|---------------------|------------------|
| Original completion | 5.953" | 8.535" |
| New completion | 5.953" | 8.535" |

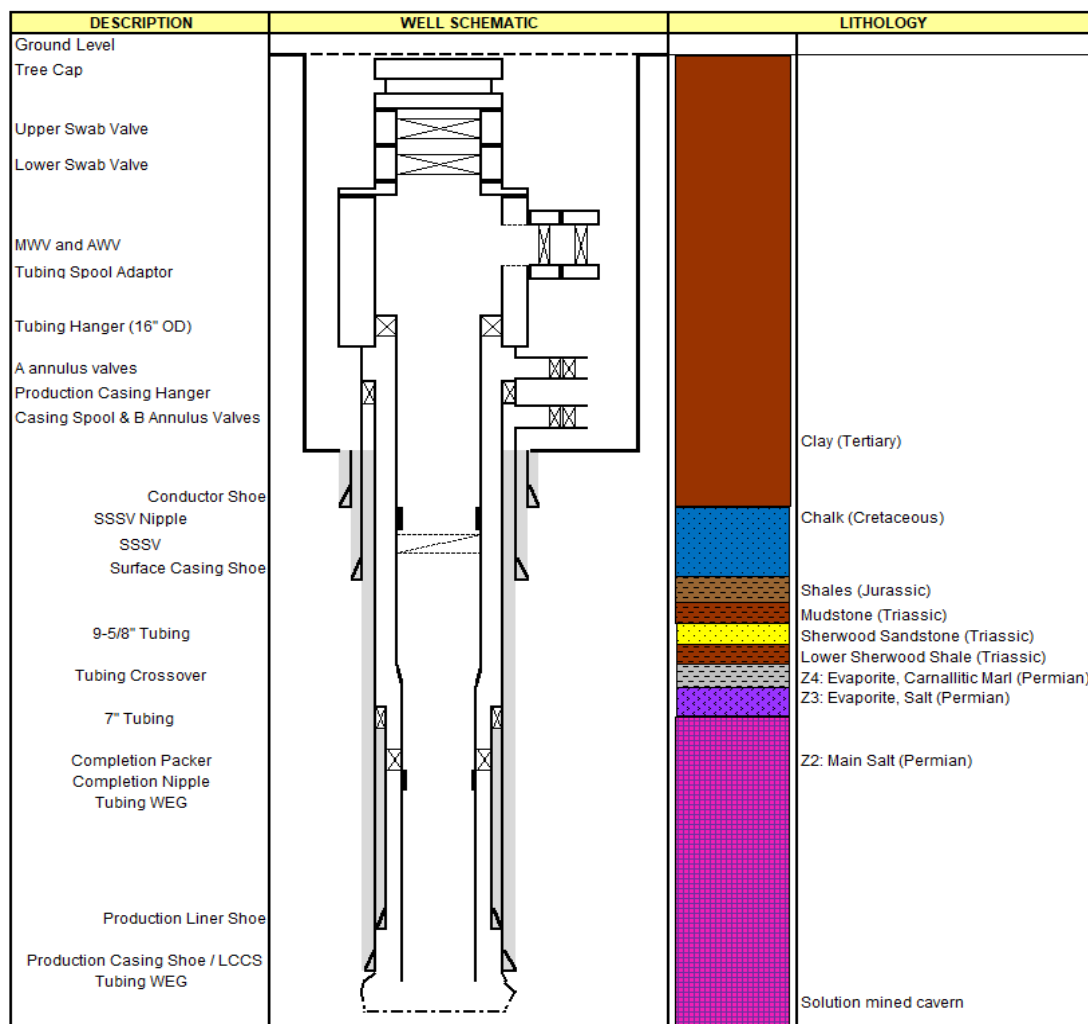


Figure 2 - Existing Completion Schematic

On discussions with the OEM, the high expansion bridge plug had not been qualified as gas-tight to V0 (ISO 14310) and it was agreed to change the plug rubber element to Hydrogenated Acrylonitrile Butadiene (HNBR) rubber as this had shown greater resilience to the movement of the rubber element when setting and un-setting the plug.

On review of the well conditions and on agreement with the client and OEM, the V0 qualification test (ISO 14310) on the high expansion bridge plug was performed to the parameters detailed in

| Test Spec | Test Criteria | Comments |
|----------------------|-------------------------|---|
| ISO 14310 Validation | V0 | |
| Temperature (Min) | 30 Deg C | Previous minimum qualification temp, confirmed via WellCAT modeling after lub & bleed |
| Temperature (Max) | 66 Deg C | 1.1 safety factor over the LCCS temperature |
| Pressure | 2250 psi | 1.1 safety factor over planned “dry” recompletion cavern pressure, with suitable margin for lub & bleed |
| Setting Casing | 9 5/8”, 53.5lb/ft, P110 | |

Table 4 below.

Table 4 - Plug V0 Qualification Test Requirements

| Test Spec | Test Criteria | Comments |
|----------------------|-------------------------|---|
| ISO 14310 Validation | V0 | |
| Temperature (Min) | 30 Deg C | Previous minimum qualification temp, confirmed via WellCAT modeling after lub & bleed |
| Temperature (Max) | 66 Deg C | 1.1 safety factor over the LCCS temperature |
| Pressure | 2250 psi | 1.1 safety factor over planned “dry” recompletion cavern pressure, with suitable margin for lub & bleed |
| Setting Casing | 9 5/8”, 53.5lb/ft, P110 | |

The test ensured that the plugs adhered to the requirements of BS EN ISO 14310:2008, to the V0 grade from this standard. The test requires two gas pressure reversals (above/below) and one temperature cycle, which results in five cycles with a zero-bubble acceptance criteria. The tests performed are provided in Table 5 below.

Table 5 - Plug Qulaification Test Paramiters

| Cycle No. | Temperature | Pressure | Direction |
|-----------|-------------|----------|-----------|
| 1 | 66°C | 2250 psi | Below |
| 2 | 66°C | 2250 psi | Above |
| 3 | 66°C | 2250 psi | Below |
| 4 | 30°C | 2250 psi | Below |
| 5 | 66°C | 2250 psi | Below |

Pull Test

- Following the fifth cycle but while the plug was still in the heated condition, the plug was retracted to the 'pull' position, left for 40 minutes to allow the element to relax, and then pulled through a 5.325" restriction (0.125" greater than pre-set OD of 5.200", and smaller than the minimum completion restriction) with a relatively small force (~1,100 lb) to retrieve the element through the restriction.
- With tension removed, the element diameter was recorded as 6.360" (161.43mm) as is shown in Figure 3 below.
- Inspection of the elastomer showed it to be largely in good condition, with no axial cracking present. There was still a reasonable surface area around the circumference of the elastomer across which there had been a good contact with the casing wall.
- There were some small radial tears where the elastomer was bonded to the steel packer fixture, these tears were found to be caused by the jarring impact loads acting on the bond when unsettling/stretching the element.



Figure 3 - Plug After Qualification Test

Shearable Barrier

The client required that the BOP used should have the ability to: recover the existing tubing hanger (16.75" OD), shear the 9-5/8" tubing and seal against THP in the event there was a failure of both the cavern isolation well barriers.

A review of the market indicated that there were a few suitable rental BOP (18-3/4" and 20-3/4") for the recovery of the 16.75" OD tubing hanger, located in the Middle East, but due to logistics it was elected to refurbish a legacy BOP system from a stacked semi-submersible drilling rig, as the BOP was located in the UK.

Figure 4 shows the status of the BOP



prior to refurbishment and Figure 5 shows the BOP stack after completion of the refurbishment.

The shear test was performed before committing to the refurbishment of the BOP and completion of the 5 yearly recertification.

Figure 4 - 18-3/4" Double BOP before Refurbishment



The shear test was performed on the 18-3/4", 15k, NOV, SLX Double BOP, c/w 14" Pos-lock and 18" Boosters. As is shown in Figure 4 the BOP was superficially in poor condition. To establish the suitability of the stack for the project, a shear test was conducted (referencing API 16A) to prove the capacity of the BOP to shear and seal against the 9-5/8" completion and dual encapsulated (2 x 1 1/4" x 0.049", Inconel A825) control line in the worst-case scenario that the dual barriers to the cavern inventory fail, prior to committing to the refurbishment and 5 Yearly recertification of the BOP. The shear test was repeated 3 times, with the hydraulic pressure required to cut the 9-5/8" tubular (2,400-2,450 psi) within the rig contractors 3,000 psi accumulator pressure. After each cut the shear seal BOP ram was successfully pressure tested to 5,000 psi for 10 min.

Figure 5 - 18-3/4" BOP Stack Post Refurbishment

After each test the cut tubing was recovered from the BOP, visually inspected and measured to confirm the maximum width of the cut joint. The largest width measurement was 14-3/16", which is less than the clearance within the BOP stack and HWO rig, so would not cause recovery issues if required during operations.

Figure 6 shows the double BOP on the test stump with the 9-5/8" tubing secured within the double BOP and the cut 9-5/8" tubing after the shear test.



Figure 6 - BOP Shear Test Photos

Workover Rig

The HWO contractor manufactured a suitable substructure to support the rig and BOP at the client's site and a large bore work window to permit the laying out of the 16.75" OD tubing hanger assembly, on recovery as it could not be pulled through the HWO unit and laid out conventionally from the work basket. With this equipment manufactured a stack-up test of the HWO unit was performed at the contractor's yard to confirm the rig-up prior to mobilisation to site.

Plug Installation

This section provides a summary of the plug installation, reviewing some of the issues encountered and the recommendations for future "dry" recompletion operations. Figure 7 below shows the configuration of the well after installation of the plugs.

The key steps undertaken were:

- Rigged up intervention equipment (venting & wireline) onto the well
- Cut packer mandrel with cutter toolstring and cut the tailpipe below the packer to permit the installation of the upper and lower plug.
 - Used a no-go on a completion nipple, for spaceout for the cuts
 - Used an adjustable sub to permit field adjustments of the space out
- Installed the lower plug and inflow tested plug with cavern gas
- Lubricated and bled tubing to 70:30 Water / MEG.
- Installed the upper plug and pressure tested from above, verification of the test with wireless barrier verification tool.
- Installed and tested nipple plug/junk basket in the SSSV (3rd plug set to act as a debris barrier during rig and wellhead operations).

Issues

- Spaceout amended to suit actual completion dimensions based on CCL / Caliper log.
- Spaceout sub, set with shear pin and on recovery from the tubing cut the shear pin was found to be sheared, so it was unclear the exact depth that had been cut. Changed Spaceout sub to grub screws to remove issue for future packer mandrel cutting.

Recommendations

- Post operations the OEM has qualified the high expansion bridge plug to 3,000 psi, so inflow test against full cavern differential is now possible.
- Bleeding to atmosphere would permit top fill of the tubing in future operations, removing the complications and pressure cycles of the lube & bleed.
- Use of an intelligent/wireless controlled valve within the plug assembly, allowed setting the upper and lower plug on top of each other, removing the risk of hydraulic effects impacting the setting of the upper plug due to the small volume of fluid between the plugs.
- The use of the barrier verification device enabled independent testing of the upper plug.

| DESCRIPTION | WELL SCHEMATIC | LITHOLOGY |
|---------------------------------|----------------|---|
| Ground Level | | |
| Tree Cap | | |
| Upper Swab Valve | | |
| Lower Swab Valve | | |
| MVV and AWV | | |
| Tubing Spool Adaptor | | |
| Tubing Hanger (16" OD) | | |
| A annulus valves | | |
| Production Casing Hanger | | |
| Casing Spool & B Annulus Valves | | Clay (Tertiary) |
| Conductor Shoe | | |
| Nipple Plug & Junk Basket | | Chalk (Cretaceous) |
| SSSV | | |
| Surface Casing Shoe | | |
| 9-5/8" Tubing | | Shales (Jurassic) |
| Tubing Crossover | | Mudstone (Triassic) |
| 7" Tubing | | Sherwood Sandstone (Triassic) |
| Completion Packer | | Lower Sherwood Shale (Triassic) |
| Completion Nipple | | Z4: Evaporite, Carnallitic Marl (Permian) |
| Tubing WEG | | Z3: Evaporite, Salt (Permian) |
| Upper High Expansion Plug | | Z2: Main Salt (Permian) |
| Intelligent barrier valve | | |
| Lower High Expansion Plug | | |
| Intelligent barrier valve | | |
| Production Liner Shoe | | |
| Production Casing Shoe / LCCS | | Solution mined cavern |

Figure 7 – Plug Installation Schematic

Recompletion

This section provides a summary of the completion recovery and completion installation operation, reviewing some of the issues encountered and the recommendations for future “dry” recompletion operations.

The key steps undertaken were:

- Removed tree valves and installed BOP/Rig crossover.
- Installed BOP, riser and commissioned HWO rig (see Figure 8).
- Ran 9-5/8" landing string and un-set tubing hanger.
- Recovered completion, monitoring well using a trip tank.
- Performed CBL/calliper logs using open hole equipment.
- Set 13-3/8" bridge plug on the first full production casing joint below the cellar (3rd plug set to act as a debris barrier, during rig and wellhead operations).
- Rigged down HWO unit, BOPs and riser
- Removed existing tubing spool and inspected starterhead flange.
- Installed new 13-5/8" tubing spool.
- Installed BOP/Rig crossover, BOP, riser and commissioned HWO rig.
- Recovered 13-3/8" bridge plug.
- Performed wireline brush run to prepare the production liner for setting the new production packer.
- Ran new completion with HWO rig, testing the tubing hanger seals, SSSV control line and tubing against a nipple plug pre-installed above the packer.
- Recovered nipple plug from the completion.
- Installed a bridge plug below the packer and set production packer hydraulically.
- Recovered bridge plug from below packer.
- Rigged down HWO unit, BOP and riser.
- Installed new production tree assembly
- Hydro and gas tested production tree & flowline.



Figure 8 - HWO Rig-up

Issues

- BOP/Rig crossover found to be machined out of tolerance for the H26 Techlok clamp.
- Alignment of the rig on well centre had to be conducted visually due to the design of the substructure, this would have required nipping down of the BOP in the event the rigs substructure was misaligned with the BOP/well centre.
- The wing valve design prevented the full recess of the studs during installation, increasing critical path working and manual handling – Review valve design to ensure the flange design permits the full stud to be fitted/recessed to aid installation and removal.
- Completion assembly lengths found to require staging through the HWO unit, due to the length of crossovers, flow couplings and pups used.
- Pressure test charts found to have the centre hole misaligned, resulting in a false pressure rise/fall indication due to chart eccentricity – Use of digital pressure recorders used to remove this issue.

Recommendations

- Cutting of the packer release mandrel with wireline tools prior to mobilisation of the workover unit, worked well.
- The full BOP & Workover rig stack-up testing prior to mobilisation of equipment to site is recommended, as this will identify conflicts and constructability issues before operations commence.
- Recommend that the substructure is designed to be moved (lifted or skidded) in one piece with an alignment guide, as this would remove the risk of miss alignment of the rig with well centre (it was estimated that miss alignment could have caused 24 to 36hrs of non-productive time).
- Recovery of the high expansion bridge plugs was thought to be one of the key risks of the project. For the new completion a permanent packer solution was selected, as it had a larger ID, than the available retrievable packers. But in the event of an issue with the permanent packer the recovery and installation of a back-up assembly would be more complicated. For future operations this selection criteria should be reviewed, as it was found that the plug elements passed through the completion restrictions without issues during recovery.
- Prior to procurement of long lead items, hold a review with the selected rig contractor to determine if the planned equipment can be run efficiently and if amendments to the completion design would reduce complexities during installation.
- Back-up equipment (crossovers, test pumps, power packs, power tongs, etc) was found to be cost effective at preventing down time during operations and was a worthwhile investment.
- It is recommended to prepare the studs and nuts that will be broken with wire brush, thread die and penetration fluid.
- Digital pressure recorders found to be more efficient and accurate for pressure testing operations and is recommended for all future operations.

Plug Recovery

This section provides a summary of the plug recovery operation, reviewing some of the issues encountered and the recommendations for future “dry” recompletion operations. Figure 10 below shows the configuration of the well with the new completion after recovery of the plugs.

The key steps undertaken were:

- Completed surface commissioning of the wellhead control panel
- Rigged up intervention equipment (venting, pumping & wireline) onto the well
- Recovered upper plug (see Figure 9, showing slips and element to be in very good condition) in two runs:
 - Electric line using a powered toolstring to stretch the element.
 - Braided line to permit jarring to unseat the slips and as a contingency during recovery to surface.
- Unset lower plug element and equalised pressure across packer, using electric line.
- Displaced fluid within the tubing into the cavern by venting and injection of nitrogen.
- Recovered lower plug using braided line.
- Final gas testing and commissioning of the wellhead, control panel and plant systems.
- Handed over well to the operator



Figure 9 - Recovered Upper High Expansion Plug (Slips & Element)

Issues

- Cavern pressure and the hydrostatic column of the fluid above the bridge plug were in equilibrium, this coupled with the small annular clearance between the unset plug and the production liner, hindered displacement of the well fluids into the cavern and the gas migration to surface.
- Hay pulley anchor (5MT) block found to move during jarring operations – Investigations found that water/MEG or wireline grease had reduced the static friction between the anchor block and the concrete wellpad permitting the anchor block to move during jarring.

Recommendations

- The high expansion bridge plug with HNBR rubber element was recovered without issues, and the system would be recommended for future “dry” recompletions within similar well and completion configurations.
- The use of 70:30 Water / MEG prevented hydrate formation during the plug equalisation process.
- Planning to displace the fluid column with nitrogen would reduce the time taken to flip the fluid above the lower plug to gas prior to plug recovery.
- Use of 2x (5MT) anchor blocks bolted together is recommended for future operations on existing sites and for new sites permanent hard points for securing the Hay pulley for wireline interventions is recommended.

| DESCRIPTION | WELL SCHEMATIC | LITHOLOGY |
|---------------------------------|----------------|---|
| Ground Level | | |
| Tree Cap | | |
| Upper Swab Valve | | |
| Lower Swab Valve | | |
| MVV and AWV | | |
| Tubing Hanger | | |
| A annulus valves | | |
| Production Casing Hanger | | |
| Casing Spool & B Annulus Valves | | Clay (Tertiary) |
| Conductor Shoe | | |
| SSSV Nipple | | Chalk (Cretaceous) |
| SSSV | | |
| Surface Casing Shoe | | Shales (Jurassic) |
| 9-5/8" Tubing | | Mudstone (Triassic) |
| Tubing Crossover | | Sherwood Sandstone (Triassic) |
| 7" Tubing | | Lower Sherwood Shale (Triassic) |
| Completion Packer | | Z4: Evaporite, Carnallitic Marl (Permian) |
| Completion Nipple | | Z3: Evaporite, Salt (Permian) |
| Tubing WEG | | Z2: Main Salt (Permian) |
| Production Liner Shoe | | |
| Production Casing Shoe / LCCS | | Solution mined cavern |

Figure 10 - New Completion Schematic

Project Schedule (Planned vs Actual)

The planned project duration for the single well was 75.0 days, assuming 25% non-productive time over the estimated trouble-free times. The actual time for the re-completion of the single well was 75.1 days (including 12% recorded NPT). The actual well operations broadly followed the expected timings. Table 6 below provides a summary of the single well "dry" recompletion performance.

Both wells handed back to the client ahead of the project completion milestone, permitting the client to increase the sites operational storage capacity in advance of the winter peak period. The overall project cost was within the project cost estimate tolerances, where this was delivered during a period of disruption in the supply chain due to the impact of COVID 19 and increasing rates due to market conditions impacted by the geopolitical events in 2022.

Issues

- Operations were impacted with weather due to the reliance on mobile cranes.
- The compact and operational nature of the clients site meant that the rig-up and rig-down durations took longer than expected.
- Planned timings were based on batching operations, so that there were no simultaneous operations on the two wells. During the project there were times when operations were conducted on both wells at the same time, but due to the compact nature of the site the use of simultaneous operations was not found to provide the expected efficiencies so was minimised as much as possible.

Recommendations

- Ensure planned timings are not based on contractor's optimistic mobilisation and de-mobilisation estimates.
- Although planned timings matched actual timings the actual NPT rate was half of what was estimated, so it is recommended to carefully consider trouble free timings and NPT events / rates in future operations planning.
- Where operations on multiple wells are planned, it is recommended to batch operations (complete wireline operations on well A then B, before moving on to the next operations) to increase operational efficiency by focusing on a single operation at a time.

Table 6 - "Dry" Recompletion Performance

| Operations | Planned Days (Trouble Free) | Planned Days (Including NPT) | Actual days (Including NPT) |
|------------------------|--------------------------------|---------------------------------|--------------------------------|
| HEX Installation | 12.00 | 15.00 | 14.10 |
| "Dry" Recompletion | 36.00 | 45.00 | 46.00 |
| HEX Recovery | 12.00 | 15.00 | 15.00 |
| Total Durations | 60.00 | 75.00 | 75.10 |

Conclusions

Both wells returned to full gas storage service ahead of schedule and within the project budget with no HSE incident during the workover operations.

The project demonstrated that the “dry” recompletion method can be used to replaced completions in salt cavern gas storage wells, on an operational Tier 1 COMAH gas storage site without affecting gas storage operations.

Nomenclature

| | |
|-------|--|
| BOP | Blowout Preventer |
| CCL | Casing Collar Locator |
| COMAH | Control of Major Accident Hazards Regulations |
| HNBR | Hydrogenated Acrylonitrile Butadiene Rubber |
| HSE | Health Safety & Environmental |
| LCCS | Last Cemented Casing Shoe (production casing shoe) |
| MEG | Mono Ethylene Glycol |
| NPT | Non-Productive time |
| SAP | Sustained Annulus Pressure |

References

- Lennox.A, et al, Practical considerations when selecting recompletion method (dry/wet) in underground cavern storage UK, Solution Mining Research Institute; Proc. tech. conf , 22-24 September (2020)
- Engmann, M. & Tenbrock, A., ‘Dry’ Recompletion of a Cavern Storage Well’, Solution Mining Research Institute; Proc. tech. conf , 24-25 September, (2018)
- Bernhardt.H, Flooding and Recompletion Project of Salt Cavern To-8 LI. Torup, DK, Solution Mining Research Institute; Proc. tech. conf , 5-6 May, (2014)

Exploring for unlocked subsurface potential by integration of historic and modern data: The case of a forgotten Flysch reservoir within the Vienna Basin (Austria) discovered almost a century ago

R. Möbius, A. Gauer, F. Tosoratti
OMV, Vienna, Austria

Abstract

Brown Fields are rarely attractive for major capex investments. Even studies commonly only focus on opex optimization. However, brown fields often have huge data sets available which were collected over decades. Additionally, also the surface infrastructure is in place. When being integrated with modern data both can reveal a significant treasure. The massive amount of data, comparatively low investment costs and proven knowledge of production history including pitfalls make brown field development an opportunity for cost-efficient and low-risk production.

Aside from economical reasons why such reservoirs should attract more attention, other good reasons are that the huge amount of data being already present, though commonly stored in archives, makes them ideal playgrounds to study future energy solutions. When production facilities are still in place, ideas can be directly tested in the field. At least as long as the reservoirs are still accessible. Furthermore, as facilities do not need to be rebuilt, the environmental impact of such projects is low compared with green field development.

An example of an Austrian Flysch reservoir is presented: it consists of a structurally complex fractured reservoir with extremely low matrix permeability and over nearly a hundred years data has been gathered.

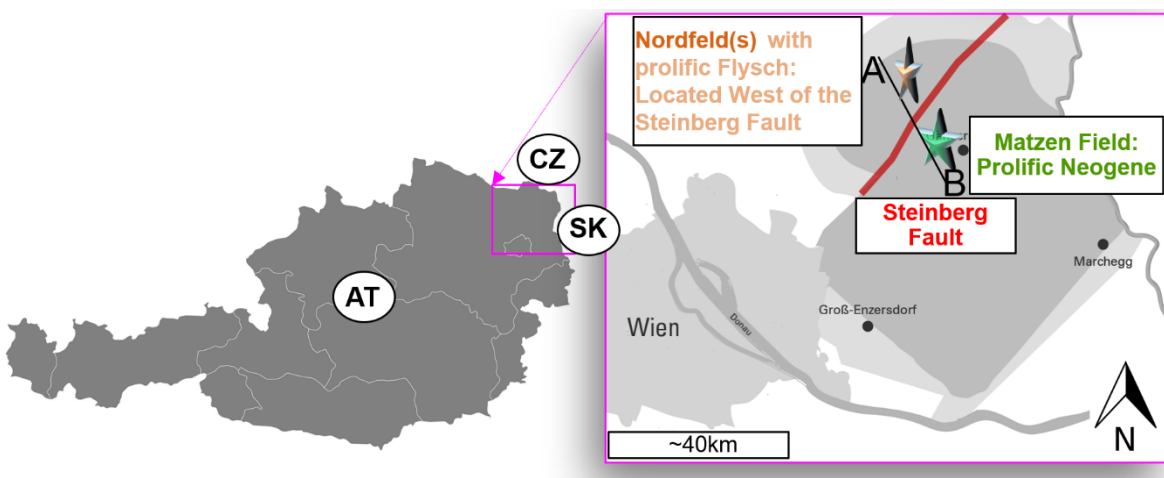


Fig.1: Location of the prolific Flysch reservoir in the “Nordfeld”.

Introduction

The Flysch reservoir in the Vienna Basin is composed of more than 1000 m thick, deep-water sandstone and shale intercalations. They contain an at least 300 m thick section of proven hydrocarbons. The prolific compartments are commonly less than 100 m in width and length and spread over 10s of kilometers in the so called “Nordfeld”. Hydrocarbon presence is not limited to the Austrian part of the Vienna Basin and continues towards the Czech and the Slovakian side of the Vienna Basin.

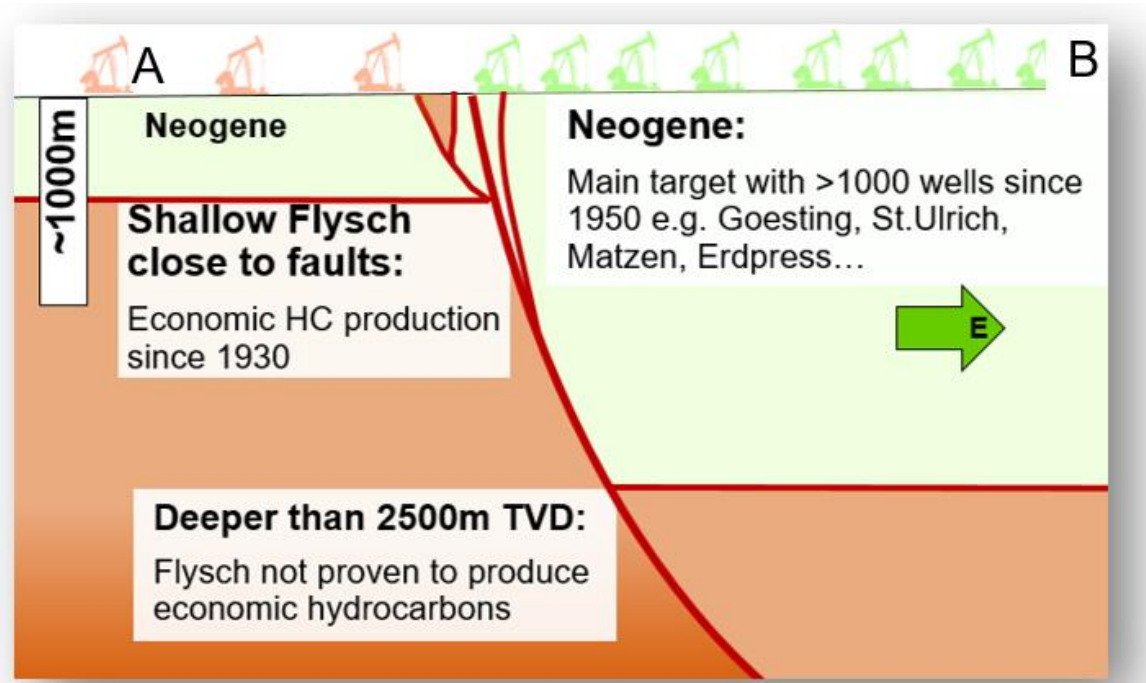


Fig.2: Schematic cross-section across the “Nordfeld”.

History of the Austrian Flysch Play

The first hydrocarbons were found in 1929. Commercial production started in the early 1930s resulting in almost a century of production with over 50 MMbbl of oil and 30 Bcf of natural gas extracted. Nevertheless, recent studies indicate substantial additional amounts of so far bypassed hydrocarbons. Due to the depth of typically less than 1500 m TVDss these can be recovered by comparatively simple, onshore infill wells. Such was proven by a well drilled in 2018, which produced almost pure oil for more than a year. This well has confirmed that regardless of the well location being less than 100 m away from several highly prolific wells, economic oil production can be still achieved.

Challenges

It is commonly not economic to collect comprehensive data sets during the late-stage development of brown fields. Therefore, it is of higher importance to optimize the usage of existing data by integration of modern and historic data sets. With time, more than 700 wells were drilled into the reservoir. Consequently, data situation per well ranges from a simple self-potential log and hand-written reports to highly modern and advanced logging tools calibrated to core data. During the last years the different historic data sets were screened and used to locate well locations. To do so, these were gathered, partially digitized and re-interpreted. Subsequently these were integrated with modern, locally present high-quality data to refine existing models. Available 3D seismic was re-processed and likewise used for well placement, as notes in historic well reports were. Such side notes and observations often pointed to locations with an estimated open fracture system or sub-seismic faults. These are crucial to exploit this reservoir. Such hints were sense-checked using modern data sets. Of particular help were comments about technical or geological well failures.

Key Characteristics:

- ▶ Sand beds extend the field size and are, without fault presence, laterally correlatable.
- ▶ Matrix is composed of medium-sized, grey quartz sandstones with 5-15% porosity.
- ▶ Matrix permeability is often below 0,1md.
- ▶ **Fractures** are common, but **only partially open** reflecting the diagenetic overprint.

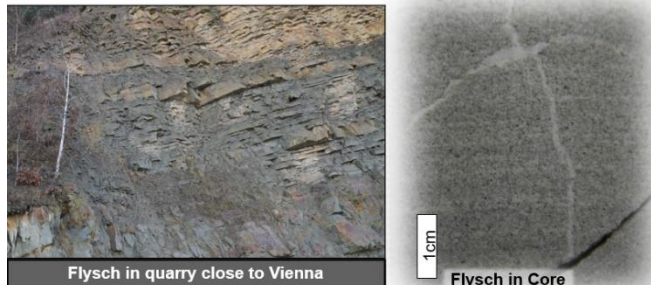
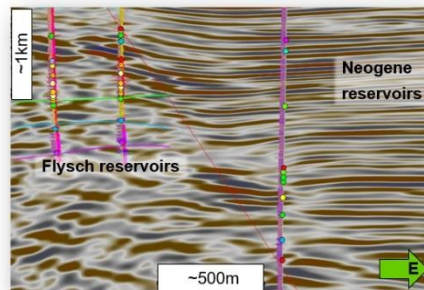


Fig.3: Typical characteristics of the Austrian Flysch reservoir.

Recent Development

From a purely technical perspective, the reservoir remains challenging. Nevertheless, good reasons exist that economic value is still high. This led to a comprehensive economic review in 2021 resulting in the initiation of a phased, clearly structured field-redevelopment plan starting with its first well campaign in 2023.

Remaining challenges are:

- 1) How to overcome drilling risk caused by highly depleted compartments being located adjacent to over-pressured compartments with initial hydrocarbon saturations.
- 2) Well planning in a structurally complex area with limited to poor seismic imaging, possibly due to the presence of several cross-cutting fault systems.
- 3) How to locate areas with open fracture systems.
- 4) How to best orient the well in respect to the different fracture orientations and how to keep these open and connected to the wellbore while drilling and after completing the well.
- 5) Risking and reserves allocation per well is complex. Exact compartment boundaries are difficult to map, and drained volumes depend on the direction of open fracture systems.

On the positive side:

- 1) The shallow depth of the reservoir and its location onshore results in moderate drilling costs.
- 2) Supporting data such as pressure can often still be extracted from productive wells.
- 3) Close-by outcrop data of the same formation exist.
- 4) Huge amounts of data were collected over the years which can be calibrated with spot-wise gathered modern data.

Consequently, even though most of the data are not state of the art, these still support the success of future wells. Infrastructure is available, and application of selected modern technologies can boost productivity of single wells. Usage of artificial intelligence systems or campaign drilling can compensate for the increased single well risk. Multidisciplinary data integration is still ongoing to further optimize the value and knowledge of this area.

Summary

Flysch reservoirs in the Vienna Basin represent an excellent living subsurface laboratory how to integrate modern and historic data to support both conventional hydrocarbon development and to de-risk alternative energy applications within an area of still existing surface and subsurface infrastructure. An example is given how economic value of brown fields can be increased when multidisciplinary data collected over more than nine decades are successfully integrated. Optimized usage of existing infrastructure and the increase of recovery factors result in an environmentally sensitive redevelopment approach by keeping existing, marginally economic hydrocarbon fields active and therefore accessible for future energy solutions.

Geological realization screening using Python script for reservoir simulation: First results of application on Mittelplate simulation model

L. Lin
Wintershall Dea Deutschland GmbH

Abstract

The Mittelplate oilfield is Germany's largest and most productive oil field, on-stream since 1987, located in the national park and UNESCO World Heritage Wadden Sea – the tidal flats of the Elbe Estuary. The oilfield is producing from four reservoirs – the Jurassic Dogger Beta, Gamma, Delta and Epsilon sandstone – with currently 27 production wells (offshore & onshore) and 10 injection wells (offshore). Reservoir simulation models have been conducted to ensure applicable production forecast and determine optimal development concepts. Although after more than 35 years of production, different parts of the reservoir zones still exhibit uncertainties that have strong influences on the dynamic behaviors.

In order to represent the uncertainties, more than hundred geological realizations were initially created based on geostatistical algorithm. However, it is usually very time-consuming to run all the realizations and thus very challenging to finalize the dynamic modeling process within tight time schedule. Therefore, as a reservoir engineer, how to select representative geological realizations before implementing reservoir simulation, becomes one important question to be answered.

Introduction

This presentation will provide you an insight of first python application results on screening 50 geological realizations for Mittelplate reservoir simulation.

Python application for geological realization screening

Python scripts have been applied to generate distance matrix, which describes how similar two realizations are in terms of critical geological properties. The distance matrix is then used to map all geological realizations into a Euclidean space, using a so-called multidimensional scaling technique. A small sub-set of representative realizations are selected using python script of kernel k-means clustering algorithm. Finally, only the selected representative realizations will be conducted for reservoir simulation instead of the full set of geological realizations. This will reduce the computation time significantly.

Conclusion

This python application on geological realization screening supports reservoir engineers to find good starting realizations to proceed with the comprehensive history matching process.

References

C.S and J.C., Computer Science (2008): Uncertainty Quantification Using Distances and Kernel Methods – Application to a Deepwater Turbidite Reservoir

EOR Barenburg: Pilot-Verlauf & -Ergebnisse

J. Kalunka

ExxonMobil Production Deutschland GmbH, Hannover, Germany

Polymerflutung ist eine Methode der „Enhanced Oil Recovery (EOR)“, bei der eine Polymerlösung in eine Lagerstätte injiziert wird, um die Viskosität der Injektionsphase zu erhöhen, die Flut-Effizienz zu verbessern und letztendlich die Ölproduktion zu steigern. Obwohl die Technologie bereits seit einiger Zeit bekannt und erprobt ist, gab es mehrere Projekte, darunter auch in der deutschen E&P-Industrie, die nur gemischte Ergebnisse aufzeigen konnten. Um das Potenzial dieser Technologie weiter zu testen wurde vor kurzem wurde in einem ca. 70 Jahre alten deutschen Ölfeld mit mehr als 98% Verwässerung eine Pilotphase dieser Art mit vielversprechenden Ergebnissen durchgeführt.

In der Pilotphase wurde eine Polymerlösung in zwei Injektionsbohrungen injiziert während Ölproduktion, Druck und mehrere andere Parameter genau überwacht und aktiv getestet wurden. Durch die enge Zusammenarbeit zwischen Projekt- und Betriebsmitarbeitern und die daraus resultierenden Designoptimierungen der Anlagen wurde eine erstklassige Verfügbarkeit erreicht und gezeigt, dass diese Art der Injektion ein ebenso erfolgreiches wie gewinnbringendes Konzept sein kann.

Insgesamt zeigte die Pilotphase, dass Polymerflutungen die Ölproduktion aus hochpermeablen Lagerstätten signifikant erhöhen können sowie wertvolle Informationen über optimale Injektionsraten und die Polymerkonzentration für zukünftige Projekte liefern können. Potenziell kann diese Technologie auf andere mature Ölfelder in Deutschland und der ganzen Welt angewendet werden, insbesondere auf solche, die nahe dem Ende ihrer produktiven Lebensdauer sind oder dieses bereits erreicht haben.

CO₂-EOR in stark zerklüfteten Karbonatlagerstätten – Eine Fallstudie

M. Amro¹, S. Reichmann², C. Freese¹, H. Alkan¹

¹Technische Universität Bergakademie Freiberg, Germany, ²GASAG Gruppe, Berlin, Germany

Abstract

Mit Blick auf die globale Nachfrage nach Energie muss die Ölindustrie weitere innovative Technologien entwickeln, um diese möglichst umweltschonend zu decken. Trotz der wachsenden Bedeutung erneuerbarer Energie und dem Streben nach mehr Klimaschutz hat die Energie aus fossilen Quellen auf absehbare Zeit einen festen Platz im weltweiten Energiemix. Mit Hilfe von EOR-Verfahren wird versucht ein maximales Förderpotential für Erdöl aus Lagerstätten umweltschonend auszuschöpfen.

In diesem Beitrag wird am Beispiel einer stark geklüfteten KW-Lagerstätte im Nahen Osten das Potential der Anwendung von CO₂ zur Produktionssteigerung vorgestellt. Im Rahmen einer „Pre-Screening“ Studie konnte gezeigt werden, dass in dieser seit mehr als 70 Jahren produzierenden Lagerstätte alle wasserbasierten EOR-Methoden aufgrund der hohen Heterogenität und des sehr hohen Anteils an Mikroporen wenig Chancen haben. Stattdessen wird ein CO₂-EOR-Verfahren als erfolgversprechendste Methode für diese Lagerstätte empfohlen.

CO₂-Mischtrieb ist eine der effektivsten EOR-Methoden und bedeutet, dass CO₂ und Öl unter den herrschenden Bedingungen mischbar sind. Jedoch hängt deren Erfolg stark von den Lagerstätteneigenschaften ab. In der vorgestellten Lagerstätte kam nur die nicht mischbare CO₂-Anwendung in Frage. Deren Erfolg hängt hauptsächlich vom Quellverhalten des Öls als dominantem Effekt ab, der neben der Volumenzunahme auch zur Reduzierung der Viskosität und der Grenzflächenspannung führt und somit eine Verbesserung der Entölung bewirkt. Das Quellverhalten wird hauptsächlich von der CO₂-Löslichkeit in das Öl bei dem herrschenden niedrigen Druck in der Lagerstätte limitiert.

Zunächst wird über Swelling-Experimente berichtet, die das Ziel hatten, das Quellverhalten des Öls in Abhängigkeit verschiedener Gaszusammensetzungen zu charakterisieren. Der Einfluss der CO₂ induzierten Quellung auf die Viskosität des Rohöls und die Grenzflächenspannung werden vorgestellt. Der Einfluss von in der Lagerstätte vorkommenden Begleitgasen wird bewertet. Coreflood-Experimente vervollständigen die Untersuchungen, in deren Ergebnis eine vorläufige Bewertung der inkrementellen Ölgewinnung vorgenommen werden soll. Innovative Maßnahmen zur Mobilitätskontrolle von CO₂ wie Schaumfluten im heterogenen Lagerstättenkörper finden ebenso Berücksichtigung.

Die Swelling-Experimente und die modellgestützte Schätzung des inkrementell gewonnenen Öls ermöglichen eine Diskussion über den Kohlenstoff-Fußabdruck des CO₂-EOR-Prozesses insgesamt. Es wurde eine CO₂-Bilanz erstellt, in der die Injektion von Begleitgasen, das zurückgewonnene und recycelte CO₂ sowie die potenziell emittierten Kohlenstoffemissionen infolge des zusätzlich gewonnenen Brennstoffs berücksichtigt wurden. Es wurden Maßnahmen zur Optimierung des CO₂-Fußabdrucks erarbeitet, die vom Eigentümer der Felder für die weitere Entwicklung des Feldes berücksichtigt werden.

Einleitung

Alle wichtigen Wirtschaftsprägnoseinstitute sowie die großen Ölgesellschaften und die OPEC

gehen davon aus, dass Öl und Gas in den kommenden Jahrzehnten die wichtigsten Energieträger bleiben werden und dass ihr derzeitiger Anteil von rund 60 % am globalen Energiemix aufgrund der wachsenden Weltbevölkerung und der weltweiten wirtschaftlichen Entwicklung auch im Jahr 2050 noch bestehen wird. Im Gegensatz dazu wird erwartet, dass die Energieversorgung aus Kohle und Kernenergie zurückgehen wird. Aus diesen Gründen hat das Interesse an EOR-Methoden, die darauf abzielen, die Ausbeute aus ausgereiften konventionellen und unkonventionellen Ölreservoirs zu verbessern, zugenommen.

Der Großteil der weltweiten Ölreserven ist in Karbonatlagerstätten gespeichert. Derzeit gibt es zwar mehrere EOR-Verfahren, die sich bei der Verbesserung der Ölgewinnung aus Karbonatlagerstätten als wirksam erwiesen haben. Die praktische Anwendung einiger dieser Verfahren hat sich jedoch aufgrund hoher Kosten und teilweise negativer Auswirkungen auf die Umwelt als schwierig erwiesen.

In diesem Beitrag steht die Anwendung des CO₂-EOR Verfahren in einer Lagerstätte im Nahen Osten im Mittelpunkt. Sie findet als emissionsminimierende Methode aktuell weltweit mehr Anwendung als jede andere EOR-Methoden. Insbesondere ist die Eignung des CO₂-EOR in dieser Erdöllagerstätte zu betrachten sowie die Optionen zur späteren CO₂-Injektion in die ausgeforderte Lagerstätte. Ein besonderer Focus liegt auf dem Vergleich der Wirkung von CO₂ und CH₄ bzw. N₂ auf die Entölung.

Feldbeschreibung

Die betroffene Lagerstätte ist in der gesamten Region von Oman bis in den Nordirak als ölhöfig bekannt (Sadooni und Alsharhan, 2003) und besteht aus mehreren Schichten. Eine dieser Formationen ist Maaddud-Formation und war nach der Ablagerung verschiedenen Spannungsregimen ausgesetzt. Diese Spannungen führten zu einer Vielzahl von seismischen und subseismischen Ereignissen, daraus entstanden unterschiedlich orientierte Hauptstörungen. Eine davon ist die N-S-Störungen, die in direktem Zusammenhang mit der Bildung der vorherrschenden N-S-länglichen Antiklinalstruktur der Formation stehen (Samahiji und Chaube, 1987).

Die zweite ist NW-SE-orientiert und steht im Zusammenhang mit der Zagros-Orogenese in der persischen Region und vor 150 Millionen Jahren begann (Agard et al., 2011; Smith und Parakh, 2016).

Die Maaddud Formation ist ein stark heterogenes, geschichtetes und geklüftetes Karbonatreservoir. Die Formation wird in den oberen und unteren Bereich unterteilt, die durch eine dünne Tonschicht getrennt sind. Diese stellt nur lokal eine hydraulische Barriere dar. Das Deckgebirge, das die ölführenden Formationen von der darüber liegenden, wasserführenden Formation trennt, wurde während der Injektion selektiv durch größere Risse infolge hoher Drücke beschädigt.

Diese Änderung des lokalen Spannungsfeldes führte vermutlich zu einer hydraulischen Öffnung der Klüfte und damit zu einem lokalen Eindringen von Gas in die überlagernde Formation. Für die darunterliegende Nahr Umr Formation deuten die Anfangsdrücke und Öl Zusammensetzungen auf eine anfängliche Verbindung zwischen dieser und der unteren Formation hin. Diese Verbindung beruht vermutlich auf einem bestehenden Kluftsystem, durch die im Laufe der Fördergeschichte eine wechselseitige Migration von Lagerstättenfluiden beobachtet wurde.

Zurzeit wird mittels Injektion von CH₄ in die sekundäre Gaskappe (Gasinjektion Schwerkraftdrainage) Öl gewonnen. Dieses Verfahren erweist sich als ein effizienter Mechanismus in der Lagerstätte. Jedoch beträgt die aktuelle Restölsättigung ca. 70%. Das Potential für die Erhöhung der Ölgewinnung ist somit sehr hoch. Neben der Wasserinjektion wurden weitere EOR-Methoden wie die Leichtöl-Dampfflutung (LOSF) und die nicht mischbare WAG (IWAG) in dem Feld erprobt, aber eingestellt, da keine erkennbaren positiven Auswirkungen beobachtet wurden (Hameed et al., 2022).

Ergebnisse der Machbarkeitsstudie

Eine am Institut durchgeführte Machbarkeitsstudie kam zu den folgenden Ergebnissen:

- Die größten Herausforderungen bei dem Einsatz von Gewinnungsmethoden in der betrachteten Lagerstätte sind das Vorhandensein von Klüften, Hohlräumen (Vugs) und der Heterogenität der Matrix, einschließlich des großen Anteils an Mikroporen und des Problems der Benetzungsbartigkeit. Vor diesem Hintergrund ist die konventionelle Förderstrategie in diesem Reservoir nur schwer anwendbar (Hameed et al., 2022).
- Nutzung des EOR-Potenzials auf Basis des Einsatzes von CO₂ wurde vorgeschlagen. Allerdings kann aufgrund der oben beschriebenen Einschränkung (max. Druck 62 bar) CO₂ als nicht mischbar mit Öl eingesetzt werden, da alle in dieser Studie verwendeten Korrelationen darauf hindeuten, dass MMP höher ist als der aktuelle sowie der initiale Lagerstättendruck.
- Folgende Verfahren wurden vorgeschlagen:
 - o CO₂-EOR-Injektion als Gas assisted gravity drainage (GAGD) in der Gaskappe
 - o CO₂ im Wechsel mit N₂-Schaum. Schaum wird als Blockierungsmittel in den Klüften betrachtet, um gas-cusping (Gasdurchbruch) zu verhindern und ein hohes Gas-Öl-Verhältnis (GOR) zu verhindern (Alkan und Göktekin, 1996).
 - o CO₂-Schaum oder N₂-Schaum als Injektionsflüssigkeit im zentralen Bereich. Die Gasinjektion kann weiterhin in nahe gelegene Bohrungen durchgeführt werden.
 - o Surfactant Alternating Gas (SAG) (Tensid als Vorspülung im Wechsel mit Gas)
- Die CO₂-Injektion könnte im betrachteten Feld effektiver sein als andere EOR-Methoden. Dies ist auf die erwähnte komplexe Struktur des Reservoirs zurückzuführen. Die wichtigsten Mechanismen der CO₂-Injektion sind in diesem Fall die Quellung und die Verringerung der Viskosität. Darüber hinaus kann die direkte Verdrängung durch CO₂ die Ölförderung unterstützen.
- In manchen Feldteilen kann die CO₂-Injektion in der Ölzone oberhalb des Öl-Wasser-Kontakt OWC als kontinuierliche Anwendung oder Huff-n-Puff eingesetzt werden.

Vorgehensweise im Labor

In der betrachteten Lagerstätte ist CO₂ nicht mit der Ölphase mischbar, was besondere Einschränkung für die laborativen Untersuchungen bedeutet. Diese werden an aus dem Feld gewonnenen Kernmaterialien bei feldähnlichen Druck- und Temperaturbedingungen durchgeführt. Dabei teilen sich die Laborversuche in drei große Blöcke auf:

- Physikalische Parameter des Öls (Viskosität, Dichte, Swelling, IFT)
- Petrophysikalische Eigenschaften des Gesteins (Porosität in Abhängigkeit von Lösungsmitteln, Porengrößenverteilung, Abbildungen im Vergleich zu anderen Lagerstätten...)
- Flutversuche

Später werden diese durch abschließende Feldtests durch den Auftraggeber ergänzt. Neben der Bestimmung von druck- und temperaturabhängigen Dichte und Viskosität ist das Quellverhalten des Öls bei unterschiedlichen CO₂ Partialdrücken ein wichtiger Parameter für die Planung der EOR-Maßnahmen.

Die Quellung wurde in einem mit Öl gefüllten Zylinder in CO₂ Atmosphäre bei unterschiedlichen Drücken beobachtet. Die Veränderung der Höhe der CO₂-Öl-Grenzfläche in Folge der Quellung wird mit einem akustischen Sensor detektiert. Bei dieser Methode werden die Differenzen zwischen den Signallaufzeiten in Volumenänderungen umgerechnet. Das experimentelle Verfahren wurde für drei verschiedene Gaszusammensetzungen

durchgeführt. Die erzielten Ergebnisse wurden mittels Autoklavenversuchen (Pressure decay) zur Bestimmung der Volumenzunahme des gleichen Öls abgeglichen.

Eine weitere Methode zu Bestimmung der Quellung ist die Tropfenkonturanalyse (Drop Shape Analysis, DSA), in der das sich ändernde Volumen eines hängenden Tropfens unter CO₂ Druck mittels Bildanalyse bestimmt wird.

Für die Laboruntersuchung wurde originales Kernmaterial der Lagerstätte präpariert. Zu diesem Zweck stehen dem Institut über 45 Liner repräsentativer Bohrkerne der Lagerstätte zur Verfügung. Die petrophysikalischen Eigenschaften des Gesteins werden an durch Soxhletextraktion gereinigtem Bohrkern vorgenommen. Zu diesem Zweck wurde zunächst das wirkungsvollste Extraktionsmittel identifiziert (Abb. 1). Von den gereinigten Gesteinsproben wurde die Reindichte und Porenradienverteilung (Abb. 2) ermittelt. Von jedem Liner wird dazu eine Mischprobe entnommen, so dass eine teufenabhängige Aussage getroffen werden kann

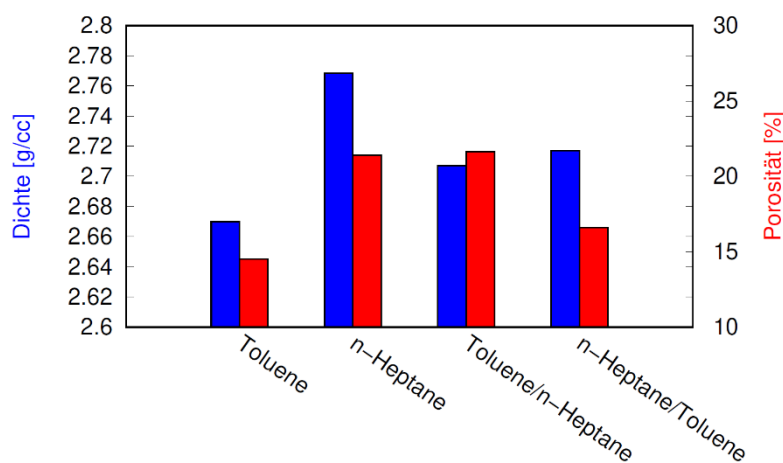


Abbildung 1: Dichte und Porosität nach Soxhletextraktion mit verschiedenen Lösungsmitteln.

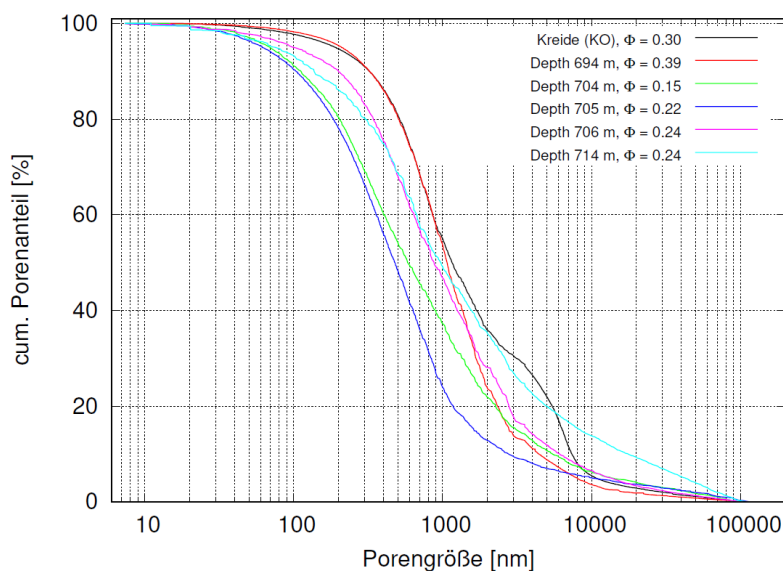


Abbildung 2: Porenradienverteilung und Porosität des Lagerstättenmaterials

Für die Durchströmungsversuche werden die Kerne in einem Kernhalter bei Lagerstättenbedingungen mit Wasser, CO₂, N₂ und CH₄ durchströmt. Das produzierte Öl wird aufgefangen und mengenmäßig erfasst. Zwischen den einzelnen Durchströmungen liegen

Ruhephasen, in denen die Probe mit einem der Gase bzw. einer Mischung aus ihnen unter Druck eingeschlossen ist. Bei der Durchströmung der Proben kann nicht nur die Fluidart variiert werden, sondern auch die Reihenfolge dieser. Auf diese Weise können eine Vielzahl von Behandlungsmöglichkeiten simuliert werden und später mit der produzierten Ölmenge korreliert werden.

Zusammenfassung

- Das Vorhandensein von Rissen und Heterogenität stellt eine große Herausforderung für den Einsatz von EOR-Methoden dar, insbesondere in Karbonatlagerstätten.
- Die Ermittlung der Porenradienverteilung an Proben unterschiedlicher Teufen zeigt, dass der Anteil der Mikroporen zwischen 50 bis 80% liegt. Somit bleibt ein großer Teil des Öls in der Matrix gebunden und kann nicht in die Klüfte fließen.
- Die wichtigsten Mechanismen der CO₂-Injektion sind in diesem Fall die Quellung und die Verringerung der Viskosität.
- Die Quellung-Experimente zeigen deutlich die Volumenzunahme insbesonders mit reinem CO₂. Diese verringert sich im Falle des Vorhandenseins von CH₄ und N₂.
- Die Flutversuche haben das Ziel, das bestgeeignete Verfahren zur Injektion von CO₂ zu identifizieren.
- Die ersten Flutversuche zeigen, dass CO₂ zur Teilmobilisierung des Öls unter den Lagerstättenbedingungen geeignet ist.

Referenzen

- Agard, P. et al. (2011) 'Zagros orogeny: A subduction-dominated process', *Geological Magazine*, 148(5–6), pp. 692–725. doi: 10.1017/S001675681100046X.
- Alkan, H. and Göktekin A. (1996) 'Experimental Investigation of Foam Flow Through Synthetic Fractures' Oil Gas-European Magazine 3/1996.
- Hameed, M. et al. (2022) 'Reservoir Performance Analysis of Eighty-Four Years of Immiscible Gas Injection in a Matured Carbonate Reservoir, Bahrain Field.', paper SPE 211348, presented at the ADIPEC held in Abu Dhabi, UAE, 31 October – 3 November 2022.. DOI 10.2118/211348-MS.
- Sadooni, F. N. and Alsharhan, A. S. (2003) 'Stratigraphy, microfacies, and petroleum potential of the Ma Ruddud Formation (Albian-Cenomanian) in the Arabian Gulf basin', *American Association of Petroleum Geologists Bulletin*, 87(10), pp. 1653–1680. doi: 10.1306/04220301111.
- Samahiji, J. A. and Chaube, A. N. (1987) 'Evolution of Bahrain Field in Relation To Western Arabian Gulf Basin.', *Society of Petroleum Engineers of AIME, (Paper) SPE*, (623 m), pp. 97–107. doi: 10.2118/15697-ms.
- Smith, S. and Parakh, S. (2016) 'Carbonate reservoir field experiments in extreme steam conditions, Bahrain field', *Society of Petroleum Engineers - SPE EOR Conference at Oil and Gas West Asia, OGWA 2016*. doi: 10.2118/179772-ms.

Stimulation der Geothermiebohrung Geretsried – Operativer Ablauf und Herausforderungen beim Technologietransfer aus der KW-Industrie

R. Tegeler¹, T. Backers²

¹Tegeler Energy, Berlin, Germany, ²Ruhr-Universität Bochum, Institut für Geologie, Mineralogie und Geophysik Lehrstuhl Ingenieurgeologie/Felsmechanik, Bochum, Germany

Im Herbst 2021 wurde im Rahmen von Forschungsprojekt ZoKrateS eine Hydraulische Stimulation an der Geothermiebohrung GEN-1ST-A1 durchgeführt. Im Verlauf der operativen Arbeiten wurde die Horizontalsektion mit einer „Multistage Stimulation Completion“ komplettiert und anschließend hydraulisch behandelt. Insgesamt konnten drei von vier Stages erfolgreich stimuliert und in Summe mehr als 330 Tonnen Stützmittel in die geklüfteten Bereiche des Malm eingebracht werden. Erste Analysen der Flowback-Phase deuten darauf hin, dass eine signifikante Verbesserung des Zuflussverhaltens im Bohrlochnahmbereich erzielt werden konnte. Der folgende Vortrag gibt einen Überblick über die operativen Arbeiten und die damit verbundenen technischen Herausforderungen. Wenngleich es sich bei Multistage Gel-Stimulationen mittlerweile um ein Standardverfahren in der KW-Industrie handelt, hat Projekt ZoKrateS aufgezeigt, dass eine Anwendung in der Tiefengeothermie teilweise mit Einschränkungen behaftet ist. Hier besteht ggf. weiterer F&E-Bedarf im Bereich Technologietransfer.

Geothermische Nachnutzung von Kohlenwasserstoffbohrungen durch tiefe Erdwärmesonden

N. Koltzer¹, M. Sporleder^{1,2}, J. Schoenherr³, S. Steininger¹, F. Wellmann^{1,4}, R. Bracke^{1,5}, P. A. Kukla⁶

¹Fraunhofer-Einrichtung für Energieinfrastrukturen und Geothermie IEG, Bochum, Germany,

²Brandenburg University of Technology Cottbus-Senftenberg BTU, Department of Electrical and Thermal Energy Systems, Cottbus, Germany, ³ExxonMobil Production Deutschland GmbH, Hannover, Germany, ⁴RWTH Aachen University, Computational Geoscience, Geothermics and Reservoir Geophysics (CGGR), Aachen, Germany, ⁵Geothermal Energy Systems, Ruhr University Bochum, Bochum, Germany, ⁶RWTH Aachen University, Geological Institute, Energy and Mineral Resources, Aachen, Germany

Die Motivation der Machbarkeitsstudie ist die geothermische Nachnutzung von Kohlenwasserstoffbohrungen als Wärmequelle in der kommunalen Wärmeversorgung. Dazu wird hier die Möglichkeit der Umkomplettierung alter und zur Verfüllung stehender Gasbohrungen zu tiefen Erdwärmesonden (TEWS) untersucht. Die mögliche Verlängerung des Wertschöpfungszeitraums von Explorations- und Produktionsbohrungen durch „Nachförderung“ erneuerbarer Wärmeenergie und der verminderte CO₂-Fußabdruck durch Einsparung neuer Tiefbohrungen sind Treiber dieses Konzepts.

In dieser Studie werden die zu erwartende Leistung umkomplettierter TEWS und die daraus errechneten Wärmegestehungskosten für Verbraucher mit Hilfe von Modellen quantifiziert. In einem ersten Projektabschnitt wird mit numerischen Modellen die Effizienz von koaxialen TEWS über eine Betriebszeit von 30 Jahren berechnet. Die zu erwartende thermische Entzugsleistung liegt zwischen 200 kW und 400 kW und kann durch Optimierung betrieblicher Parameter, sowie durch einen innovativen Ausbau, auf bis zu 600 kW angehoben werden, was jedoch mit einer Reduzierung der Vorlauftemperatur einher geht. Diese Werte sind im Vergleich deutlich höher als in bereits installierten Anlagen und deuten auf das große Potenzial dieser Wärmequellen hin. Die Untersuchung der Sensitivitäten verschiedener Parameter zeigt, dass die Ausbautiefe, die Erhöhung der Fließrate und das Herabsetzen der Rücklauftemperatur den größten Einfluss bei der Optimierung der TEWS haben. Im zweiten Projektabschnitt wurde der Wärmebedarf um zwei exemplarisch gewählte Kohlenwasserstoffbohrungen kartiert und Wärmegestehungskosten durch Wärmenetzmodellierungen berechnet. Die Ergebnisse zeigen, dass die Kosten vergleichbar sind mit anderen Energieträgern wie Biomasse aber auch mit den derzeitigen Gaspreisen. Die Entfernung zum Verbraucher spielt hier eine entscheidende Rolle, wobei durch die sehr hohe Qualität der Wärmequelle von bis zu mehr als 70 °C Vorlauftemperatur eine Wärmeversorgung über mehrere Kilometer hinweg möglich ist.

Mit dieser Studie kann das große Potenzial von Altbohrungen als qualitativ hochwertige Wärmequelle für eine kommunale Wärmeversorgung als ein wichtiger Teil der Wärmewende aufgezeigt werden. Die Nachnutzung durch TEWS überzeugt durch ein Minimum an geologischen Risiken, da sie aufgrund der Vorkenntnisse bei der vorangegangenen Kohlenwasserstoffproduktion weitgehend reduzierte Unsicherheiten aufweisen. Zudem werden die Bohrkosten als größter Posten der Investitionskosten bei der Etablierung geothermischer Anlagen eingespart. Das Potenzial der Nachnutzung zahlreicher alter Bohrlokalisationen für die geothermische Nutzung wird als sehr hoch erachtet.

Large scale heat pumps and geothermal energy – an ideal couple for a greener heating scenario

J. Schäfer, N. Wenn, C. Hüttl

Siemens-Energy, Erlangen, Germany

While climate change and security of supply are calling for substantial investment and innovation to drive the energy transition, the heating sector still relies heavily on fossil fuels.

However, technological advancements in geothermal energy exploration have increased the feasibility and affordability and hence the attractiveness of geothermal heating.

Likewise large scale heat pumps are experiencing increased attention and political support to become a key element to greenify Europe's district heating networks and industry.

The complementarity of heat pumps with renewable heat generation technologies such as geothermal but also solar and waste heat recovery allows for a wide range of application for very large heat pumps.

The presentation features interesting configurations and benefits of large industrial heat pumps in combination with geothermal energy as well as with a variety of processes within the oil and gas industry.

Lessons learned from a geothermal well test with associated sour gas in a former gas well in the Vienna Basin

M. Maierhofer, N. Romich, T. H. Hollman
OMV Exploration & Production GmbH

Abstract

The city of Vienna intends to become carbon-neutral by 2040. To reach this ambitious goal, geothermal energy will play a crucial role and should become a dominating technology to produce the required energy for district heating. The geothermal gradient in the Vienna Basin is about 3°C per 100 meters. The Northern Calcareous Alps beneath the basin have the potential to deliver hot water between 90°C and 180°C to the district heating network. Besides high temperatures, a formation with sufficient permeabilities, to extract high flow rates, is crucial for a successful hydro-geothermal project.

In 2022 a geothermal well test was executed to acquire more information about the rock and fluid properties to better quantify the potential. A former gas production well, which has been drilled into the 2800m deep target formation, was selected to reduce expenditures. This well is located few kilometers north-east of the Vienna city limits and therefore provides a possible close access point to the district heating network of the city.

A complex workover operation was necessary to access the fractured dolomite. The well was perforated from 2800 to 2873m in the aquifer below the initial gas-water contact and completed with a 4 ½" tubing.

After the acid stimulation, 2800m³ saline formation water was produced via coiled tubing lift at a rate of up to 40m³/h. The produced water was temporarily stored in 43 closed containers, as the associated gas contains H₂S. Finally, it was re-injected with up to 120m³/h into the same formation. The test objectives were amongst others determining key reservoir parameters and obtaining downhole fluid samples. Those were fully achieved.

The production and injection test delivered encouraging results. The inflow performance was excellent, low drawdowns below one bar were observed during the main flow period with 20m³/h. The calculated permeability is in the order of 500mD. Reservoir temperature is 102°C, the well head temperature increased up to 80°C during the test. The analyzed fluid samples of the formation fluid show an average gas-water ratio of 3,5Sm³/Sm³. The associated gas contains about 6mol% of H₂S and 15mol% of CO₂. A salinity of about 30.000ppm was measured in the formation water. Precipitations during the production test were mainly corrosion products, like iron sulfide (FeS). However, also some quartz and calcite materials were detected.

We recommend using high resolution gauges for geothermal well tests to avoid data smoothing. This might be required if high permeable formations with moderate rates are tested.

Introduction

Geothermal potentials can be better quantified by acquiring information about the rock properties, especially permeability and fluid data. To get this data a geothermal well test was executed in 2022. To reduce expenditures, a former gas production well, which has been drilled into the target formation, was selected. This well is located few kilometres north-east of the Vienna city limits. For the successful execution of geothermal heat projects, it is important to have possible off takers close to geothermal projects. The city of Vienna has

already an extensive district heating network in place. Therefore, a close access point to the district heating network was a crucial criterion for the well selection.

From a geological point of view, the test took place in the “Hauptdolomit” formation. This formation is a huge mainly water bearing fractured dolomite layer. It is in a depth range between 2500 and 6500m (see Figure 1), with formation temperatures of up to 180°C. Permeabilities are around 50mD, however they could also reach several hundred mD, which makes it interesting for extracting geothermal energy. (Oteleanu, Pelz, König, & Loisl, 2021)

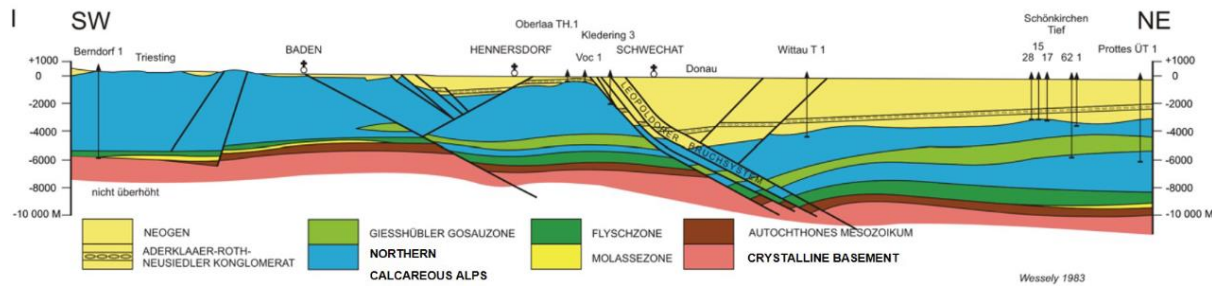


Figure 1: SW-NE Geological section across the Leopoldsdorfer Fault (Wessely, 1983)

Well Test Design

In the late 1960s the well has produced sour gas from the “Hauptdolomit”. In the end, the well was perforated and produced gas from the “Karpat”, a sandstone reservoir of the neogene basin fill. A complex workover operation was necessary to again access the 2800m deep target formation. The well was perforated from 2800 to 2873m in the aquifer below the initial gas-water contact of the Hauptdolomit and was completed with a 4 ½" tubing.

After the successful workover, the well test was performed. The test equipment consisted of a coiled tubing which was used to stimulate the well with 40m³ acetic acid and lift the fluid by injecting nitrogen during the flow periods and a well test unit which measured and processed the produced water and gas. The main components were the choke manifold, a separator, flow meters, knock out vessels, closed storage tanks and flares (see Figure 2).

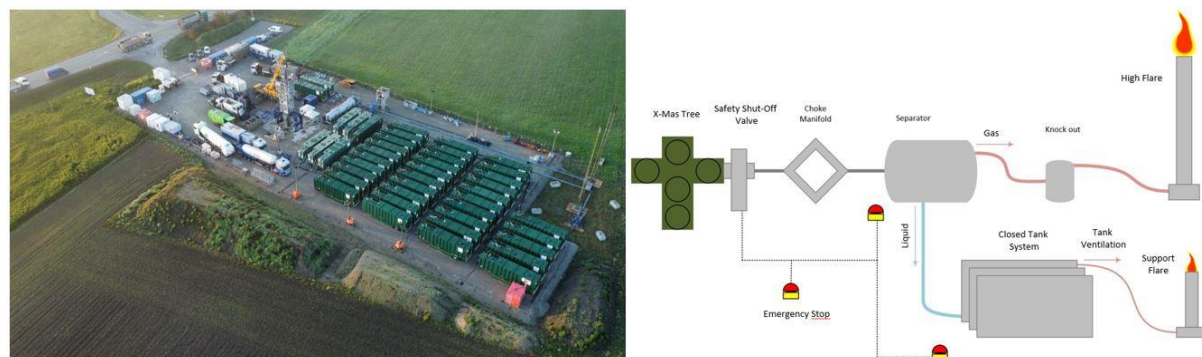


Figure 2: Overview of the well site during the production test (left) and schematic of the well test facilities (right)

During the test, saline formation water was produced, temporarily stored above ground in 43 closed containers and then re-injected into the formation. The goal was to determine key reservoir parameters to quantify the geothermal potential and obtain fluid samples to acquire valuable data for the development of potential geothermal plants.

A carefully designed test program was required to derive as much information as possible. Table 1 shows the production test design. The test program consisted of several flow and shut-in periods. After the main pressure build-up phase (PBU) 4 downhole water samples

were taken with slickline and a special sampling tool to get pressurized and uncontaminated fluid samples, which is crucial for the geochemical and PVT study.

Table 1: Production well test design

| Flow Period | Duration [h] | Rate [m³/h] | Volumes [m³] |
|------------------|----------------------|------------------------------------|--------------|
| Clean-up Flow | 12-24 | Increasing flow rate up to 25 m³/h | 300 |
| Intermediate PBU | 18-36 | 0 | 0 |
| Main Flow Period | 96 | 20 | 1920 |
| Main PBU | 96 | 0 | 0 |
| High-rate period | 12 | 40 | 480 |
| Total | 264 (~11days) | | 2700 |

The design ensured to meet the main well test objectives:

- Determine permeability x height (kh), Skin (S), reservoir pressure (p_r)
- Generate a 2-point inflow-performance ratio (IPR) to estimate the maximum inflow from the formation
- Take surface and downhole fluid samples for geochemical, materials & corrosion and PVT studies
- Determine flow barriers or reservoir boundaries within the radius of investigation

After the production test the produced water was reinjected from the closed storage tanks via a pump into the same formation. The injection rate was 60m³/h and 120m³/h, respectively. During the injection test, downhole gauges measured pressure and temperature continuously.

Besides, four seismometers were installed to measure seismic events before, during and after the test. One seismometer was located on the well site, the other three were positioned in distances of 2-3 km around the well site in an equilateral triangle.

Test results and discussion

The well test operation was conducted safely and efficiently, with no safety incidents and uncontrolled releases during the test. The technical test objectives were fully achieved. The inflow performance was excellent, low drawdowns below one bar were observed during the main flow period. The productivity index (PI) for water was about 32m³/h/bar, which exceeded the expectations. Reservoir pressure is slightly under hydrostatic, whereas reservoir temperature is 102°C, resulting in a geothermal gradient of 3,27°C/100m. The well head temperature during the high-rate period (40m³/h) increased up to 80°C. The temperature loss to the surrounding system at these low rates was quite significant. Furthermore, the injected nitrogen to lift the fluid, cooled down the produced hot water. Usually, geothermal wells are produced at much higher production rates and with ESPs (Electrical Submersible Pump). In such wells, the temperature loss is very low.

The quality of the data was sufficient for a conclusive well test interpretation. Only the early time was distorted due to the pulling out of the coiled tubing from the wellbore before shutting in the well. As a surface shut-in was performed, fluid segregation between gas and formation water led to noisy data in the beginning. The apparent half unit slope is an indication of a fractured and/or stimulated well. The middle time is in good agreement with various pressure build-ups and of good quality. The negative skin is in line with the stimulated well. The infinitive acting radial flow (IARF) period starts from ~30hr into the build-up. The kh (permeability x height) is about 16.000mDm. The late time shows no boundary effects or signs of depletion (see Figure 3)

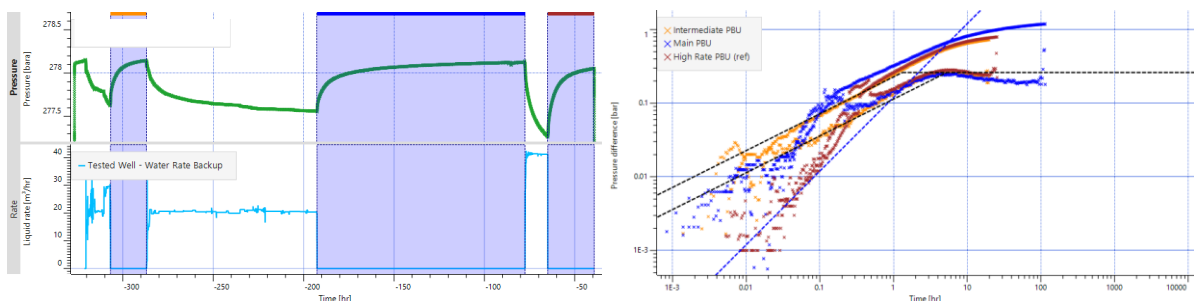


Figure 3: Downhole pressure data and rates during the production test (left) and log-log plot including all three pressure build-ups (right)

The data from the injection test (fall-off test) is in good agreement with PBUs (Pressure-Build-Ups) from the production test. The skin during injection is slightly increased, which is in line with expectations as the injected fluid contains some precipitations. The result of kh was 24.000 mDm and this is slightly higher than in the build-up periods.

They analyzed fluid samples of the formation fluid show an average gas-water ratio of $3,5 \text{ Sm}^3/\text{Sm}^3$. The associated gas contains about $6\text{mol}\%$ of H_2S and $15\text{mol}\%$ of CO_2 . A salinity of about 30.000 ppm was measured in the formation water. Precipitations during the production test were mainly corrosion products, like iron sulfide (FeS). However, also some quartz and calcite materials were detected.

Conclusion

The production and injection test delivered encouraging results for further development of hydrothermal plants in the “Hauptdolomit” formation of the Vienna basin. An experienced workforce on OMV and contractor side was also critical to manage the complex workover, the testing operations as well as the handling of sour gas and hot fluids.

The production behaviour of the well was strongly improved by acid stimulation of the fractured dolomite. Near wellbore inflow increased strongly by dissolving calcite and hence opening the existing fracture network.

One of the most important knowledge gains of this test was an uncontaminated and pressurized formation water sample. Therefore, a lot of effort was put into getting a proper sample at reservoir conditions for laboratory analysis. With that in hand, the correct gas composition, undisturbed of the injected nitrogen from the lifting operations, could be determined and a scaling study could be performed.

The produced fluid contained H_2S , therefore a closed tank system was required to safely store the formation water. The closed tanks with a capacity of 70 m^3 per unit as well of the size of the well location limited the total production volume to around 2800 m^3 . Furthermore, it was necessary to mix the produced hot water with cold formation water to not exceed the maximum allowed temperature in the coated storage tanks of 60°C . This increased the complexity of the operations.

On the other hand, storing the formation water on the surface and re-injecting it afterwards delivered valuable information about the injectivity and allowed a comparison with productivity.

Artificial lifting of the formation water is possible with an ESP or with Coiled Tubing by injection of nitrogen. The advantage of the second option is that it allows for an acid wash with Coiled Tubing and that it offered a higher flexibility on the production rates. On the downside it should be mentioned that it turned out to be challenging to maintain stable rates

and a hard shut-in procedure is not possible with this method as the Coiled Tubing has to be pulled out of the well. If the goal of such a test would be to determine the well capacity, an ESP would be recommended.

To get better data on early time pressure behaviours a downhole shut-in tool which allows for a quick and hard downhole shut-in would be recommended. On the other hand, operational flexibility would get lost. Furthermore, a production logging tool (PLT) during the injection period would show the contribution of each individual zone in the reservoir.

We also recommend using higher resolution gauges for geothermal well tests to avoid data smoothing. This might be required if high permeable formations with moderate rates are tested.

References

- Oteleanu, A., Pelz, K., König, M., & Loisl, J. *The NCA and their Geothermal Potential in the Vienna Basin*. Vienna: OMV. (2021)
- Wessely, G. *Zur Geologie und Hydrodynamik im südlichen Wiener Becken und seiner Randzone*. Wien: Mitteilungen der Österreichischen Geologischen Gesellschaft, 76, 27–56.(1983)

Influence of Capillarity on Salt Precipitation during Primary CO₂-Brine Displacement

B. Jammernegg¹, T. Schollenberger², J. Hommel², B. Flemisch², H. Ott¹

¹Montanuniversität Leoben, Department of Petroleum Engineering - Chair of Reservoir Engineering, Leoben, Austria, ²Universität Stuttgart, Institut für Wasser- und Umweltsystemmodellierung, Stuttgart, Germany

Geological storage of CO₂ is currently considered as the most promising large-scale option to avoid emissions by industrial activities. As suitable subsurface containers, oil and gas reservoirs and the more abundant saline aquifers are considered. The injection of dry or under-saturated supercritical CO₂ into water-bearing formations leads to the formation of a dry-out zone due to evaporation/dissolution of the resident brine into the injected fluid and, thus, potential precipitation of formerly dissolved brine constituents. If minerals precipitate within the pore space of a rock formation, porosity and permeability are negatively affected, which potentially impairs injectivity. Even though the impairment of injectivity poses both operational and financial challenges, minor attention has been dedicated to this research area so far. What is the size of the affected zone itself? What is the impact of capillarity on the fluid transport therein?

In this presentation, the responsible evaporation of brine and fluid transport mechanisms are outlined and discussed, as well as the potential reduction of the formation permeability and with it the injectivity. A remaining important question is the zone of counter-current flow in the direction of the wellbore, which determines the amount of salt that potentially precipitates in the near-wellbore area and the accompanied porosity reduction. Current reservoir simulation tools are not accounting for this effect because they typically do not capture evaporation kinetics. Earlier studies indicate that in certain cases the respective permeability can be reduced by several orders of magnitude (Ott et al., 2021), which comes close to a loss of the injection well.

We approach this question with numerical simulations to determine the size of the zone affected by the undersaturated CO₂ that allows for salt to be transported toward the injector and the major parameters governing this zone and their dependencies as well as the fluid transport therein. We are currently developing and testing a reservoir simulation module based on DuMuX capable of describing reaction kinetics. In parallel, we built up a meter-scale core flood experimental setup that allows us to extract fluid saturation profiles and solid saturation (precipitation) via CT imaging of core samples. Besides that, by monitoring the differential pressure, we can determine changes in permeability and with it changes in injectivity.

This study aims to establish an experimental/numerical workflow to forward simulate, respectively design, and to history match experiments with a reservoir simulator to upscale the results to the field scale. The work is currently in progress – the applied workflow will be outlined in detail.

Development of a Well Delivery Process for CO₂ Injection Wells

K. Krueckert

Wintershall Dea AG, Global Well Construction, Hamburg, Germany

The emission of greenhouse gases are the dominant cause for the climate change observed over the last centuries, and the increased carbon dioxide (CO₂) concentrations in the atmosphere play the most prominent role in the observed warming. To mitigate adverse consequences of climate change, reduction of greenhouse gases is goal of political initiatives globally like the Paris Agreement. Generation of CO₂ can be hard to abate and thus capturing CO₂ and its geological storage is seen as important measure to counteract further increase of CO₂ in the atmosphere; carbon capture and storage (CCS) can facilitate the mitigation of climate change on a global scale.

Wintershall Dea has ambitious climate targets and is aiming for Net Zero emissions by 2030 with strong commitment to sustainable development, transparency, and a low-carbon future. As Wintershall Dea builds on its gas portfolio by developing hydrogen capabilities, CCS will be an essential element of the sustainable development plan by providing a mitigation pathway for Scope 3 emissions as defined in the Paris Agreement.

CO₂ injector wells play a central role in CCS as they connect the CO₂ capture facilities topsides with the geological storage sites downhole, mostly depleted hydrocarbon reservoirs or saline aquifers. These wells have to deal with a variety of challenges. Any well penetrating the cap rock in the storage site poses a significant risk for the long-term containment of CO₂. Injector wells will be exposed to harsher conditions than other wells of the projects (e.g. monitoring wells) in terms of pressure, CO₂ concentration and temperature variance.

Technical key challenges for CO₂ injector wells are identified as:

- Handling of nearly pure CO₂ as fluid
- Variance in CO₂ stream
- Phase management
- Long-term well integrity
- Monitoring requirements

Whereas the well design should allow for CO₂ injection at rate which makes the overall CCS project economically viable.

The presentation illustrates the development of a well delivery process for CO₂ injector wells. Many lessons can be learned from the comprehensive experience of the oil and gas industry in terms of safe and efficient well design, management and operations. Therefore, the newly developed process for CO₂ injector wells follows the principle of the established processes for delivering oil and gases production wells, however, considers the specific requirements of CCS projects.

Importance of Proper Curing and Aging of Cements in Laboratory Testing for CCS Applications

T. Mandt¹, O. Czuprat², A. Fogden³

¹Wintershall Dea GmbH, Global Well Construction, Hamburg, Germany, ²Wintershall Dea Technology & Service Center GmbH & Co. KG, Drilling Fluids & Cement Testing Laboratory, Barnstorf, Germany, ³Wintershall Dea Technology & Service Center GmbH & Co. KG, Digital Rocks, Barnstorf, Germany

Abstract

Carbon capture and subsequent geological storage requires wellbore cement that is resistant to CO₂ for at least several centuries. Conventional API Class oil-well cement based on Portland cement is thermodynamically unstable against CO₂. Previous laboratory studies have shown that the carbonation reactions often cause destabilization and formation of fractures. However, published findings vary greatly, owing to the multitude of methods used to prepare cement samples for studying their interaction with corrosive environments.

In the course of the EUDP-coordinated research project Greensand Phase II, a systematic trial matrix of cement types (API and non-API) and additives have been mixed and cured in sample cells under actual downhole conditions. These samples for lab testing were cured at reservoir pressure and temperature, since the alternative of hardening under atmospheric conditions would not represent the reality and would render the cement more sensitive to CO₂ attack.

Complementary slurry characterization ensured that all formulations met oilfield specifications in terms of density, rheology, thickening time and compressive strength development. Subsequently, the cement plugs were aged in synthetic formation water under reservoir conditions to generate a comparable degree of maturation, regardless of the specific cement type and formulation. Each cement plug was prepared as unconfined as well as confined in steel pipe.

Prior to final aging under CO₂-containing environments for varying durations, every single plug was non-destructively 3D imaged by X-ray micro-CT to ensure reproducible homogeneity without defects and to characterize the pre-testing state. Post-aging micro-CT imaging with 3D pre-post alignment and complementary SEM analysis were performed to detect the type, severity and localization of the CO₂-induced changes. More than 250 cement plugs were produced and processed using this workflow within the project to date.

First results from the research project are presented and a concluding outlook will be given.

Introduction

Geological storage of CO₂ typically relies on the presence of an impermeable rock layer, which can act as a caprock, situated above the reservoir formation. The caprock is penetrated by wells which potentially can act as communication pathways for CO₂ from the reservoir towards the surface. An important role plays the cement which is supporting casing and forms a barrier with low permeability and high geo-mechanical strength. It prevents leakage, but must be able to withstand the conditions imposed by the CO₂ injection.

The project Greensand Phase 2 is to deliver a CO₂ storage pilot test, in the Nini Field, Danish

North Sea. If successful, this will enable storage of $\frac{1}{2}$ to $1 \frac{1}{2}$ million tons of CO₂ by 2025 and 4 to 8 million tons CO₂ by 2030 in the depleted oil fields of the Siri Area. Project Greensand allows Denmark to reach its ambitious climate target in 2025 and 2030.

For the demonstration CO₂ is captured in Belgium and transported in ISO containers by ship to the Nini platform, where the O₂ is pressurized and injected into the NA-05 well of the Nini West reservoir (Figure 1). The pilot project will monitor the pilot injection as per regulations.

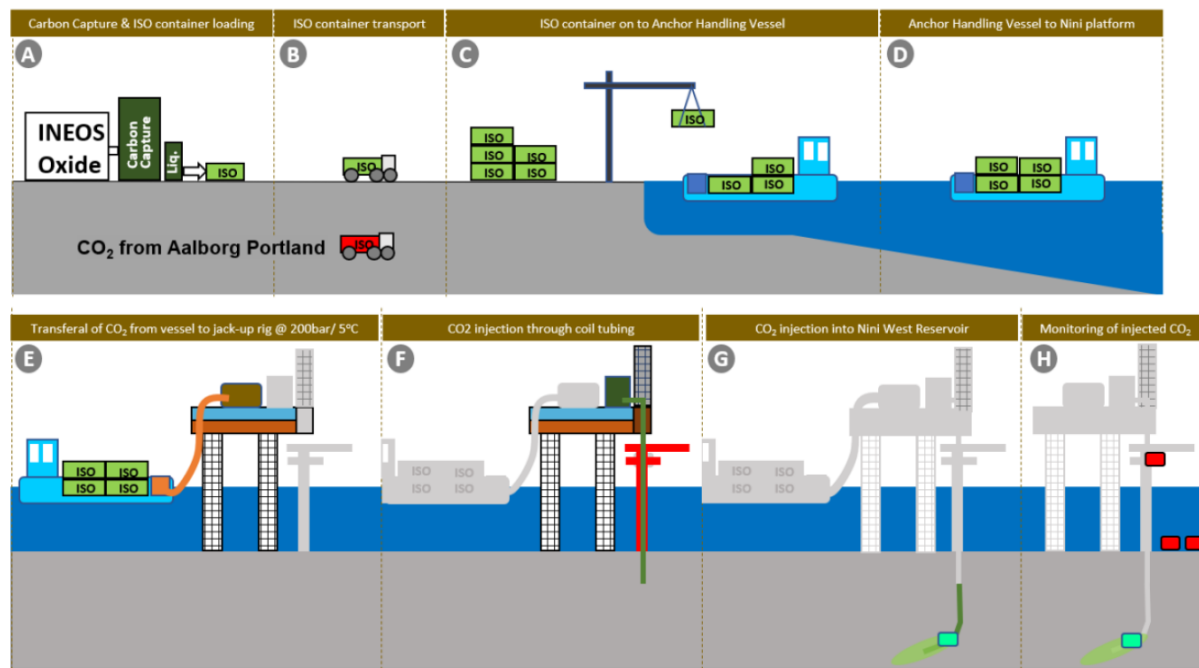


Figure 1: Purpose of Project Greensand Phase 2 is to make a system prototype demonstration in an operational environment. CO₂ will be shipped to the Nini Platform, and injected into the Nini West Reservoir. Additional CO₂ will be provided by Aalborg Portland (red truck in (B)) and additional monitoring technologies will be qualified (red boxes in (H)).

In Project Greensand Phase 2 CO₂ storage is the qualifying step, in the process of maturing the first CO₂ storage site in Denmark. The purpose is to mature the safe, low-emission and cost-effective long-term storage of CO₂ in the Nini Field by 2025, to the next level.

Carbon capture and subsequent geological storage requires wellbore cement that is resistant to CO₂ for at least several centuries. Contact with CO₂ can impact the integrity of the well cement by dissolution (generating porosity/permeability for fluid flow) or alterations which lower the mechanical strength of the material, thus increasing the risk of fracturing.

If dissolution is substantial, it can create sufficient porosity and permeability for fluid flow and lower the capillary threshold pressure for CO₂ entry into cement pore spaces [1]. Conversely, carbonate precipitation can result in porosity and permeability decrease [2,3],, lowering the risk of CO₂ leakage and slowing the alteration rate. 2) Alterations can affect the mechanical strength of the material, increasing or decreasing the risk of fracturing [2]. Both scenarios can result in conduits for migration of buoyant supercritical CO₂ or, if a pressure gradient exists, CO₂ charged water.

Conventional API Class oil-well cement based on Portland cement is considered thermodynamically unstable against CO₂. Previous laboratory studies have shown that carbonation reactions often cause destabilization and formation of fractures. However, published findings vary greatly, owing to the multitude of methods used to prepare cement samples for studying their interaction with corrosive environments.

Impact of Curing and Aging Conditions on Cement Plug Quality

Several methods of plug manufacturing have been reported in the literature. Lesti et al. have casted their investigated slurries in cylindrical plastic containers and cured in synthetic reservoir fluid under atmospheric conditions for two weeks [4]. Afterwards the plastic containers were removed and the cement cores cured for another 28 days at elevated temperature and pressure (90 °C and 400 bar) in the synthetic reservoir fluid. These samples which were cured in the afore mentioned two steps were then taken to carbonation experiments.

Multiple cracks were reported because of reaction with CO₂ after 6 months for the following cement systems:

- a) Class G + inorganic filler/stabilizer (A)
- b) Class G + Latex (C)
- c) neat Class G (D),

whereas the blast-furnace based system incl. EFA-filler (B) appeared to be more resistant to CO₂.

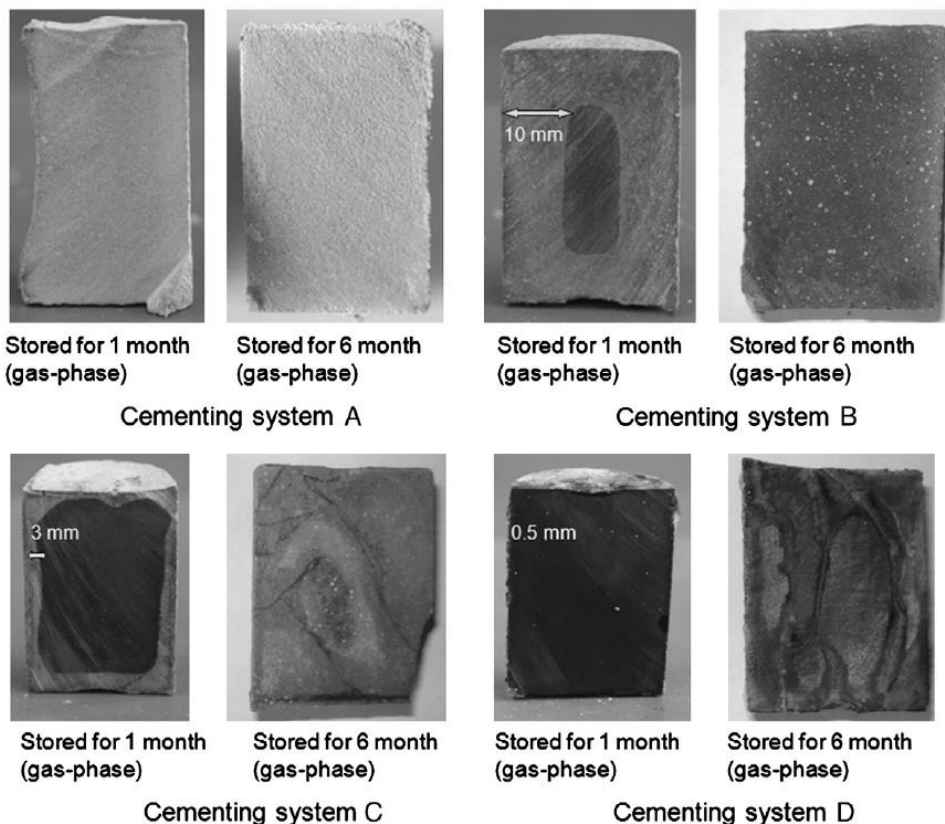


Figure 3: Cement plugs of different systems after aging in CO₂ [4].

Kutchko et al [5] produced cylindrical cement samples (12 mm x 130 mm) and cured same in 1% NaCl solution under 150 bar and 50 °C for 28 days to simulate the hardening of cement in contact with a saline aquifer at 1300 m depth. Afterwards the samples were partially submerged in 1% NaCl solution and the autoclave pressurized with CO₂ to 150 bar and 50 °C.

No further non-destructive damage survey was done prior the exposure to CO₂. After the treatment in CO₂ samples were cut into ~1 cm slices, and polished for electron and optical microscopy analysis and micro hardness testing as described in [5]. For permeability measurements larger cores (50.8 mm by diameter and 40 mm length) with same cement recipe were produced the same way. The intention of the work was to compare the resistance of 35/65 Pozzolan against 65/35 Pozzolan Cement.

Kutchko et al.[5] evaluated the reaction of Portland cement with CO₂, and from their laboratory testing determined the reaction rates are sufficiently slow as to not be a concern over the timeframe of decades. It should be noted that Kutchko's experiments were run with Slug Cement with densities between 1,70 sg – 1,75sg.

The progress of the carbonatization is depending on the diffusion of the CO₂ through the cement. Slowing down the diffusion means in primarily to reduce the pathways through the cement. An increase of the Particle/Water ratio meaning the increase of cement density is most likely a very efficient method to extend the lifetime of the seal.

Barlet-Gouedard [6] measured the degradation rate by diffusion of supercritical CO₂ of less than one centimetre per year. That would mean that a cement sheet from the formation to the casing steel would be eventually in several years crossed, but the degradation of a cement seal along the axis of the well in the caprock could take very long, even assuming that the process of degradation could progress with constant speed and the captured CO₂ would might not be react to something else.

These examples were selected to show that the imaginations of the degeneration velocity of cement still vary widely. To get a better understanding of the matter and to make results comparable it is necessary to describe the preparation of samples and the method of contamination precisely. Micro CT imaging is a very useful tool to make changes in the cement structure visible, especially sample scanning prior and after the CO₂ ageing helps to understand processes in the rock.

Analytical Scope

In the course of the EUDP-coordinated research project Greensand Phase II, a systematic trial matrix of cement types (API and non-API) and additives have been mixed and cured in sample cells under actual downhole conditions. These samples for lab testing were cured at reservoir pressure and temperature, since the alternative of hardening under atmospheric conditions would not represent the reality and would render the cement more sensitive to CO₂ attack. Boersheim et al. [7] showed that both permeability and porosity decreased upon curing under pressure and temperature. Similar observations were made in the Wintershall Dea TSC lab when cement samples cured under atmospheric conditions tend to have gas bubbles and showed cracks.

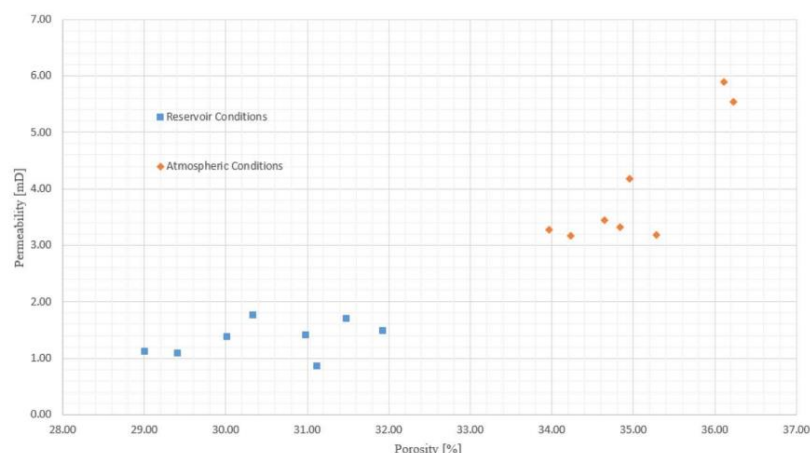


Figure 2 Porosity and permeability values for cement G samples - (Red) Cured at atmospheric conditions (Blue) Cured at reservoir conditions [7]

Complementary slurry characterization ensured that all formulations met oilfield specifications in terms of density, rheology, thickening time and compressive strength development. Each cement plug was prepared as unconfined as well as confined in steel pipe.

Subsequently, the cement plugs were aged in synthetic formation water under reservoir conditions to generate a comparable degree of maturation, regardless of the specific cement type and formulation. It was ensured that the samples did not dry out, but always remained saturated so that no salt precipitated, nor cracks formed. Pressurizing the samples to downhole conditions and releasing the pressure afterwards were conducted carefully over two days to prevent them from failing due to internal overpressure.

Prior to final aging under CO₂-containing environments for varying durations, every single plug was non-destructively 3D imaged by X-ray micro-CT to ensure reproducible homogeneity without defects and to characterize the pre-testing state. This proved to be a very effective in the later interpretation of the samples, as it gave the opportunity visually to compare the samples before and after the exposure to CO₂. Beside that, the preparation of samples always implies that a certain percentage were prepared with some internal failure (e.g. cracks). As in most cases, but also in our investigation, the ageing capabilities for CO₂-containing atmospheres are the bottleneck in regard of number of samples which can be treated.

Post-aging micro-CT imaging with 3D pre-post alignment and complementary SEM analysis were performed to detect the type, severity and localization of the CO₂-induced changes. More than 250 cement plugs were produced and processed using this workflow within the project to date.

Selection of cement types and Plug Fabrication

In the course of the project Greensand Phase 2, 3 major cement types and formulations were produced at Wintershall Dea's Technology & Service Center and subsequently exposed to CO₂ containing atmospheres:

- a) Class G
- b) Class G + Latex
- c) Blast-furnace cement (non-Portland based) + reactive filler

The experimental work relied on three steps:

- i) Production/curing of cement plugs
- ii) brine aging of the plugs to allow time for the reactions within the cement to occur, and
- iii) experiments with the plugs, brine and CO₂.

Between curing, brine aging and before experiments, all plugs were kept wet in sealed containers ensuring that the pore space of the cement was water saturated at all times. After the curing, the plugs were immersed in the respective mixing water, whereas after brine aging and the CO₂ experiments, the surrounding fluid was synthetic formation brine.

For the Class G formulation (a), the respective legacy formulation of the TAIL slurry for the 9 7/8" intermediate casing was used as basis. For comparison, a variation with Latex as additive (b) and a non-Portland based blast-furnace cement (c).

All slurries were mixed and characterized according to API Recommended Practice RP 10B-2 ensuring that the slurries are in alignment with their original specifications and can be considered "fit-for-purpose" for field application.

To simulate downhole conditions during the curing process, cylindric molds (Figure 3) filled with the cement slurry are placed in an HPHT Consistometer.



Figure 3: Mold for cement slurry curing: left = disassembled, middle = filled with cement slurry and right = closed with a lid.

The standard curing time was chosen based on the actual compressive strength development. After 96 hours at Nini West reservoir conditions (60 °C, 200 bar), the compressive strength development has reached its plateau. After the curing is completed, the cured cement cylinders are cut into smaller plugs and kept wet in the mixing water prior to subsequent analysis and aging (Figure 4).



Figure 4: Cement samples before (top) and after cutting (bottom).

Ageing of Cement Samples

The cement plugs are aged under conditions present in the Nini West reservoir: 200bar pressure, 60° Celsius and synthetically produced Nini formation brine. To distinguish if future changes in material properties are caused by the formation brine or the presence of CO₂ the samples are altered in two steps. First, they were aged for 28 days in base Nini formation brine without CO₂, followed by 120 days of alteration in the presence of CO₂.

Base brine ageing

The base brine ageing is conducted in an autoclave system consisting of steel pressure cells, a heating cabinet and two Vindum pumps (Figure 5). To avoid corrosion in the pressure cells the cement plugs are individually packed into sealed Latex gloves filled with formation brine (Figure 6). Each pressure cell contains three samples. To exclude air the pressure cells are filled with tap water. Because of the Vindum pumps the temperature in the heating cabinet can be raised in parallel with the pressure. To prevent damage on the samples in the beginning and end of the experiment the temperature and pressure conditions are changed slowly over a period of 24 hours.

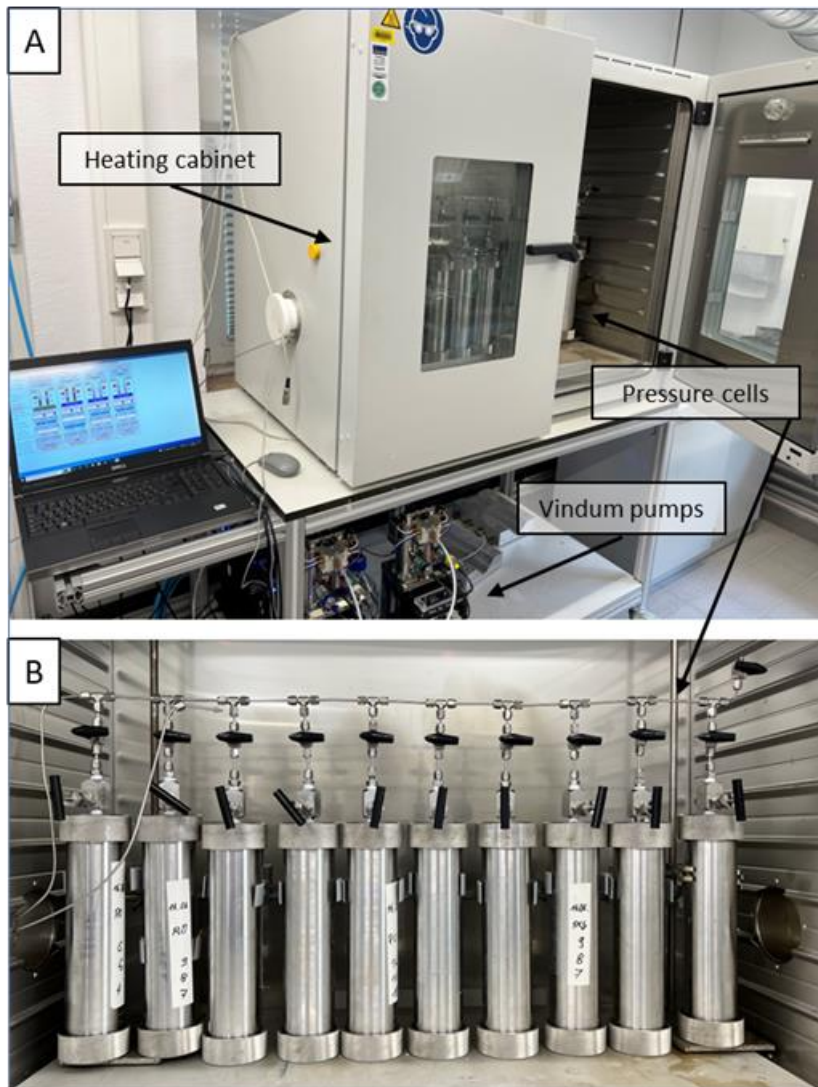


Figure 5: Autoclave system used for base brine aging.

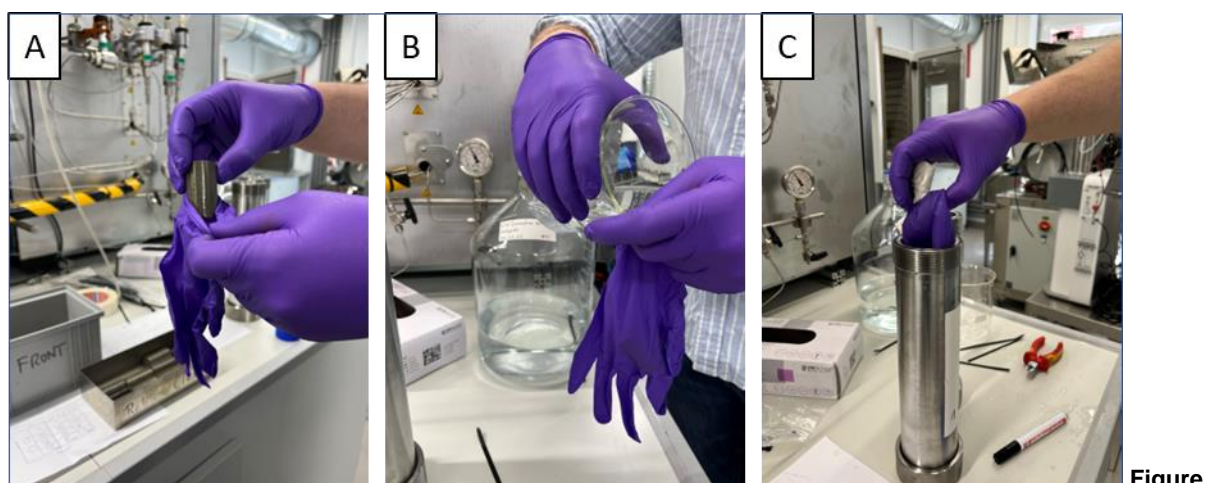


Figure 6: Sample preparation for base brine ageing. Cement plugs are individually packed into Nitril gloves filled with synthetic Nini formation brine .

Figure

Ageing in CO₂

The CO₂ ageing is performed in Hastelloy C276 pressure cells (Figure 7). In total this cell can hold 25 cement plugs divided on five baskets stacked on top of each other into the cell. During the alteration experiment the cell gets filled half and half with CO₂ saturated formation brine and CO₂ gas. Therefore, during the experiment the lowest two baskets are submerged in the brine while the upper two baskets are in contact with gas. The samples in the middle basket are in contact with both fluids. Because of size and weight limitation the pressure cell could not fit in the heating cabinet used for the base brine ageing experiments. To ensure a constant temperature over the period of 120 days the pressure cell was immersed in a 250 liter heated water tank. To avoid sample damage we increased the temperature and pressure at the beginning of the experiment separately. First we submerged the pressure cell in the 60°C water tank and applied 60bar of pressure. After 24 hours the pressure increased to 100bar because of the heat expansion of the water. In a second step we added CO₂ gas till we reached 200 bars of pressure. At the end of the experiment we reduced the temperature of the water tank till room temperature (22°C after 24 hours) before we used a needle valve to reduce the pressure slowly over a period of eight hours.



Figure 7: Setup used for cement ageing in presence of CO₂.

- [1] Carey 2013. Geochemistry of wellbore integrity in CO₂ sequestration. Rev. Mineral. Geochem. 77, 505-539.
- [2] Fabbri et al., 2009. Effect of carbonation on the hydro-mechanical properties of Portland cements. Cem. Concr. Res. 39, 1156-1163.
- [3] Jung and Um, 2013. Experimental study of potential wellbore cement carbonation by various phases of carbon dioxide during geologic carbon sequestration. Appl. Geochem. 35, 161-172.
- [4] M. Lesti et al. / Cement and Concrete Research 45 (2013) 45–54
- [5] Kutchko, B. et al.: CO₂ Reaction with Hydrated Class H Well Cement under Geologic Sequestration Conditions: Effects of Flyash Admixtures, National Energy Technology Laboratory, United States, 2008
- [6] Barlet-Gouédard, V., Rimmelé, G., Goffé, B. and Porcherie, O. 2006. Mitigation strategies for the risk of CO₂ migration through wellbores, paper IADC/SPE 98924, presented at the IADC/SPE Drilling Conference, Miami, Florida, 21-23 February
- [7] Boersheim et al. Experimental Investigation of Integrity Issues of UGS Containing Hydrogen, 81st EAGE Conference and Exhibition, London, England 2019

Comprehensive Guidelines On The Suitability Criteria Of Cementitious Materials For Carbon Capture And Storage (CCS) In Oil Wells

E. Congiu¹, T. Mandt², K. Dideriksen³, F. Canonico⁴, H. Plack⁵, E. Boccaleri⁶, C. Cassino⁷, G. Paul⁸

^{1,6}Dip.to per lo Sviluppo Sostenibile e la Transizione Ecologica, Università del Piemonte Orientale, Vercelli, Italy

²Wintershall Dea AG, Hamburg, Germany

³Geological Survey Of Denmark & Greenland University of Copenhagen, Copenhagen, Denmark

⁴Built - Buzzi Unicem Innovation Lab and Technology, Vercelli, Italy

⁵Buzzi Unicem, Dyckerhoff, Global Well Cement, Wiesbaden, Germany

^{7,8}Dip.to di Scienze ed Innovazione Tecnologica, Università del Piemonte Orientale, Alessandria, Italy

Abstract

In order to reduce atmospheric greenhouse gases, capturing and storing of carbon dioxide underground is considered as the most effective, low-cost, long-term and safer approach. Depleted oil and gas wells are a suitable geologic site for storage and can offer stability and effective CO₂ trapping. However, cement used in oilwell drilling, under CCS applications, is exposed to extreme conditions as high temperatures, high pressures and acid, salt and CO₂ attack. There have been reports of leakage incidents associated to cement degradation and failure of the integrity of the cement sheath. On the other hand, as a systematic retrieval of samples is impossible and lab-scale simulation is extremely difficult, there are very few representative studies reported in the literature that firmly address the key features for a long-term cement integrity on wells operating in supercritical state. In addition, once possible, experiments carried out on real samples extracted directly from exhausted oil wells and laboratory experiments provide conflicting data due to mismatch between the simulated lab scale conditions and the real well conditions. A comprehensive literature survey highlights that the types of cement providing an effective long-term barrier for CO₂ storage underground are Portland cement of Class H or G according to API and ISO specification. To withstand extreme conditions and high depths, class G and H cement can be profitably modified by adding additives, such as pozzolan. One of the main methods of effectively increase the strength of cement subjected to HTHP conditions is to add silica flour in 35/40% BWOC. Extreme and harmful conditions for cementitious binders, however, are not only high temperatures and pressures, but also the ground level temperature (there are oil fields in extremely cold areas) and the need of cement formulation to bear these environmental conditions as well as the temperature gradient in depth. For these conditions, special cements with a gypsum/Portland mix and the addition of sodium chloride (12%) are commonly used. In some regions a pozzolanic additive, Class F Fly ash, is the most common mineral additive used in well cement formulations. Other kind of problems can occur due to the presence of brines containing sulfates which are usually solved or lessened by the use of high-sulfate-resistant (HSR) well cements. Concerning CO₂, the best method to face its attack is related to the reduction of porosity and permeability which can be done in the easiest way by reducing the water-to-cement (-to-binder) ratio. With regard to the general resistance of Portland cements to CO₂ the formation of Ca(OH)₂ during cement hydration is considered as the weakest part. Any material added to Portland cement which reduces the amount of formed Ca(OH)₂ improves the CO₂ stability. Quite commonly this is achieved by adding pozzolanic material.

Introduction

To try to keep global warming within a threshold of +1.5°C, as envisioned by the 2015 Paris Agreement, it is not enough just to limit or zero emissions, but it also becomes crucial to eliminate the CO₂ already in the atmosphere due to emissions over the past 200 years as a result of high fossil fuel use¹. The European Union in 2019 made formal commitments to

reduce net greenhouse gas emissions by at least 55 percent by 2030, compared to 1990 levels, and to achieve carbon neutrality, so-called "zero emissions" by 2050. Complete elimination of CO₂ emissions is difficult to achieve so different solutions are needed to reduce its concentration in the atmosphere. Among these certainly play an important role are those using the strategy of CO₂ capture and storage (CCS) or capture and reuse (CCU).

CCS consists of three main steps: the capture, transport, and storage of carbon dioxide. Effective CO₂ capture and separation as well as delivery/transportation technologies are currently under study, but a key issue is the proper and safe storage in suitable reservoirs. Geological sites are good candidates, but the key aspects are adequate capacity, good isolation from the surrounding environment and a stable geological condition that guarantees its integrity in the time. The arrangement of the basins depends on their location as well as on their characteristics. Possible CO₂ storage sites are oil and gas fields, fields exploited with Enhanced Oil and Gas Recovery technology, salt formations sites, abandoned mines, basaltic formations, clayey formations soaked in oil and gas.

Commonly oil or gas wells used for injecting CO₂ in depleted gas or oil fields are cemented with Portland cement-based slurries. A crucial aspect here is the proof of such material on its long-term stability in an environment of CO₂ under downhole conditions, i.e. under pressure and temperature in order to ensure a proper durable sealing and avoid leakages².

There are very few representative studies reported in the literature that addresses the long-term cement integrity under a combination of pressure and temperature along with chemically challenging downhole conditions. Testing cement under real conditions is essential but extremely difficult due to physical limits (pressure, temperature), chemical aspects (composition) and time (years).

The main objectives of this research activity are to provide an overview of the existing studies, related to well characteristics, temperature effects, pressure effects, attack by acids and salts in addition to the CO₂ concentration in the well, under the point of view of well cements and their degradation under HTHP conditions.

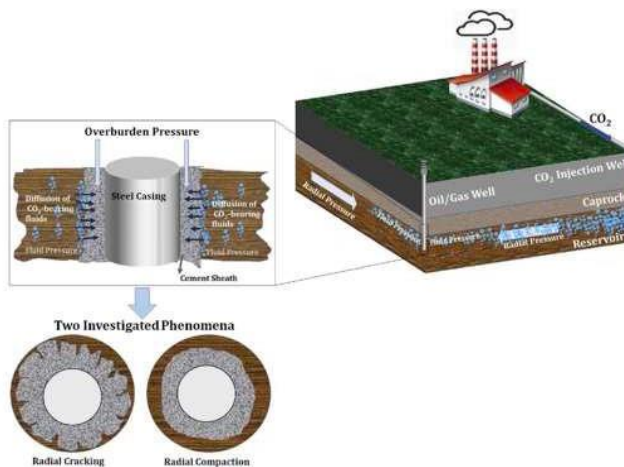
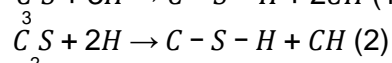
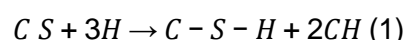


Figure 1. Cross section of oil well. This figure shows the pipeline, the cement envelope and the caprock.³

Effects of CO₂ on cement properties

The reactions involve the formation of carbonic acid and its interaction with the Ca(OH)₂ present in the cement after hydration (scheme 1,2,3) forming calcium bicarbonate. The dissolved calcium bicarbonate reacts with the alkali constituents to form calcium carbonate and water. This causes a decrease of pH to about 8.5 and this can damage the metal piping in contact with the cement matrix, opening the way to possible corrosion.



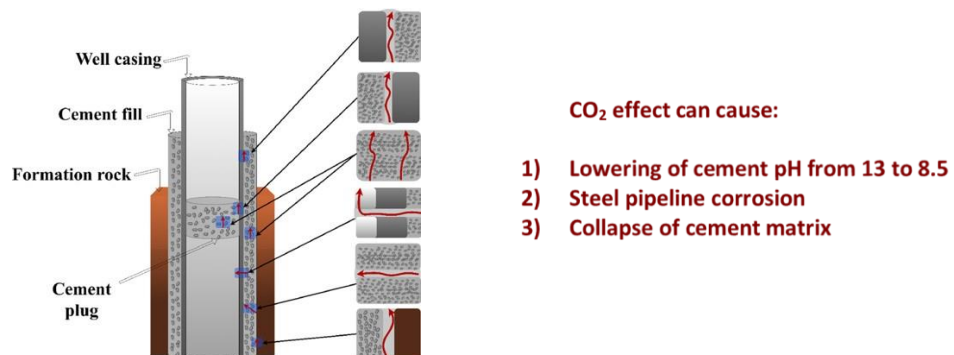


Scheme 1,2,3.

The net result of CO₂ degradation is an increased porosity and permeability and decreased compressive strength. In the wellbore, this can result in a loss of corrosion protection of the casing and a loss of zonal isolation. Carbon dioxide corrosion of Portland cements is thermodynamically favored and, therefore, cannot be completely prevented as long as CO₂ has permanent and free access to the Portland cement used.

According to the scientific literature, beneficial aspects to control the effects of contact with CO₂ in the cement wellbore are:

- Addition of a pozzolanic material (and/or fly ash) to the cement.
- Reduction of the water/cement ratio (densification) to reduce the permeability of the cement matrix.
- Addition of latex to increase the effectiveness of sealing^{2,4}.

Figure 2. Possible pathways of CO₂. ⁵

Effects of the geophysical conditions on well suitability

Among the factors that may reduce/prejudge the suitability of the well for CCS, temperature and/or pressure conditions, as well as temperature gradients need to be carefully considered. It is known from literature² that hydrostatic pressure and temperature increase with increasing depth. Both have an effect on hydration and with respect to temperature also on stability of cement. From decades of experience, cement is known to be highly resistant to many combinations of temperature and hydrostatic pressure, if necessary, reducing the effect of degradation with the help of adding mineral additives, e.g. silica for borehole temperature above 110 °C.

Effects of the chemical conditions on well suitability

Temperature and pressure, however, are not the only factors that can lead to degradation. Depending on the well site there may be various conditions of pH, which inside the cement matrix is usually close to the value 12. However, it could go down depending on attacks by acids. An example is the presence of sulfuric acid which, due to acidizing workover, is present in oil fields and shows a strong attack (Barlet-Gouédard et al.⁶, Duguid et al.⁷, Gan et al.⁸). Another important factor is the presence of salts such as NaCl, among the various ideal sites for CO₂ storage, old salt deposits that are currently empty have been considered, the

presence of salt could adversely affect the life of the cement without considering the likely additional effect to other factors².

Two effects:

- 1) harmful salts/brines in formation fluids chemical attack
- 2) salt concentration differences between inside and outside the cement matrix (= leaching/dissolution)

Effects of improper cement slurry design on well suitability

Other factors are related to the cement matrix that can lead to the formation of any porosity, gaps, and cracks with critical effects on carbon dioxide leakage. For example, an incorrect percentage of water and cements, usually too much mix water, leads to higher porosity in the matrix and an increased likelihood of CO₂ migration as well as increased chemical degradation. Supplementary cementitious materials (such as fly ash, blast furnace slag, natural pozzolan, etc.), if used in unproper quantities or if materials unsuitable for exposure to supercritical conditions can increase the probability of matrix failure⁴.

Apart from improper cement slurry design also operational aspects can compromise CO₂ tightness of a well, e.g. improper cleaning of borehole walls i.e. remaining filter cake from drilling mud.

Discussion

It becomes essential to evaluate the different factors that can change cement properties for well operations under high temperature and pressure conditions through literature and laboratory experiments.

In the following paragraphs, some strategies will be presented to try to limit the degradation of the cement matrix by CO₂ and other factors dependent on the well candidate selected for CCS application.

Statistically Portland cements of Class H or G (porosity of 25 to 30% and permeability of 21 μD to 1 μD), are considered to be the cements that show the highest resistance to attack by CO₂ under supercritical conditions⁹.

Regarding the effects of pozzolan a majority of sources confirm: the addition of up to 50% fly ash to API Classes H and G inhibits CO₂ entry into cement microstructure. Thus, Portland cement-based well systems can prevent significant migration of CO₂ from reservoirs for long periods of time (at least decades)¹⁰. It is essential to conduct laboratory experiments directly on cement samples exposed to realistic well conditions for many years and extracted from the oil wells (Figure 3) (Crow et al.¹¹).

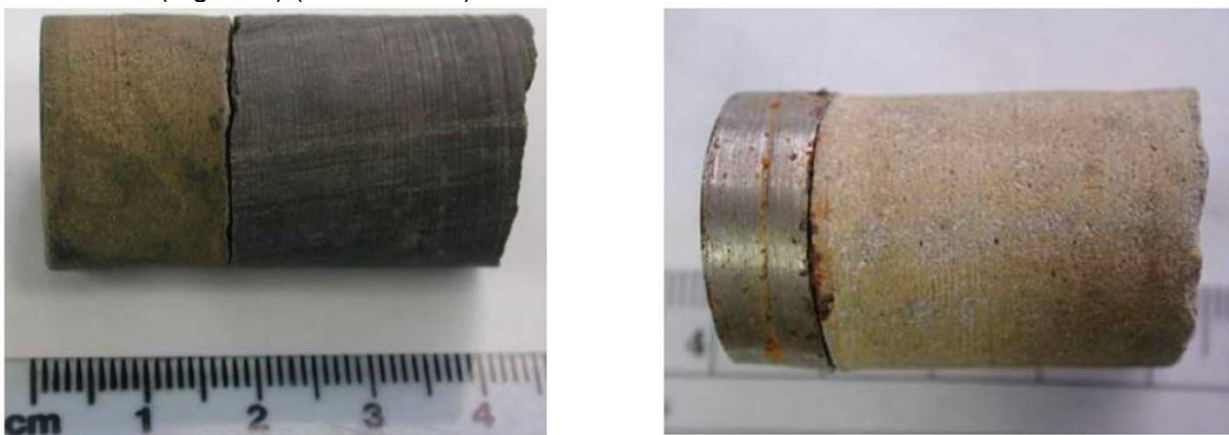


Figure 3. Photograph of cores from a 30 year old exhausted Dakota well showing the tight fit at interface between cement and formation (left panel) as well as between casing and cement (right panel).¹¹

Temperature and pressure Effects

Increasing depth within the Earth's crust, following temperature gradient, the amount of potentially CO₂ increases, which induces the breakdown of portlandite and C-S-H in cement as well as increased precipitation of calcite and amorphous silica. We recommend the use of different and more specific cement formulations according to the various well depths.

Usually, silica flour with 35 percent concentration is used to eliminate the strength retrogression phenomenon, but it has been observed that in a CO₂-rich environment it is advisable to reduce the concentration of the additive material to 20 percent.

To solve the low-temperature problem, one solution seems to be the use of special cements with a gypsum/Portland mix and the addition of sodium chloride.^{4,2}

Additive effect

Some authors investigated the use of nano-scaled materials for improving CO₂ stability of Portland-cement based slurries for well cementing: adding nanosilica (n-SiO₂) in suitable amount improves the rheological and mechanical properties of the cement, while the porosity and permeability decreases by 33 and 99%, respectively. After being exposed to CO₂ for longer period, the n-SiO₂ amount had no expressive influence on the compressive strength, and all the n-SiO₂ cement systems performed better than the standard cement at HPHT conditions (Abid et al.¹², Kutcho et al.¹³, Duguid et al.¹⁰, Laudet et al.¹⁴, Hatami et al.¹⁵).

The best result for the compressive strength, the capillary permeability, and other, mechanical properties were observed when 1.25 wt% nanoalumina was used (Tiong. et al.¹⁶).

Adding Nanotitania could reduce the porosity from 11 to 9%, but it is not suitable for CO₂ sequestered sites due to its instability under high-temperature and high-pressure conditions (Tiong et al.¹⁷, Lee et al.¹⁸, Chang et al.¹⁹).

Nanoclay reduces the porosity and water absorption, is cheap, but shows no pozzolanic activity.

Basalt powder (BP) can be used, as a mineral additive, in cement paste, modifying the fundamental cement properties such as microstructure (porosity and permeability), mechanical, and chemical resistance. Disadvantages: formulations with a high BP content (≥ 0.5 wt.%) demonstrated characteristics that may not recommend their application in CCS wells since they presented, under extreme conditions, high porosity low resistance to CO₂, and mechanical properties that were compromised by the carbonation process.²

In some regions the pozzolan additive, Class F fly ash, is the most common additive used in cement for well-sealing in oil-gas field operations. Pozzolan-cement blends (35:65 and 65:35 vol/vol) exposed to supercritical CO₂ and CO₂-saturated brine underwent only slight cement carbonation after 30 years.

Effect of sulphatic waters

Formation brines containing sulfates are well considered and managed in oilwell cement formulations, as sulfate are one on the most destructive agents for Portland cements.

For this issue, commonly cement used contain very low C₃A amounts and are therefore classified as High Sulfate Resistant (HSR).

Some studies suggest that in the simultaneous presence of CO₂ and sulfate brines, CO₂ attack is much less severe than that in the system without additional sulfate and even mitigate the deterioration of the cement's strength and elastic modulus.²⁰

As well, Class H Portland cement were reacted in brines containing 0.05 M sulfate and/or magnesium ions under both GCS (Geologic CO₂ sequestration) (50 °C and 100 atm CO₂) and control (50 °C and atmospheric pressure) conditions. Slower cement carbonation rates were observed in the presence of sulfate because of gypsum precipitation on cement surfaces.

Under GCS conditions, the dissolved CO₂ lowered the pH of the solution surrounding cement surfaces, thus favoring the formation of gypsum over calcite on cement surfaces, while the

high pH condition in pore solution inside cement favors the formation of calcite over gypsum. The presence of magnesium had no significant effect on cement degradation under GCS conditions, as brucite, magnesium carbonates and magnesium calcite did not form, due to the low pH at cement surface and the limited diffusion of Mg into cement inner layers.²¹

Presence of salt

The results of laboratory tests conducted with slurries of different salt concentrations showed that the contact of the cement matrix with the salt interface improves with increasing salt concentration in the cement. Although no dissolution occurs when using a salt saturated slurry, these slurries are quite difficult to design with the desired properties of compressive strength development, sedimentation, free water, fluid loss. Cement slurries used for salt formation often contain NaCl up to saturation level. At the same time, in salt formations sites, different ionic concentrations can compromise cement integrity due to dissolution/osmotic forces.² Experimental studies²² have shown that a CO₂-rich brine first affects the steel surface, causing the leaching of Fe²⁺ ions in solution and inducing the precipitation of FeCO₃ on the steel surface (corrosion phenomenon). This corrosion layer has protective characteristics and can retard the progress of the corrosion front. If it proceeds on the surface of the cement, two processes occur: (i) the dissolution of Portlandite, which increases the pH and calcium (Ca) concentration in the medium, and (ii) the carbonation process of the cement, which leads to the formation of calcium carbonate (CaCO₃), thus reducing the porosity of the material.

Conclusion

Capturing and underground storing of carbon dioxide is considered as the most effective, low-cost, long-term and safe approach. Depleted oil and gas wells are a suitable geologic medium for storage and can offer stability and effective CO₂ trapping. However, cement when used for CCS applications is exposed to extreme conditions: high temperatures, high pressures, acid effects, brine effects and CO₂ attack. More importantly, to ensure compliance with specification and application specific requirements, as in the case of wells for CO₂ storage, testing cement formulations under representative downhole condition is essential.

Following the literature survey, it was found that the best cement classes that can create a long-term barrier for CO₂ storage underground are Portland cements of API Classes H or G according to API Specification 10° and ISO 10426-1. Both cement classes are characterized as "basic well cements" and commonly used in the field in combination with various chemical and mineral additives, as examples for the latter, among others, pozzolans or silica flour or nanosilica, some of them to make the cement slurry formulation to withstand extreme conditions such as high temperatures and other challenging downhole conditions.

The best method so far to counter CO₂ attack seems to be the addition of a pozzolanic material, e.g. Type F fly ash, to the Portland cement containing formulation, which reduces the amount of formed Ca(OH)₂ in the cement matrix and thus improves its CO₂ stability.

- (1) Nature (London, United Kingdom) Volume: 534 Issue: 7609 Pages: 631-639 Journal; Article; Research Support, Non-U.S. Gov't 2016 DOI: 10.1038/nature18307. *Paris Agreement Climate Proposals Need a Boost to Keep Warming Well below 2 °C.*
- (2) Erik B.Nelson, Dominique Guillot. *Well Cementing*, Second Edition.; Schlumberger.
- (3) Bagheri, M.; Shariati Pour, S. M.; Ganjian, E. Prediction of the Lifespan of Cement at a Specific Depth Based on the Coupling of Geomechanical and Geochemical Processes for CO₂ Storage. *International Journal of Greenhouse Gas Control* **2019**, 86, 43–65. <https://doi.org/10.1016/j.ijggc.2019.04.016>.
- (4) The ChevronTexaco and BP Cement Manual, 2002.
- (5) Freire, A. L.; José, H. J.; Moreira, R. de F. P. M. Potential Applications for Geopolymers in Carbon Capture and Storage. *International Journal of Greenhouse Gas Control* **2022**, 118, 103687. <https://doi.org/10.1016/j.ijggc.2022.103687>.
- (6) Barlet-Gouédard, V.; Rimmelé, G.; Porcherie, O.; Quisel, N.; Desroches, J. A Solution against Well Cement Degradation under CO₂ Geological Storage Environment. *International Journal of Greenhouse Gas Control* **2009**, 3 (2), 206–216. <https://doi.org/10.1016/j.ijggc.2008.07.005>.
- (7) Duguid, A.; Radonjic, M.; Bruant, R.; Mandecki, T.; Scherer, G.; Celia, M. THE EFFECT OF CO₂

- SEQUESTRATION ON OIL WELL CEMENTS. 5.
- (8) Gan, M.; Zhang, L.; Miao, X.; Wang, Y.; Fu, X.; Bai, M.; Li, X. Micro-CT Characterization of Wellbore Cement Degradation in SO₄²⁻-Bearing Brine under Geological CO₂ Storage Environment. *Geofluids* **2019**, *2019*, 1–10. <https://doi.org/10.1155/2019/5164010>.
 - (9) Crow, W.; Carey, J. W.; Gasda, S.; Brian Williams, D.; Celia, M. Wellbore Integrity Analysis of a Natural CO₂ Producer. *International Journal of Greenhouse Gas Control* **2010**, *4* (2), 186–197. <https://doi.org/10.1016/j.ijggc.2009.10.010>.
 - (10) Duguid, A.; Scherer, G. W. Degradation of Oilwell Cement Due to Exposure to Carbonated Brine. *International Journal of Greenhouse Gas Control* **2010**, *4* (3), 546–560. <https://doi.org/10.1016/j.ijggc.2009.11.001>.
 - (11) Crow, W.; Brian Williams, D.; William Carey, J.; Celia, M.; Gasda, S. Wellbore Integrity Analysis of a Natural CO₂ Producer. *Energy Procedia* **2009**, *1* (1), 3561–3569. <https://doi.org/10.1016/j.egypro.2009.02.150>.
 - (12) Abid, K.; Gholami, R.; Mutadir, G. A Pozzolanic Based Methodology to Reinforce Portland Cement Used for CO₂ Storage Sites. *Journal of Natural Gas Science and Engineering* **2020**, *73*, 103062. <https://doi.org/10.1016/j.jngse.2019.103062>.
 - (13) Kutchko, B. G.; Strazisar, B. R.; Lowry, G. V.; Dzombak, D. A.; Thaulow, N. Rate of CO₂ Attack on Hydrated Class H Well Cement under Geologic Sequestration Conditions. *Environ. Sci. Technol.* **2008**, *42* (16), 6237–6242. <https://doi.org/10.1021/es800049r>.
 - (14) Laudet, J.-B.; Garnier, A.; Neuville, N.; Le Guen, Y.; Fourmaintraux, D.; Rafai, N.; Burlion, N.; Shao, J.-F. The Behavior of Oil Well Cement at Downhole CO₂ Storage Conditions: Static and Dynamic Laboratory Experiments. *Energy Procedia* **2011**, *4*, 5251–5258. <https://doi.org/10.1016/j.egypro.2011.02.504>.
 - (15) Hatami, S.; Hughes, T. J.; Sun, H.; Roshan, H.; Walsh, S. D. C. On the Application of Silica Gel for Mitigating CO₂ Leakage in CCS Projects: Rheological Properties and Chemical Stability. *Journal of Petroleum Science and Engineering* **2021**, *207*, 109155. <https://doi.org/10.1016/j.petrol.2021.109155>.
 - (16) Tiong, M. Cement Degradation in CO₂ Storage Sites: A Review on Potential Applications of Nanomaterials. *Journal of Petroleum Exploration and Production Technology* **2019**, *12*.
 - (17) Tiong, M.; Gholami, R.; Abid, K.; Ekhlasur Rahman, M. Nanomodification: An Efficient Method to Improve Cement Integrity in CO₂ Storage Sites. *Journal of Natural Gas Science and Engineering* **2020**, *84*, 103612. <https://doi.org/10.1016/j.jngse.2020.103612>.
 - (18) Lee, B. Y.; Kurtis, K. E. Influence of TiO₂ Nanoparticles on Early C3S Hydration. *Journal of the American Ceramic Society* **2010**, *93* (10), 3399–3405. <https://doi.org/10.1111/j.1551-2916.2010.03868.x>.
 - (19) Chang, C.-F.; Chen, J.-W. The Experimental Investigation of Concrete Carbonation Depth. *Cement and Concrete Research* **2006**, *36* (9), 1760–1767. <https://doi.org/10.1016/j.cemconres.2004.07.025>.
 - (20) Li, Q.; Lim, Y. M.; Jun, Y.-S. Effects of Sulfate during CO₂ Attack on Portland Cement and Their Impacts on Mechanical Properties under Geologic CO₂ Sequestration Conditions. *Environ. Sci. Technol.* **2015**, *49* (11), 7032–7041. <https://doi.org/10.1021/es506349u>.
 - (21) Guo, J.; Cao, B.; Steefel, C. I.; Chen, J.; Hu, Y. Effects of Sulfate and Magnesium on Cement Degradation under Geologic CO₂ Sequestration Conditions. *International Journal of Greenhouse Gas Control* **2017**, *63*, 118–125. <https://doi.org/10.1016/j.ijggc.2017.04.017>.
 - (22) Celia, M. A.; Bachu, S.; Nordbotten, J. M.; Bandilla, K. W. Status of CO₂ Storage in Deep Saline Aquifers with Emphasis on Modeling Approaches and Practical Simulations: STATUS OF CO₂ STORAGE IN DEEP SALINE AQUIFERS. *Water Resour. Res.* **2015**, *51* (9), 6846–6892. <https://doi.org/10.1002/2015WR017609>.

Decentralised energy supply with fuel cells and green hydrogen

F. Lehmann¹, M. Michael¹, U. Beyer², S. Scheffler²

Texulting GmbH¹, Fraunhofer Institute for Machine Tools and Forming Technology²

Abstract

Decentralised energy supply with hydrogen is the goal of the project "HyTrA - Hydrogen Tryout Area", which is being carried out together with the "Hydrogen Taskforce" of the Fraunhofer Institute for Machine Tools and Forming Technology IWU Chemnitz as part of the funding programme "Export Initiative for Green and Sustainable (Environmental) Infrastructure of the Federal Ministry for the Environment, Nature Conservation, Building and Nuclear Safety (BMUV)".

Here, hydrogen could be produced decentrally from renewable energies and used for stationary reconversion into electricity by means of fuel cells. With these so-called microgrids, there is the possibility of combating energy poverty and supplying companies in South Africa and Namibia with sufficient and sustainable energy. In addition, the currently widespread generators, which are mostly diesel-based, could be gradually replaced and a significant contribution made to reducing CO₂ emissions. In addition, these microgrids can also guarantee a stable, continuous and area-wide energy supply in conurbations. This would support the development of structures that ensure continuous medical care and industrial production and services. But construction sites or drilling rigs could also be supplied with green energy on a decentralised basis in rural areas. This would also lead to immense social benefits, promote economic development, and prevent ecological overexploitation and economically motivated migration.

To achieve this, it is necessary to create aggregates for microgrids that are both robust and effective and can be flexibly deployed for different application scenarios. At the same time, the scalability must allow the system to "grow" with increasing demand. The most important aspect and the greatest challenge, however, is to ensure economic production that guarantees cost parity with the current fossil alternatives. In this way, the basis that will eventually lead to the market introduction of hydrogen-based microgrids and, ultimately, to their acceptance by the population.

Introduction

Renewable energies such as solar energy, wind energy, hydropower and biomass are low-emission and help reduce greenhouse gas emissions that contribute to global warming. They replace fossil fuels such as coal, oil and gas, which release large amounts of greenhouse gases when burned. Using renewable energy can reduce emissions of carbon dioxide and other greenhouse gases, helping to slow climate change and preserve the planet for future generations. The transition to renewable energy is therefore an important component of climate protection measures at national and international level.

There are many benefits to using renewable energy, but there are also some challenges and problems that come with it. These are some of the most important problems:

Unpredictability: The availability of renewable energy sources such as solar, wind and hydro can fluctuate and be unpredictable. This can lead to fluctuations in electricity supply and make renewable energy planning and integration difficult.

Costs: Although the cost of renewable energy has decreased in recent years, it is still higher than the cost of fossil fuels such as coal and gas. This may mean that some countries or companies can-not afford to switch to renewable energy.

Storage: Storing renewable energy is a challenge because most renewable energy sources do not generate electricity continuously. There are ways to store renewable energy, such as battery storage or pumped storage power plants, but they are not yet as effective or cost-efficient as desired.

Grid stability: The integration of renewable energy into the electricity grid can lead to instabilities, as the generation of electricity from renewable sources can be fluctuating and unpredictable. This requires careful planning and coordination to ensure that the power grid remains stable.

Environmental impacts: Although renewable energy is generally considered environmentally friendly, it can also have negative impacts on the environment. For example, large wind turbines or solar power plants can alter landscapes and affect wildlife.

Dependence on raw materials: Renewable energy requires the use of raw materials such as lithium, cobalt, and rare earths to produce batteries and other components. The availability and extraction of these raw materials can also be associated with environmental problems and social challenges.

Storing renewable energy in hydrogen can be a solution to some of the challenges of renewable energy. Hydrogen can be used as an energy storage medium, as it can be converted into electricity and heat in a fuel cell or combustion engine when needed. This can help solve the problem of un-predictable availability of renewable energy sources, as hydrogen can be used as an energy storage device to store energy when it is available and then release it when it is needed. Another advantage of hydrogen as an energy storage device is its high energy density. Compared to batteries, hydrogen can store a larger amount of energy and keep it for longer periods of time.

The potential applications for hydrogen based self-sufficient MicroGrids are diverse. For example, there is yet untapped potential especially in rural, often remote, and difficult-to-access areas in developing and emerging countries. Here, hydrogen could be produced decentral from renewable energy and used for stationary reconversion into electricity by means of fuel cells. With H2 microgrids, there would be an opportunity to combat energy poverty and to supply these regions with sufficient and sustainable energy. In addition, generators that are currently widely used, mostly based on diesel, could be gradually replaced and a substantial contribution to reducing CO2 emissions could be realised. In addition, these microgrids can also guarantee a stable, continuous, and comprehensive energy supply in conurbations. This would support the development of structures that guarantee not only continuous medical care but also industrial production and services. This would also lead to immense social benefits, promote economic development, and prevent ecological overexploitation and economically motivated migration.



It is necessary to create aggregates for microgrids that are robust and effective and can be used flexibly for different application scenarios. At the same time, scalability must allow the system to "grow along" with increasing demand. The most important aspect and the greatest challenge, however, is to ensure economic production that guarantees cost parity with the current fossil alternatives. In this way, the basis can be created that will ultimately lead to a market ramp-up of hydro-gen-based microgrids and ultimately to acceptance by the population.

This is the task of the HyTrA (South Africa) and HygO (Namibia) projects funded by the German Federal Ministry for the Environment, Nature Conservation, Nuclear Safety and Consumer Protection.

Both projects are briefly described below.

HyTrA – Hydrogen Tryout Areal



Supported by:



Federal Ministry
for the Environment, Nature Conservation,
Nuclear Safety and Consumer Protection

based on a decision of
the German Bundestag



Project partners:

texulting

Fraunhofer
IWU

Funding Code:

67EXI5556B

67EXI5556A

Duration: 01.12.2021 – 30.11.2023 | Target Country: South Africa

The project focuses on the development of a compact 8 kW hydrogen microgrid. The aim is to create an effective, robust, and cost-parity alternative to the polluting, fossil-fuelled generators that play a central role in South Africa as emergency power generators or to support the unstable, non-area-wide energy supply. The compact hydrogen microgrid unit includes complete power-to-power sector coupling. This includes solar cells for the generation of climate-neutral energy. Used in the electrolyser, this green energy will be used to split water and produce hydrogen and oxygen. Storage units allow for staggered use. Finally, the hydrogen can be used for reconversion to electricity by the integrated fuel cell. This produces electricity and water. The water is recycled for electrolysis in a closed system.

The focus is on the use and networking of different components that ensure hydrogen production, storage, and reverse power generation for a decentralised power supply independent of the temporary availability of renewable energies.

A modular, closed structure is essential here, which allows the system to be largely maintenance-free, flexibly scalable, and variably adaptable.

The technical development will be accompanied by various socio-economic and socio-ecological activities. The microgrid itself should also act as a showcase for hydrogen technology and arouse the interest of local companies to take on parts of the component production, assembly, or installation. The information and training provided will heighten awareness of environmental aspects and fundamentally contribute to the acceptance of hydrogen.

With this economic and social combination, HyTrA makes it possible not only to consider hydrogen in terms of climate policy, but also to develop it in terms of sustainable value creation. This substantially intensifies the possibilities of using new solutions to bring about a profound transformation of energy systems in emerging countries. Nationally and internationally comparable regions should be motivated to realise structural and cultural change in a similarly positive way. In addition, the Social Development Goals (SDG) 7 - Renewable Energy, Goal 8 - Good Jobs and Economic Growth, 9 - Innovation and Infrastructure, 13 - Climate Action and 17 - Partnerships to Achieve the Goals are directly addressed.

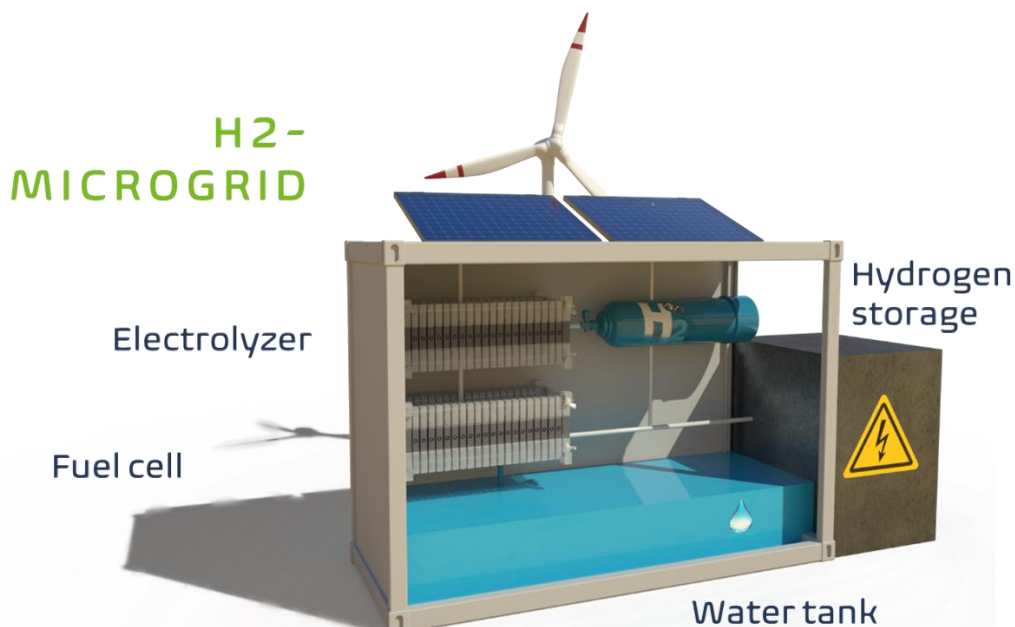


Figure 1: HyTrA H2-Microgrid

HygO – Hydrogen and Oxygen Biotope



www.hygotech

Supported by:



based on a decision of
the German Bundestag



Project partners:

texulting



Fraunhofer
IWU



Funding Code: 67EXI6502

Duration: 01.01.2023 – 31.12.2025 | Target Country: Namibia

Creating microgrids that are robust and effective and can be used flexibly for different application scenarios is a solution for the energy transition. At the same time, their scalability must allow the system to "grow" in line with increasing demand. The most important aspect and the greatest challenge, however, is to ensure economic production that guarantees cost parity with the current fossil alternatives. In this way, the basis can be created that will ultimately lead to a market ramp-up of hydrogen-based microgrids and ultimately to acceptance by the population. Furthermore, the branding "Made in Germany", which continues to be used worldwide as a seal of quality and innovation both for classic export goods in mechanical and plant engineering and increasingly for GreenTech products, is to be used to establish a Hydrogen & Oxygen Biotope Namibia (HygO) for microgrids in Namibia. The central component of HygO is the robust microgrid designed for the South African market in the HyTrA project, in which an electrolyser for hydrogen production and a fuel cell stack for reverse power generation are compactly combined.

The decisive innovation is that the HygO microgrid will also have an additional circuit for biological-mechanical water treatment. The general scarcity of water in connection with hydrogen production is a decisive influencing factor for the breakthrough of hydrogen technology in Namibia. The HygO microgrid thus gains additional importance and relevance for the intended region of application.

The microgrid was designed from the outset with a closed water cycle for reasons of resource efficiency. This means that if the microgrid is filled once with clean water, this becomes hydrogen ("waste": pure oxygen) in the electrolysis process, which later becomes water again ("waste": energy) in the fuel cell stack with the addition of air-oxygen. This is then fed back into the electrolysis process, thus closing the energy generation-water cycle. Clean drinking water is generally scarce in Namibia and Africa and is therefore a very valuable resource. It is reluctantly used in technical processes, as this is often socially unacceptable. In contrast, polluted water, so-called "dirty water", is much more common and also available in sufficiently high quantities. For this reason, the oxygen released during electrolysis, combined with other filter technologies, is to be used to treat industrial water from dirty water in parallel with the electrolysis process. The addition of oxygen, the "waste product" of electrolysis, causes bacteria in the dirty water to multiply in general. They thus become active and promote water treatment, e.g. by destroying carbon and other pollutant particles.

- Microgrids are a solution for the energy transition, must be robust, effective, flexible and scalable
- Economic production with cost parity to fossil alternatives is the biggest challenge
- The HygO project in Namibia aims to establish a Hydrogen & Oxygen Biotope with hydrogen-based microgrids
- The HygO microgrid is a combination of electrolyser and fuel cell stack with a closed water loop for resource efficiency
- The HygO microgrid has another loop for bio-mechanical water treatment to save clean water and be socially acceptable
- The oxygen released during electrolysis is used with filter technologies to treat industrial water from "dirty-water".

Microgrid Technology

The micro-grid is a small, self-sufficient power grid for various applications. All the necessary components of the micro-grid are located in a transportable housing, for example a shipping container. The solar cells on the roof of the container convert the solar energy of the sunlight into electricity. This electricity is used to produce hydrogen and oxygen from fresh water in the electrolyser. The hydrogen is compressed and stored in suitable gas cylinders. If electricity is required, the hydrogen can be converted back into electricity by feeding in ambient air (oxygen) via a fuel cell stack. The waste product is water. This is stored in a tank and made available for electrolysis as required. This creates a closed water circuit that only needs to be filled at the beginning and then operates almost loss-free. Therefore, no fresh water needs to be added during operation.

The structure and the components used are shown in Figure 2.

The microgrid itself can be extended by various modules. Among other things, a wastewater treatment unit that uses the oxygen produced for the biological treatment of wastewater and sewage into service water. In addition, a cooling module can be added that enables food to be stored for longer periods of time.

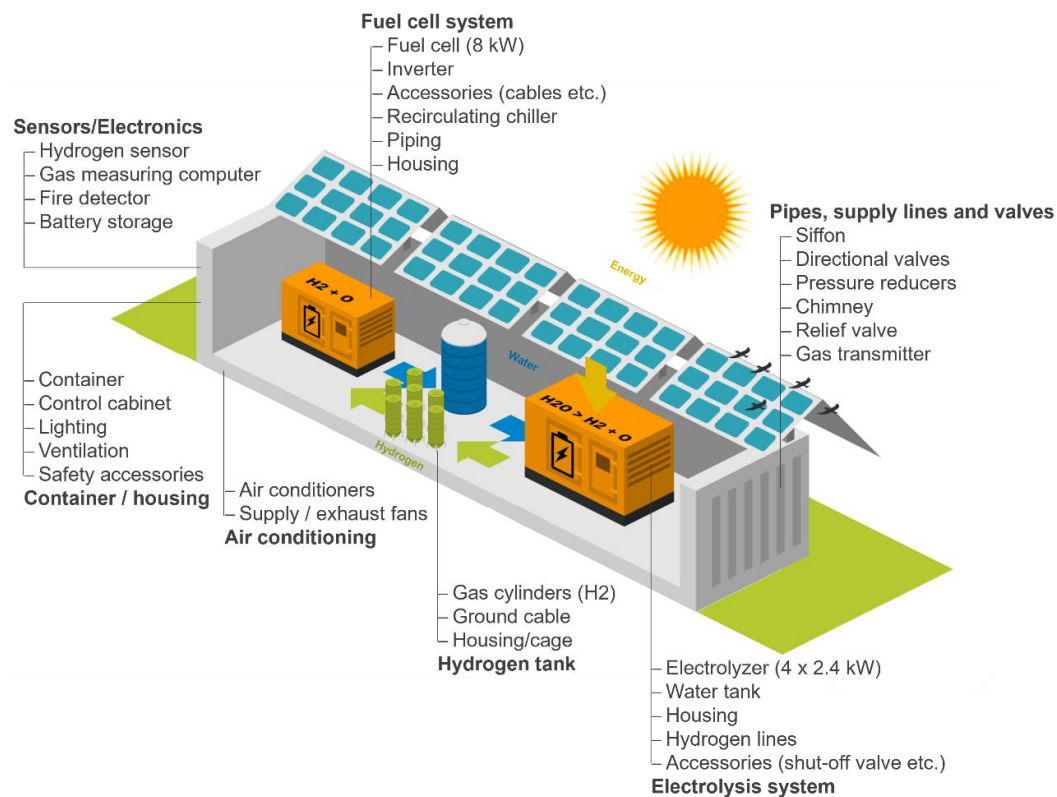


Figure 2: design of the microgrid

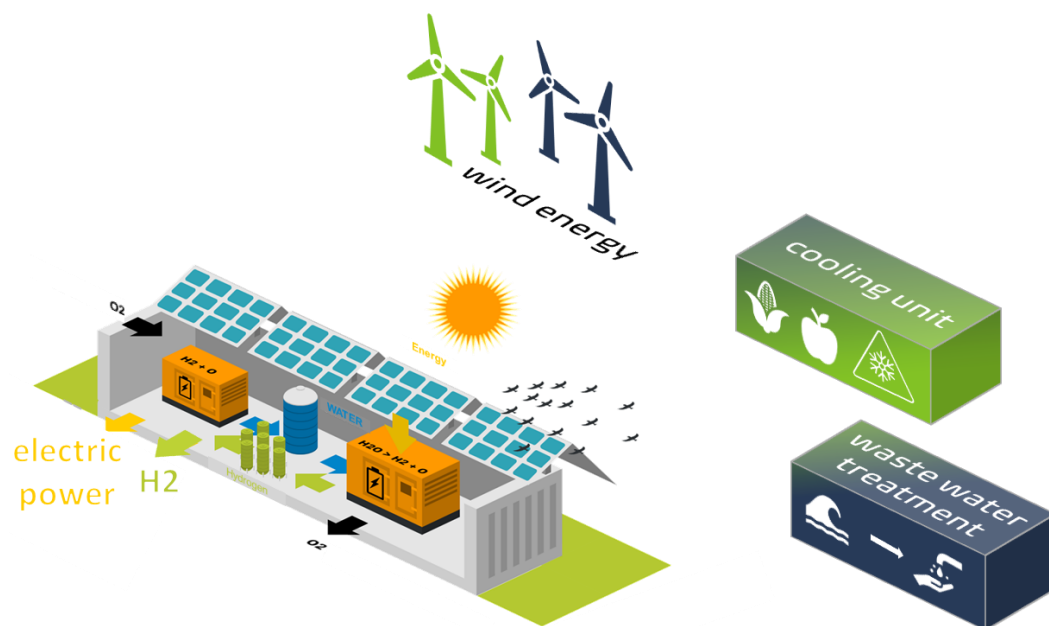


Figure 3: extension options of the microgrid

Objective

The project partners of the two projects are pursuing two main goals in both projects.

On the one hand, the technology of the microgrid is to be further developed in such a way that microgrid systems are created which reliably and permanently provide the required electricity at the location and which are also robust, low-maintenance, cost-effective, mobile and durable. To this end, prototypes of the individual systems are being built and tested. The knowledge gained from both projects will flow into the subsequent product development. In parallel, the participating companies are developing a business plan for later commercialisation. This includes the establishment of a supplier and partner network in the respective countries. The aim is to establish a joint value chain that will enable the microgrids to be built locally.

In addition, further use cases will be defined and the resulting requirements for the system will be worked out. The future business model will consist of various building blocks:

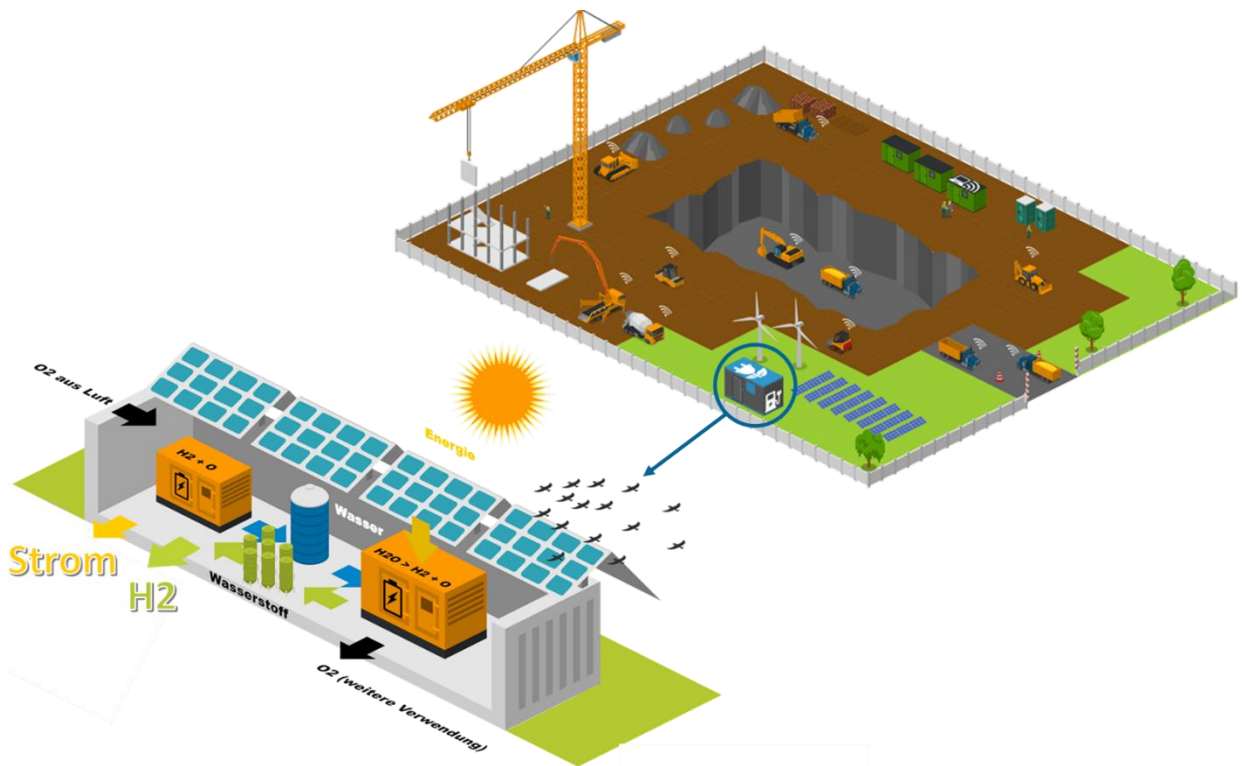
- Design of the requirements and the system for the respective use case
- Construction and procurement of the microgrids
- Embedding the microgrid in existing infrastructure
- Commissioning and maintenance
- Training and further education of employees
- Disposal and recycling

Use case mobile solution for a construction site

Today, the power supply of mobile construction machinery is predominantly based on combustion engines, in which the chemical energy bound in liquid fuels is used to provide mechanical power. In its energy concept, the German government has formulated the central goal of achieving greenhouse gas neutrality by 2045 [1].

In general, therefore, a trend towards CO₂-reducing drive technologies can be observed in all industrial sectors, which are implemented in different ways. The need for and commitment to electromobility in Germany is also becoming increasingly noticeable in the rather conservative area of mobile machinery (which relies on proven solutions), so that construction machinery and system manufacturers are beginning to offer hybrid and electrified drive concepts. For machines in the small power range (< 50 kW), accumulators are usually used as energy storage. For construction machinery of higher power classes, the use of hydrogen as an energy carrier and fuel cells as energy converters can fill the niche between modern battery technology and alternative eFuel technology.

An important prerequisite for the future operation of battery-electric and hydrogen-based construction machinery is the local supply and refuelling infrastructure at the construction site. For this purpose, decentralised mobile charging and refuelling systems must be established, as is also the case with construction site refuelling using diesel tanker trucks. A particular challenge is posed by construction sites that cannot be supplied with electricity or hydrogen via the power grid due to their location. This applies, for example, to construction projects on greenfield sites, on motorways or in unpaved terrain (no access for trucks with hydrogen possible). Here it is necessary to enable self-sufficient energy and hydrogen production directly on site.



However, this solution is not only suitable for construction sites, but also for other fields of application. For example, a drilling rig could be supplied with energy independently.

Sources

- [1] Die Bundesregierung: "Klimaschutzgesetz", <https://www.bundesregierung.de/breg-de/themen/klimaschutz/klimaschutzgesetz-2021-1913672>, Zugriff: 24.02.2023

Reaktivierung & Transition im Nachbergbau: Wie gelingt ein erfolgreicher Umschwung von traditioneller Ressourcennutzung zu erneuerbaren Energien?

J. Tiganj

Research Center of Post-Mining at the THGA University Bochum, Reactivation & Transition, Bochum, Germany

Das Thema Nachbergbau gewinnt in Zeiten von Klimawandel und Nachhaltigkeit global immer mehr an Bedeutung. Dazu gehört nicht nur der Umgang mit dem nachbergbaulichen Erbe durch ein adäquates Grubenwassermanagement oder Umweltmonitoring. Vielmehr braucht es auch Konzepte für eine erfolgreiche Transition in betroffenen Bergbauregionen. China als größtes Bergbauland der Welt bietet hier einen wichtigen Bezugspunkt. In kohleintensiven Regionen ist die Wirtschaftlichkeit eng mit der Kohleindustrie verknüpft. Der Strukturwandel erfordert additive Politiken und Umstrukturierungen, um einerseits innovative Umwandlungsmöglichkeiten wie die Integration erneuerbarer Energien in bestehende Bergwerke zu schaffen. Andererseits folgt auf Werksschließungen die Arbeitslosigkeit ehemaliger Arbeiter. Hier wiederum bedarf es der Schaffung alternativer Beschäftigungsmöglichkeiten und neuer Anreize, um die Folgen für Bürger und Umwelt zu minimieren. Um neue Lösungsansätze für die oben beschriebenen Probleme zu schaffen, werden im Rahmen des aktuellen EU-Projekts „POTENTIALS – Synergistic potentials of end-of-life coal mines and coal-fired power plant, along with closely related neighbouring industries: update and readoption of territorial just transition plans“. Basierend auf betriebswirtschaftlichen Analysen, gepaart mit technischen und bergbautechnischen Aspekten, werden Konzeptentwürfe entwickelt. Am Ende sollen Szenarien auf verschiedene Standorte mit unterschiedlichen Besonderheiten anwendbar gemacht werden, wodurch eine neue Nutzung des Bergbauerbes ermöglicht wird. Das Projekt läuft noch und die Ergebnisse sind noch nicht endgültig, aber es gibt bereits eine Reihe möglicher Szenarien. Diese werden derzeit geprüft [1]. Dennoch kann festgestellt werden, dass es unerlässlich ist, stillgelegte Werke wiederzuverwenden, um mehrere Faktoren zu unterstützen: Effiziente Nutzung vorhandener Ressourcen, Kostensenkung, Schaffung alternativer Arbeitsplätze, Schutz des Industrieerbes, Modernisierung der Geschichte, Nachhaltigkeit und grüne Entwicklung. Der Antrieb hinter dieser Forschung besteht weitgehend darin, aktiv zu einer grünen und lebenswerten nachhaltigen Zukunft für alle beizutragen, sowohl national als auch international. In diesem Bereich gibt es noch viele Forschungslücken, die gefüllt werden müssen. Wissenstransfer basierend auf deutschen Erfahrungen, als Nachbergbauland hinsichtlich der Steinkohle und der eng verzahnten Forschung mit europäischen Partnern kann eine Assimilation begünstigen und aus vorherigen Konsequenzen positiv profitiert werden. Da China der dominierende Akteur in der Energiebranche ist und über enorme Reserven von notwendigen Ressourcen verfügt, sei es Kohle oder Seltene Erden, kann dies zu einem globalen grünen Wandel beitragen.

References:

[1] POTENTIALS, (2023), Potentials Project focuses on..., <https://potentialsproject.eu/>

Digitale Transformation – Wie neue Technologie die Mitarbeiter inspirierte, den Betrieb eines mehr als 80 Jahre alten Öl & Gasfeld zu modernisieren!

M. Bernold

OMV Austria Exploration & Production GmbH, PSO - Production System Optimization,
Gänserndorf, Austria

Neben all den Technologien, die in den letzten Jahrzehnten in der Öl- und Gasindustrie Einzug gehalten haben, steht gerade bei der Produktion und Förderung dieser wichtigen Energieträger immer noch der Mensch im Mittelpunkt. Noch immer ist das operative Personal („Blue Collar Workers“) essenziell, da sie durch regelmäßige Anlagenrundgänge, Sondenkontrollen und Routineinspektionen mit ihrer über Jahre hinweg gewonnenen Erfahrung, prozessrelevante Gefahren frühzeitig erkennen, auf geänderte Betriebsbedingungen reagieren und auch die teilweise noch so kleinen und unscheinbaren Zeichen deuten und größere Gefahren oder Schäden unterbinden.

Natürlich wird auch in unserem Unternehmen versucht, all jene zuvor beschriebenen Prozesse zu digitalisieren und zum Teil mit künstlicher Intelligenz zu ersetzen, was mehr und mehr gelingt. Das Ergebnis dieser Entwicklung ist jedoch, dass die vielfältigen Aufgaben der Anlagenbetreiber, Schichtarbeiter, Fördermeister oder Facharbeiter, auf immer weniger Schultern verteilt werden müssen.

Genau hier setzt das „Agile Field Operations“ Konzept der OMV Austria GmbH an. 2016 als Digitalisierungsprojekt gestartet, um Routineinspektionen auf Sonden und Anlagen via Tablet zu erfassen und entsprechend zu dokumentieren, hat sich aus dieser Idee ein ganzes Programm entwickelt, welches es sich zur Aufgabe gemacht hat, bestehende Prozesse für das Feldpersonal zu modernisieren und zu vereinfachen.

Schlagworte die Angestellte & Mitarbeiter tagtäglich hören, möchte man meinen. Also wo liegt der Unterschied zu all den vielen Digitalisierungsmaßnahmen, die es rund um den Globus in scheinbar jedem Unternehmen gibt?

Wir haben in den letzten beiden Jahren eine Entwicklung erlebt, dass immer mehr Mitarbeiter von sich aus mit neuen Ideen auf uns zu kamen, wie wir ihre tägliche Arbeit verbessern und erleichtern können. So wurden die realisierten Apps am Tablet über die Jahre immer mehr und die Zusammenarbeit der verschiedenen Abteilungen und Fachbereiche immer enger und integrierter.

Es hat sich gezeigt, wie wichtig es ist nahe am Geschehen zu sein, und wie man durch die Einführung neuer Technologie auch die Innovationskraft und Kreativität seiner „jahrelangen“ Mitarbeiter wieder in Schwung bringt. Genau diese Erfahrungen und welche Applikationen sich in unserem Unternehmen daraus entwickelt haben wollen wir in diesem Vortrag mit Ihnen teilen.

Flood-induced seismicity in the Ruhr area – a geomechanics perspective

T. Niederhuber¹, B. Müller², T. Röckel³, M. Rische⁴, F. Schilling²

¹Karlsruhe Institute of Technology, Institute of Applied Geosciences, Technical Petrophysics, Karlsruhe, Germany, ²Karlsruhe Institute of Technology, Institute of Applied Geosciences, Technical Petrophysics, Karlsruhe, Germany, ³Piewak & Partner GmbH, Bayreuth, Germany, ⁴Ruhr Universität Bochum, Institut für Geologie, Mineralogie und Geophysik, Bochum, Germany

The Ruhr area is characterised by centuries of intensive coal mining. After the closure of the last mines, their controlled flooding began. The Floodrisk project investigates ground uplift, stress changes due to pore pressure changes and the reactivation potential of faults to explain induced seismicity. A particular focus is on monitoring and investigating in detail the relationship between mine water level rise, tectonic stress and induced seismicity in the Haus Aden catchment. Since 2014, mine water levels measured at the pumping stations of the central drainage system have been available for this region. This includes data from the post-mining phase through to flooding.

Highest seismicity during mining was observed in the area of the former "Bergwerk Ost". Ruhr University of Bochum has installed a network of 30 short-period seismic stations spaced between 0.5 and 3.5 km apart. The stations cover an area of about 160 km². They allow continuous monitoring of seismicity. By using the method of relative localization in combination with the dense network, it was possible to improve the precision of the measurements to a lateral resolution of less than 100 m. This detailed localisation of earthquakes made it possible to study the spatial and temporal evolution of earthquake clusters due to rising mine water levels.

The main underground waterways are the former adits which are surrounded by safety pillars of the mine. Since the permeability of the rock is rather low, the rising mine water affects the surroundings of the adits first and the mined-out sections. Over 2200 induced events have been localized since the start of flooding, showing spatial clustering. However, the majority of events occurs about 300 m below the main pillars between the longwall mining panels.

The geomechanical investigations are based on a compilation of the regional stress state in the eastern Ruhr area. We re-evaluated hydraulic fracturing tests that had been carried out to minimize rock bursts. The results were compared with stress orientations from independent sources (stresses in deep boreholes and earthquake source mechanisms). The new map of the spatial distribution of stress orientations shows a rather homogeneous stress pattern with very few locations where stress orientations deviate significantly from the average of N 154°E.

The second focus of the geomechanical approach is a 3D numerical model of stress concentration due to stress arching effects: Based on the geometry of the pillars, shafts and longwall panels, a generic FE numerical model was developed for a section of the Heinrich Robert mine using the collected stress data for model calibration. Increased vertical stresses within and below the pillars were observed as a result of stress arching. As the horizontal stress changes below the mining level are small, this results in increasing differential stresses which, with rising mine water, may lead to the observed events 300 m below the mining level.

The importance of studies on the mitigation of environmental impacts in the Santos Basin Region: Focus on pre-salt oil and gas activities

F. Oliveira¹; M. Oliveira¹, A. Nascimento²

¹Universidade Estadual Paulista – UNESP – Faculty of Engineering and Sciences, Guaratinguetá; Master in Engineering,

²Universidade Federal de Itajubá (UNIFEI) – Brazil, Institute of Mechanical Engineering; Energy Group.

Abstract

After the pre-salt discovery and the beginning of the petroleum extraction in the coastal region of Brazil, a lot of research is being developed on this subject, mainly focusing on oil & gas exploration and production activities. As well as, eventual researches related to environmental impacts. However, in addition to works on the technology used to extract oil from the pre-salt region, studies are also being conducted on the impacts that this activity will result in. This project has the objective of showing the importance of studies on the reduction of the impacts. Focusing on the Santos Basin region and the consequences, even though the impacts happen in the entire coastal region covered by the pre-salt layer. It is necessary to analyze the impacts related to environmental sustainability, in addition to the social and economic impacts. Through this study, an action plan can be created and put into practice and implemented by means of public policies and by private companies.

Keywords: Sustainability, Environmental Impact, Pre-salt, Petroleum and Natural Gas.

Introduction

Oil is responsible for a large part of global energy production. With many uses and applications, this fossil fuel is the raw material that makes up various products such as plastics, footwear and cosmetics. A flammable and oily substance that has been used by mankind for thousands of years, from embalming the dead, paving roads, waterproofing homes and lighting. The production and extraction of oil cause significant environmental impacts. The production phase being the most aggravating (MARTINS et al., 2015).

Within the energy market in Latin America, pre-salt discoveries are among the most relevant today. Even with the economy weakened by the damage caused by the New Coronavirus pandemic, we can observe an increase in the productivity of the withdrawal of a barrel of oil on the national scene in the last 10 (ten) years and even in the year 2020, in which the pandemic worsens.

According to the Brazilian National Agency of Petroleum, Natural Gas and Biofuels (ANP) "in 2020, Brazil had a record in the production of oil and natural gas, totaling 3.74 million barrels of oil equivalent per day (boe / d). 2.94 million barrels of oil per day (bbl/d) and 127.4 million cubic meters of natural gas per day (m³/d) were produced. This is an increase of 52.71% compared to 2010 (2.45 boe/d)."

It is a demonstration of the growth and development of the Brazilian energy sector, specifically the oil & gas industry, which shows a great opportunity for business and foreign investment in the petroleum sector in the national scenario and specifically in the area selected for this study, the Santos Basin region. And within this area it can be highlighted one of the main regions for our study, the Metropolitan Region of Baixada Santista.

The Santos Basin is the largest offshore sedimentary basin in the country, with a total area of over 350,000 square kilometers, extending from Cabo Frio (Rio de Janeiro state) to Florianópolis (Santa Catarina state). It is in this region that the Santos Basin Pre-Salt Pole is located, which brings together the largest producing fields in the country, such as Tupi and Búzios (PETROBRAS, 2022).



Figure 1 – Location of marine and land basins, distributed throughout Brazil. Source: PETROBRAS (2022).

The increase in oil production is also due to the discoveries made in relation to the pre-salt which, according to the National Agency of Petroleum, Natural Gas and Biofuels (ANP), covers the coastal layer from the state of Espírito Santo to the state of Santa Catarina. In Figure 3, the highlighted area is the Tupi Field, in the Santos Basin, whose reserves range from 5 to 8 billion barrels of quality (light) oil, which represents approximately 50% of Brazil's current reserves, with an estimated total of 15 billion barrels (PETROBRAS, 2021).

The oil found at this location is considered light, averaging 28 degrees API (American Petroleum Institute). According to this classification, the closer to 50 degrees the better the quality of the oil, and it is also considered of better quality than the average commercial oil found in Brazil, as it allows a better refining process. According to Adriano Pires, director of the Brazilian Infrastructure Center (CBIE) - as light oil (less dense) has the best quality, it is the most sought after. This oil allows producing nobler products, such as naphtha used in petrochemicals, better quality of fuels, among others. Another advantage, for light oil, is the fact that for denser oil, the refining operation costs much more and requires more expensive technology from companies in the sector (ANP, 2022).

In addition to the good market quality of the oil, according to Petrobras details presented in its reports published in its main website, it is possible to understand the great potential of the Santos Basin and the Tupi field (PETROBRAS, 2021). Based in some ANP data shown in Figure 4, in 2020 the national oil production reached the record mark of 3,740,612.09 barrels of oil equivalent per day. Another finding by the agency is that this is an increase of 5.22% compared to 2019 (3,554,976.06 boe/d) and 52.71% compared to 2010 (2,449,563.04 boe/d). That is, the last decade had a constant increase in production, with the exception of

the years 2012 and 2018.

As it is an economically attractive market, the flow of people has been making the region's economic activity grow. There can be seen already a lot of national and international investment in this region, both in the oil and natural gas industry and in the areas of hotels, events, civil construction and the entire sector that involves the urban structure. Mobilizing a series of activities in different sectors of the economy, the oil and gas industry directly and indirectly generates income and jobs, affecting many other economic and social aspects of the country and especially of the region, also by means of environmental impacts.

In this way, the tendency is to aggravate the social and environmental impacts generated by this flow in the coastal regions located in the vicinity of regions with activities related to oil and natural gas. The cities in the region have a strong tourism as a whole, due to the fact that geographically all cities are coastal, which attracts many tourists in search of their natural beauties. They also have been attracting business tourism, due to their intense economic activities in several areas, but mainly oil and gas activities in this entire region that is within the pre-salt region (GASPAR, 2018).

Even though it is a non-renewable natural resource, oil is a source of energy widely used in society today. Its exploitation generates irreparable impacts on nature and the environment and, therefore, government agencies have required an environmental licensing process on the part of companies involved in the oil and gas sector chain. So that these impacts can be minimized in the best possible way (FERREIRA, 2019).

Environmental issues

Throughout history, human beings are shown to be the great enemy of their own environment. But in a way, it is also his great ally. And it is not new that the struggle for environmental preservation conflicts with the economic interests of our current society.

More detailed researches should be carried out on the environmental impacts caused by the oil and gas industry in the Santos Basin region and consequently on alternatives to mitigate these impacts. As society's needs are growing, along with economic development and increasing industrialization, the probability of accidents occurring during exploration, extraction, transportation or refining in the oil and gas industry is greater, as activities are becoming increasingly more and more intense. Accidents followed by contamination can arise through oil spills from oil tankers, accidents on platforms and occasional leaks in pipelines (RIOS, 2014 apud ALMEIDA, 2018).

According to Almeida (2018, p. 13) "If there is an accident, the environment will suffer consequences that could last for many years and, generally, accidents that occur in the marine environment cause greater impacts since the oil can travel long distances". The author also mentions that if this oil reaches the coastal zone, it will contaminate mammals, molluscs, algae, fish and seabirds, in addition to causing damage to human health.

The Infrastructure and Environment Secretariat of the State of São Paulo (SIMA/SP) defines mitigation as actions that reduce or remedy harmful impacts on the fauna and flora of the region, as well as the anthropic environment (SÃO PAULO. SIMA, 2022). Environmental compensation may be an option for areas already impacted, such as the Metropolitan Region of Baixada Santista.

Knowledge of the history between Brazilian society and nature becomes necessary for

understanding the beginning of environmental conservation. At the “beginning” of national history, the very name - Brazil - arises from the exploration of brazil wood (“pau-brasil”), which was practically extinct. The colonizers, not satisfied with everything they had already explored, started to plant sugar cane and then coffee, producing them on a large scale, in this way they were the main devastators of forests in Brazil.

Royal Charters of the Portuguese Crown in 1797 was one of the first measures to contain forest devastation, which was more concerned with the lack of wood for shipbuilding than with nature conservation. In 1937, the first national park was created in Itatiaia, with the purpose of encouraging scientific research and offering leisure to urban populations. Environmental preservation has its emergence through economic interests, with scientific research and visitation being its main factors. From the 1960s onwards, with rapid deforestation, mainly in the Amazon, and the expansion of agricultural frontiers, several conservation units were created. The Amazon National Park was then created in 1974, which in the following year provided for the creation of new conservation units in the region by the II National Development Plan (DIEGUES, 1994).

In 1989, the Brazilian Institute for the Environment and Renewable Natural Resources (IBAMA) was created, to whom the establishment and administration of the Conservation Units was passed. However, in 1992, a new proposal was sent to Congress with the plan for the National System of Conservation Units (SNUC), enacted in 2000 in the Constitution. In Brazil, the emergence of environmental laws is crucial for the preservation of its vast area. In view of this, SNUC defines a conservation unit in its Art. 2nd paragraph I (BRASIL. LAW 9.985 OF JULY 18, 2000).

Conservation Units are areas specially created with the aim of preserving and/or conserving a certain asset, be it an element of fauna, flora or landscape. There are several types of Conservation Units, and some have greater potential for environmental preservation. And other types for the tourist use of their space, since, through a management plan and a public use plan, they allow controlled visitation within their area (MENEZES, 2022).

Law 9985 of July 18, 2000 institutes the SNUC, which establishes criteria and norms for the creation, implantation and management of conservation units. Taking into account article 7 of this law (The conservation units that are part of the SNUC) established in the constitution, two types of conservation units with specific characteristics are placed: Full Protection Units and Sustainable Use Units (SILVA, 2019).

In order to administratively and economically strengthen conservation units without losing their main focus (environmental protection), this work seeks to strengthen the mandatory ties between oil and gas exploration companies and environmental preservation institutions. It is essential for an institution to survive in the current market, the need for adequate strategic planning and financial resources, as well as an analysis of its surroundings. For conservation units, which are involved in the economic environment and depend on their administration to remain active, it is no different, even in the case of non-profit units.

In this way, the management of the Conservation Unit, through an effective strategy that uses its public use correctly, can have an administration that brings financial sustainability to the Unit. Since the resources coming from the government are not enough for the protection of the area. Allying projects and financial resources with the oil and gas industry can be a way to mitigate environmental impacts (GODOY, 2019).

Studies on the reduction of environmental impacts

The object of study proposed here is the Santos Basin region, this coastal region extends from the city of Cabo Frio in the state of Rio de Janeiro to Florianópolis in the state of Santa Catarina. In addition to covering a significant economic area of the Santos Basin, the Metropolitan Region of Baixada Santista, this area has 9 (nine) municipalities ranging from Peruíbe to Bertioga. As the main municipality and headquarters, we have the city of Santos, where one of the most important port complexes in Brazil is located, in addition, the Industrial Park of Cubatão is also a region that is economically of great importance for the region (PITTERI, 2012).

In order to gather the desired information, analyzes can be made through observations in cities and places, which are and possibly will be affected environmentally, socially and economically by the oil exploration and production activity. Observation is a data collection technique to obtain information, it also examines facts or phenomena that one wishes to study, being a basic element of scientific investigation used in field research (MARCONI; LAKATOS, 2005). Because it is a very extensive area, only the most relevant industries and Conservation Units for the study can be visited.

It is also important to note that the controlling company of oil and natural gas activities in Brazil is PETROBRAS (Petróleo Brasileiro S/A), a publicly traded state-owned company, whose majority shareholder is the Brazilian government. The company operates in the energy sector in exploration and production, refining, marketing and transport of oil and natural gas, petrochemicals and other energy sectors. It also conducts studies in the environmental and socioeconomic areas, so its database and all the information provided were taken into account in this project.

The method approached for the work has been the case study, which DALMAZO (2013, p. 49) defines case study as the “deep study of a unit in its own complexity and dynamism, providing relevant information for decision making”. With this, a history of oil and natural gas exploration and production activities and their environmental impacts in the Santos Basin can be created, describing it from its creation to the present day, containing critical analyses. Interviews were conducted with managers, entrepreneurs, technicians and various other involved. Among the bodies taken into account for carrying out the entire research, we can mention:

- Secretary of the Environment of the State of São Paulo (SM).
- Secretary of Tourism for Santos and São Vicente.
- Municipalities of the cities of the Santos Basin.
- Universities in the region and mainly the UNESP São Vicente campus.
- Environmental Company of the State of São Paulo (CETESB).
- Brazilian Institute of Environment and Renewable Natural Resources (IBAMA).

For the implementation and operation of an oil exploration or production project, the responsible company must analyze in detail the environmental impacts related to the enterprise. The environmental licensing process is a legal obligation, which must follow the guidelines and rules for its execution, such as Federal Law 6938/81, Complementary Law 140/2011 and CONAMA Resolutions 001/86 and 001/86. 237/97. (LIMMER, 2018).

In the licensing process, the environmental studies are prepared by the company in charge and delivered to the environmental agency for analysis and approval. For each stage of licensing there are specific studies to be prepared (IBAMA, 2022). “In order to subsidize the

preliminary license stage, given that the undertaking has a significant environmental impact, the entrepreneur sends the Environmental Impact Study (EIA) and respective Environmental Impact Report (RIMA) to Ibama. For the other enterprises, more simplified studies are required." (PETROBRAS, 2022).

These studies are essential to support the definition of the necessary mitigating and compensatory measures during the implementation, operation and deactivation of projects that impact the environment. The RIMA, currently prepared by Petrobras, specifically for the Santos Basin, can be used as a bibliographic source for the study.

As a form of study, one can analyze the results and also the effectiveness of the projects currently underway in the Santos Basin, Petrobras' RIMA Step 3, for example, provides as a mitigation measure required by the federal environmental licensing process monitored by IBAMA (Brazilian Institute for the Environment and Renewable Natural Resources) the programs and projects below:

- Pollution Control Project (PCP);
- Invasive Exotic Species Prevention and Control Project – Petrobras (PPCEX-PETROBRAS);
- Workers' Environmental Education Project (PEAT);
- Marine Biota Monitoring Project for Seismic Activity;
- Environmental Education Program (PEA);
- Santos Basin Regional Social Communication Program (PCSR-BR);
- Project for Monitoring the Impact of Platforms and Vessels on Avifauna in the Santos Basin (PMAVE).

In addition to mitigation measures, Petrobras also carries out programs and projects in the environmental area of characterization, emergency, compensation and monitoring in the Santos Basin.

The Federal government and the Brazilian states are administratively weakened, incapable of formulating, implementing and evaluating, in an orderly and effective manner, their public policies. This happens, not only due to the new world economic reality caused by the pandemic that started in 2020, but also due to the history that imposes a series of limitations on developing countries, thus not allowing the State to perform its functions satisfactorily. Additionally, we can mention that such functions are poorly performed due to the involvement of corruption and the technical inability of public managers (SILVA, 2019).

Another aspect involved in a large undertaking such as oil production in the pre-salt layer is the "feeling of inexorability" of such an undertaking, which ends up imposing that indigenous (local) communities should not fight for their rights. This is due to the fact that this sensation inhibits attitudes of the affected local community, as the positive economic aspects involved are seen as more important than the environment and culture (GASPAR, 2018).

It is considered that the projects underway to mitigate the environmental impacts caused by the oil and gas industry in the Santos Basin region, carried out obligatorily by the Brazilian environmental licensing law, are being executed in a vague and disassociated way. It is believed that the oil industry only puts into practice its projects related to the environment and social, so that the licensing is approved, but such projects are not effective.

Research should also be carried out with the purpose of analyzing the connection between the existing Conservation Units and the mitigation projects already executed and in execution by the obligatory environmental licensing. Analyzing its direct and indirect financing,

administration and operation relationships between the Conservation Units and the oil and gas industry. It is observed below in Figure 06, that in all four states that make up the Santos Basin there are Conservation Units, especially in the State of São Paulo.

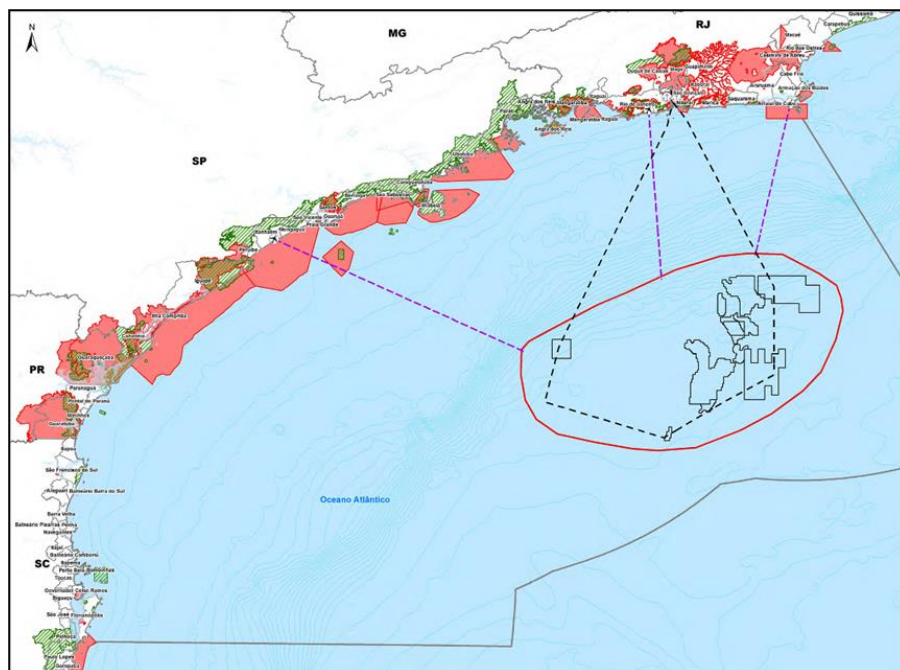


Figure 2 – Conservation Units present in the Santos Basin. (Environmental Impact Report - RIMA PETROBRAS, 2022).

Environmental risks in the Santos Basin are imminent and a reality, as are the impacts on populations affected by the process, such as fishermen and traditional communities, and also caused by tourism in the region. Economic impacts related to the prevention and repair of environmental damage deserve to be highlighted. (GASPAR, 2108). These future and current environmental, economic and social impacts that may be caused in the pre-salt region and the Santos Basin being within the region affected by the pre-salt, prove the need to reduce these impacts.

In addition to the impacts caused by the oil and natural gas industry, the flow of people and urbanization will be major aggravating factors not only for the environment, but also for the local and native population of the region. At the moment, there is no definition by the companies and political entities involved of all the part that will be affected by the production and exploration of oil and natural gas in the region, whether the affected part is offshore (not continental or at sea), which is where the pre-salt wells are located, or where there is no oil exploration and production (onshore or continental).

Even with oil exploration activities and the economic activities involved rising in the region, the economic benefits are also evident, but the environmental consequences will have to be reduced and the social consequences will have to be controlled. Autochthonous communities lose their cultural essence with the large flow of people.

The delay in regulating environmental laws in Brazil is a culture that has to be changed. A historical fact that proves this was the incident that happened on January 18, 2000 in Guanabara Bay in Rio de Janeiro with the rupture of a Petrobras pipeline. Then, plans for responses to emergencies in Brazil regarding the oil spill began to be structured. It was only after the incident that Law No. 9966 was enacted that same year, which provides for the

prevention, control and inspection of pollution caused by the release of oil and other harmful substances in waters under national jurisdiction (NORONHA; FERREIRA; PINTO, 2018).

Acknowledgment

The authors would like to thank the financial support from the National Agency for Petroleum, Natural Gas and Biofuels - ANP -, the Financier of Studies and Projects - FINEP - and the Ministry of Science, Technology and Innovation - MCTI through the ANP Human Resources Program for the Oil and Gas Sector Gas – PRH-ANP/Finep 34.1.

Conclusion

This work is extremely important so that private and public companies from the region know how to deal in advance with the new environmental, social and economic situation to which the Santos Basin has been subject in the past years. It is necessary to have an action plan that minimizes the environmental impacts. Consequently, a well-designed study with all methodology and schedule will help private industry and public policy actions. Which will also bring a better use of public resources destined to this area. The studies are expected to provide an analysis that can contribute to future plans for sustainable environmental preservation in the region and encourage international bodies and companies focused on the oil and gas chain that are interested in the effective implementation of environmental standards. And also bring financial resources for projects in the environmental area.

The work aims to clarify the local society about the importance of Conservation Units. So that in this way, the local population can put pressure on public policy actions. In order to serve as a guide and even a model for future projects to be carried out in the socio-environmental field, this research can be used in the future by Non-Governmental Organizations (NGOs), public and private institutions.

Sustainable development is the great challenge of modern society, so it is necessary to prepare a study on the sustainability relationship between the pre-salt oil industry and the Conservation Units, together with the Santos Basin community.

References

- [1] ALMEIDA, Júlia Cintra. Avaliação da Biodegradação do Petróleo com Microalgas em Águas Marinhas Contaminadas por Petróleo. Monografia apresentada ao Curso Graduação em Oceanografia, Instituto de Geociências, Universidade Federal da Bahia, p. 61. Salvador. (2018)
- [2] AGÊNCIA NACIONAL DO PETRÓLEO, GÁS NATURAL E BIOCOMBUSTÍVEIS (ANP). Brasília: DF. [viewed date: February 2022]. Available from: <<https://www.gov.br/anp/pt-br>>. (2021)
- [3] ANDRADE, M. M. Introdução à metodologia do trabalho científico. 6^a. Ed. São Paulo: Atlas. (2003)
- [4] ANDRÉ, Marli Eliza Dalmazo Afonso de. Etnografia da prática escolar. São Paulo: Papirus. (2013)
- [5] ASSOCIAÇÃO BRASILEIRA DE NORMAS TÉCNICAS. NBR 14724: informação e documentação – trabalhos acadêmicos - apresentação. Rio de Janeiro. (2011)

[6] BRAGA, B. Introdução à engenharia Ambiental. São Paulo: Prentice-Hall, 2002. 305p.: il. ISBN 8587918052. (2002)

[7] BRAZIL, Lei nº 6.938, de 31 de agosto de 1981. Constituição da República Federativa do Brasil, Brasília. 2000. [viewed date: July 2022]. Available from: < http://www.planalto.gov.br/ccivil_03/leis/l9985.htm >. (2022)

[8] BRAZIL, SNUC, Lei nº 9985/00, (2000) Sistema Nacional de Unidades de Conservação. Constituição da República Federativa do Brasil, Brasília. 2000. [viewed date: July 2022]. Available from: < http://www.planalto.gov.br/ccivil_03/leis/l9985.htm >. (2022)

[9] BRAZIL. AGÊNCIA METROPOLITANA DA BAIXADA SANTISTA. Plano Diretor de Turismo da Baixada Santista. Santos. (2002)

[10] BRAZIL. MINISTÉRIO DE TURISMO. Ecoturismo: orientações básicas. Brasília: Ministério do Turismo, 60 p. (2008)

[11] DIAS, R. A. Impactos da substituição de equipamentos na conservação de energia. Guaratinguetá, 94p. Dissertação (Mestrado em Engenharia Mecânica) – Faculdade de Engenharia, Campus de Guaratinguetá, Universidade Estadual Paulista. (1999)

[12] DIEGUES, Antonio Carlos Sant'Ana. O mito moderno da natureza intocada. São Paulo, NUPAUB/USP. (1994)

[13] ECONOMIA IG. [viewed date: November 2021]. Available from: <http://economia.ig.com.br/empresas/infraestrutura/poco-de-75-mil-metros-amplia-fronteira-do-presal/n1237714960821.html> (2021)

[14] FERREIRA, L. M.; SILVA, A. M.; DA SILVA, L. C.; DA SILVA, L. M. Um estudo de caso dos Impactos e Desastres Ambientais da Implantação da Refinaria de Petróleo ao longo do litoral de Ipojuca e Cabo de Santo Agostinho. Revista Gestão e Sustentabilidade Ambiental. Florianópolis, v. 8, n. 3, p.736-759, jul/set. (2019)

[15] GASPAR, Natália Moraes, Organização política de populações tradicionais costeiras frente à indústria petrolífera: caiçaras, quilombolas e indígenas do litoral sudeste do Brasil e a exploração do petróleo da camada pré-sal. Trabalho apresentado na 31ª Reunião Brasileira de Antropologia, realizada entre os dias 09 e 12 de dezembro de 2018, Brasília/DF. (2018)

[16] GODOY, Larissa Ribeiro da Cruz e LEUZINGER, Márcia Dieguez. O financiamento do Sistema Nacional de Unidades de Conservação no Brasil: características e tendências. Revista de informação legislativa, v. 52, n. 206, p. 223-243. (2019)

[17] GONÇALVES, A. e GRANZIERA, M. L. M. (Organizadores). Petróleo, gás e meio ambiente / [recurso eletrônico]. Programa de Mestrado em Direito Ambiental e Internacional Universidade Católica de Santos. Santos: Editora Universitária Leopoldianum, 195 p. (2012)

[18] GOVERNO DO ESTADO DE MINAS GERAIS. Plano de Manejo do Parque Estadual do Itacolomi. Belo Horizonte. (2021)

[19] GOVERNO DO ESTADO DE SÃO PAULO. INFRAESTRUTURA E MEIO AMBIENTE.

[viewed date: July 2022] Available from:
<<https://www.infraestruturameioambiente.sp.gov.br/>> (2022)

[20] HENKELS, Carina. Identificação de aspectos e impactos ambientais: proposta de método de aplicação. 139f. Dissertação (Mestrado em Engenharia de Produção) - Programa de Pós-Graduação em Engenharia de Produção, UFSC, Florianópolis. (2002)

[21] HINRICHES, R. Energia e meio ambiente. São Paulo, CENGAGE Learning. [viewed date: October 2021] Available from <<http://www.revistadomeioambiente.org.br/>> (2010)

[22] IBP. Instituto Brasileiro do Petróleo. [viewed date: November 2021] Available from: <<https://www.ibp.org.br/observatorio-do-setor/snapshots/cadeia-do-setor-petroleo/>> (2021)

[23] INSTITUTO ESTADUAL DE FLORESTAS (IEF). [viewed date: July 2022] Available from: <<http://www.ief.mg.gov.br/>> (2022)

[24] LAKATOS, E. M. e MARCONI, M. A. Fundamentos de metodologia científica. 6.ed. São Paulo: Atlas. (2005)

[25] LIMMER, Flavia da Costa. O Licenciamento Ambiental da Indústria Petrolífera. Revista Brasileira de Direito do Petróleo, Gás e Energia, v. 5, n.1, p. 225-242. (2018)

[26] LORA, E.E.S. Prevenção e Controle da Poluição nos setores energético, industrial e de transporte. 2. ed. Rio de Janeiro: Editora Interciência. 481p. ISBN 85-7193-066-X. (2002)

[27] MARTINS, S. S. et al. Produção de petróleo e impactos ambientais: algumas considerações. HOLOS, v. 6. (2015)

[28] MENEZES, Gláucio Costa de. Meio ambiente e sociedade [livro eletrônico]: Análises, Diálogos e Conflitos ambientais / organização Neide Kazue Sakugawa Shinohara. Campina Grande: Editora Amplla, 2 v. (2022)

[29] MILLER, T. Ciência ambiental. São Paulo, CENGAGE Learning. (2007)

[30] NORONHA, Iruam Rodrigues de; FERREIRA, Maria Inês Paes; PINTO, Augusto Eduardo Miranda. Riscos e Danos ambientais Associados às Atividades da Cadeia Produtiva do Petróleo: Instrumentos de Comando e Controle para Mitigação dos Impactos de Vazamentos de Óleo. R. gest. sust. ambient., Florianópolis, v. 7, n. 1, p. 596-613, jan./mar. (2018)

[31] PETROBRAS. Pré sal. Uma nova fronteira. [viewed date: November 2021] Available from: <<http://www.petrobras.com.br/minisite/presal/pt/uma-nova-fronteira/>> (2021)

[32] PITTERI, S. Competências Territoriais para o Desenvolvimento: uma análise sobre a Região Metropolitana da Baixada Santista (RMBS) / Sirlei Tereza Pitteri Vieira – São Caetano do Sul: USCS. (2012)

[33] REIS, L.; Fadigas, E; CARVALHO, C. Energia, recursos naturais e a prática do desenvolvimento sustentável. BARUERI, Manole. (2005)

[34] RIMA/ETAPA 3, Estudo de Impacto Ambiental e Relatório de Impacto Ambiental da Bacia de Santos, Polo PreSal Etapa 3. [viewed date: June 2022] Available from: <<https://www.comunicabaciadesantos.com.br>> (2022)

[35] SECRETARIA DE MEIO AMBIENTE E DESENVOLVIMENTO SUSTENTÁVEL (SEMAD). [viewed date: June 2022] Available from: <http://www.semad.mg.gov.br> (2022)

[36] SILVA, A. R.; MELLO, J. S. Viabilidade de políticas públicas no sistema nacional das unidades de conservação da natureza - SNUC (LEI Nº 9.985/2000). Revista Processus de Políticas Públicas e Desenvolvimento Social, [S.I.], v. 1, n. 2, p. 71-107, nov. (2019)

Celsius Energy: an industrial, digital native geoenergy solution to accelerate the deployment of low-carbon heating and cooling

G. Sosio, C. Merino

Celsius Energy, Clamart, France

Celsius Energy is a technology company with the mission to decarbonize the building HVAC industry by designing and developing shallow geothermal energy installations. A Celsius Energy system consists of three elements: a borehole heat exchanger (BHE), a heat pump for both heating and cooling, and a digital geoenergy management solution.

The first system was built in Clamart, France, in 2020 [1]. Dozens of other installations have been designed and built for different types of uses and operating requirements, from single buildings to district heating networks. Celsius Energy has already drilled more than 120 wells in several countries, including 6 completed borehole exchangers at customer sites.

One of the key features of Celsius Energy systems is the geometry of the BHE, including both vertical and inclined wellbores. Inclined wells, and in particular a star-shaped layout (pioneered by the GZB center in Bochum), allow reducing drastically the surface footprint of an installation, making it possible to implement a geothermal exchanger in contexts such as urban areas or existing buildings where vertical wells alone would not be feasible.

Celsius Energy takes advantage of the extensive industrial expertise of its parent company SLB to provide technical solutions and operating procedures to improve the reliability of its solution while reducing its implementation cost and time. For instance, controlling the trajectory of the wells is crucial to avoid wellbore collision, to remain within the boundaries of the property plot and to optimize the energy extracted by the inclined wells. The use of adequate drilling techniques and equipment ensures that well trajectories do not deviate from the well plan, and well placement algorithms developed by Celsius Energy guarantee that the most efficient BHE geometry is designed and can be updated in real time during the operations. The installation steps of a Celsius Energy system will be described during the talk.

On the other hand, Celsius Energy has developed tailor-made digital solutions to model, monitor and manage the system. The geoenergy management solution is instrumented with sensors and controls for IoT operation, including fiber-optic DTS and building management sensors; it uses sensor input, external information and past records for digital performance management. Also, integrated modelling tools have been developed in-house to describe the different components of the system with the desired level of detail, compare their behavior to the observed data and refine the dimensioning of each installation [2].

The application of industrial experience to the development and operation of GSHP systems and the development of fully digital energy management and modelling tools allow Celsius Energy to build robust, reliable and efficient systems in contexts where traditional installations would not be feasible.

References:

- [1] Thierry, S. et al., (2021), The “Celsius Energy System”: a low surface footprint ground source heat pump system for collective buildings in urban environments, GRC Transaction, 1097-1121, 45
- [2] Parry A., Varadarajan P.A., Demichel C., Simon M., Thierry S., Sosio G., (2022), : Modelling and benchmarking the behavior of closed-loop borehole heat exchangers with inclined wells: the Celsius

DGMK/ÖGEW Frühjahrstagung 2023
DGMK/ÖGEW Frühjahrstagung 2023

Energy system, Proceedings of the European Geothermal Congress (Berlin, 17-21 October 2022),
Berlin

Numerical Simulation of Bio-Geo-Reactive Transport during UHS - A Modelling Approach

S. Hogeweg, B. Hagemann, L. Ganzer

Clausthal University of Technology, Institute of Subsurface Energy Systems, Clausthal-Zellerfeld, Germany

Abstract

The increased share of renewable energy sources leads to larger fluctuations of energy availability but also increases the significance of energy storage. Large scale hydrogen storage in the subsurface may hence become a vital element of a future sustainable energy system because stored hydrogen is an energy carrier that will be available on demand. Large capacities of hydrogen can be stored in porous formations such as former gas fields or gas storages, while caverns will contribute with high deliverability. However, the storage of hydrogen induces unique processes on fluid-fluid and rock-fluid interactions (for example, bio- and geochemical reactions), which may affect the efficiency of the storage.

In the present study, a numerical model describing the two-phase multicomponent flow in porous media, including bio- and geochemical reactions, is developed. The proposed model extends an existing model in the open-source simulator DuMux describing the bio-reactive transport process considering methanogenesis and sulfate-reduction by geochemical reactions. Based on the kinetic formulation, the hydrogen-driven reduction of pyrite to pyrrhotite with the production of harmful hydrogen sulfide is modelled. Due to limited literature data, a simplified model describing the conversion process is used, and artificial rates are defined. Preliminary simulations on a semi-artificial geological model show the potential hydrogen consumption and consequently lead to a reduced withdrawal of stored hydrogen. Furthermore, changes in mineral composition can be observed, though with a minor impact on the petrophysical parameters.

Within the scope of the study, the established numerical model is validated and improved by accompanying laboratory experiments to assess the risk of hydrogen conversion during UHS. Finally, field scale simulations with actual field data are planned to be conducted.

Introduction

The increasing share of renewable energy sources with characteristic fluctuations amplifies the demand for sustainable energy storage. Here, hydrogen storage in porous rocks in the subsurface offers a suitable potential to balance seasonal changes in production and demand at a large scale to fulfil the anticipated demand for storage in a decarbonized future energy system. The storage of natural gas, with a history of more than 100 years, can be assumed to be well understood. However, hydrogen possesses unique properties influencing the storage process. While the displacement process is impacted by the low viscosity and density of hydrogen, resulting in phenomena such as viscous fingering, bio- and geochemical reactions will lead to changes in the fluid composition. Hydrogenotrophic microorganisms such as methanogenic archaea and sulfate-reducing bacteria could consume hydrogen and may even produce harmful hydrogen sulfide.

Furthermore, geochemical reactions have been observed [1]–[3]. For instance, the reduction of pyrite to pyrrhotite resulting in the production of hydrogen sulfide is expected to be critical. An integrated modelling approach composed of experimental and numerical simulation work is suitable to assess the risk of these reactions. This study extends a mathematical model developed for Underground Hydrogen Storage (UHS) by geochemical reactions and is afterwards implemented in the open-source simulator DuMu^x.

The mathematical model for bio-geo-reactive transport in porous media

The mathematical model for bio-geo-reactive flow is an extension of the mathematical model developed by Hagemann [4], initially developed to simulate microbial processes during UHS. The enhanced model considers two-phase multicomponent reactive transport on the continuum scale (Darcy scale) with an additional compositional solid phase. Here, the mole balance for the fluid components can be expressed as follows:

$$\frac{\partial \phi(\rho_g c_g^k S_g + \rho_w c_w^k S_w)}{\partial t} + \nabla \cdot (\rho_w c_w^k u_w + J_w^k + \rho_g c_g^k u_g + J_g^k) = q^k$$

where ϕ is the porosity, ρ is the molar density in mol/m³, c^k is the molar concentration of component k , S is the saturation of the phase, u is the advective flux in m/s, and J is the diffusive/dispersive flux in mol/(m² · s). The subscript indicates the phases gas (g) and water (w), and the superscript k defines the component.

The mass balance for the solid phase can be expressed as follows:

$$\rho^s \frac{\partial \phi_s}{\partial t} = q^k$$

Where ρ^s is the molar mass of the pure solid component k in mol/m³, ϕ_s is the volume fraction of the solid component S .

On the continuum scale, the advective flow can be described by Darcy's law for each phase, including the term for gravitational influence:

$$u_i = - \frac{K k_{ri}}{\mu_i} (\nabla P_i - \hat{\rho}_i g), \quad i = g, w$$

where K is the absolute permeability in m², k_{ri} is the relative permeability of the phase i , μ_i is the dynamic viscosity of the phase in Pa · s, ∇P_i is the pressure gradient along the flow path in Pa/m, $\hat{\rho}_i$ is the density in kg/m³, and g is the gravitational acceleration in m/s².

The transport due to molecular diffusion is expressed as follows:

$$J_i^k = -\rho_i D_{\text{diff},i}^k \nabla c_i^k, \quad i = g, w$$

where $D_{\text{diff},i}^k$ is the effective molecular diffusion coefficient in m^2/s and ∇c_i^k is the concentration gradient along the flow path in $1/\text{m}$.

To obtain a system of balance equations, the sum of all saturations and the sum of all component concentrations in each phase have to be one:

$$\sum_i S_i = 1 \quad \sum_k c_i^k = 1 \quad i = g, w$$

Besides the bio-geochemical reactions, the storage operation consisting of injection and production through wells is considered in the source/sink term:

$$q^k = q_{\text{bio}}^k + q_{\text{geo}}^k + q_{\text{well}}^k$$

To consider the presence and activity of microorganisms, the interdependent growth and conversion must be modeled. The population kinetics are influenced by the growth and decay of microbes:

$$\frac{\partial(n \cdot S_w \cdot \phi)}{\partial t} = \psi^{\text{growth}} \cdot n \cdot S_w \cdot \phi - \psi^{\text{decay}} \cdot n \cdot S_w \cdot \phi$$

where n is the microbial density in $1/\text{m}^3$, ψ^{growth} is the growth rate in $1/\text{s}$, and ψ^{decay} is the decay rate in $1/\text{s}$.

The growth depends on the quantity of available substrate, as described by the double Monod model:

$$\psi^{\text{growth}} = \psi_{\text{max}}^{\text{growth}} \left(\frac{c_w^{S1}}{\alpha_{S1} + c_w^{S1}} \right) \left(\frac{c_w^{S2}}{\alpha_{S2} + c_w^{S2}} \right)$$

where $\psi_{\text{max}}^{\text{growth}}$ is the maximum growth rate in $1/\text{s}$, c_w^S is the mole concentration of substrate S in the aqueous phase, and α_S is the half velocity constant.

To mimic the reduction of population size in case of insufficient substrate supply, the decay is introduced as follows:

$$\psi^{\text{decay}} = b \cdot n$$

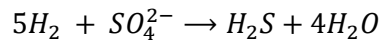
where b is the decay factor in m^3/s .

Depending on the growth, the reactive components are consumed and produced by the following equation:

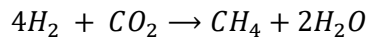
$$q_{\text{bio}}^k = \phi \gamma_{\text{bio}}^k \frac{\psi^{\text{growth}}}{Y} n \cdot S_w$$

where γ_{bio}^k is the stoichiometric factor and Y is the yield factor in $1/\text{mol}$. Generally said, conversion rates increase with increasing growth and smaller yield factor.

Within this work the focus is placed on the biochemical sulfate-reduction and methanation. Sulfate-reducing bacteria are living organisms consuming hydrogen and sulfur (SO_4^{2-}) and simultaneously discharging water and hydrogen sulfide. The stoichiometric equation is as follows:



Methanogenic archaea consume hydrogen and carbon dioxide and produce methane and water. The simplified metabolism reaction takes place according to the Sabatier reaction:



Regarding geochemical reactions, two approaches are commonly used: 1) equilibrium models, which are suitable for fast reactions as the reaction is expected to be at equilibrium; 2 kinetic models, where reactions are slower (strong dependency on time) and can therefore be described by a reaction rate [5].

Geochemical effects are considered in the source term in analogy to microbial reactions. However, instead of having a pseudo component that governs the reaction, the reactants in the solid and liquid phases initiate the conversion. In the present study, the implementation of the geochemical reactions is realized with a kinetic model. A generic and straightforward method is a concentration-based model, where the concentrations of the present reactants govern the rate. The following assumes that the reaction is comparatively slow and irreversible, allowing a kinetic implementation similar to [6].

$$q_{\text{geo}}^k = \gamma_{\text{geo}}^k \cdot \kappa \cdot \prod_n^{r_w} \phi \cdot S_w \cdot c_w^n \cdot \prod_n^{r_s} (1 - \phi) \cdot c_s^n$$

where γ_{geo}^k is the stoichiometric factor, κ is the reaction rate in $\text{mol}/(\text{m}^3 \cdot \text{s})$, r_w is the number of reactants in the aqueous phase, and r_s is the number of reactants in the solid phase.

Regarding mass balance, the geochemical reactions affect the porosity, which impacts the permeability. To satisfy the mass equilibrium, the following mathematical relation is used:

$$\phi = \phi_0 - \sum_n^{r_s} \phi_n$$

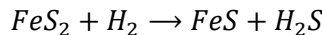
where ϕ_0 is the reference porosity (initial pore fraction without reactive solid components) and ϕ_n is the pore fraction filled with the solid reactive component ϕ_n .

The impact of the changed porosity on the permeability is modelled by the Kozeny-Carman-relationship.

$$K(\phi) = K_0 \cdot \left(\frac{1 - \phi_0}{1 - \phi} \right)^2 \cdot \left(\frac{\phi}{\phi_0} \right)^3$$

where K_0 is the reference permeability of the inert solids in m^2 .

For the specific case of pyrite-to-pyrrhotite reduction, the stoichiometric equation can be expressed as follows:



Following the mathematical model, the implementation of the source/sink for the geochemical reaction yields:

$$q_{\text{geo}}^k = \kappa \cdot \gamma_{\text{geo}}^k \phi c_w^{H_2} \cdot S_w \cdot (1 - \phi) \cdot c_s^{FeS_2}$$

Numerical implementation in the open-source simulator DuMu^x

The previously developed mathematical model is afterwards implemented in the open-source simulator DuMu^x. DuMu^x is in development by the University of Stuttgart (Institute of Modelling Hydraulic and Environmental Systems) since 2007, based on Distributed and Unified Numerics Environment (DUNE) and comes as an additional module to mimic the fluid flow in the subsurface, including chemical reactions. DuMu^x is the abbreviation for “DUNE for Multi-{Phase, Component, Scale, Physics, ...} flow and transport in porous media” [7], [8]. DuMu^x does not offer any Graphical User Interface (GUI) and is coded in C++. However, a better adjustment of chemical reactions and other effects than in commercial simulators can be realized. With promising results, Hagemann [4] implemented the first biochemical reactions caused by microbial activities during UHS. The following implementation of the UHS scenario is an extension of the previously developed UHS benchmark scenario [9].

A fluid system covering the relevant components is developed. It comprises two phases (water and gas), which are composed of six components: water (H_2O), methane (CH_4), hydrogen (H_2), carbon dioxide (CO_2), nitrogen (N_2), and hydrogen sulfur (H_2S). Apart from the chemical components, two types (sulfate-reducing and methanogenic) of microorganisms are implemented as additional pseudo components, which do not affect the fluid viscosity and density. The characteristic growth parameters are based on literature values [10], [11]. Regarding the solid system, three components are introduced: pyrite, pyrrhotite, and as an inert phase, quartz. The rate for the geochemical reaction is currently artificial and may over- or underestimate the velocity of the reaction. Here, the rates have to be validated on lab and field-scale.

A corner-point grid based on a semi-artificial geological structure (cf. Figure 1) is used for the spatial discretization of the simulation. It consists of 44652 (61x61x12) grid cells with a dimension of 50 m x 50 m (x- and y-direction) and varying thickness. The petrophysical properties (porosity and permeability) are distributed heterogeneously, and the permeability is additionally defined as anisotropic. The average porosity is 15%, and the mean horizontal permeability is 143 mD ($k_v \sim 3$ mD), which can be observed in some sandstone formations in Northern Germany (permeability distribution based on a modified poro-perm-correlation).

The system is initialized with a pressure of $P_{GWC} = 81.6$ bar at the gas-water-contact at a depth of 1210 m. A transition zone is established by the capillary pressure (Brooks-Corey parameter $\lambda = 2.0$, $P_e = 0.1$ bar [12]) separating the gas and water zone. The initial gas composition in the gas zone is defined as natural gas. Furthermore, the initial pyrite concentration is set to 0.1% and the sulfate content in the liquid phase is 0.0003375.

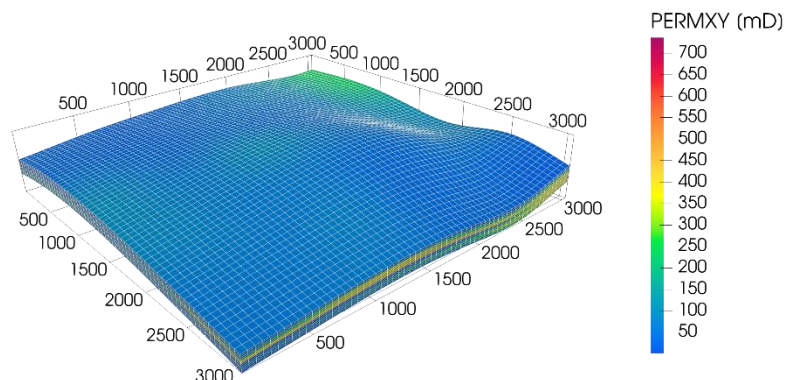


Figure 1: General overview of the geological structure (here: horizontal permeability)

In the present study, the schedule comprises two sections: 1) Conversion from natural gas storage into UHS and 2) Regular storage operation. In both sections, the injection/production occurs along a single well located in the centre of the structure. The injected gas composition remains constant (10% H₂, 90% natural gas). The first section, the conversion cycle, is characterized by a bottom-hole-pressure controlled injection which is incrementally increased from 90 bar to 102 bar (step size: 4 bar) to increase the reservoir pressure and raise the hydrogen content in the storage. Four cycles of 60 days with one month idle time between each cycle are performed. After the conversion cycles, regular storage cycles are conducted. The regular operation consists of alternating injection and production with a constant rate of $q = 293.13 \text{ mol/s} = 6 \cdot 10^5 \text{ Sm}^3/\text{day}$. The duration of the injection is identical to the withdrawal (90 days) to equalize the cumulative volumes. Similar to the conversion cycles, the regular storage cycles are separated by idle times.

Results

One of the crucial parameters during UHS is the gas composition of the withdrawn gas (see Figure 2). In the present study, the hydrogen fraction decreases with increasing cycle numbers. There are two main reasons for this observation: 1) gas mixing with the initial gas and 2) biogeochemical reactions. The impact of these reactions is also visible in Figure 3, where the consumption rate of each reaction is depicted. Regarding the geochemical reactions, the conversion rate increases strongly with hydrogen injection. However, during regular storage cycles, the global conversion rate decreases caused by the reduced pyrite concentration. A similar trend is also noticeable for the sulfate-reducing microorganisms, where sulfate progressively becomes a limiting substrate and diminishes the activity of the sulfate-reducing bacteria. Contrary to the sulfate-reduction process, the methanation seems constant over the storage period as neither hydrogen nor carbon dioxide (natural gas component) is limited. Next, the spatial distribution of the parameters is analyzed. Figure 4 represents the gas phase's hydrogen mole fraction after the last injection cycle. As expected, the highest concentrations close to the injection concentration are observed near the well. In general, the concentration decreases with increasing distance from the well. A similar spatial distribution can be observed for the volume fraction of pyrite (cf. Figure 5), just with the inverse behaviour. This observation is expected as the geochemical reaction decreases the pyrite content in the solid phase, and the highest hydrogen concentrations are achieved close to the well.

Regarding biochemical reactions (see Figure 6), only low hydrogen contents are required to lead to a maximum microbial density of approx. 58 times the initial for the methanogenic species. However, these observations regarding bio-geochemical reactions strongly depend on the specific growth parameters (biochemical) and reaction rate (geochemical). In particular, the geochemical reaction rate is influenced by significant uncertainties, and the model has to be calibrated by experimental results.

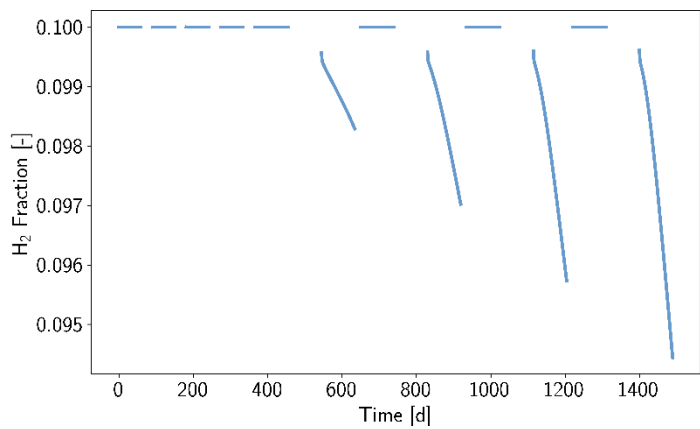


Figure 2: Hydrogen fraction in the withdrawal stream versus time

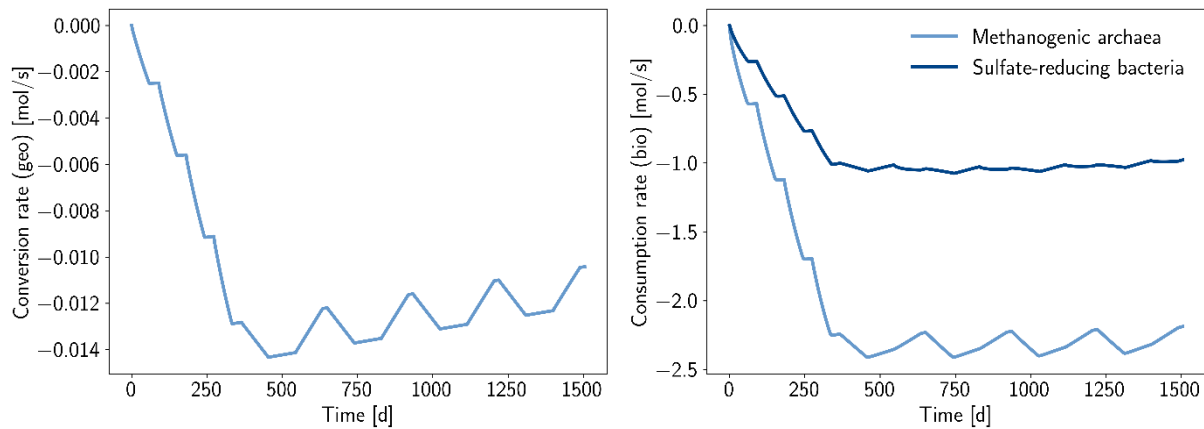


Figure 3: Hydrogen conversion rates from geo- and biochemical reactions versus time

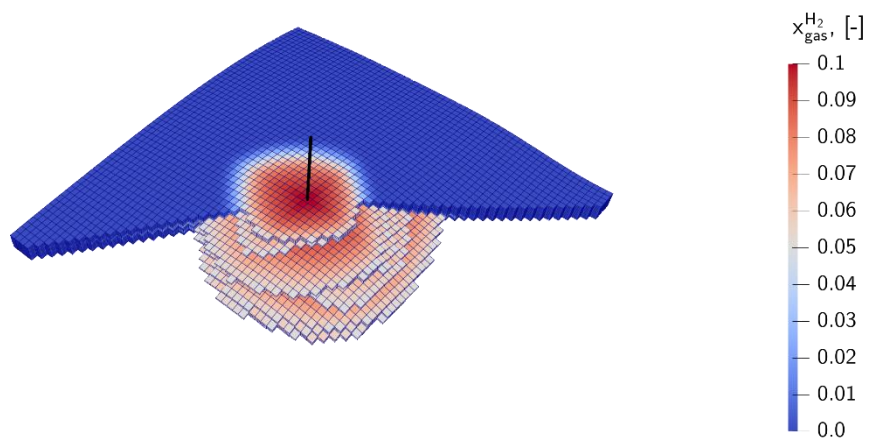


Figure 4: Hydrogen concentration after the last injection cycle

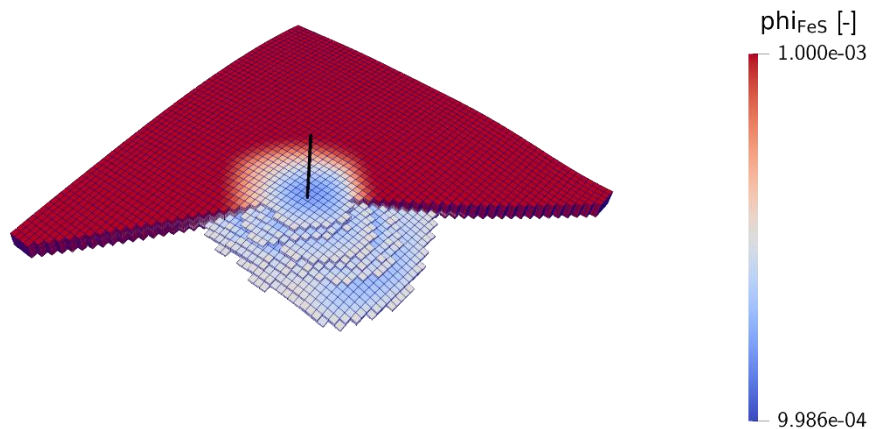


Figure 5: Pyrite concentration after the last injection period

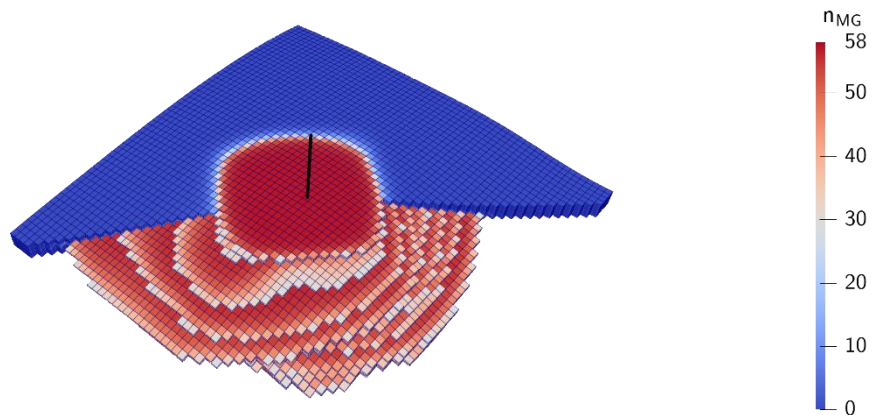


Figure 6: Spatial distribution of methanogenic microorganisms

Summary

With increasing interest in UHS, modelling unique hydrogen-related processes becomes more critical to efficiently predict and operate an UHS. Within this study, a mathematical model was developed describing the bio-geo-reactive transport in the subsurface and successfully implemented into the open-source simulator DuMu^x. This model considers the presence of methanogenic and sulfate-reducing microorganisms progressively consuming hydrogen and other substrates. The extension of geochemical reactions is focused on reducing pyrite-to-pyrrhotite, which leads to changes in the fluid and solid phases. The temporary loss into the initial gas and the permanent loss due to bio-geochemical reactions could be observed within the first simulation scenarios. However, laboratory experiments must be used to calibrate the reaction parameters.

After calibrating the model with more data, the resulting realization in DuMu^x allows to predict and optimize the operation of UHS scenarios.

Code availability

The implementation in the open-source simulator DuMu^x is available in its persistent form [13] and dynamically in a Gitlab repository [14].

Acknowledgement

This project has received funding from the Fuel Cells and Hydrogen 2 Joint Undertaking (now Clean Hydrogen Partnership) under grant agreement No 101006632. This Joint Undertaking receives support from the European Union's Horizon 2020 research and innovation programme, Hydrogen Europe and Hydrogen Europe Research.

References

- [1] N. Heinemann *et al.*, "Enabling large-scale hydrogen storage in porous media – the scientific challenges," *Energy Environ. Sci.*, vol. 14, no. 2, pp. 853–864, 2021, doi: 10.1039/D0EE03536J.
- [2] L. Truche *et al.*, "Clay minerals trap hydrogen in the Earth's crust: Evidence from the Cigar Lake uranium deposit, Athabasca," *Earth Planet. Sci. Lett.*, vol. 493, pp. 186–197, 2018, doi: 10.1016/j.epsl.2018.04.038.
- [3] V. Reitenbach, L. Ganzer, D. Albrecht, and B. Hagemann, "Influence of added hydrogen on underground gas storage: a review of key issues," *Environ. Earth Sci.*, vol. 73, pp. 6927–6937, 2015.
- [4] B. Hagemann, *Numerical and Analytical Modeling of Gas Mixing and Bio-Reactive Transport During Underground Hydrogen Storage*, 1. Auflage., vol. Band 50. in Schriftenreihe des Energie-Forschungszentrums Niedersachsen, vol. Band 50. Göttingen: Cuvillier Verlag, 2018. [Online]. Available: <https://ebookcentral.proquest.com/lib/gbv/detail.action?docID=5218530>
- [5] N. Hassannayebi, S. Azizmohammadi, M. Lucia, and H. Ott, "Underground hydrogen storage: application of geochemical modelling in a case study in the Molasse Basin, Upper Austria," *Environ. Earth Sci.*, vol. 78, no. 5, p. 177, 2019, doi: 10.1007/s12665-019-8184-5.
- [6] A. S. Abd and A. S. Abushaikha, "Reactive transport in porous media: a review of recent mathematical efforts in modeling geochemical reactions in petroleum subsurface reservoirs," *SN Appl. Sci.*, vol. 3, no. 4, p. 401, 2021, doi: 10.1007/s42452-021-04396-9.
- [7] B. Flemisch *et al.*, "DuMux: DUNE for Multi-(Phase, Component, Scale, Physics,...) Flow and Transport in Porous Media," *Adv. Water Resour.*, vol. 34, no. 9, pp. 1102–1112, 2011, doi: 10.1016/j.advwatres.2011.03.007.
- [8] T. Koch *et al.*, "DuMux 3 – An Open-Source Simulator for Solving Flow and Transport Problems in Porous Media with a Focus on Model Coupling," *Comput. Math. Appl.*, 2020, doi: 10.1016/j.camwa.2020.02.012.
- [9] S. Hogeweg, G. Strobel, and B. Hagemann, "Benchmark study for the simulation of Underground Hydrogen Storage operations," *Comput. Geosci.*, vol. 26, no. 6, pp. 1367–1378, Dec. 2022, doi: 10.1007/s10596-022-10163-5.
- [10] B. Hagemann, L. Ganzer, and M. Panfilov, "Field Scale Modeling Of Bio-Reactions During Underground Hydrogen Storage," presented at the ECMOR XVI - 16th European Conference on the Mathematics of Oil Recovery, Barcelona, Spain, in Proceedings. Barcelona, Spain: EAGE Publications BVNetherlands, 2018. doi: 10.3997/2214-4609.201802116.
- [11] G. Strobel, B. Hagemann, M. Wirth, and L. Ganzer, "Pore-Scale Modeling of Microbial Growth in A Two-Phase Saturated Porous Medium," vol. 2020. European Association of Geoscientists & Engineers, pp. 1–14, 2020. doi: 10.3997/2214-4609.202035171.
- [12] R. H. Brooks and A. T. Corey, "Hydraulic Properties of Porous Media and Their Relation to Drainage Design," *Trans. ASAE*, vol. 7, no. 1, pp. 0026–0028, 1964, doi: 10.13031/2013.40684.
- [13] S. Hogeweg and B. Hagemann, "Data for: HyUSPRe - Work Package 6 - Validated open-source reservoir modelling software that can simulate coupled flow, geochemical and microbiological processes in a porous reservoir under operational hydrogen storage conditions." GRO.data, 2023. doi: 10.25625/GNHQ93.

[14] S. Hogeweg, “GitLab Repository - dumux-hyuspre.” Apr. 11, 2023. [Online]. Available: <https://gitlab.tu-clausthal.de/asho13/dumux-hyuspre/>

Experimental investigations and development of a correlation to characterize the diffusion process of hydrogen and methane during UHS

J. Michelsen, S. Hogeweg, B. Hagemann, N. Langanke, L. Ganzer

Technische Universität Clausthal, Germany

Abstract

Renewable energy sources are becoming increasingly important during the current energy transition. The growing share of renewable energy sources problematically leads to fluctuations challenging the entire energy system. To keep the balance between energy demand and production in the future, and therefore to maintain energy availability, excess energy can be converted into hydrogen, stored and thereby acts as a buffer. Porous reservoirs, such as depleted natural gas fields, offer a good potential to store hydrogen in appropriate quantities. A reliable and effective storage operation requires a fundamental understanding of the mixing processes between the injected hydrogen and residual/cushion gas, supporting the deliverability of the storage. Besides the pressure-driven advective flux, mechanical dispersion and molecular diffusion influence the progressive mixing with the initial gas, typically natural gas. In the present study, experimental investigations are performed to determine gas-gas diffusion coefficients of the binary hydrogen-methane system. Here, diffusion experiments using a novel pseudo-stationary approach with reservoir rock samples at typical storage conditions (temperatures and pressures) are performed. Evaluations of the experiments showed effective diffusion coefficients for the system to lie within a range of $5.00 \cdot 10^{-9}$ to $3.71 \cdot 10^{-7} \text{ m}^2/\text{s}$.

A temperature and pressure dependent correlation is developed to predict effective diffusion coefficients for the porous rock samples. Furthermore, the experimental results are used to establish an additional correlation describing the interdependence between bulk and porous medium diffusion. This relationship depends on petrophysical properties such as porosity, permeability, and tortuosity. For the correlation, the polynomial regression approach is used; nevertheless, more general forms can be produced by measuring other binary gas constellations. The achieved correlation can be used in various models, such as the simulation of underground hydrogen storages on field scale.

Introduction

Over the course of the ongoing energy transition, underground energy storage is expected to become increasingly important to manage the fluctuations in the production of renewable energy from wind and solar. Underground hydrogen storage (UHS) in porous reservoirs in the subsurface is a new technology that can help to transition to a low carbon society and mitigate climate change. Several knowledge gaps have been identified that must be addressed to enable the implementation of hydrogen storage in porous media. One particular area of uncertainty is the H_2 fluid flow behaviour in porous media, which determines the hydrogen recovery, thereby ultimately affecting the economic feasibility of the storage operation. For underground hydrogen storage the mixing behaviour of the injected hydrogen and residual natural gas, which is mainly methane, in porous reservoirs plays an important role. One of the processes which influences the mixing of the gases is molecular diffusion (Figure 1). Molecular diffusion is a mixing process that is driven by concentration gradients.

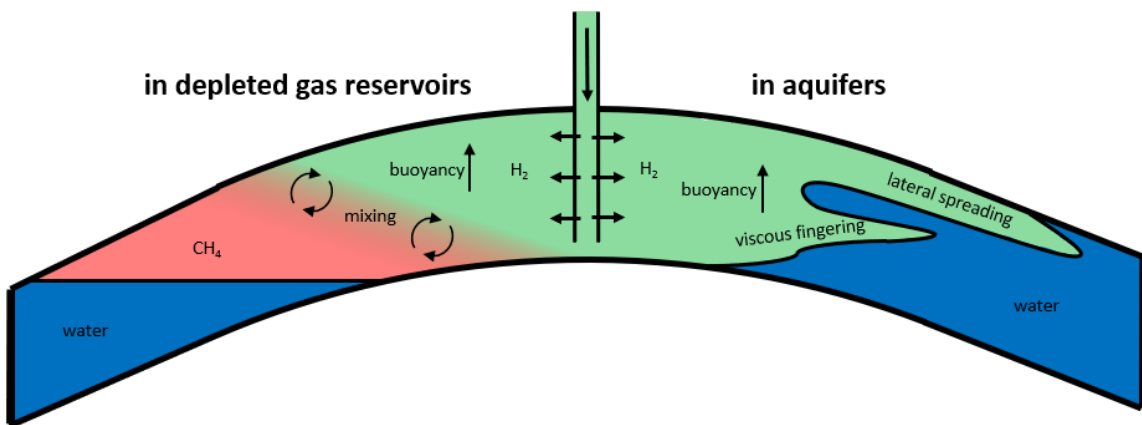


Figure 1. Sketch of gas mixing and hydrodynamic effects in an underground hydrogen storage

The aim of this work was to investigate the flow behaviour of hydrogen in a porous reservoir with laboratory experiments concerning the molecular diffusion. Besides the experimental measurements the processing of the experimental data for the use in numerical models was also part of this work. Based on the experimental results a correlation was built, which describes the interdependence between bulk and porous medium diffusion.

Molecular diffusion of hydrogen in the gas phase

Diffusion is a physical process that is driven by concentration differences and thus can occur even without pressure differences. It can take place under both stationary and unsteady conditions. The difference between the two conditions is that stationary diffusion occurs at a constant rate, while the unsteady diffusion rate is a function of time. Both diffusion conditions can be described using Fick's laws and can be used to measure the diffusion coefficient. Fick's first law states that the diffusive flux is directly proportional to the concentration gradient (Ho and Webb, 2006).

In a porous medium the diffusivity is usually reduced compared to the free gaseous diffusivity because the gas has less space and must travel a longer distance through it. Factors which are influencing the effective diffusivity are porosity, tortuosity and the presence of other fluid phases in the pore space. For binary systems the diffusive flux of gas components in a porous medium can be described by the following relation:

$$J_{\text{diff}}^k = -\rho D_{\text{eff}} \nabla c^k$$

where J_{diff}^k is the diffusive flux of component k in $\text{mol}/\text{m}^2/\text{s}$, ρ is the molar density of gas in mol/m^3 , D_{eff} is the binary effective diffusion coefficient in m^2/s and ∇c^k is the gradient of the mole fraction of component k .

Knudsen diffusion occurs when the mean free path of the gas molecules is comparable to or larger than the pore sizes of the porous medium. As a result, the molecules collide more frequently with the pore walls than with each other. Knudsen diffusion can be characterized by the Knudsen number, K_n . A Knudsen number greater than 10 indicates Knudsen diffusion. In this case, collisions between molecules and the pore wall are dominating. To find out if Knudsen diffusion is an issue in the experiments which are carried out within this study, the Knudsen number is calculated by using the following equation (Bear, 2018):

$$K_n = \frac{\lambda}{l_{pm}}$$

λ is the mean free path of the molecules in m and l_{pm} is the characteristic length dimension of the void space, here the pore diameter, in m. When assuming a mean free path of $6.6 \cdot 10^{-8}$ m and a mean pore diameter of $5 \cdot 10^{-5}$ m for a Bentheimer sandstone, which is one of the samples used for the measurements, the Knudsen number is $1.32 \cdot 10^{-3}$. Consequently, Knudsen diffusion does not play a role in the measurements here.

Experimental setup and procedure

The measurement of molecular diffusion is performed with a binary diffusion setup. The diffusion measurement method was modified after Wicke and Kallenbach (1941). The main component of the setup is a core holder, which is designed for rock samples with a length of up to 6 cm and a diameter of 3 cm, as shown in Figure 2.

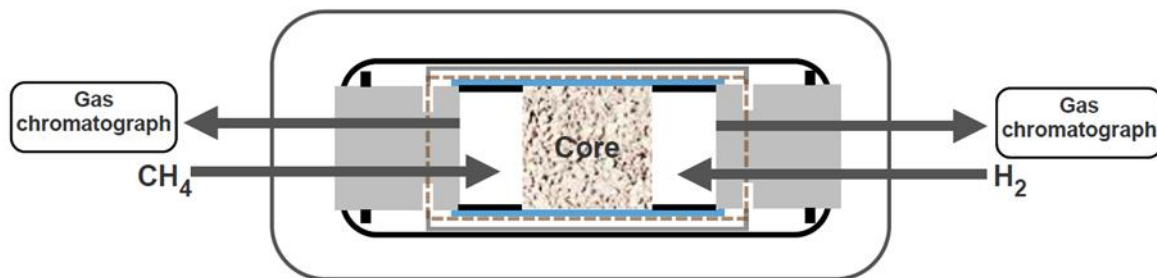


Figure 2. Sketch of the core holder

The rock sample, two hollow cylinders, two targets and two end pieces are first installed in a Viton sleeve and then in the core holder.

When a low diffusion rate is expected, a stationary method is used. Here, both hollow cylinders, which work as chambers, have the same volume. During the diffusion measurement the chambers are flooded with the sample gases, on the left side with methane and on the right side with hydrogen. The injection of the gases is controlled by high-pressure syringe pumps which are regulating gas filled floating piston chambers. The pressure in the chambers are regulated by pressure regulators, which are connected to the chamber outlets. Behind the left back pressure regulator, the composition of the outflowing gas is constantly analysed by a micro gas chromatograph.

For measurements with higher diffusion rates a quasi-stationary method is used. In this method one chamber contains a much larger volume than the other one. The large chamber must have a multiple of the volume in relation to the pore volume of the rock sample. The large chamber has one inlet. Prior to the measurement the chamber is filled with hydrogen gas and pressurised. On the other side of the sample is the target, which has one inlet and one outlet. During the experiment methane is injected into the cell via this inlet. The injection is again controlled by a syringe pump, which drives a floating piston chamber. This floating piston chamber is filled with methane. At the outlet of the target there is a backpressure regulator installed, which regulates the pressure in the diffusion cell to a constant value during the measurement. Behind the backpressure regulator again a gas chromatograph analyses the composition of the outflowing gas continuously. A sketch of the complete experimental setup for both configurations is shown in Figure 3.

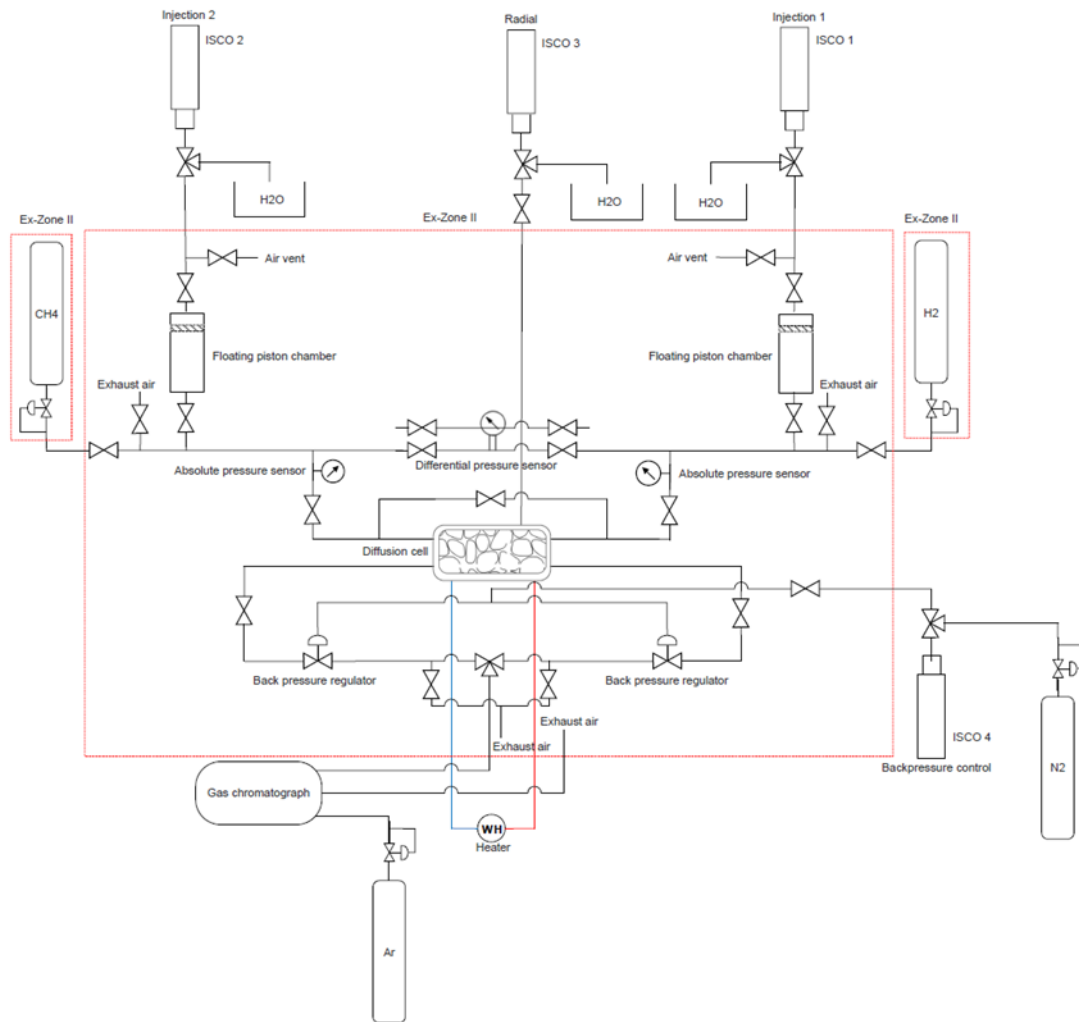


Figure 3. Sketch of the experimental setup for diffusion measurement

The measurement of an effective diffusion coefficient is performed using the following four steps:

1. Sample installation: The cylindrical sample of the porous material is inserted into a Viton sleeve together with the chambers, targets, and end pieces, and installed in the diffusion measurement cell. The diffusion measurement cell is connected to the measuring device. For the measurement of a water-saturated sample, there is an additional step prior to the installation into the measurement cell. The sample is saturated with distilled water externally under vacuum in a desiccator. The sample was pushed into a Viton sleeve and compressed air was used to displace the water and obtain a residual saturation. The resulting saturation was determined by weighing the sample directly before starting the experiment and afterwards.
2. Leakage test: The radial pressure and the measuring pressure are gradually increased to the desired values. The radial pressure should be 1.5 times or at least 50 bar higher than the measuring pressure. A leak test with nitrogen is carried out for at least 2 hours, during which the leakage rate should be no more than 0.5 % of the later injection rate.
3. Preparation:
Stationary measurement

As a first preparation step, the two floating piston chambers are filled with the samples gases (hydrogen and methane). The two chambers are flooded with the sample gases to

displace impurities and contamination. One chamber should be filled with >99.9 % hydrogen and the other one with >99.9 % methane. Then both chambers are pressurized up to the measuring pressure.

Quasi-stationary measurement

The chambers and the sample are flowed through with hydrogen from a gas cylinder. The purity of the outflowing gas is repeatedly analyzed with the process gas chromatograph. Again a gas purity of over 99.9 % should be ensured. The chambers and sample are then pressurized up to the desired measuring pressure with hydrogen. This is done via a gas booster at higher pressures. The floating piston chamber is filled with methane. Again, a gas purity of over 99.9 % must be ensured, which is achieved through repeated flushing. Filling to the desired measuring pressure is also done via the gas booster.

4. Measurement:

Stationary measurement

Injection at a constant rate on both sides is started and the shut-off valves on both sides are opened. The composition of the outflowing gas is continuously analysed with the process gas chromatograph.

Quasi-stationary measurement

Injection of methane is started at a constant rate, and the shut-off valve separating the diffusion measurement cell and the floating piston chamber is opened. The composition of the outflowing gas is again analyzed with the process gas chromatograph every three minutes.

Rock samples

For the diffusion measurements in total seven storage rock samples were selected. Additionally, one Bentheimer sandstone sample from a surface quarry was selected as a reference sample. All used samples and their properties are listed in Table 1. The porosity was measured by a gas pycnometer (micromeritics AccuPyc II 1340) using helium. The permeability was measured in a core flooding cell using nitrogen. The radial pressure during the permeability measurements was 20 bar and the gas pressure approx. 10 bar. As "mean pressure" the arithmetic mean between the minimum and maximum (allowable) operating pressure at reference depth (e.g. mid-point of the reservoir) was defined. Alternatively, for locations which were not used as gas storage before, the mean pressure is defined as $0.75 \cdot p_{\text{init}}$ (initial reservoir pressure).

Table 1. Selected rock samples for the diffusion measurement

| Sample site/ formation | Lithology | Porosity [%] | Permeability [mD] | Dry density [g/cm³] | Site conditions | |
|---------------------------|-----------|-----------------|----------------------|---------------------------|---------------------------|---------------------|
| | | | | | Mean pressure [bar] | Temperature [°C] |
| Bentheimer sandstone | Sandstone | 24.7 | 2500 | 1.99 | - | - |
| Chattian Sand | Sandstone | 29.9 | 71.0 | 1.90 | 106 | 50 |
| Aquitanian formation | Sandstone | 26.8 | 157.6 | 1.99 | 53.5 | 25 |
| Pliocene Sands | Sandstone | 31.7 | 718.6 | 1.83 | 88.3 | 45 |
| Ebes Fm. | Limestone | 19.9 | 23.6 | 2.19 | 140.5 | 107 |
| Ujfalu Fm. 1 | Sandstone | 32.1 | 288.2 | 1.84 | 116.5 | 86 |

| | | | | | | |
|--------------------|-----------|------|-------|------|--------|----|
| Detfurth formation | Sandstone | 27.4 | 263.1 | 1.93 | 287.25 | 96 |
| Rough Rotliegendes | Sandstone | 17.6 | 17.2 | 2.20 | 203 | 92 |

Interpretation and calculation of effective diffusion coefficients

Stationary conditions

For diffusion measurements where steady-state conditions were reached the interpretation and the calculation of effective diffusion coefficients was done according to Chen, Katz and Tek (1977). Based on Fick's first law they derived the following equation:

$$D_e = \frac{N_b Z}{A (C_{\text{right}}^{H_2} - C_{\text{left}}^{H_2})}$$

where N_b is the molar rate of H_2 diffusing through the sample in mol/s, Z is the length of the sample in m, A is the cross-sectional area of the sample in m^2 and C are molar concentrations in mol/m^3 . The molar density (or total molar concentration) of the gas is calculated under pressure and temperature by using the ideal gas law. For the molar hydrogen concentration this value is multiplied by the mole fraction measured by the gas chromatograph:

$$C^{H_2} = c_g^{H_2} \frac{p}{RT}$$

where $c_g^{H_2}$ is the mole fraction of H_2 in the gas phase, p is the pressure in Pa, R is the universal gas constant in $\text{J}/\text{K/mol}$ and T is the temperature in K.

Quasi-stationary conditions

Alternatively, a one-dimensional numerical simulation model was used to obtain the effective diffusion coefficient by a model fitting process when steady-state conditions were not reached. A numerical simulation model was implemented in COMSOL Multiphysics. The model solves the following partial differential equation, which is based on Fick's second law, in a one-dimensional domain (cf. Figure 4):

$$\frac{p}{RT} \phi \frac{\partial c}{\partial t} = \frac{p}{RT} D \frac{\partial^2 c}{\partial x^2}$$

where p is the measurement pressure in Pa, R is the universal gas constant in $\text{J}/(\text{mol} \cdot \text{K})$, T is the measurement temperature in K, ϕ is the porosity of the sample, c is the molar fraction of hydrogen, D is the effective diffusion coefficient in m^2/s .

Chamber 1 ————— Chamber 2



Figure 4. One-dimensional domain for the simulation of diffusion measurements

The following differential equations describe the boundary conditions. On the left side, no hydrogen is injected, but hydrogen which is transported into the chamber by diffusion flows out:

$$\frac{pV_l}{RT} \frac{\partial c_l}{\partial t} = -qc_l + \frac{p}{RT} DA \nabla c_1$$

where V_l is the volume of the left chamber in m^3 , q is the injection rate in mol/s , A is the end face of the rock sample, ∇c_1 is the space derivative of the hydrogen concentration at position 1, c_l is the hydrogen concentration in the left chamber. On the right side, a similar differential equation is solved:

$$\frac{pV_r}{RT} \frac{\partial c_r}{\partial t} = -\frac{p}{RT} D A \nabla c_2$$

where V_r is the volume of the right chamber in m^3 , ∇c_2 is the spatial derivative of the hydrogen concentration at position 2 and c_r the hydrogen concentration in the right chamber.

As an example, Figure 5 shows a comparison of a measurement with the simulation model. This measurement was done at 125 bar and 40 °C. The determined effective diffusion coefficient is $1.25 \cdot 10^{-7} \text{ m}^2/\text{s}$.

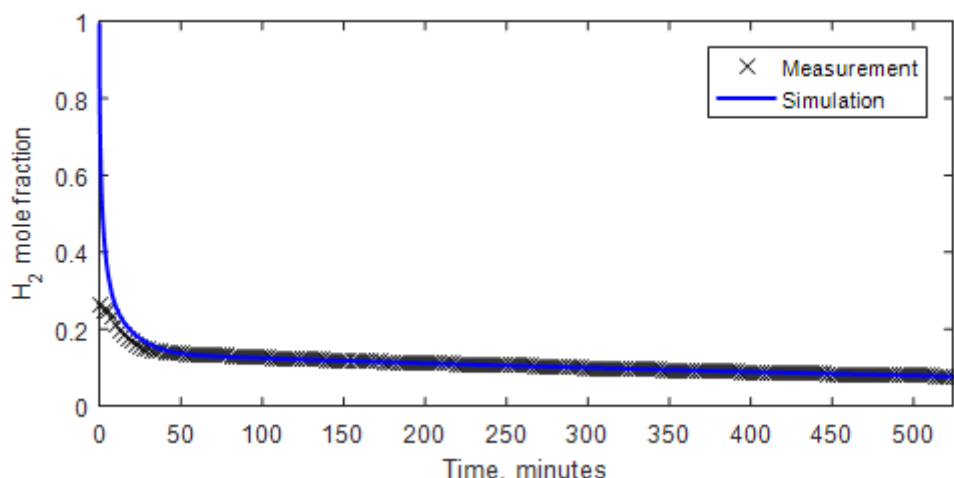


Figure 5. Comparison of the simulation results with the measurement

Results and discussion

As reference conditions for the diffusion measurements a pressure of 100 bar and a temperature of 40 °C was chosen. All samples were measured at these conditions. In addition, every sample was measured at the respective site conditions. The Bentheimer sandstone sample was used to investigate the influence of pressure, temperature and water saturation on diffusion. Altogether, 32 diffusion measurements were performed covering a pressure range of 10 to 287.5 bar and a temperature range of 25 to 100 °C. All measurement results are shown in the Appendix.

Figure 6 to Figure 8 show the behaviour of the effective diffusion coefficient in dependence of pressure, temperature and water saturation for the Bentheimer sandstone sample.

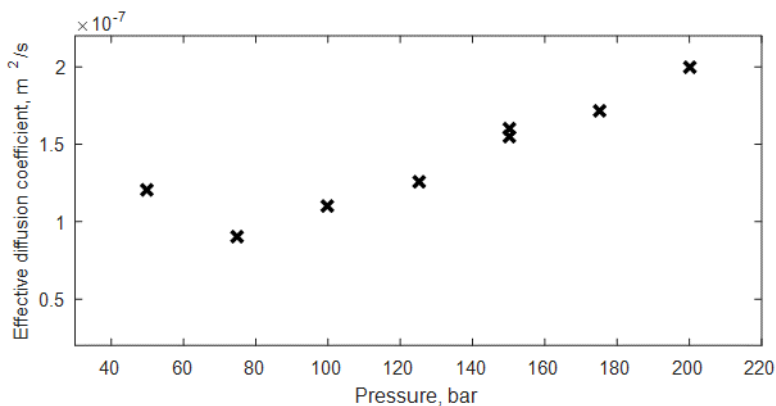


Figure 6. Effective diffusion coefficient vs. pressure for the Bentheimer sandstone sample at 40 °C

As in the plot depicted, the effective diffusion coefficient decreases with increasing pressure, in the lower pressure range. The smallest effective diffusion coefficient occurs at a pressure of 75 bar. At pressures above 75 bar the effective diffusion coefficient increases with higher pressure.

The following equation (Helmig, 1997) for the effective diffusion coefficient D_{pm} is a combination of the formula by (Vargaftik, 1975) for the description of the Fickian diffusion coefficient of binary gases and the model by (Millington and Quirk, 1961):

$$D_{pm} = \phi^{4/3} S_g^{10/3} D^0 \frac{p_0}{p_g} \left(\frac{T}{T_0} \right)$$

Based on this equation it can be assumed that the effective diffusion coefficient is inversely proportional to pressure, a behaviour as it appears between the two data points at 50 and 75 bar. However, the measurements show a different trend for higher pressures. From 75 to 200 bar there is a clear rising trend. A similar dependence of the diffusion coefficient on pressure was observed by Guevara-Carrion et al. (2019) for the binary system of CH₄ and CO₂.

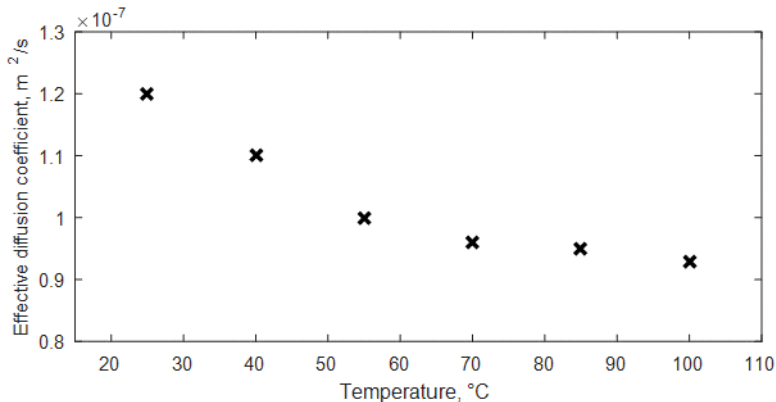


Figure 7. Effective diffusion coefficient vs. temperature for the Bentheimer sandstone sample at 100 bar

The effective diffusion coefficient shows a decreasing trend with increasing temperature. This trend is the opposite than expected but it was also observed by Guevara-Carrion et al. (2019) along certain pathways in the supercritical region.

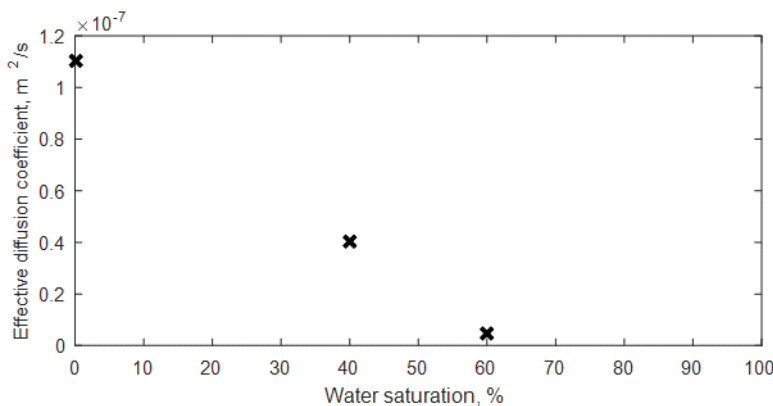


Figure 8. Effective diffusion coefficient vs. water saturation for the Bentheimer sandstone sample at 100 bar and 40 °C

As water saturation increases, there is clear decrease in the effective diffusion coefficient, with the dry core sample having the highest effective diffusion coefficient of $1.10 \cdot 10^{-7} \text{ m}^2/\text{s}$, the sample with 40 % water saturation having $4.00 \cdot 10^{-8} \text{ m}^2/\text{s}$, and the 60 % water saturation sample having $5.00 \cdot 10^{-9} \text{ m}^2/\text{s}$. This aligns with the expectation that an increased water saturation reduces the pore space available for gas diffusion in the rock sample, and is consistent with the Millington and Quirk correlation.

Application of the experimental results in numerical reservoir simulations

The performed experiments allow a more accurate prediction of the flow processes on a larger scale. Here, numerical simulations on field scales are an established method to match and forecast the operation of gas storages allowing the process to be optimized. The following presents the workflow from the laboratory to input parameters for numerical simulations.

Before the experimental data can be built into the simulator, a more general characterization of the molecular diffusion has to be developed. Generally, the diffusive flux in reservoir simulators is described as follows:

$$F_D^k = -\rho_{m,g} \cdot D_{pm}^k \cdot \nabla c_g^k$$

where F_D^k is the diffusive flux in $\text{mol}/(\text{m}^2 \cdot \text{s})$, $\rho_{m,g}$ is the molar density of the gaseous phase in mol/m^3 , D_{pm}^k is the diffusion coefficient of component k in the porous media in m^2/s , and c_g^k is the mole fraction of component k in the gaseous phase.

Considering a system composing two components, the effective binary diffusion coefficient is typically modelled during numerical simulation based on the following relationship:

$$D_{pm}^{AB} = \phi \cdot \tau \cdot S_g \cdot D^{AB}$$

where ϕ is the porosity, τ is the tortuosity factor of the porous medium, S_g is the gas saturation and D^{AB} is the binary diffusion coefficient in m^2/s .

Here, the experimental results are used to establish a model describing the molecular diffusion in rock samples at storage conditions. Existing models of binary diffusion coefficients are often limited to ambient to low pressures and temperatures. Therefore, a model with the following relationship is developed:

$$D_{pm}^{AB}(p, T, \phi, k, S_g) = \phi \cdot S_g \cdot \tau(\phi, k, S_g) \cdot D^{AB}(p, T)$$

In general, the modelling approach can be divided into two parts: 1) the development of a correlation describing the tortuosity factor based on various samples with varying properties at the same temperature and pressure conditions; 2) the establishment of correlation to predict binary diffusion coefficients of methane-hydrogen independently of the porous medium with changing temperature and pressure. The correlation based on the petrophysical properties is shown in Figure 9.

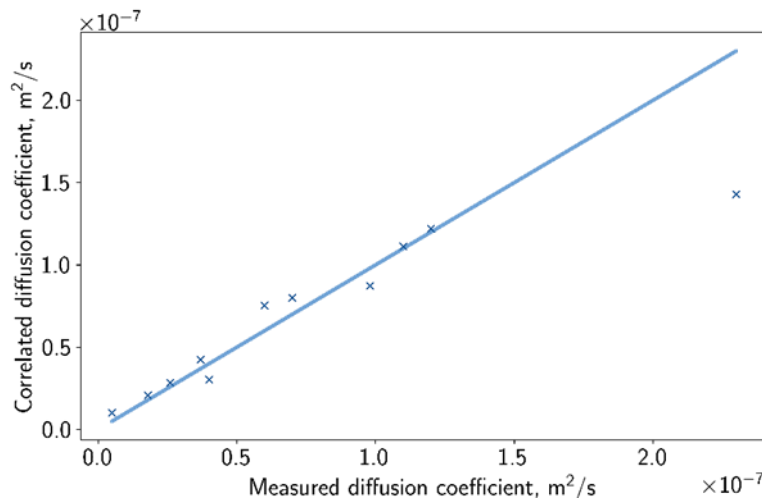


Figure 9. Correlation of diffusion coefficient based on various rock samples varying in petrophysical properties and saturation at reference conditions (100 bar, 40 °C)

A proper match, indicated by correlated values close to the identity line, was achieved with the following empirical relationship:

$$D_{pm}^{AB} = \phi^2 \cdot S_g^2 \cdot k_{\text{eff}}^{\frac{1}{5}} \cdot 3.4 \cdot 10^{-4} \text{ } m^2 / (\text{m}^{\frac{2}{5}} \cdot \text{s})$$

where the porosity and saturation are given in fractions and the effective permeability in m^2 . The Fullers method (Fuller et al., 1969) was selected due to its reported good accuracy at lower pressure and temperatures and evaluated at $T= 40 \text{ } ^\circ\text{C}$ and $P=10 \text{ bar}$ to obtain a reference bulk diffusion coefficient. With this reference value, the samples' tortuosity factor can be determined, leading to the general formulation:

$$D_{pm}^{AB} = \phi \cdot S_g \cdot \tau \cdot D^{AB}$$

$$\tau = \phi \cdot S_g \cdot k_{\text{eff}}^{\frac{1}{5}} \cdot 176.916 \text{ } m^{-\frac{2}{5}}$$

Next, a correlation for the binary diffusion coefficient was constructed. A polynomial regression second degree (2x2y) was used to describe the effective diffusion coefficient (measured) in dependency of pressure and temperature (See Figure 10).

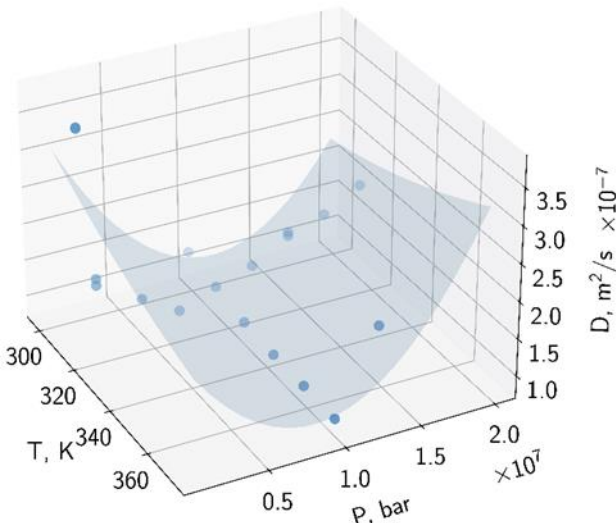


Figure 10. Effective diffusion coefficient in dependency of pressure and temperature of the Bentheimer Sandstone sample – dotted: experimental data; surface: polynomial regression

Using the first correlation, the polynomial function can be transformed, allowing the characterization of the binary diffusion coefficient. Here, the following parameters were achieved:

$$D^{AB}(T, p) = \beta_1 + \beta_2 \cdot T + \beta_3 \cdot p + \beta_4 \cdot T^2 + \beta_5 \cdot T \cdot p + \beta_6 \cdot p^2$$

$$\begin{aligned} \beta_1 &= 3.61069 \cdot 10^{-5} \text{ m}^2/\text{s} & \beta_4 &= 1.67793 \cdot 10^{-10} \text{ m}^2/(\text{s} \cdot \text{K}^2) \\ \beta_2 &= -1.46672 \cdot 10^{-7} \text{ m}^2/(\text{s} \cdot \text{K}) & \beta_5 &= 2.95155 \cdot 10^{-15} \text{ m}^2/(\text{s} \cdot \text{K} \cdot \text{Pa}) \\ \beta_3 &= -1.74842 \cdot 10^{-12} \text{ m}^2/(\text{s} \cdot \text{Pa}) & \beta_6 &= 3.71863 \cdot 10^{-20} \text{ m}^2/(\text{s} \cdot \text{Pa}^2) \end{aligned}$$

This function was fitted to the measured effective diffusion coefficients with the Bentheimer sandstone sample at various conditions. To extend the region of validity three additional measurements were conducted (10 bar/40 °C, 20 bar/40 °C, 150 bar/85 °C). The measurements with the storage site samples under reference and storage conditions were used as a test set to assess the developed correlations' accuracy. Table 2 presents the results of this comparison.

Table 2. Overview of relative errors of the correlation regarding the test set

| Exp. no | Sample | T [°C] | P [bar] | Measured diff. coeff. [m²/s] | Correlated diff. coeff. [m²/s] | Relative error [%] |
|---------|----------------------|--------|-----------|------------------------------|--------------------------------|--------------------|
| 1 | Chattian sand | 40 | 100 | $7.00 \cdot 10^{-8}$ | $8.00 \cdot 10^{-8}$ | -14.3 |
| 2 | Chattian sand | 50 | 106 | $6.50 \cdot 10^{-8}$ | $7.55 \cdot 10^{-8}$ | -16.2 |
| 3 | Aquitanian formation | 40 | 100 | $6.00 \cdot 10^{-8}$ | $7.54 \cdot 10^{-8}$ | -25.7 |
| 4 | Aquitanian formation | 25 | 53.5 | $1.10 \cdot 10^{-7}$ | $1.32 \cdot 10^{-7}$ | -19.8 |
| 5 | Pliocene sand | 40 | 100 | $2.30 \cdot 10^{-7}$ | $1.43 \cdot 10^{-7}$ | 37.9 |
| 6 | Pliocene sand | 45 | 88.3 | $2.00 \cdot 10^{-7}$ | $1.48 \cdot 10^{-7}$ | 26.1 |
| 7 | Ebes fm. | 40 | 100 | $2.60 \cdot 10^{-8}$ | $2.84 \cdot 10^{-8}$ | -9.4 |
| 8 | Ebes fm. | 107 | 140. 5 | $1.70 \cdot 10^{-8}$ | $4.22 \cdot 10^{-8}$ | -148.3 |

| | | | | | | |
|----|--------------------|----|------------|----------------------|----------------------|--------|
| 9 | Ujfalu fm. | 40 | 100 | $1.20 \cdot 10^{-7}$ | $1.22 \cdot 10^{-7}$ | -1.7 |
| 10 | Ujfalu fm. | 86 | 116. 5 | $1.10 \cdot 10^{-7}$ | $1.22 \cdot 10^{-7}$ | -10.8 |
| 11 | Detfurth formation | 40 | 100 | $9.80 \cdot 10^{-8}$ | $5.55 \cdot 10^{-8}$ | 43.3 |
| 12 | Detfurth formation | 96 | 287. 25 | $1.70 \cdot 10^{-7}$ | $4.32 \cdot 10^{-7}$ | -153.9 |
| 13 | Rough Rotliegendes | 40 | 100 | $1.80 \cdot 10^{-8}$ | $2.09 \cdot 10^{-8}$ | -16.0 |
| 14 | Rough Rotliegendes | 92 | 203 | $9.00 \cdot 10^{-9}$ | $6.51 \cdot 10^{-8}$ | -623.1 |

In general, the reproducibility shows a good accuracy with less than 50 %, with some exceptions. Remarkable are experiments 8, 12, and 14, where the relative error is higher than 100 %. The remarkable deviations were samples measured at the experimental matrix's higher boundaries and exceeding these conditions. Furthermore, the binary diffusion coefficient is overestimated for these cases; therefore, the process is more substantial than observed. Regarding the significant deviation of 623 % for the Rough Rotliegendes sample, the temperature is located at the upper boundary, the pressure exceeds the upper limit, and the permeability is the lowest of the entire measurement series. In this region, the established correlation seems to be inaccurate, leading to a higher error. Nevertheless, the established correlation allows the reproduction of the observed molecular diffusion coefficients for sandstone samples in a pressure and temperature range of 10 to 200 bar and 25 to 100°C.

Conclusions

In total 32 measurements of molecular diffusion with reservoir rock samples were performed and interpreted. The influence of pressure, temperature and water saturation was investigated using a Bentheimer sandstone as reference sample. The determined effective gaseous diffusion coefficients varied between $5.00 \cdot 10^{-9}$ and $3.71 \cdot 10^{-7} \text{ m}^2/\text{s}$. The results showed clear trends, but deviations were observed from conventional correlations at pressures above 75 bar and for the dependence on temperature at 100 bar. The decreasing trend of effective diffusion coefficient with increasing water saturation fits the expectation. The comparison of effective diffusion coefficients for different samples at reference conditions indicated that the effective diffusivity increases with porosity and permeability.

The developed correlations can be implemented into numerical simulators to predict the mixing effects during hydrogen storage in the subsurface. However, many commercial simulators are limited in their level of adaption, and only the binary diffusion coefficient can be implemented. Here, the presented modelling has to be modified. Further, additional measurements with different gas components, such as carbon dioxide or nitrogen, could lead to a more general model instead of a polynomial regression.

Acknowledgement

This project has received funding from the Fuel Cells and Hydrogen 2 Joint Undertaking (now Clean Hydrogen Partnership) under grant agreement No 101006632. This Joint Undertaking receives support from the European Union's Horizon 2020 research and innovation programme, Hydrogen Europe and Hydrogen Europe Research.

Additionally, this project is a cooperation with the DMT and we acknowledge funding by the TÜV Nord AG.

References

- Bear, Jacob (2018): Modeling phenomena of flow and transport in porous media. Cham: Springer (Theory and applications of transport in porous media, volume 31).
- Chen, Lillian Lung-yu; Katz, Donald L.; Tek, M. Rasin (1977): Binary gas diffusion of methane-nitrogen through porous solids. *AIChE Journal* 23 (3), pp. 336–341.
- Fuller, Edward N.; Ensley, Keith; Giddings, J. Calvin (1969): Diffusion of halogenated hydrocarbons in helium. The effect of structure on collision cross sections. *The Journal of Physical Chemistry* 73 (11), pp. 3679–3685.
- Guevara-Carrion, Gabriela; Ancherbak, Sergiy; Mialdun, Aliaksandr; Vrabec, Jadran; Shevtsova, Valentina (2019): Diffusion of methane in supercritical carbon dioxide across the Widom line. *Scientific reports* 9 (1), p. 8466.
- Ho, Clifford K.; Webb, Stephen W. (Eds.) (2006): Gas Transport in Porous Media. Dordrecht: Springer Netherlands (SpringerLink Bücher, 20).
- Millington, R. J.; Quirk, J. P. (1961): Permeability of porous solids. *Transactions of the Faraday Society* 57, p. 1200.
- Soukup, Karel; Schneider, Petr; Šolcová, Olga (2008): Comparison of Wicke–Kallenbach and Graham's diffusion cells for obtaining transport characteristics of porous solids. *Chemical Engineering Science* 63 (4), pp. 1003–1011.
- Vargaftik, Natan B. (1975): Tables on the thermophysical properties of liquids and gases. In normal and dissociated states. 2. ed. Washington: Hemisphere Publ (Advances in thermal engineering, 4).
- Wicke, E.; Kallenbach, R. (1941): Die Oberflächendiffusion von Kohlendioxyd in aktiven Kohlen. *Kolloid-Zeitschrift* 97 (2), pp. 135–151.

Appendix

Effective molecular diffusion coefficients

Table 3. Data set of effective diffusion coefficients

| Measurement no. | Sample site/formation | Lithology | Porosity [%] | Permeability [mD] | Pressure [bar] | Temperature [°C] | Water saturation [%] | Effective diffusion coefficient [m²/s] |
|-----------------|-----------------------|-----------|--------------|-------------------|----------------|------------------|----------------------|--|
| 1 | Bentheimer sandstone | Sandstone | 24.7 | 2500 | 10 | 40 | 0 | 3.71·10 ⁻⁷ |
| 2 | Bentheimer sandstone | Sandstone | 24.7 | 2500 | 20 | 40 | 0 | 1.64·10 ⁻⁷ |
| 3 | Bentheimer sandstone | Sandstone | 24.7 | 2500 | 50 | 40 | 0 | 1.20·10 ⁻⁷ |
| 4 | Bentheimer sandstone | Sandstone | 24.7 | 2500 | 75 | 40 | 0 | 9.00·10 ⁻⁸ |
| 5 | Bentheimer sandstone | Sandstone | 24.7 | 2500 | 100 | 40 | 0 | 1.10·10 ⁻⁷ |
| 6 | Bentheimer sandstone | Sandstone | 24.7 | 2500 | 125 | 40 | 0 | 1.26·10 ⁻⁷ |
| 7 | Bentheimer sandstone | Sandstone | 24.7 | 2500 | 150 | 40 | 0 | 1.55·10 ⁻⁷ |
| 8 | Bentheimer sandstone | Sandstone | 24.7 | 2500 | 150 | 40 | 0 | 1.60·10 ⁻⁷ |
| 9 | Bentheimer sandstone | Sandstone | 24.7 | 2500 | 175 | 40 | 0 | 1.72·10 ⁻⁷ |
| 10 | Bentheimer sandstone | Sandstone | 24.7 | 2500 | 200 | 40 | 0 | 2.00·10 ⁻⁷ |
| 11 | Bentheimer sandstone | Sandstone | 24.7 | 2500 | 100 | 25 | 0 | 1.20·10 ⁻⁷ |
| 12 | Bentheimer sandstone | Sandstone | 24.7 | 2500 | 100 | 55 | 0 | 1.00·10 ⁻⁷ |
| 13 | Bentheimer sandstone | Sandstone | 24.7 | 2500 | 100 | 70 | 0 | 9.60·10 ⁻⁸ |
| 14 | Bentheimer sandstone | Sandstone | 24.7 | 2500 | 100 | 85 | 0 | 9.50·10 ⁻⁸ |
| 15 | Bentheimer sandstone | Sandstone | 24.7 | 2500 | 100 | 100 | 0 | 9.30·10 ⁻⁸ |
| 16 | Bentheimer sandstone | Sandstone | 24.7 | 2500 | 150 | 85 | 0 | 1.49·10 ⁻⁷ |

| Measurement no. | Sample site/formation | Lithology | Porosity [%] | Permeability [mD] | Pressure [bar] | Temperature [°C] | Water saturation [%] | Effective diffusion coefficient [m²/s] |
|------------------------|------------------------------|------------------|---------------------|--------------------------|-----------------------|-------------------------|-----------------------------|--|
| 17 | Bentheimer sandstone | Sandstone | 24.7 | 2500 | 100 | 40 | approx. 40 | 4.00·10 ⁻⁸ |
| 18 | Bentheimer sandstone | Sandstone | 24.7 | 2500 | 100 | 40 | approx. 60 | 5.00·10 ⁻⁹ |
| 19 | Chattian Sand | Sandstone | 29.9 | 71 | 100 | 40 | 0 | 7.00·10 ⁻⁸ |
| 20 | Chattian Sand | Sandstone | 29.9 | 71 | 106 | 50 | 0 | 6.50·10 ⁻⁸ |
| 21 | Aquitianian formation | Sandstone | 26.8 | 157.6 | 100 | 40 | 0 | 6.00·10 ⁻⁸ |
| 22 | Aquitianian formation | Sandstone | 26.8 | 157.6 | 53.5 | 25 | 0 | 1.10·10 ⁻⁷ |
| 23 | Pliocene Sands | Sandstone | 31.7 | 718.6 | 100 | 40 | 0 | 2.30·10 ⁻⁷ |
| 24 | Pliocene Sands | Sandstone | 31.7 | 718.6 | 88.3 | 45 | 0 | 2.00·10 ⁻⁷ |
| 25 | Ebes Fm. | Limestone | 19.9 | 23.6 | 100 | 40 | 0 | 2.60·10 ⁻⁸ |
| 26 | Ebes Fm. | Limestone | 19.9 | 23.6 | 140.5 | 107 | 0 | 1.70·10 ⁻⁸ |
| 27 | Ujfalú Fm. 1 | Sandstone | 32.1 | 288.2 | 100 | 40 | 0 | 1.20·10 ⁻⁷ |
| 28 | Ujfalú Fm. 1 | Sandstone | 32.1 | 288.2 | 116.5 | 86 | 0 | 1.10·10 ⁻⁷ |
| 29 | Dettfurth formation | Sandstone | 27.4 | 27.4 | 100 | 40 | 0 | 9.80·10 ⁻⁸ |
| 30 | Dettfurth formation | Sandstone | 27.4 | 27.4 | 287.25 | 96 | 0 | 1.70·10 ⁻⁷ |
| 31 | Rough Rotliegendas | Sandstone | 17.6 | 17.2 | 100 | 40 | 0 | 1.80·10 ⁻⁸ |
| 32 | Rough Rotliegendas | Sandstone | 17.6 | 17.2 | 203 | 92 | 0 | 9.00·10 ⁻⁹ |

Biostratigraphic evaluation of data from the Mittelplate oilfield (NW Germany)

B. Holstein¹, C. A. Schneider², H. Bolten³

¹IntegBiostrat, Wedemark, Germany

²Wintershall Dea, Technology & Service Center, Barnstorf, Germany,

³Wintershall Dea Deutschland GmbH

Abstract

In the framework of a comprehensive field study, all available biostratigraphic data from Early Cretaceous to Middle Jurassic age of the Mittelplate oilfield was checked and evaluated. Old recordings of microfossil analyses, which partially reach back to the 1990s, were revised for consistency and afterwards harmonized. All available microfossil counting information was transferred to a consistent data format. In total biostratigraphic data from approximately 50 wells was available.

Older microfossil spellings were updated to scientific notations and emendations, using the latest available literature. By means of a complex data query and a standardized section (all stratigraphic units were matched and a general thickness for each was created), a micropaleontological generalised range-chart for the whole field was compiled.

As primary tool “Excel®” spreadsheets were used and with help of visual basic functions the operational mode of a small database functionality was obtained. This allows to select a specific microfossil and to execute a query. As a result, each occurrence of the microfossil within any well can be displayed.

In a second step, the complete dataset was exported into the biostratigraphic software “StrataBugs®” (www.stratadata.co.uk). This software allows to combine the data with other significant well data like gamma ray logs, lithology, wellsite stratigraphy or casing depths.

Within “StrataBugs®” different charts were compiled: an overview chart with all wells, which helped to identify effectively biostratigraphic data gaps, and a second chart, which allows to select specific microfossils, being displayed in all wells. This provides an overview of the field wide occurrences facilitating the identification of index fossils. Based on the large database, the ranges and respectively the abundance maxima of some index microfossils were revised. All biostratigraphic relevant events were compiled in a stratigraphic framework.

The created dataset will be constantly updated and a paleoenvironmental assessment conducted. Future well site biostratigraphic analyses (“biosteering”) will benefit through a more confident stratigraphical assignment of the drilled horizons.

Introduction

The Mittelplate field operated by Wintershall Dea is Germany's largest oil field and is placed in coastal tidal flats at the mouth of the River Elbe estuary, about 20 km northeast of Cuxhaven. It is located in the Westholstein Jura Trough with its flanking salt walls Oldenswort and Büsum.

Since the beginning of the field development, biostratigraphic support in a large extend, although not continuous and not for all wells, was supplied (Figure 1). In more than 30 years, more than 5400 micropaleontological analyses were carried out, using ditch cuttings as well as core material. The samples are typically treated with hydrogen peroxide (H_2O_2) for disaggregation. The sieved and dried residue is analyzed under the microscope for microfaunal as well as accessory elements that might serve as possible stratigraphic indicators (e.g. sphaerosiderite, coal, pyrite, bioturbation fillings).

The biostratigraphic application in Mittelplate is based on the occurrences or disappearances of certain microfaunal assemblages and individual taxa that can often be correlated over large parts of NW-Germany. Important microfossil groups are calcareous and agglutinated foraminifera, ostracods, siliceous diatoms and radiolarians, as well as organic-walled megaspores.

The existing micropaleontological data was available in different formats, and sometimes only accessible in an analogue format. Only few, mainly older wells had been truly biostratigraphically correlated and microfossil ranges compared and evaluated. Additionally, during this time progress was made regarding the stratigraphical and micropaleontological knowledge of the German Jurassic system (e.g., Brand & Mönnig, 2010).

It became imperative to harmonize the complex set of analyses making it available in an up-to-date database and software environment. At the same time, when applicable, the micropaleontological nomenclature from new literature was implemented and new stratigraphic assignments incorporated.

Biostratigraphic knowledge of the Mittelplate field is exceptionally meaningful for supporting drilling activities through applied biostratigraphy ("biosteering"). Well pathfinding and correction through long horizontal sections, verification of casing points and redirecting when faults are drilled have a significant impact on successful drilling. The better the biostratigraphic dataset, the more reliable and accurate age assignments of drilled sediments become.

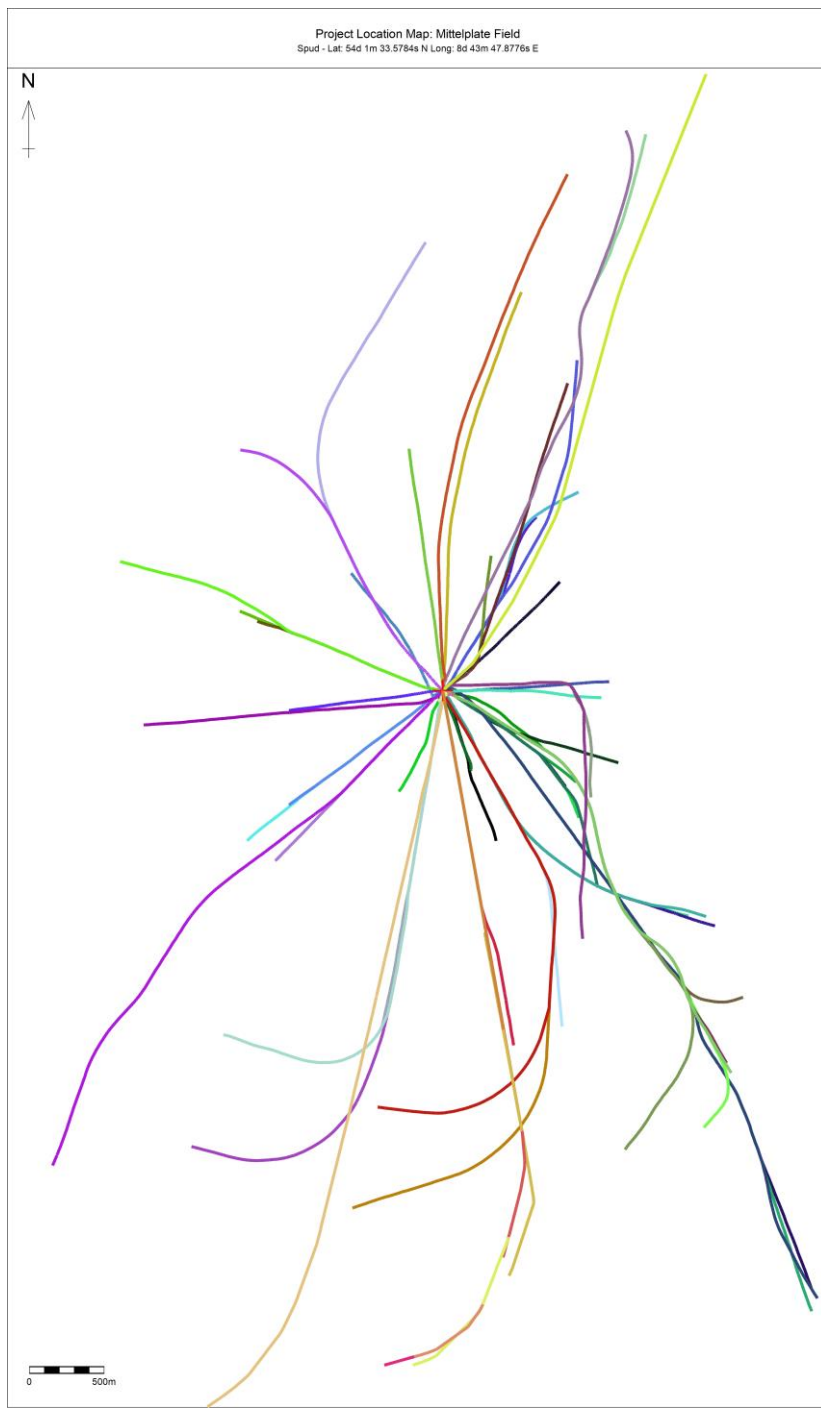


Figure 1: Map projection of studied wells. It points out the complexity of the well framework within the Mittelplate oil field.

Initial position – available data evaluation and preparational steps

At the beginning of this study, a thorough assessment of the available data was performed. Each well within the Mittelplate Field was checked for biostratigraphic analyses and existing micropaleontological slides. The available data was checked for consistency. Partly, the oldest documentation (handwritten counting sheets) is incomplete. The analyses had been documented in various formats, as

- Handwritten micropaleontological counting sheets
- Text files and Excel spreadsheets
- Printed reports
- “StrataBugs” projects

To gain an optimal summary of data availability and quality, a framework of all Mittelplate field wells including wells with no biostratigraphic analyses was created with “StrataBugs”. This software can record, store, manipulate and display biostratigraphical and geological data including wireline logs and graphic lithologies. This framework allows a quick assessment for which wells and stratigraphical intervals data gaps are existent.

Biostratigraphic data harmonization

This step was crucial for the successful outcome of the project, as the comparability of biostratigraphic data significantly depends on a uniform micropaleontological nomenclature. In some cases, different publishers used different (working) names for the same microfossils in these three decades. Where necessary, the original micropaleontological slides were reviewed.

Older microfossil spellings and assignments, used by former scientific publishers like Plumhoff (1963), were updated to scientific notations and emendations, using the latest available literature. For example, the ostracod working name *Terquemula* sp. 99 was originally described as *Lophodentina?* sp. 99 Brand, and is nowadays addressed as *Dolocythere tuberculata* (Luppold, 2012). There is also a similar species from Britain from the same age interval (Lord et al., 2020).

At first, a reference microfossil name file was created. This file stores the microfossil name, a numerical ID and further metadata (e.g., age, paleoenvironment). Then an Excel spreadsheet with a uniform structure for all micropaleontological analyses was created. This uniform structure ensures that queries interpreting ranges of microfossils within the dataset run properly. Thereby the microfossil ID ensures, that all microfossil names have the identical spelling.

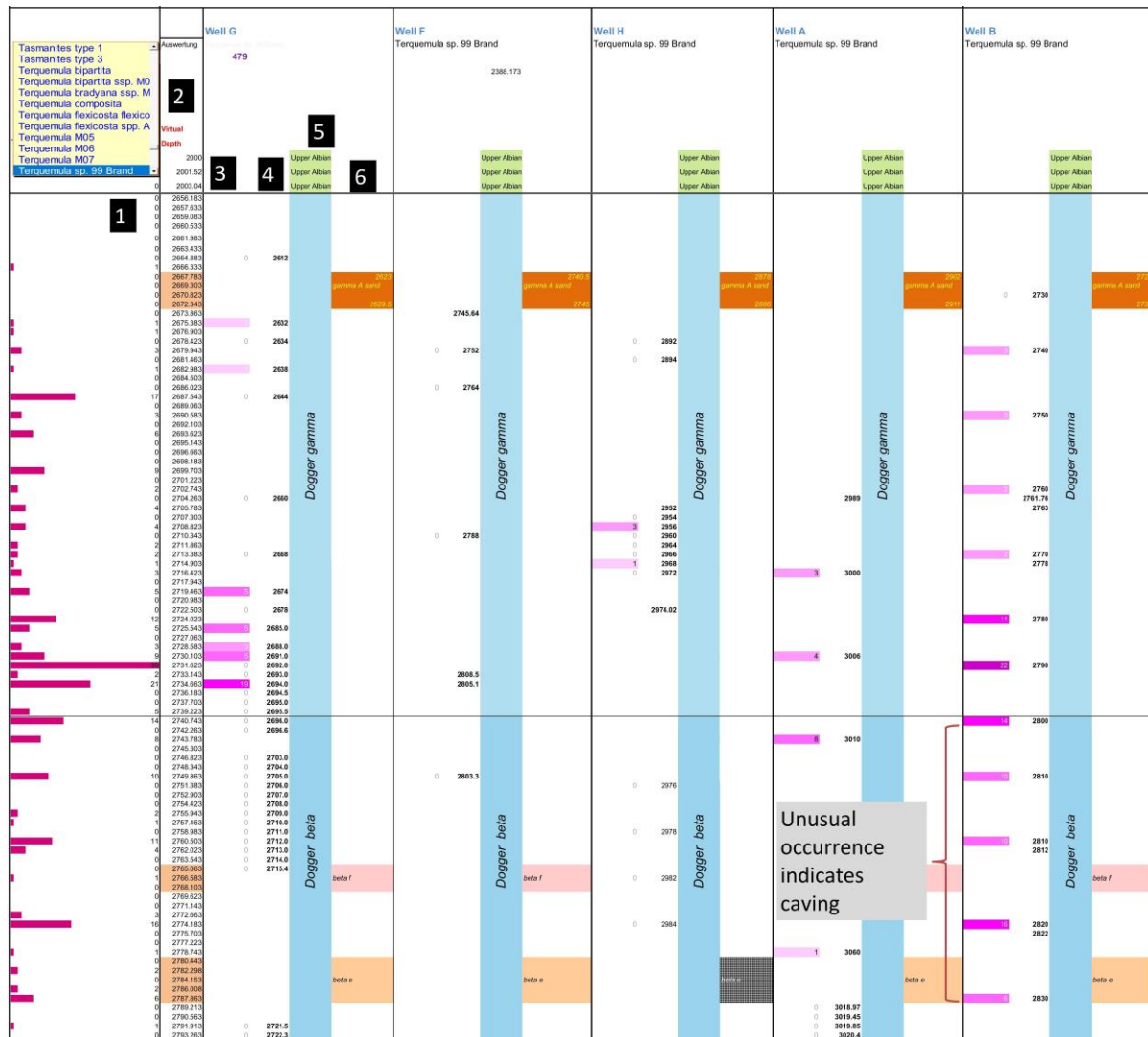
All handwritten microfossil counting sheets were transformed to Excel spreadsheets. Already existing Excel microfossil counting spreadsheets were revised and converted. Micropaleontological data stored solely in “StrataBugs” was exported as Excel files and equally transformed. At the end of this step, all biostratigraphic data originating from the different data sources obtained the same format.

Microfossil range query

The purpose of the range query is to create a fast overlook of field wide microfossil occurrences and ranges. For the sake of reproducibility, only wells with a relatively non-disturbed stratigraphic succession have been selected.

Within a complex Excel spreadsheet, all selected wells were aligned, and one well with a nearly vertical drilling path was selected for the standard thickness of the stratigraphic intervals. The stratigraphic tops and bases of the other wells were adapted to this standard well and the samples were drawn into an equivalent position. Consequently, all wells within the chart contain samples with the true depth, which is allocated to a second virtual depth.

This allows a comparative display of the stratigraphic range of a certain microfossil in all wells (Figure 2).



“Strata Bugs” the dataset can be filtered and displayed as desired. It is possible to select all microfossils, setting up groups with most important microfossils (markers), or to display single species (Figure 4).

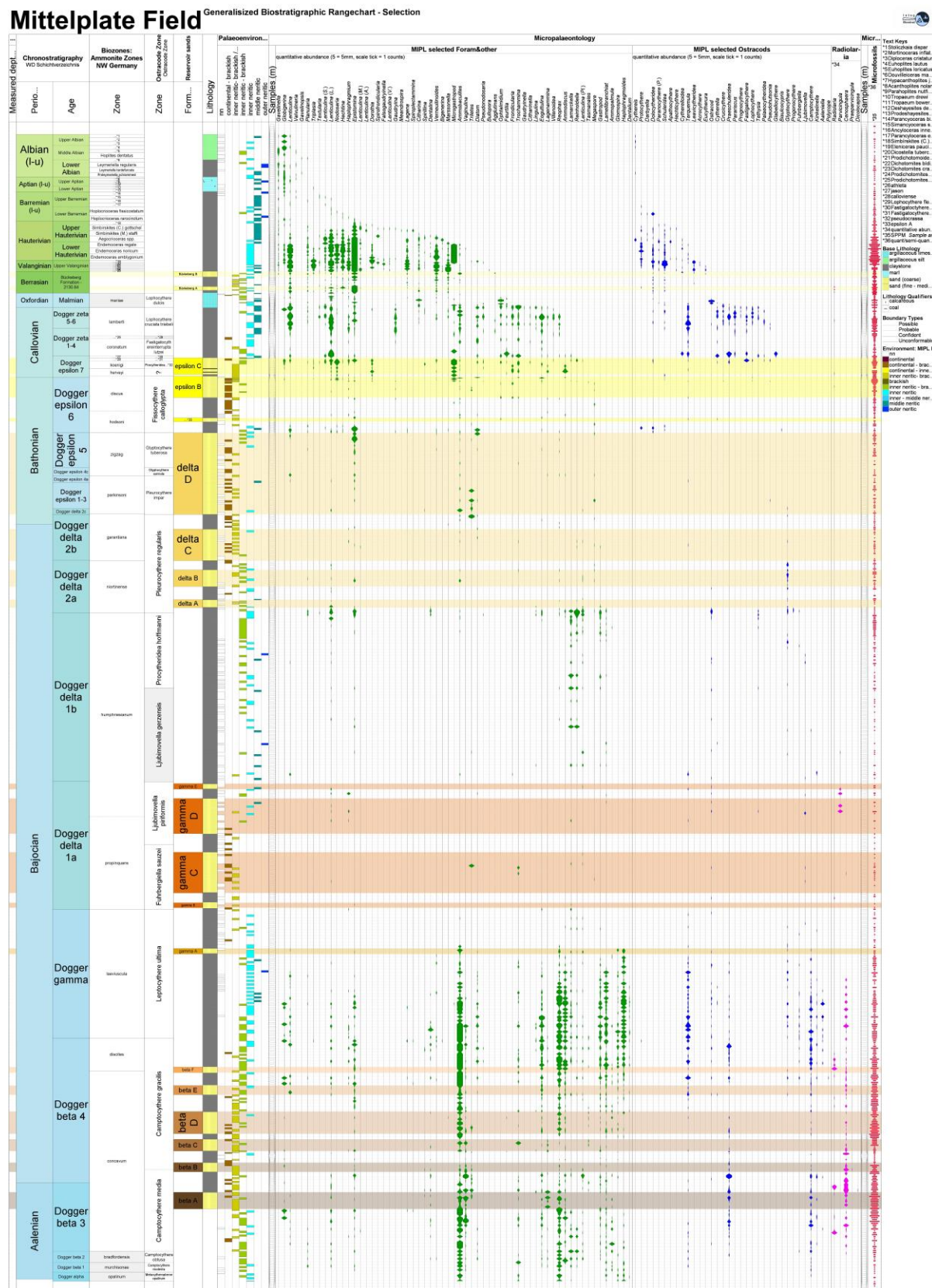


Figure 3: Generalized field wide range for the Mittelplate Field, Lower Cretaceous – Dogger beta. The microfossil countings (only a selection of taxa) reflect the accumulative abundance through all wells. The column with red fillings at the right side of the chart displays the quantity of analyses for the specific stratigraphic horizon.

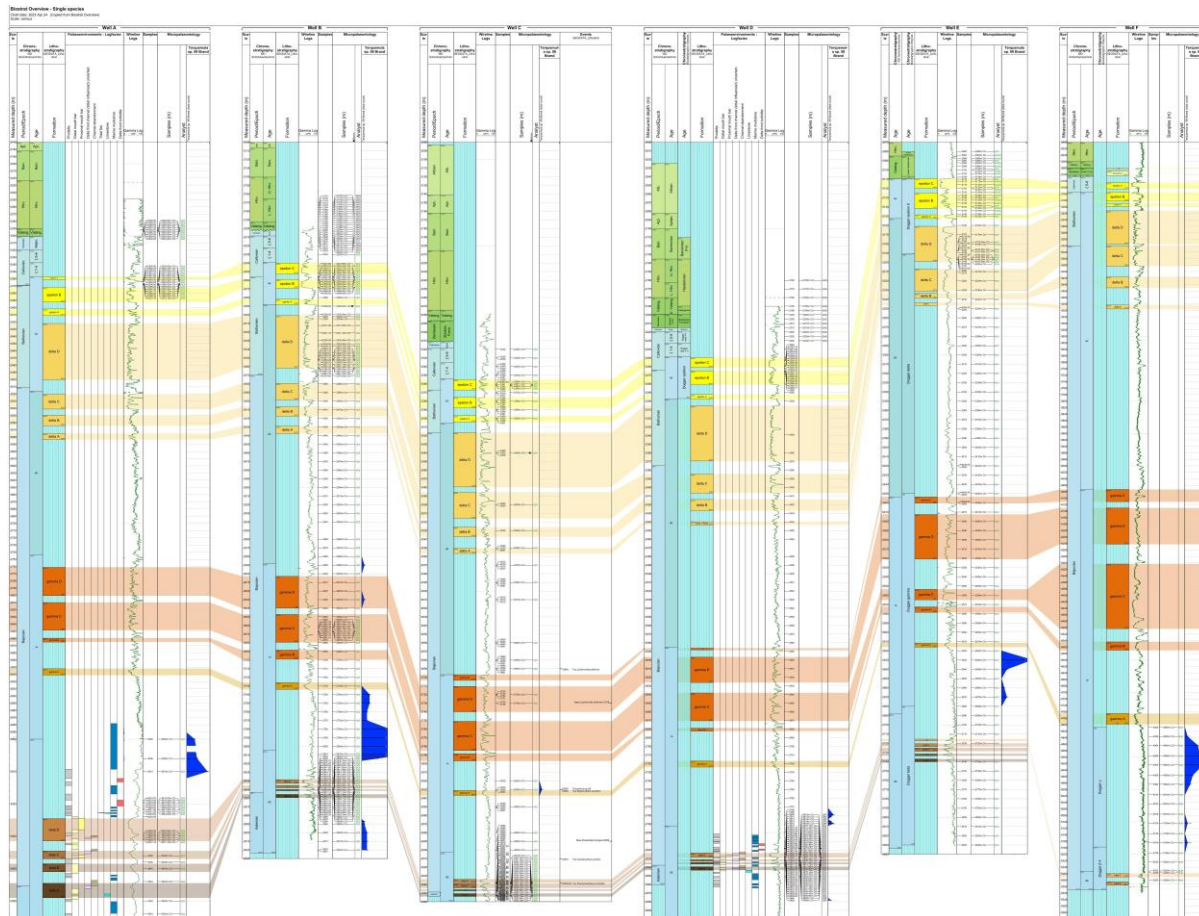


Figure 4: Extract from microfossil range chart of the Mittelplate Field created with “StrataBugs”. In this example the stratigraphic valuable species *Terquemula* sp. 99 is selected and displayed through all wells (blue colour). This chart also helps to identify effectively biostratigraphic data gaps. All well names have been anonymized.

Results and outlook

For the first time in the Mittelplate Field, all biostratigraphic analyses carried out were consolidated and evaluated applying a consistent approach. The combination of data preparation and analysis with Excel and graphic implementation for displaying range charts with “StrataBugs®” provides a profound toolbox for biostratigraphic interpretations on a field-wide scale.

An overview of the field wide occurrences allows the proper identification of index fossils with stratigraphic value. Based on the extended database, the ranges and respectively the abundance maxima of already used index microfossils were revised, and many others have

been identified. All biostratigraphic relevant events were compiled in a stratigraphic framework.

Several, in particular rare microfossils retain their provisional working names, due to absent scientific identification and shortage of time in a dynamic E&P business. Their chronostratigraphic assignment and value remain vague or unclear. Stepping up the efforts in the identification of these microfossils could further enhance the knowledge of the chronostratigraphic zonation of the Mittelplate field.

The created dataset will be constantly updated and a paleoenvironmental assessment conducted. Future well site biostratigraphic analyses (“biosteering”) in Mittelplate will benefit through a more confident stratigraphical assignment of the drilled horizons.

References

- Arbeitskreis deutscher Mikropaläontologen (Hrsg.) (1962): Leitfossilien der Mikropaläontologie, Berlin, Gebrüder Borntraeger.
- Brand, E. & Mönnig, E. (2010): Beiträge zur Stratigraphie von Deutschland: Litho- und Biostratigraphie des Mittel-Jura (Dogger) in Bohrungen Norddeutschlands. – Schriftenreihe der Deutschen Gesellschaft für Geowissenschaften, 54, 5–74.
- Lord, A.R., Cabral, M.C., and Danielopol, D.L. (2020): Sieve-type normal pore canals in Jurassic ostracods: A review with description of a new genus. *Acta Palaeontologica Polonica*, 65 (2), 313–349.
- Luppold, W. (2012): Ostracod assemblages from the Middle Jurassic of NW Germany with special reference to the Sowerbyi ammonite Zone (Early Bajocian, Jurassic) – N. Jb. Geol. Paläont. Abh. 266/3, 217–238.
- Plumhoff, F. (1963): Die Ostrakoden des Oberaalenium und tiefen Unterbajocium (Jura) des Gifhorner Troges, Nordwestdeutschland. – Abh. Senckenb. Naturforsch. Ges, 503, 1–100.
- StrataData Ltd (2014): Stratabugs 2.1 software (<https://www.stratadata.co.uk/>)

Anforderungen und Realisierung eines Monitoringsystem zur Überwachung der Axiallastsituation in Bohrungs- Komplettierungen.

Beschreibung der zum Einsatz kommenden Systeme

K.Pfeifer, Antje Hansen-Stichel, D.Maut

UGS GmbH, Mittenwalde, Germany

Kurzfassung

Eine Speicherbohrung unterliegt über ihren gesamten Betriebszyklus unterschiedlichen Belastungen. Für die Bewertung von verschiedenen Betriebszuständen und Betriebsparametern hinsichtlich der Bohrungsintegrität ist der Abgleich mit zulässigen Werten erforderlich.

Die UGS- GmbH hat für diese umfänglichen Betrachtungen die Berechnungssoftware **SEW (Safety Evaluation of Wells)** entwickelt. Mit dieser lässt sich die Integrität von Bohrungen für unterschiedliche Lastfälle bewerten und zulässige Grenzwerte für einzelne Betriebsparameter ableiten. Über einen Abgleich von rechnerisch ermittelten, zulässigen Parametern mit tatsächlich gemessenen Werten, wird ein sicherer und stets beherrschbarer Zustand für den Betrieb von Bohrungen sichergestellt.

Neben der standardmäßigen Überwachung von Druck- und Temperaturwerten, ermöglicht das kontinuierliche Überwachen von Axiallasten an eingebauten Rohrtouren eine unmittelbare Abbildung der Spannungssituation im Bohrungsausbau und stellt somit ein zusätzliches Monitoringsystem für den Nachweis bzw. die Sicherstellung der Bohrungsintegrität dar. Durch das Erfassen von tatsächlich Lastwerten im Bohrungsausbau ist wiederum ein Abgleich zu theoretischen Annahmen und Berechnungsgrundlagen möglich.

Neben den Lastwechseln im Bohrungsbetrieb werden auch die Spannungsänderungen mit Lasteintrag auf die Verrohrung/UT-Ausrüstung erfasst, wie z.B. durch plastisches Verhalten Salinar oder Konvergenzeinfluss im Kavernenbau. Neben einer kontinuierlichen Überwachung und dem Nachweis eines bestimmungsgemäßen Betriebs ist es möglich, Rückschlüsse auf den Integritätszustand der Bohrung nach unvorhergesehenen In-Situ Ereignissen wie z. B. Firstbruch, Gebirgsschlag oder andere (mikro)seismische Ereignisse zu ziehen. So zeigt ein Praxisbeispiel, dass über den Einsatz eines Spannungsmesssystems nach einem Salzfall belegt werden konnte, dass es zu keiner unzulässigen Lasterhöhung in der Komplettierung gekommen ist. Aufgrund der vorliegenden Daten eines vor Ort installierten und kontinuierlichen messenden Monitoringsystems, waren somit aufwendige Untertagetests und Messungen zur Bestätigung der Bohrungsintegrität nicht erforderlich.

Die UGS-GmbH hat Messsysteme und -verfahren zur Erfassung der axialen Belastung in Bohrlochkomplettierung entwickelt und zum Einsatz gebracht.

Die **DMS**-Systeme (**Dehnmessstreifen**) sowie hydraulische Lösungen (**TCMS** - **Tension Control and Monitoring System**), welche in die Abfangung der Rohrtouren in den Kavernen- bzw. Sondenkopf integriert sind zählen zu den direkten Messverfahren und müssen vor oder im Zuge einer Komplettierung installiert werden.

Indirekt messende Systeme (z. B. das **TMS** - **Tension Monitoring System**) können redundant im Bereich Kavernen- bzw. Sondenkopf installiert werden. Durch das Erfassen der Laständerungen im Bereich Förderrohrtour, letzte zementierte Rohrtour, Ankerrohrtour können Rückschlüsse auf die In-Situ Lastsituation im Bohrungsausbau gezogen werden.

1. **Dehnmessstreifen (DMS)**, zum Überwachen der Axiallast sind diese direkt an der Ankerrohrtour und/oder an der Förderrohrtour appliziert.
2. Das **Tension Monitoring System (TMS)** ist ein kombiniertes, redundant messendes System. Es besteht aus applizierten DMS an der Ankerrohrtour und einem zwischen der Unterseite des Grundflansches und der Bohrkellersohle unter Vorspannung installiertem Rahmen (TMS Frame) der Teile der wirkenden Axiallast der Ankerrohrtour auf Wägezellen ableitet.

3. Das **Tension Control and Monitoring System (TCMS)** wird als Hohlkolbenzylinder direkt als Bestandteil des Bohrlochkopfes integriert. Die Messung erfolgt anhand des im Zylinder wirkenden hydraulischen Druckes mittels Drucksensoren.

Durch den Einsatz von Monitoringsystemen zur kontinuierlichen Erfassung von Axiallasten lassen sich:

- Aktuelle Axiallastzustände der Rohrtouren messen und dokumentieren
- Der bestimmungsgemäße Betrieb nachweisen
- Frühzeitig hohe Belastungen der Förderinstallation erkennen und Gegenmaßnahmen einleiten
- Langzeitauswirkungen durch geologische und betriebliche Einflüsse erfassen.
- Technische als auch gebirgsmechanische Berechnungs-Modelle können verifiziert werden.

Abstract

A storage well is subject to different loads over its entire operating cycle. For the evaluation of different operating conditions and operating parameters with regard to the well integrity, the comparison with permissible values is necessary.

UGS GmbH has developed the **SEW (Safety Evaluation of Wells)** calculation software for these comprehensive considerations. With this software, the integrity of wells can be evaluated for different load cases and permissible limit values for individual operating parameters can be derived. By comparing calculated permissible parameters with actual measured values, a safe and always controllable condition for the operation of wells is ensured.

In addition to the standard monitoring of pressure and temperature values, the continuous monitoring of axial loads on installed casings enables a direct mapping of the stress situation in the borehole lining and thus represents an additional monitoring system for proving or ensuring the integrity of the borehole. By recording actual load values in the borehole support, a comparison with theoretical assumptions and calculation bases is possible.

In addition to the load changes in the drilling operation, the stress changes with load application on the casing / subsurface equipment are also recorded, such as plastic behavior Salinar or convergence influence in the cavern construction. In addition to continuous monitoring and proof of intended operation, it is possible to draw conclusions on the integrity state of the well after unforeseen in-situ events such as ridge break, rock burst or other (micro)seismic events. For example, a practical example shows that the use of a stress measurement system after a salt fall proved that there was no unacceptable load increase in the completion. Due to the available data of an on-site installed and continuous measuring monitoring system, costly underground tests and measurements to confirm the well integrity were therefore not necessary.

UGS- GmbH has developed and deployed measurement systems and methods to record the axial stress in borehole completions.

The **strain gauge systems (SGS)** as well as hydraulic solutions (**TCMS - Tension Control and Monitoring System**), which are integrated in the interception of the pipe tours in the cavern or probe head, belong to the direct measuring methods and must be installed before or in the course of a completion.

Indirect measuring systems (e.g. the **TMS - Tension Monitoring System**) can be installed redundantly in the cavern or probe head area. By recording the load changes in the area of the production pipe run, last cemented pipe run, anchor pipe run, conclusions can be drawn about the in-situ load situation in the borehole support.

1. strain gauges system (**SGS**), for monitoring the axial load, are applied directly to the anchor pipe run and/or to the production pipe run.
2. The Tension Monitoring System (**TMS**) is a combined redundant measuring system. It consists of applied strain gauges on the anchor pipe run and a frame installed between the underside of the base flange and the bottom of the borehole under preload, which transfers parts of the acting axial load of the anchor pipe run to load cells.
3. the Tension Control and Monitoring System (**TCMS**) is integrated as a hollow piston cylinder directly as part of the wellhead. Measurement is based on the hydraulic pressure acting in the cylinder by means of pressure sensors.

By using monitoring systems to continuously record axial loads, it is possible to:

- Measure and document current axial load conditions of the pipe tours
- Prove that the system is operating as intended
- Detect high loads on the conveying installation at an early stage and initiate countermeasures
- Record long-term effects due to geological and operational influences.
- Technical as well as rock mechanical calculation models can be verified.

Einleitung

Speicher- und Förderbohrungen unterliegen im Verlauf verschiedener Lebenszyklen unterschiedlichen Betriebsbelastungen und Einflüssen. Integritätsbewertungen von Bohrungen, Gefährdungsanalysen, Lebensdauerbetrachtungen sowie ein Bohrungsintegritätsmanagement sind etablierte Bestandteile eines sicheren Bohrungsbetriebs.

Entsprechend Bohrungstyp, geologischen Randbedingungen und Betriebsfahrweisen sollen Barrieren (Abbildung 1) in einer Bohrung einen sicheren Betrieb gewährleisten und einen unkontrollierten Umstieg von Medien aus einer Bohrung verhindern. Überwachungs- und Monitoringsysteme gewährleisten einen kontrollierten, bestimmungsgemäßen Betrieb. Integritätsbewertungen haben die Zielstellung, unter Ansatz der Betriebsparameter bzw. der zu erwartenden Belastungsenvelopen für jeden Lebenszyklus die Eignung der Barrieren bzw. Barrierefälle zu prüfen und ggf. nachzuweisen.

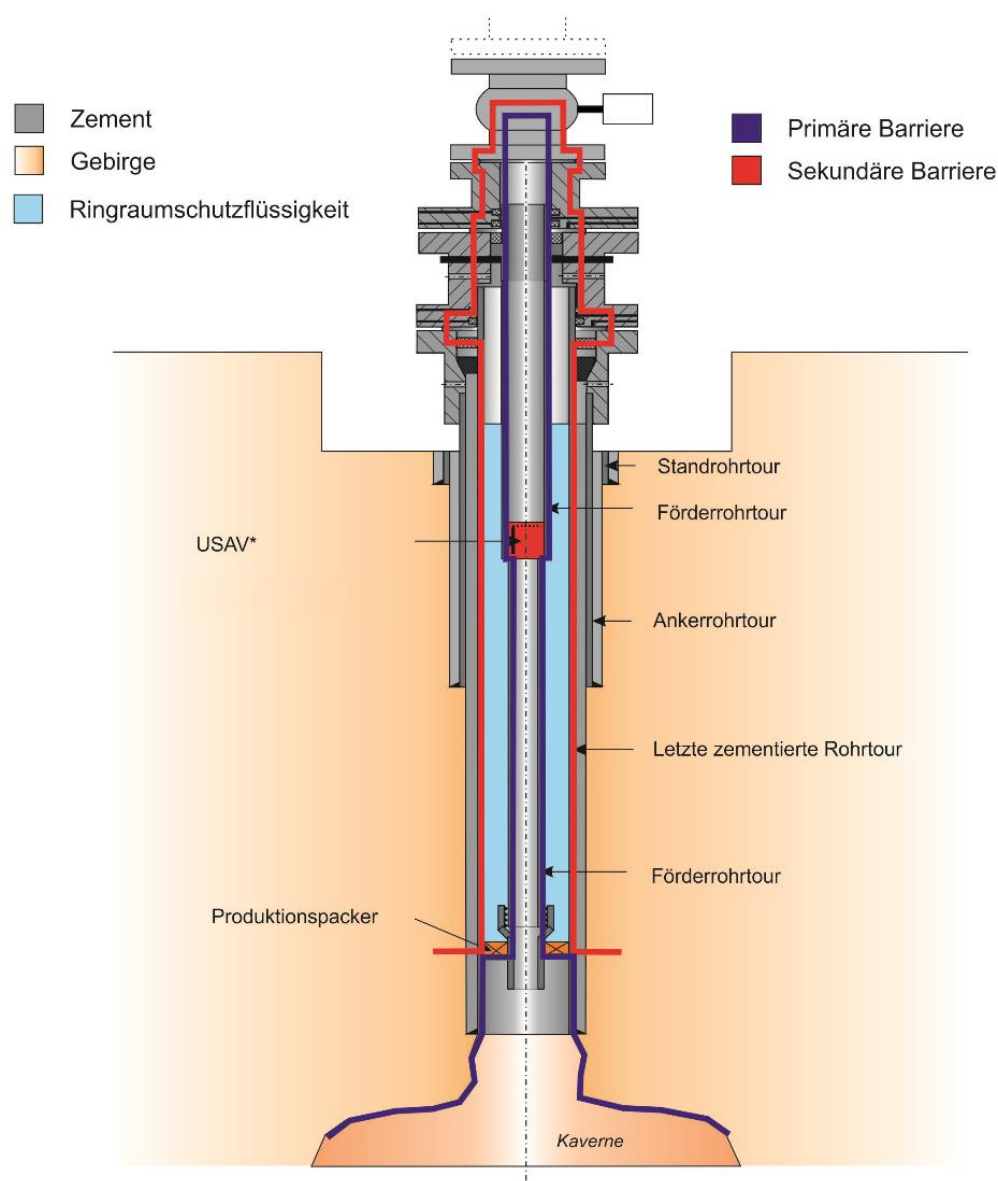


Abbildung 1: Barrierenschema, Beispiel Kavernenbohrung

Integritätsbewertung

Mit der zyklischen Durchführung von Integritätsbewertungen werden alle Barriere Elemente hinsichtlich ihrer belastungsgerechten Auslegung untersucht und bewertet.

Die Berechnungs- und Bewertungsgrundlagen einer Bohrungsbewertung bilden unter anderem die u.a. API 5C3, die DIN EN ISO 16530-1:2017, die aktuelle BVOT: Veröffentlichung LBEG Niedersachsen vom 17.05.2022 und der BVEG: Leitfaden Bohrungsintegrität ; 07.2021 aber auch ggf. vorhandene betreiberspezifische Managementhandbücher - Well Integrity Management.

Für die Anwendung und Umsetzung der DIN EN ISO 16530-1:2017, der BVEG: Leitfaden Bohrungsintegrität, sowie der aktuellen BVOT („Bohrloch-TÜV“) werden in Abhängigkeit vom Bohrungstyp für die Integritätsbewertung von Bohrungen Lebenszyklen, Barrieren und Barriere-Elemente spezifiziert.

Die Bewertungsbasis sind Betriebsdaten, thermodynamische Analysen, Daten zur Geologie und Gebirgsmechanik, Daten zum Bohrungsausbau, der Untertagekomplettierung und der Bohrlochkopfausrüstung sowie zu vorhandenen Mess-, Test- und Monitoringprogrammen.

Die UGS GmbH nutzt für die komplexe Bohrungsbewertung auch die Software SEW (Safety Evaluation of Wells). In dieser Software werden alle bohrungsspezifischen Angaben aus einer vorliegenden Datenbasis integriert.

Als Ergebnis umfangreicher Lastfallberechnungen in SEW werden Sicherheitsbeiwerte für verschiedene Belastungsarten (Außendruck, Innendruck und Axialbelastung) für jede Rohrtour ausgegeben, bzw. zulässige Betriebsparameter / Grenzwerte ermittelt, z.B. MAASP. Ergebnisse aus Bohrlochmessungen können auch wiederkehrend in die Berechnungen einfließen. In Trendanalysen werden Prognosen zum Verlauf der Sicherheitsfaktoren in Abhängigkeit von bohrungsspezifischen Korrosionsabträgen berechnet.

Weiterführend können auf Grundlage der SEW-Berechnungen für Betreiber „Ampelsysteme“ hinsichtlich zulässiger Belastungen für Betriebsparameter entwickelt werden.

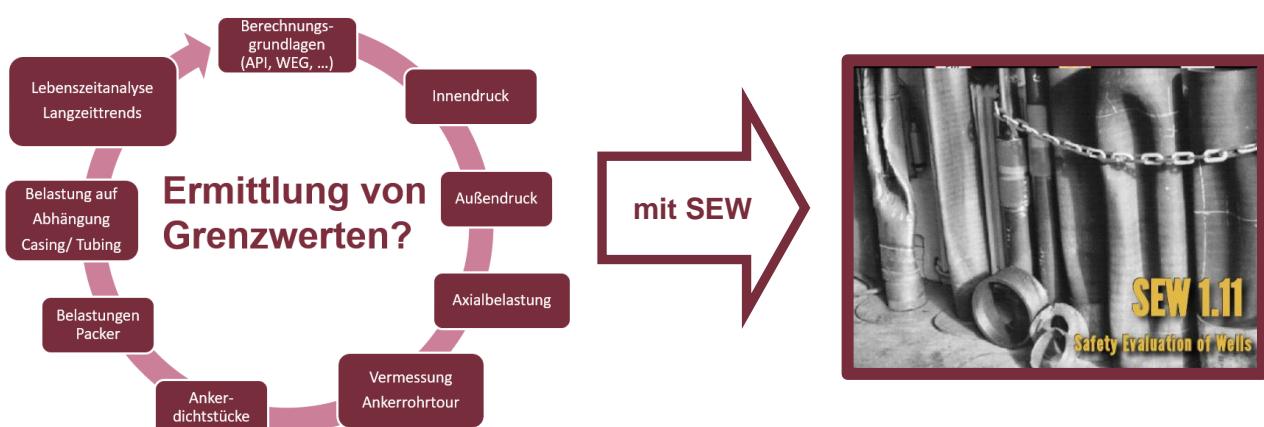


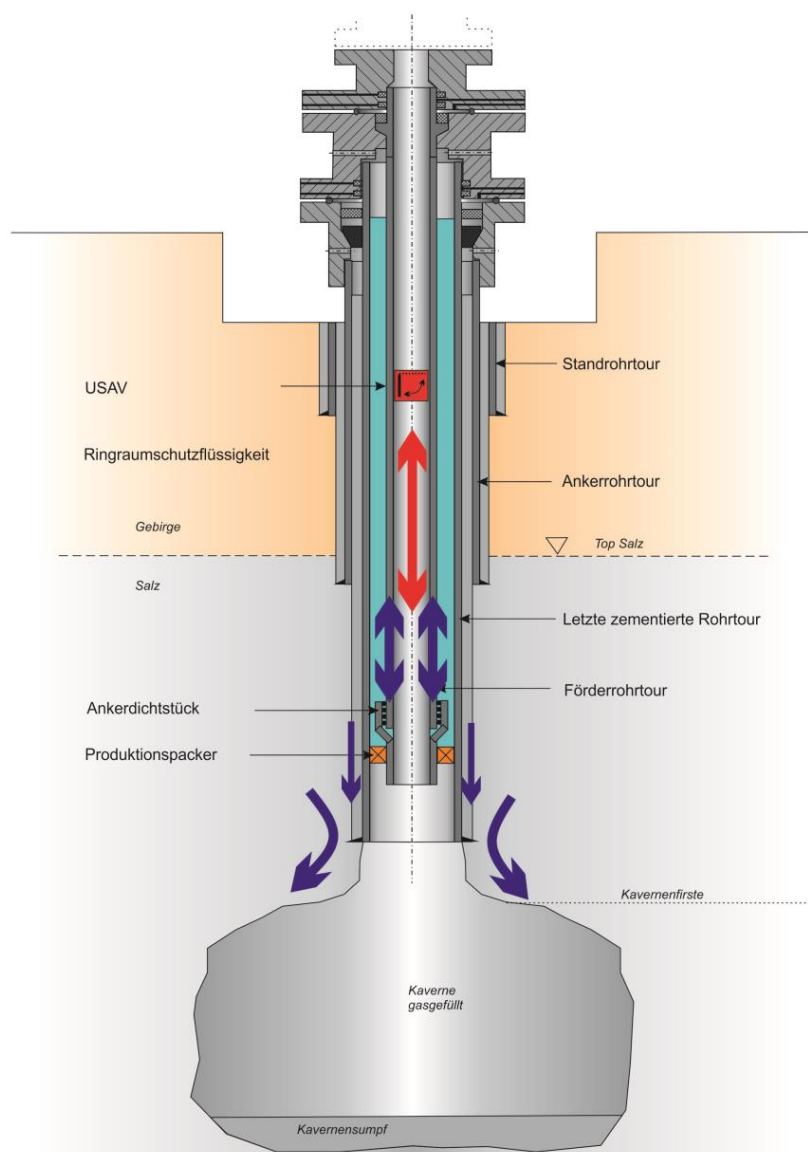
Abbildung 2: UGS-Berechnungs-Software SEW (© UGS)

Voraussetzung des Bohrungsausbau

Voraussetzung für die Messung von Axiallasten in einer Komplettierung ist eine unter Vorspannung im Bohrlochkopf abgesetzte Förderrohrtour (FRT). Betriebsbedingte Änderungen des Dehnungszustands der FRT (z.B. durch Temperatureinflüsse) bewirken somit eine Änderung des axialen Lastzustandes der FRT (Änderung der Vorspannung).

Die in die Bohrung eingebrachte letzte zementierte Rohrtour (LzRT) wird mit Hilfe eines Zementmantels fest mit den geologischen Schichten verbunden. Somit werden alle Kräfte, die in den Schichten auftreten oder durch diese verursacht werden, über den Zementmantel in die Rohrtour übertragen und ändern damit den vorherrschenden Spannungszustand. Bei Kavernenbohrungen kann eine solche Kraft bspw. durch die Konvergenz der Salzschichten verursacht werden.

Durch die Verbund LzRT-Packer-FRT werden summarisch Dehnungsänderungen aufgenommen.



Die Abbildung 3 zeigt die schematische Darstellung der Bohrungsinstallation einer Gaskaverne mit betriebsbedingten Laständerungen in der Förderrohrtour (Pfeil rot), wirkender Konvergenz im Salz (gekrümmte blaue Pfeile) und die Übertragung der Kraft (gerade blaue Pfeile) vom Gebirge über die letzte zementierte Rohrtour in den Packer und von dort aus weiter über die Förderrohrtour bis nach Oberlage in den Bohrlochkopf.

Abbildung 3: Schematische Darstellung einer Gaskavernenkomplettierung mit wirkenden Kräften

Da im Bohrlochkopf alle Gewichts- und Betriebslasten der Rohrtouren abgefangen werden, ist die Installation von Axiallast- Messsystemen in diesem Bereich vorgesehen.

Systeme für das Axiallastmonitoring

Für die Gewährleistung des sicheren Betriebes einer Bohrung ist die Überwachung und Dokumentation der vorhandenen Betriebsparameter erforderlich. Die aufgenommenen Messwerte werden dazu mit zulässigen Werten abgeglichen. Zulässige Axiallastparameter sind Ergebnisse von Integritätsbewertungen.

Mit den von der UGS GmbH entwickelten Monitoringsystemen können zusätzliche Informationen zum axialen Lastzustand in einer Bohrung erfasst werden.

Durch eine Auswertung der kontinuierlich aufgenommenen Messwerte kann der bestimmungsgemäße Betrieb einer Bohrung dokumentiert und auch gegenüber Behörden belegt werden.

Zusätzlich ist ein Abgleich des Spannungszustand in einer Komplettierung bzw. Förderrohrtour nach unvorhergesehenen Ereignissen (z.B. Firstbrüchen) zum ursprünglichen Lastzustand möglich und kann als Indikator für mögliche auftretende ereignisbezogene Laständerungen genutzt werden. Im Umkehrschluss lässt sich ggf. auch nach dem Ereignis nachweisen, dass untertätig keine unzulässigen Belastungen aufgetreten sind (Vorher-Nach-Vergleich).

Die im nachfolgenden Abschnitt aufgezeigten Systeme sind für die Messung der genannten Axialbelastung bzw. deren Änderung als Abgleich mit der Ausgangssituation entwickelt worden und bilden in Verbindung mit den Betriebsdaten Druck und Temperatur die Grundlagen für die Auswertung der Axialbelastungen.

- **DMS – Dehnmessstreifen (Ankerrohrtour/Casing)**

Die einfachste Möglichkeit für das Messen der in der Installation auftretenden Axiallast besteht darin, die Dehnmessstreifen direkt auf der Ankerrohrtour/dem Casing zu applizieren. Die Ausführung erfolgt dabei in einer Wheatstone'schen Brückenschaltung (siehe Abbildung 2).

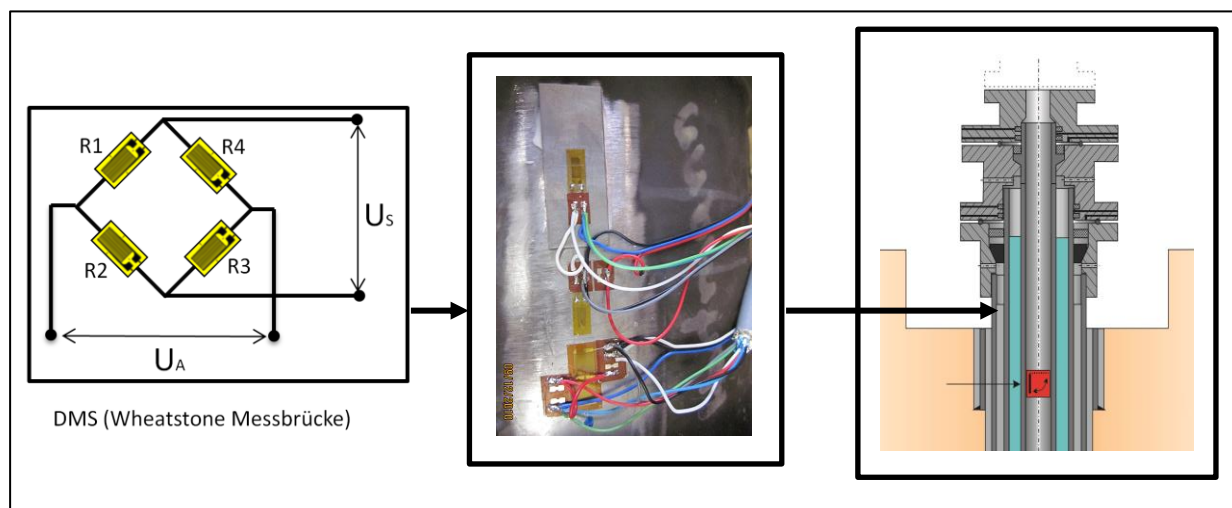


Abbildung 4: Schemadarstellung einer DMS-Applikation auf der Ankerrohrtour/dem Casing

Ein großer Vorteil dieser Applikation ist eine routinierte Verfahrensweise zur Installation der DMS. Sie können sowohl bei neuen als auch an existierenden Bohrungen zum Einsatz kommen. Der Kalibrierungsaufwand bei bestehenden Bohrungen ist allerdings als umfangreicher einzustufen, da für die Kalibrierung der DMS unterschiedliche Betriebszustände angefahren werden müssen. Für Neubohrungen oder Rekomplettierungen kann eine Kalibrierung im Zuge der Arbeiten unmittelbar vor Ort erfolgen.

- **DMS – Dehnmessstreifen (Förderrohrtour/Hanger)**

Eine weitere Möglichkeit für die Überwachung der Axiallasten ist die Messung direkt am Hänger der Förderrohrtour. Hierfür werden Dehnmesstreifen auf dem Hänger appliziert und ebenfalls in einer Wheatstone'schen Brücke miteinander verschalten.

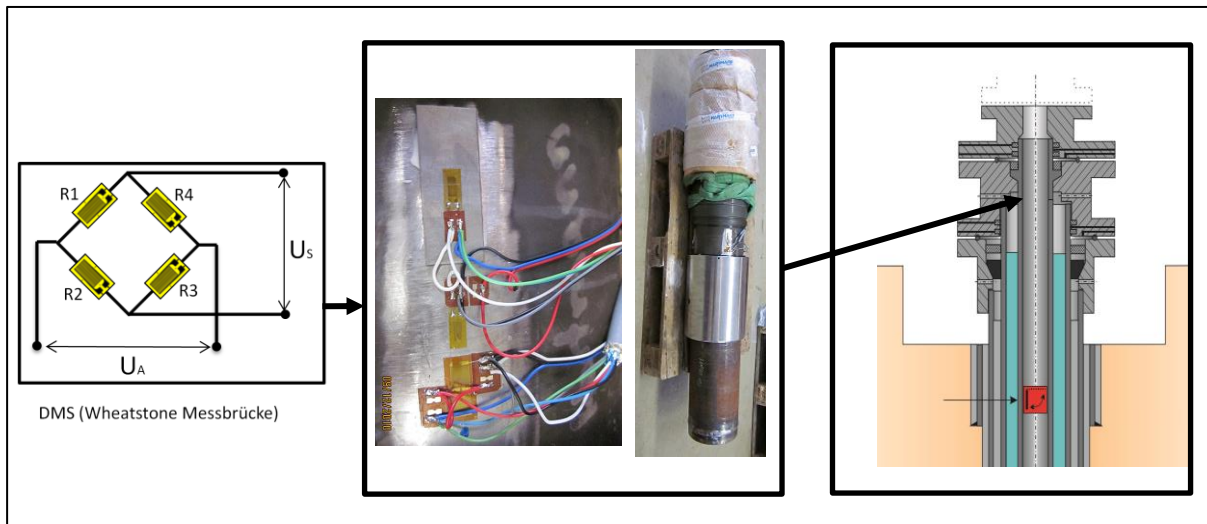


Abbildung 5: Schemadarstellung einer DMS-Applikation auf dem Hänger der Förderrohrtour

Die Applizierung der DMS am Hänger gestaltet sich anders als an der Ankerrohrtour aufwendiger, da eine Schutzhülse vorzusehen ist, aus der die Messkabel der DMS nach außen geführt werden. Dadurch ist eine nachträgliche Applikation von Dehnmesstreifen auf dem Hänger nur in Verbindung mit sehr hohem Aufwand zu realisieren (Rekomplettierung). Unter 6a.

- **Tension Monitoring System (TMS)**

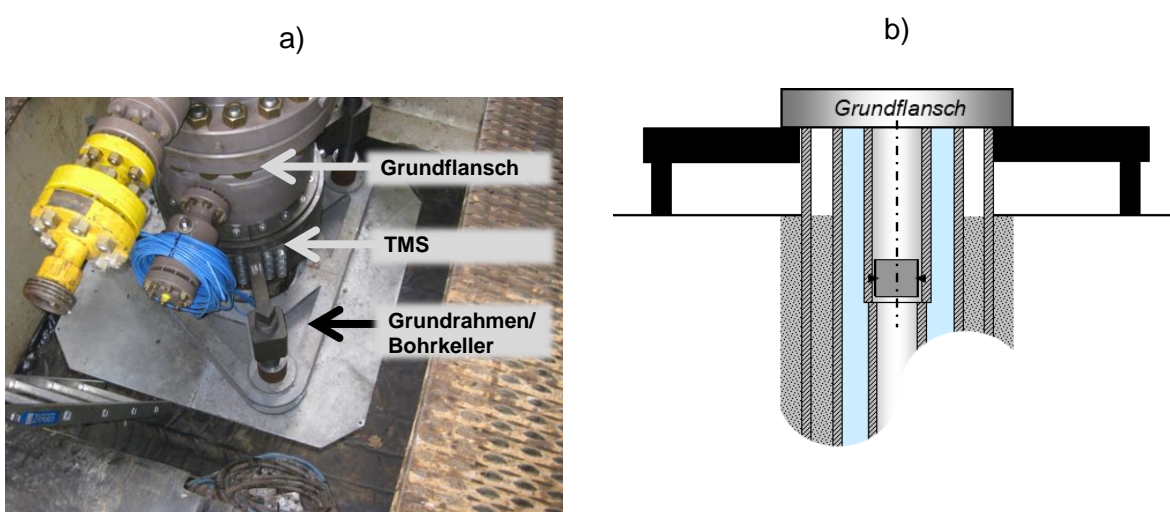


Abbildung 6a) und 6b): Installation eines TMS am Bohrlochkopf (6a) sowie eine schematische Darstellung des TMS installiert am Grundflansch (6b)

Das Tension Monitoring System (TMS) ist ein kombiniertes, redundant messendes System. Es besteht einerseits aus applizierten DMS an der Ankerrohrtour und zusätzlich aus einem zwischen der Unterseite des Grundflansches und der Bohrkellersohle unter Vorspannung installiertem Rahmen (TMS- Frame), über den Teile der wirkenden Axiallast der Ankerrohrtour auf Wägezellen ableitet werden. Durch die beiden verschiedene Messprinzipien ist stets ein Plausibilitätsabgleich möglich.

Für eine bessere Kraftverteilung auf der Kellersohle besitzt das Messsystem zusätzlich einen Grundrahmen. Die in Abbildung (6a) aufgezeigte Grafik zeigt ein TMS- Frame installiert zwischen Grundflansch und Kellersohle. Zusätzlich ist in Abbildung (6b) eine schematische Darstellung des installierten Messsystems dargestellt.

Das TMS lässt sich von außen auch während des laufenden Betriebs installieren. TMS-Systeme sind seit 2017 installiert und in Betrieb. Die Rekalibrierung der Dehmessstreifen gestaltet sich ebenso wie bei den DMS auf der Ankerrohrtour.

- **Tension Control and Monitoring System**

Auf Grund der kontinuierlichen Weiterentwicklung von Systemen zur Axiallastmessung folgte als Konsequenz die Forderung einer Erweiterung der Funktionalität, so dass nicht nur die Axiallast gemessen, sondern die Belastung in der Rohrtour gesteuert und aktiv beeinflusst werden kann.

Der Zugewinn im Vergleich zu den zuvor gezeigten Messsystemen besteht darin, dass zusätzlich zur Messung der Axialkraft ein aktives Eingreifen und somit eine kontrollierte Erhöhung oder Reduzierung der Lasten erfolgen kann.

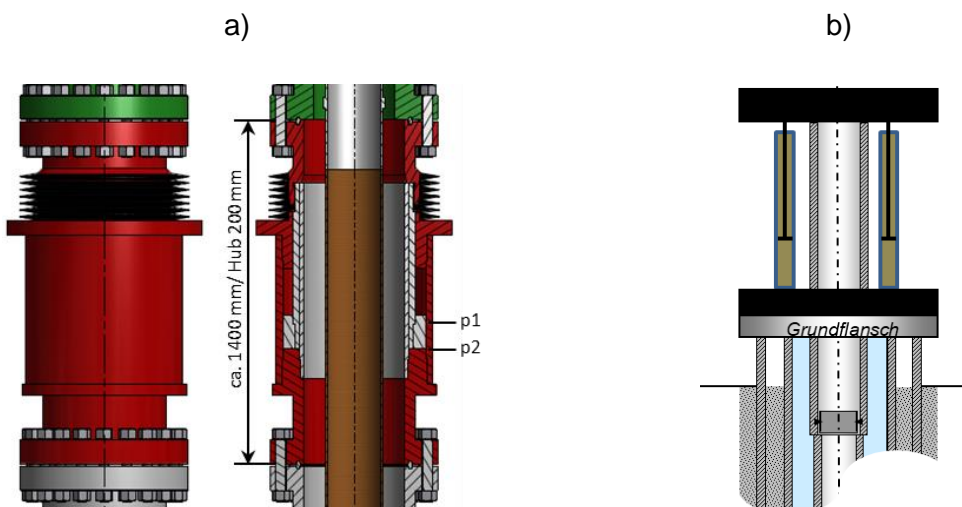


Abbildung 7 a) und b): *Details des Hohlkolbenzylinders in a), in b) ist die schematische Darstellung eines am Bohrlochkopf installierten TCMS.*

Die Ausführung des TCMS erfolgt als Hohlkolbenzylinder, der mittels zweier Flanschanschlüsse als Bauteil im Bohrlochkopf integriert wird. Der Aufbau kann der Schnittzeichnung Abbildung (7a) bzw. dem Schema in Abbildung (7b) entnommen werden.

Das System wird als fester Bestandteil oberhalb des Grundflansches installiert. Durch den Aufbau wird die Belastung der Rohrtour direkt in das TCMS geleitet und kann dort als Druckänderung mittels eines Drucksensors, gemessen werden.

Auf Grund des System-Aufbaus kann die Nachkalibrierung des Messsystems durch einen einfachen Wechsel des Drucksensors erfolgen.

Eine alternative Möglichkeit für den Einsatz des TCMS besteht darin, dass sich während des Betriebes der Hohlkolbenzylinder in einem drucklosen Zustand befindet und nur für die Messung der Axiallast mit Druck beaufschlagt wird. Die Druckbeaufschlagung erfolgt dabei solange bis ein Wegmesssystem anschlägt. Aus dem dabei ermittelten Druckwert kann die wirkende Kraft abgeleitet werden.

Zum gegenwärtigen Zeitpunkt befindet sich das TCMS als solches noch in der Entwicklung.

Erfahrungen im Feldeinsatz

Die Erfahrung der vorangestellten Messsysteme umfasst ein Zeitraum von bis zu mehreren Jahrzehnten.

Die **DMS** sowohl an der Anker- als auch an der Förderrohrtour werden bereits seit 1995 erfolgreich auf Kavernenspeichern eingesetzt und liefern zuverlässig Messdaten. Umfangreiche weitere Erfahrungen mit dem Messsystem konnten an einem Versuchsstand, mit der Möglichkeit zur Einstellung definierter Belastungssituation, gemacht werden. Unter anderem konnten dabei durch Versuche der Einfluss des Tagesganges der Temperatur sowie die Umlagerung von Eigenspannungen aufgezeigt werden.

Das in 2015 entwickelte **TMS** wurde bis zum jetzigen Zeitpunkt mehrfach installiert. Bei allen Installationen ist ein redundantes DMS- System auf der Ankerrohrtour appliziert. Infolge der bisherigen kürzeren Einsatzzeit liegen gegenwärtig die Erfahrungen in der Aufzeichnung der Axiallasten bei Einbau, Inbetriebnahme und ersten Zyklen im Speicherbetrieb im Zeitraum unter 10 Jahren.

Da sich das **TCMS** gegenwärtig in der Entwicklungsphase befindet, sind keine Felderfahrungen vorhanden. Wie bereits genannt, konnte das Grundprinzip des Messsystems schon mehrfach in anderen Anwendungsfällen, z.B. hydraulische Hebeeinrichtung (Casing Jack), eingesetzt werden.

Auswertungen

Die Bewertung und Analyse der Messdaten unterscheidet sich in den Routinen der Datenauswertung aus dem Langzeitmonitoring.

- Unter Betriebsmonitoring wird die Überwachung und Dokumentation des aktuellen Istzustandes während des Betriebes verstanden, das heißt, die aufgezeichneten Messdaten werden direkt genutzt und mit den zulässigen Daten abgeglichen.

- Das Langzeitmonitoring dient zur Erfassung von Langzeitverhalten axialer Einflüsse. Dabei werden über einen längeren Zeitraum aufgezeichnete Messdaten analysiert und von den Betriebseinflüssen bereinigt. Je länger der Aufzeichnungszeitraum, umso genauer fällt z. B. die Aussage über das geomechanische Verhalten aus. Ein Langzeitmonitoring ist für die Überwachung eines bestimmungsgemäßen Betriebes in der gesamten Betriebszeit einer Bohrung ausgelegt. Darüber hinaus lassen sich aus den betriebsbedingt und geomechanisch verursachten und messtechnisch erfassten Einflüssen Analogien auf Axiallastbeanspruchungen vergleichbarer Bohrungen ableiten.

In der nachfolgenden Abbildung 8 ist der Verlauf der gemessenen relativen Dehnung für einen Zeitraum von ca. 6 Jahren (Langzeitmessung) dargestellt. Die in der Grafik zusätzlich eingeführte Gerade (schwarze Linie) zeigt den Anstieg der gemessenen Axialbelastung durch geologische Einflüsse (Δx) über die Zeit. Betriebseinflüsse sind hier herausgerechnet.

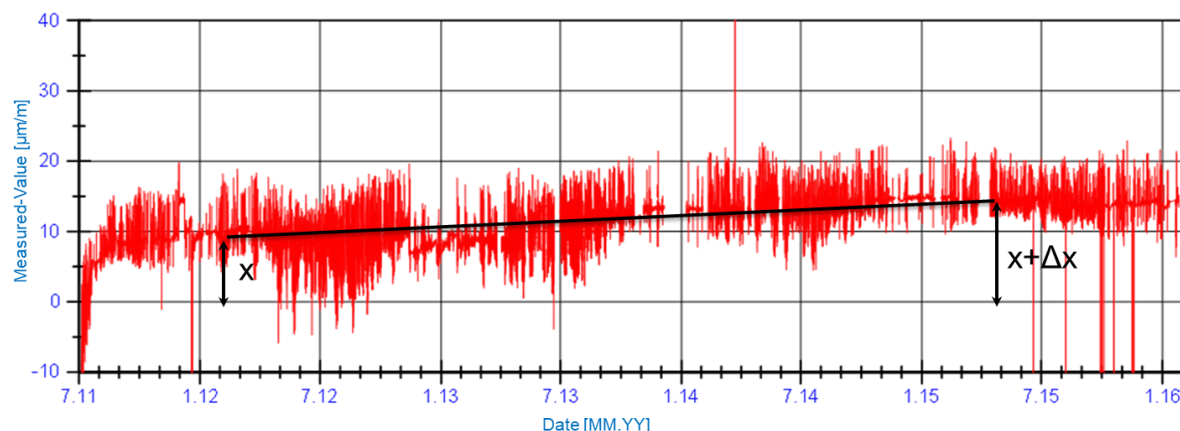


Abbildung 8: Langzeitmessung der relativen Dehnung in einer Rohrtour

Abbildungsverzeichnis

| | | |
|------------------------|--|----|
| Abbildung 1: | Barrierenschema, Beispiel Kavernenbohrung | 4 |
| Abbildung 2: | Software SEW (© UGS) | 5 |
| Abbildung 3: | Schematische Darstellung einer Gaskavernenkomplettierung mit wirkenden Kräften..... | 6 |
| Abbildung 4: | Schemadarstellung einer DMS-Applikation auf der Ankerrohrtour/dem Casing.... | 7 |
| Abbildung 5: | Schemadarstellung einer DMS-Applikation auf dem Hänger der Förderrohrtour.. | 8 |
| Abbildung 6a) und 6b): | Installation eines TMS am Bohrlochkopf (6a) sowie eine schematische Darstellung des TMS installiert am Grundflansch..... | 8 |
| Abbildung 7 a) und b): | Details des Hohlkolbenzylinders in a), in b) ist die schematische Darstellung eines am Bohrlochkopf installierten TCMS. | 9 |
| Abbildung 8: | Langzeitmessung der relativen Dehnung in einer Rohrtour | 11 |

Aktueller Forschungsstand zur thermischen Wasserstoffgewinnung aus ausgeförderten Erdöllagerstätten

J. F. Bauer, M. Amro

Institut für Bohrtechnik und Fluidbergbau, Technische Universität Bergakademie Freiberg, Freiberg, Deutschland (Germany)

Abstract

Basierend auf dem Vortrag zur Wasserstoffgewinnung aus Erdöllagerstätten von der letzten DGMK-Frühjahrstagung soll in diesem Jahr eine Fortsetzung der vorgestellten Forschung präsentiert werden. Aus den vorgestellten drei Verfahren (Thermische Wasserstoffgewinnung, Biogeneration und dunkle Fermentation) erwies sich nur die thermische Wasserstoffgewinnung als aktuell technisch und wirtschaftlich durchführbar. Daher fokussiert sich zurzeit die Forschung des Instituts für Bohrtechnik und Fluidbergbau an der TU Bergakademie Freiberg auf dieses Thema.

In diesem Vortrag wird nach einer kurzen Einführung zum Verfahren das aktuelle Untersuchungsdesign sowie der Forschungsablauf zur thermischen Wasserstoffgewinnung dargestellt. Dazu wird auch die Frage zur simulativen Umsetzung sowie zu relevanten Bewertungsfragestellungen diskutiert. Weiterhin werden Dimensionen der Forschung an der TU Bergakademie Freiberg sowie die relevanten Verknüpfungen unter den einzelnen Bereichen aufgezeigt.

Aus der aktuellen Forschung erfolgt die Ergebnisvorstellung von Lagerstättensimulationen im mittleren Maßstab (Meter) sowie eine Bewertung einzelnen thermischen Verfahren der Wasserstoffgewinnung. Basierend darauf wird der „best case“ detailliert analysiert sowie relevante Schlussfolgerung für die heterogene Lagerstättensimulation gezogen. Anhand einer Parameterstudie veränderlicher Parameter sowie einer Sensitivitätsanalyse vordefinierter Parameter werden relevante Einflussgrößen identifiziert und analysiert. Weiterhin wird die Unsicherheit der Simulationen diskutiert und im Rahmen der Möglichkeiten quantifiziert. Der Vortrag endet mit einer Zusammenfassung sowie einem Ausblick auf weitere Forschungsaktivitäten.

1. Einleitung

Die Energiewende und der damit verbundene steigende Bedarf an erneuerbaren Energieträgern hat in den letzten Jahren zu einer verstärkten Fokussierung auf die Wasserstoffproduktion geführt. Dabei rückt auch die Nutzung ausgeförderter Lagerstätten als potenzielle Wasserstoffquelle zunehmend in den Fokus der Forschung. Der Anteil ausgeförderter Lagerstätten nimmt weltweit kontinuierlich zu, was die Bedeutung dieser alternativen Wasserstoffquelle unterstreicht.

In diesem Beitrag werden aktuelle Forschungsergebnisse zur Wasserstoffgewinnung aus ausgeförderten Lagerstätten vorgestellt. Der Schwerpunkt liegt dabei auf Untersuchungen mittels Simulationen und Literaturanalysen. Es werden verschiedene Simulationsmodelle vorgestellt und diskutiert, die dazu dienen, die Effizienz und Nachhaltigkeit der Wasserstoffgewinnung aus ausgeförderten Lagerstätten zu bewerten. Durch die Zusammenführung der aktuellen Forschungsergebnisse soll ein umfassender Überblick über den derzeitigen Stand der Wasserstoffgewinnung aus ausgeförderten Lagerstätten gegeben werden.

2. Lagerstättentechnische Simulation

Um im Lagerstättensystem die Vorgänge angemessen abbilden zu können, werden für die chemischen Reaktionen die Konzentrationen der Komponenten benötigt und für die thermofluiddynamischen Fließprozesse in der Lagerstätte das Verhalten der aus den Komponenten gebildeten Phasen. Da Erdöl aus vielen verschiedenen Verbindungen besteht, und für dieses System zum einen keine reaktionskinetischen Beschreibungen vorliegen und zum anderen der Berechnungsaufwand zu hoch ist, wird dieses zu Pseudokomponenten zusammengefasst. Im folgenden Kapitel wird das in dieser Arbeit genutzte Modell vorgestellt und die Auswahl näher begründet. Des Weiteren werden die mathematisch-physikalischen Zusammenhänge näher dargestellt, welche in der Simulation verwendet wurden.

2.1. Modellierung des Fluidsystems

Die Genese des verwendeten Fluidsystemmodells ist in Abbildung 1 dargestellt und zeigt die Entwicklung des häufig verwendeten Belgrave-Schemas (Belgrave et al., 1993) durch Erweiterungen von (Yang und Gates, 2009) für Gasphasenreaktionen sowie für die Wasserstoffbildung durch (Babushok und Dakdancha, 1993, Guntermann, Gudenu und Mohtadi, 1982) in (Kapadia et al., 2013). Der Nachweis der lagerstättentechnischen Anwendbarkeit wurde über einen erfolgreichen History Match an den Lagerstättenversuchen von (Hajdo, Hallam und Vorndran, 1985) durch (Kapadia et al., 2013) unter Verwendung der zusätzlichen Modelle von (Kapadia et al., 2012) und (Kapadia, Kallos und Gates, 2013) erbracht. Dieses Schema stellt das einzige validierte Fluidsystem für die Lagerstättenmodellierung dar, welches sich auch in der Anwendung längerfristig bewährt hat.

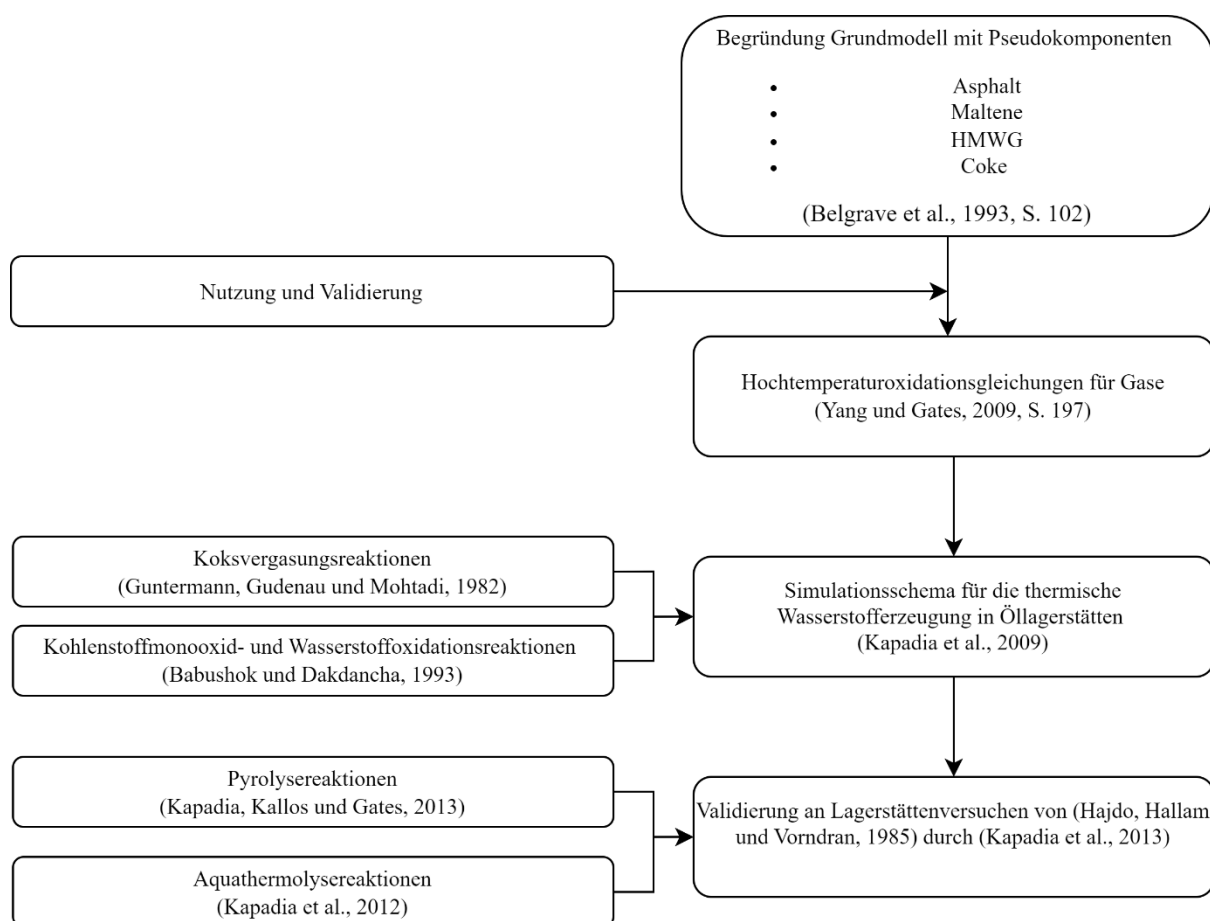


Abbildung 1: Genese des verwendeten Fluidmodells für die Simulation

2.2. Evaluierungsgrundlagen von simulativen Untersuchungen

Die Evaluierung von simulativen Untersuchungen basiert einerseits auf der Bewertung der numerischen Berechnungsmethodik selbst sowie der Ergebnisse der numerischen Simulation. Abhängig von der numerischen Berechnungsqualität wird die Unsicherheit der Simulationen quantifiziert.

Die hier vorgestellten Simulationen stellen die Grenze der simulativen Lösbarkeit mittels der bekannten Softwareprodukte dar, da der Prozess neuartig ist und durch extreme Bedingungen (Temperaturen oberhalb des Boudouard-Gleichgewichtes - $>700^{\circ}\text{C}$, Wechsel von Injektionsregimen, schnelle Abkühlung und Abführung der Gasphase) erst seine Wirkung entfaltet. Daher wird in dem Kapitel zunächst evaluiert, welche Vorgänge simulativ zum aktuellen Stand der Technik abbildbar sind sowie welche Belastbarkeit deren Ergebnisse (Unsicherheitsanalyse) haben. Aktuell ist die Forschung zur numerischen Abbildung dieses Prozesses noch nicht abgeschlossen, insbesondere weil die Entwicklung von eigenständigen Simulationsschemen stets eine Validierung an einer Lagerstätte erfordert, denn die Untersuchungen sind an Bohrkernen mit anschließendem History Match nicht ausreichend.

2.2.1. Numerische Berechnung

Anhand der Ergebnisse der numerischen Berechnungsschritte wird vom Solver automatisch ein Materialbilanztest durchgeführt. Dieser gibt programmintern Aufschluss über die Genauigkeit der numerischen Abbildung einzelnen Komponenten in dem System. Insbesondere, für die chemischen Prozesse mit hohen auftretenden Temperaturen und vielen unterschiedlichen Phasenverhalten ist dieser Test essenziell. Bekanntlich treten bei der in-situ combustion hohe bis sehr hohe Materialbilanzfehler auf; diese sind vor allem auf die komplexe Abbildung von den unterschiedlichen PVT-Eigenschaften der Gemische sowie die schnelle und zugleich von vorneherein nicht materialbilanzausgeglichene Reaktionskinetik zurückzuführen. Um die einzelnen Simulationen hinsichtlich ihrer weiteren Verwertbarkeit sowie Belastbarkeit zu bewerten, müssen diese mittels Kriterien der numerischen Berechnungsqualität bewertet werden.

Die konkreten Fehlerbewertung basieren dabei auf der Sichtung der Simulationsergebnisse und den jeweiligen Prozentsätzen des Materialbilanzfehlers, zur Qualifizierung sind bei temporär auftretenden Effekten einmalige oder kurzfristige Überschreitungen ausreichend.

2.3. Unsicherheitsanalyse

Die Unsicherheit der Simulation kann in vielen Dimensionen abgeschätzt werden. Entscheidend ist dabei die Definition der Unsicherheit, hier ist diese die Abweichung der Simulation zur realen Durchführung des Verfahrens. Die Unsicherheit der Berechnungen ist qualitativ anhand der Genese der Berechnungsmethode sowie der Berechnung an sich festzustellen. Quantitativ ist die Unsicherheit dagegen deutlich schwieriger abschätzen.

2.3.1. Durchgeführte Lagerstättenprozesse & Messmethoden

Grundsätzlich stammen die Daten für das hier verwendete Fluidsystem aus Lagerstättenversuchen von (Hallam und Donnelly, 1993, Hajdo, Hallam und Vorndran, 1985, Hallam et al., 1989). Dabei wurde mittels der eindimensionalen Messung von Produktionsdaten über die Zeit (mit gelegentlicher Gaschromatographie) die Datenerfassung durchgeführt. Das Verfahren, welches stark diskontinuierlich funktioniert, wurde somit weder dreidimensional repräsentiert noch in der Gänze erfasst. Eine Messung von Lagerstättentemperaturen oder eine Untersuchung von Bohrkernen nach der Verbrennung zum Rückschluss auf relevante Prozesse wurde nicht durchgeführt. Die sich daraus ergebende Unsicherheit ist nicht quantitativ messbar.

2.3.2. History Match und Modellaufbau

Im Rahmen der numerischen Regression der Ergebnisse („History Matching“) wurden die eindimensionalen Daten mithilfe der gewonnen Lagerstättenparameter sowie einem stark vereinfachten Lagerstättenmodell durch Optimierung von reaktionskinetischen Parametern durch (Kapadia et al., 2013) angenähert. Dieses induktive Vorgehen ist einerseits beschränkt durch die vorhandenen Daten sowie das genutzt Modell, als auch die Genauigkeit der Annäherung. Dabei wirkt insbesondere das Fluidmodell mit kinetischen Hemmungen

verzehrend auf Temperaturen und die damit verbundenen variablen Reaktionsenthalpien. Die daraus resultierende Unsicherheit kann anhand der gegebenen Daten auf ca. 50% geschätzt werden, allerdings kann diese aufgrund von den genannten Faktoren signifikant höher liegen, nur ist diese dann nicht mehr quantifizierbar.

2.3.3. Numerische Modellierung

Grundsätzlich ist die numerische Berechnung aufgrund der vorherig genannten fehlerbehafteten Modellbildung kritisch zu betrachten. Dabei sind modellinhärente Fehler aufgrund der Singularität des bestehenden Modells für diese Simulationen als nicht quantifizierbar bzw. validierbar zu betrachten. Die Genauigkeit von dreidimensionalen Phasen- und Komponententransportgleichungen kann im Rahmen des mathematischen Massebilanztests durchgeführt werden. Dabei werden Fehler durch massentechnisch unausgeglichenene Reaktionen sowie numerisch instabile Berechnungssituationen (hohe Temperaturgradienten, komplexe und schnelle Reaktionsnetzwerke, viele Komponenten mit entsprechend häufigem Phasenwechsel, komplexe und instabile Gleichgewichte) erzeugt. Hohe Fehlerquoten sind gerade bei in-situ combustion Simulationen durchaus einkalkuliert und üblich, dies ist durch die zugrundeliegenden und bereits stark fehlerbehafteten Modelle begründet (grundsätzlich wird dies auch beim Vergleich verschiedener Modelle für die in-situ combustion deutlich, diese sind grundsätzlich stark unterschiedlich). Diese sind teilweise mittels genaueren, und extrem zeit- und rechenaufwendigen, Methoden reduzierbar, fallen aber in der Regel unterhalb der genannten Unsicherheit des Modells aus.

Aufgrund der extremen Unsicherheit ist Optimierung dieser Faktoren unerheblich, solange der größte Unsicherheitsfaktor nicht minimiert werden kann. Auf die simulative Sicherheit (Berechnungsgenauigkeit) abzustellen, ist für die Bewertung der simulativen Abbildbarkeit zulässig, ist aber keinesfalls ein Maß für die Unsicherheit im Sinne der Differenz Simulation - Realität. Grundsätzlich sind für die genannten Zahlen daher Fehlertoleranzen bis zu 70% anzunehmen, insbesondere auch in Bezug auf die Übertragbarkeit auf die Realität.

2.4. Geförderte Gaskomponenten

Um Simulationsergebnisse von schematischen Berechnungen bewerten zu können, kann aufgrund von den veränderten Bedingungen nicht mit einer Bewertung wie für eine gesamte Lagerstätte gerechnet werden. Um die Fälle trotzdem bewerten zu können und Erkenntnisse über die weitere Verfahrensauswahl zu treffen, werden die Verfahren hier zunächst anhand der geförderten Gase bewertet.

3. Prozessanalyse

Aufgrund von simulative Restriktionen (Zeit, Rechenpower, Genauigkeit) ist eine Vorevaluierung der jeweiligen Reaktionsschemen auf numerische Anwendbarkeit sowie auf die Wirksamkeit der jeweiligen Prozesse durchzuführen. Diese dient der Auswahl von geeigneten Fahrweisen für die Lagerstättensimulation mit Heterogenität.

Dafür wurden jeweils drei unterschiedliche geometrische Reservoir (Einbohrloch, zwei horizontale Bohrlöcher, zwei vertikale Bohrlöcher), drei unterschiedliche Prozessarten (Reine Verbrennung, Gas-Wasser, Gas-Wasserdampf) sowie je zwei unterschiedliche Injektionsmittel (Luft, sowie aufbereitete Luft mit 95% Sauerstoff) simuliert und bewertet. Zur Vermeidung von Fehlern durch komplexe und unrealistische Randbedingungen werden alle Verfahren mit ausreichendem horizontalem Abstand der Bohrungen zum Rand simuliert. Dazu wird auf nicht gleichskalierte Randblöcke zurückgegriffen. Die untersuchten Prozessvarianten sind in Tabelle 1 dargestellt.

Tabelle 1: Untersuchte Prozessvarianten

| Grundprozess /Oxidationsmittel | Reine combustion in-situ | Oxidationsmittel alternierend mit Wasser | Oxidationsmittel alternierend mit Dampf |
|--------------------------------|--------------------------|--|---|
| Luft | Air_ISC | Water_Air | Steam_Air |
| Angereicherte Luft | Oxy_ISC | Water_Oxy | Steam_Oxy |

3.1. Einbohrlochverfahren

Die Auswertung simulativer Ergebnisse teilt sich auf in die Analyse der geförderten Gase, sowie der energetischen Betrachtung.

Anhand von Abbildung 2 kann die Förderung der relevanten Gase nachvollzogen werden. Dabei ist die Förderung von relevanten Gasen (HMWG, CH₄, H₂) für die Verfahrensbewertung in erster Sicht wichtig. Die Förderung von Wasserstoff tritt während der Versuche mit alternierender Injektion von Wasser und Sauerstoff insbesondere auf, wenn auch insgesamt mit nur geringen Mengen (~10⁴ Sm³). Weiterhin sind Verfahren mit alternierender Injektion mit Dampf ebenfalls geeignet Wasserstoff zu produzieren, allerdings vergleichend betrachtet in deutlich geringeren Mengen.

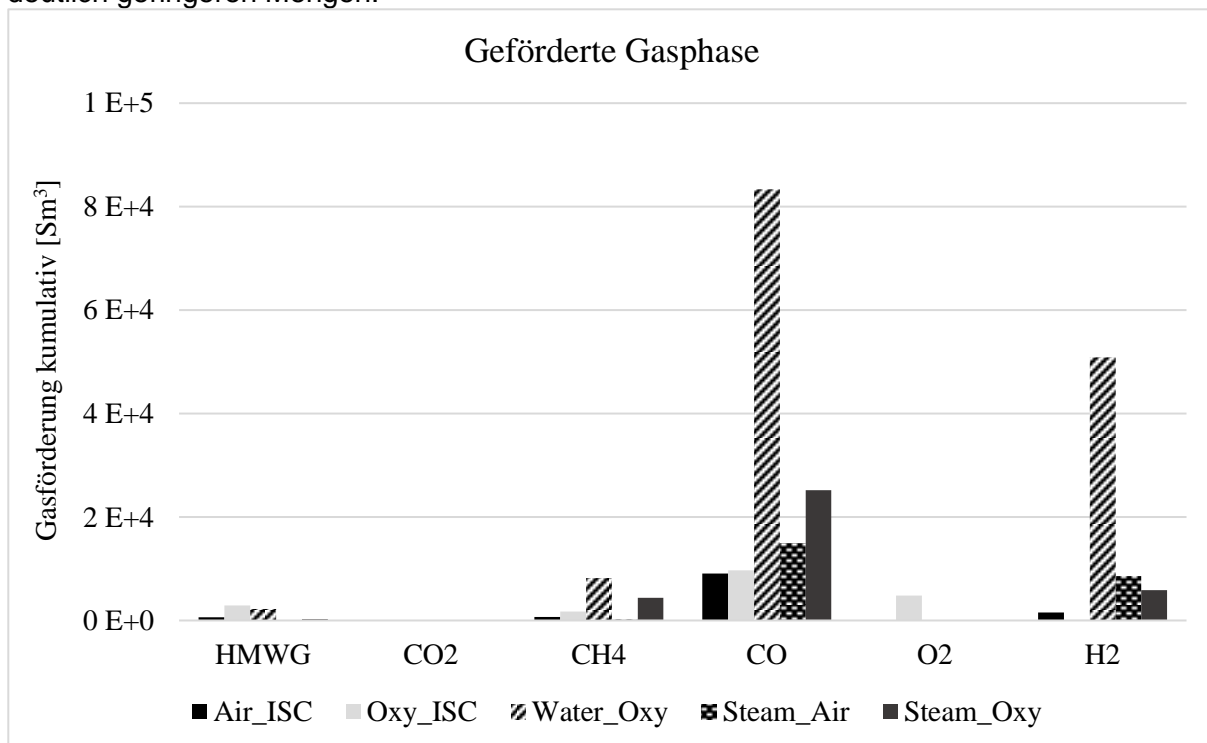


Abbildung 2: Geförderte Gasbestandteile am Einbohrlochschemma

3.2. Zweibohrlochverfahren mit vertikalen Bohrungen

Eine Wasserstoffförderung im abbildungsbaren Maße kann nur bei vertikalen Bohrlochschemas nach Ausschluss der nicht-simulierbaren Fragestellungen nur bei einer alternierenden Wasser-Oxidationsmittel-Injektion festgestellt werden. Die Mengen an Kondensatgasen sowie Methan sind dagegen im Rahmen der Verfahrenssimulation nicht eindeutig einer solchen alternierenden Injektion zuzuordnen. Signifikant ist hier die deutlich höhere Kohlenstoffmonoxid (CO) sowie Sauerstoffförderung (O₂) im Falle von einer Aufbereitung von Sauerstoff (aufbereiteter Luft).

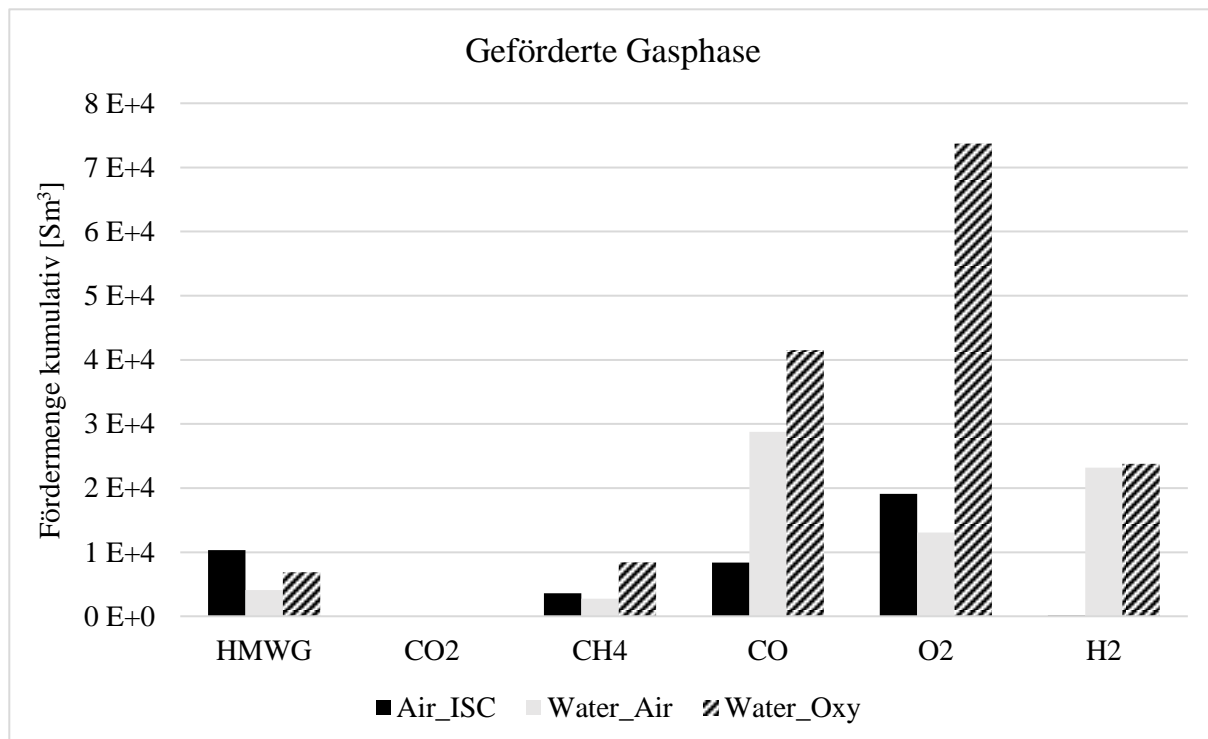


Abbildung 3: Geförderte Gasbestandteile bei Anwendung am vertikalen Zweibohrlochschemma

3.3. Zweibohrlochverfahren mit horizontalen Bohrungen

Anhand von Abbildung 4 wird deutlich, dass für die Wasserstoffproduktion lediglich das Verfahren der alternierenden Injektion von Wasser und Luft infrage kommt. Dieses produziert zwar weniger Kondensatgase als die alternierende Dampfinjektion sowie die herkömmliche *in-situ combustion*, stellt aber eindeutig das beste Verfahren dar. Auffallend ist in dem Gasförderungsplot die Korrelation zwischen der Förderung von Kohlenstoffmonooxid und Wasserstoff.

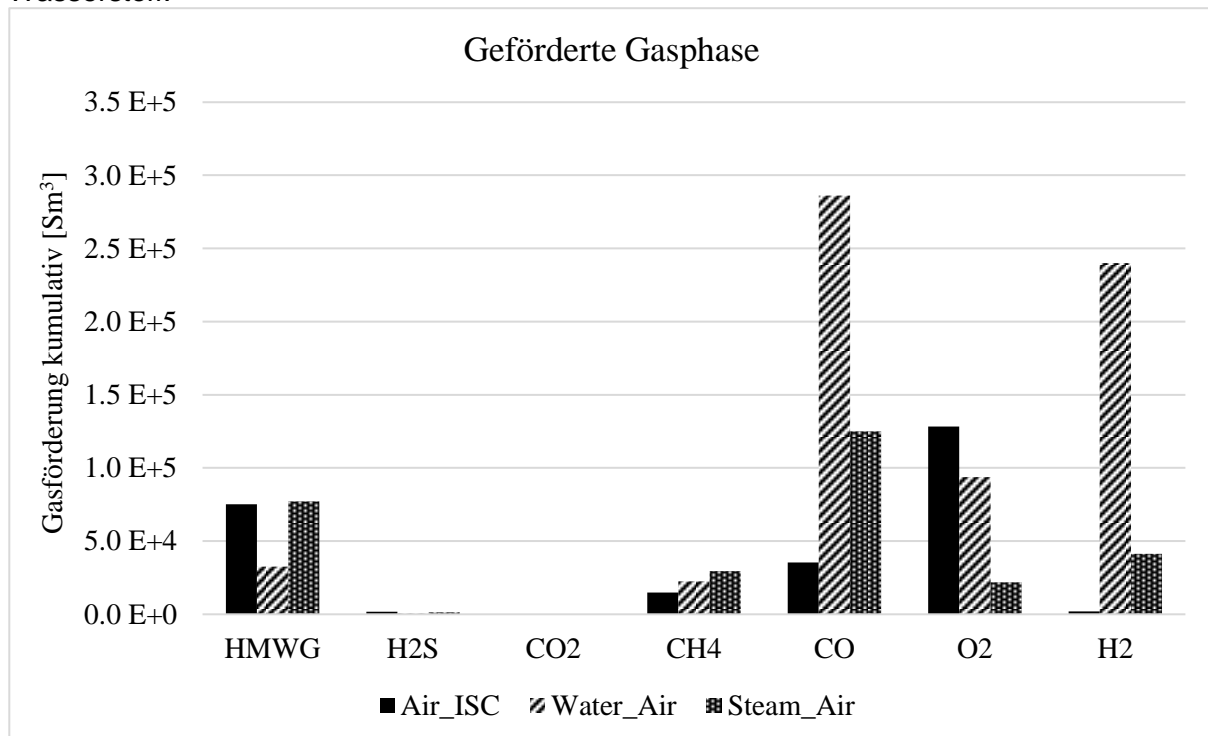


Abbildung 4: Geförderte Gasbestandteile bei Anwendung am horizontalen Zweibohrlochschemma

4. Analyse best case der Verfahren und Bohrungsschemen

Aufgrund von Simulationsdaten sollte auf die horizontale Injektion von Wasser-Air zurückgegriffen werden als bester Fall bzw. relevanter Untersuchungsfall. Die geförderten Wasserstoffmengen liegen bei vergleichbaren Domains um ca. eine Größenordnung höher als für die anderen Schemen. Die grundsätzliche Bedeutung der alternierenden Injektion spiegelt sich dabei in allen Testschemen wider.

Identifikation relevanter Bereiche bzw. Zeitphasen

Zur Analyse relevanter Effekte muss zunächst der relevante Bereich der Förderung des Wasserstoffs eingegrenzt werden. Dieser wird in Abbildung 5 als Bereich F bezeichnet. Anhand von der Abbildung wird deutlich, dass zum ersten Wechsel von Luft auf Wasserinjektion eine kurzzeitige und starke Förderung von Wasserstoff auftritt. Gleichzeitig tritt eine starke Förderung von Kohlenstoffmonoxid auf, welche auf eine gemeinsame Entstehung der Gase hinweist.

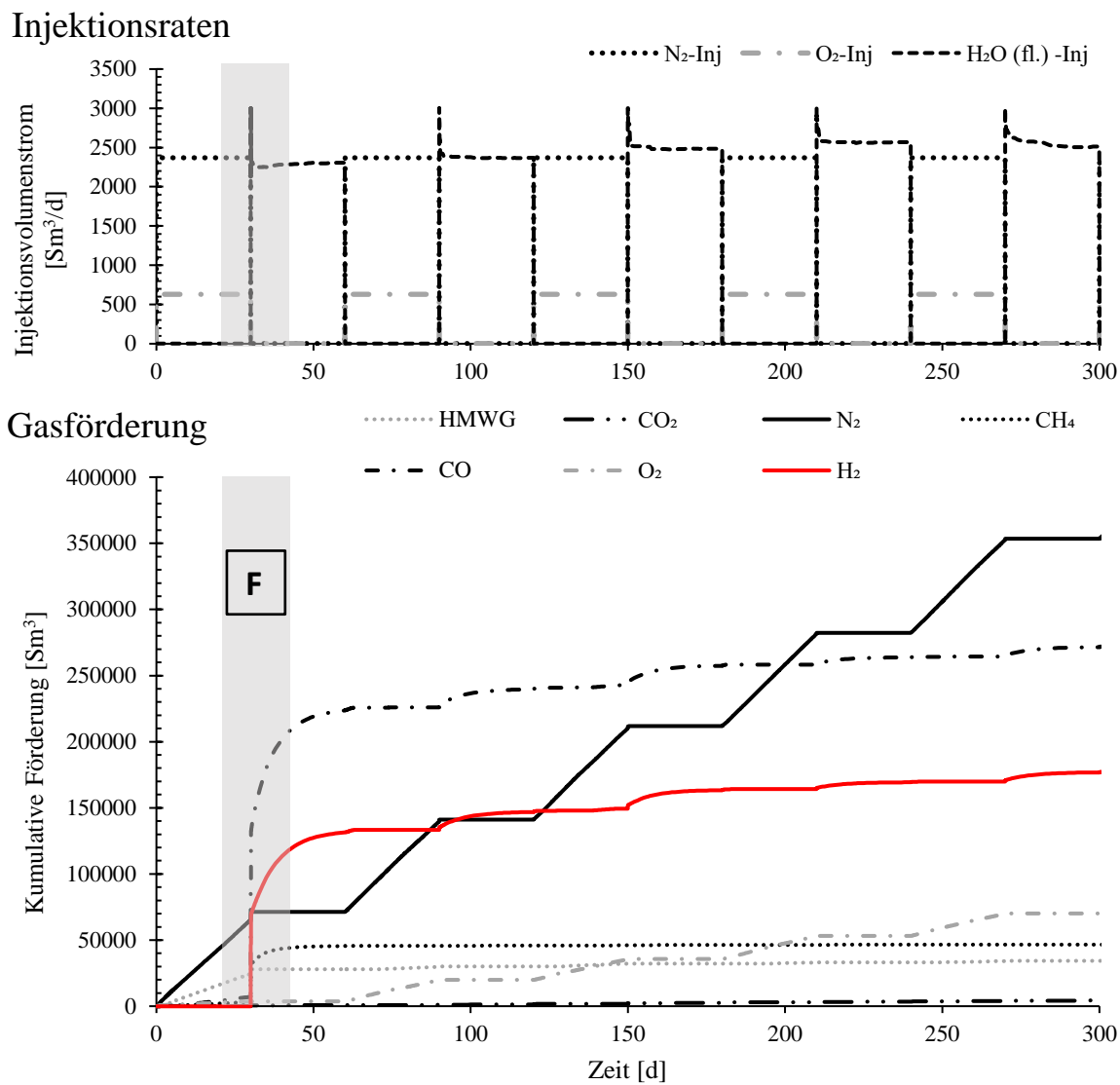


Abbildung 5: Injektionsparameter und geförderte Gasphasen der alternierenden Wasser-Luft-Injektion an der horizontalen Domain

Im weiteren Verlauf der Untersuchung geht die Förderung von Wasserstoff zurück und tritt jeweils beim Wechsel der Injektionsmittel zur Wasserphase auf, erreicht allerdings nicht mal mehr annähernd den erstmals erzeugten Peak.

4.1. Analyse der 3D-Daten zur Wasserstoffbildung

Um die Fragestellung genauer zu analysieren, wurden Analysen zum Verhalten der Fluide im Moment der Wasserstoffentstehung (mit dem Start der Wasserinjektion) durchgeführt. Dafür sind einige relevante Prozesse chronologisch in Abbildung 6 dargestellt. Dort sind sechs nummerierte Verlaufsbilder mit einem Schnitt der relevanten Lagerstätte dargestellt. Das jeweils rechte Bildbestandteil zeigt die Temperatur zwischen den beiden Bohrungen in der Simulationsdomain. Das jeweils linke Element stellt in Blau die Strömungslinien der injizierten Wasserphase dar, und in Gelb Volumenelemente in denen der globale Wasserstoffanteil größer als 10% ist. Nachfolgend sind die Bilder in ihrer Reihenfolge in Bedeutung beschrieben: In Bild 1 ist der Zustand vor Beginn der Wasserinjektion. Eine Wasserstoffbildung ist nirgends festzustellen, der Prozess verbraucht produzierten Wasserstoff unmittelbar wieder. In manchen Bereichen der Lagerstätte erreicht die Temperatur Werte knapp unter 700°C. Diese Bereiche liegen unterhalb des Produktionsbohrloches.

In Bild 2 beginnt die Wasserinjektion und kühlte die durchströmten Bereiche (zunächst nur den direktesten Weg) unmittelbar ab, auf ca. 600°C im wärmsten Bereich.

In Bild 3 findet eine Wasserstoffbildung rund um den abgekühlten Kern statt. Diese ist neben den vom Wasser durchströmten Bereichen und befindet sich in einem Temperaturbereich von ca. 400-500°C.

Die Wasserstoffbildung setzt sich fort, der gebildete Wasserstoff wird fast direkt durch das Produktionsbohrloch gefördert.

Die Strömungslinien der Wasserstoffinjektion zeigen einen größeren durchströmten Bereich in dem erneut eine Wasserstoffbildung durch die Kommunikation mit bislang nicht betroffenen Gegenden der Lagerstätte erreicht wird. Die Lagerstätte kühlte in den durchströmten Bereichen weiter ab.

Die durchströmten Bereiche nehmen weiter zu und die Lagerstätte kühlte sich in vielen Bereichen so stark ab, dass die Bildung von Wasserstoff stark abnimmt. Die Wasserstoffbildung beschränkt sich auf Bereiche ohne Wasserphase mit Temperaturen von mehr als 300°C.

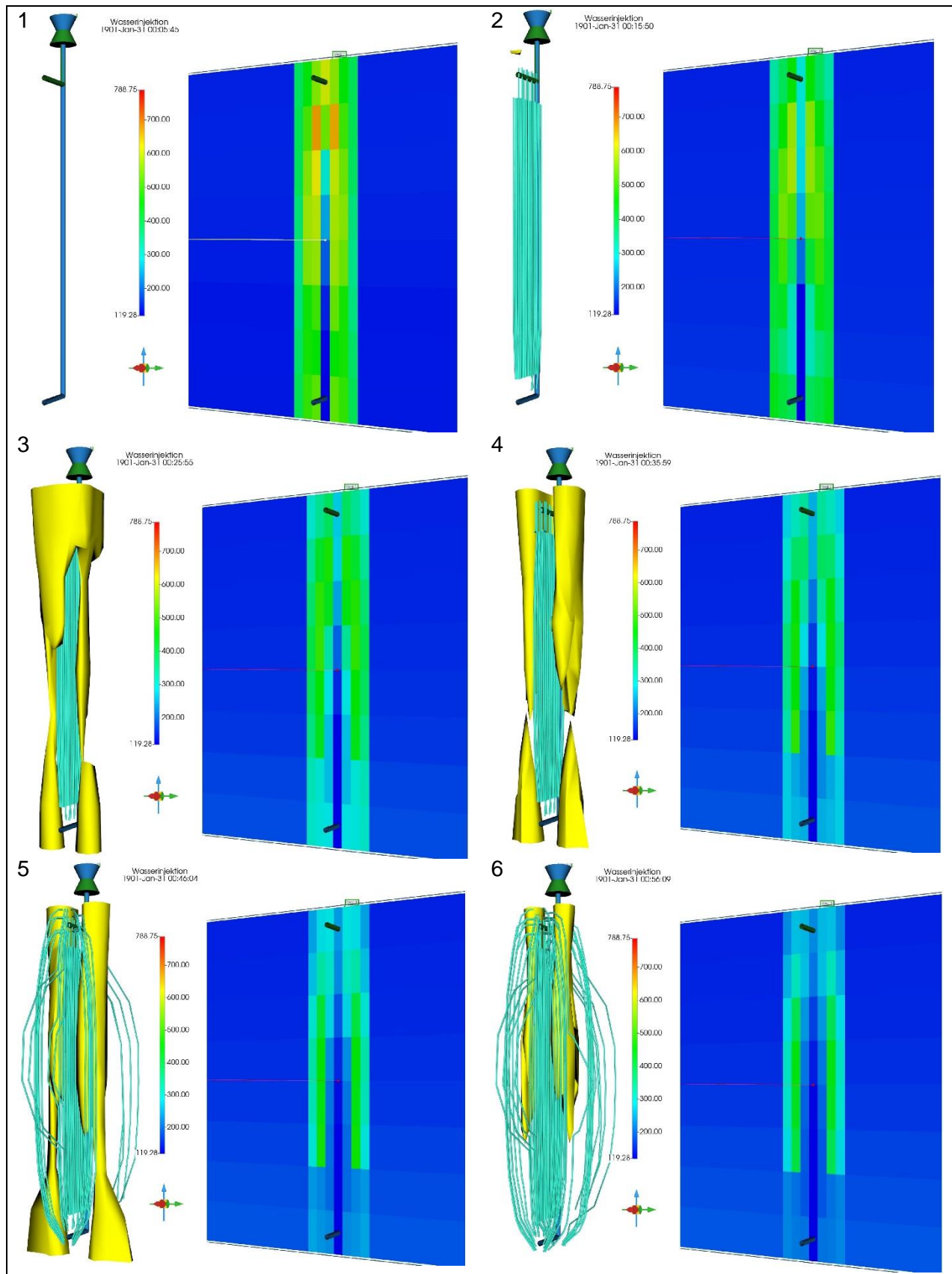


Abbildung 6: 3D-Analysen zur Wasserstoffbildung

4.2. Analyse der räumlichen Reaktionen zur Wasserstoff- bzw. Synthesegasbildung in den relevanten Bereichen

Anhand der vorhergehenden Analysen wird deutlich, dass die Wasserstoffproduktion nur bei dem Wechsel der Injektion von Luft zu Wasser auftritt. In Abbildung 7 wird eine wasserstoffsgebildende Zone zunächst über die gesamte Betrachtungszeit analysiert. Dazu wird diese in die Zonen A-F eingeteilt.

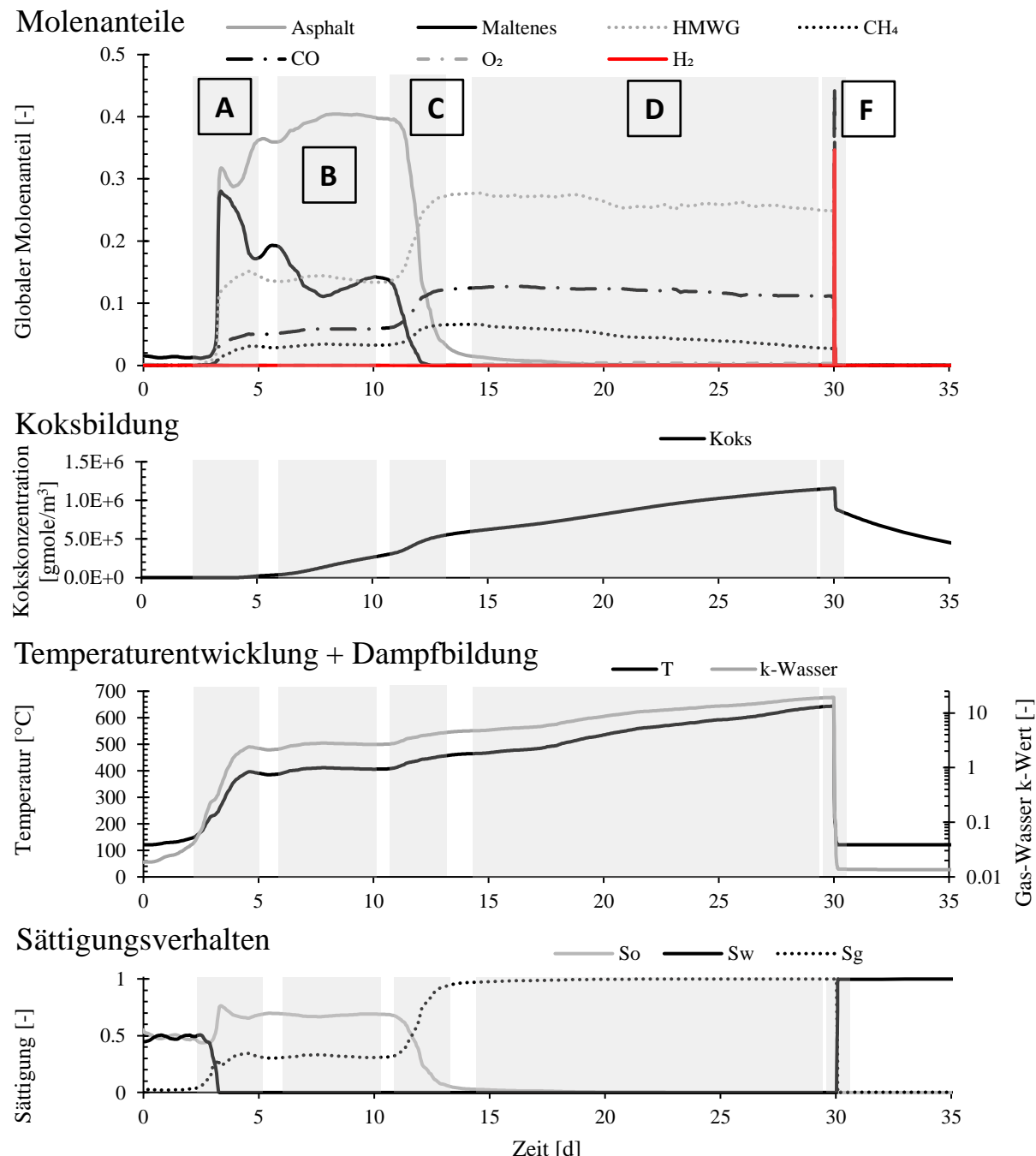


Abbildung 7: Analyse des Verfahrens anhand einer wasserstoffsgebildenden Zone; globaler Zeithorizont

Zone A stellt in der Graphik die Entzündung mit der Verdampfung der Wasserphase sowie der Ausbildung einer Gasphase dar. Insbesondere im Plot der globalen Molenanteile ist die Bildung einer Ölbank klar ersichtlich. Die Phase B zeigt stellt die Phasen mit der Herausbildung von Cracking-Reaktion innerhalb der Ölphase dar. In Phase C reagieren die vorhandenen Komponenten im Rahmen einer vollständigen Vergasung vor allem zu Kondensatgasen,

Methan und Verbrennungsgasen. Phase E stellt die Bildungsphase von Koks mit weiterer Erhitzung durch anliegende Schichten und die Nähe der Verbrennungsfront dar. In Phase F tritt peakartig die Wasserstoffbildung auf, in Verbindung mit einer Verringerung der Koksmenge sowie einer Abkühlung der Zone durch die Wasserinjektion, welche die Gasphase komplett verdrängt.

In Abbildung 8 wird die Phase F kleinteiliger und genauer untersucht. Diese ist dabei in die Unterkategorien F.1-F.4 eingeteilt. Die Phase F.1 stellt dabei die Phase dar, in der das injizierte Wasser zwar die Zone noch nicht erreicht hat, allerdings der Wasserdampf bereits als Zone auftritt und in den betrachteten Bereich strömt. Der vorhandene Wasserdampf führt innerhalb der betrachteten Zone zur Bildung von Kohlenstoffmonooxid und Wasserstoff (F.2) und Methan. Diese Reaktionen in Phase F.3 werden durch das Auftreten der flüssigen

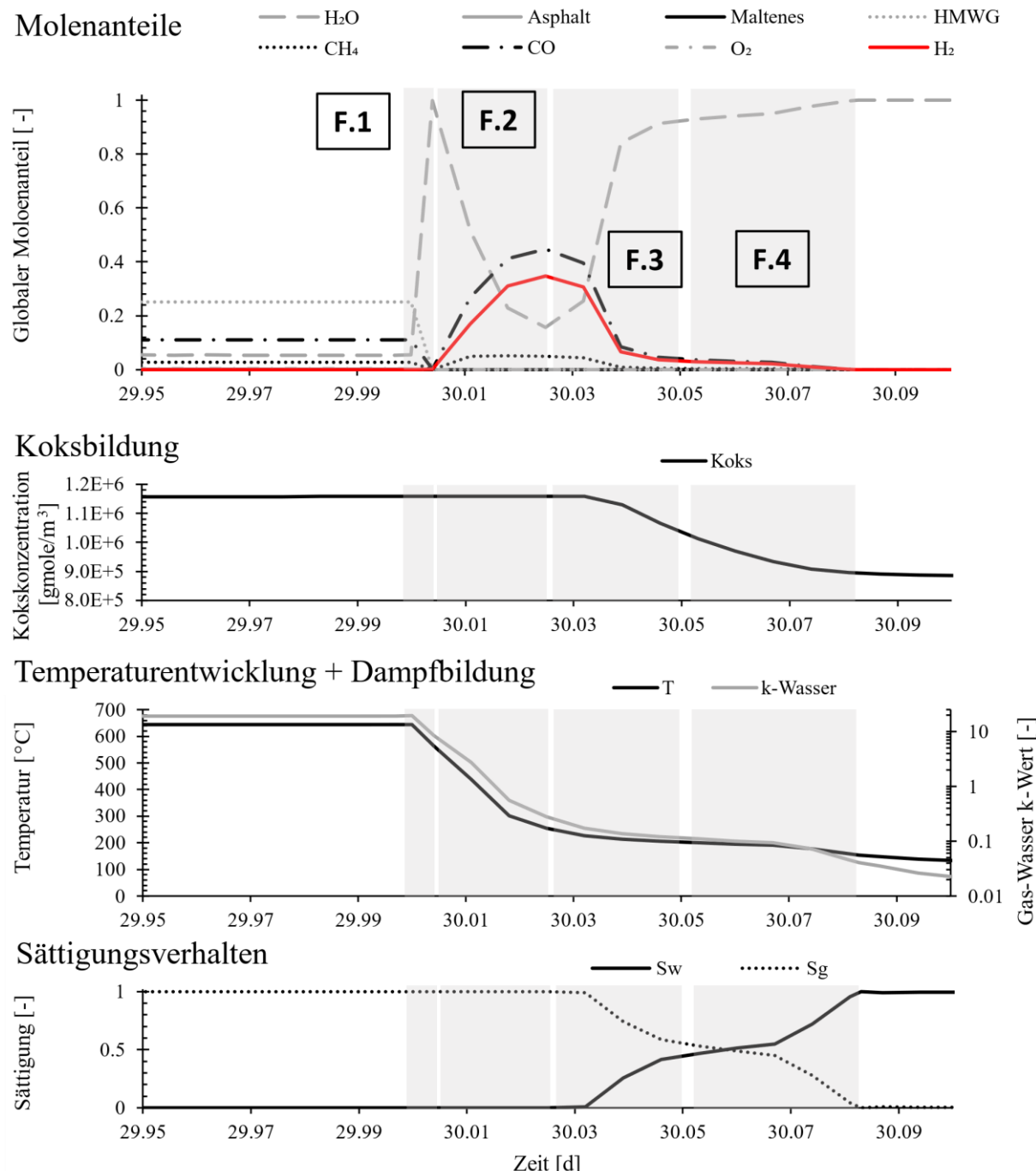


Abbildung 8: Analyse des Verfahrens anhand einer wasserstoffbildenden Zone; lokaler Zeithorizont

Wasserphase sowie der damit verbundenen Temperaturreduktion beendet und alle weiteren Reaktionen kinetisch gehemmt. Während dieses Prozesses erfolgt die Reaktion des Wasserdampfes mit dem Koks zur Bildung weiteren Wasserstoffes. In Phase F.4 wird die vorhandene Gasphase durch die hineinströmende Wasserphase verdrängt und durch die stark abgesenkten Temperatur kinetisch gehemmt.

4.3. Sensitivitätsanalyse

Im Rahmen der Sensitivitätsanalyse wurden die einzelnen beeinflussbaren und nicht beeinflussbaren Parameter hinsichtlich ihrer Auswirkung auf die Wasserstoff-, Methan- und Kondensatgasmenge untersucht. Die Simulationen wurden anhand von normalisierten Parametern regressiert und dargestellt.

Sensitivitätsanalyse beeinflussbarer Parameter

Im Rahmen der Sensitivitätsanalyse der beeinflussbaren Parameter wurden als wichtige Einflussparameter die Fließrate des Gases, die Zeitspanne bis zum Wechsel des Injektionsmediums sowie die Injektionstemperatur, der Druck im Produktionsbohrloch sowie die Fließmenge des Wassers identifiziert. Die Fließmenge des Gases sowie die Wechselzeit haben bei Vergrößerung einen positiven Wert auf den geförderten Wasserstoff (Abbildung 9), wohingegen die Injektionstemperatur sowie der Bohrlochsohlendruck leicht negativ auf die Wasserstoffmenge wirken. Die Fließrate des Wassers wirkt sich dagegen stark negativ aus, da diese eine zu schnelle Abkühlung innerhalb der Reaktionszone bewirkt und somit die Reaktionen kinetisch hemmt.

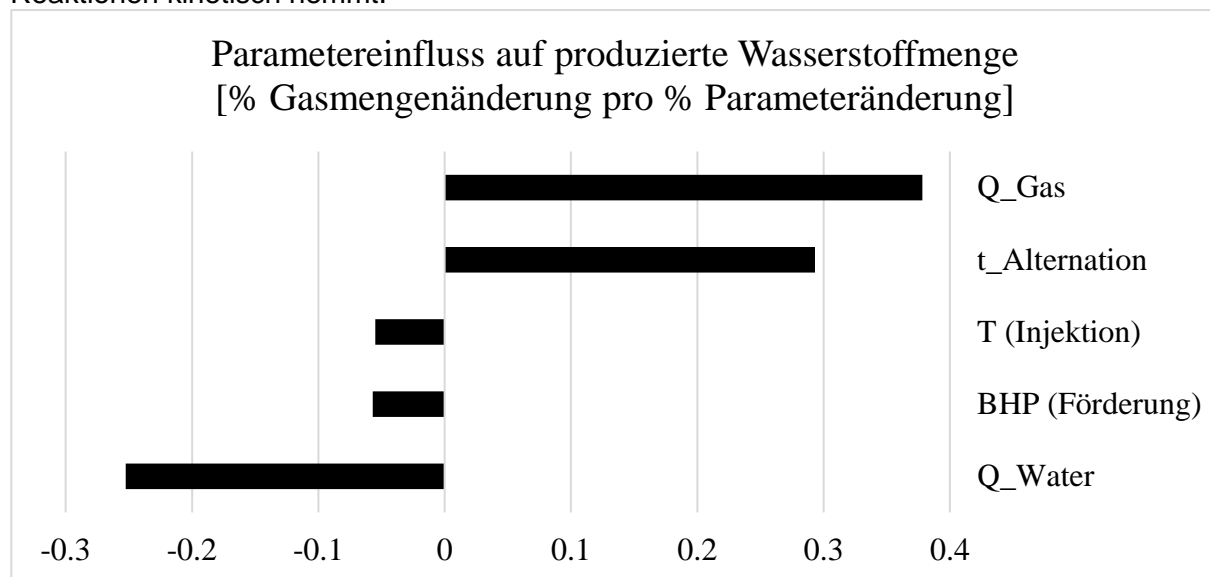


Abbildung 9: Parametereinfluss auf die produzierte Wasserstoffmenge
Sensitivitätsanalyse nicht beeinflussbarer Parameter

Als nicht beeinflussbare Parameter in der Lagerstätte wurden die Ölsättigung, die initiale Lagerstättentemperatur, die Wassersättigung (im Falle von nicht nur ölgesättigten Lagerstätten), die horizontale und vertikale Permeabilität sowie die Porosität der Lagerstätte identifiziert.

In Abbildung 10 ist die analysierte Sensitivität der Parameter für die Wasserstoffförderung dargestellt. Dabei wirkt die Ölsättigung als der stärkste Parameter positiv auf die Wasserstoffförderung, dies ist zurückzuführen auf die höhere erreichbare Temperatur sowie die größere Menge reaktionsfreudigen Materials in der Lagerstätte. Die initiale Temperatur wirkt ebenfalls fördernd, wenn auch in geringerem Maße. Diese verringert die notwendige Erwärmung durch Luftinjektion und ermöglicht weiterhin die Reaktionen auch im nicht erwärmten Zustand besser. Die Wassersättigung (bzw. substituierte die Gassättigung nicht reaktiver Gase) zu Beginn des Verfahrens stellt keinen relevanten Einflussfaktor dar. Höhere Permeabilität sowie Porosität verringern die Wasserstoffförderung ebenfalls, der Einfluss ist hierbei auf die höhere Verbrennungsgeschwindigkeit sowie die effektivere Stoffdispersion im

Medium zurückzuführen. Dabei ist die Permeabilität in Richtung der Verbrennungsfront (hier die vertikale) erwartungsgemäß relevanter für die Verringerung der Wasserstoffförderung.

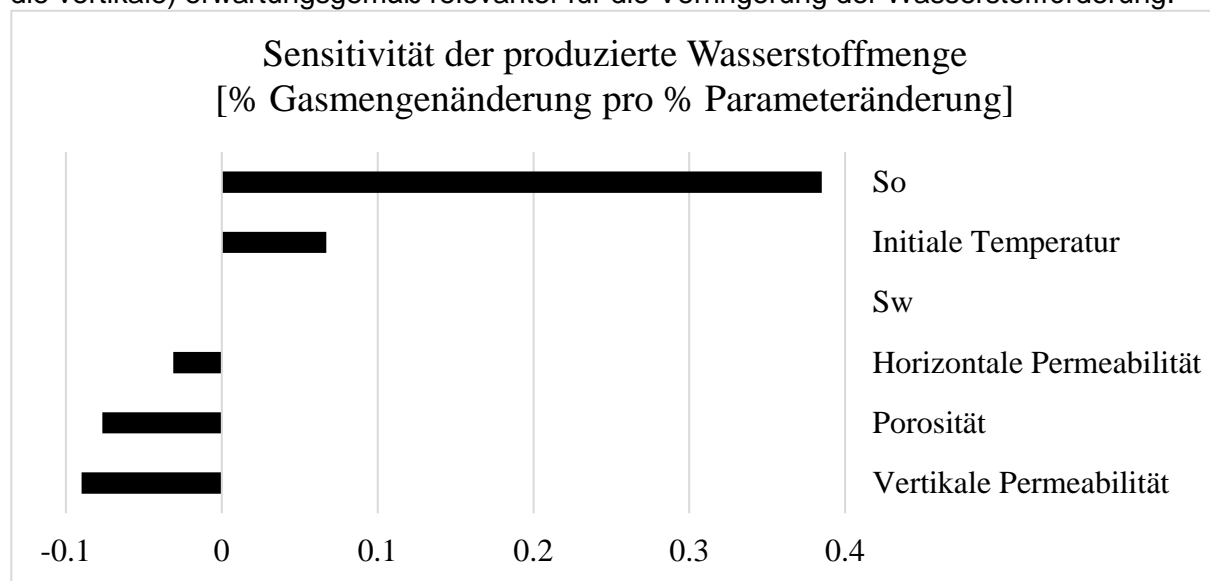


Abbildung 10: Sensitivität der produzierten Wasserstoffmenge

5. Optimaler Algorithmus zur Wasserstoffförderung aus Lagerstätten

Anhand der vorherigen Ergebnisse sind die folgenden Faktoren als maximierend für die Wasserstoffgewinnung anzusehen:

- Temperaturen bei denen der Anteil des CO deutlich höher ist als des CO₂
- Cracking statt Verbrennungsreaktionen, zur höheren Koksbildung
- Wasserphase trifft auf heiße Bereiche und wandelt fast direkt als Heißdampf die vorhandenen Koksbestandteile um
- Sauerstoffatmosphäre möglich ohne kinetische Hemmung (kurz vorher noch möglichst hohe Temperatur) vor dem Auftreten Wasserinjektion verbrauchen
- Wasserstoffhaltiges Gas (Synthesegas) sollte möglichst durch schnelle Abkühlung nach der Erzeugung kinetisch gehemmt werden, um Reduktionsreaktionen zu vermeiden, und anschließend mit hoher Sweep-Effizienz aus der Lagerstätte gefördert werden
- Möglichst große Wasserstoffmenge beim ersten Zyklus, weitere Zyklen begünstigen aufgrund der Reaktionskinetik und der Ansteuerungsgeschwindigkeit (Entzündung nicht mehr an der Bohrung, sondern an der alten, gelöschten, Front) geringere Fördermengen hochwertiger Gase.
- Die Injektion von Luft kann teilweise höhere Drücke bzw. langsamere Verbrennungen herbeiführen, allerdings ist der Effekt des Stickstoffes einerseits durch sein Volumen zu einer schnelleren Überschreitung der kritischen Gassättigung bei noch nicht vergasten Lagerstättenbereichen als auch durch die Herabsetzungen der Partialdrücke reaktiver Komponenten als vorteilhaft zu bewerten.
- Ein Höhenunterschied zwischen Injektionsbohrung und Produktionsbohrung wirkt sich wasserstoffbildungsförderlich aus.

Daraus lassen sich die folgenden Prozessparameter für einen möglichst effizienten Prozess ableiten:

- Im Bestfall enthält der Prozess nur einen Injektionszyklus. Dadurch kann die Wasserstoffmenge am effektivsten maximiert werden.
- Die Temperatur während der Verbrennung muss möglichst schnell möglichst hoch eingestellt werden. Dies kann durch entsprechend hohe (nahe dem Fracdruck) und schnelle Luftpumpe durchgeführt werden. Luft hat dabei insbesondere aufgrund der inertien Eigenschaften des Stickstoffes vorteilhafte Eigenschaften gegenüber aufbereiteter Luft.
- Bei Erreichen eines möglichst großen und koksgefüllten Areals mit Temperaturen

oberhalb ca. 700°C muss mit möglichst hohem Druck eine Wasserinjektion durchgeführt werden. Die Produktionsbohrung ist vom Druck so einzustellen, dass die Förderung vor allem eine Abführung der Gase ermöglicht.

- Lagerstätten mit einem Höhenunterschied zwischen Injektor und Producer sind zu bevorzugen.

6. Diskussion

Grundsätzlich müssen die Ergebnisse des vorliegenden Kapitels unter der Prämisse der Bedingungen gesehen werden. So sind aus Gründen des simulativen Aufwandes und der Klarheit nur drei unterschiedliche Bohrungspositionen genauer untersucht worden. An diesem wurden insgesamt je 6 verschiedene Verfahrensvarianten getestet. Da jedoch das zugrunde liegende Modell der thermo-numerischen Fluidabbildung in seiner Anwendbarkeit beschränkt ist, mussten einige der Verfahren als nicht simulativ abbildbar von der genaueren Evaluation ausgenommen werden.

Anhand der simulierten Bereiche wurden Kriterien für ein Verfahren mit maximaler Förderung an Wasserstoff bei energetischer Effizienz erarbeitet. Die dort verwendeten Werte sind aufgrund der erheblichen Simulativen Unsicherheit, welche für Verfahren dieser Art industrieüblich sind, übermäßig genau bzw. suggerieren eine Genauigkeit, welche simulativ nicht widergespiegelt wird.

Um die Fragestellung nach den wasserstoffbildenden Verfahren weitergehend zu evaluieren, wurden die simulativen Ergebnisse des ergiebigsten Falles („best case“) zunächst global anhand von der Förderung, sowie anschließend lokal anhand von simulativen 3D-Ergebnissen und Stoffbilanzen innerhalb zentraler Zonen analysiert. Anhand von dieser Analyse konnte der wasserstoffbildende Prozess auf den Wechsel der Injektion des Oxidationsmittels hin zum Wasser terminiert werden. Die Wasserstoffbildung ist dabei auf einen nur kurzfristig vorhandenen physiko-chemischen Zustand reduziert und erfordert dort eine schnelle Abkühlung zur kinetischen Hemmung und eine zügige Abführung der Gase. Weiterhin ist die Bilanz der geförderten Gase nur für den ersten Wechselzyklus als effizient zu beurteilen.

Um die Einflussfaktoren auf die Förderung von energiereichen Gasen weiter zu untersuchen, wurde eine Sensitivitätsanalyse durchgeführt. Diese teilt sich auf in veränderbare Komponenten, welche üblicherweise, während der Verfahren beeinflusst werden können (z.B. Injektionstemperatur), sowie unveränderliche Komponenten, welche durch die natürlich gebildete Lagerstätte vorhanden sind (z.B. Porosität und Permeabilität). Die Sensitivitätsanalyse ist bei als Indikation zu betrachten, unter der Einschränkung der verwendeten Parametergrenzen und simulativer Interferenzen. Zur Validierung der Sensitivitätsanalyse wurde die Vorhersagequalität spezifisch geprüft.

Basierend auf diesen Ergebnissen wurden Schlussfolgerungen zur Maximierung der Fördermenge aus der Lagerstätte gezogen. Diese basieren auf der Evaluierung der simulierten Verfahren in den Testschemen und zeigen klar die Vorteilhaftigkeit eines einmaligen Luft-Wasser-Prozesses mit Höhendifferenz zwischen den Bohrungen. Weiterhin wurde die Erreichung einer hohen Temperatur als zentraler Einflussfaktor für die Wasserstoffförderung identifiziert.

7. Zusammenfassung & Ausblick

Das vorgelegte Paper fast den aktuellen Stand der Forschung zur thermischen Wasserstoffgewinnung in ausgeförderten Erdöllagerstätten zusammen. Dabei wird insbesondere der Prozess der Wasserstoffbildung als Folge der alternierenden Injektion von Luft und Wasser hervorgehoben. Dieser wurde hinreichend genau analysiert anhand von ZusammensetzungsvARIABLEN und weiteren Parametern. Basierend darauf werden die Prinzipien für die Bereitstellung von Wasserstoff analysiert und erläutert.

Aufgrund der Notwendigkeit ist die Forschung zur Weiternutzung von ausgeförderten Erdöllagerstätten ein spannendes und aktuell wichtiges Forschungsgebiet. Die thermische Nutzung von Erdöllagerstätten stellt für diese Diskussionen einen wichtigen Ansatz dar, welcher aktuell durch weitere Forschung untersucht wird.

Literatur

- BABUSHOK, V.I. und an DAKDANCHА, 1993. Global kinetic parameters for high-temperature gas-phase reactions. *Combustion, Explosion and Shock Waves*, **29**(4), 464-489. ISSN 1573-8345.
- BELGRAVE, J., R.G. MOORE, M.G. URSENBACH und D.W. BENNION, 1993. A Comprehensive Approach to In-Situ Combustion Modeling [online]. *SPE Advanced Technology Series*, **1**(01), 98-107. ISSN 1076-0148. Verfügbar unter: doi:10.2118/20250-PA
- GUNTERMANN, K., H.W. GUDENAU und M. MOHTADI, 1982. Mathematical modeling of the in situ coal gasification process.
- HAJDO, L.E., R.J. HALLAM und L. VORNDRAN, Hg., 1985. *Hydrogen Generation During In-Situ Combustion*. SPE Western Regional Meeting. All Days.
- HALLAM, R.J. und J.K. DONNELLY, 1993. Pressure-Up Blowdown Combustion: A Channeled Reservoir Recovery Process [online]. *SPE Advanced Technology Series*, **1**(01), 153-158. ISSN 1076-0148. Verfügbar unter: doi:10.2118/18071-PA
- HALLAM, R.J., L.E. HAJDO, J.K. DONNELLY und P.R. BARON, 1989. Thermal Recovery of Bitumen at Wolf Lake [online]. *SPE Reservoir Engineering*, **4**(02), 178-186. SPE Reservoir Engineering. Verfügbar unter: doi:10.2118/17022-PA
- KAPADIA, P.R., J. WANG, M.S. KALLOS und I.D. GATES, 2012. New thermal-reactive reservoir engineering model predicts hydrogen sulfide generation in Steam Assisted Gravity Drainage [online]. *Journal of Petroleum Science and Engineering*, **94-95**, 100-111. ISSN 09204105. Verfügbar unter: doi:10.1016/j.petrol.2012.06.030
- KAPADIA, P.R., J. WANG, M.S. KALLOS und I.D. GATES, 2013. Practical process design for in situ gasification of bitumen [online]. *Applied Energy*, **107**, 281-296. ISSN 0306-2619. Verfügbar unter: doi:10.1016/j.apenergy.2013.02.035
- KAPADIA, P.R., M.S. KALLOS und I.D. GATES, 2013. A new kinetic model for pyrolysis of Athabasca bitumen [online]. *The Canadian Journal of Chemical Engineering*, **91**(5), 889-901. ISSN 0008-4034. Verfügbar unter: doi:10.1002/cjce.21732
- YANG, X. und I.D. GATES, 2009. Combustion Kinetics of Athabasca Bitumen from 1D Combustion Tube Experiments [online]. *Natural Resources Research*, **18**(3), 193-211. ISSN 1520-7439. Verfügbar unter: doi:10.1007/s11053-009-9095-z

Verfolgung der Flüchtigen 200° Isotherm in Norddeutschland

W. A. Heins¹, S. M. Masterton²

¹Getech Group plc, Houston, United States of America, ²Getech Group plc, Leeds, United Kingdom

Die Suche nach geothermischer Energie wird in Deutschland heiß, da die Energiekosten in die Höhe schießen und die Versorgung angesichts des anhaltenden Krieges in der Ukraine unsicher bleibt. Im Oberrheingraben, wo die Temperaturen am höchsten sind, und im Molassebecken um München, wo am intensivsten gebohrt wird, ist das Risiko einer geothermischen Exploration relativ geringer. In Norddeutschland sind die Temperaturen nicht niedrig und die historische Bohraktivität sehr hoch, aber das Erkundungsrisiko bleibt unbedeutend hoch, da die öffentlich zugängliche Temperaturdatenbank, die aus historischen Bohrungen für Kohlenwasserstoffe zusammengestellt wurde, sehr wenig Licht auf die Tiefen und Temperaturen wirft, die für die beste Fernwärmeeffizienz erforderlich sind, oder die für viele industrielle Anwendungen oder zur Stromerzeugung ausreichen.

In einem repräsentativen Gebiet historischer Öl- und Gasbohrungen in Niedersachsen greift das geothermische Informationssystem GeotIS auf 3462 Temperaturmessungen aus 1509 einzelnen Bohrungen zurück. Nur 150 oder ~4 % der Temperaturmessungen weisen Werte über 150 °C auf. Fast 70 % der Beobachtungen sind flacher als 2000 m. Die relativ spärlichen Messungen, die tief und heiß sind, zeigen, dass es eine starke geografische und stratigraphische Variabilität des geothermischen Gradienten gibt, die wahrscheinlich Variationen in der Krustendicke, der Wärmeproduktion des Grundgebirges, der Wärmeleitfähigkeit, und der Flüssigkeitszirkulation widerspiegelt.

Ein rein statistischer Ansatz zur Temperaturextrapolation oder -interpolation kann keine angemessene Auflösung der erwarteten Temperaturen in der Tiefe für eine effektive Verringerung des Explorationsrisikos liefern. Kommerzielle Lösungen, die 1D-Physik mit groben Annäherungen an die Geologie kombinieren, können nur dabei helfen, Möglichkeiten auf regionaler Ebene zu untersuchen und Einblicke in einige der Faktoren zu geben, die die Variabilität auf lokaler Ebene beeinflussen können. Das Beste, was wir mit den Daten, die wir haben, machen können, ist die Kombination von 3D-Physik und Geologie. Lokale Modellierung, die spärliche Temperaturdaten verwendet, um Ergebnisse einzuschränken, die aus detaillierten geologischen Interpretationen von Bohrlöchern, seismischen und anderen geophysikalischen Daten erwartet werden, basierend auf vernünftigen Annahmen zur Wärmeerzeugung und Wärmeleitfähigkeit für diese Geologie, hat die besten Chancen, Temperaturen in der Tiefe mit der Auflösung vorherzusagen die eine rationale wirtschaftliche Entscheidungsfindung unterstützen können.

Diagenetic controls and reservoir quality of tight limestones from the Upper Cretaceous

J. A. Ölmez, B. Busch, C. Hilgers

Karlsruhe Institute of Technology, Structural Geology & Tectonics, Karlsruhe, Germany

Abstract

This study focuses on the reservoir quality prediction in former high porosity limestones from the Upper Cretaceous Campanian of the Münsterland Cretaceous Basin in NW Germany (Ahlen-Fm., Beckum Submember), as they unconformably overlie Upper Carboniferous coal-bearing strata. For this study, outcrop analyses were carried out and samples were taken in a vertically stacked profile, focusing on a better understanding of the variability and controlling factors of reservoir properties in tight limestones. The results can be applicable to assess the potential interaction of rising mine-water and future potential for regional geothermal use. Petrophysical (He-pycnometry, Klinkenberg-corrected air permeability and p-wave velocity) and petrographic data sets (transmitted and reflected light microscopy, point-counting and cathodoluminescence) were linked with diagenetic alteration and the detrital composition to understand the controls on reservoir quality. Porosity ranges between 1.0% to 18.7% and permeability from <0.0001 mD to 0.2 mD, while p-wave velocity ranges between 2089 m/s and 5843 m/s. The detrital dominated limestones consist of mostly micrite, calcispheres and partly clay laminae. Mechanical compaction leads to porosity and permeability loss due to grain rearrangement, deformation of fossils (e.g., calcispheres and foraminifera), and ductile clay mineral laminae. Mechanical compaction is recorded by elliptically deformed calcispheres and foraminifera, and formation of compaction bands around clay laminae. Bacterial sulfate reduction leads to formation of frambooidal pyrite and marcasite in clay laminae and former hollow fossils and additionally provide the formation of calcite cements. Subsequent early diagenetic authigenic mineral precipitation of inter- and intragranular sparry ferroan calcite reduces porosity and permeability. The studied lithologies can be considered as seals for potentially rising mine-water levels and may limit their potential for geothermal utilization. However, rocks were fractured during burial forming larger veins filled by ferroan calcite and/or strontianite. Later, open fractures overprinted the rocks and veins and thus may enhance the reservoir quality if formed during exhumation.

Visualisation of microbial activities in reservoirs during UHS based on real-rock micromodels

C. Cheng, B. Busch, M. von Dollen, J. A. Ölmez, C. Hilgers

Institute of Applied Geosciences, Karlsruhe Institute of Technology (KIT), Karlsruhe, Germany

Abstract

Hydrogen, converted from renewable energy sources, provides a feasible route map to balance the daily up to seasonal fluctuation between renewable energy supply and consumer demand. However, storing such a large volume of hydrogen (G-TWh) safely and economically remains a big challenge for achieving net-zero emission targets for the future. The concept of underground hydrogen storage (UHS) in porous formations is promising since depleted hydrocarbon reservoirs and aquifers are widespread worldwide. Unlike underground natural gas (mainly methane) storage, hydrogen is the perfect electron donor for microbes, and thus microbial metabolisms can consume and convert hydrogen into other molecules, e.g., methanogenesis, $H_2 + CO_2$ to methane, causing the loss and contamination of hydrogen. Another concept is geo-bio-methanation, converting hydrogen to methane directly in the subsurface for stable long-term storage. Both concepts need a thorough understanding of microbial activities in porous rocks. Questions, including, 1) does microbial growth reduce reservoir performance? 2) is there any effect of minerals and pore microstructures on microbial activities? 3) how do static and flow conditions affect microbe distribution? need to be better elucidated. In this study, we develop an unconventional real-rock micromodel configured with a thin rock layer in a transparent microfluidic chip to visualise microbial growth under a fluorescence microscope. The real-rock micromodels will fill the drawback of the lack of mineral difference and real pore structures. This workflow and platform may hence open new possibilities in studying microbial metabolism in geo-materials and the potential interactions.

Comparative Analysis of Well Drilling Techniques for Natural Resources Access and Energy Recovery

T. Maluf, N. Nascimento, A. Nascimento

Universidade Estadual Paulista - UNESP, PRH-ANP/Finep 34.1, Guaratinguetá, Brazil

The development of today's society depends directly on the exploitation of natural resources and their use in different fields, from direct consumption on a daily basis for different activities and final use.

Some of these resources

deserve to be highlighted because of their vital importance for society's development, such as groundwater, oil, and gas, while others deserve attention for representing alternative solutions in some specific situations, including

access to white hydrogen and energy production from geothermal systems. Although different in essence, all the resources mentioned have one characteristic in common: all are extracted from the underground through well drilling.

That being the case, the work developed aims at expanding the knowledge about exploration processes through a basic comparative analysis of drilling costs and techniques for accessing these resources.

All the analyses are based on a consistent literature review of relevant sources, covering technical economical aspects along with details of equipment employed, drilling methods used, characteristics of well completion, and characteristics

the involved elements (chemical and physical characteristics). From this study, similarities were observed in terms of drilling mechanisms, but due to differences in properties between the resources, there are some

particularities in each of the processes, especially related to the necessary well length and equipment's materials, reflecting most in the associated costs. In terms of exploratory process overall, it could be observed its direct

relation to the physical and chemical properties of each type of resource, ultimately associated with their process of formation/storage in the underground.

KEYWORDS: Comparison. Drilling. Natural Resources. Groundwater. Geothermal. Oil and Gas.

Drilling Geothermal wells, challenges, and solutions

F. Zapata Bermudez, J. Zajaczkowski
Archer Oiltools AS, Stavanger, Norway

Abstract

In addition to new geothermal wells construction, well re-entry on existing geothermal steam producers or injectors is one of the strategies for cost optimization (workover), including cut and pull casing to reline them with new completion strings that extend the life expectancy of the well. For drilling, completion, or intervention operations the geothermal industry is bridging the gap with cutting edge technologies in reservoir barriers, slot recovery, side-tracks, annular barriers, stage cementing tools and wellbore cleaning solutions that are considered “ground-breaking” in the geothermal project’s optimization.

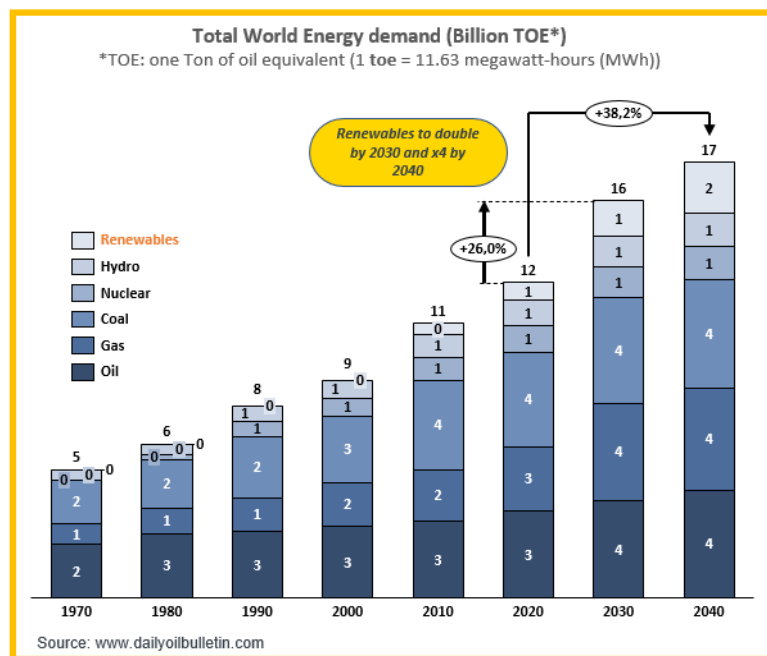
The objective of this abstract is to address the process of drilling a Geothermal well for steam production, including annular barriers that can be installed to seal possible annular leaks to maintain well integrity. Since Annulus integrity and fluid losses are one of the biggest challenges facing the geothermal industry, the cementing operations play a critical role on the success of a geothermal well. The plans for future adaption in the Geothermal industry for high-performance primary and multistage cementing operations are in place to improve the annular seal integrity in each geothermal well. This abstract will demonstrate tangible case studies from the more than 200 high-temperature geothermal wells drilled in Iceland and the global learnings from drilling wells with depths reaching 4630m and 450degC. This current geothermal drilling knowledge and the future to improve the drilling process are a perfect match for this forum. Knowledge transfer with more than 200 high-temperature geothermal wells drilled in Iceland and the global learnings from drilling wells depths reaching 4630mt and 450degC around the world in New Zealand, Nicaragua, Dominica, Montserrat, Philippines, Azores, Germany, Denmark, Switzerland, Djibouti, and St. Vincent.

Introduction

In the energy mix many models predict a steady growth in energy consumption between 1% to 1.5% per year through 2040 and the renewables and natural gas are the largest contributors to energy supply growth through 2040 while Oil, hydro and nuclear are steady (Oil growth 1% per year through 2040) then coal consumption increases a small amount; however, more efforts need to be made to replace this polluting source of energy.

By exploring the subsurface potential beyond the traditional fossil fuels, renewables energies such as geothermal appear as one of the options for humanity to make the energy transition happen in the decades to come. By 2030 the expectations are to double the energy demand from renewables sources and to growth by 4 times in 2040¹.

Drilling wells for geothermal is a challenging task, reaching deeper and hotter wells to extract the required steam and to drill wells to reinject the water at lower temperatures. Through the years there has been many challenges and solutions that are learnings to make the drilling process more efficient and lower the cost per well.

Figure 1: Global Energy Demand B-TOE¹

Geothermal energy is one of the most fast-growing renewable energy resources to generate electricity and/or heating and cooling while producing very low levels of greenhouse-gas (GHG) emissions. Geothermal energy is stored in rock as trapped vapor or liquids, such as water or brines; these geothermal resources can be used for generating electricity and for providing heat (and cooling). Electricity generation usually requires geothermal resources temperatures of over 100degC.

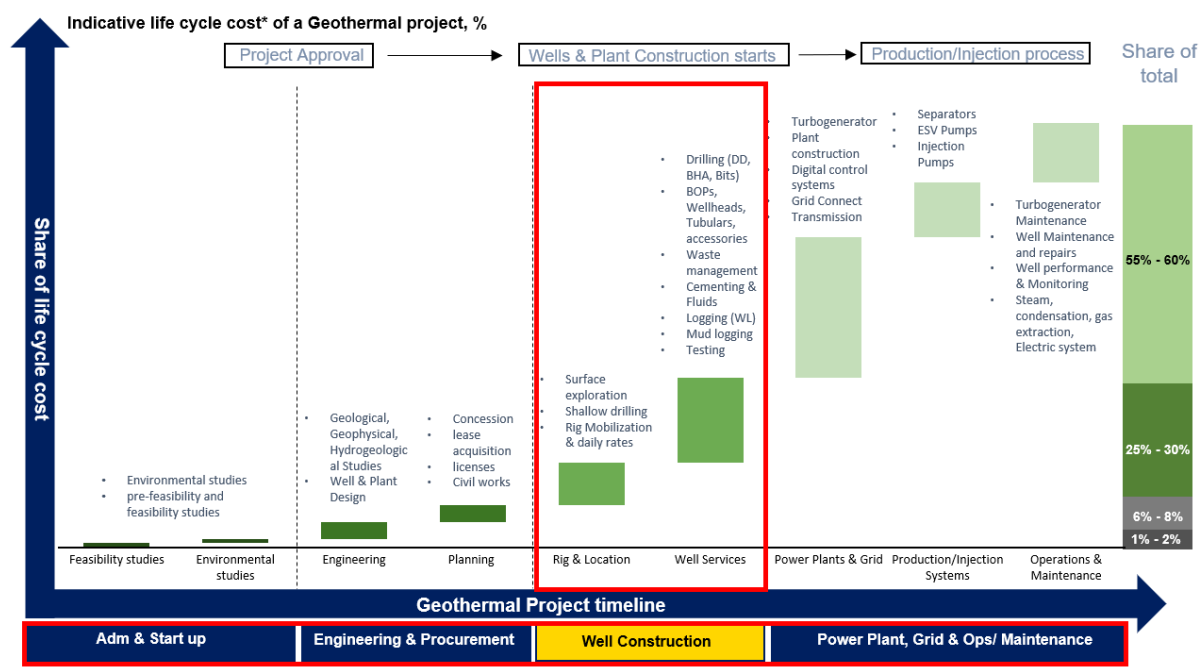
Tectonic plates and earth interior heat are key for creating the geothermal enthalpies and heat, this underground hydrothermal system feeds reservoirs with hot water systems below boiling point (due to pressure) that can be reached by drilling techniques like the ones used in the oil and gas industry, however it is important to highlight that a geothermal reservoir is quite different from an oil or gas reservoir, or even a ground freshwater reservoir as the geothermal system depend on heat flow and geological setting (permeability).

Depending on reservoir pressure and temperature; geothermal plants can be fed with two-phase flow, hot brine, steam, or both, also known as **Dry steam, Flash steam, and Binary cycle**:

- **Dry Steam Plants:** These were the first type of plants creating electricity from geothermal. They use underground steam to directly turn the plant's turbines.
- **Flash Steam Plants:** These are the most common plants. These systems pull deep, high pressured hot water that reaches temperatures of 182°C (360°F) or more to the surface. This water is transported to low pressure chambers, and the resulting steam drives the turbines. The remaining water and steam are then injected back into the reservoir source from which they were taken.
- **Binary Cycle Plants:** This system passes moderately hot geothermal water through out a liquid, usually an organic fluid, that has a lower boiling point. The resulting steam from the organic liquid drives the turbines. This process does not produce any emissions and the water temperature needed for the water is lower than that needed in the Flash Steam Plants 121°C - 182°C (250°F – 360°F).

1. Geothermal Projects life cycle

Challenge: The capital intensity and expenditure (CAPEX) upfront is the biggest hurdle for the geothermal projects to become a reality, with the power plant, grid construction and operations being more than the 60% of total CAPEX plan. In terms of geothermal well construction and drilling costs, it could range between 25 to 30% of the total CAPEX, with the biggest challenge on the drilling activities and success rates to produce steam/hot water; for example, in the O&G industry, operators could make economical projects with 10% of success rates on wet wells (containing oil and gas) but in the geothermal projects, operators need 90% success with steam or hot water production from wells.

Figure2: Archer² and Iceland Drilling's Geothermal project cycle³

Solution: as described in the Figure1, the global demand for energy is on a sharp increase and sources may need to be diverse with a mind set to make a more sustainable energy mix with less greenhouse effects for the planet. In this effort Europe is leading the energy transition with 5,5GWth⁴ installed capacity of geothermal electricity generating a turnover on utility sales of more than €1B/yr. The total CAPEX to growth the geothermal market globally is expected to growth from \$4B in 2020 to \$7B by 2025⁴ allowing many more geothermal projects to become economical with a global average of 7MWh per well drilled.

To overcome the challenge of drilling success for geothermal wells, experience in the market is the key solution. Iceland is a country well known for being the leaders in geothermal projects in the country as the geothermal energy is 4 times more powerful than solar energy in the country. These facts have made Iceland Drilling (Jarðboranir³) the most experience geothermal drilling company globally, with close to 300 geothermal wells drilled since 1970, thereof 200 for the last 10 years in all kinds of environments, in well depths up to 4.630 meters and temperature up to 450°C. Iceland Drilling provides hydraulic onshore rigs with the highest safety standards by a high degree of automation. The rigs are undoubtedly the most modern rig equipment on the market today, characterized by low noise emission, limited area required for operation and low height of the telescopic mast. The high flexibility combined with high mobility increase the efficiency of the drilling projects and make operations on remote, small, and sensitive locations possible. Iceland Drilling operates 7 rigs, sizes from small truck-mounted rigs for core drilling up to rigs with 3.500 kN lift capacity.

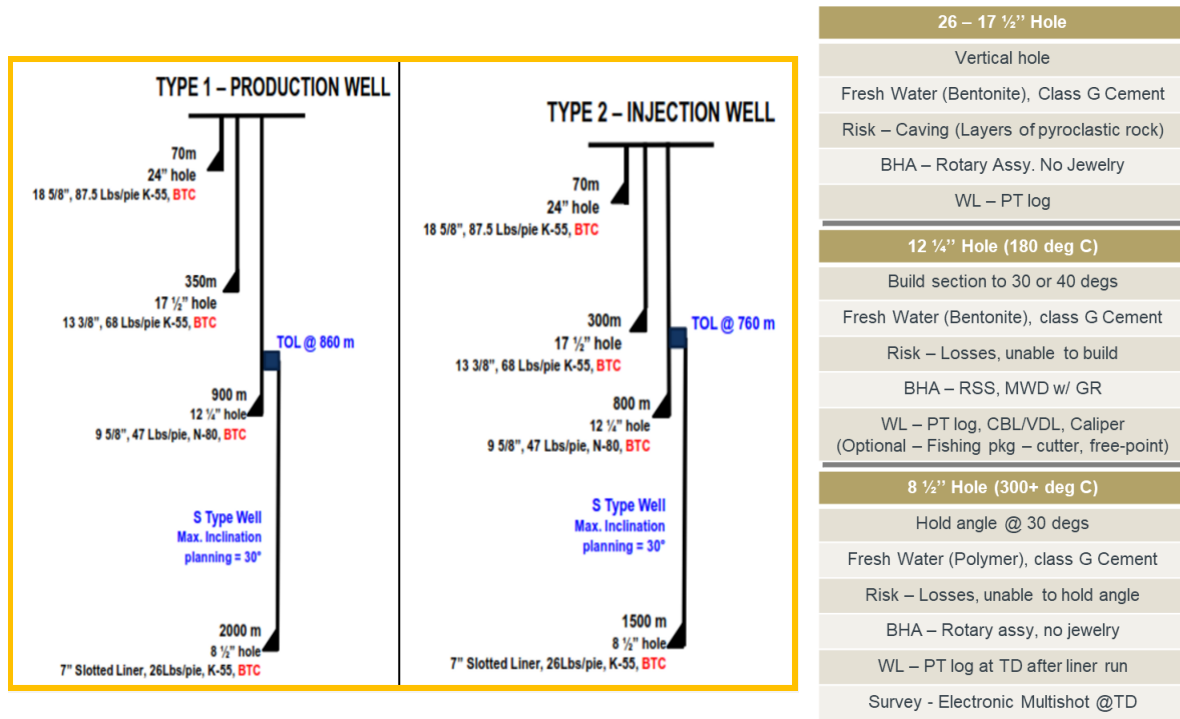


Figure3: Typical Geothermal and Injector well design and Drilling Program

More geothermal projects can become viable with few tactics, such as *Integrated drilling solutions*, in this way the geothermal industry is becoming more cost effective in the project delivery, meaning that drilling companies can procure all the different materials and services needed for the drilling operation. Secondly, *direct project investment* from drilling contractors, as some drilling companies have in their scope of business a possibility of investing in the project that they are participating in. e.g., a step-in equity investment was in the 1,000MW Corbetti project in Ethiopia from a drilling contractor from Iceland.

Since well construction can range between 25 to 30% of the total project's CAPEX, standardizing the geothermal wells, when applicable, for drilling process is a good tactic to gain efficiencies. Typically, a 24" surface casing, 13-3/8" Intermediate casing, 9-5/8" production casing and normally a slotted (pre-perforated) 7" liner as presented in Figure3 are the norm. These casings are typical sizes used in the oil industry, which immediately gives access to the geothermal industry for the downhole Oiltools, completions accessories and technologies that fits from surface casings to production casings where temperatures are lower than the steam reservoirs.

2. Optimizing Geothermal Drilling, Completions & Intervention Operations with Downhole Oiltools Technologies

Challenge: During the geothermal wells construction, or during the well re-entry (workover) on existing geothermal steam producers or injectors, using the know how and technologies from oil field services companies is one of the strategies required to tackle the challenges on geothermal completion reline for well life extension, whipstocks systems to drill lateral exit windows, and techniques to abandon properly non-economical steam reservoirs, and since annulus integrity and fluid losses are one of the biggest challenges facing the geothermal industry, the cementing technologies play a critical role on the success of a geothermal well.

Solution: the geothermal industry needed to merge the drilling know how from the experiences gained in Iceland with the innovative technologies from the oil field services bridging the gap in this way between geothermal and oil field services. The current portfolio offered in the O&G sector can optimize the geothermal operations in both segments, power generation and district heating, where drilling, completion and well intervention operations need efficient solutions and optimized products to keep the well construction cost under control.

In addition to new wells construction, well re-entry/repurposing on existing geothermal steam producers or injectors is one of the strategies for cost optimization, including cut and pulled casing to reline them with modern completion strings that extend the life expectancy of the well. For drilling, completion, or well intervention operations the geothermal industry is bridging the gap with cutting edge technologies in reservoir barriers, slot recovery, sidetracks and whipstocks systems, mechanical annular barriers, stage cementing tools and wellbore cleaning solutions that are considered “groundbreaking” in the geothermal project's optimization.

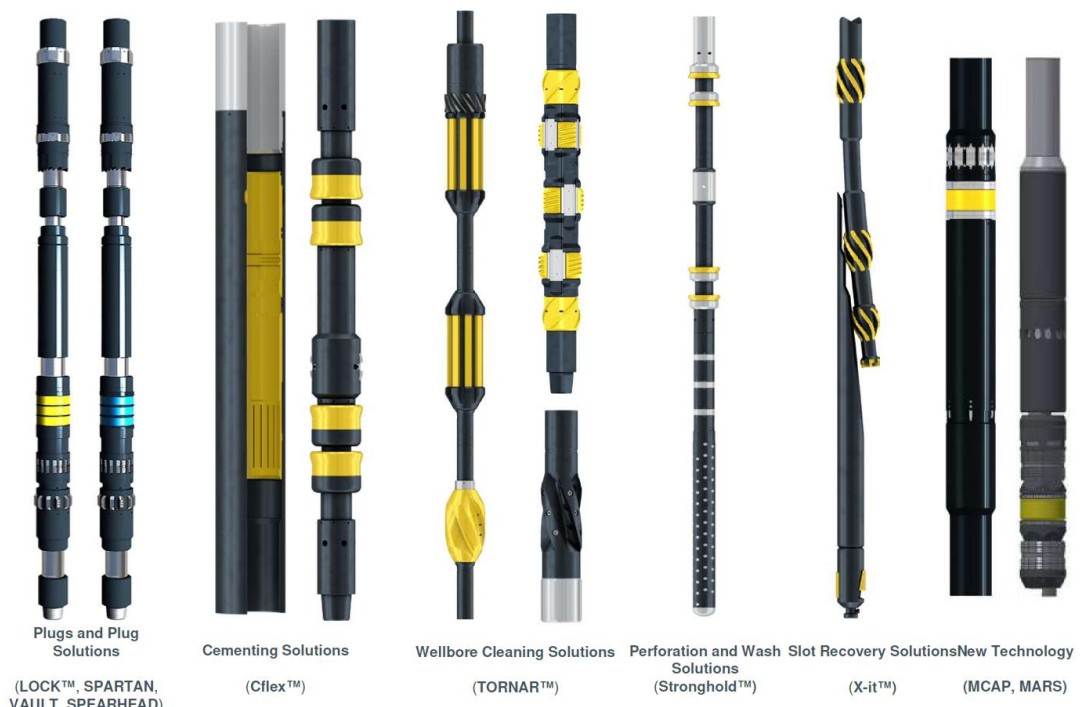


Figure 4: Archer² Drilling, Completions & Intervention portfolio

During installation of new casing strings, the mechanical annular packers can be installed to seal possible annular leaks to maintain well integrity since annulus integrity is one of the biggest challenges facing the geothermal industry. Multistage cementing solutions enables high-performance cementing operations improving the annular seal integrity in the well.

During well interventions, the single trip cut and pull system allows an efficient casing string(s) removal to allow drilling sidetracks using the whipstocks technologies. For wells not producing geothermal steam/brine anymore, they must be sealed-off properly using the cross-sectional cement and annular barriers acting as an absolute seal and cement cap to avoid leakages to the surface. As result, geothermal operators in Europe, Southeast Asia Latin America and Africa have already benefited from these technologies during well construction or well re-entry, delivering a more cost-effective operation.

3. Whipstock Successfully Expedited Large-Bore, Dual String Casing Exit

in a Geothermal well in Europe.

Challenge: A Company drilling on Geothermal wells in Continental Europe required a clean, full-gauge window and rathole for side-tracking with an 8 1/2" directional drilling assembly in a geothermal well. The exit window would be through dual strings of 13 3/8" & 18 5/8" casing, at 607 mMD. This was an old well with limited well information, no casing tallies and uncertain cement conditions on the outside of the casing.

Solution: A 13 3/8" cased hole whipstock mechanical system was run with a 12 1/4" Single Trip Tri-mill spaced out with an additional 12 1/4" Utility Mill configuration. There was no requirement to orient the whipstock prior to setting. The whipstock assembly was then run, and anchored. The anchor was triggered on top of a cement plug. The single trip mill was released from the whipstock and window milling commenced with a combination of using rig top drive and a downhole mud motor due to limitations of the drilling rig. The window and rathole were successfully milled. The mills were found to be within acceptable gauge loss tolerance, and in excellent condition when back on surface. The subsequent 8 1/2" OD drilling assembly passed through the window and drilled ahead the planned 8 1/2" section.

The whipstock System enabled the drilling company to lock the whipstock assembly against the casing wall during milling, drilling, and completion. Ensuring that the whipstock did not impact operations. A 12 1/4" window was provided at 616 mMD, and the exemplary execution of the dual string-exit solution enabled the drilling company to return to drilling operation and to avoid skidding the rig and redrilling the well.

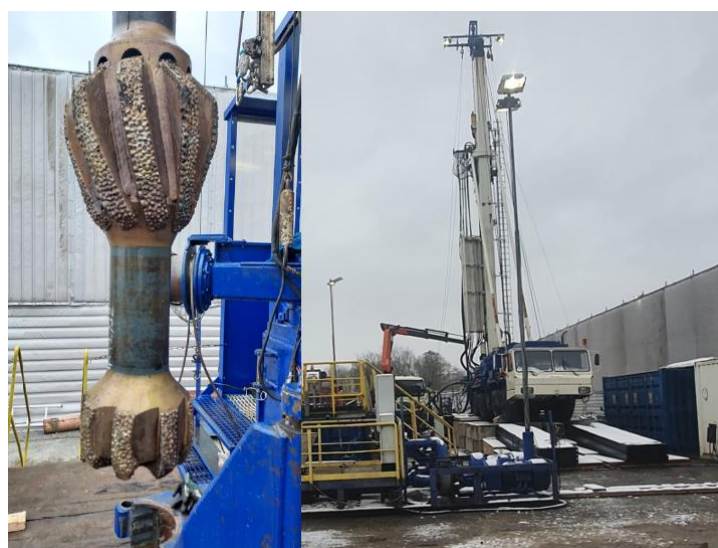


Figure5: Archer's X-it® system & Fangmann Energy Services⁵

4. Repurposing a Geothermal well by exiting the 9-5/8" casing in a challenging environment in Europe.

Challenge: in the geothermal wells drilling, reusing the slot is economically more attractive than drilling new wells; for this reason, abandoning non-producing sections and then side-tracking at the production 9-5/8" casing with no cement behind the casing in a geothermal well becomes a challenging operation.

Solution: after abandonment of a lower geothermal well section not producing steam anymore, drilling-out a lateral window in the 9-5/8" casing using a whipstock system in a single run became a challenge. The window milling was performed very efficiently, and mills returned

to surface 100% in gauge and in excellent condition. The casing exit was in a challenging environment with no cement outside the casing in the kick-off interval.

An 8 ½" Motor (1,5 deg. bend) Directional BHA was used to drill a "pocket" of 25 m to avoid tracking the old wellbore, this assembly entered the window & drilled the planned section without any issues, and then an 8 ½" RSS Directional Drilling BHA was utilized to complete the 8 ½" section, this BHA also entered the window without any problems.



Figure6: Archer's X-it® system

5. Stuck BHA and parted drill-string recovery in a geothermal well

Challenge: Tools and equipment could get lost in the hole for a variety of reasons. In drilling operations, common causes of fishing are a result of a twist-off or parted drill string, or a stuck pipe problem result of formation differential pressures or formation collapse. On geothermal wells, some fishing jobs can go on for months before the fish is retrieved, and after a period, the cost of fishing operations and rig time becomes prohibitive. For a drilling geothermal operator, that was stuck with a 17 ½" directional BHA at 841m, became a challenge to recover the BHA after trying many other means unsuccessfully.

Solution: When drilling a 17 ½" section in a complex geothermal well with high temperatures and fluid issues, an operator working in drilling geothermal wells, picked up the drill-string to ream the hole, resulting in a stuck BHA. Rotation and vertical movement were all lost. When attempts to free string failed, a special recovery plan needed to be in place to free up the stuck BHA.

The drill-string was manipulated free with a combination of jarring, torque technics, and pumping water, soap, and air down the drill-string. During well cleaning operations, the drill-string got stuck again, and drill-string parted unexpectedly while working string due to fatigue. The fishing assembly was run in, and the fish engaged with a tool overshot. Again, the stuck

string was work free with a combination of jarring, string manipulation and pumping water, soap, and air down the string.

The freed BHA was pumped and worked out of the well due to drag and excessive returns of cement. At surface, the BHA was visually inspected, and a 100% recovery was confirmed.

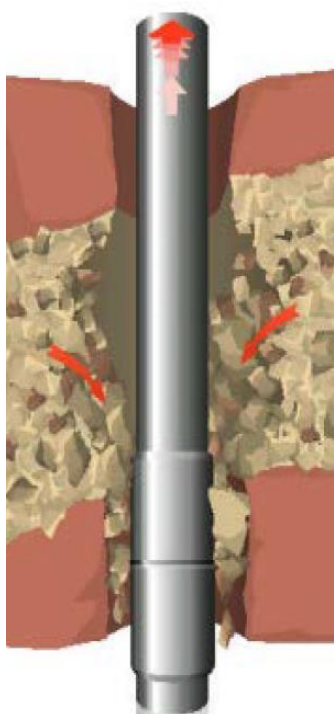


Figure7: Stuck pipe problem results of formation collapse



Figure8: Overshot to fishing drilling pipe

6. Multistage cementing in geothermal wells

Challenge: a geothermal operator in the Southeast Asia needed to cement the annular in 3 geothermal wells with known fluid losses. A high-performance multistage cementing operation improving the annular seal integrity in the 3 geothermal wells was a requirement for the production casing as there were plenty fluid losses experienced during the drilling process, then a primary and secondary cementing job were planned.

Solution: a multistage cement tool and open hole packer solution proposed was a 2-stage cement job utilizing an inner string that would allow efficient, accurate and effective placement of cement around all target zones. The primary job was performed through an supplied tag in float system allowing the packer to be set and the multistage cementing tool opened before the 1st stage cement set up.

The open hole packer situated just above the loss zone, was then set, to isolate the losses and provide a fundament for the column of the 2nd stage cement job. After the packer setting, the multistage cementing tool, directly above it, was opened with the inner string cementing tool and excess cement was circulated out from the first job. A 2nd stage cement job was then performed through the multistage cement tool above the open hole packer, providing the ideal well integrity in an scenario of fractured zones that created fluid losess during the cementing operation as described in figure9.

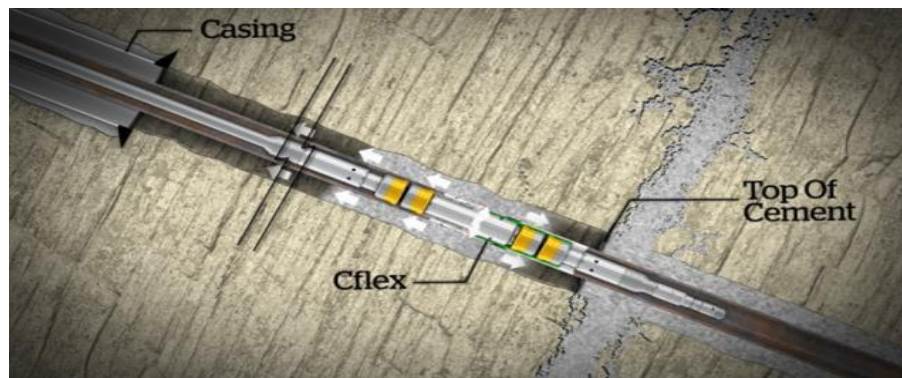


Figure9: Archer's CFLEXt® system 2nd stage cementing due to fluid losses

Conclusions:

- Geothermal drilling can easily benefit from the technologies from the oil and gas industry.
- 25% to 30% of the total capex is for drilling new wells (producers & injectors), experience, know-how and integrated well services from the drilling contractor are key for the success of any project.
- Majority of the new wells drilled for dry steam or flash steam have reservoir temperatures above 175°C (350°F) that are the maximum temperatures in the O&G industry, however many of the completions, downhole tools and accessories can be used at depths where temperatures are more accessible (depending on the temperature gradients).
- Geothermal new wells drilling efficiencies are available only if close contact between operators, drilling contractors and service companies happen during the well design.
- O&G technologies fit the existing wells repair and interventions (workover) needs in the geothermal space making the projects more cost effective.

References:

- [1] Dailyoilbulletin and the global energy demand – dailyoilbulletin.com
- [2] Archer Oiltools - Downhole tools for Geothermal – archerwell.com
- [3] Iceland Drilling – Geothermal drilling specialist - jardboranir.is
- [4] RYSTAD Energy, Norwegian data analitics – rystadenergy.com
- [5] Fangmann Energy Services – Geothermal services- fangmannenergyservices.com

Optimize and de-risking the execution of Geothermal wells through real-time drilling interpretation

P. Ferrando, N. Abolins
SLB Company, Paris, France

Abstract

In a costly geothermal well construction environment, effective communication is essential for decision-making to ensure safe optimization of operational sequences, drilling performance, and wellbore assurance, resulting in consistent delivery of wells according to plan. It is crucial to establish a close and efficient loop between the stakeholders on the rig and office. Remote decision-makers require information based on the analysis and processing of rig data to take efficient action when operations deviate from the prepared drilling program.

As modern well construction becomes increasingly complex due to technical challenges and economic constraints especially where the drilling is an important part of the geothermal project, operators strive to improve performance by remotely interpreting real-time well operations data. The approach varies depending on the operator and the well's challenges.

To meet customers' needs, our service is tailored to their processes and workflows, expertise level, and technical challenges. This service provides customized workflows and dedicated applications based on the well's technical challenges, enabling each customer to achieve their drilling objectives. Ultimately, the service aims to promote safety by early prevention and mitigation of drilling hazards and continuous improvement in well construction performance.

To enable our clients to drill safer, faster, and more cost-effectively in geothermal wells, we have developed a dedicated workflow and communication protocol between our remote interpretation team and the execution team on the rig.

Introduction

The primary goal of drilling geothermal wells is to execute the drilling program safely and efficiently, while staying within the allocated budget. Typically, the cost of drilling a well accounts for 35 to 50 percent of the total capital costs of a geothermal project. Achieving this objective requires reducing non-productive time and ensuring compliance with environmental regulations. Drilling operators are constantly exploring new drilling methods to increase efficiency and reduce drilling time. The entire well construction process must be examined, from planning to post-drilling activities, to ensure continuous improvement in well execution.

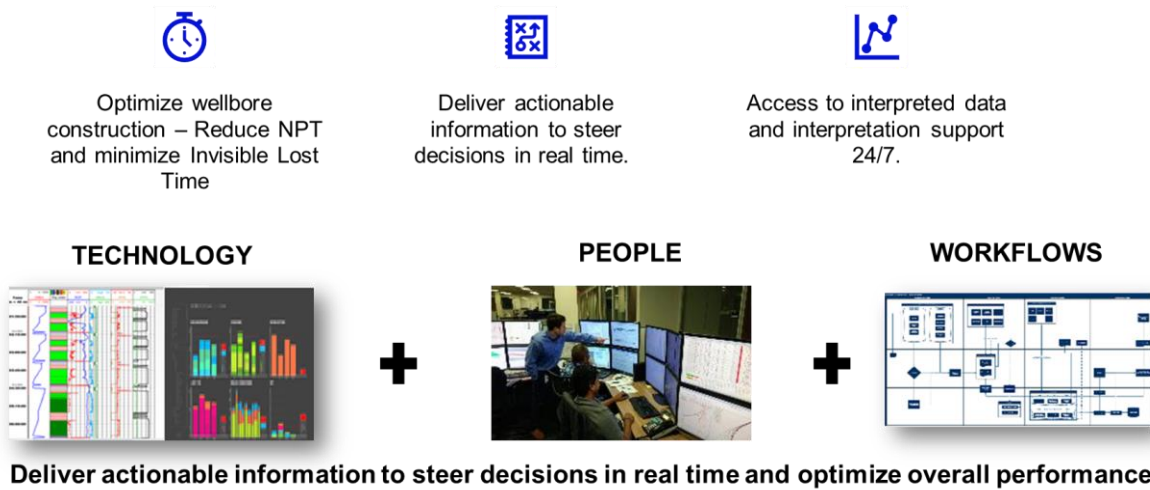
One of the major drilling problems encountered in geothermal drilling is lost circulation, which refers to the loss of drilling fluid to pores or fractures in the rock formations being drilled. This issue can lead to wellbore instability, pack-off, and stuck pipe, making it crucial to closely monitor mud properties and ECD management to prevent it and prevent flat time.

This paper discusses how real-time interpretation services can be used to continuously de-risk the well execution process. The paper describes the workflows used to control all drilling services provided on the rig during the geothermal well execution. It also provides a clear overview and summary of what was achieved and how it was done, and can be communicated to government institutions if required.

Real-time interpretation services are essential to ensure insurance coverage for drilling activities, particularly in areas close to cities.

The remote interpretation service is a combination of software suites, tailored workflows, and well-trained operational analysts who support end-to-end well delivery through planning, operational surveillance, performance diagnostics, and optimization.

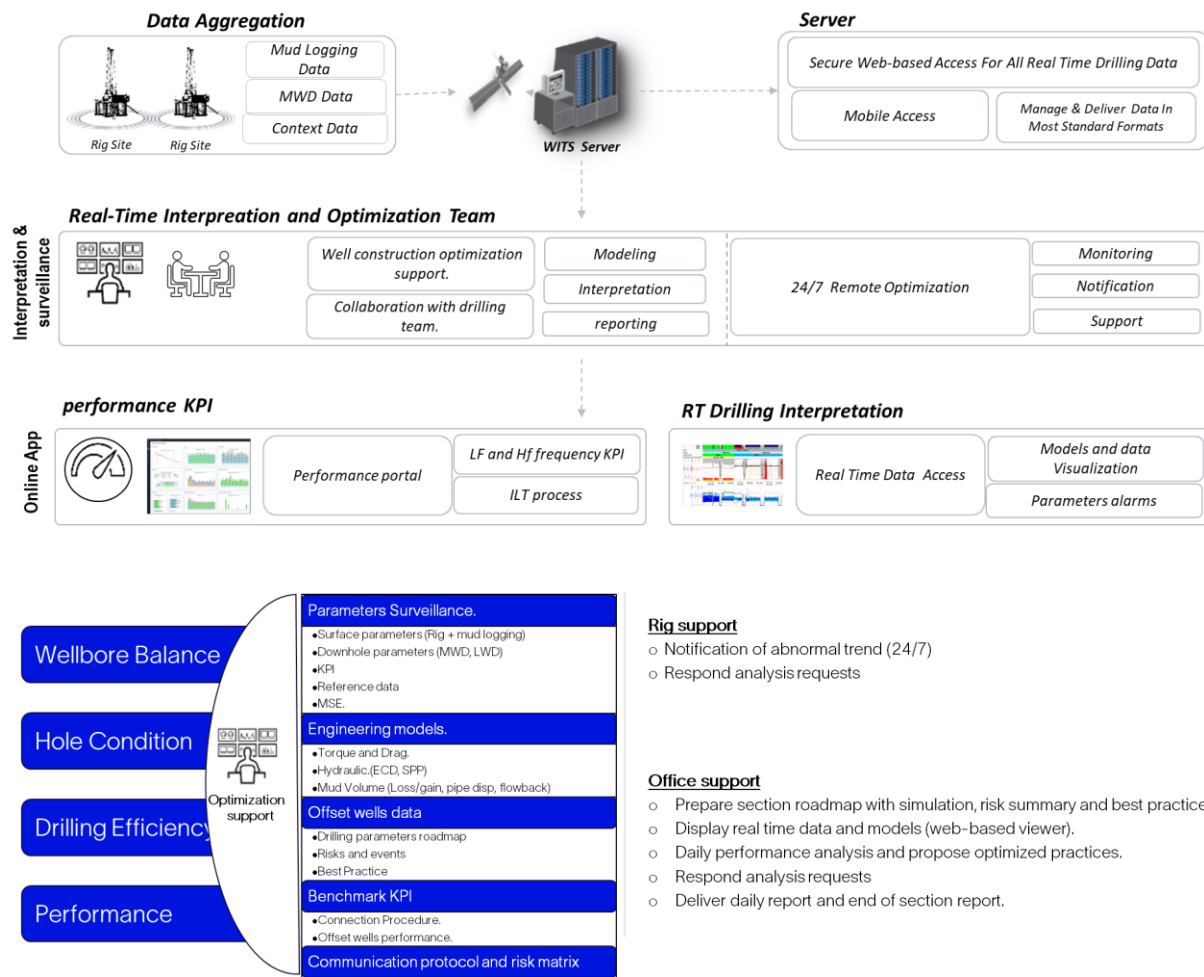
The general workflow involves real-time data streaming and visualization, well modeling and optimization, 24x7 remote monitoring and surveillance, and well performance analytics. These workflows transform real-time data into actionable information and encourage collaboration between multi-disciplinary teams to increase efficiency.



Deployment Solution - Data streaming and Visualization

Real-time data streaming provides a seamless connection between essential information and the right people. This technology aggregates, distributes, and visualizes well data - including surface mudlogging and downhole drilling data - providing valuable insights into rig operations from remote office locations. Real-time data transmission utilizes WITSML protocol which is the main standard of data sharing in the industry.

The real-time data is stored on a unified platform that enables the monitoring of rig operations and facilitates knowledge acquisition among well engineering and subsurface people. By updating Drilling models, drilling experts can make rapid and informed decisions.



The real-time interpretation and optimization team utilize advanced analytics to transform real-time data into meaningful and actionable information. Proprietary logic, capable of automatically detecting 17 types of rig activities, is embedded into the monitoring application to segregate live data into greater granularity before being fed into live computation of torque and drag and hydraulics models. The monitoring section is staffed by optimization specialists drawn from both logging while drilling and surface data logging disciplines who work 24x7. Their primary focus is to act as a second set of eyes and provide intervention and recommendations to rigs in order to improve efficiency and reduce operational risks. By incorporating the results of optimized well design and offset benchmarked performances, the optimization specialists ensure that each activity falls within operating margins and investigate any deviations in wellbore conditions. Real time monitoring display, tailored based on activity types, are shared with drilling supervisors to facilitate effective communication between rig and office and enable quick knowledge exchange to aid the decision-making process. In addition to monitor the data for warning signs of operational hazards, the optimization specialists also highlight areas for improvement in each operation that can be reduced in time based on allowable operating margins and pre-agreed performance targets.

During the performance and optimization tasks, the interpretation team perform correlative analysis of historical data for drilling and completion performance benchmarking and tracking. The performance computation tools utilize the identical rig states detection engine built into the monitoring application, aggregate data from multiple sources, including surface logging data and daily operation reports. By statistically comparing activities and measuring effective micro-KPIs, the tools identify invisible lost time and underperforming activities, as

well as best practices.

This approach enables teams to spend less time on data mining and more time understanding performance limitations by comparing with a global dataset. The daily operation performance benchmarking process facilitates performance-related discussions among the team during morning meetings, allowing for greater improvement of drilling efficiency and reduction of invisible lost time (ILT) without compromising hole conditions.

Planning stage

During the planning stage, the interpretation team collaborated with the customers to develop a tailored communication protocol aimed at mitigating risks during the well execution process. This key documented process outlines the potential risks, optimal strategies, and benchmarks for each section of the well, and is prepared in coordination with the client drilling team.

By providing streamlined communication to key personnel, this protocol helps prevent early changes or deviations from the expected model, reducing non-productive time and ensuring timely completion of the project. In short, an effective communication protocol is crucial for de-risking the well execution process and maximizing productivity.

The team is extracting and analyzing information from multiple wells in the database and using engineering models to create a drilling roadmap that provides an accurate outlook of the subject well. This roadmap includes expected drilling parameter ranges, anticipated risks, and time estimates for each section.

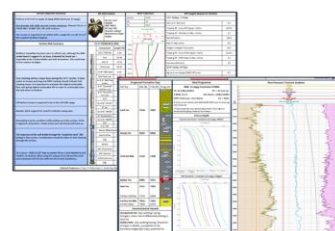
During the execution phase, the dynamic roadmap is used to ensure that the drilling parameters remain within the optimal range. This guidance helps to minimize destructive drilling dynamics and maximize penetration rates, which ultimately leads to a more efficient and effective drilling process. In summary, the team's use of the drilling roadmap is a key factor in ensuring the success of the drilling operation.

Planning Stage

Communication protocol

- It is developed and agreed upon with the client as well as the alert criteria for abnormal well condition

Comm. Protocol Collaboration



- Road Map**
- Gather Qc'd data from historical wells
 - Synchronize by top of formation on subject well trajectory
 - Analyze statistic
 - Create parameters envelop.
 - Compare with design limiters.

Road Map & Comm. Protocol Risks Identification

Well Execution

The interpretation team plays a central role in all aspects of well construction, from initial planning and design optimization to well operation advisory services, performance tracking, and the final review of lessons learned. To facilitate digitalization in this environment, we

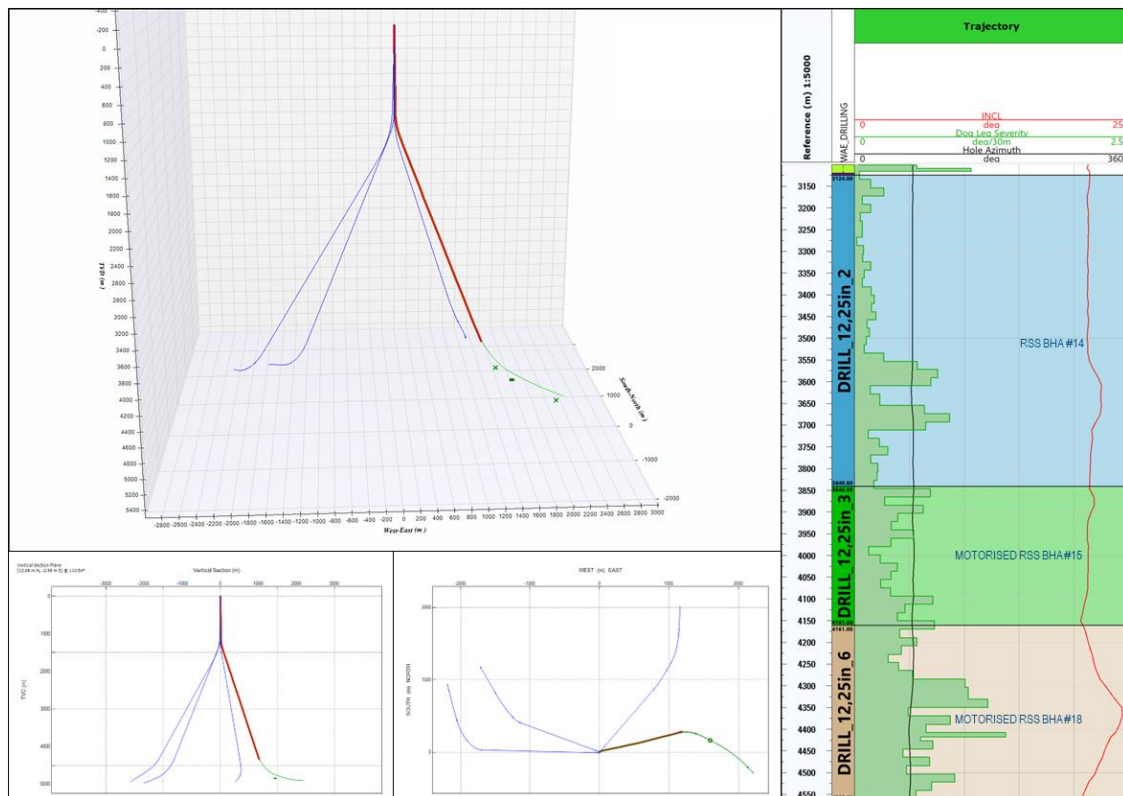
have implemented several key workflows:

- Standardization of performance measuring and reporting procedures to ensure consistency and sustainability in the performance improvement process.
- Automation of existing digital workflows, including performance tracking and reporting of key metrics.
- Managing performance-driven demand through detailed analysis of historical well information.
- Improving ECD management through Torque and Drag tracking, mud properties tracking, and surge and swap calculation.
- Enhancing the Drilling Efficiency & Optimization workflow.

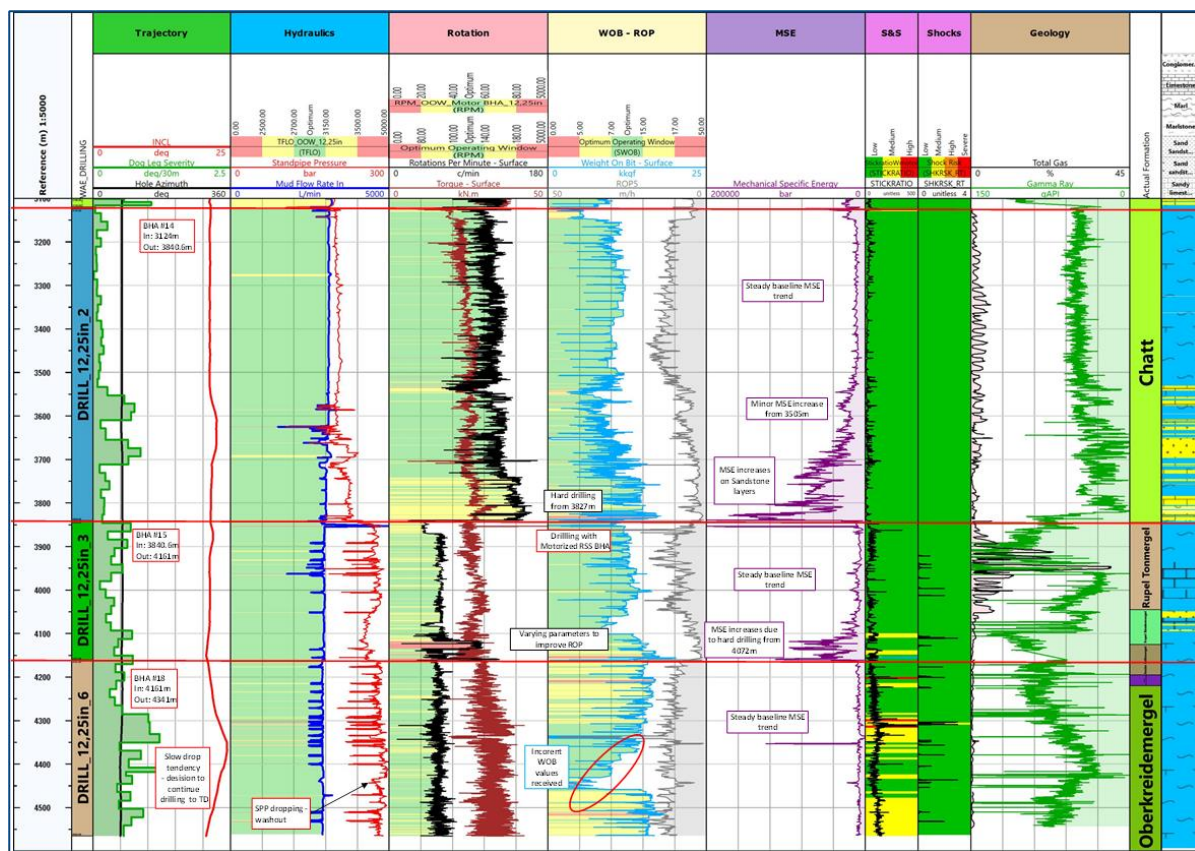
By executing these workflows, we aim to streamline operations and improve overall performance, while leveraging data-driven insights to inform decision-making and drive continuous improvement.

Example of deliverables provided for Geothermal well done in Germany

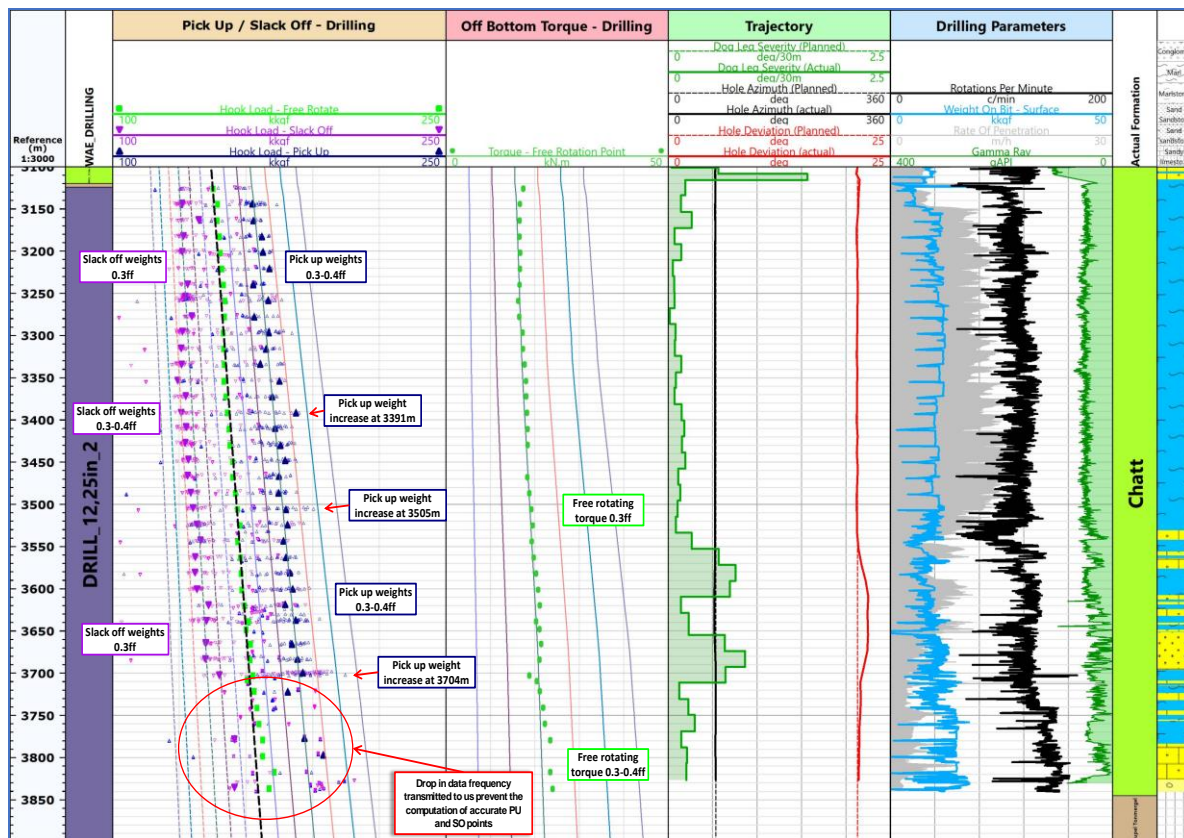
Trajectory Monitoring (global overview):

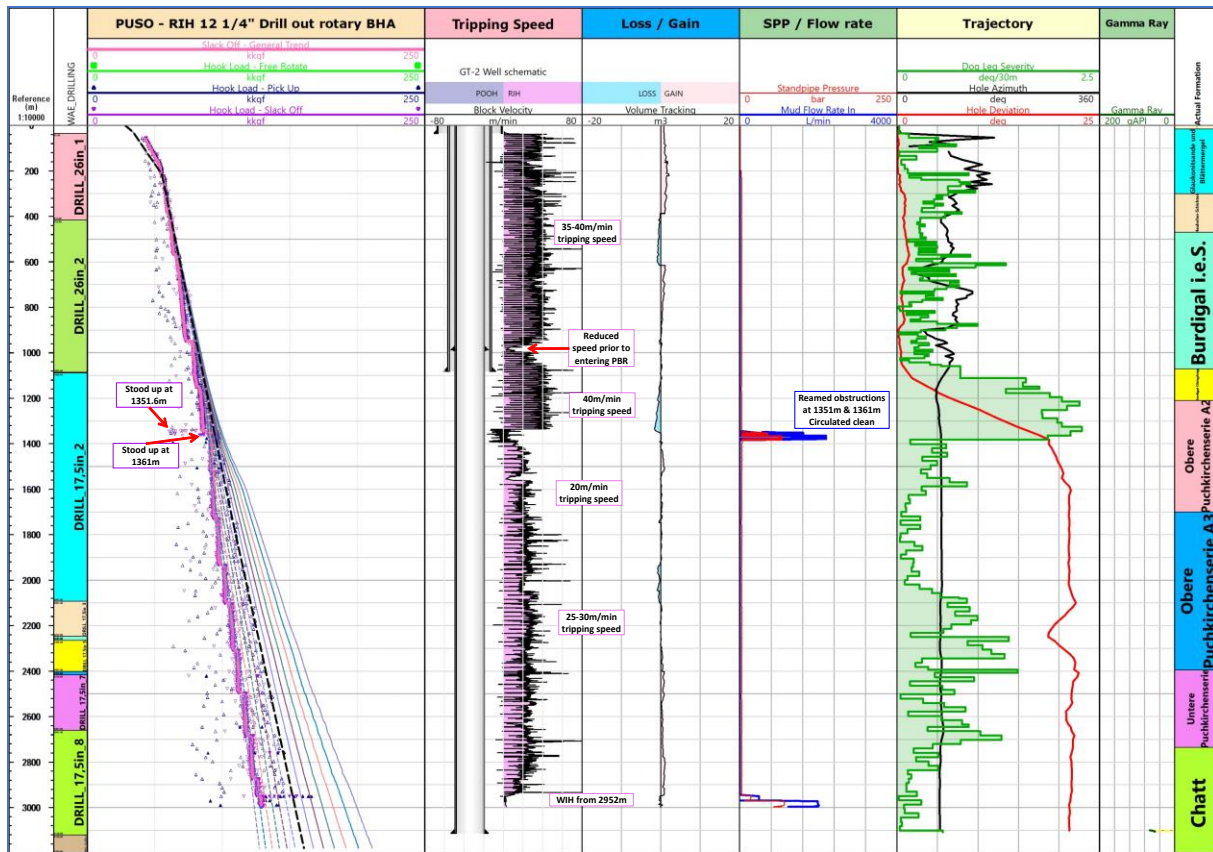


Drilling Tracking (12.25" Section overview):



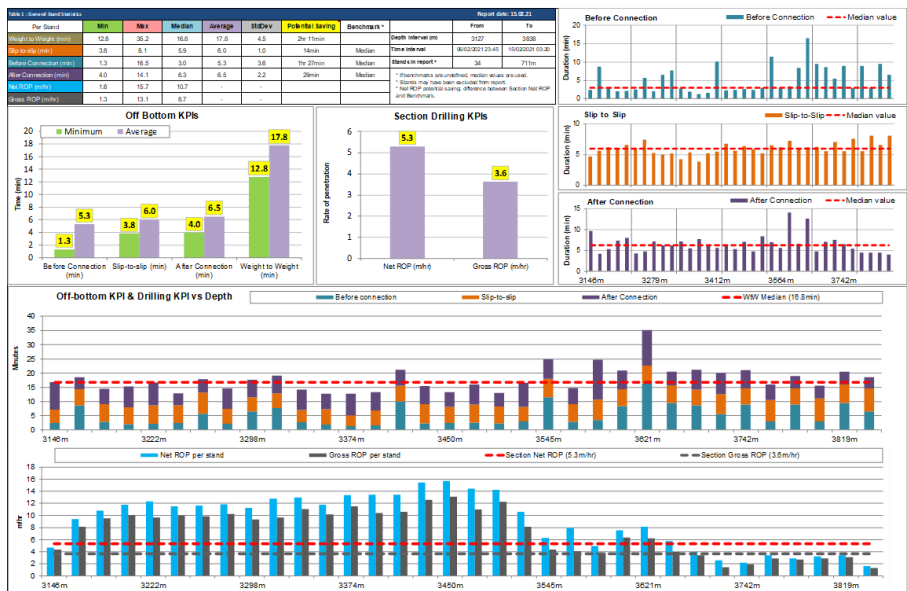
Torque and Drag tracking – Drilling and Tripping (12.25" Section overview)::





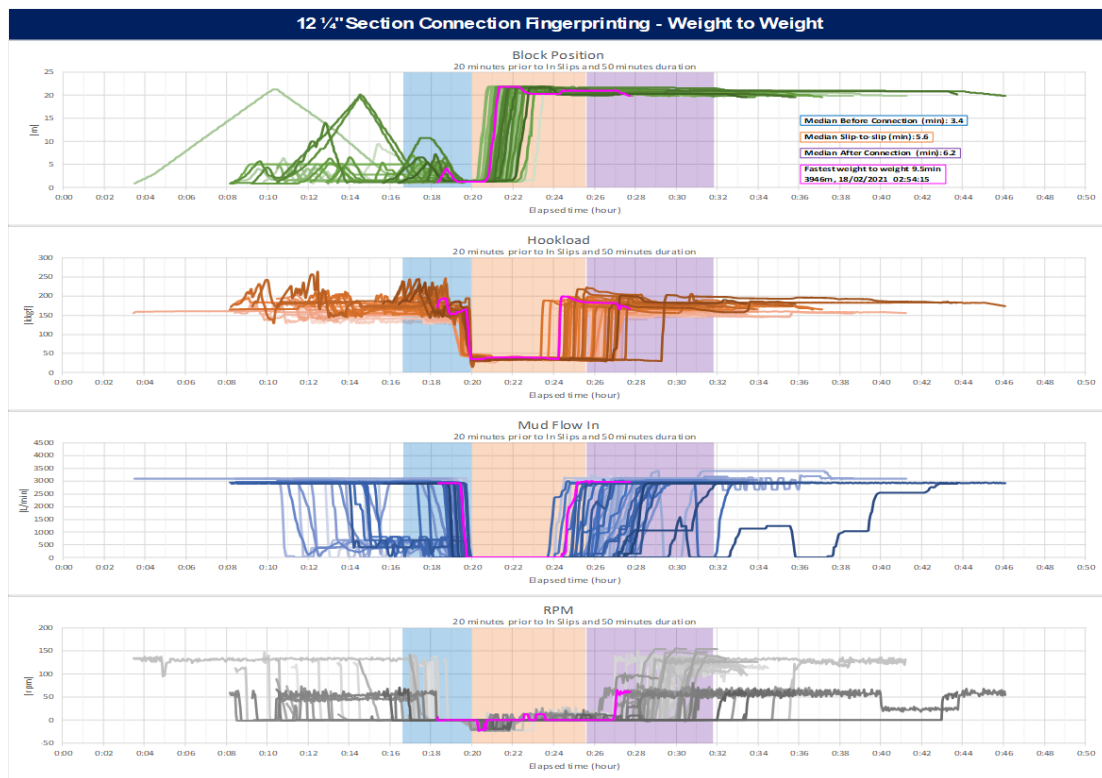
Performance Traking (12.25" Section overview):

12 1/4" SECTION - DRILLING AND CONNECTION STATISTICS – BHA #14



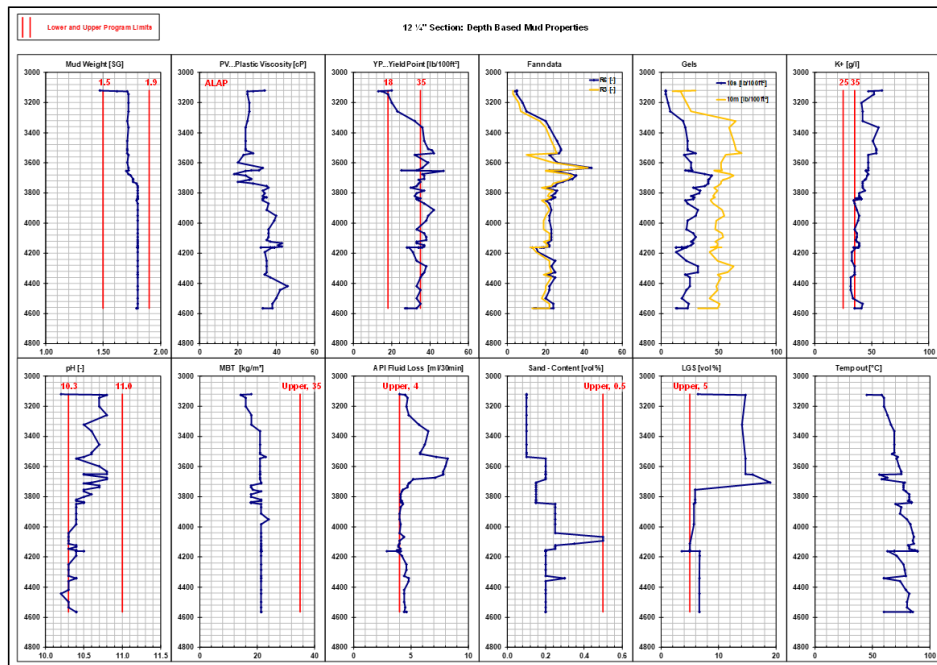
12 1/4" section, BHA #14:

- Before Connection practice was generally inconsistent with the greatest variance when compared to Slip to Slip and After Connection practices. Backreamed full stand at 3xxx m due to increasing PUW trend. Slip to Slip times were very consistent for the entire run.
- Net/Gross ROP per stand trends were relatively consistent at the beginning of this run with 12-16m/hr Net ROP per stand until 3xxxx m where hard abrasive sands encountered which led to significant reductions in ROP. No significant divergence between Net and Gross ROP per stand was observed indicating very little time was spent off-bottom for the stands selected on this run.



Mud Properties checking versus limits defined in time and depth (12.25" Section overview:

12 1/4" SECTION - MUD PROPERTIES VS DEPTH

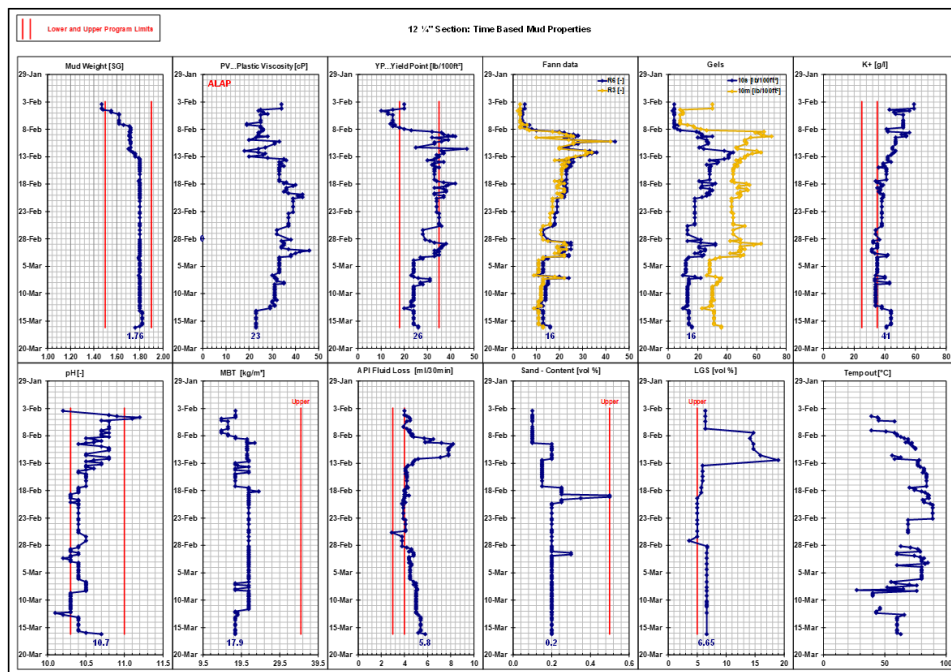


Mud properties deviating from their specifications from the onset of the 12 1/4" section, particularly for the LGS content due to the reutilisation of 17 1/2" section mud which was out of specs.

From ~3700m, mud treatment was intensified and allowed to restore the mud to its intended properties.

| Mud Properties | Fluid Specifications |
|-----------------------|----------------------|
| Active Mud kg/L 50 °C | 1.5 1.90 |
| PV cps @ 50 °C | ALAP |
| YP lbs/100 ft² | 18 35 |
| HTHP | 0 4 |
| Sand % | 0 0.5 |
| LGS % | 0 5 |
| MBT | 0 35 |
| pH | 10.3 11 |

12 1/4" SECTION - MUD PROPERTIES VS TIME



Following reaching TD a wireline run was attempted with no success. The toolstring was held up at 3920m. A C/O BHA was therefore run in hole to check the hole condition as well as the presence of junk and condition the mud prior to run the 9 5/8" liner.

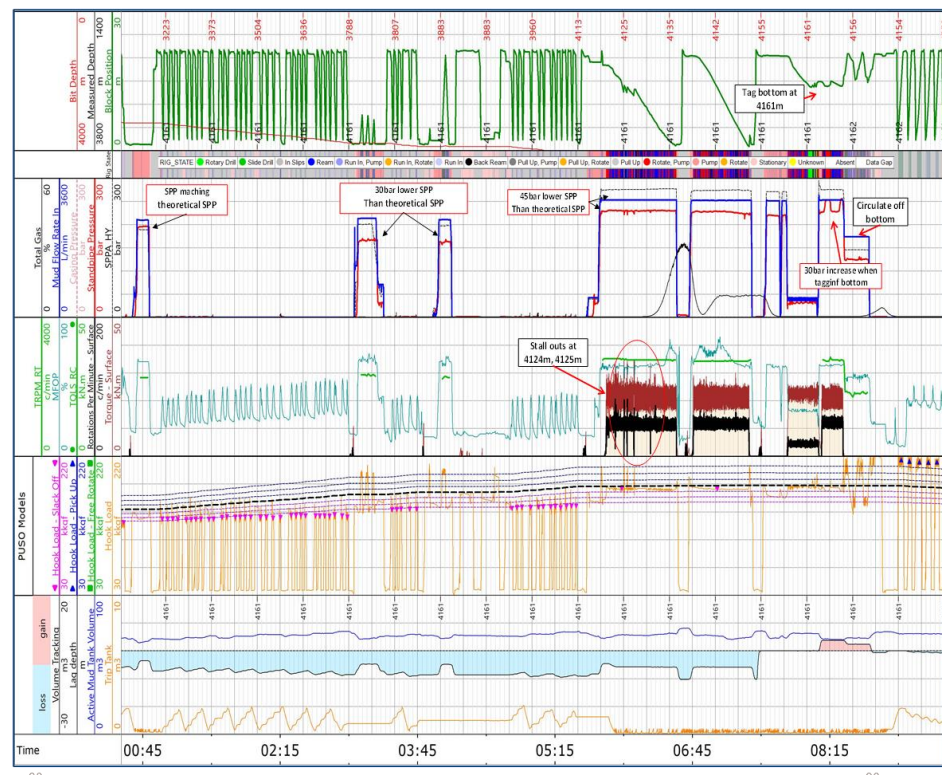
At TD, the well was circulated to mill and remove potential junk from the well (wireline centralizer and drill pipe protectors).

As illustrated in the plot on the left, the mud was kept within the specified rheology parameters from the 13th February.

The 9 5/8" liner was subsequently run in hole and cemented with no issue.

Some Key Events capture and analysis (12.25" Section overview):

12 1/4" SECTION - EVENT PLOT – PRESSURE LOSS/TWIST OFF

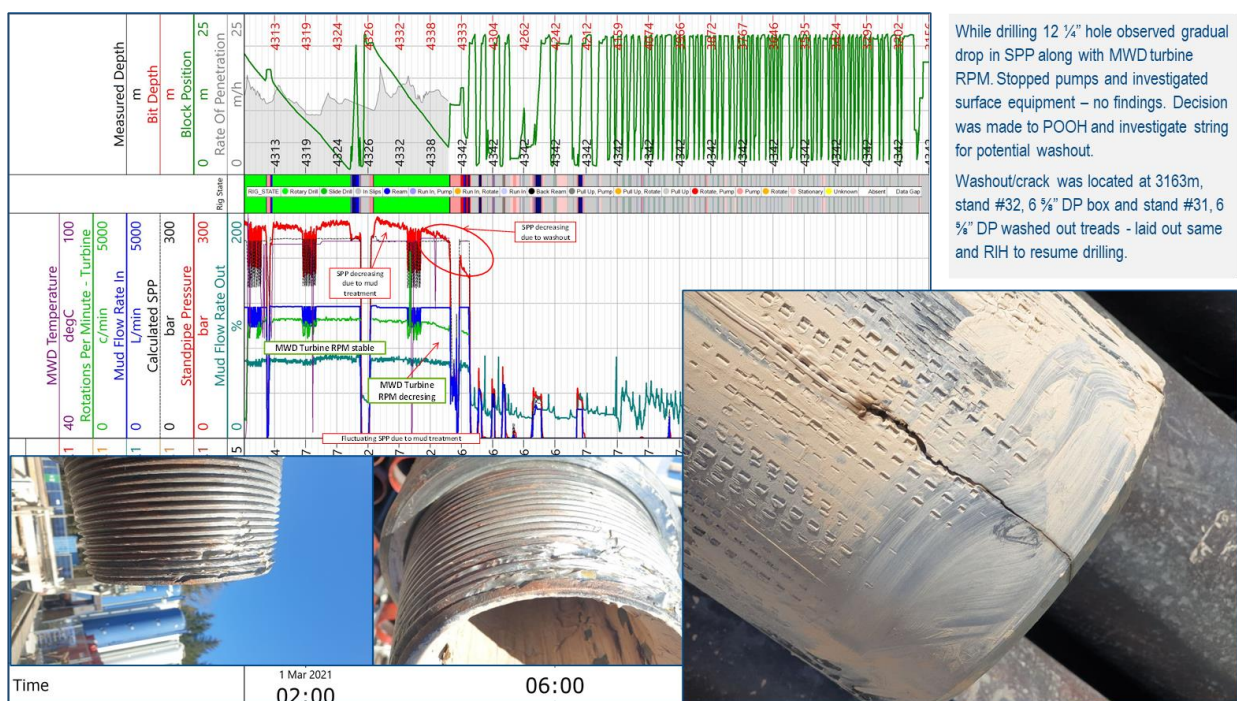


Whilst RIH with BHA #16, the pipe was filled up every 10 stands and circulation was broken every 700m - all pressures matched the theoretical values until reaching 3800m. When breaking circulation observed loss of 30 bar. The BHA was ran in hole as all surface equipment was checked. Once again, 3 stands off bottom, the pressure was found to be less than anticipated. The assembly was carefully reamed down with reduced parameters 450 rpm, and 20 RPMs. Depth was checked on the last connection and bottom was tagged with 2-3 tons with a couple of bars increase in pressure. The assembly was picked off bottom, parameters were increased to drilling parameters and the string was lowered to tag bottom. As weight was increased to 5.6 kkgf an immediate increase in pressure of 25-30 bars was observed, with no signs of progress or weight being drilled off. The decision was made to pull to surface to check the BHA.

On surface, the filter sub pin was found to be broken. The pin had sheared in the PowerDrive box. The PowerDrive and PDC bit were left in the hole.



12 1/4" SECTION - EVENT PLOT – WASH OUT AT 6 5/8" DP



While drilling 12 1/4" hole observed gradual drop in SPP along with MWD turbine RPM. Stopped pumps and investigated surface equipment – no findings. Decision was made to POOH and investigate string for potential washout.

Washout/crack was located at 3163m, stand #32, 6 5/8" DP box and stand #31, 6 5/8" DP washed out treads - laid out same and RIH to resume drilling.

Results and Evaluation:

The combination of a remote interpretation team has yielded significant results in mitigating drilling risks and establishing optimal benchmarks for geothermal well drilling in selected areas. To maintain consistency in results and ensure the drilling team and rig crew remain focused on execution, it is crucial to continue using this innovative approach.

After executing their new approach at the geothermal well, the interpretation team summarized the opportunities and lessons learned. These insights will be used to optimize future well drilling plans during the campaign.

Potential saving by section for future well:

| END OF SECTION REPORT – OPTIMIZATION AND OPPORTUNITIES FOR FUTURE WELLS | | | SAVINGS PER SECTION | |
|---|---|---------------------|---------------------|------------|
| 26" SECTION | Operational Performance – Drilling | Potential Saving | Hours | Days |
| | The main opportunity for optimisation of future wells is to improve the stability of mud properties. | 18.5 hours | 81,1 h | 3,37 d |
| | Consistency: if all the connections had been lasting the median weight to weight time, 2.6 hours would have been saved over the section. | 2.6 hours | | |
| 17 1/2" SECTION | Operational Performance – Flat time | Potential Saving | 315,9 h | 13,20 d |
| | Condition mud prior to proceed to cement job. | 67.0 hours | | |
| | Operational Performance – Drilling | Potential Saving | | |
| | The main opportunity for optimisation of future wells is to drill the section in one run. Average time spent to change each BHA: 34.6hrs.. Total time spent tripping and MU or L/D BHA: | 207.3 hours | | |
| | Consistency: if all the connections had been lasting the median weight to weight time, 6.12 hours would have been saved over the section. | 6.12 hours | | |
| | Operational Performance – Flat time | Potential Saving | | |
| | Clean out run after the wireline tools could not be run to TD. | 33.5 hours | | |
| | Condition mud prior to run the 13 3/8" run | 41.5hours | | |
| | Operational Performance - Drilling Events | Estimated Lost Time | | |
| | DDR#22, Wash out in 5.5in DP body at 924 m. L/O single and ran back to bottom to continue drilling. | 6.50 hours | | |
| 12 1/2" SECTION | DDR#69, Look for and repair leak observed while pressure testing liner. | 6.50 hours | 317,4 h | 13,22 d |
| | DDR#73, Investigate leak observed during pressure test. Noticed the upper sealing ring on plug tester has been destroyed. | 15.5 hours | | |
| | Operational Performance – Drilling | Potential Saving | | |
| | The main opportunity for optimisation of future wells is to drill the section in one run. Time spent changing BHAs: | 99.25 hours | | |
| 8 1/2" × 9 1/2" SECTION | Fishing operations after the bit and PD assembly snapped off BHA#16 | 116.25 hours | 3,8 h | 0,16 d |
| | Consistency: if all the connections had been lasting the median weight to weight time (16.8min), 4.14 hours would have been saved over the section. | 4.14 hours | | |
| | Operational Performance – Flat time | Potential Saving | | |
| | Clean out run after the wireline tools could not be run to TD. | 81 hours | | |
| 6 1/2" × 8 1/2" SECTION | Issues with MFT wireline tools. | 16.75hours | 63,2 h | 2,63 d |
| | Operational Performance – Drilling | Potential Saving | | |
| | Consistency: if all the connections had been lasting the median weight to weight time, 1.0 hours would have been saved while drilling. | 1.0 hours | | |
| | Consistency: if all the connections had been lasting the median weight to weight time, 1.75 hours would have been saved while hole opening. | 1.8 hours | | |
| | Operational Performance – Flat time | Potential Saving | | |
| | Cleared pack off at 4683m. | 1 hour | | |
| | Operational Performance – Drilling | Potential Saving | | |
| | Consistency: if all the connections had been lasting the median weight to weight time, 2.75 hours would have been saved while drilling. | 2.75 hours | | |
| | Consistency: if all the connections had been lasting the median weight to weight time, 1.4 hours would have been saved while hole opening | 1.4 hours | | |
| | SUB TOTAL | 4.15 HOURS | | |
| | Operational Performance – Flat time | Potential Saving | | |
| | Stop drilling, UTFT. Resume after conversation between SLB & HAS | 2 hours | | |
| | 50bar pressure loss while enlarging 6 1/2" hole to 8 1/2". Bullnose bit lost in hole. Fishing trip required to recover fish. | 57 hours | | |
| | TOTAL POTENTIAL SAVINGS | | | 781 h 33 d |

Conclusion

The Real-time interpretation team is a proactive approach to enhance the services of traditional real-time service at rig site. It involves the implementation of a state-of-the-art collaboration between rig and town that incorporates advanced automation and digitalization workflows, alongside existing data communication and visualization tools. This enables more proactive well design, operational monitoring, and performance optimization, resulting in improved well construction efficiency. With early detection of non-productive time (NPT) and invisible lost time (ILT) events, the interpretation team drives towards better well delivery. Furthermore, the integration of a performance-driven approach cultivates a performance mindset in the client organization, rather than relying solely on a rig team. This embeds a new way of working that allow to drill in safely manner and in the budget allocated the Geothermal well.

Experimental determination of the capillary pressure to assess hydrogen integrity in completion systems

N. Perozo, P. Jaeger

Technische Universität Clausthal, Institute of Subsurface Energy System, Clausthal-Zellerfeld, Germany

In order to quantify the risk of storing hydrogen in underground facilities, the materials belonging to a wellbore completion (cement and steel) are analyzed by using laboratory tests in presence of hydrogen at elevated pressures and temperatures. Penetrated and diffused hydrogen produces negative effects on materials. In steels, embrittlement is caused by hydrogen diffusing in atomic form through defects and interstitial spaces of the material's lattice. Recombined molecular hydrogen occupies more space, inducing cracking and severely affecting the mechanical properties.

On the other hand, the impact hydrogen has on the cements' integrity can be estimated by determining the capillary effect of this gas when being in contact with the reservoir water initially present in the cement pores. It is considered a loss of integrity in the completion once the pressurized hydrogen completely displaces the reservoir water from the pores. Gas break-through tests enable to determine the capillary pressure associated with the loss of cement storage integrity. During the test program, the cement composition was continuously improved by using different additives and by being able to adjust the cement hydration process to the real situation in the field, resulting in a continuous increase of the capillary pressure, which translates into an increase of the gas tightness of the completion system. The results obtained from the tests along with their interpretation have been confirmed by additionally determining the capillary pressure from experimental data on the interfacial tension between the fluids as well as contact angles on the solid materials involved at reservoir conditions.

Einsatz der FMEA-Methode zur Bewertung der Integrität untertägiger Kavernenspeicher

N. Bachmann¹, D. Boernecke²

¹Fraunhofer IEG, Betriebssicherheitsmanagement, Bochum, Germany, ²Fraunhofer IEG, Tiefbohrtechnik und Completion, Bochum, Germany

Zur Dekarbonisierung der Energieerzeugung ist es notwendig, sowohl die Differenz zwischen Angebot und Nachfrage als auch die Volatilität bei der Erzeugung durch geeignete Speichermethoden zu überbrücken. Hierdurch steigt derzeit die Bedeutung für stoffliche und energetische Untertagespeicher. Um die gesellschaftliche Akzeptanz für diese Form der Speicherung zu erhöhen und einen sicheren Betrieb zu ermöglichen, ist die Gewährleistung der Integrität zwingend notwendig[1].

Die bisherigen Risikobewertungen fokussieren sich in erster Linie auf mögliche Undichtigkeiten innerhalb der Primär- und Sekundärbarriere sowie auf die Gefahrenabwehr ohne eine detaillierte Fehleranalyse auf Bauteilebene vorzunehmen. Empfehlenswert ist es jedoch die Barrieren in ihre Barriereelemente zu untergliedern und eine Funktions- sowie Fehleranalyse für alle Ebenen des Systems durchzuführen. Hierdurch wird es möglich durch präventive Maßnahmen potenzielle Fehlfunktionen vor dessen Auftreten zu vermeiden[2].

Eine Methode mittels derer solch eine Analyse durchgeführt werden kann, ist die FMEA-Methode (Failure Mode and Effects Analysis). Während diese gängigerweise in der Automobil- und in der Luftfahrtindustrie eingesetzt wird, um Qualitäts- und Sicherheitsaspekte zu bewerten, findet die FMEA in der Risikobewertung von Bohrungen und untertägigen Speichern bisher kaum Anwendung. Dabei bietet die FMEA als semi-quantitative Methode zur Risikoanalyse die Möglichkeit, potenzielle Fehlfunktionen anhand der Bedeutung, Auftritts- und Entdeckungswahrscheinlichkeit zu bewerten, um somit eine Aussage über die Bauteile mit den potenziell höchsten Risiken zu treffen und geeignete Maßnahmen abzuleiten[3][4]. Limitation ergeben sich bei der Anwendung der FMEA, wenn es darum gehen soll Fehlerketten und Wechselwirkungen zwischen Barriereelementen zu analysieren. In diesen Fällen bedarf es als Ergänzung zur FMEA weiterer Methoden, wie z.B. der FTA (Fault Tree Analysis).

Durch Bauteilprüfungen im Labor und durch die Auswertung von Versagensursachen einzelner Bohrungselemente unter Realbedingungen lässt sich mittels der FMEA eine umfangreiche Datenbasis aufbauen, welche eine kontinuierliche Verbesserung der Bauteilkonzeption und der Sicherheitskonzepte ermöglicht. Weiterhin lassen sich die bisher gesammelten Erfahrungen aus der untertägigen Gasspeicherung im Sinne des Lessons Learned auf neue Anwendungsgebiete wie z.B. die untertägige Speicherung von Wasserstoff übertragen.

References:

- [1] Stolten, D., Grube, T., & Weber, M., (2012), Wasserstoff–Das Speichermedium für erneuerbare Energie
- [2] Torbergsen, H. E. B., Haga, H. B., Sangesland, S., Aadnøy, B. S., Sæby, J., Johnsen, S. & Lundeteigen, M. A., (2021), An introduction to well integrity, Members of the Norwegian Oil and Gas Association's Well Integrity Forum (WIF) and Professors at NTNU
- [3] DIN e.V. (Hrsg.), (2006), DIN EN 60812:2006, Analysetechniken für die Funktionsfähigkeit von

DGMK/ÖGEW Frühjahrstagung 2023

Systemen – Verfahren für die Fehlerzustandsart- und – auswirkungsanalyse (FMEA), Beuth-Verlag, Berlin

[4] Lipol, L. S., & Haq, J., (2011), Risk analysis method: FMEA/FMECA in the organizations, International Journal of Basic & Applied Sciences, 74-82, 11(5)

Experimental simulation of bit-rock interaction to study and analyze the effect of stick-slip vibrations on a drillstring

Aditya Sharma and Catalin Teodoriu
The University of Oklahoma

Stick-slip is a drilling dysfunction in which the bottom-hole-assembly (BHA) periodically stops rotating whereas the surface RPM is still operating at the set point. This results in a torque build up followed by release of energy during which the bit RPM can shoot up to ten times the RPM at the surface. This phenomenon is very harmful to the drilling equipment specially to the drill bit and greatly increases the non-productive time (NPT). In this extended abstract an experimental lab scale setup to study stick-slip is described. The setup is one of the largest in the world among its type and is equipped with multiple sensors and actuators and a high speed data acquisition system to help analyze stick-slip in a controlled laboratory setup. To simulate the bit-rock interaction a unique arrangement of electro-mechanical actuators and rotary encoders is designed and used in conjunction with the mathematical bit-rock models available in literature.

Setup Overview

To conduct an experimental study of drilling vibrations a laboratory scale drilling test rig equipped with several sensors and actuators has been designed to simulate the process of oil well drilling. A National Instruments cDAQ data acquisition device is used to fetch real time data the sensors and to control the actuators. The control system software is designed using National Instruments LabVIEW. A detailed description of the setup is presented in a previous work (Sharma et al. 2020).

The setup since has been upgraded to facilitate the testing of drilling dynamics in directional wells. The setup is now capable of simulating wells with vertical, curved and horizontal sections. An actuation mechanism had also been designed to replicate various curved section geometries. A schematic overview of the setup overview is shown in figure 1.

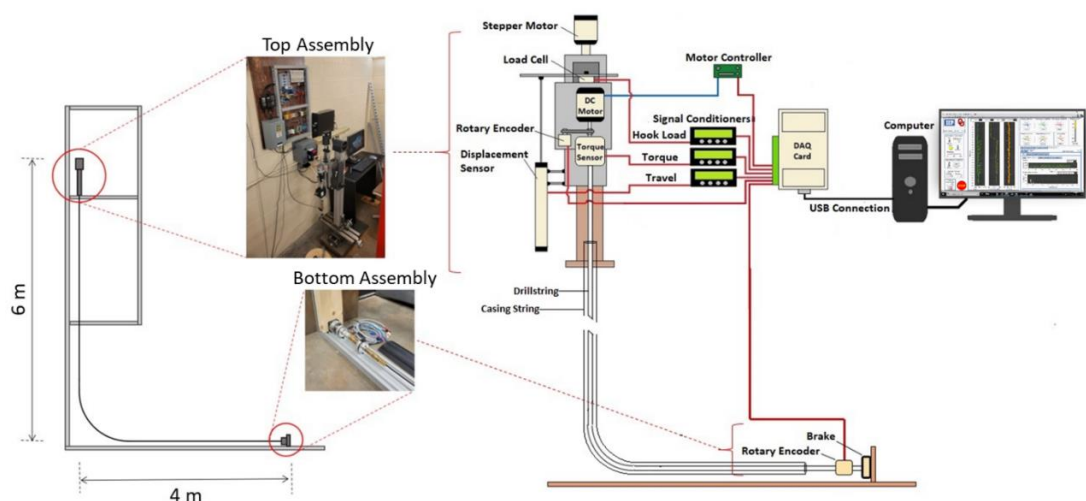


Figure 1. Setup Overview

Figure 2 shows the arrangement of the top assembly which also highlights the unicity of our setup: the ability to trip in and out of the well, hence enabling a real time weight on bit control.

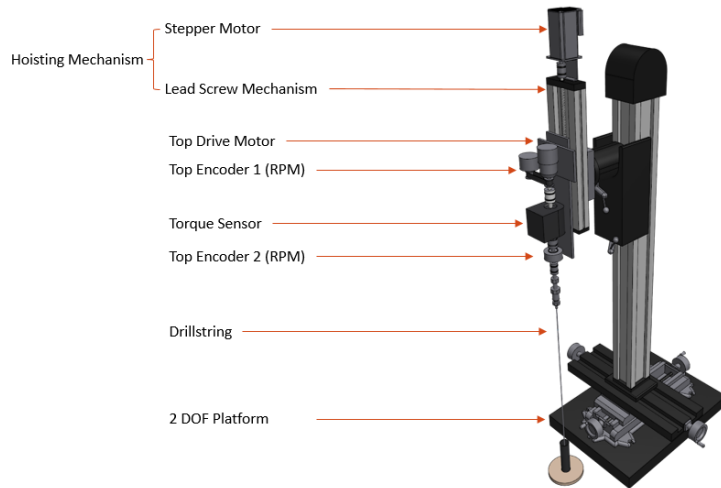


Figure 2. Top Assembly

Methodology

To simulate the bit-rock interaction a unique arrangement of electro-mechanical actuators and rotary encoders is designed and used in conjunction with a mathematical bit-rock model (Rudat and Dashevskiy 2011). A relationship between the applied weight on bit 'W', and the resulting torque on bit 'T', at a given bit RPM 'ω' is as follows:

$$\mu = \frac{3T}{D_B W} \quad \dots \dots \dots (1)$$

Here ' μ ' is the coefficient of friction at the bit-rock interface and ' D_B ' is the diameter of the drill bit. The coefficient of friction can be represented as a function of the bit RPM by the following equation:

$$\mu(\omega) = a_1 + (a_2 - a_1)e^{-\frac{|\omega|}{a_3}} \quad \dots \dots \dots (2)$$

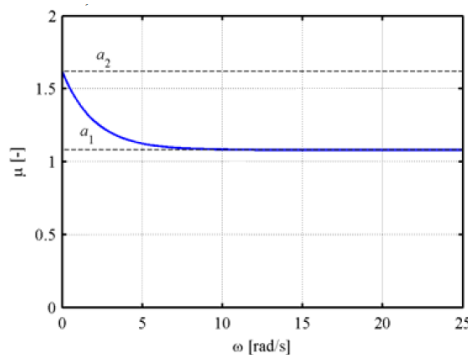


Figure 3. Friction coefficient μ as a function of bit RPM ω (Rudat and Dashevskiy 2011)

where a_1 , a_2 and a_3 represent the Coulomb friction, static friction and the slope of the decaying curve respectively. Changing the values translates to changing the type of formation being drilled, see the figure 3. Using equations 1 and 2 the torque on bit can be calculated as:

$$T = \frac{\mu(\omega) D_B W}{3} \quad \dots \dots \dots (3)$$

Equation 3 is implemented using LabVIEW, where a torque output is produced by an electro-mechanical brake in response to a RPM feedback generated by a rotary encoder. The hardware implementation of the bit-rock model is shown in figure 4.

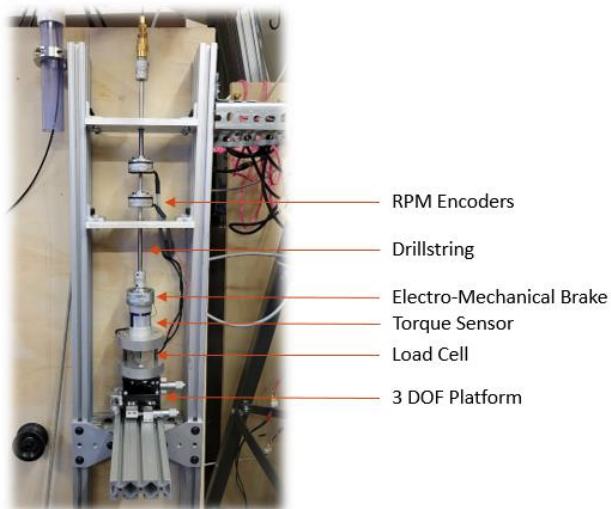


Figure 4. Hardware implementation of the bit-rock model

Conclusions

A unique digital/mechanical twin of a bit-rock interaction has been designed and constructed.

The new bit-rock interaction model enables accurate repeatability of bit-rock interaction situations without the fear of bit wear and thus alteration of bit response.

References

- Rudat, Jens , and Dmitriy Dashevskiy. 2011. "Development of an Innovative Model Based Stick/Slip Control System." SPE/IADC Drilling Conference and Exhibition. Amsterdam, The Netherlands: SPE.

Sharma, Aditya , Saket Srivastava, and Catalin Teodoriu. 2020. "Experimental Design, Instrumentation, and Testing of a Laboratory-Scale Test Rig for Torsional Vibrations— The Next Generation." Energies 13 (18): 4750.

Large-scale underground energy storage: A key technology for carbon neutrality in China and Germany

Yachen Xie^{1,2}, Xuning Wu^{1,3}, Zhengmeng Hou^{1,4}, Zaoyuan Li³, Jiashun Luo^{1,3}, Christian Truitt Lüddeke¹, Liangchao Huang^{1,4}, Wei Sun^{5,6}

¹ Institute of Subsurface Energy Systems, Clausthal University of Technology, Clausthal-Zellerfeld, Germany

² State Key Laboratory of Geomechanics and Geotechnical Engineering, Institute of Rock and Soil Mechanics, Chinese Academy of Sciences, Wuhan, China

³ National Key Laboratory of Oil and Gas Reservoir Geology and Exploitation, Southwest Petroleum University, Chengdu, China

⁴Sino-German Research Institute of Carbon Neutralization and Green Development, Zhengzhou University, Zhengzhou, China

⁵Faculty of Land and Resources Engineering, Kunming University of Science and Technology, Kunming, China

⁶ Yunnan Key Laboratory of Sino-German Blue Mining and Utilization of Special Underground Space, Kunming , China

Abstract

Since its carbon peak in 1990, Germany's energy productivity related to GDP has increased by 60 %, and the share of renewable energy generation is nearly 12 times greater. Numerous energy spatial-temporal complementarities, such as energy efficiency, green buildings, renewable energy power systems, hydrogenation, electrification, increasing usage of smart technology, and electricity future marketization have contributed to achieving a power grid input/output balance. Even underground energy storage sites are currently used for natural gas, Germany has set the goal to use green hydrogen as a medium to promote sector coupling by using energy multiple conversion and reconversion technologies. Germany has established an underground storage plan for 73 billion kWh of green hydrogen in 2045. Meanwhile, Germany's electricity storage demand is expected to reach 45 ~ 90 billion kWh in 2030. In comparison, China's annual electricity consumption is about 11 times that of Germany's. China's electricity storage demand is 500 ~ 1,000 billion kWh in 2030 and 6,000 ~ 7,000 billion kWh in 2060. Therefore, we propose a clean large-scale energy system based on smart sector coupling (ENSYSCO), which uses digital technologies such as artificial intelligence and big data to couple energy production, storage, transport and utilization intelligently. To achieve large-scale energy storage, which is the most essential part of ENSYSCO, we develop four underground energy storage modes. By analyzing the characteristics, challenges, typical cases, and potentials of every mode in China, we illustrate that the pilot projects of regenerative enhanced geothermal system and pumped-storage hydropower in mines should be conducted in China to lay the technical and economic foundation for a wide-scale replication. Due to the strict requirements on site selection, especially for underground hydrogen storage in salt caverns and depleted hydrocarbon reservoirs, the authors suggest that extensive geological surveys should be conducted to promote project implementation.

1 Introduction

From the mid-19th century onward, there has been a 1.1°C increase in the global average temperature, with approximately 0.2°C of this increase occurring in the past ten years. This escalation in temperature has contributed to heightened glacier melting, rising sea levels, and intensified extreme weather events such as heavy rainfall and flooding, all of which have had substantial repercussions for both human society and natural ecosystems [1]. To

alleviate the consequences of global warming, prompt and coordinated efforts on an international level are imperative. As such, nations worldwide are endeavoring to curtail greenhouse gas emissions through collaborative agreements. Notably, at the 21st United Nations Climate Change Conference in 2015, 178 parties collectively endorsed the Paris Agreement on Climate Change [2]. As illustrated in Figure 1, carbon dioxide, along with other greenhouse gases such as methane and fluorocarbons, constitutes the principal driving forces of climate change, posing a critical global challenge [3]. Fossil fuels, predominantly coal, oil, and natural gas, account for more than 75% of global greenhouse gas emissions and nearly 90% of carbon dioxide emissions. Conversely, renewable energy sources like solar, wind, hydro, and geothermal power produce no greenhouse gas emissions, rendering them a more environmentally responsible and sustainable energy alternative. A transition from fossil fuels to renewable energy is essential in decelerating the progression of climate change [4-6]. Advancing the transition towards a green and low-carbon energy system, as well as establishing a renewable energy-centric power infrastructure, are crucial components of achieving carbon neutrality.

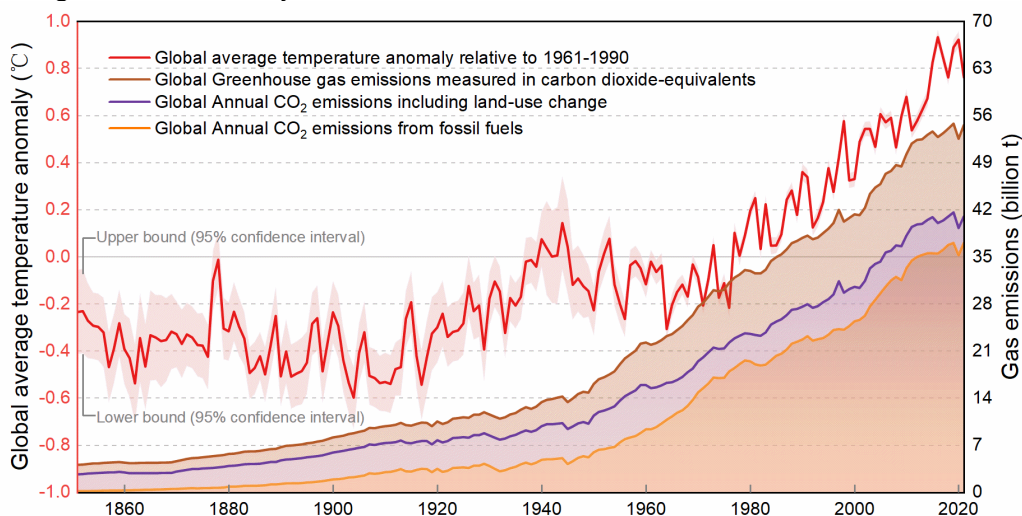


Figure 1. Global average temperature and GHG emissions (sources from the World Bank). Due to the variability of renewable energy, its supply is not always stable, posing a challenge to the stability and reliability of the energy system [7]. In the time dimension, some energies are affected by periodic and more random climate and weather fluctuations (i.e., hydropower, wind, and solar power). If a lot of green electricity is available on particularly sunny or windy days, the amount of electricity produced can exceed actual demand. In the space dimension, geographic and global circulation patterns predominantly control the weather in different regions, contributing to significant differences between locations for the same energy source, especially for wind and solar resources. A significant characteristic of future energy systems is the distributed production of renewable energy. Different types of renewable energy power plants will be located in geographic locations with higher production potential, depending on environmental conditions [8]. Therefore, the development of energy storage technologies is crucial to solving the problem of the instability of renewable energy generation. Large-scale underground energy storage is an advanced energy storage technology that can convert electricity into other forms of energy (such as compressed air, liquid, or thermal energy) for storage and then convert it back to electricity when needed. This energy storage method has many advantages, including high efficiency, flexibility, and environmental friendliness. Large-scale underground energy storage is considered a key technology for overcoming the variability of renewable energy generation. It can store surplus electricity and release energy during peak demand periods, helping to ensure the stable operation of the power grid, improve the utilization efficiency of renewable energy, and reduce waste, thereby promoting the popularization and development of renewable energy.

2 Renewable Energy Generation and Storage

2.1 Electricity Structures in Germany and China

Finding the optimal equilibrium between economic development and carbon mitigation has persistently posed a significant challenge for policymakers. This delicate balancing act requires careful consideration of trade-offs in order to achieve sustainable growth without exacerbating environmental concerns. Germany has handled this problem well. Policy guidelines such as the complete phase-out of nuclear energy, the phase-out of coal, and the continuous promotion of renewable energy have resulted in a significant change in Germany's energy structure from fossil energy to renewable and clean energy. The utilization of renewable energy sources compensates for the negative impact of carbon reduction.

Before the energy transition, the German power plant park was based primarily on traditional generation plants based on a broad, regionally diversified, predominantly fossil fuel mix (hard coal and brown coal, nuclear energy, natural gas, mineral oil products, hydroelectric power, etc.). The energy transition changes the composition of the German power plant park. The number of power plants using renewable energy is increasing. Power plants with high greenhouse gas emissions are taken off the grid. Unlike other countries, Germany did not strongly develop hydropower, which has many problems (such as environmental and ecological damage, displacement of local communities). As shown in Figure 2, solar and wind energy have become the most dominant forms of renewable energy generation in Germany. In 2020, Germany's newly installed photovoltaic capacity is nearly 5 million kilowatts, the highest level since 2012. In addition, federal directives state that 2% of the country's land area will be used for onshore wind energy development, and the permitting process should be simplified and accelerated. In the future, the capacity of renewable energy generation plants will be further expanded.

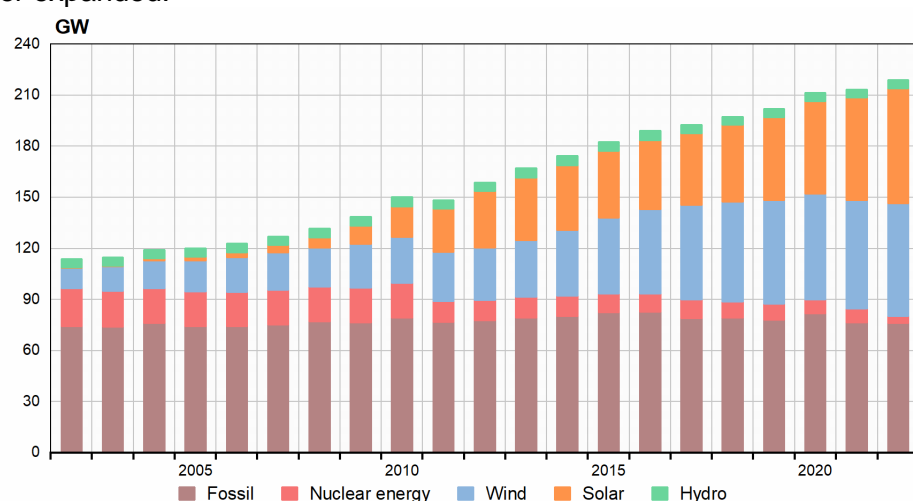


Figure 2. Installed capacity for electricity generation in Germany ([9]).

China has also adopted active measures to reduce carbon emissions and has made some achievements in the development of renewable energy. Over the past 40 years of reform and opening up, China's economy has experienced significant growth. However, ecological and environmental issues have emerged as weak links, posing a threat to China's sustainable development. Environmental protection, international public opinion, trade competition, energy security and other factors have jointly promoted China's carbon emission reduction and energy transition. On September 22, 2020, Chinese President Xi Jinping announced that China will reach its carbon peak by 2030 and become carbon neutral by 2060. China is one of the largest carbon dioxide emitters in the world, but the Chinese government has formulated a series of measures, including expanding the use of renewable energy, reducing the consumption of fossil fuels, and establishing a carbon trading market, etc., to achieve its carbon neutrality goal.

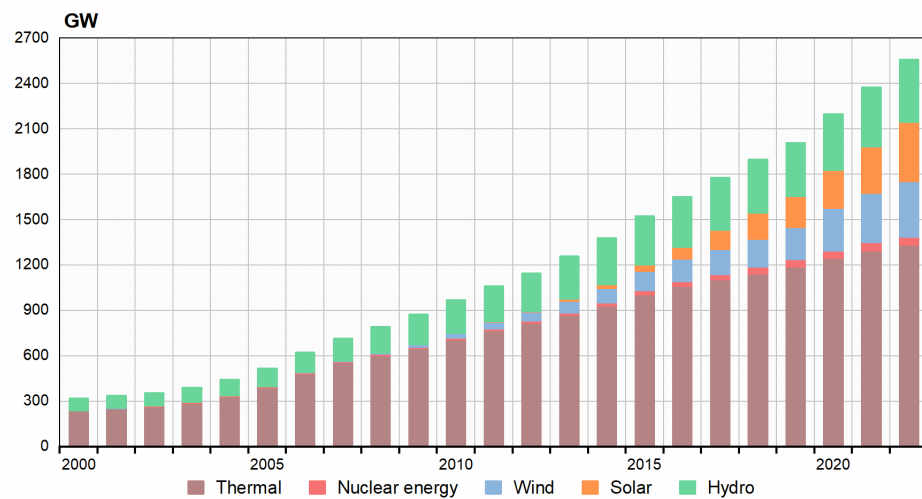


Figure 3. Installed capacity for electricity generation in China (sources from China National Bureau of Statistics).

The most notable change is the increased installed capacity from renewable energy, which has increased more than 14-fold since 2000. Various renewable energy sources have grown at different rates. The fastest is photovoltaics, which have grown to match wind and hydro in just a decade since they were first recorded in 2009. Unlike Germany, China has kept both hydro and nuclear power and both have maintained a steady growth trend. Due to China's abundant water resources and mature water power technology, as well as reliable electricity output, hydro power was the first to be developed as an important component of China's clean energy development. It is worth noting that thermal power still accounts for a large proportion of China's electricity structure. The Chinese government has taken a series of measures to phase out thermal power and promote clean energy, such as issuing policies to encourage enterprises to transform thermal power units into renewable energy power units, promoting thermal power desulfurization, denitrification, and dust removal, and promoting the upgrading of thermal power generation technology. With China's increasing awareness of environmental protection and sustainable development, it is believed that China will gradually phase out thermal power and popularize clean energy.

Although renewable energy has been rapidly developed with a significant increase in installed capacity, it has not been fully utilized. As shown in Figure 4, from 2017 to 2022, China's installed capacity of renewable energy doubled to 12.13×10^8 kW. However, renewable energy generation increased by only 58.8%, and its share of total electricity production increased by only 5.2%. Germany faces similar issues, even more severe. From 2017 to 2022, the installed capacity of renewable energy has increased by 32.7%, but the electricity generation has only increased by 17.6%. This shows that renewable energy has not been fully utilized, and the problems of abandoning wind, water and solar energy are very prominent. Therefore, it is necessary to pay special attention to the efficient utilization of renewable energy power generation, and to improve the multi-energy complementarity and underground storage of renewable energy.

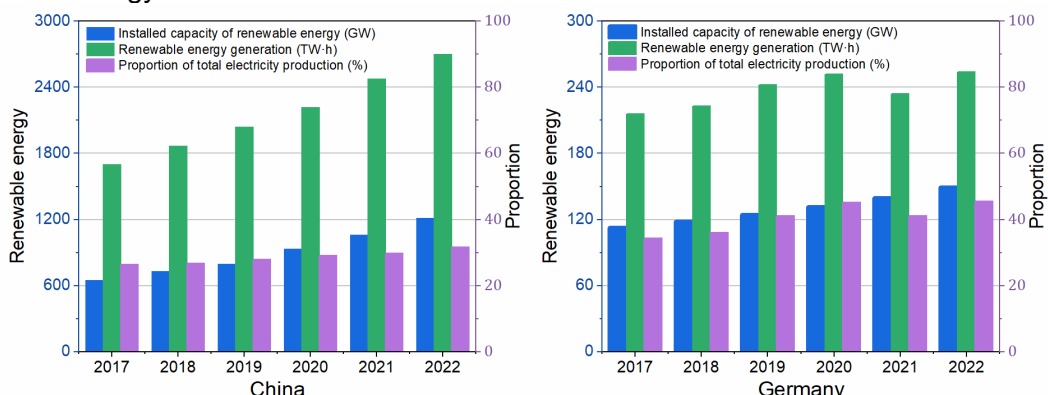


Figure 4. renewable energy power generation in China and Germany (sources from China National Bureau of Statistics and the World Bank).

Renewable energy will play a key role in the new power system. Renewable energy generation in China accounted for 31.6% of the total electricity production in 2022 (Figure 4) and is expected to reach 85% by 2060. At that time, wind and solar power will generate nearly 2.6×10^{13} kWh (approximately 25% comes from energy storage coupled with power to X, in which more than 80% are expected to be generated by large-scale underground energy storage, accounting for 20% of total). Germany, as one of the leading global countries, its share of renewable energy power generation near 50% in 2022. Benefited by the well-organized German Power Future (from 15 minutes to 10 years), smart energy system, and sufficient storage capacity, Germany's power system still operates reliably. According to estimates, Germany's electricity storage demand will be 4.5×10^{10} kWh ~ 9×10^{10} kWh in 2030. In comparison, China's annual electricity consumption is about eleven times that of Germany's. As a result, the demand of reserved power in China would be 5×10^{11} kWh ~ 1×10^{12} kWh in 2030, and 6×10^{12} kWh ~ 7×10^{12} kWh in 2060 corresponding to 70% ~ 82% of the total electricity consumption of 8.5×10^{12} kWh in 2021 (Table 1). Therefore, massive demand is anticipated for implementation of large-scale (especially underground) energy storage technologies (Figure 6), and it will play a vital role in China's future energy system.

2.2 Power to X and energy storage

In response to the unstable nature of renewable energy generation, Power-to-X [10] technology provides a transformative solution. The basic principle of Power-to-X technology is to use renewable energy to generate hydrogen through water electrolysis, and then synthesize hydrogen with carbon dioxide and other substances to produce energy products such as chemicals and fuels. X represents various products, processes, technologies, and applications. It can be understood as a means of converting electric energy into energy carriers, heat, cold, products, or raw materials. It is a generalized term for different types of power generation, including natural gas, liquid, fuel, chemical, and thermal power generation. Figure 5 shows the three common power sources for X. Power-to-X technology converts renewable energy into chemical energy for long-term storage and sustainable use.

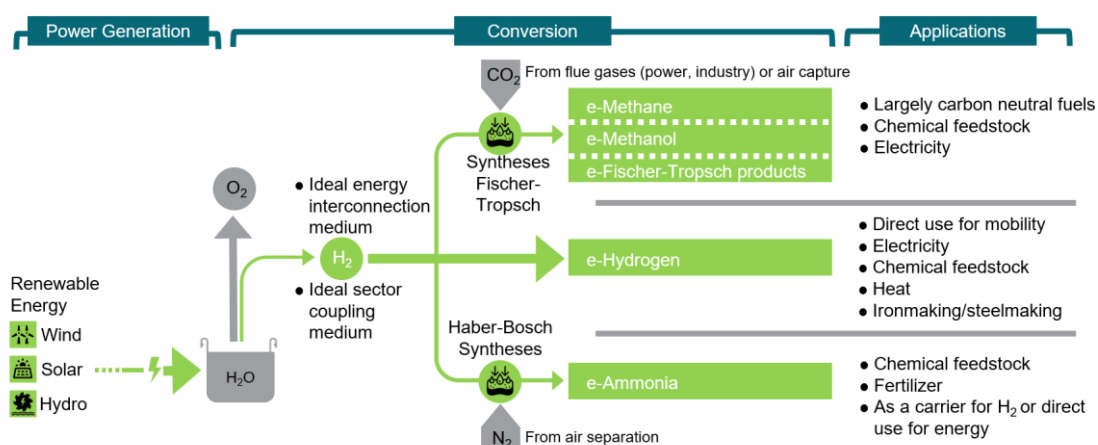


Figure 5. Three pathways of Power-to-X (Electricity based molecular hydrogen, methanol and hydrocarbons as well as ammonia) (modified from [11]).

The Power-to-X technology and large-scale underground energy storage complement and promote each other. Power-to-X technology can provide storable chemicals for large-scale underground energy storage, which can be stored as energy storage media in underground reservoirs, thus improving the efficiency and reliability of underground energy storage. At the same time, large-scale underground energy storage can also provide energy storage media for Power-to-X technology by storing chemicals in underground reservoirs, thereby guaranteeing the energy supply for Power-to-X technology.

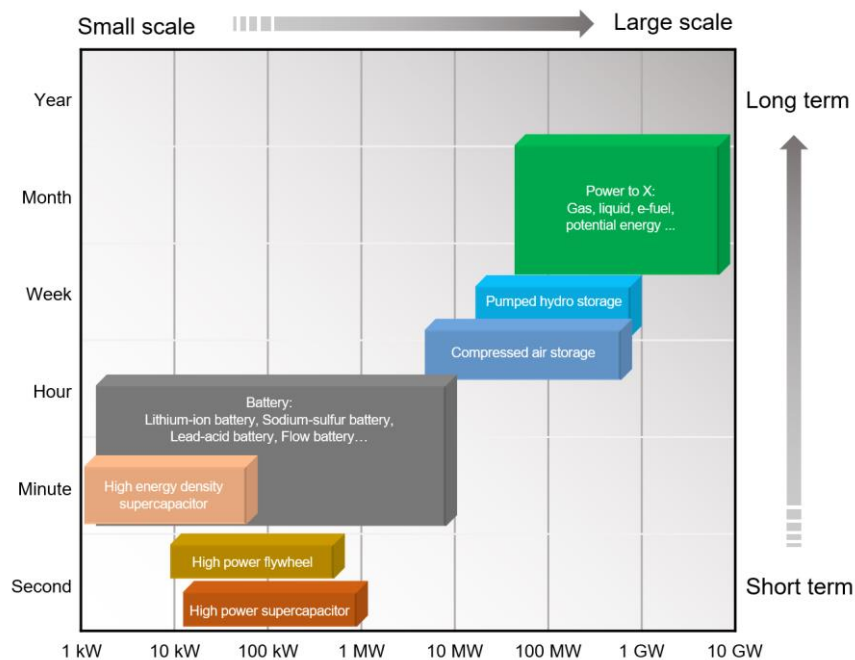


Figure 6. Comparison of various energy storage technologies.

Compared to the aboveground energy storage technologies (e.g., battery, flywheel and supercapacitor, compressed air and pumped hydropower storage), the underground energy storage (UES) technologies (especially underground storage of renewable power to X (gas, liquid and e-fuels) and pumped-storage hydropower in mines (PSHM)) are more favorable due to their large-capacity (more than 10^{12} kWh) and long-term (a few months) storage characteristics (Figure 6). Comparatively, UES is safe, efficient, and low-cost with the following six functions: peak regulation, frequency regulation, phase regulation, energy storage, backup system, and black start. Furthermore, UES can effectively reduce the land requirement and damages to ecosystem (Table 1). The synergies effect is also crucial in coordinating UES with the rapid-response and flexible-deployment aboveground energy storage technologies. Obviously, to ensure the efficient and stable operation of the energy system in accomplishing carbon neutrality goals, there is an urgent need of developing large-scale (especially underground) energy storage technologies rapidly. In this paper, we proposed four insightful portfolios that can integrate renewable UES coupled with power to X.

Table 1. Characteristics and potentialities of various energy storage technologies.

| Type | Energy storage technology | Main characteristics | Technology maturity | Potential (10^8 kWh) | |
|---------------------------------|--|---|--|---------------------------------|---------------|
| | | | | 2030 | 2060 |
| Above ground | Pumped-storage hydropower | Fast response, high efficiency, long life and long discharge time, large scale | Mature | 3300 | 8900 |
| | Batteries, flywheels, super capacitors, etc. | Fast response, high efficiency, flexible deployment | Mostly mature | 1500 | 3800 |
| | Pumped-storage hydropower in mines | Fast response, high efficiency, large scale, long life and long discharge time, little external influence | Pilot, but mostly mature | — | 11300 ~ 13500 |
| Under-ground | Salt cavern | Hydrogen | Long discharge time, large scale, little external influence | Pilot abroad, but mostly mature | 5000 |
| | | Methanol, e-fuels | | Mature abroad | 5800 |
| | Geothermal | Shallow | Long heat release time, large scale, little external influence (climate) | Mostly mature | 5300 ~ 21000 |
| | | Deep | | Pilot | 2700 ~ 11000 |
| Depleted hydrocarbon reservoirs | Natural gas | Large scale, low cost | Mature | 2500 ~ 4000 | 6000 ~ 9600 |
| | Biomethanation | Large scale, low cost of underground methanation, storage of renewable methane, | Theoretical stage | — | 58200 ~ 67300 |

| CCUS, carbon circular economy | | | |
|---|--------------------------------|--------------------------------|--|
| Total power demand / Power storage demand | 14000 ~ 15000/ 5000 ~ 10000 | About 300000/ 60000 ~ 70000 | |
| Total potential | — | 118800 ~ 157700 | |

3 Four modes of large-scale underground energy storage

3.1 Regenerative enhanced geothermal system

The enhanced geothermal system with integrated cogeneration and energy storage is combined with green power heating technology to store renewable energy in the form of thermal energy. It can realize the graded and recycling utilization of geothermal energy, and can consume renewable wind and solar energy in an efficient and high proportion way. Use surplus green electricity to heat the exchange medium and inject it into deep geothermal reservoirs, combining large-scale wind and solar conversion with underground energy storage (Figure 7). The innovative concept of regenerative EGS with both functions of electricity and heat production (Model I) and storage of renewable wind/solar energy (Model II).

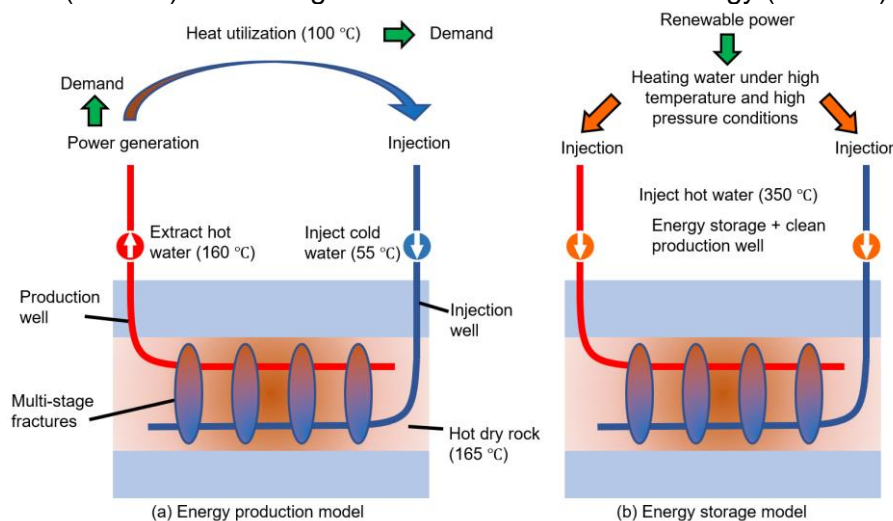


Figure 7. Schematic diagram of EGS integrated with cogeneration and energy storage (modified from [12]).

A numerical simulation study based on Germany's GeneSys geothermal energy storage project demonstrated that REGS significantly promotes the usage and storage of renewable energy, as well as extending the system's lifetime. Results show that with an injection rate of 144 L/s and a utilization rate of 90%, the annual power generation potential in the early stage reaches 49.14 GW·h, and the cumulative output within 30 years exceeds 1200 GW·h [13]. China's shallow geothermal energy, deep hydrothermal resources, and hot dry rock resources are incredible, accounting for 7.9% of the world's reserves, with an annual availability of 3.06×10^{18} kWh and a huge renewable power consumption capacity [14]. According to calculations, only 5% to 15% of wind and solar power can realize geothermal heat storage of about 8.0×10^{11} kWh ~ 3.2×10^{12} kWh through the power to heat technology by 2060. Out of which, the shallow geothermal energy storage potential mainly used for heating/cooling is 5.3×10^{11} kWh ~ 2.1×10^{12} kWh, while the potential of a deep renewable geothermal system for cogeneration is 2.7×10^{11} kWh ~ 1.1×10^{12} kWh.

3.2 Pumped-storage hydropower in mines

Pumped-storage hydropower is one of the most effective methods to ensure the safe, stable and economical operation of the power system and to release the bottleneck in the development of clean energy such as large-scale wind power. However, due to the influence of terrain, environmental protection, investment and other factors, it will become more and more difficult to build above-ground pumped storage hydropower plants. In view of the large and widely distributed abandoned mines [15, 16], the construction of pumped-storage hydropower in mines (PSHM) using mine caverns and tunnels as multi-stage water storage reservoirs has broad prospects for application. From the perspective of ecology and

environment, the use of underground abandoned space to build pumped storage power plants has a positive effect on the prevention and control of disasters in underground mining areas and ecological restoration of mines. From an economic perspective, the construction of pumped-storage hydropower in mines utilizes the original abandoned underground space, which can greatly reduce the construction investment [17]. In addition, compared with surface reservoirs, the pumped-storage hydropower in mines has less evaporation of water resources, and has groundwater sources as supplements, which can better solve the problem of water sources.

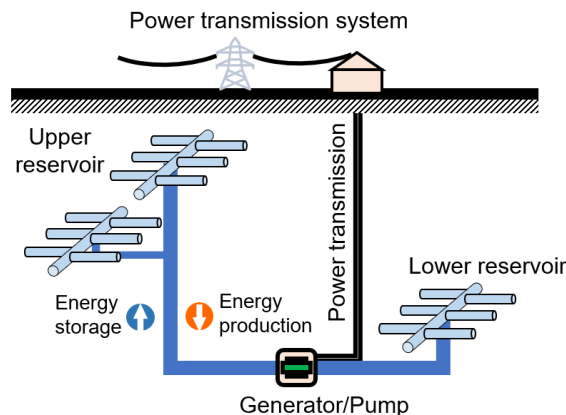


Figure 8. Schematic diagram of pumped storage in underground mines.

PSHM enables water storage, energy storage, power generation, water cycle, and renewable energy development and utilization. When there is excess electricity supply, water is pumped to the upper reservoir and the surplus electricity is converted into gravitational potential energy. When the demand for electricity increases, water is released from the upper reservoir to generate electricity by gradually flowing down to the lowest reservoir. Thus, the gravitational potential energy of water is converted back into electricity and fed back to the grid (Figure 8). PSHM is characterized by a short response time (minutes and seconds), long working life (40–60 years) and high energy efficiency (up to 80%) [18].

A 2×10^3 MW semi-underground pumped storage power plant at Mount Hope is planned to be built in New Jersey, USA in this century. The upper reservoir is an artificially excavated pool with an area of 22.3 km^2 , and the lower reservoir is an underground abandoned mine. Preliminary estimation of its effective reservoir capacity is $6.2 \times 10^6 \text{ m}^3$ [19]. Germany's Saxony Energy Research Center plans to use the abandoned Upper Harz metal mine roadway to build a fully underground pumped storage power plant (preliminary installed capacity of 1×10^2 MW). China has an abundance of abandoned mines with considerable development potential. According to studies, PSHM constructed only from abandoned coal mines (up to 2014) yields $7.25 \times 10^9 \text{ kW}\cdot\text{h}$ [16]. In addition, the volume of available metal mines is $1.2 \times 10^8 \text{ m}^3$ in Yunnan Province. PSHM can accomplish an annual power generation capacity of $3.29 \times 10^{10} \text{ kW}\cdot\text{h}$ [83], while it is $6.70 \times 10^{10} \text{ kW}\cdot\text{h}$ in Henan Province [20], and China's total potential ranges from 1.13×10^{12} to $1.35 \times 10^{12} \text{ kW}\cdot\text{h}$ based on rough computational conversion.

3.3 Underground hydrogen storage in salt cavern

Hydrogen is considered as a green energy carrier when it is produced solely from renewable energy, which is not only a potential medium for large-scale energy storage, but also a bridge connecting electricity, heating/cooling and transportation (sector coupling). Underground hydrogen storage (UHS) is regarded as the most economic and safest option for large-scale utilization at different time scales [21]. Salt caverns have suitable physicochemical and mechanical properties to ensure safe and efficient storage even at high pressures, therefore, salt caverns are ideal storage site for highly-pure hydrogen [22-24].

As shown in Figure 9, UHS in salt caverns refers to underground systems of artificial caverns built in rock salt to store gas or liquid energy sources (such as hydrogen, natural gas, compressed air and oil). UHS in salt caverns can not only reach the energy carrier and carbon cycle in nature, but also store all renewable clean gaseous and liquid energy sources under the Power to X.

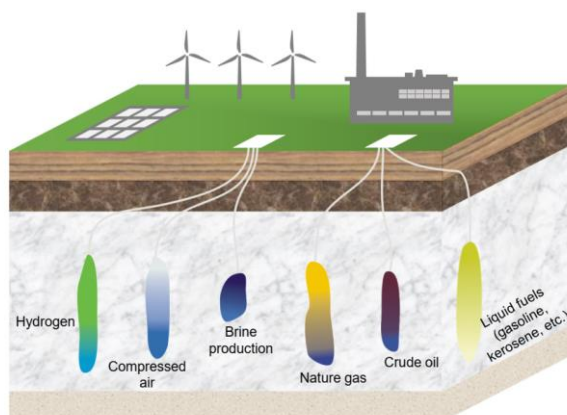


Figure 9. Schematic diagram of multi-functional rock salt cavern storage.

At present, the UHS in salt caverns technology in European and American countries is basically mature, and salt caverns have nearly 60 years of operating experience for oil and gas storage. Since 1972 in the UK (Teesside in Yorkshire), the Sabic Petroleum company has been storing almost pure hydrogen (95% of H₂, 3%–4% of CO₂) in three shallow salt caverns (at a depth of 400 m) [25, 26]. In Texas, USA, three deeper located caverns are operated by ConocoPhillips (Clemens), Praxair (Moss Bluff), and Air Liquide (Spindletop), and they are utilized in the petrochemical industry. Their dimensions and shape basically correspond to that of modern natural gas caverns. For instance, the Clemens salt dome has a cylindrical shape. It is 300 m high and has a diameter of 49 m. The newest Spindletop cavern (operating since around 2017) is currently the largest hydrogen storage facility in the world. The cavern in Moss Bluff is connected to the Praxair Gulf Coast pipeline network with a total length of several hundred kilometers, covering the hydrogen demands of Texas and Louisiana [27].

The capacity and potential of UHS in salt caverns are tremendous. For instance, the northern German basin has 269 underground rock salt structures with a storage capacity of approximately 1.6×10^{12} kW·h through UHS. Liu et al. [28] expect hydrogen storage of up to 3.69×10^{10} kW·h using only 4×10^7 m³ of the salt cavern capacity in Jiangsu Province, China by 2050. In China, the volume of salt caverns has exceeded 1.3×10^8 m³ with an annual increment of over 5×10^6 m³. It has the potential of about 5×10^{11} kW·h for hydrogen storage in 2030, and it is expected to reach 1.05×10^{12} kW·h in 2060. The prospects for methanol storage are even more significant with an estimate of 5.8×10^{11} and 1.21×10^{12} kW·h in 2030 and 2060, respectively.

3.4 Bio-methanation in depleted hydrocarbon reservoirs

Underground gas storage (UGS) has a critical impact on peak shaving and energy security in the natural gas supply chain. China's demand for natural gas remains huge, and it is currently in the golden age for large-scale UGS construction. Depleted hydrocarbon reservoirs (DHR) capable of storing gas (impure hydrogen, natural gas, compressed air and carbon dioxide) are widely distributed in China and offer significant energy storage potential [29]. In the process of using depleted hydrocarbon reservoirs for hydrogen storage, hydrogen exacerbates various microbial metabolisms in the subsurface. Four metabolisms were identified to play an important role during the storage of hydrogen: the methanogenesis, acetogenesis, iron-reduction and fermentation [30]. Three of the stated metabolisms can be considered as negative side effects, but the methanogenic metabolism can be used as an in-situ conversion process for an underground bio-reactor. Therefore, depleted hydrocarbon reservoirs can be used as giant natural biochemical reactors to synthesize methane (renewable natural gas).

The underground bio-methanation technology is directly related to underground gas storage or underground hydrogen storage. The induction and catalysis of micro-organisms (methanogenic archaea) by injecting impure H₂ and proportional CO₂ into DHR exploited the storage capacity of the porous subsurface, and it allowed methane conversion to take place in situ. The gas, consisting mainly of methane and hydrogen, can then be extracted and further processed through production wells (Figure 10). The underground bio-methanation system in depleted hydrocarbon reservoirs can realize the production, flexible storage and utilization of

renewable natural gas [31]. This UES mode effectively couples zero (negative) emission economic utilization of impure hydrogen, CO₂ recycling and sequestration, underground natural gas synthesis and storage, as well as geothermal parallel development, thus promoting the development of a low-carbon circular economy[32].

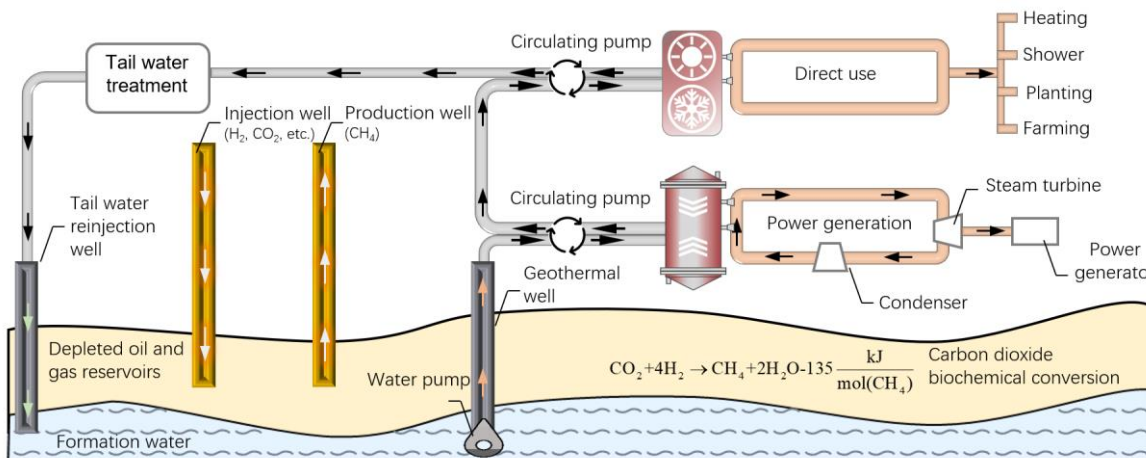


Figure 10. Carbon dioxide biochemical conversion and geothermal utilization system

Numerous research projects have been launched during the last decades, which concern the cyclic storage of energy in the form of hydrogen, methane, compressed air or heat or the permanent disposal of carbon dioxide. The Argentinean company Hychico S.A. began researching the storage of hydrogen in depleted hydrocarbon reservoirs in 2010. Field tests were carried out by operating different hydrogen-natural gas storage cycles using a porous reservoir in a depth of 815 m, and it was observed that some of the stored hydrogen was converted to methane. Changes in gas components were also observed in town gas storage reservoirs, especially the increase in CH₄ concentration caused by methanation reactions, which was reported by the Czech Republic and Germany [33].

Recent estimates suggest that China's natural gas storage capacity in 2060 will reach 1.2×10^{11} m³, with corresponding storage potential of 6×10^{11} to 9.6×10^{11} kW·h. Moreover, biomethanation presents an unprecedented opportunity for development and has significant potential as a key carbon-negative technology. According to preliminary studies, China's wind power is projected to reach 1.42×10^{13} kW·h in 2050. If fully utilized for hydrogen production and underground biochemical synthesis of methane with CO₂, an electricity capacity generated via re-electrification of 5.82×10^{12} to 6.73×10^{12} kW·h can be achieved (energy efficiency ranges from 41.1% to 47.5%).

4 Summary

The transition from fossil fuels to renewable energy is essential to mitigate climate change. However, renewable energy sources often exhibit supply instability, making energy storage technology crucial for their effective utilization. Large-scale underground energy storage (UES) presents an efficient and flexible method for storing surplus electricity production and releasing it during periods of peak demand. Utilizing the UES can ensure the stable operation of the power grid, enhance the utilization efficiency of renewable energy, and minimize waste, thereby promoting the widespread adoption and development of renewable energy. Four UES technology portfolios have been proposed to meet China and Germany's renewable energy storage needs at the national level.

We believe that carbon neutrality can be achieved through the development of renewable energy and the integration of key technologies such as coupling power-to-X with large-scale underground energy storage (e.g., in mines, salt caverns, depleted hydrocarbon reservoirs, and geothermal reservoirs). While there have been some successful instances of large-scale underground storage of renewable energy, in conjunction with power-to-X, these implementations are predominantly confined to hydrogen and compressed air storage in rock

salt caverns. Nevertheless, there remains considerable scope for enhancing energy efficiency and economic benefits. It is imperative that policymakers escalate fundamental research in pertinent scientific fields and accelerate experimental investigation and technological development. The early adoption of industrial standardization and the widespread implementation of large-scale UES technologies are vital to attaining the carbon-neutrality goals.

Acknowledgment

This work is funded by Henan Institute for Chinese Development Strategy of Engineering & Technology (No. 2022HENZDA02), the Science & Technology Department of Sichuan Province (No. 2021YFH0010), High-End Foreign Experts Program of the Yunnan Revitalization Talents Support Plan of Yunnan Province, and the China Scholarships Council (No. 202008080235).

References:

- [1] Van Aalst M.K.: The impacts of climate change on the risk of natural disasters. *Disasters*. 30. 5 [2006].
- [2] United N.: What is the Paris Agreement? <https://unfccc.int/process-and-meetings/the-paris-agreement> [2023].
- [3] Gil Alana L.A., Monge M.: Global CO₂ emissions and global temperatures: Are they related. *International Journal of Climatology*. 40. 6603 [2020].
- [4] Xie Y., Qi J., Zhang R., Jiao X., Shirkey G., Ren S.: Toward a Carbon-Neutral State: A Carbon–Energy–Water Nexus Perspective of China’s Coal Power Industry. *Energies*. 15. 4466 [2022].
- [5] Hou Z., Luo J., Xie Y., Wu L., Huang L., Xiong Y.: Carbon Circular Utilization and Partially Geological Sequestration: Potentialities, Challenges, and Trends. *Energies*. 16. 324 [2023].
- [6] Hou Z., Xiong Y., Luo J., Fang Y., Haris M., Chen Q., Yue Y., Wu L., Wang Q., Huang L., Guo Y., Xie Y.: International experience of carbon neutrality and prospects of key technologies: Lessons for China. *Petroleum Science*. 2023.
- [7] Hu J., Li Y., Wörman A., Zhang B., Ding W., Zhou H.: Reducing energy storage demand by spatial-temporal coordination of multienergy systems. *Applied Energy*. 329. 120277 [2023].
- [8] Zhengmeng H., Wentao F.: An Integrated Framework to Better Fit Future Energy Systems—Clean Energy Systems Based on Smart Sector Coupling (ENSYSCO) (In Chinese). *Advanced Engineering Sciences*. 54. 5 [2022].
- [9] Energy-charts:Net installed electricity generation capacity in Germany, https://energy-charts.info/charts/installation_power/chart.htm?l=en&c=DE&chartColumnSorting=default&year=-1 [2023].
- [10] Sternberg A., Bardow A.: Power-to-What? – Environmental assessment of energy storage systems. *Energy & Environmental Science*. 8. 389 [2015].
- [11] Schnettler A.: At the Dawn of the Hydrogen Economy. <https://www.powermag.com/siemens-dawn-hydrogen-economy/>, <https://www.powermag.com/siemens-dawn-hydrogen-economy/> [2022].
- [12] Hongyuan Y.: The Adjustment of Trump Government’s Climate Policy and Its Implications. (Chinese). *Pacific Journal*. 26. 25 [2018].
- [13] Haris M., Hou M.Z., Feng W., Mahmood F., Saleem A.B.: A regenerative Enhanced Geothermal System for heat and electricity production as well as energy storage. *Renewable Energy*. 197. 342 [2022].
- [14] Frondel M., Kaeding M., Sommer S.: Market premia for renewables in Germany: The effect on electricity prices. *Energy Economics*. 109. 105874 [2022].
- [15] Lu K., Hou Z., Sun W., Zhang S.: Potential evaluation and construction key technologies of pumpedstorage power stations in mines of Yunnan Province. (In Chinese). *Advanced Engineering Sciences*. 54. 136 [2022].
- [16] Xie H., Hou Z., Gao F., Zhou L.: A new technology of pumped-storage power in underground coal mine: Principles, present situation and future. (Chinese). *Journal of China Coal Society*. 40. 965 [2015].
- [17] Luo K., Shi W., Cao F., Ma X.: Preliminary study on construction of pumped storage power

- station by using abandoned mines. (Chinese). *Energy of China.* 40. 42 [2018].
- [18] Rehman S., Al-Hadrami L.M., Alam M.M.: Pumped hydro energy storage system: A technological review. *Renewable and Sustainable Energy Reviews.* 44. 586 [2015].
- [19] Li J., Yi C., Gao S.: Prospect of new pumped-storage power station. *Global Energy Interconnection.* 2. 235 [2019].
- [20] Cao C., Hou Z., Xiong Y., Luo J.: Technical routes and action plan for carbon neutral for Yunnan Province. (In Chinese). *Advanced Engineering Sciences.* 54. 37 [2022].
- [21] Małachowska A., Łukasik N., Mioduska J., Gębicki J.: Hydrogen Storage in Geological Formations—The Potential of Salt Caverns. *Energies.* 15. 5038 [2022].
- [22] Fang Y., Hou Z., Yue Y., Ren L.: A new concept of multifunctional salt cavern hydrogen storage applied to the integration of hydrogen energy industry. (Chinese). *Advanced Engineering Sciences.* 54. 128 [2022].
- [23] Yang C., Wang T., Li Y., Yang H., Li J., Qu D.A., Xu B., Yang Y., Daemen J.J.K.: Feasibility analysis of using abandoned salt caverns for large-scale underground energy storage in China. *Applied Energy.* 137. 467 [2015].
- [24] Hou Z.: Mechanical and hydraulic behavior of rock salt in the excavation disturbed zone around underground facilities. *International Journal of Rock Mechanics and Mining Sciences.* 40. 725 [2003].
- [25] Blanco H., Faaij A.: A review at the role of storage in energy systems with a focus on Power to Gas and long-term storage. *Renewable and Sustainable Energy Reviews.* 81. 1049 [2018].
- [26] Lord A.S.: Overview of Geologic Storage of Natural Gas with an Emphasis on Assessing the Feasibility of Storing Hydrogen. Sandia National Laboratories (SNL). 28. 975258 [2009].
- [27] Tarkowski R.: Underground hydrogen storage: Characteristics and prospects. *Renewable and Sustainable Energy Reviews.* 105. 86 [2019].
- [28] Liu W., Zhang Z., Chen J., Jiang D., Wu F., Fan J., Li Y.: Feasibility evaluation of large-scale underground hydrogen storage in bedded salt rocks of China: A case study in Jiangsu province. *Energy.* 198. 117348 [2020].
- [29] Hou Z., Xie H., Zhou H., Were P., Kolditz O.: Unconventional gas resources in China. *Environmental Earth Sciences.* 73. 5785 [2015].
- [30] CORD-RUWISCH R., SEITZ H.J., CONARD R.: The capacity of hydrogenotrophic anaerobic bacteria to compete for traces of hydrogen depends on the redox potential of the terminal electron acceptor. *Archives of microbiology.* 149. 350 [1988].
- [31] Xiong Y., Hou Z., Xie H., Zhao J., Tan X., Luo J.: Microbial-mediated CO₂ methanation and renewable natural gas storage in depleted petroleum reservoirs: A review of biogeochemical mechanism and perspective. *Gondwana Research.* 2022].
- [32] Hou Z., Xiong Y., Liu J., Cao C.: Strategy, technical route and action plan towards carbon peak and carbon neutrality in Henan Province. (Chinese). *Advanced Engineering Sciences.* 54. 23 [2022].
- [33] Strobel G., Hagemann B., Huppertz T.M., Ganzer L.: Underground bio-methanation: Concept and potential. *Renewable and Sustainable Energy Reviews.* 123. 109747 [2020].

Fluvio-deltaic facies interpretation using 3D-seismic attributes analysis and unsupervised machine-learning algorithm: strategy to reduce geothermal exploration risk in the North German Basin

L. Bello¹, H. von Hartmann², M. Franz¹, I. Moeck^{1,2}

¹University of Göttingen, Geoscience Center - GZG, Göttingen, Germany, ²Leibniz Institute for Applied Geophysics, Hannover, Germany

The application of machine learning algorithms for reservoir characterization and prospect identification in seismic data is becoming standard practice in the exploration industry. This technique has proven useful in identifying patterns in the data that might be overlooked by the interpreter. In addition, it improves reservoir predictions and characterization at a lower computational cost.

In this study, we evaluate the fluvio-deltaic facies of the Upper Triassic Exter formation in the North German Basin. We apply a workflow consisting of three main stages: 3D-Seismic Interpretation; seismic attributes analysis for the identification and delineation of the fluvio-deltaic system; and clustering of the fluvio-deltaic facies.

For seismic facies clustering we apply an unsupervised machine learning algorithm based on waveform segmentation of seismic amplitude data. Furthermore, to evaluate the evolution of deltaic complexes, we implemented the stratal slicing technique through the resulting waveform segmentation and the generated attributes volumes.

Results allow understanding and delineation of a number of fluvial architectural elements in the study area, i.e. lateral shifting of individual channels contributing to the formation of channel belt reservoirs within the Rhaetian Deltaic System.

These results contribute significantly to reducing the risk of geothermal exploration in the North German Basin by proposing for the first time a way to improve the prediction of Rhaetian reservoirs on a local scale based on seismic methods.

Hydrothermal und petrothermal: “TRENDS” – und ein Rückblick

H. Behrens¹, J. Ghergut¹, M. Sauter¹, C. Haas², T. Winter², K. Zosseder²

¹Universität Göttingen, Geowissenschaftliches Zentrum, Dept. Tiefe GeoReservoir

²Technische Universität München, Dept. Hydrogeologie und Geothermie

Abstract

Zu den Ergebnissen des **BMW-Projektes “TRENDS”** (“Tracer-assisted evaluation of fluid transport and reservoir lifetime – is the expansive deployment of geothermal projects in ‘Malm’ formations beneath the Greater Munich Area sustainably scalable?”, 2014–2021, FKZ: **0325515**) zählen der tracergestützte Nachweis des petrothermalen Charakters eines ursprünglich als hydrothermal erschlossenen Reservoirs und die tracergestützte Prognose dessen thermischer Lebensdauer, sowie Befunde zur eingeschränkten Anwendbarkeit und Parametersensitivität sogenannter “Push-Pull”-Tests (*single-well injection-withdrawal*) mit Konservativtracern und Empfehlungen zum Design abgewandelter Einbohrlochtestverfahren für geothermische Reinjektions- bzw. Produktionsbohrungen. Trotz kongruenter Lebensdauerprognosen aus den inzipienten Produktionstemperaturtrends und den (halbwegs ‘vollständig’ erfassten) Tracersignalen, bleibt die Mehrdeutigkeit (*parameter interplay*) bei der Inversion hydrogeologischer Parameter aus beiden Signalarten für das als petrothermal befundete Malmreservoir frustrierend groß. Unerlässlich zur Eingrenzung des Parameterspielraums ist die erneute (gezielte!) Anwendung hydraulischer Testkonzepte mit Signalauswertung wie von T. Tischner (2020) vorgeschlagen. Um genuin-hydrogeologische Parameter (wie: Matrixporosität, effektive Aquifermächtigkeit, Kluftdichte, Kluftaperturen und -flächen, ggf. Kluftraumporosität) zu ermitteln, sind Push-Pull-Tests mit Konservativtracern alleine eher ungeeignet; mehr noch, sie wirken sich einschränkend und potentiell gefährdend aus mit Blick auf mittel- bis langfristig zu-erfassende Tracersignale aus großräumigen Thermalwasserkreislaufmarkierungen, welchen eine sehr viel größere Bedeutung für das Reservoirmanagement zukommt. Hingegen empfehlen sich Endotracer-Push-Pull-Tests unter Verwertung der bereits im Thermalwasserkreislauf zirkulierenden Tracer in deren mittlerem Tailing-Stadium und der ‘intermittierenden’ (mehr oder weniger periodisch wiederkehrenden) Gelegenheit von Bohrlochbehandlungen als Mittel zur quasi-kontinuierlichen Beobachtung des Reservoir-Langzeitverhaltens. Im BMWi-Vorhaben “TRENDS” sollten zweckmäßige (*multi-well, single-well, dual-tracer*) Fluidmarkierungsverfahren entwickelt und ein dediziertes Tracertestprogramm initiiert werden, für dieses Gebiet mit großräumig nachgewiesenen Hydrothermalressourcen (Malm-Formationen im Großraum München), um im Zuge deren expansiver Erschließung durch eine Vielzahl neuer Bohrungen, angesichts zunehmender hydraulischer und thermischer Interferenz unter ‘benachbarten’ Thermalwasserkreisläufen, ungünstige, potentiell-gefährdende Reservoirentwicklungen frühzeitig zu erkennen und quantitativ zu bewerten, um ihnen beizeiten, durch Anpassungen im Reservoirbetrieb und/oder an der Bohrloch(multipletten-)konfiguration, entgegensteuern zu können. Das **BMW-K-Verbundprojekt “GFK-MONITOR”** (“Fiber-optic sensing and tracer tools deployed for a versatile all-round monitoring of reservoir operation to secure durable geothermal plant integrity”; sub-project E: “Rationed artificial-tracer allocation in interfering fluid turnover loops with multiple injection spots”, FKZ: **03EE4036E**) bietet die Chance, dank tracerunabhängiger Verfahren zur Abbildung der Hohlräumstruktur (Fluidwegsamkeiten) und u. U. sogar des Strömungsfeldes in Realzeit (variabler Fließgeschwindigkeiten) zumindest im näheren Bohrlochumfeld, jene den Einbohrloch-Push-Pull-Tracersignalen inhärente Parametermehrdeutigkeit zu verringern, insbesondere die berüchtigte »hartnäckige Äquivalenz« zwischen transportwirksamer Porosität und Dispersivität »aufzuknacken«.

Aufgabenstellung im BMWi-Projekt “TRENDS”

Wie nachhaltig lässt sich ein gerade erschlossenes Geothermalreservoir bewirtschaften? Diese Frage lässt sich mit klassischen geophysikalischen und hydraulischen Methoden nicht beantworten. Die mögliche Betriebsdauer (Lebensdauer) des Reservoirs hängt von Fluidtransportgrößen ab, die nur über Tracertests (TT) messbar sind.

Malm-Grundwasserleiter im Molassebecken sind für die Geothermie mit verhältnismäßig geringem Fündigkeitsrisiko zu erschließen, im Vergleich zu den Petrothermalsystemen des Norddeutschen Beckens. Ihre Lebensdauer ist jedoch ungleich schwieriger zu prognostizieren. Zweifelsfrei erscheint vorab nur, dass im Zeitmaßstab der Fluidverweilzeiten (Jahre, Jahrzehnte oder länger) mit Wechselwirkungen zwischen den einzelnen Nutzungen des Malmaquifers durch Geothermieranlagen zu rechnen ist, die sich möglicherweise überlagern; zunächst dürften diese Effekte hydraulisch, später auch hydrogeochemisch und (viel) später auch thermisch erkennbar werden. Solche Entwicklungen (“Trends”) gilt es, frühzeitig zu erkennen, zu quantifizieren und ihnen ggf. gegenzusteuern.

Gegenstand des BMWi-Projekts “TRENDS” war die Entwicklung und Anwendung einer hierfür geeigneten *multi-well* und *single-well* (*mw*, *sw*) Tracertestmethodik, sowie die Initiierung eines dedizierten Tracertestprogramms für das Malm-Molassebecken im Münchner Großraum. Das Testprogramm sollte in Anbetracht der zu-erwartenden Signalüberlagerungen aus mehreren individuellen Traceranwendungen mit besonderer Sorgfalt dimensioniert werden. Geeignete hydrogeologische Konzeptmodelle und mathematische Transportmodelle liefern hierfür die Grundlagen. Die Aufgaben des Projekts umfassten im Einzelnen:

- Aufbau deterministischer Multikontinua-(Diskret-(Hybrid-))Modelle der heterogenen Zielreservoire
- Erarbeiten von Szenarien zur TT-basierten Lebensdauerprognose für geklüftetporöse Reservoir variablen Verkarstungsgrades, typisch für geothermisch-genutzte Malmaquifere im Molassebecken
- Entwicklung analytisch-numerischer Verfahren zur *mw*-basierten Erfassung von Speicher-Durchfluss-Verteilungen (SDV) im Aquifermaßstab, und zur SDV-gestützten Transportparameterinversion
- Design und Dimensionierung von *swTT* und *mwTT* zur Quantifizierung lebensdauer-kontrollierender Reservoirparameter bei verschiedentlich konfigurierten Bohrloch-systemen
- Pilotanwendung von *swTT* und *mwTT* an einem ausgesuchten Standort (Bohrloch-triplette), ggf. unter Einbeziehung thermosensitiver Tracer und der damit am Standort Pullach bis 2013 gemachten Erfahrungen
- Erarbeitung standortübergreifender Empfehlungen zum TT-gestützten Reservoir-monitoring und -management (über das Ende der Projektlaufzeit hinaus).

Die Stadtwerke München planen weitere und größere Geothermieranlagen im wachsenden urbanen Großraum, die aus Malmaquiferen in 3–6 km Tiefe (unter Berücksichtigung eines etwaigen, erwartungsgemäß ‘nicht prägenden’ Einflusses durch tektonische Verwerfungen) gespeist werden sollen. Beim Forschungsbedarf verschiebt sich der Schwerpunkt von Fragen der Bohrtechnik und Reservoirerschließung hin zu Themen der thermohydraulischen Nachhaltigkeit bei langfristigem gleichzeitigem Betrieb mehrerer Dutzend geothermischer Bohrungen im gesamten Malm-Molasseraum. Geophysikalische Verfahren liefern dabei kaum Aussagen zur *Lebensdauer* eines Geothermalsystems und hydraulische Methoden stoßen im Malm-Molassebecken wegen hoher Speicherkoefizienten sowie wegen hoher Durchlässigkeiten in den Auflockerungsbereichen von anliegenden Störungszonen an die Grenzen ihrer Aussagefähigkeit. Nur TT können Fluidverweilzeit- und SDV ermitteln, deren

Kenntnis für eine *standortübergreifend-nachhaltige* Bewirtschaftung der geothermischen Ressource unerlässlich ist. Darüber hinaus können swTT lokal wichtige Daten liefern, als Grundlage für technische Maßnahmen zur Erhöhung der (hydraulischen, hydrogeomechanischen, hydrogeochemischen) Lebensdauer von Reinjektionsstellen, nicht zuletzt auch zum Aufspüren ‘pathognomonischer’ Verschiebungen in Porositäts-Permeabilitäts-Verhältnissen als Frühwarnelement hinsichtlich induzierter Seismizität [1].

Zwischen der thermischen Lebensdauer T_{thermal} und der Fluidverweilzeit(-verteilung) T_{fluid} in einem Thermalwasserkreislauf besteht [2, 3] ein starker (monotoner) funktioneller Zusammenhang (cf. Abb. 1-oben). Andere Aspekte der ‘Nachhaltigkeit’ (Abb. 1-mittig) eines Thermalwasserkreislaufs hingegen weisen bis dato weniger eindeutige Korrelationsmuster mit T_{fluid} auf, obwohl die zugrundeliegenden THMC (gekoppelten) Prozesse, insbesondere im Zusammenhang mit induzierter Seismizität [1], sowohl vom kumulativen Fluidumsatz als auch von dessen Rate (implizit von T_{fluid}) abhängig sind.

Die Vorstellung einer großräumigen *mw-“Tracertomographie”* zur Parametrisierung heterogener (in 2D oder 3D) *distributed-parameter*-Modelle der markierten Reservoirs hat kaum Erfolgssicht, in Anbetracht des übergroßen Malmaquifervolumens sowie der Unstetigkeit, auch räumlich wechselnder Thermalwasserkreisläufe, die in einem “hoch-dynamischen” bzw. sehr labilen “Marktumfeld” betriebenen werden müssen.

In der zweiten Hälfte der Projektlaufzeit verschob sich die Aufgabenstellung von der tracer-gestützten Wärmebergbauprognoze [2, 3] hin zur sogenannten “*joint inversion*” gemessener Tracer- und Temperatursignale [4].

“Malm goes petrothermal?” – nicht wirklich ...

Ein überraschendes Projektergebnis ist der tracerbasierte Nachweis eines petrothermalen Charakters und einer petrothermal-dynamischen Fließratensensitivität in einem sonst *par-excellence* hydrothermalen Teilgebiet.

Ferner, diese zunächst als hydrothermal konzipierte Reservoirerschließung stellt nach unserer Einschätzung Deutschlands bis dato erfolgreichste Petrothermalprojekt dar. Der petrothermale Anteil des hier erschlossenen Reservoirs ist sogar höher, als bei den bislang erfolgreichsten Demonstrations- und Pilotvorhaben in klassischen Petrothermie-Domänen.

Die tracerbasiert ermittelte transportwirksame ‘Kluft’öffnungsweite (ca. 1/8 bis 1/6 Meter) ist eindeutig zu klein, um noch mit der “Aquifer-auskeilend”-Hypothese kompatibel zu sein; die ermittelte Mächtigkeit (4–7 Km) ist wiederum zu hoch, um einem einzelnen “Hydrofrac” zugeschrieben zu werden. In frühen Betriebsstadien ist allerdings die Aktivierung ungünstig ausgerichteter Klüfte (potentieller Verwerfungen?) entlang der Bohrlochdubletteachse möglich [3], infolge von Spannungsfeldrotation durch poroelastische Effekte; die Bohrloch-dublette wirkt zur frühen Betriebsstunde wie eine ‘Blattverschiebung’, d. h. wie ein *strike-slip* Herdprozess, was ggf. auch erklären würde, warum solche Klüfte bei der geophysikalischen Exploration nicht detektierbar waren und auch im hydraulischen Testprogramm an Einzelbohrungen zunächst keine Signale erzeugen konnten.

Die Übereinstimmung gemessener Tracer- und Temperatursignale (vgl. Abb. 2 und Abb. 3) mit einem Einzelkluftmodell (‘single fracture’) erscheint sogar prägnanter als bei den bisherigen Petrothermie-Standorten.

Zugleich erweist sich der bei Tracersignalinversion noch bestehende Parameterspielraum als unerheblich für die weitere ‘Wärmebergbau’-Prognose (Abb. 2), deren Spielraum deutlich enger ausfällt und mit höherer Wärme-Ausbeute, als nach einem Hydrothermalmodell zunächst erwartet. Diese weitgehende ‘Harmlosigkeit’ einer sonst auf Modellaufbau-Ebene frustrierenden Parameter-‘Indifferenz’ ist wiederum typisch für ein petrothermales Verhalten, wie auch die fließratenabhängige SDV-Dynamik.

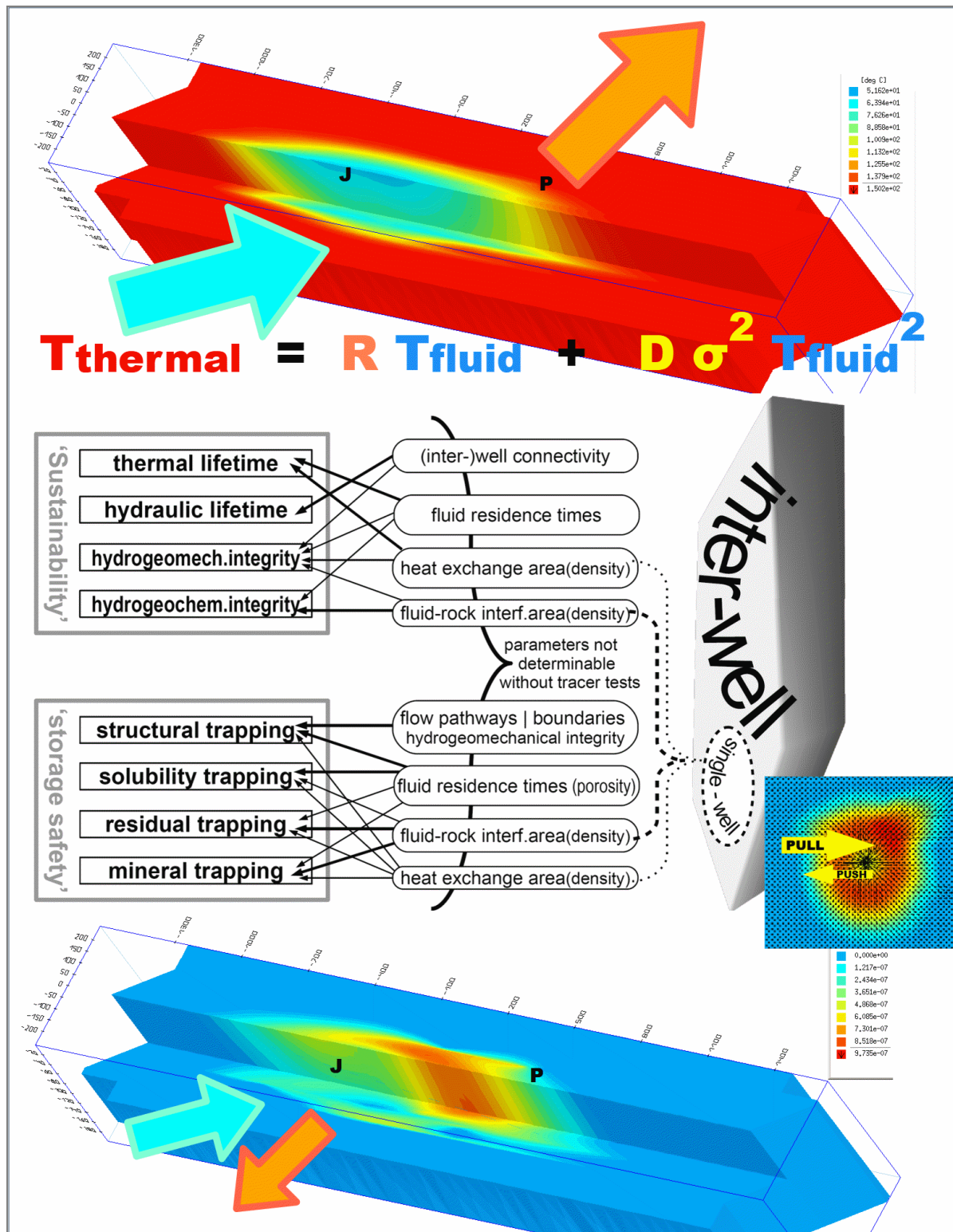


Abb. 1: Reservoireigenschaften und -parameter, deren Bestimmung über *iw(mw)TT* und/oder *swTT* angestrebt wird; tracertestmethodische Übertragbarkeit von Fragen der »Nachhaltigkeit« (Lebensdauer) geothermischer Reservoir auf Fragestellungen der Kapazität und Integrität geologischer Untergrundspeicher

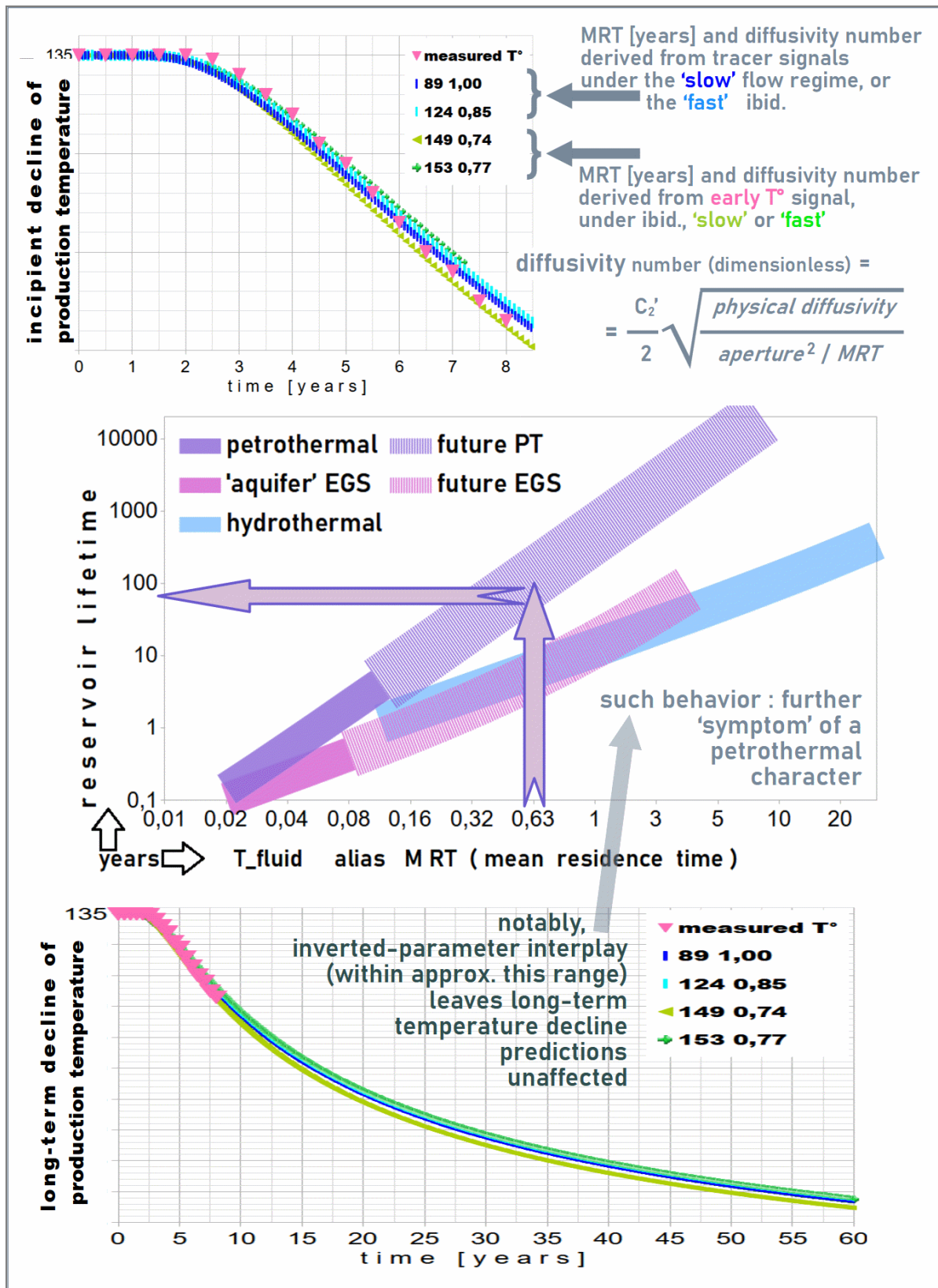


Abb. 2: Tracergestützte Neuermittlung des petrothermalen Charakters des Malmreservoirs; cf. auch die fließratenabhängige SDV-Dynamik in [10]

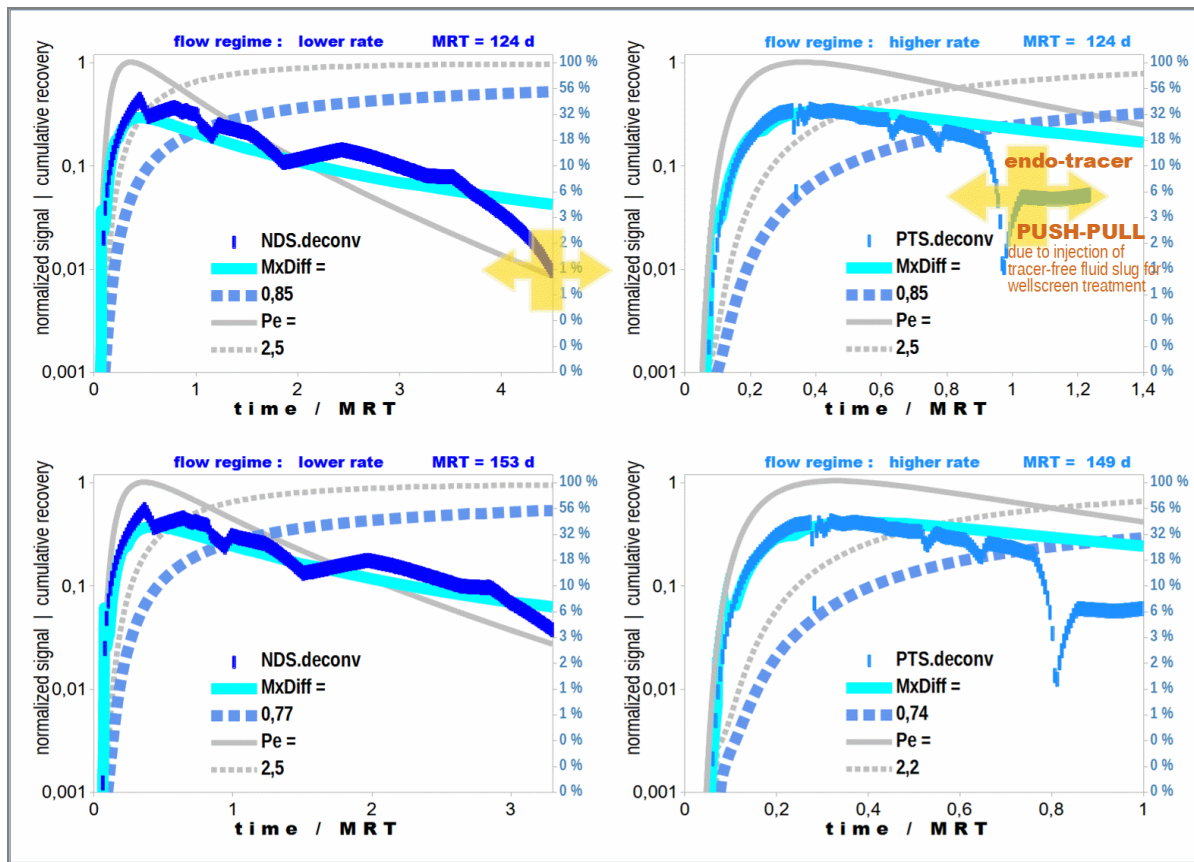


Abb. 3: Parameterinversion durch Kluftmodellanpassung an die gemessenen Tracersignale: mittlere Verweilzeit (*mean residence time* MRT), Pécletzahl und Diffusivitätsparameter (Pe und MxDiff, beide dimensionslos). Gemessene Tracersignale in Dunkelblau (links, erster Tracer, eingespeist bei niedrigerem Fluidumsatz) und Mittelblau (rechts, zweiter Tracer, eingespeist ca. 21 Monate später bei erhöhtem Fluiddurchsatz). In Hellblau ist jeweils die Modellanpassung dargestellt. Die nicht-stetigen Änderungen in den gemessenen Tracersignalen resultierten aus kurzzeitigen tracerfreien Fluidslug-Injektionen (Bohrlochbehandlungen). Unter gewissen Voraussetzungen lassen sie sich wie ein push-pull-TT interpretieren, wobei der im Thermalwasserkreislauf bereits länger (im mittleren Tailingstadium) zirkulierende künstliche Tracer jeweils wie ein »EndoTracer« fungiert; Details in [10,11]. In Grau ist das mit jeweils gleichen MRT- und Pe-Werten, jedoch ohne Matrixdiffusion simulierte Signal dargestellt. Die Differenz zwischen der hellblauen ($MxDiff > 0$) und grauen ($MxDiff = 0$) Kurve ist ein Maß für die Bedeutung der Matrixdiffusionsprozesse im Reservoir. Gleichfarbig gestrichelte Kurven stellen den kumulativen Tracermengenrückgewinnungsfaktor dar (in %, Achse jeweils rechts).

Empfehlungen zu Design und Dimensionierung sogenannter “Push-Pull”-Tests

Anders als bei Thermalwasserkreislaufmarkierungen [2], wo die Dimensionierung der Tracerzugabe sich nach eindeutigen Anforderungen richtet, hängt diese bei sog. “Push-Pull”-Tests (*single-well injection-withdrawal*, cf. [5, 6]) einerseits von den betriebs-/bohrlochoperativen Möglichkeiten bzw. Einschränkungen (begrenzte Fluidvolumina für “Push”- und/oder “Pull”-Stadien, begrenzte Shut-in-Dauer, beschränkte Fluidbeprobungsmöglichkeiten *downhole* falls freier Auslauf oder “Pull”-Volumen zu gering), andererseits vom mit dem Push-Pull-Test angestrebten Erkenntnisgewinn, bzw. von einem auf nicht-/advektive Parameter gerichteten Augenmerk [7, 8], wie in Abb. 4 summarisch dargestellt.

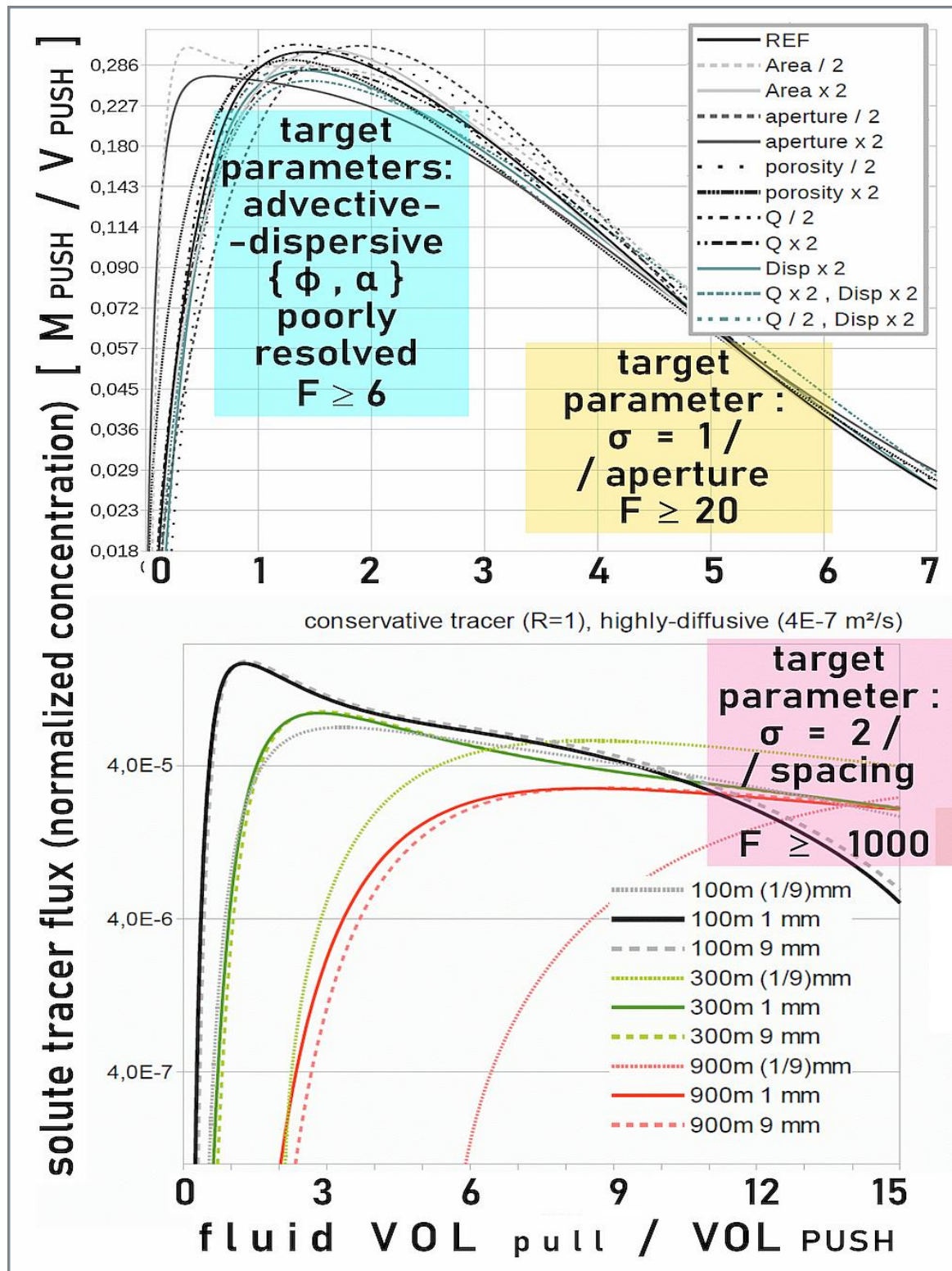


Abb. 4: Empfehlungen zur Push-Pull-Testdimensionierung, basierend auf Tracersignalsimulationen für Poren-Kluft-Reservoirmodelle in Anlehnung an Pilotstandorte – Diagrammelemente aus [5, 6, 7, 8] angepasst – abhängig vom angestrebten Erkenntnisgewinn und von bohrlochoperativen Fluidvolumenbegrenzungen für Pull- und/oder Push-Stadien

Die einzuspeisende Tracermenge M_{PUSH} muss immer ein Mehrfaches des Produkts zwischen dem gesamten Fluid-“Push”-Volumen (V_{PUSH}) und der (i. d. R. Fernlabor-instrumentellen) Bestimmungsgrenze (BG) der gewählten Tracerspezies betragen, etwa

$$M_{PUSH} = (b \square BG) \square (p \square V_{PUSH}) \square F$$

mit den dimensionslosen Faktoren

b : mindestens 10–15

p : mindestens 3

F : mindestens 6 für die Bestimmung advektiver Parameter { Porosität ~ Dispersivität }

F : mindestens 20 für die Bestimmung von Kluftaperturen

F : mindestens 300 für die Bestimmung langzeitwirksamer Grenzflächenparameter,

wobei sich insbesondere mit Letzterem prohibitiv hohe Tracermengen ergeben, die dann am Praktikabelsten mit Tracerspezies realisierbar werden, deren Nachweis, on-site oder (ggf. zusätzlich präparativ) nachgelagert Labor-instrumentell über belastbar detektierbare und empfindlich quantifizierbare Radioaktivität erfolgt. Den Simulationen anderer Autoren [9] zufolge, erscheinen zur Bestimmung langzeitwirksamer Grenzflächenparameter sogar um eine bis drei Größenordnungen höhere Mengenfaktoren erforderlich; ob diesen langzeit-asymptotischen Grenzflächenparametern, die bei der Beurteilung der Barrierefunktion von geringst-permeablem und zugleich hoch-porösem Gestein im Umfeld eines geologischen Endlagers von zentraler Bedeutung sind (wie beim in [9] betrachteten Culebra-Dolomit der WIPP von New Mexico), eine vergleichbar hohe Relevanz für das Management eines Geothermalreservoirs zukommt, ist indes umstritten.

Zur Ermittlung genuin-hydrogeologischer Parameter (wie: Matrixporosität, effektive Aquifer-mächtigkeit, Kluftdichte, Kluftaperturen und -flächen, ggf. Kluftraumporosität) sind Push-Pull-Tests mit Konservativtracern alleine grundsätzlich ungeeignet, aufgrund unauflösbarer Mehrdeutigkeiten [5–8] zwischen advektiven und non-advektiven Parametern bei deren Inversion aus messbaren Pull-Signalen; zudem wirken sie einschränkend und potentiell gefährdend hinsichtlich mittel- bis langfristig zu-erfassender Tracersignale aus großräumigen Thermalwasserkreislaufmarkierungen, welchen für das Reservoirmanagement eine sehr viel größere Bedeutung zukommt. In Kombination mit den im BMWK-Verbundvorhaben “**GFK-MONITOR**” (“*Entwicklung eines ganzheitlichen Monitorings mit Unterstützung der Glasfaserkabeltechnologie und Tracertechnik zur Verbesserung der Systemintegrität von Geothermieanlagen*”, Teilvorhaben 03EE4036E: “*Gesamtfrachtkontrolle künstlicher Tracer in großräumig wechselwirkenden Thermalwasserkreisläufen*”) entwickelten Verfahren zur Abbildung der Fluidwegsamkeiten und ggf. des Fließgeschwindigkeitsfeldes im Umfeld der Testbohrung eröffnet sich eventuell eine Möglichkeit zur Einengung advektiver Parameter und damit zur näheren Bestimmung der ‘übrigen’, non-advektiven Parameter.

Von großem Wert hingegen sind Push-Pull-Tests, um das physikochemische Verhalten sogenannter “thermosensitiver”, “oberflächensensitiver” oder aber [6] “dual-reaktiver” Tracer (kandidaten-)spezies unter Reservoirbedingungen realiter in-situ zu überprüfen und ggf. neu zu quantifizieren. Mit “dual-reaktiven” Spezies wiederum ließe sich die Äquivalenz advektiver und non-advektiver Parameter im Pull-Signal aufbrechen, wie in [6] theoretisch dargelegt.

An geothermischen Reinjektionsbohrungen empfehlen sich vielmehr “Push–Shut-in”–Tests mit zumindest kampagnenartiger, wenn möglich längerfristiger Temperaturfassung *down-hole* (tiefenaufgelöst). Für geothermische Produktionsbohrungen hingegen empfehlen sich “Dilute-and-Retrieve”–Tests mit den bereits lange zuvor, im Rahmen von Thermalwasserkreislaufmarkierungen eingespeisten Tracerspezies, in ihrem mittelfristigen *tailing*-Regime als sogenannte ‘Endotracer’ [10, 11] fungierend, wie mit Pfeilen in Gelb in Abb. 3 skizziert.

Wenn das "Pull"-Volumen zu klein bzw. die "Pull"-Dauer zu kurz ist (wie in der Praxis, notgedrungen, nicht selten der Fall zu sein droht) bleibt auch mit "bestens qualifizierten" Tracerspezies die Mehrdeutigkeit non-/advektiver und insbesondere der kluftbezogenen Parameter bestehen. Bei zu-geringem "Push"-Volumen (geringem Fluid-Eindringradius in die Formation) verstärkt dieser Effekt die ohnehin begrenzte räumliche Repräsentativität der gewonnenen Parameterbeziehungen.

Die Durchführung von "Push-Pull"-Tests mit künstlichen Tracerspezies an geothermischen Produktionsbohrungen, noch bevor Tracersignale aus großräumigen Thermalwasserkreislaufmarkierungen eindeutig detektierbar werden, stellt ein nicht hinnehmbares Risiko dar. In späteren Stadien, wenn TWK-Signale eindeutig werden, entschärft sich der Zielkonflikt. Aus den gleichen Gründen ist auch bei Reinjektionsbohrungen im frühen, gewissermaßen noch 'explorativen' Betriebsstadium, wo die Eventualität einer Bohrlochfunktionsumwandlung (Produktion statt Reinjektion) noch nicht ausgeschlossen ist, Zurückhaltung hinsichtlich des Einsatzes künstlicher Tracer geboten.

Fazit

Unter Ausnutzung der bereits im Thermalwasserkreislauf zirkulierenden 'Endotracer' [10, 11] in deren mittlerem *tailing*-Stadium und der 'intermittierenden' (mehr oder weniger periodisch wiederkehrenden) Gelegenheit von (erweiterten) 'Bohrlochbehandlungen' bietet sich eine dankbare Möglichkeit zur quasi-kontinuierlichen Beobachtung des Reservoirverhaltens im Umfeld einer geothermischen *Produktionsbohrung* (besonders im 'reiferen' Betriebsstadium, wo mit signifikanten Auswirkungen thermohydraulischer, thermohydromechanischer und hydrogeochemischer Prozesse zu rechnen ist), da die für Thermalwasserkreislaufmarkierungen eingesetzten Tracerspezies über längere Zeiträume signifikant empfindlicher nachweisbar bleiben, als elektrische Leitfähigkeitsunterschiede am Fluid oder Konzentrationsunterschiede gängiger isotopen-/geochemischer Fluidtracer. Limitierender Designfaktor für 'Endotracer'-Push-Pull-Tests ist dabei meistens die Volumenbegrenzung sowie die ggf. erforderliche chemische Konditionierung (mit erhöhten Kosten und ohnehin im Zielkonflikt mit einer etwaigen Lf-Nutzung als Tracer) des "Push"-Fluids, angesichts der Gefahr induzierter Wasser-Gesteins-Wechselwirkungen, die später zu Ausfällungen im Umfeld der Bohrung führen können.

Literatur

- [1] Shapiro, S. A.: *Fluid-induced seismicity*. Cambridge University Press (2015)
- [2] Ghergut, J., Behrens, H., Licha, T., Sauter, M.: *Stanford Geotherm. Procs.*, SGP-TR-198, 309–315 (2013)
- [3] Behrens, H., Ghergut, J., Sauter, M., Wagner, B., Wiegand, B.: *Stanford Geotherm. Procs.*, SGP-TR-216, 195–201 (2020)
- [4] Behrens, H., Ghergut, J., Sauter, M.: *Stanford Geotherm. Procs.*, SGP-TR-224, 1–10 (2023)
- [5] Ghergut, J., Behrens, H., Sauter, M.: *Stanford Geotherm. Procs.*, SGP-TR-198, 295–308 (2013)
- [6] Ghergut, J., Behrens, H., Sauter, M.: *Stanford Geotherm. Procs.*, SGP-TR-198, 326–335 (2013)
- [7] Ghergut, J., Behrens, H., Bensabat, J., Sauter, M., Wagner, B., Wiegand, B.: *Stanford Geotherm. Procs.*, SGP-TR-213, 170–180 (2018)
- [8] Ghergut, J., Behrens, H., Sauter, M.: *Geothermics*, 63, 225–241 (2016)
- [9] Haggerty, R., McKenna, S. A., Meigs, L. C.: *Water Resour. Res.*, 36(12), 3467–3479 (2000)
- [10] Ghergut, J., Bedoya-González, D. A., Bensabat, J., McDermott, C. I., Wagner, B., Wiegand, B., Sauter M.: *Stanford Geotherm. Procs.*, SGP-TR-214, 217–227 (2019)
- [11] Behrens, H., Ghergut, J., Sauter, M.: *Stanford Geotherm. Procs.*, SGP-TR-218, 130–135 (2021)

Lithiumgewinnung im Thermalwasserkreislauf – wie es mitunter zu Fehlprognosen kommt

J. Ghergut, B. Wiegand, H. Behrens, M. Sauter

Universität Göttingen, Geowissenschaftliches Zentrum, Dept. Tiefe GeoReservoir

Abstract

Bei der geothermischen Co-'Erzeugung' eines Fluidinhaltsstoffes wie Lithium kann zunächst ein konservativer Transport desselben im Thermalwasserkreislauf angenommen werden. Damit wird auch der Transport eines beliebigen konservativen Tracers, der dem Thermalwasserkreislauf künstlich beigeimpft wurde, nahezu 1:1 repräsentativ für den Lithiumtransport, bis auf etwaige Matrixdiffusionsunterschiede, welche allerdings eine tracerbasierte Prognose des Lithiumtransports nicht nennenswert »verfälschen«, zumal die nominellen Diffusionskoeffizient-Unterschiede, bei ionischen Spezies in wässriger Lösung, durch deren Hydratisierung stark gedämpft werden. Sonstige Transportparameter sind für das natürliche Lithium und den künstlichen Tracer praktisch gleich, nur die Anfangs- und Randbedingungen (beim Thermalwasserkreislaufszenario mit Co-'Erzeugung') unterscheiden sich. Damit lässt sich der Lithiumtransport bzw. die Lithium-Abreicherung (*depletion*) im zirkulierenden Fluid durch Konvolution seiner 'Reinjektions'-Randbedingung mit dem Green'schen Kernel des künstlichen Tracersignals beschreiben bzw. vorhersagen, sofern ein auswertbares, halbwegs 'vollständiges' (und im Reservoir unter dem gleichen Fließregime gewonnenes) Signal eines künstlichen Tracers bereits vorliegt. Dieses Vorgehen wird hier anhand von Mustersignalen, in Anlehnung an bereits durchgeführten Geothermalreservoirmarkierungen (Tracertests) im Norddeutschen Becken und im Oberrheingraben demonstriert. Dabei zeigt sich, dass frühe Beobachtungen zur Lithium-'Ergiebigkeit' einer geothermischen Dublette keinen belastbaren Prädiktor der späteren Gesamtausbeute darstellen. Aber auch die künstlichen Tracersignale können insofern irreführend wirken, dass sie die 'fernen' Randbedingungen einer etwaigen geogenen Lithium-Nachlieferung nicht erfassen können.

Aufgabenstellung im BMWi/BMWK-Projekt "UNLIMITED"

Parallel zur Erfassung künstlicher Tracersignale und deren Auswertung oder Nachbildung im Rahmen analytischer oder numerischer Reservoirmodelle, werden im BMWi/BMWK-Projekt **UNLIMITED** ("Untersuchungen zur Lithiumproduktion aus heißen Tiefenwässern in Deutschland", FKZ: 03EE4023E) auch standortunabhängige Verfahren entwickelt, um die Nachhaltigkeit (**N**) der Li-Gewinnung im Thermalwasserkreislauf (TWK) tracergestützt zu bewerten und weiterhin quantitativ vorherzusagen. **N** umfasst gegenläufige Beiträge:

- |> einerseits hydraulisch bedingte **N**-Verluste durch Rezirkulation abgereicherter Fluide,
- |> andererseits ggf. durch Wasser-Gestein-Wechselwirkungen induzierte **N**-Gewinne.

Quantifizierbar sind Letztere vorzugsweise durch natürliche Tracer, Erstere vielmehr durch künstliche Fluidmarkierung (Tracertests) im TWK.

Die Li-Ausbeute als Funktion der Zeit bzw. des kumulativen Fluidumsatzes ergibt sich [1, 2] als Summe dreier Terme, von welchen nur der erste in frühen Betriebsstadien messbar ist: ein linearer Anstieg mit dem Fluidumsatz, proportional mit der Konzentrationsdifferenz: Li-Konzentration im anfangs ungestörten natürlichen Reservoirfluid, abzüglich seiner Residualkonzentration im 'verbrauchten' und reinjizierten Fluid. Letztere hängt vom oberflächig angewendeten Li-Extraktionsverfahren ab, stets Gegenstand von standortspezifischen Anlagenoptimierungen sowie von allgemeinem technischem Fortschritt.

Standortunabhängige Befunde

Wir können nun quantitativ darstellen, wie der erste Term mitunter irreführend wirkt, wenn er über längere Zeiträume der Li-Ausbeuteprognose zugrundegelegt wird. Mittel- bis langfristig wird der lineare Anstieg in Wirklichkeit zunehmend gebremst (Abb. 1: dunklere Blautöne) durch unvermeidliche, hydraulisch bedingte Rezirkulationsverluste, d. h. durch allmählich fortschreitende Li-Abreicherung im TWK. Möglicherweise – jedoch eher ausnahmsweise – werden solche Verluste kompensiert durch Freisetzung ‘frischer’ Li-Ionen aus dem umliegenden Gestein.

Tracertests ermöglichen eine standortübergreifend standardisierte Prognose des hydraulisch bedingten Verlustterms, unabhängig von Verfügbarkeit und Parametrisierung (Kalibrierung) etwaiger (numerischer) Reservoirmodelle für den jeweiligen Standort.

Anhand normierter Typkurven (Abb. 2) zeigt sich ferner, dass vom gemessenen Tracer-signal, im Endeffekt, nur die normierten verweilzeitstatistischen Momente nullter und erster Ordnung zählen:

Mom.0 = R% = asymptotischer Rückgewinnungsfaktor des Tracers,
mit (1 - R) als »Öffnungswinkel« des TWK interpretierbar

Mom.1 = MVZ = mittlere Verweilzeit des Tracers im Reservoir
oder RUV = Reservoir[fluid]umsatzvolumen
[im Angelsächsischen eher geläufig:
MRT = mean residence time ,
TOV = reservoir turnover volume]

Mom.2, als Maß für die Fließfeldheterogenität, äquivalent mit dem Kehrwert der Pécletzahl (1/Pe) in allen Abbildungen beeinflusst die Li-Ausbeute nur zeitweise, meist nicht länger als 5xMVZ. Abb. 2 zeigt eine etwas größere Pe-Spannweite (1 bis 10) als Abb. 1 und Abb. 3, wobei niedrige Werte auch einen stärkeren Einfluss durch Matrixdiffusionsprozesse und/oder verstärkte Strömungsdivergenz im Umfeld von Störungszonen charakterisieren können).

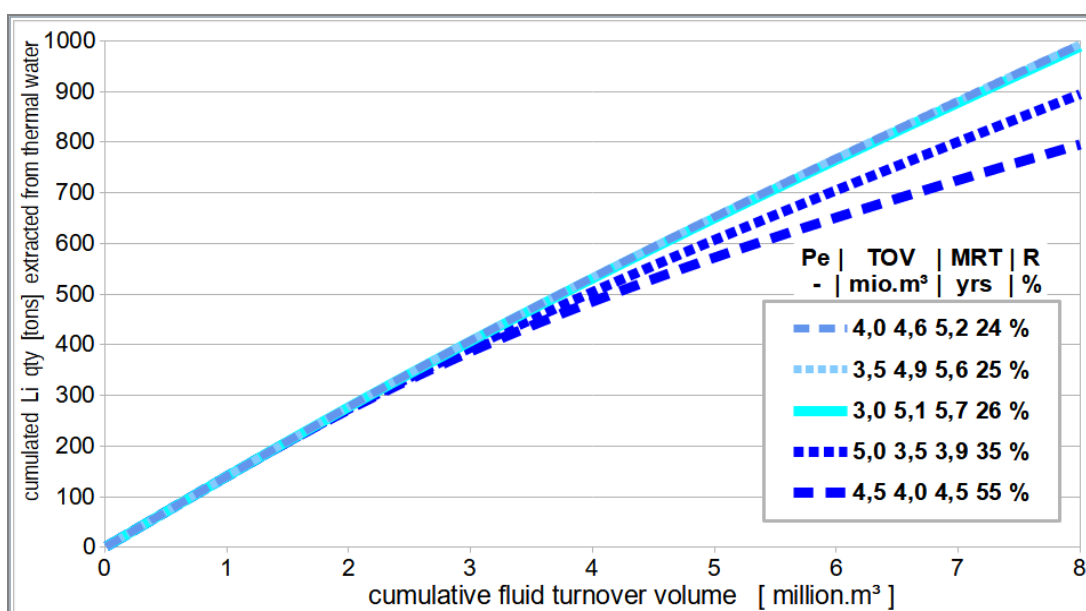


Abb. 1: Lithium-Ausbeute für Reservoirs unterschiedlicher Größe (Reservoirumsatzvolumen TOV oder mittlere Fluidverweilzeit MRT), Heterogenität (1/Pe) und TWK-Öffnungswinkel (1-R)

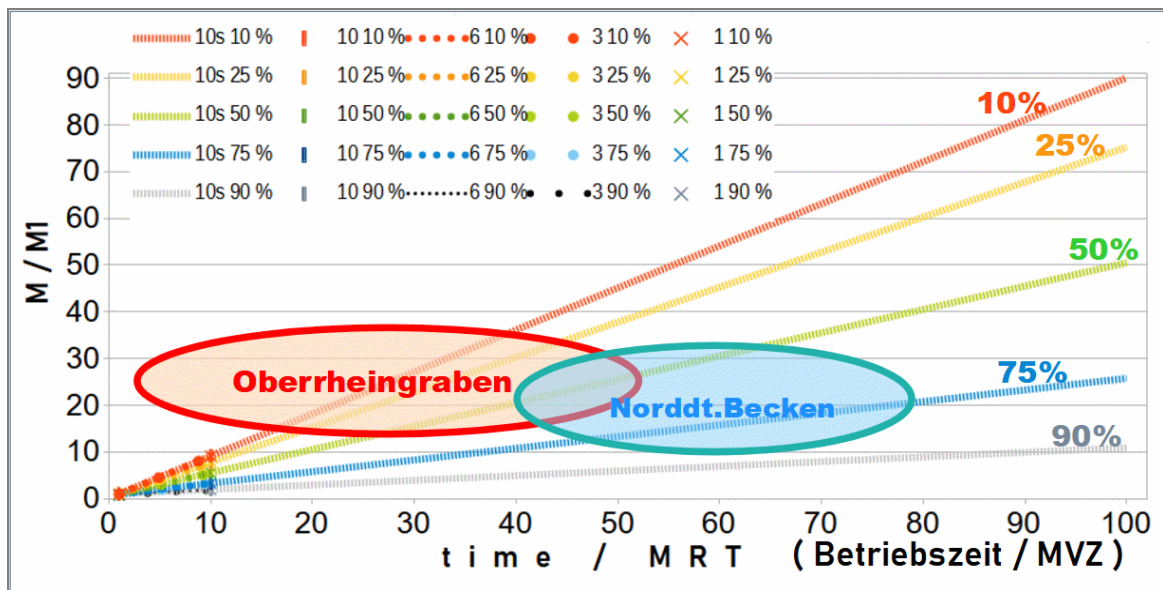


Abb. 2: Lithium-Ausbeute, normiert durch den Anfangsgehalt (M_1) eines ersten TWK-“Durchlaufs” (RUV bzw. TOV), als Funktion der Betriebszeit, normiert durch die mittlere Fluidverweilzeit

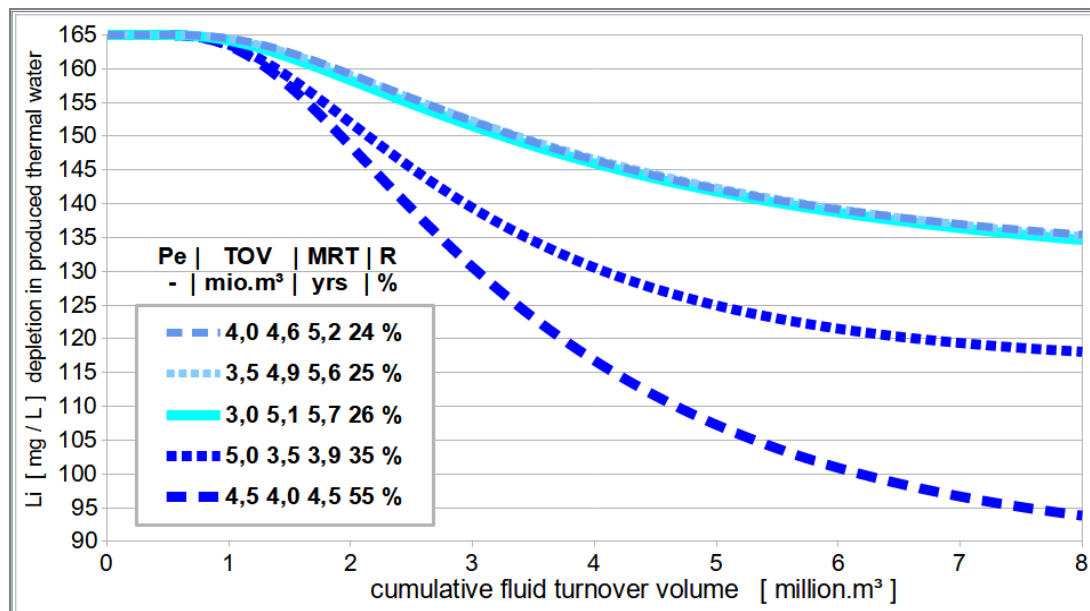


Abb. 3: Li-Abreicherung im Thermalwasserkreislauf unter den gleichen Bedingungen wie in Abb. 1

Der zeitliche Verlauf der Li-Abreicherung im Thermalwasserkreislauf (Abb. 3) zeigt zwar sehr deutliche Unterschiede, je nach den (tracerbasiert-ermittelten) Werten für die Fluidverweilzeit (MVZ, MRT) bzw. das Reservoirumsatzvolumen (RUV, TOV). Intuitiv würde man erwarten, dass hauptsächlich diese Reservoirgröße die Li-Gesamtausbeute bestimmt, denn »so viel« Lithium wäre sozusagen »insgesamt drin«. Mittel- bis langfristig zeigt sich jedoch, dass der Tracerrückgewinnungsfaktor (R%) diese Reservoirgröße »übersteuert«, d. h. ein kleineres Reservoir mit größerem (1-R)-Wert eine höhere Li-Ausbeute liefert, als ein größeres Reservoir mit kleinerem (1-R)-Wert (vgl. Abb. 1).

Fazit

Für die konservative Li-Ausbeuteprognose kommt es nicht auf eine akkurate modellmäßige Nachbildung aller Reservoirdetails, sondern nur auf Randbedingungen und Permeabilitätskontraste an, welche den asymptotischen Tracerrückgewinnungsfaktor kontrollieren. Die Fluidverweilzeit- oder Speicher-Durchfluss-Verteilung im Reservoir unter den Bedingungen (*forced-gradient* Strömung) des Thermalwasserkreislaufs ist von zentraler Bedeutung für die Wärmearausbeute und die thermische Lebensdauer des Reservoirs. Auf die Gesamtausbeute eines im Thermalwasserkreislauf co-‘erzeugten’ Fluidinhaltsstoffes wie Lithium wirkt sie sich nicht nennenswert aus; hingegen der Tracerrückgewinnungsfaktor, der die Wärmebergbauprognose nur nachrangig beeinflusst, ist für die stoffliche Gesamtausbeute entscheidend.

Was auch quasi-‘vollständig’ vorhandene künstliche Tracersignale leider nicht vermitteln können, sind etwaige Nachlieferungsraten des natürlichen Fluidinhaltsstoffes an fernen Reservoirrändern und/oder an inneren Grenzflächen sowie aus dem umliegenden Gestein durch die im (Dubletten-)Zirkulationsverfahren hervorgerufenen (und infolge fortschreitender Abreicherung zunehmenden) Konzentrationsgradienten.

Literatur

- [1] Behrens, H., Ghergut, J., Sauter, M., Wagner, B., Wiegand, B.: *Stanford Geotherm. Procs.*, SGP-TR-223, 200–210 (2022)
- [2] Ghergut, J., Wiegand, B., Behrens, H., Sauter, M.: *Stanford Geotherm. Procs.*, SGP-TR-224, 1–9 (2023)

CompReact: Compositional Simulation of Reactive Transport in CO₂ Storage

M. Wirth, W. Yan

Technical University of Denmark

Carbon capture and storage (CCS) is a key strategy for reducing greenhouse gas emissions and mitigating climate change. The process involves capturing CO₂ from various sources and storing it in geological formations, but the long-term stability and safety of CO₂ storage sites are not yet fully understood. The CompReact project, funded by Innovation Fund Denmark under the INNO-CCUS research partnership, aims to improve our understanding of CO₂ storage by developing advanced simulation techniques that can capture the complex chemical reactions that occur when CO₂ is injected into subsurface reservoirs.

The project focuses on developing high-resolution numerical models that can simulate how CO₂ interacts with the rock matrix, fluids, and other geochemical components in the storage reservoir. The models account for the transport of fluids, gases, and heat, as well as the chemical reactions between CO₂ and the minerals in the reservoir. The researchers plan to develop a next-generation compositional CO₂ storage simulator with multiphase geochemical reactions that is applicable to various geological reservoir types, including aquifers and depleted petroleum reservoirs, and dramatically improved in terms of efficiency and robustness.

To achieve this, the researchers plan to utilize novel RAND-based multiphase reaction algorithms that have recently been developed at DTU. The algorithms treat phase and chemical equilibrium simultaneously and are particularly suited to situations with many phases and reactions, such as CO₂ storage. The developed simulator will be able to handle both near-wellbore and reservoir-scale simulations during the injection and post-injection periods, with a general non-isothermal formulation to account for local operational issues.

The project involves two work packages, focusing on the development of a highly-efficient compositional reactive simulator and large-scale simulation coupled with GEOSX. The new GEOSX simulator will be applied to long time-scale post-injection simulations with coupled geomechanics, allowing for the analysis of pressure and stress variation and CO₂ plume development. This project is and the coupling of the two work packages is a collaboration with Stanford University.

In summary, the CompReact project aims to develop a highly efficient and reliable CO₂ storage simulator with multiphase geochemical reactions that will be applicable to various geological reservoir types. The novel RAND-based algorithms developed at DTU will be utilized to provide a new formalism for compositional CO₂ storage simulation with multiphase reactions. The coupling with GEOSX will create synergy based on complementary expertise, allowing for the analysis of pressure and stress variation and CO₂ plume development during long-term simulations. This project will significantly contribute to technical risk assessment and support the realization of a sustainable carbon-neutral energy system.